THE DYNAMIC ORGANIZATION OF PROTEINS IN THE SYNAPTIC BOUTON

Dissertation

for the award of the degree

"Doctor rerum naturalium"

of the Georg-August-Universität Göttingen

within the doctoral program "Molecular Biology"

of the Georg-August University School of Science (GAUSS)

submitted by

Sofiia Reshetniak

from Kherson, Ukraine

Göttingen 2021

Thesis Advisory Committee

Prof. Dr. Silvio Rizzoli, *Institute of Neuro- and Sensory Physiology, University Medical Center Göttingen*

Prof. Dr. Reinhard Jahn, *Laboratory of Neurobiology, Max Planck Institute for Biophysical Chemistry*

Prof. Dr. Andreas Janshoff, *Department of Biophysical Chemistry, Institute for Physical Chemistry*

Members of the Examination Board

1st Reviewer: Prof. Dr. Silvio Rizzoli, *Institute of Neuro- and Sensory Physiology, University Medical Center Göttingen*

2nd Reviewer: Prof. Dr. Reinhard Jahn, *Laboratory of Neurobiology, Max Planck Institute for Biophysical Chemistry*

Further members of the Examination Board

Prof. Dr. Andreas Janshoff, *Department of Biophysical Chemistry, Institute for Physical Chemistry, Georg August University Göttingen*

Prof. Dr. Nils Brose, *Department of Molecular Neurobiology, Max Planck Institute of Experimental Medicine*

Dr. Sarah Adio, *Department of Molecular Structural Biology, Institute for Microbiology and Genetics, Georg August University Göttingen*

Prof. Dr. Carolin Wichmann, *Institute for Auditory Neuroscience & InnerEarLab, University Medical Center Göttingen*

Date of oral examination: 13.10.2021

TABLE OF CONTENTS

SUMMARY

Protein availability is crucial for maintaining cellular processes. In synapses, the identities and functions of proteins involved in neurotransmission are well known. Their spatial distribution, copy numbers, and lifetimes have also been thoroughly investigated. However, little information is available on their mobility and its regulation. In this thesis, I have addressed this issue by analyzing the mobility of 45 diverse proteins in the synapses of primary hippocampal neurons. Relying on the fluorescence recovery after photobleaching (FRAP) technique, I have measured the mobility of proteins in the axons and synapses of living neurons. The FRAP results were then combined with electron microscopy data and *in silico* simulations to extract detailed information on protein mobility. The results provided diffusion coefficients for the analyzed proteins in various locations of the synapto-axonal compartment, demonstrating generally lower mobility in the synapses compared to the axons, and, as expected, lower mobility for membrane proteins as compared to soluble proteins. The main parameters affecting protein mobility were determined to be synaptic geometry and binding to the synaptic vesicles.

I then aimed to further investigate the role of the synaptic vesicles in the regulation of synaptic protein mobility. An *in vitro* approach was employed to measure the diffusion of purified synaptic proteins in the presence or absence of synaptic vesicles in a cell-free system, using fluorescence correlation spectroscopy (FCS). The results demonstrated a major impact of the synaptic vesicles on protein mobility, but implied that other parameters, such as the spatial organization of the synaptic vesicle cluster, also play a role in determining protein mobility in the synapse. Combined with previous observations, these results suggest a fundamental role of the synaptic vesicle cluster in the organization and maintenance of synaptic morphology and physiology.

The generated data provide quantitative information on the mobility (expressed as a fraction of mobile molecules and their diffusion coefficients) and distribution of major synaptic proteins (including key SNAREs, endo- and exocytosis co-factors, and cytoskeletal components) in synapses, the synaptic vesicle cluster, and axons. This represents the most detailed view of the dynamic organization of proteins in the synaptic bouton presently available and was used to generate a representational visual rendering of protein mobility in the synaptic bouton.

Additionally, the quantitative data provided here can be used while generating computational models of synaptic physiology, allowing for models of higher precision than were previously possible. For example, these data have been used to computationally analyze the involvement of dynamin and clathrin in the endocytosis of synaptic vesicles. By considering the mobility rates and copy numbers of the corresponding proteins, such analysis explained why clathrin-independent pathways of vesicle retrieval must be employed to maintain the spontaneous network activity. This example demonstrates how the mobility data can be used to obtain additional information on synaptic processes that were difficult to address in the past. The generated database of synaptic protein mobility data will be useful not only for laboratories specializing in the modeling and system biology of synapses, but also for investigations of individual proteins, and the generated visualizations can also be used for educational purposes. As such, the results presented here have a broad spectrum of potential applications.

INTRODUCTION

Apart from the primitive *Porifera*, who were the first group to branch off of the *Metazoa* evolutionary tree, all animals have a nervous system. A common feature that is indispensable for any, no matter how primitive, neural system is the presence of cell contacts between the neural cells, neurons. These contacts allow information to be tranduced from one neuron to another, which is a prerequisite for coordinated and regulated responses to the environmental stimuli, bodily movements, and organ functioning, including the higher neural functions such as memory, cognition, and speech.

The connections between the neurons are known as synapses, of which there are two types: electrical and chemical. An electrical synapse is formed by gap junctions that directly connect the cytoplasm of two neurons. In this case, the signal is transduced from one cell to another directly in a form of an action potential via an ion flow through the gap junctions. This allows fast and synchronous neurotransmission but lacks directionality as well as amplification and modulation possibilities.

The chemical synapses compose the majority of the synapses in the central neural system, and this work is focused specifically on this type of synapses. In these synapses the action potential does not travel directly from cell to cell, since neurons remain completely separated by their membranes, but must be converted into a chemical signal.

A typical chemical synapse consists of a presynaptic terminus (a presynapse or a synaptic bouton) on an axon of one cell, which is apposed to a postsynaptic terminus (a postsynapse or a dendritic spine) on a dendrite of another cell. The pre- and postsynapse are separated by a narrow space (approximately 20 nm wide), called the synaptic cleft. An action potential causes the synaptic bouton to release neurotransmitter stored in synaptic vesicles (SV), which then diffuses trough the synaptic cleft and is recognized by post-synaptic receptors, resulting in de- or hyperpolarization of the postsynaptic membrane.

Neurotransmitter release in response to stimulation is a key feature of the chemical synapses, and the site where it occurs, the synaptic bouton, is one of the most intensively studied structures of an animal body. While being small in size and often located meters away from the cell body, these structures operate seemingly autonomously. They are able to maintain and finely control the molecular processes that lead to both the fastest reflexive reactions of an animal, and to the most complex behavioral and cognitive presentations. While the general molecular mechanisms of the presynaptic neurotransmission and the composition of the synaptic bouton are well known, it is not clear how the temporal requirements of respective reactions are fulfilled. Starting with the basics, with only a few exceptions, we do not know the rates of protein mobility in the presynapse, and, consequently, we do not know how protein supply within the presynapse is sustained and regulated.

In this section I will summarize the information we have on the synaptic boutons, including their composition and organization, and the available quantitative data on the protein requirements for maintaining synaptic activity. I will then discuss how the proteins can be delivered to the synapse and to

their respective target locations within the presynapse, and what information we have on the protein mobility rates in neurons. I will finish the introduction by highlighting which important aspects remain unknown and explain how I intended to address these in my PhD project.

The following two chapters, presented in a form of published articles, will describe two sets of experiments I performed to answer the questions posed. The first one focuses on the measurements of protein mobility rates in the presynapses of living neurons and evaluates the global protein dynamics in the presynapses. The second one uses an *in vitro* approach to validate the findings on the role of the synaptic vesicles in the regulation of synaptic protein mobility.

I will conclude with the Discussion section, where I will discuss possible interpretations and implications of the findings, and present possible future uses of the obtained data.

No parts of this work included experiments on the postsynaptic side of the synapse, and in all the sections the term "synapse" is mainly used to refer to the synaptic bouton only.

The synaptic bouton

Morphology and composition

Synaptic boutons present as widened regions of an axon and can be found both at the ends of the axons as well as along them (so called *en passant* synapses). Depending on their location, synapses can substantially vary in size and shape (Innocenti and Caminiti, 2017; Rollenhagen and Lübke, 2006). Synapses of the cultured hippocampal neurons are on the smaller side of this range and were estimated to have a volume of 0.122 ± 0.106 μm^3 (Schikorski and Stevens, 1997), which roughly corresponds to a diameter of 0.5 – 1.5 µm.

While not being defined by a membrane enclosure, synapses maintain a specific protein and organelle composition (Figure 1), which distinctly differentiates them from the rest of the axon. This being said, identifying synapses in the first electron microscopy images used to be a challenging task in the past (Palay, 1956). At that time the concept of a synapse was largely physiological, while their morphology was not yet understood. However, the very first electron microscopy observations quickly accumulated information on a number of structures that are characteristic of all synapses and unequivocally differentiate them from other parts of a neuron.

One defining component of the presynapse is a protein-rich area found next to the plasma membrane, closely apposed to the postsynaptic membrane of the dendritic spine. This area, termed the active zone (AZ), is the site where the neurotransmitter release occurs. The AZ contains a number of proteins that are crucial for different steps of presynaptic neurotransmission. Various molecules of cellular adhesion (Chavis and Westbrook, 2001; Missler and Südhof, 1998; Mizoguchi et al., 2002; Rougon and Hobert, 2003; Shapiro and Colman, 1999; Walsh and Doherty, 1997) align the release site with the postsynaptic density (PSD) of the postsynapse. Voltage-gated calcium channels (Haydon et al., 1994; Kawasaki et al., 2004; Robitaille et al., 1990) allow local changes in Ca^{2+} concentration, which cause vesicle release.

Plasma membrane SNARE molecules (SNAP25, syntaxin), while are not restricted to the active zone and are found in the axonal plasma membrane throughout (Garcia et al., 1995), are directly required for vesicle fusion at the active zone (Jahn and Grubmüller, 2002; Jahn and Scheller, 2006; Montecucco et al., 2005; Rizo and Südhof, 2002). Multiple scaffolding proteins (Muncs, Piccolo, Bassoon, RIM, RIM-BPs) arrange all these components at the active zone and regulate vesicle priming, docking, and release (Brose et al., 1995; Dieck et al., 1998; Fenster et al., 2000; Wang et al., 1997, 2002).

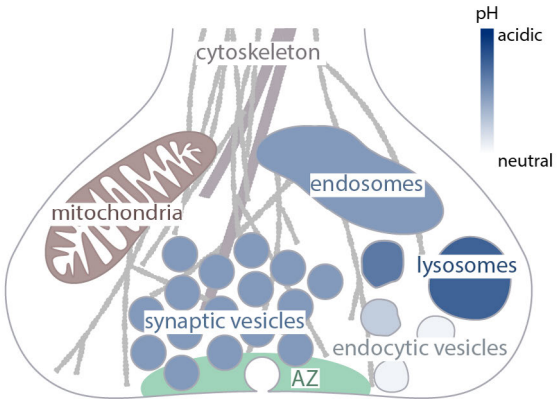

Figure 1. Components of the synaptic bouton. The synaptic bouton contains synaptic vesicles organized into a synaptic vesicle cluster, organelles of the endo-lysosomal pathway, mitochondria, and various cytoskeletal components. A prominent protein-reach area termed the Active Zone is the site where exocytosis of the SVs and release of the neurotransmitter occurs. Figure from Reshetniak and Rizzoli, 2019.

Another component that was used to identify synapses in the early studies is mitochondria (Palay, 1956), which were observed to accumulate at the synapses in larger numbers than in the axons. Synapses require ATP for multiple processes related to the neurotransmitter release and since synapses can be found meters away from the cell body (for example the neuromuscular synapses in distal limb muscles of large mammals), they must rely on local mitochondria for energy supply. It has been later shown that on average each synapse contains one mitochondrion (Sakata and Jones, 2003), which occupies up to 1/3 of the synaptic volume (Verstreken et al., 2005; Wilhelm et al., 2014), although synaptic mitochondria tend to be smaller in size compared to the ones found elsewhere (Chavan et al., 2015). At the same time, some studies show that about half of the synaptic boutons lack mitochondria (Chavan et al., 2015; Shepherd and Harris, 1998). Such synapses, however, can transiently recruit axonal mitochondria in an activity-dependent manner (Chang et al., 2006; Shepherd and Harris, 1998), indicating that local mitochondria are required for synaptic activity.

The positioning of mitochondria within the synapse is likely maintained by cytoskeletal components, including microtubules, which are also associated with the SVs and the active zone (Bird, 1976; Chan and Bunt, 1978; Gordon-Weeks et al., 1982; Graffe et al., 2015; Perkins et al., 2010). A more abundant cytoskeletal protein, actin, is suggested to form two distinct populations of microfilaments. It is found as a component of the active zone cytomatrix (Bloom et al., 2003), where it may form a barrier regulating

vesicle release (Morales et al., 2000), as well as surrounding SVs (Richards et al., 2004; Sankaranarayanan et al., 2003; Shupliakov et al., 2002), potentially being involved in their recycling.

Among other components that are not specific to synapses but are found there are endoplasmic reticulum (Bouchard et al., 2003; Harris et al., 2015), which is mainly thought to serve as an intracellular storage of calcium, but may also be involved in the regulation of synaptic plasticity (Singh et al., 2021), ribosomes (Crispino et al., 1997), which may be required for local protein synthesis (Crispino et al., 2014; Hafner et al., 2019; Scarnati et al., 2018; Younts et al., 2016), and various endosome-like structures, which are probably involved in the sorting of synaptic and other endocytic vesicles (Heuser and Reese, 1973).

Lastly, the most prominent component of the presynapse are the synaptic vesicles. These are small spherical vesicles approximately 40 nm in diameter that contain a neurotransmitter and fuse with the plasma membrane upon stimulation (Schikorski and Stevens, 1997). They are not functional anywhere else but are indispensable for synaptic function and concentrate at the presynapses in great numbers. SVs are not dispersed throughout the synapse but are all kept together in a structure termed the synaptic vesicle cluster. This cluster is easily identified in the electron microscopy images and maintains specific composition, which is discussed in more detail in the following section.

The synaptic vesicle cluster

The synaptic vesicle cluster is found in close proximity to the active zone and, depending on the synapse type, may contain from several dozens to hundreds of thousands of synaptic vesicles. The vesicles are linked together by soluble proteins, which collectively make up the cytomatrix of the synaptic vesicle cluster. The key component of this cytomatrix is synapsin – a phosphoprotein that is able to form dimers that bind the SVs (Monaldi et al., 2010). The phosphorylation status of synapsin is modulated by the intracellular concentration of calcium (Krueger et al., 1977), and affects the ability of synapsin to cluster the vesicles (Greengard et al., 1993), which indicates that vesicle clustering is linked to synaptic activity. Synapsin also binds cytoskeletal elements such as actin, spectrin, and microtubules (Cingolani and Goda, 2008; Greengard et al., 1993; Hilfiker et al., 2005), and it was suggested that synapsin clusters the SVs by anchoring them to the cytoskeleton. Early electron microscopy data showed that the synaptic vesicle cluster contains a network of short filaments, or tethers, that connect vesicles to each other. These tethers were suggested to consist of synapsin and actin (Hirokawa et al., 1989; Landis et al., 1988). However, no long microfilaments were found within the cluster, and some tethers persisted in synapses of mice lacking all isoforms of synapsin (Siksou et al., 2007), challenging the view that synapsin binding to actin cytoskeleton is the mechanism of vesicle clustering.

In addition to synapsin, several other proteins that might play a role in the vesicle clustering are found in the synaptic vesicle cluster. Many of these proteins are endocytosis co-factors, such as amphiphysin (Evergren et al., 2004), intersectin, dynamin (Evergren et al., 2007), and epsin (Jakobsson et al., 2008). Various interactions are possible between these proteins since many of them contain multiple protein- or lipid-binding domains. For example, amphiphysin contains both SH3 and BAR domains, and intersectin contains EH, SH3, DH, PH and C2 domains. These two proteins alone may interact with each other,

synaptic vesicle membranes, and proteins of the SVs, and could, in principle, cause vesicle aggregation. Synapsin, in turn, contains a proline-rich motif (PRM) which can be recognized by the SH3 domains of the above-mentioned proteins, and it has been suggested that these interactions are the driving mechanism for synaptic vesicle clustering (Figure 2, Shupliakov et al., 2011).

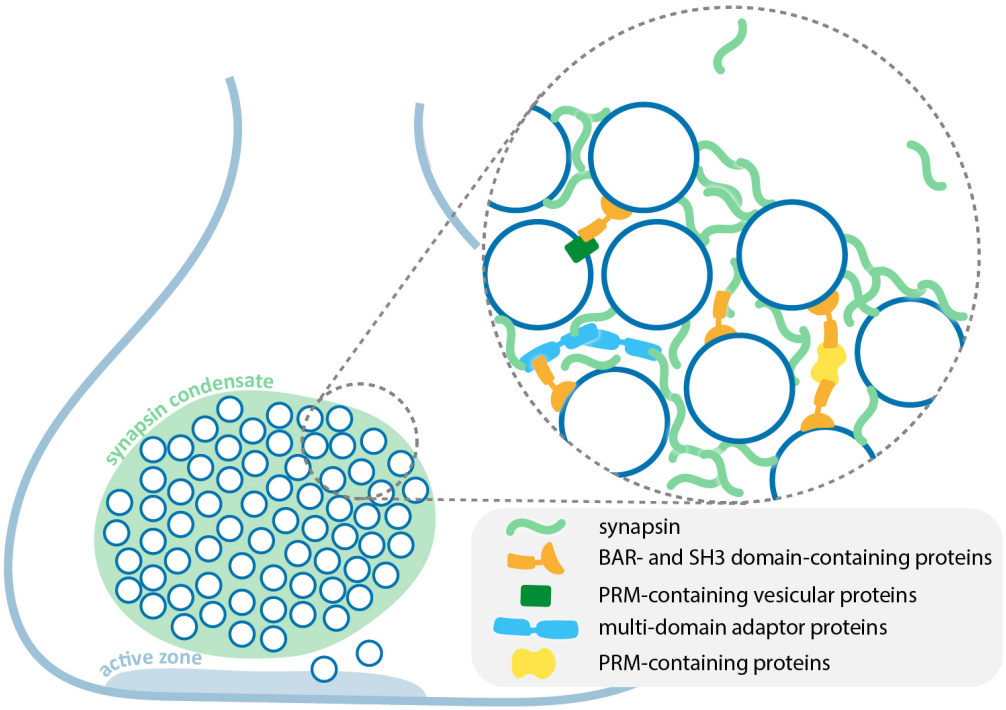

Figure 2. Proposed mechanisms of the synaptic vesicle clustering. Synaptic vesicles are clustered in the vicinity of the active zone. Due to the ability to form multiple weak interactions between its intrinsically disordered regions, synapsin (light green) can form condensates via liquid-liquid phase separation. Synapsin is also a strong SV binder and can recruit vesicles to the formed condensate, which results in a formation of a synaptic vesicle cluster. Multiple interactions result in the recruitment of other soluble proteins that can also contribute to the maintenance of the SVs cluster. BAR and SH3 domain-containing proteins (orange) can bind synaptic vesicles and PRMs of soluble (yellow) or vesicular (dark green) proteins, as well as synapsin. Adaptor proteins containing multiple protein-protein interaction domains can link vesicles via interactions with each other, synapsin, synaptic vesicles or other proteins. These multivalent interactions keep vesicles clustered while allowing mobility within the cluster.

The more recent studies, however, demonstrated that disruption of SH3-PRM interactions does not inhibit vesicle clustering, indicating that other mechanisms play a more important role (Pechstein et al., 2020). The suggested alternative for the synaptic vesicle cluster formation is synapsin-driven liquid-liquid phase separation (LLPS) of the vesicles and vesicle-binding proteins (Milovanovic and Camilli, 2017). It has been shown that synapsin can form a distinct liquid phase by itself, and can also promote segregation of SH3-containing proteins as well as lipid vesicles (Milovanovic et al., 2018). This segregation relies of the intrinsically disordered region of synapsin, can recruit soluble proteins of the synaptic vesicle cluster, and allows specific clustering of synaptophysin-containing vesicles in non-neuronal cells (Hoffmann et al., 2021; Park et al., 2021; Pechstein et al., 2020; Wu et al., 2020), providing a possible mechanism for the synaptic vesicle cluster formation *in vivo*.

The idea that the SV cluster is formed and maintained via liquid-liquid phase separation is supported by several observations. SVs are clustered tightly with a clear cluster border, without any mechanical barriers present. At the same time, the vesicles are mobile within the cluster, and can be exchanged between clusters (Betz et al., 1992). Such behavior would be expected in a liquid condensate, that is maintained by transient multivalent interactions, but would be unlikely if the vesicles were linked to a rigid scaffold. Proteins that can participate in the required multivalent interactions are highly enriched in the synapses (Wilhelm et al., 2014). Synapsin specifically is the most abundant protein in the synaptic bouton, and is highly synapse-specific (Cesca et al., 2010; Fassio et al., 2011; Südhof et al., 1989). It does not participate in vesicle fusion or endocytosis and its domain structure is consistent with the idea of it undergoing LLPS. The intrinsically disordered region of synapsin is similar to such of other proteins known to participate in the LLPS (Molliex et al., 2015; Patel et al., 2015). Additionally, synapsin condensates have been shown to fuse with each other (Milovanovic et al., 2018), which is a behavior that is characteristic of liquid phase condensates. Another important feature of liquid phase formation is its reversibility, which is also observed in the case of the SV cluster. Clustering of synaptic vesicles can be manipulated by changing synapsin phosphorylation state, and can be reproduced with *in vitro* synapsin-vesicle condensates (Milovanovic et al., 2018).

While synapsin-driven LLPS of the synaptic vesicle cluster becomes more widely accepted as a mechanism of the SV cluster formation and maintenance, the role of other proteins cannot be disregarded. Despite SH3-PRM recognition being shown to not be the key interaction leading to synapsin-SV LLPS (Pechstein et al., 2020), it is probably still important for the SV cluster maintenance and regulation of its composition. Additionally, some proteins may play a crucial role in supporting the synapsin-induced LLPS. For example, vesicular protein synaptophysin has been shown to be necessary to induce synapsin-dependent vesicle clustering in COS7 cells (Park et al., 2021).

In addition to mentioned above, many other soluble proteins are found in the synaptic vesicle cluster and on the SVs, including CSP, NSF, clathrin, Hsc70, RIM2 and others (Denker et al., 2011; Murthy and De Camilli, 2003; Takamori et al., 2006; Wilhelm et al., 2014). They are not required for vesicle clustering and it was suggested that in fact the function of the majority of the vesicles in the cluster is to provide storage for these proteins (Denker et al., 2011; Shupliakov, 2009). Under physiological conditions, only 10-20% of the SVs present in a synapse are involved in recycling (Van der Kloot, 2003). This fraction of the vesicles is termed the recycling pool, and for a long time the role of the remaining majority of vesicles, the reserve pool, was not understood. They could serve as a reserve storage of the neurotransmitter, but since vesicles do not appear to exchange their contents with each other (at least in the cholinergic preparations that have been mostly studied in relation to this aspect), and since most of the vesicles are never released, such a storage of a neurotransmitter would be effectively useless. The soluble proteins bound to the SVs, on the contrary, can be released from the synaptic vesicle cluster to participate in their respective functional processes, and then can be stored again in the synaptic vesicle cluster until needed, instead of diffusing out of the synapse. In this regard, the buffering role of the excess SVs appears to be more tenable and provides an explanation of how the proteins required for the synaptic function are retained in the synapse (Denker et al., 2011).

Protein requirements in synaptic function

If the synaptic vesicle cluster acts as a storage of proteins involved in synaptic function, why such a storage would be required in the first place? To answer this question, here I will discuss protein requirements for some key processes of the synaptic vesicle cycle. I will not focus on the details of the molecular mechanisms behind and will not discuss the whole cycle, but rather provide an overview of the qualitative and quantitative protein requirements of different steps (summarized in Table 1) and will compare them to the protein availability in the synapse.

Neurotransmitters are released via exocytosis of synaptic vesicles. The fundamental principle of membrane fusion is the interaction between SNARE proteins found on the fusing membranes (Jahn and Grubmüller, 2002). Three such molecules are involved in the synaptic vesicle exocytosis: VAMP2 (synaptobrevin 2), SNAP25 and syntaxin 1, which together form one SNARE complex. Different studies report different number of SNARE complexes to be necessary for a single vesicle fusion event, typically ranging between 1 and 10 with the commonly accepted number to be 1-3 complexes per fusion (van den Bogaart et al., 2010; Hua and Scheller, 2001; Karatekin et al., 2010; Mohrmann et al., 2010; Shi et al., 2012; Sinha et al., 2011). A single synaptic vesicle contains ~70 copies of VAMP2 (Takamori et al., 2006). SNAP25 and syntaxin 1 are found on the plasma membrane and there are approximately 27 000 copies of SNAP25 and 20 000 copies of syntaxin 1 in the synapse (Wilhelm et al., 2014). By considering the surface areas of a synapse and the active zone, one can estimate that there are at least 600 molecules of each syntaxin 1 and SNAP25 at the active zone, which would be sufficient to simultaneously release about a half of all the vesicles present in the synapse if no other factors are considered.

Although SNAREs alone can, in principle, drive membrane fusion (Weber et al., 1998), in the cellular environment other proteins are needed for adequate vesicle release. Proteins such as Munc13 and Munc18 bind inactive SNAP25-syntaxin 1 heterodimers (Guan et al., 2008; Weninger et al., 2008) and are required for syntaxin transition from closed to open conformation and vesicle priming (Basu et al., 2005; Medine et al., 2007; Richmond et al., 2001; Rickman et al., 2010; Shen et al., 2007). Since a single molecule might act on several SNARE complexes sequentially, it is generally difficult to estimate how many copies of a soluble protein are required for vesicle fusion. In the case of Muncs it is likely that one copy of each is required for each SNARE complex since Muncs must remain bound to their partners to perform their function. Similarly, one copy of complexin must be bound to each SNARE complex to prevent fusion before Ca^{2+} influx (Tang et al., 2006). Unlike SNAREs, which are the most abundant proteins in the synapse, these auxiliary proteins are present in much smaller numbers. On average there is only one molecule of the most abundant SNARE co-factor, Munc18, per 7 molecules of SNAP25 (Wilhelm et al., 2014). Although the total number of these molecules is still significantly higher than the number that can participate in a single fusion event, their relative sparsity implies that the distribution of these proteins must be more carefully regulated to ensure that they are found at a proper location and are not all bound to the excess SNAREs outside of the active zone. This issue would be even more pronounced for less abundant proteins, such as for example CSPα, a chaperone required for SNAP25 stability (Sharma et al., 2011) and loss of which causes early mortality (Fernández-Chacón et al., 2004), of which there are less than a thousand copies in the whole synapse (Takamori et al., 2006; Wilhelm et al., 2014).

Table 1. Functions and approximate required copy numbers of some key proteins involved in the SV fusion and retrieval.

Protein	Category	Function	Required copy numbers
 VAMP2	vesicular SNARE	Component of a SNARE complex	1-3 per fusion event
 SNAP25	plasma membrane SNARE	Component of a SNARE complex	1-3 per fusion event
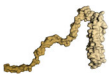 Syntaxin	plasma membrane SNARE	Component of a SNARE complex	1-3 per fusion event
 Munc13	exocytosis co-factor	Promotes syntaxin transition from closed to open conformation	1 per SNARE complex
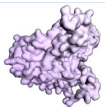 Munc18	exocytosis co-factor	Mediates SNARE complex assembly priming	1 per SNARE complex
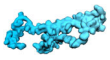 Complexin	exocytosis co-factor	Inhibits spontaneous exocytosis	1 per SNARE complex
 Synaptotagmin	vesicular calcium sensor	Displaces complexin, facilitating $Ca2^{+}$-triggered fusion	1 per SNARE complex
 NSF	exocytosis co-factor	Disassembles SNARE complex	6 per SNARE complex
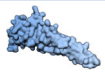 αSNAP	exocytosis co-factor	Facilitates SNARE complex disassembly	2 per SNARE complex
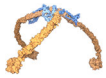 Clathrin (heavy + light chains)	endocytic	Forms a clathrin coat	100-300 per vesicle
 Dynamin	endocytic	Catalyzes membrane fission	>52 per vesicle
 Hsc70	endocytosis co-factor	Mediates the uncoating of clathrin-coated vesicles	50-150 per vesicle
 Auxilin	endocytosis co-factor	Recruits Hsc70 during uncoating	50-150 per vesicle

After fusion, the SNARE complex, now residing on the plasma membrane, must be disassembled. For this 6 copies of NSF (one hexamer) and 2 copies of αSNAP are required per SNARE complex (White et al., 2018). The membrane material of the synaptic vesicle then must be retrieved from the plasma

membrane via endocytosis. Several modes of endocytosis exist and may be used in the synapses (Chanaday and Kavalali, 2018; Smith et al., 2008; Soykan et al., 2016). The classical clathrin-dependent endocytosis relies on an assembly of multiple proteins, including FCHo, Eps15, intersectin, AP2, AP180, epsin, and others, which together promote a formation of a clathrin-coated pit. Membrane fission then follows, which relies on an enzyme dynamin recruited by BAR domain containing proteins, including amphiphysin and endophilin. The formed clathrin-coated vesicle must then be stripped of clathrin with the help of a chaperone Hsc70 and co-factors, before it can undergo endosomal sorting and recycling. Although it might be difficult to quantify the copy number requirements of these proteins for endocytosis of one vesicle, some of them have been estimated in the past. At least 36 triskelions, each consisting of 3 clathrin heavy chains and 3 clathrin light chains, are required to form one clathrin-coated vesicle, while some can use up to 100 triskelions (Cheng et al., 2007; McMahon and Boucrot, 2011). For membrane fission, at least 52 copies of dynamin are required (Faelber et al., 2011; Shnyrova et al., 2013). At least one Hsc70 per 2 triskelions is required for the uncoating to begin (Böcking et al., 2011), and one auxilin molecule is needed to recruit each Hsc70 (Rothnie et al., 2011; Ungewickell et al., 1995).

Overall, the known copy numbers of proteins required to exo- and endocytose one synaptic vesicle comprise only a small fraction of what is present in the synapse. However, in addition to the mentioned above issue of proper localization, the temporal requirements must also be considered. First, more than one vesicle is often released by a synapse. In the primary hippocampal cultures it has been estimated that during spontaneous activity about 6 vesicles are released every 10 seconds (Truckenbrodt et al., 2018). One such burst would consume ~8% of all available dynamin in a synapse, while higher numbers would be required during continuous stimulation due to more release events happening in a shorter time. While the proteins can be repeatedly reused, they are still removed from the functional pool for the time they are involved in release or retrieval of a given vesicle, with the whole cycle taking around 30 seconds (Aravanis et al., 2003; Jähne et al., 2021). Of these 30 seconds, less than 1 ms is required for the membrane fusion itself (Schneggenburger and Neher, 2000), suggesting that the actions and availability of all the co-factors involved in the preceding and following events may be the time-limiting aspect of vesicle recycling. Taken together, this explains why the synaptic vesicle cluster would need to store some of these proteins, and why there is an apparent excess of proteins in the synapse. At the same time, this raises a question of whether the available copy numbers of any specific protein might be the limiting factor for the synaptic vesicle cycle progression.

Protein mobility

Protein availability is crucial for any cellular process, but it is not sufficient for the proteins to exist in adequate amounts, they also have to be able to efficiently reach the locations where they are required. Many proteins in the cell have specific signal sequences that target them to their respective organelles, where membranes may restrict their diffusion only to this compartment. No such signal sequences and diffusion barriers exist for synaptic proteins. In addition, synapses have limited protein synthesis capabilities and rely on protein supply from the cell body. In this section I will summarize the current view of the processes that allow synaptic proteins to reach their target locations.

Protein delivery to the synaptic bouton

Majority of the synaptic components are delivered to the synaptic boutons via anterograde axonal transport, which is also the mechanism by which the distinct composition of axons and dendrites is maintained (Farías et al., 2015). This process largely relies on proteins from the kinesin superfamily - microtubule-associated molecular motors that preferably move towards the plus-end of microtubules (Hirokawa, 1998). Since microtubules in the axon are aligned with their plus end facing the axon tip (Stepanova et al., 2003), this ensures directed transport of kinesins' cargoes from the cell body towards the synapses. Two modes of active axonal transport are classically distinguished: slow (less than 10 mm/day) and fast (50-400 mm/day). Membranous organelles are transported via fast axonal transport, while soluble proteins are transported via slow axonal transport. Despite such a distinction in speeds and cargoes, both modes rely on the same motors (Terada et al., 2010; Verhey et al., 2001). The difference is attributed to stronger association of vesicular cargoes with motors (via various adaptor proteins), compared to soluble proteins, which are predominantly co-transported with vesicles due to their interactions with the vesicular proteins (Scott et al., 2011; Tang et al., 2013). The average speed of kinesin movement is approximately 1 μm/s, although not all organelles travel at the maximum speed and mitochondria, for example are transported at ~0.4 μm/s (Tang et al., 2012). Two major groups of vesicles deliver synaptic components via fast axonal transport: components of the SVs are packed and transported in synaptic vesicle precursor vesicles, while proteins of the active zone are delivered by piccolo-bassoon transport vesicles (Ahmari et al., 2000; Sabo and McAllister, 2003; Shapira et al., 2003; Tao-Cheng, 2007). At the same time, some proteins of the active zone are co-transported with the synaptic vesicle precursor vesicles, and the transport of the two vesicle types is coordinated (Bury and Sabo, 2011; Maas et al., 2012; Wu et al., 2013). The frequency of active transport events appears to be low, with about 2 vesicle precursors per minute being transported per micrometer of the initial axonal segment in *Caenorhabditis elegans* (Maeder et al., 2014).

Known mobility rates in the synapse

While the mechanisms of protein delivery from the cell body to the synapse are well known, little information is available on protein movements within the synapse. The mobility of synaptic vesicles has been investigated in the past, and is thought to be maintained by passive diffusion (Graydon et al., 2014; LoGiudice et al., 2008; Tokuoka and Goda, 2006). At rest, only a small population of the vesicles is mobile (Gaffield et al., 2006; Jordan et al., 2005; Shtrahman et al., 2005), likely corresponding to the recycling pool, with a diffusion coefficient of ~0.003 $\mu m^2/s$ (Gaffield et al., 2006; Lee et al., 2012). At the same time, the mobility rates differ between different types of synapses (Rea et al., 2004; Rothman et al., 2016). The mobility of the SVs is modulated by synaptic activity (Gaffield et al., 2006) and probably depends on the synaptic vesicle-binding proteins found in the synaptic vesicle cluster, particularly synapsin (Orenbuch et al., 2012), but is not significantly affected by disruptions of the cytoskeleton (Jordan et al., 2005). Additionally, the exchange of mature SVs between the synapses (Darcy et al., 2006; Herzog et al., 2011; Staras et al., 2010) is not affected by mechanisms regulating intrasynaptic vesicle mobility, indicating that intrasynaptic and intersynaptic vesicle mobility are maintained by distinct mechanisms (Kamin et al., 2010).

Intrasynaptic mobility of only few individual proteins, mainly limited to the plasma membrane or SV proteins has been analyzed. Analysis of the mobility of synaptotagmin on the plasma membrane showed limited diffusion that increased upon stimulation, indicating presence of mechanisms that limit mobility of vesicular components on the plasma membrane (Kamin et al., 2010). The plasma membrane SNARE syntaxin 1 exhibits quick exchange between synapses and adjacent axonal regions, but generally has slower diffusion in synapses (Ribrault et al., 2011). The mobility of VGLUT1 has been measured *in vivo* and in culture (Herzog et al., 2011), but these measurements reflect the mobility of the whole SVs where VGLUT1 resides. The majority of the works on individual protein mobility are focused on the postsynapses. There, multiple studies investigated the mobility of various membrane receptors (Borgdorff and Choquet, 2002; Dahan et al., 2003; Groc et al., 2004; Jacob et al., 2005; Meier et al., 2001; Tardin et al., 2003), signaling molecules (Shen and Meyer, 1999), and molecules of cellular adhesion (Chamma et al., 2016; Fu and Huang, 2010). These studies report distinct populations of receptors with different diffusion kinetics in a range 0.01-0.1 $\mu m^2/s$, lower mobility on the postsynapses compared to the extrasynaptic surface of the dendrite, and note that activity reduces the mobility of postsynaptic receptors (Ehlers et al., 2007).

Methods to study protein mobility

One of the reasons for the limited data availability on protein mobility in the presynapse is technical challenges of obtaining such data. Most of the methods used to obtain highly detailed information on the composition and organization of the synapse are not compatible with live imaging, or have low temporal resolution, making it impossible to use them to investigate protein dynamics.

The majority of the studies mentioned above rely on single particle tracking (Figure 3A) – an imaging technique where tracks of individual molecule or particle movement are recorded over time and used to calculate the diffusion coefficients (Liu et al., 2016; Schmidt et al., 1996). The direct observation of the particle of interest provides not only speed of its movement, but also additional details on its behavior, allowing to detect whether the particle moves continuously or with stops, whether its speed is constant or changes over time, and whether there are any preferences for the specific path the particle takes. On the other hand, observing individual particles has its limitations: first, the tracks of different particles must be distinguishable, so relatively low labeling density is required. At the same time, to withstand prolonged imaging, the fluorescent label used must be highly photostable. Typically this issue is solved by labeling the protein of interest with an antibody coupled to a quantum dot – a bright and photostable nanoparticle (Walling et al., 2009). This approach, however, can only be used for plasma membrane proteins, or proteins of the SVs if a quantum dot small enough to be endocytosed is used (Lee et al., 2012).

To measure diffusion of soluble proteins, fluorescence correlation spectroscopy (FCS, Figure 3B) can be used instead (Schwille, 2001). FCS analyses fluorescence fluctuations in a small volume (femtoliters) and requires nano- to picomolar concentrations of a fluorophore. These fluctuations reflect molecules entering and leaving the detection volume and are analyzed by temporal autocorrelation. The resulting autocorrelation function is then fitted to an appropriate equation to extract diffusion coefficients. To be able to detect cytoplasmic proteins using this approach, the proteins need to be tagged by fluorescent

moieties, for example by fusing them with fluorescent proteins. Due to the high sensitivity of this method, cellular autofluorescence and light absorption and scattering within the cell significantly increase the risk of detecting artifacts. Autocorrelation curve analysis poses an additional challenge as using an equation that does not correctly describe the behavior of the analyzed protein would result in erroneous diffusion coefficients. Two works that used FCS to measure mobility of the SVs report diffusion coefficients that differ by an order of magnitude (Jordan et al., 2005; Shtrahman et al., 2005), indicating that, especially in the case of complex behaviors, FCS might provide unreliable results in synapses.

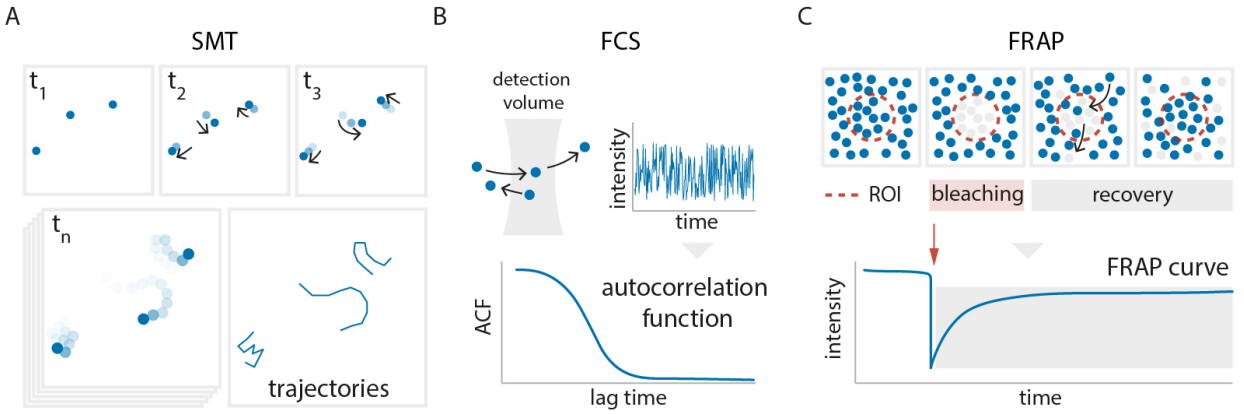

Figure 3. Commonly used methods to analyze protein mobility. A, single molecule tracking (SMT): movement of individual particles is directly observed over a period of time. Their positions are recorded in each frame and are used to generate a track of particle movement. The obtained trajectory can be used to calculate diffusion coefficients. **B**, fluorescence correlation spectroscopy (FCS): fluorescence intensity is measured in a small detection volume. As single particles enter and leave the detection volume, fluctuations in fluorescence intensity are recorded in real time. An autocorrelation function of the recorded intensity changes is generated, which is used to calculate diffusion coefficients and fluorophore concentration. **C**, fluorescence recovery after photobleaching (FRAP): a region of interest is bleached with a high intensity laser pulse. The fluorescence recovery caused by protein movement is recorded over time. Recorded recovery curve then used to calculate the time constants and the immobile fractions.

As opposed to previous two methods, fluorescence recovery after photobleaching (FRAP, Figure 3C) and fluorescence loss in photobleaching (FLIP) detect bulk protein motion in a large volume (Ishikawa-Ankerhold et al., 2012). These methods rely on the irreversible photobleaching of fluorophores and can be used with genetically encoded fluorescent tags or with chemical dyes. The latter can be used for the plasma membrane or vesicle proteins, or, in the case of membrane-permeable dyes, can be combined with click-chemistry to label proteins that are never exposed on the plasma membrane (Cambier et al., 2020; Milles et al., 2012). In FRAP, a region of interest is bleached with a high intensity laser pulse, and then monitored over time. As proteins diffuse and non-bleached fluorescent ones enter the bleached region, the signal recovers. The speed of recovery reflects the speed of protein diffusion. In FLIP, the region of interest and the bleached region are separate. The bleaching region is repeatedly bleached over the course of the experiment and the fluorescence changes are recorded in the region of interest. As the proteins diffuse from the region of interest and get bleached, loss of fluorescence is detected.

FRAP is a simple and widely used method which does not require specialized equipment, labor- or cost intensive labeling approaches or otherwise complicated experimental procedures but has some

limitations. Due to the potential phototoxicity effects, care must be taken not to cause damage to the cells. In synapses, FRAP experiments are also challenging due to the small size of synapses and the method being diffraction limited. Also, interpretation of FRAP experiments poses additional challenges. Typically FRAP results are reported as time constants – time that it takes for the fluorescence to recover to a certain percentage of the initial level. This time might differ depending on the experimental conditions and does not provide a direct measure of molecular motion speed, as a diffusion coefficient does. Commonly used approaches to extract diffusion coefficients from FRAP data (Axelrod et al., 1976; Blumenthal et al., 2015; Kang et al., 2012) assume specific geometry of the bleached region, which is supposed to be completely surrounded by the non-bleached cellular material and to not occupy too large of a fraction of the cell. In the case of hippocampal synapses these conditions are not met due to the synaptic geometry, as new material can only enter from two entry points from the narrow axon, making currently existing approaches unusable to extract accurate data.

In addition to the methods used to measure protein mobility, the used model system is important for data interpretation. Dissociated neuronal cultures are typically used to study neuronal physiology, since they are comparably easy to prepare, manipulate, and image, and allow analyzing processes within living neurons. At the same time, while they provide a fair representation of protein behavior *in vivo*, the mechanisms behind this behavior are challenging to dissect when working with living cells. The complex cellular composition and organization make it difficult to determine factors influencing protein behaviors. This is especially true for synapses, which have a unique geometry that cannot be easily modified without risking the integrity of synaptic physiology. As such, it would be impossible to determine which components or parameters affect protein mobility in synapses. These would be easier to identify in a cell-free *in vitro* system, composition and organization of which can be finely controlled by an experimenter. As an example, the mechanisms of synapsin-induced phase separation were analyzed using an *in vitro* setting (Milovanovic et al., 2018). There, salt composition, proteins present, their concentrations or domain structure could be manipulated to determine effects of each factor. At the same time, *in vitro* results cannot always be reproduced *in vivo*, and some aspects of cellular composition might be difficult or impossible to reconstitute artificially. Considering these arguments, a combination of both approaches would be optimal to analyze mobility of synaptic proteins.

Topicality of this work

Open questions related to synaptic function and protein mobility

Despite numerous efforts to understand various aspects of the dynamics and mobility of synaptic components, many questions remain unanswered. First, only a handful of proteins were analyzed in terms of their mobility in living neurons. The absence of a comprehensive dataset of the diffusion coefficients of synaptic proteins does not allow evaluating the overall rate of protein mobility in the boutons. While the available data demonstrate certain mobility tendencies for some proteins, it is not clear to which extent this is extended to the overall protein dynamics. Similarly, since mobility of only a few proteins is known, very few comparisons between different proteins can be made, making it

impossible to deduce what factors might influence the mobility of a certain protein and determine its behavior.

While the movement rates and the mechanisms remain unknown, it is also not clear how the protein mobility relates to the synaptic activity. I have discussed the protein requirements during synaptic activity above, and it is clear that there are mechanisms that ensure timely delivery of all the necessary proteins to the functionally relevant sites such as the active zone, however, it is not known whether this delivery is ensured via directed transport within the synapse, or whether it can be maintained by random diffusion.

In this regard, we also do not know how protein mobility and transport are regulated in the synaptic boutons. As discussed above, the synapse maintains its composition and organization distinct from such of the rest of the axon without being separated by any membranes. Thus, no obvious physical barriers for protein diffusion exist in the compartment, and no signal sequences are known that would target soluble proteins to the synapse or different parts thereof. Nonetheless, some regulatory mechanisms must exist to ensure correct localization and movement rates of various proteins.

The movement rates and their differences between proteins can be crucial for synaptic physiology. First, the mobility rates must be sufficient to maintain sufficient supply of proteins to the active zone. However, the differences in the copy numbers of different proteins must also be considered. Theoretically, more abundant proteins might be easier to be delivered to the active zone compared to the less abundant ones given they have the same movement rates. In the case of drastically different mobility behaviors, they might be equally effective in reaching their target locations, or even the less abundant one might surpass the more abundant one. This raises a question of whether the delivery rates of certain proteins can be a limiting factor for endo- and exocytic events, therefore determining the maximal activity rate the synapse can maintain.

Another question to be answered concerns the role of the synaptic vesicle cluster in determining protein mobility. The cluster is known to bind and retain multiple soluble proteins, but it is not clear how this binding affects the overall movement of proteins in the synapse. The vesicle cluster can maintain its distinct composition, presumably through multiple protein-protein interactions. We do not know, however, whether this can be fully attributed to protein interactions with the SVs within the cluster, or if other cellular components might play a defining role in facilitating such interactions.

Aim of this thesis

In my PhD project I aimed to address the questions posed above by generating a quantitative overview of the mobility of synaptic proteins. First, I planned to establish an experimental workflow protocol that would allow a direct comparison of the mobility of a large set of various proteins in living neurons. The sought protocol had to be (1) technically feasible to be repeated hundreds of times, to allow sufficient number of experiments for dozens of different proteins to be analyzed; (2) include minimal interference with the cellular physiology; (3) have no or minimal variation of any experimental parameters between different proteins analyzed, including protein labeling approaches. I then aimed to use the established protocol to measure the mobility of a diverse selection of 45 synaptic proteins, in synaptic boutons and

axons of living primary hippocampal neurons, and to analyze the differences and trends of the obtained mobility parameters.

Second, I planned to extract diffusion coefficients from the measured mobility rates. In the case of performed FRAP experiments, it required a custom computational analysis that would take synaptic geometry into account. Unlike FRAP parameters, diffusion coefficients directly describe the movement speed of individual protein molecules and therefore I planned to use the diffusion coefficients for further analysis. By obtaining the diffusion coefficients for all the analyzed proteins in different locations, I aimed to generate a database of quantitative data on synaptic protein mobility that can be compared with results obtained by other investigators, using different experimental approaches, and can be introduced as parameters in computational models of synaptic physiology.

In addition to obtaining the diffusion coefficients, I aimed to determine which factors affect protein mobility in the axons and the synaptic termini. Among others, I planned to focus on the role of the interactions with the SVs and determine whether and how association with the SVs affects protein mobility in the synapses.

To further investigate the role of the synaptic vesicles, I then aimed to determine the effect of the synaptic vesicle binding on the protein mobility in the absence of other cellular components. For this I needed to establish a simplified and controllable *in vitro* approach, where the mobility of individual purified proteins can be measured in the presence or in the absence of immobilized purified SVs. I then planned to use this approach to measure the effect of the SVs on the mobility of several different proteins and compare the obtained results with the ones obtained on living cells.

Ultimately, by obtaining the detailed mobility data on multiple proteins and by investigating the parameters that affect protein mobility (and, as a result, protein distribution), I aimed to start unveiling the dynamic organization of proteins in the synaptic bouton on a large scale.

CHAPTER 1. A COMPARATIVE ANALYSIS OF THE MOBILITY OF 45 PROTEINS IN THE SYNAPTIC BOUTON

Sofiia Reshetniak, Jan-Eike Ußling, Eleonora Perego, Burkhard Rammner, Thomas Schikorski, Eugenio F. Fornasiero, Sven Truckenbrodt, Sarah Köster & Silvio O. Rizzoli

Published in *The EMBO Journal*, vol. 39, no. 16, p. e104596, Aug. 2020, doi: 10.15252/embj.2020104596.

Author contribution of Sofiia Reshetniak:

- design (together with SOR and ST), performance, and analysis (together with SOR) of the experiments shown in Figs. 1, 2, 3, 4, 5, Appendix Figs. S1, S3-S14, Tables EV1, EV2;
- design (together with SOR and SK), performance (together with EP), and analysis (together with EP) of the experiments shown in Appendix Fig. S15;
- analysis and interpretation (together with SOR) of results shown in Figs. 7, 8, Appendix Figs. S16, S20, S21;
- data visualization, figure design (together with SOR), layout and generation: all main and supplementary figures, except for Fig. S15A (made together with EP);
- manuscript writing: initial draft together with SOR, refinements with all other authors.

Rights and permissions:

Formatting and contents:

The paper main text format is preserved from the journal it is published in. Page numbers conforming to this thesis page numbering have been added at the bottom of the pages. Extended view tables were reformatted to conform to the thesis format. The page 42 contains the Table of Contents for the supplementary figures and the extended view tables, as well as links to the Extended View Movies 1-4.

Resource

TRANSPARENT PROCESS OPEN ACCESS

THE EMBO JOURNAL

A comparative analysis of the mobility of 45 proteins in the synaptic bouton

Sofiia Reshetniak[1,2], Jan-Eike Ußling[1], Eleonora Perego[3], Burkhard Rammner[1], Thomas Schikorski[4], Eugenio F Fornasiero[1], Sven Truckenbrodt[1,2], Sarah Köster[3,5] & Silvio O Rizzoli[1,5,*]

Abstract

Many proteins involved in synaptic transmission are well known, and their features, as their abundance or spatial distribution, have been analyzed in systematic studies. This has not been the case, however, for their mobility. To solve this, we analyzed the motion of 45 GFP-tagged synaptic proteins expressed in cultured hippocampal neurons, using fluorescence recovery after photobleaching, particle tracking, and modeling. We compared synaptic vesicle proteins, endo- and exocytosis cofactors, cytoskeleton components, and trafficking proteins. We found that movement was influenced by the protein association with synaptic vesicles, especially for membrane proteins. Surprisingly, protein mobility also correlated significantly with parameters as the protein lifetimes, or the nucleotide composition of their mRNAs. We then analyzed protein movement thoroughly, taking into account the spatial characteristics of the system. This resulted in a first visualization of overall protein motion in the synapse, which should enable future modeling studies of synaptic physiology.

Keywords diffusion; movement; protein mobility; synapse; vesicle
Subject Category Neuroscience
DOI 10.15252/embj.2020104596 | Received 31 January 2020 | Revised 20 May 2020 | Accepted 29 May 2020 | Published online 6 July 2020
The EMBO Journal (2020) 39: e104596

Introduction

Synaptic transmission is one of the best-known cellular pathways, with most of its components being thoroughly annotated in functional terms (Koopmans *et al*, 2019). Within the synapse, the synaptic vesicle recycling pathway has been analyzed in very high detail, for several decades. This pathway involves the fusion of synaptic vesicles at the active zone (exocytosis), which is followed by the retrieval of the fused vesicle molecules (endocytosis), and by the reformation of new fusion-competent vesicles (Sudhof, 2004; Haucke *et al*, 2011; Rizzoli, 2014). The copy numbers of the molecules involved in synaptic vesicle recycling are known relatively well (Takamori *et al*, 2006; Wilhelm *et al*, 2014). Many other features of these proteins have also been analyzed in systematic studies, ranging from their overall spatial distributions (Wilhelm *et al*, 2014) to their translation in relation to synaptic function (Schanzenbächer *et al*, 2016) or to their lifetimes, both *in vitro* (Dörrbaum *et al*, 2018) and *in vivo* (Fornasiero *et al*, 2018). Such systematic studies have revealed numerous unexpected features, including strong correlations between protein functions and their lifetimes (Dörrbaum *et al*, 2018), or links between the protein and mRNA structures and a many functional parameters such as the translation rates (Mandad *et al*, 2018).

However, one important characteristic of synaptic proteins, their mobility, has not been the subject of large systematic studies. The movement of synaptic organelles, and especially of synaptic vesicles, has been thoroughly investigated (Rothman *et al*, 2016). Active transport of molecules to and from synapses has also been measured in numerous studies (Hirokawa *et al*, 2010; Roy, 2014). The movement of individual proteins in synapses has been less investigated, in studies that typically only targeted one or a handful of presynaptic molecules (e.g., Kamin *et al*, 2010; Ribrault *et al*, 2011; Albrecht *et al*, 2016). Such studies resulted in valuable insights for the respective proteins, but did not enable further analyses of, for example, protein structure in relation to synaptic mobility. Many important questions could only be approached by systematic works targeting multiple proteins simultaneously. For example, is the synaptic protein mobility determined by their size, or is their movement dominated by specific interactions with other synaptic components, rendering size effects irrelevant? As another example, several biochemical and imaging experiments have demonstrated thoroughly that the vesicle cluster binds to substantial amounts of cofactor proteins (Shupliakov, 2009; Denker *et al*, 2011a; Fornasiero *et al*, 2012; Milovanovic & Camilli, 2017). How does this relate to the protein movement? Is this effect relevant for both soluble and membrane proteins? At the same time, many functional protein parameters are known to depend on the respective protein and mRNA sequences, as mentioned above (Mandad *et al*,

1 Institute for Neuro- and Sensory Physiology and Biostructural Imaging of Neurodegeneration (BIN) Center, University Medical Center Göttingen, Göttingen, Germany
2 International Max Planck Research School for Molecular Biology, Göttingen, Germany
3 Institute for X-Ray Physics, University of Göttingen, Göttingen, Germany
4 Department of Neuroscience, Universidad Central del Caribe, Bayamon, PR, USA
5 Cluster of Excellence "Multiscale Bioimaging: from Molecular Machines to Networks of Excitable Cells" (MBExC), University of Göttingen, Göttingen, Germany
*Corresponding author. Tel: +49551395911; E-mail: srizzol@gwdg.de

2018). Could one determine such correlations also for protein movement parameters?

Such questions are difficult to explore in the absence of a large protein movement dataset. To address this challenge, we aimed to measure the mobility of multiple proteins in the synaptic bouton and in the axon. We obtained measurements for 47 proteins, including controls such as free cytosolic GFP, or membrane-bound GFP. We relied on the overexpression of GFP-tagged variants of the proteins, which is the only efficient solution when large numbers of constructs need to be analyzed. To minimize, as much as possible, the deleterious effects of GFP fusion and overexpression, we only used GFP chimeras that had been validated in the past, and we made efforts to only investigate neurons with mild expression levels. We found that the average overexpression levels ranged from ~1.2-fold to 2-fold, compared to the normal expression levels, for multiple tested proteins (albeit overexpression could reach higher values in individual neurons and synapses). We also controlled for possible connections between overexpression levels and protein mobility behaviors, and found no substantial correlations for any of the analyzed proteins. Finally, the motion measurements we obtained could reproduce well several similar measurements of (i) fluorophore-tagged native proteins and vesicles; (ii) GFP-tagged proteins expressed in mice after knock-in procedures. Overall, this suggests that our measurements reproduce well the behavior of the native proteins.

Having thus obtained a large dataset of comparative movement measurements for synaptic proteins, we proceeded to solve the questions posed above. Our results demonstrated that, for example, protein size has a very limited effect on synaptic mobility and that protein movement parameters correlate to many other cell biology parameters. We then analyzed the movement data by a modeling approach, based on the structural features of the synapses. This resulted in movement rate estimates (diffusion coefficients) for the different proteins in the axon, in the synapse, and in the vesicle cluster. These movement rates (and/or similar movement rates obtained by more complex models, which can be readily performed using our data) will be employed in the future in investigating the molecular kinetics of synaptic function (*e.g.,* exo- or endocytosis) with higher precision than currently possible.

Results

An overview of the proteins analyzed

The mobility of membrane proteins has been analyzed by quantum dot tracking in the past (e.g., Ribrault *et al*, 2011; Albrecht *et al*, 2016). As this is not a feasible labeling option for cytosolic proteins, and as its use for tracking membrane proteins in synapses has also been recently criticized (Lee *et al*, 2017), we decided to pursue this study mainly by fluorescence recovery after photobleaching (FRAP) (Axelrod *et al*, 1976). Commercial quantum dots have a relatively large size (~20 nm in diameter) and are typically coupled to their targets using antibodies (~10–15 nm in diameter). This renders the labels substantially larger than their targets, which may influence the target movement. Moreover, such labels may be unable to penetrate in areas as the synaptic cleft (Lee *et al*, 2017). GFP, with a diameter of 2–3 nm, is substantially smaller than even low-size, non-commercial quantum dots (~5–10 nm). Moreover, GFP does not require bridging molecules, as antibodies, for linking to the target protein. Therefore, GFP is expected to affect the protein behavior to a substantially lower extent than the quantum dots. We thus expressed 45 different proteins tagged with monomeric enhanced GFP (mEGFP) in mature hippocampal cultured neurons, focusing on proteins known to participate either in exo- or in endocytosis. We employed proteins whose tagging has been tested and validated in the past in various assays (Fig 1, Table EV1). All of the tagged proteins we employed have been demonstrated to localize in the expected areas, and many have been used to rescue function in cells or animals lacking the wild-type protein (Fig 1, Table EV1). We have also analyzed how proteins were differentially distributed in the synapse and in the axon, both for the tagged proteins (measuring the mEGFP fluorescence in the two compartments) and for the same untagged endogenous proteins (relying on immunostainings; Appendix Figs S1 and S2). The measurements obtained with tagged or untagged proteins correlate well, suggesting that the presence of the mEGFP moiety does not induce major effects on protein localization. Overall, we analyzed proteins involved in exo- and endocytosis, along with *bona fide* synaptic vesicle proteins, endosomal proteins, cytoskeletal components, and different trafficking proteins located both in the cytosol and in the plasma membrane (Fig 1).

The basic results: FRAP recovery rates and immobile fractions for the different proteins

Tagged proteins typically localized both to synaptic boutons and to the axonal compartment (Fig 2A and B). This enabled us to bleach both synaptic and axonal areas in live neurons, and to monitor the FRAP behavior of the proteins (Fig 2B) for both compartments. Fitting FRAP recovery curves with exponential rise to maximum equations (Fig 2C) provided recovery time constants (τ) and immobile fractions in both axons and synapses (Fig 1D–F).

These values are presented in Table EV2 and are also shown in full detail in the large Appendix Fig S3. We used neurons that were allowed to behave normally, and to fire bursts of action potentials freely (at about 0.1 Hz, Truckenbrodt *et al*, 2018). This implies that the protein motion behavior we observed conforms to conditions of mild activity, which should involve, for example, some level of release of soluble proteins from the vesicle cluster [driven by rises in the Ca^{2+} concentration and by the phosphorylation of key molecules such as synapsin (Cesca *et al*, 2010; Rizzoli, 2014; Milovanovic & Camilli, 2017)]. Heavy stimulation or activity inhibition may provide different results, but the results of such experiments would not be physiologically relevant (Denker *et al*, 2011b).

Since high expression levels can affect protein mobility (e.g., via saturation of binding sites on the cofactors of the respective proteins), we only analyzed cells with moderate expression of tagged proteins, as shown in Fig 3A–C).

Additionally, to evaluate a potential correlation between the expression levels and protein mobility, we compared the protein abundance and the time constants obtained for each individual synapse or axonal region we analyzed (Appendix Fig S5). We found no significant correlation for any of the proteins. This suggests that the mobility rates we measured are not drastically affected by the protein concentration changes produced by the expression (within the range caused by overexpression in our experiments).

	membrane / soluble	category	validation score 1	2	3	4	5
β-actin	soluble	cytoskeletal			■		
α-SNAP	soluble	exocytosis co-factor			■		
α-synuclein	soluble	vesicle tethering			■		
Amphiphysin	soluble	endocytic			■		
AP180	soluble	endocytic		■			
AP2a	soluble	endocytic				■	
Calmodulin	soluble	calcium sensor				■	
Clathrin light chain	soluble	endocytic			■		
Complexin 1	soluble	exocytosis co-factor					■
Complexin 2	soluble	exocytosis co-factor					■
CSP	soluble	exocytosis co-factor		■			
Doc2a	soluble	calcium sensor		■			
Dynamin 1	soluble	endocytic		■			
Endophilin A1	soluble	endocytic			■		
Epsin1	soluble	endocytic		■			
Hsc70	soluble	endocytic		■			
Intersectin 1-L	soluble	endocytic		■			
Munc13	soluble	exocytosis co-factor					■
Munc18	soluble	exocytosis co-factor				■	
NSF	soluble	exocytosis co-factor			■		
PIP5KIγ	soluble	endocytic				■	
Rab3a	soluble	exocytosis co-factor		■			
Rab5a	soluble	endosome-associated			■		
Rab7a	soluble	endosome-associated		■			
SCAMP1	membrane	membrane recycling	■				
Septin5	soluble	cytoskeletal		■			
SNAP23	membrane	plasma membrane SNARE	■				
SNAP25	membrane	plasma membrane SNARE			■		
SNAP29	membrane	plasma membrane SNARE	■				
SV2B	membrane	vesicular				■	
Synapsin1A	soluble	vesicle tethering			■		
Synaptogyrin	membrane	vesicular		■			
Synaptophysin	membrane	vesicular		■			
Synaptotagmin1	membrane	vesicular		■			
Synaptotagmin7	membrane	vesicular		■			
Syndapin1	soluble	endocytic					■
Syntaxin1A	membrane	plasma membrane SNARE			■		
Syntaxin16	membrane	endosomal		■			
α-Tubulin	soluble	cytoskeletal			■		
VAMP1	membrane	vesicular			■		
VAMP2	membrane	vesicular				■	
VAMP4	membrane	endosomal	■				
vATPase	membrane	vesicular		■			
vGlut1	membrane	vesicular					■
Vti1a-β	membrane	endosomal			■		

Figure 1. Overview of proteins analyzed here and previous validation of the GFP chimeras we used, according to the literature.

Protein categories according to their function and/or localization are indicated. We generated validation scores for all of the GFP-fused constructs we employed, as follows: 0) The tagged protein has not been tested before. Does not apply to any of the proteins we used. 1) The correct protein localization upon tagging is verified, but the function was not tested. 2) The correct protein localization upon tagging is verified, but function was difficult to test, due to the presence of the untagged protein. The appropriate function-related changes in the localization of the GFP-tagged proteins took place upon manipulations. 3) The appropriate protein function was verified for the tagged protein, typically in cell cultures (e.g., primary neuronal cultures). 4) The endogenous protein can be replaced by the tagged protein in cells in culture, with appropriate functional replacement. 5) The endogenous protein can be replaced by the tagged protein in living animals, with appropriate functional replacement. Most of the analyzed proteins have a score of 2 and more, meaning the correct localization and function of the tagged proteins have been shown previously. In detail, 4 proteins have a score of 1; 16 proteins have a score of 2; 14 proteins have a score of 3; 6 proteins have a score of 4; 5 proteins have a score of 5. The average score is 2.82. See Table EV1 for more details and for the references used.

We next aimed to determine whether the mobility of ectopically overexpressed mEGFP fusions would be different from that of the native proteins, or from that of knock-in proteins expressed at physiological levels (Appendix Fig S6). We compared our results with FRAP analyses of the following proteins. (i) Native synaptotagmin 1, tagged using a fluorescently conjugated antibody against its intravesicular domain, which we analyzed in the past (Kamin *et al*, 2010). (ii) Genomically labeled, knock-in vGlut1^{Venus} (Herzog *et al*, 2011). (iii) Knock-in alpha-synuclein-GFP, expressed in mouse brains at levels comparable to those observed in human disease cases (Spinelli *et al*, 2014). In addition, we also compared the FRAP curves of the proteins that are known to be exceptionally enriched in synaptic vesicles, and are not present at substantial levels in any other synaptic compartment, to FRAP curves of synaptic vesicles, obtained after labeling the vesicles with an FM dye (Shtrahman *et al*, 2005). All of these measurements were similar or nearly identical to our observations (Appendix Fig S6), which allows us to conclude that in our experimental setup neither mEGFP fusion, nor overexpression influences protein distribution and mobility in a major fashion.

The synaptic protein mobility correlates to their presence in synaptic vesicles, but not to their sizes

To extract biological insight from the FRAP experiments, we first considered the potential interactions of proteins with synaptic organelles, and especially with synaptic vesicles. A comparison of the mobility parameters of all proteins showed that proteins located in the synaptic vesicles and in endosomes have substantial immobile fractions in synapses (Fig 1E and F, Appendix Fig S4). Moreover, the FRAP time constants of the membrane proteins localized in synaptic vesicles correlated well with their enrichment in purified synaptic vesicles (Takamori *et al*, 2006, Appendix Fig S7). This confirmed the expectation that proteins that tend to localize to substantial levels in the plasma membrane had faster recovery kinetics than the proteins predominantly localized in the largely immobile vesicles (Appendix Fig S7). Interestingly, vesicular proteins also have higher time constants in axons, compared to other membrane proteins, although they are present in the axons mostly as proteins in the plasma membrane, and not as vesicles (Appendix Fig S8). An interesting case was that of VAMP4, whose recovery was substantially slower in axons than in the synapse, against the trend observed for most other proteins. VAMP4 tends to be found in endosomes in the axon, but not in the synapse, as observed in our immunostainings for this protein (Appendix Fig S2), and therefore, its axonal FRAP values are probably influenced by the slow recovery of endosomes through active transport. Additionally, a strong correlation is observed between the time constant and the immobile fraction in synapses, but not in axons (Appendix Fig S9).

We then proceeded to test whether protein mobility can be linked to previously known protein characteristics such as structure, size, or localization. We found that for membrane proteins, both the time constants and the immobile fractions correlate positively with the number of transmembrane domains (Fig 4A, Appendix Fig S10A), in agreement with an expectation that the presence of multiple transmembrane domains would slow down diffusion (Kumar *et al*, 2010). For soluble proteins, however, we did not observe a correlation between molecular weight and the

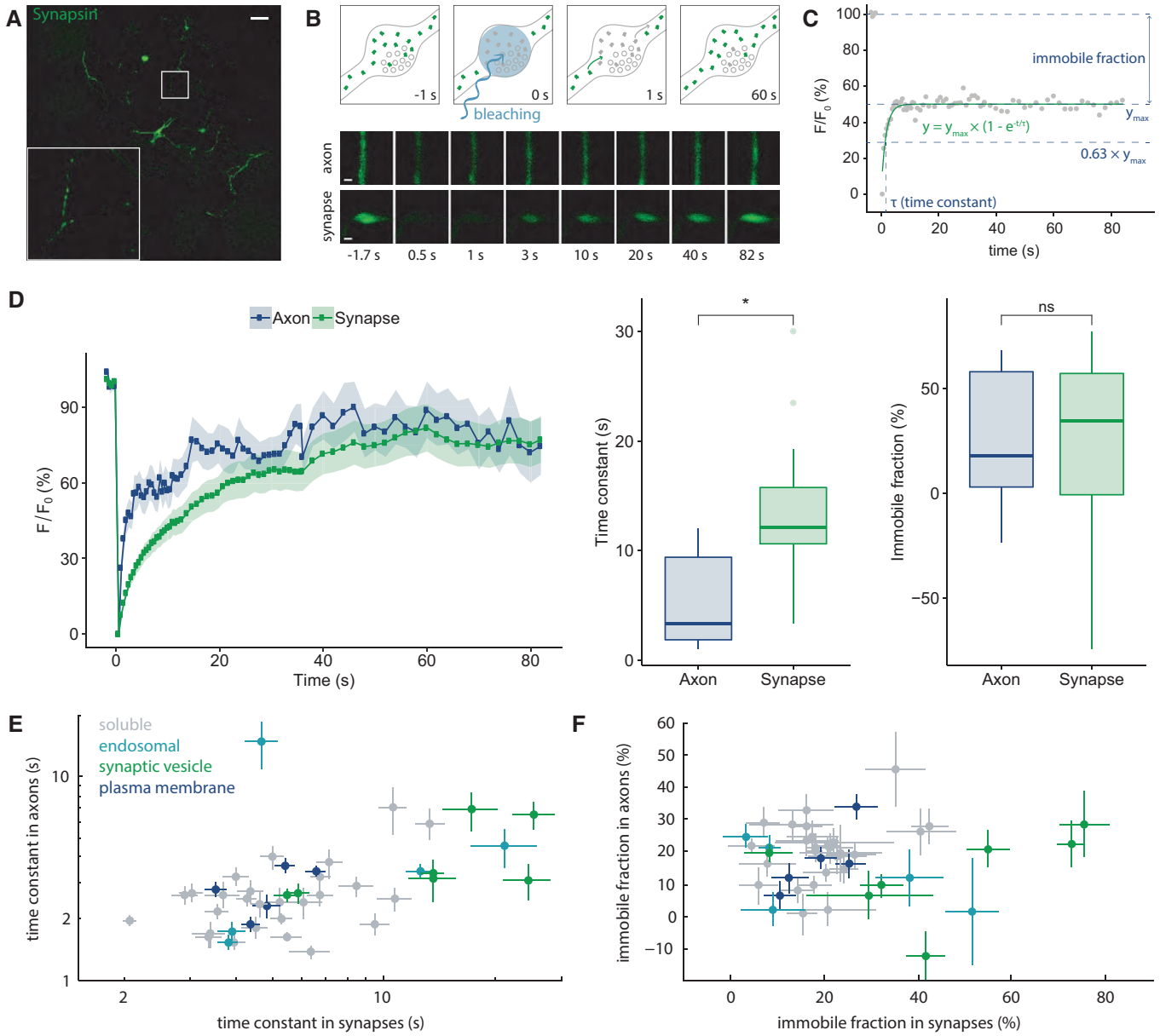

Figure 2. An overview of FRAP experiments.

A Typical wide-field image of a neuron expressing the synaptic vesicle-binding protein synapsin coupled to mEGFP. Scale bar, 100 μm.

B Top panels: a cartoon explaining the FRAP procedure. Fluorescent molecules are shown in green. The mEGFP molecules in a defined area are photobleached (gray molecules), and then, the entry of non-bleached molecules from the neighboring areas is measured. Middle and bottom panels: typical results in an axonal segment and in a synaptic bouton of a neuron expressing synapsin coupled to mEGFP. Scale bar, 500 nm.

C An explanation of the FRAP analysis procedure. The FRAP recovery curves could be well fit by single exponential functions, which provide the time constant of recovery, as well as the fraction of the molecules that is not replaced (immobile fraction).

D Exemplary results showing FRAP curves, time constants, and immobile fractions of synapsin in axons and synapses. Symbols indicate means ± SEM. The box plots are organized as follows: The middle line shows the median; the box edges indicate the 25th percentile; the error bars show the 75th percentile; and the symbols show the 90th percentile. Asterisk denotes significant difference. Wilcoxon rank-sum test with using the Benjamini–Hochberg procedure for multiple testing correction, FDR = 0.05. *N* (axons) = 17, *N* (synapses) = 24. Also presented in Appendix Fig S3.

E Time constants of all analyzed proteins in axons and in synapses. The two parameters correlate significantly, albeit not very strongly (R = 0.3182, P = 0.04). This correlation is only observed for soluble proteins (R = 0.6134, P = 0.0005), and not for membrane proteins (R = 0.0338, P = 0.9086).

F Immobile fractions in axons and synapses. No correlation was observed (R = 0.0451, P = 0.7769). Symbols indicate means ± SEM; all data are shown as box plots in Appendix Fig S3, numbers of replicates for each protein are shown in Appendix Fig S3, panels E and F are also presented in Appendix Fig S4 with protein names indicated next to symbols.

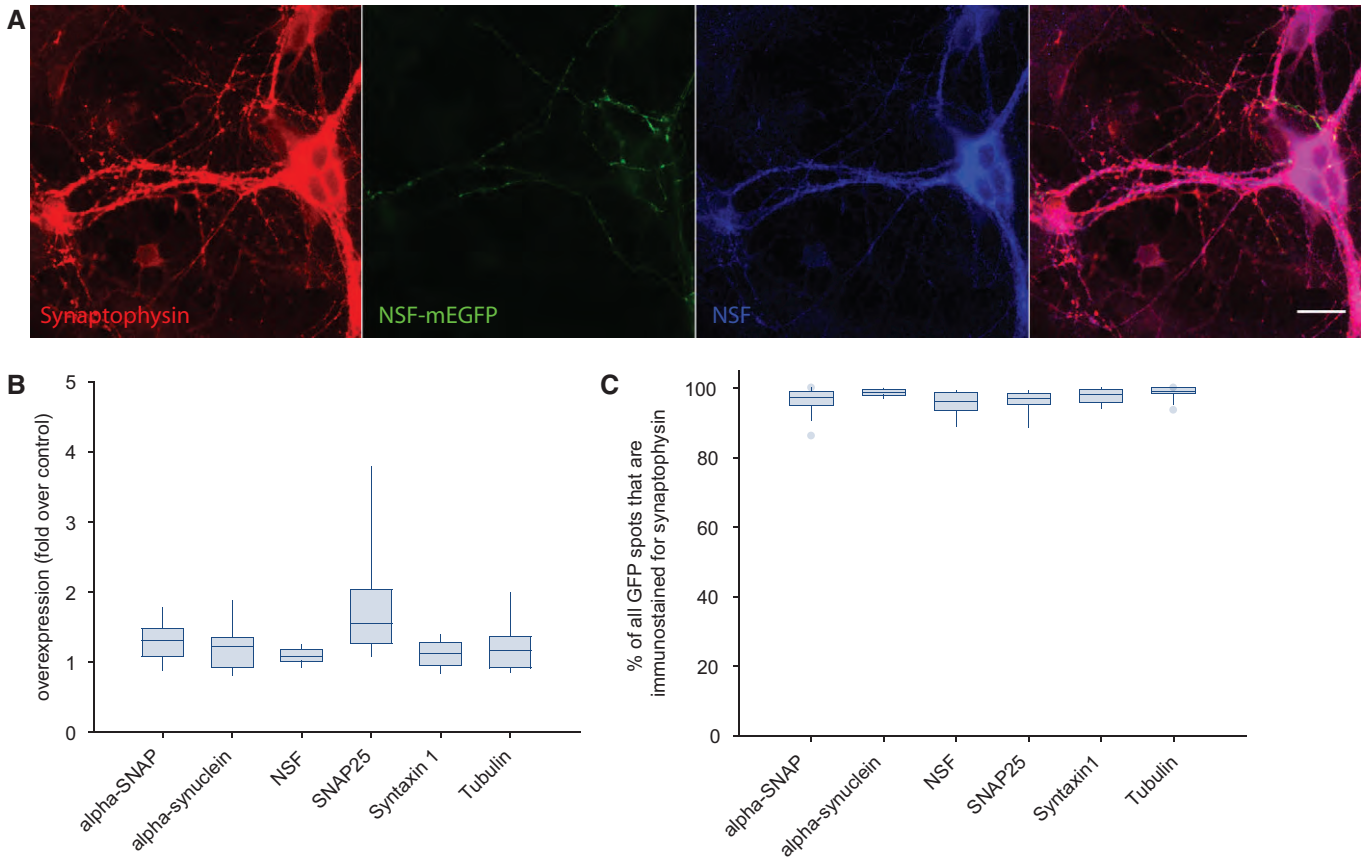

Figure 3. Analysis of protein overexpression.

A Typical images of a neuron expressing alpha-SNAP fused to mEGFP (green), which was also immunostained for the same protein (blue), and for the synaptic vesicle marker synaptophysin (red), to detect synaptic boutons. Scale bar, 20 μm.

B The levels of the proteins of interest were measured (relying on the immunostaining) in the transfected boutons, as well as in the non-transfected boutons (detected by the synaptophysin immunostaining). The overexpression levels are shown, obtained by dividing the immunostaining intensity in the overexpressing boutons by that in the non-overexpressing boutons. Only boutons with moderate expression levels have been considered in this work. *N* = 3 independent experiments, with ~6 independent fields of view (containing different neurons) per experiment.

C Percentage of GFP-positive spots that are also immunostained for synaptophysin. *N* = 3 independent experiments, with ~6 independent fields of view (containing different neurons) per experiment.

Data information: The box plots were organized as follows: The middle line shows the median; the box edges indicate the 25th percentile; the error bars show the 75th percentile.

time constant (Fig 4B), as observed, for example, in bacteria (Kumar *et al*, 2010). Another simple observation was that membrane proteins, on average, were slower compared to soluble ones, which is in good agreement with the literature (e.g. Kumar *et al*, 2010). Both protein classes showed significantly higher time constants in synapses than in axons (Appendix Fig S10B), suggesting that the synaptic environment slows the movement of both protein classes.

Synaptic protein mobility correlates to several other cell biology parameters, including structural features of the proteins and their lifetimes

We next aimed to determine whether the amino acid composition or the presence of certain structural motives can influence protein mobility. Such parameters have been linked to numerous features of the proteins in the past, such as their abundances or lifetimes (as mentioned in the introduction), which makes such a comparison also interesting for the protein mobility.

We first compared the mobility parameters of the proteins to the amino acid composition of their sequences (Appendix Fig S11). Numerous correlations were found. For example, the synapse FRAP time constant was negatively correlated with the percentage of aspartate residues in the protein sequences (Appendix Fig S12A). As it bears a negatively charged side chain, aspartate is expected to increase protein solubility, which provides an explanation for this observation. Glutamate shows a similar trend, albeit this correlation was not statistically significant (Appendix Fig S11). In contrast, we observed strong positive correlations between the percentage of phenylalanine residues in the protein sequence and the synapse FRAP time constant (Appendix Fig S11). A similarly strong influence of the phenylalanine content was observed on the immobile fraction in synapses (Appendix Fig S11, Fig 4C). The effects of this amino

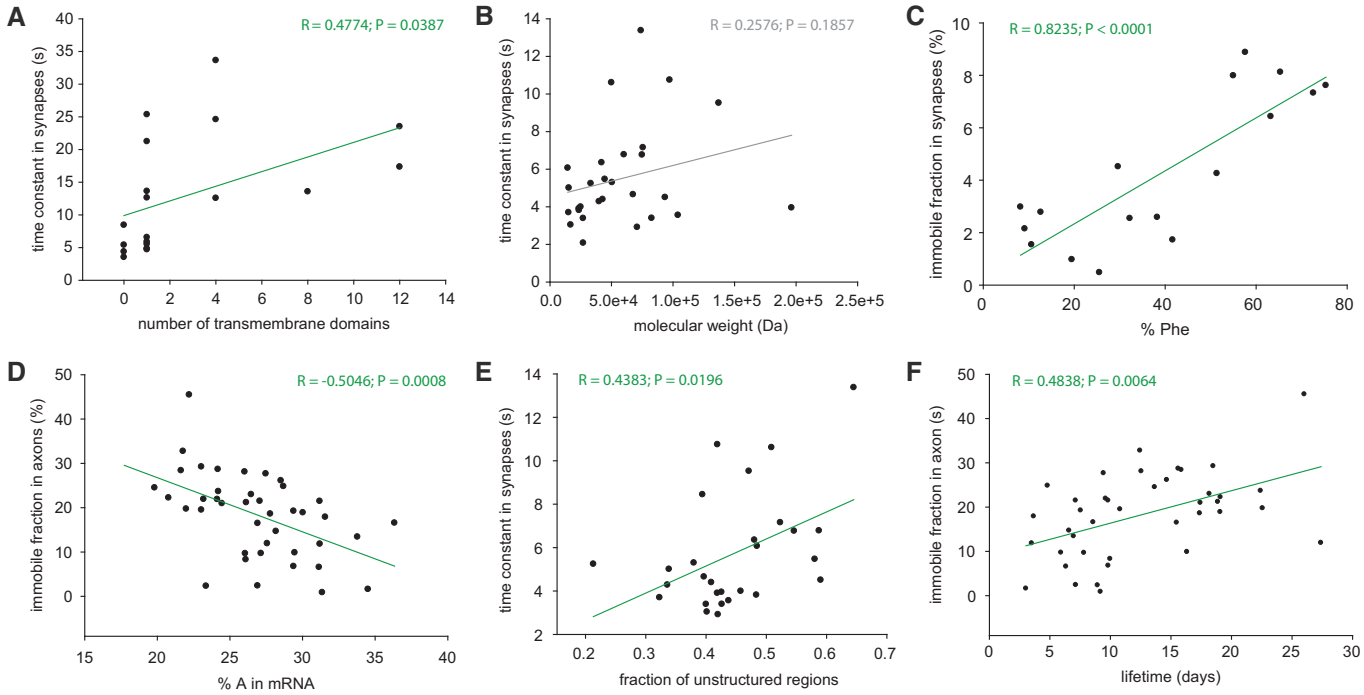

Figure 4. Correlation of protein mobility to various parameters.

A Correlation of FRAP time constants in synapses with the number of transmembrane domains, for the different membrane proteins. A significant correlation can be observed, which agrees with the previous literature, and with the expectation that proteins with large numbers of membrane domains diffuse more slowly.

B No correlation between the FRAP time constants in synapses and the molecular weight of the soluble proteins could be observed.

C Correlation between the immobile fraction in synapses (for the membrane proteins) and the percentage of phenylalanine residues in the protein sequence.

D Correlation between the immobile fraction in axons and the percentage of adenine in the mRNA sequences.

E Correlation between time constants in synapses and the predicted fraction of unstructured coils in the protein structure.

F Correlation between immobile fractions in axons and protein lifetimes. See Appendix Figs S10–S14 for more details.

acid were due to the contribution of membrane proteins, since no such correlation could be observed when only soluble proteins were considered (Appendix Fig S11). Moreover, the presence of other hydrophobic amino acids, as tryptophan, also correlated with low protein mobility in synapses. Overall, these observations are in agreement with the idea that proteins with higher numbers of transmembrane domains will contain proportionally more hydrophobic amino acids, while also being less mobile (Fig 4A, Appendix Fig S10A).

Having noted these correlations, we next turned to test whether such observations would also hold true at the mRNA level. We analyzed the correlation between mobility parameters and the percentage of different nucleotides in the respective mRNAs (Appendix Fig S13). We found significant negative correlations between the adenine percentage and the time constants in synapses and the immobile fractions, for both soluble and membrane proteins (Fig 4D, Appendix Figs S12B and S13). This is a relatively surprising observation, as none of the amino acids whose percentage correlates negatively with the protein mobility are coded by adenine-rich codons.

Overall, these observations suggest that structural parameters of the proteins (and possibly also of the respective mRNAs) may be linked to their mobility. To test this in a more direct fashion, we relied on predictions for the structured and unstructured regions in the proteins (from Mandad *et al*, 2018), and we correlated the mobility parameters with the fraction of the protein sequences that is structured (alpha-helix and beta-sheet) or unstructured (random coils). We found that the more unstructured the protein is, the less mobile it is in both axons and synapses (Fig 4E, Appendix Fig S12C). This is also supported by a relatively high (albeit not significant) correlation between the percentages of proline residues and the time constants of soluble proteins in axons (Appendix Fig S11), since prolines tend to act as breakers of secondary structures (Chou & Fasman, 1974).

Finally, we also tested less expected connections, to different cell biology parameters, including the protein lifetimes (Fornasiero *et al*, 2018; Appendix Fig S14). Remarkably, we found a significant positive correlation between immobile fraction in axons and the protein lifetimes (Fig 4F). The biological relevance of this correlation seems relatively simple. Proteins with high immobile fractions in the axon would spend long time periods here, which implies that they are more slowly transported along the axon then other proteins. The time spent during this slow transport simply adds to the total lifetime of these proteins, which renders them longer-lived than rapidly transported proteins. However, the mechanisms behind this simple hypothesis still remain to be determined.

Further considerations on alternative measurements

One criticism that these experiments could face is the exclusive use of FRAP. Other technologies could, in principle, also have been used, including fluorescence correlation spectroscopy (FCS). However, FCS measurements are difficult to interpret in the complex 3D space of the synapse (Appendix Fig S15) and resulted

in values that did not conform to the existing literature (e.g., the apparent diffusion coefficient of mEGFP was 0.9 ± 0.4 μm^2/s, which is at least 10- to 20-fold below the expected value for this molecule in cell cytosol or in synaptic boutons; see Sadovsky *et al*, 2017 and references therein, and Spinelli *et al*, 2014). These difficulties are due to a number of factors that affect FCS interpretations. First, the exact intracellular viscosity at the measurement positions is unknown, as is also the local temperature during the acquisition time (due to laser-induced heating). Second, the 2D fitting model normally used for such measurements may not be the correct choice for modeling the data, as the axon, and most of the synapses, is substantially thinner than the excitation volume. This implies that diffusion in and out of the volume in the second dimension does not occur in the measurements. As a result, FCS measurements report diffusion coefficients that do not correspond to real protein behavior. To obtain true coefficients, complex modeling procedures that take synaptic and axonal geometry into account would be required.

An alternative option for identifying the molecule movement behavior is to employ single-molecule tracking. This technique results in high-precision data and has been performed for a few presynaptic molecules, including syntaxin 1 in hippocampal neurons (Ribrault *et al*, 2011) and in *Drosophila* synaptic boutons (Bademosi *et al*, 2017), or synaptotagmin 1 in hippocampal neurons (Westphal *et al*, 2008; Kamin *et al*, 2010). The procedures to perform single-molecule tracking are substantially more difficult than FRAP or FCS, as they have relied on complex labeling using quantum dots (Ribrault *et al*, 2011), on live STED imaging close to the performance limits of the respective instrumental setups (Westphal *et al*, 2008; Kamin *et al*, 2010), or on highly specialized analysis procedures, relying on photoconvertible fluorescent proteins (Bademosi *et al*, 2017). Therefore, such procedures have not been typically employed for many proteins in any given publication, and could not be employed efficiently for the 45 proteins analyzed here. Fortunately, a detailed analysis of our own work shows that the FRAP analysis can reproduce the results provided by single-molecule tracking in hippocampal neurons, as detailed below.

Active organelle movement is a relatively rare event over the FRAP time course

Before proceeding with a thorough analysis of the FRAP data, one would need to consider the fact that FRAP does not differentiate between diffusive and active transport. Most proteins are delivered to synapses via both modes. For example, transmembrane proteins are transported actively as components of vesicles or endosomes, but they also diffuse passively in the plasma membrane. Therefore, the time constants observed in FRAP would report a mixture of the recovery of the molecule population found in the plasma membrane, and of the recovery of the population found in vesicles.

To estimate the extent to which active organelle transport would affect the FRAP observations we made, we aimed to estimate the fraction of recovery that can be caused by active transport of the organelle-bound proteins. We analyzed this experimentally by organelle-tracking experiments, again relying on the mEGFP chimeras presented above (Fig 5A). First, we calculated the fraction of each of the analyzed proteins found in organelles, as opposed to being distributed diffusely on the plasma membrane or in the cytosol. Second, we estimated the mobility of the organelles. This enabled us to determine the fraction of each molecule that is present, at any one time, in mobile organelles, which would influence the timeline of the FRAP recovery. This analysis suggested that, as expected, < 2% of cytosolic mEGFP is present in moving organelles (presumably autophagosomes produced during neurite remodeling). In general, < 10–12% of the molecules were found in moving organelles (Fig 5B, left), even for vesicle proteins, mostly due to the fact that the organelles were immobile for most of the observation time. Immobility was defined as displacements at or below the levels observed in aldehyde-fixed samples. When mobility was observed, the average movement speed was up to ~1 μm/s (Fig 5B, middle), as expected from previous studies on neuronal organelle transport (Hirokawa *et al*, 2010). The duration of each movement episode varied from 1 to ~15 s (Fig 5B, right).

Overall, these experiments imply that the contribution of active organelle transport to the FRAP recordings we obtained is limited.

A detailed analysis of the protein movement parameters obtained from FRAP imaging

The FRAP results showed here also do not report exact diffusion coefficients, but rather a comparable measure of apparent protein mobility. FRAP is notoriously difficult to analyze in terms of true molecular motion in synapses (Salvatico *et al*, 2015), and for the diffusion coefficients to be extracted from these data, the synapse geometry would also have to be considered. Albeit general FRAP interpretation models have been proposed (Kang *et al*, 2012; Blumenthal *et al*, 2015; Bläßle *et al*, 2018), they cannot be used with accuracy in a small and complex structure, as the synapse. When such models are used for our measurements, they underestimate the known motion behavior of GFP by at least 50- to 100-fold (diffusion coefficients of only ~0.2 μm^2/s both in the axon and in the synapse, Appendix Fig S16). This is probably due to the fact that the general FRAP interpretation models are designed for situations in which molecules come from large cellular areas, from all directions, and are thus unable to account for the synaptic geometry.

To interpret the FRAP results one would need a realistic model, which considers the synapse organization. We sought therefore to simulate different particle motion behaviors, with different movement speeds, in realistic synaptic space in order to find the behaviors that most closely reproduced the FRAP results. An overview of the modeling procedure is presented in Fig 6. We started by generating a 3D synapse from electron microscopy data (Fig 6A). We then moved particles in this 3D synapse, at different speeds (Fig 6B). We hypothesized that the behavior of the proteins could be approximated as the diffusive movement of particles in the synaptic space (in the cytosol or in the plasma membrane). Afterwards, we transformed the particle motion in artificial FRAP movies (Fig 6C–E), which we then compared to the original FRAP data (Fig 6F), in order to find the models that best reproduced the biological measurements. We then used these models to determine the diffusion coefficients of analyzed proteins (Fig 6G) and to generate graphical representations of their movement (Fig 6H).

To obtain a 3D synapse model, we relied on serial-sectioning electron microscopy (*e.g.*, Schikorski & Stevens, 1997, 2001). We reconstructed 30 synapses and measured their different parameters, including surface, volume, active zone area, vesicle number,

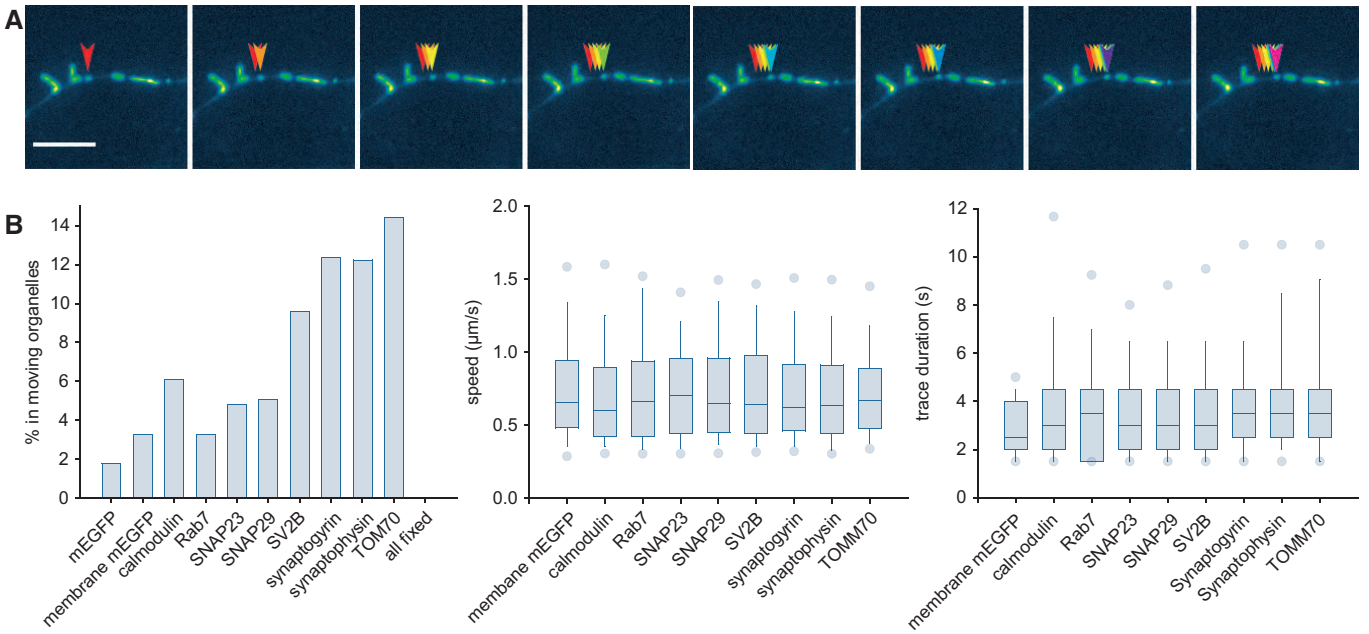

Figure 5. A tracking analysis for synaptic organelles.

A Neurons were transfected with a TOM70-mEGFP construct, to indicate mitochondria, and were visualized using an epifluorescence microscope. The arrowheads track the movement of one mitochondrion. Scale bar, 10 µm.

B The movement was analyzed using particle tracking, as indicated in Materials and Methods. The proportion of molecules found in moving organelles, the speed of movement, and the trace duration are indicated for the different proteins expressed. N = 4–10 independent analyses per condition. The box plots were organized as follows: The middle line shows the median; the box edges indicate the 25th percentile; the error bars show the 75th percentile.

vacuole number and volume, and mitochondria volume (Appendix Fig S17). We then chose a synapse that was close to the overall average for most parameters, and constructed it *in silico* with the respective axon, to a total length of ~9 µm (Appendix Fig S17A). We then used this synapse to construct Monte Carlo models of particle movement, using the simplest possible assumptions.

For membrane proteins, we placed particles in the plasma membrane of the 3D synapse model and allowed them to move in random directions, with a given average single-step velocity. The particles were allowed to move with the same velocity in the axon and in the synapse, in accordance with previous super-resolution tracking experiments we performed on the synaptotagmin 1 (Westphal *et al*, 2008; Kamin *et al*, 2010). To be able to account for slow- or fast-moving proteins, we generated models with different single-step velocities, from 25 to 200 nm per movement step.

To generate artificial FRAP movies, we placed 1,000 particles in the 3D synapse model and allowed them all to move with the same single-step velocity. A measured point-spread-function (PSF) was convoluted with each of the particles, to thus mimic the movement of 1,000 GFP-tagged protein molecules. To obtain a FRAP situation, we bleached *in silico* areas similar to those bleached in the biological experiments. We then monitored the re-entry of fluorescent (non-bleached) particles in the bleached area. The artificial movies were then analyzed exactly as the real FRAP movies. The FRAP parameters that these *in silico* movies provided were similar to those observed for most membrane proteins in real experiments. For example, the slower FRAP recovery observed in the synapse, in comparison with the axon, was also observed in the models.

For the soluble proteins, we added one more level of complexity to the model, to account for protein binding to the vesicle cluster, which is a well-known phenomenon (Shupliakov, 2009; Denker *et al*, 2011a; Milovanovic & Camilli, 2017). Particles moved with the same single-step velocity in the axon and in the synapse, as above, but they were also allowed to interact with vesicles, and to be retained on their surfaces (Fig 6B). We then combined different single-step velocities (25–250 nm per movement step) with different vesicle-retention times (from 1, meaning no retention, to 200, with particles staying on vesicles for ~200 movement steps, before coming off and moving again). This accounts for many different behaviors, such as slow or fast movement, as well as weak or strong interactions to the synaptic vesicles. The *in silico* FRAP data we obtained overlapped well with the FRAP results obtained in living neurons. Every measured protein behavior was reproduced by a specific combination of velocity and vesicle retention time, with the average difference between the measured and modeled FRAP time constants being ~5% (for FRAP in the synapse) and ~9% (for FRAP in the axon). For each combination, we calculated a diffusion coefficient using the Einstein–Smoluchowski equation and assigned the coefficients to proteins whose behaviors (FRAP recoveries) were best reproduced by the corresponding models.

A series of validations for the FRAP interpretations

The models presented above are minimalistic in nature. For example, single membrane molecules can exhibit alternating slow and rapid movement phases (Freeman *et al*, 2018), but only the average movement speed is reported here. The models also replace complex

behaviors of soluble molecules, which may include repeated binding and unbinding to several different proteins within the cluster, with one single parameter: binding to the vesicle cluster. Some proteins, such as actin, may not even bind vesicles directly, but rather actin strands or synapsin within the cluster. In spite of these shortcomings, the models should be able to address the average behavior of

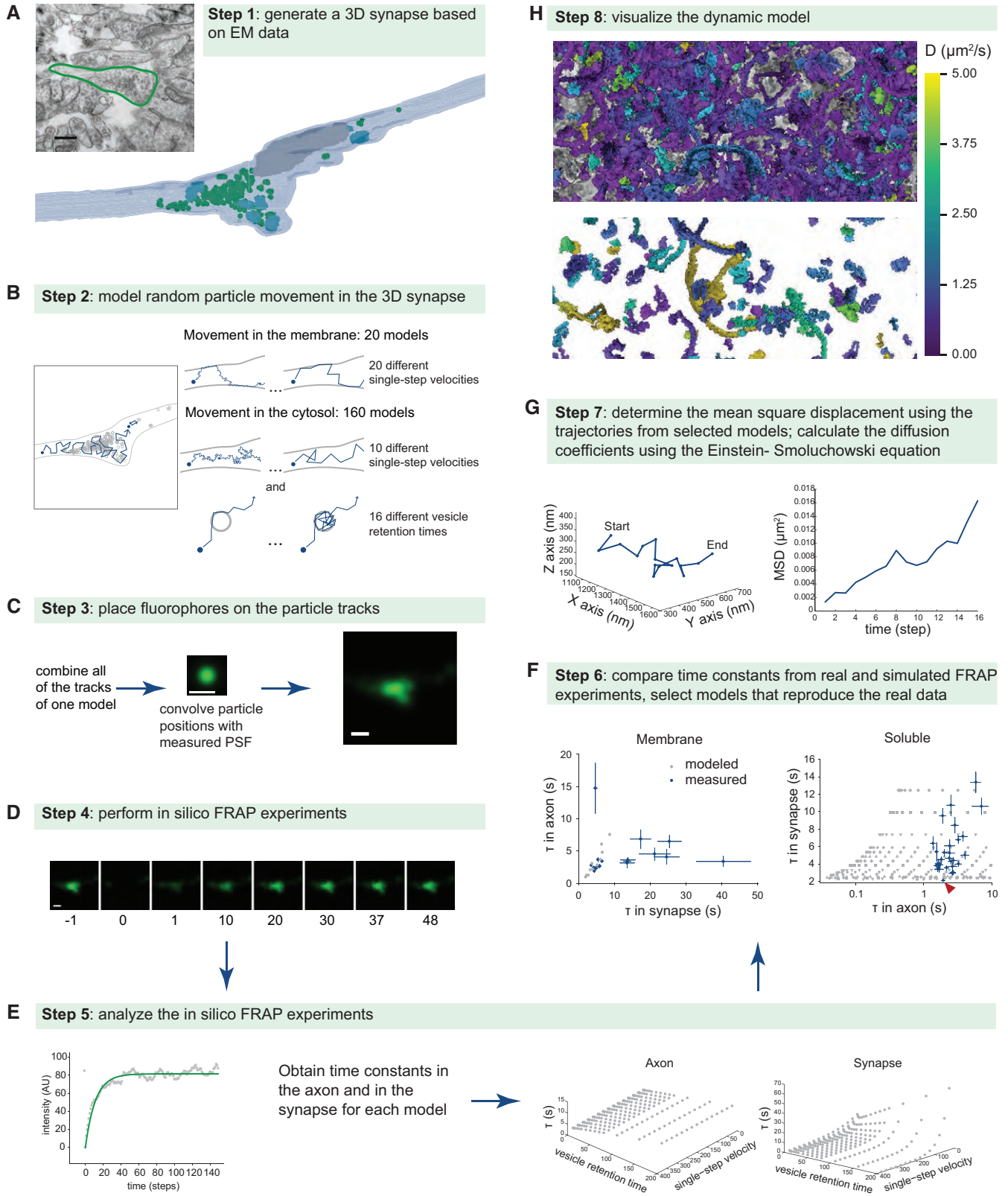

Figure 6.

Figure 6. The procedure of creating the dynamic model.

A Protein movement was modeled in a realistic synaptic 3D space, obtained from electron microscopy. Also shown in Appendix Fig S17.

B We allowed particles to move randomly with set average displacement steps (for both movement in the plasma membrane and in the cytosol) and vesicle retention times (only in the cytosol). Each model had a unique combination of the velocity and the vesicle retention time.

C All generated tracks from one model were then combined, and particle positions were convoluted with a measured PSF to produce simulated fluorescent images.

D By eliminating the fluorescence in a region similar in size to the bleaching region of real FRAP experiments, *in silico* FRAP movies were generated.

E These were then analyzed in the same manner as the real FRAP experiments.

F We selected the models reproducing the behavior of the proteins measured in live neurons by comparing the time constants obtained in the simulated FRAP experiments with the real ones. An interesting point can be observed in the right panel: the lowest blue spot (red arrowhead) represents EGFP. This is the only protein whose behavior overlaps with the lowest series of model behaviors (gray spots), which represents free motion in the synapse, without vesicle binding.

G To obtain diffusion information we calculated for these models the mean square displacements (MSD) from the tracks, and we then derived from them diffusion coefficients (D) using the Einstein–Smoluchowski equation.

H The diffusion coefficients are presented in Table EV2, while the model tracks are used to generate animated model representations (see EV movies). This panel indicates protein motion (diffusion coefficients) inside (top) and outside (bottom) the vesicle cluster in a color scheme. The top panel shows mostly vesicle-bound proteins, which have low mobility (in purple), while the space outside of the vesicle cluster contains mostly mobile proteins (green-yellow colors).

the different protein species. To test whether these models indeed report the true average behavior of the proteins, we measured or noted several independent parameters.

First, we found that the models correctly predicted that free mEGFP does not interact with synaptic vesicles (Fig 6F).

Second, the models also predicted the distribution of each protein in the synapse versus the axon. This correlated well with values obtained by immunostaining neuronal cultures for the different proteins, with a coefficient of determination (R^2) of ~0.7 (Fig 7A–C).

Third, we used the models to determine the copy number of proteins per synaptic vesicle, for the proteins that are known to reside in vesicles. This reproduced well the copy numbers measured in the past by protein biochemistry (Takamori *et al*, 2006) ($R^2 > 0.9$; Appendix Fig S18).

Fourth, we used the protein positions provided by the models to reconstruct stimulated emission depletion (STED) images for the different proteins, and we compared them with real STED images, obtained from immunostaining experiments (Fig 7D and E). The model images reproduced well the spot size and spot intensity distributions from the real images (Fig 7D–I; see Appendix Fig S2 for details on all STED immunostainings).

Fifth, the models were able to predict the fraction of membrane proteins found in the synapse, which correlated well with the enrichment of these proteins in the synaptic vesicles (Takamori *et al*, 2006; Appendix Fig S19).

Sixth, we similarly could predict the enrichment of the soluble proteins in the synaptic vesicle cluster, which correlated well with the enrichment of soluble proteins on purified synaptic vesicles (Takamori *et al*, 2006; Appendix Fig S20).

Different diffusion coefficients for the proteins analyzed here

The validations indicated above suggest that, although we used bulk measurements (FRAP) and very simple interpretation models, our results were sufficiently robust to reproduce, among other parameters, previous results on protein distributions at the nanoscale. We therefore determined diffusion coefficients for the different proteins, from the models indicated above (Table EV2). To account for possible errors in the modeling, for each protein we averaged the diffusion coefficients of the three to five models whose FRAP values were closest to those of the respective protein. The resulting means and error bars are shown in Fig 8.

They provided two further lines of validation:

First, the diffusion of several proteins conformed to previously measured values (Fig 8A). mEGFP, with a modeled diffusion coefficient of ~20 $\mu m^2/s$, is well within the range measured in many other systems (15–26 $\mu m^2/s$, with an average of ~21 $\mu m^2/s$; see Sadovsky *et al*, 2017 and references therein). Synaptotagmin 1 had a modeled diffusion coefficient of ~0.11 $\mu m^2/s$, very close to the one measured by live super-resolution tracking of antibody-tagged molecules, ~0.095 $\mu m^2/s$ (Kamin *et al*, 2010). Similarly, the axonal diffusion coefficient of syntaxin 1 (~0.22 $\mu m^2/s$) was close to the value observed by tracking quantum dot-tagged molecules (Ribrault *et al*, 2011) in axons (0.2 $\mu m^2/s$). The synaptic diffusion coefficient of syntaxin was also similar to the average coefficient measured in this work (Ribrault *et al*, 2011), albeit it was ~20% larger. This may be due to the fact that some quantum dot-tagged molecules may have been slowed in the synapse by problems with quantum dot penetration in the synaptic cleft (Lee *et al*, 2017).

Second, from the behavior of synaptic vesicle proteins we could calculate the diffusion coefficient of whole synaptic vesicles (see Materials and Methods). The resulting value, of ~0.01 $\mu m^2/s$ (Fig 8B), is well within the range measured for synaptic vesicles in hippocampal neurons in the past (average of ~0.0138 $\mu m^2/s$, taking into account the studies in Jordan *et al*, 2005; Shtrahman *et al*, 2005; Yeung *et al*, 2007; Westphal *et al*, 2008; Kamin *et al*, 2010; Lee *et al*, 2012; Rothman *et al*, 2016).

As expected from our analysis of basic FRAP parameters (Fig 4, Appendix Fig S10), the diffusion coefficients confirmed that soluble protein movement was only loosely influenced by protein size and that membrane protein movement was significantly affected by the number of transmembrane domains (Appendix Fig S21).

More interestingly, the modeling analysis we performed enabled us to produce the first realistic movies of nanoscale protein movement in the synapse. We modeled the molecular motion of all of the analyzed proteins, in a realistic synaptic setting. Movie EV1 shows several thousand cytosolic protein molecules moving within a small region next to the vesicle cluster, while Movie EV2 shows membrane proteins moving in the plasma membrane above the same region (proteins are represented according to the legend in Appendix Fig S22). Many other graphic representations could be made, including views of molecule mixing in the synapse, for the soluble (Movie EV3) or membrane proteins (Movie EV4).

Discussion

We provide here a first comparative study of protein mobility in the synaptic bouton, encompassing 45 different proteins, from different types and classes. Our results confirm several expectations, including the lower mobility of membrane proteins when compared to soluble proteins, or the lower mobility of virtually all proteins in the synapse, when compared to the axon. Other expected observations

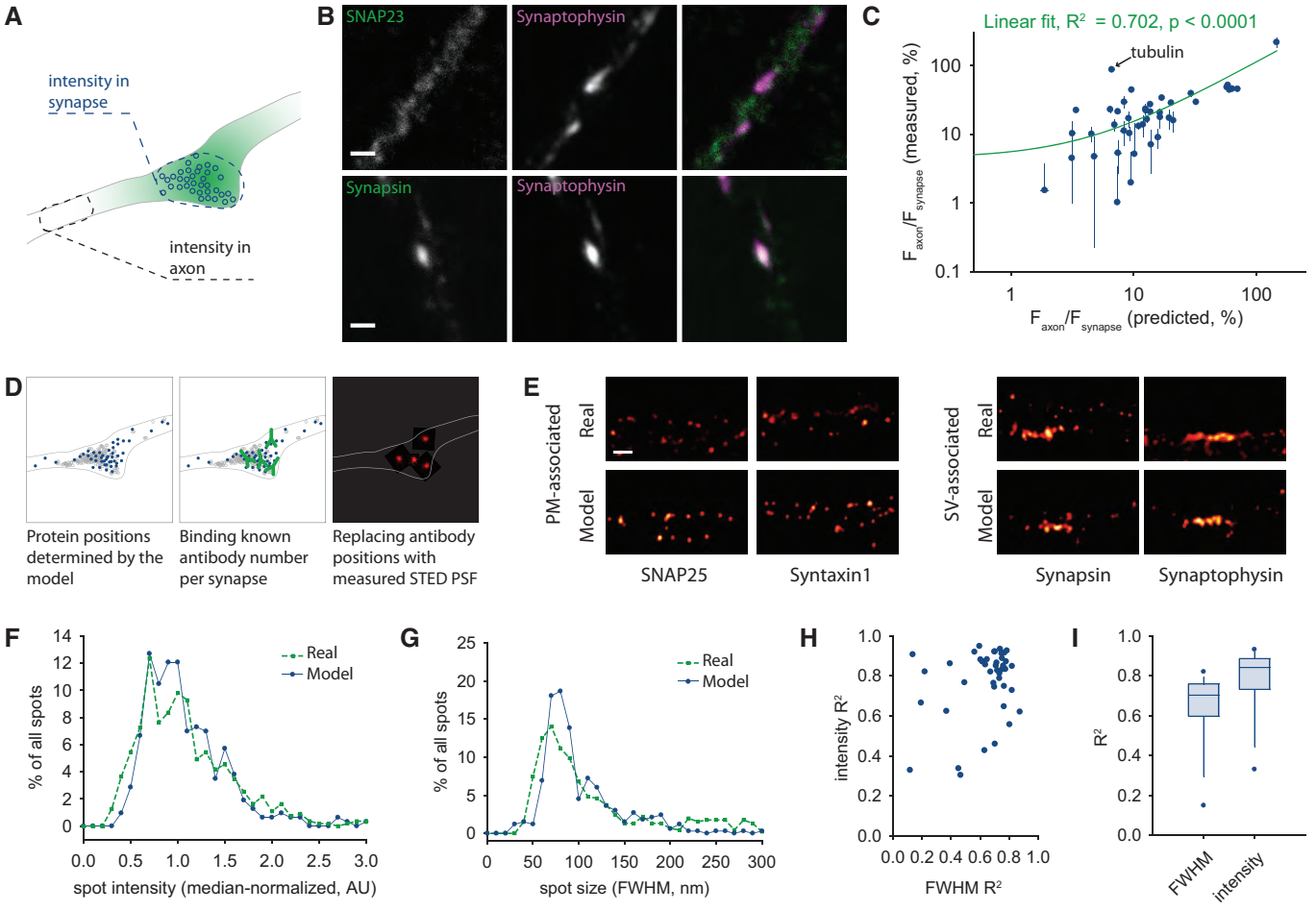

Figure 7. Modeling validations.

A We analyzed the protein distribution in synapses versus the neighboring axonal segments, both *in vivo*, by immunostaining and confocal microscopy, and in the *in silico* models, by interpreting the particle positions.

B Examples of immunostained proteins, which are present mostly in synapses (synapsin) or are distributed both in synapses and in axonal areas (SNAP23). Synapses were identified by co-immunostaining for the synaptic vesicle marker synaptophysin and for the active zone marker bassoon (not shown here). Scale bar, 500 nm.

C A correlation of the fluorescence ratios between the axonal segments and the synapses, predicted by the model and in the biologically measured data. The correlation is highly significant, with a coefficient of determination (R^2) of ~0.7. This increases to 0.8 when tubulin is removed; for tubulin, we can only model the diffusion of the free molecules, but the immunostaining reveals both the free molecules and the microtubules, implying that a poor correlation is expected for this protein. Our analysis predicts that larger amounts of free tubulin are found in the synapse, versus the axon. This is very likely, for example, due to the larger volume of the synapse, so that the model prediction appears reasonable, although it cannot be tested in this experiment. Symbols indicate mean ± SEM from at least 20 neurons, from at least 2 independent experiments.

D We relied on the model-suggested protein distributions to generate putative super-resolution images for the different proteins. Defined numbers of protein positions, corresponding to the number of antibodies that can be accommodated in these synapses for each protein (from Richter *et al*, 2018) were convoluted with a measured stimulated emission depletion (STED) PSF, thereby resulting in STED images for these proteins.

E Typical model STED images are compared to real ones, obtained by STED imaging of immunostainings. Scale bar, 500 nm. Here, we only show real (immunostained) synapses that correspond in overall size to our model synapse.

F, G The spot sizes (as full width at half maximum, FWHM) and intensities were analyzed in model synapses (using 100 different random STED images of synapses for each protein of interest) and in the real synapses (using all synapses, irrespective of size, in at least 15 different neurons from at least two independent experiments).

H, I We analyzed the correlation between the spot size and intensity distributions, in the models and in the real synapses. These are shown as a scatter plot in h, or as box plots in i (the middle line shows the median; the box edges indicate the 25th percentile; the error bars show the 75th percentile; the symbols show the 90th percentile). Overall, the models correlate very well with the real data, with coefficients of determination (R^2) of ~0.7–0.8. The number of elements quantified here is identical to the number of proteins analyzed in the STED microscopy experiments (44).

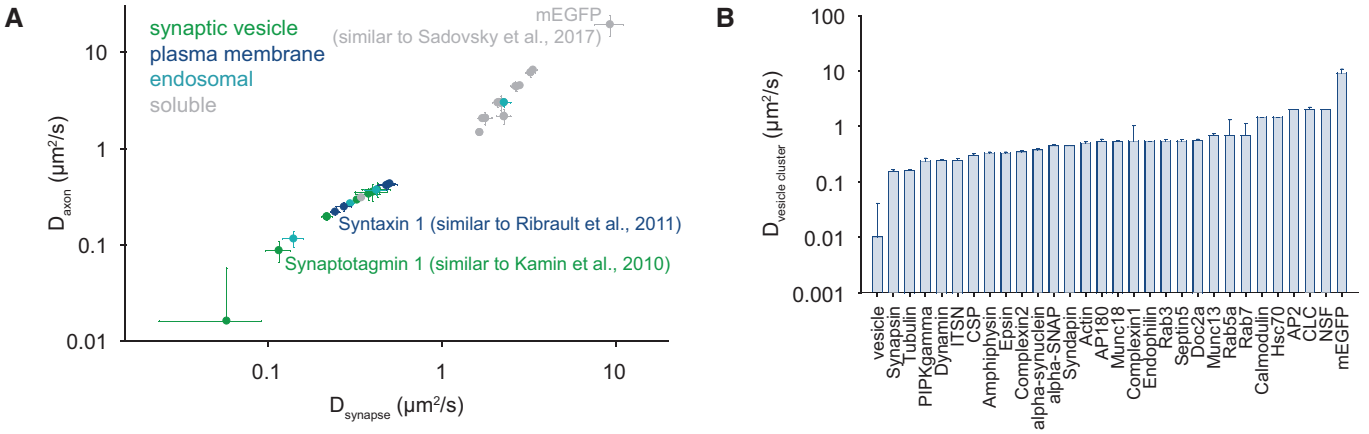

Figure 8. Modeling results.

A The diffusion coefficients obtained for the different proteins, in the synapse or in the axon. The symbols show the means ± SEM from the *in silico* models that best reproduced the data, corresponding to the range of values of 3–5 models. The values for all proteins are shown in Table EV2.

B Same as a, but for the diffusion in the vesicle cluster. For all *bona fide* synaptic vesicle proteins, this is represented by the diffusion of the vesicles themselves (back-calculated from the FRAP results of the vesicle proteins as explained in Materials and Methods). Bars show mean ± SEM, from the *in silico* models that best reproduced the data, corresponding to the range of values of 3–5 models.

were that the movement rates of the same proteins in the axon and in the synapse correlated little, presumably due to the different conditions encountered there, or that the mobility of soluble proteins was only little controlled by their molecular size. Several other observations could be made, including relations between protein mobility and structural parameters, mRNA composition, or protein lifetimes.

Our measurements, as indicated above, were performed with the caveat that the proteins we measured were more abundant than under normal (wild-type) conditions. The overexpression levels we observed were mild, but they may nevertheless contribute to artifacts, namely to an over-estimation of the mobility of individual proteins. If one protein is expressed too highly, its copy numbers saturate all binding to interacting partners, and the un-bound molecules end up moving randomly in the synapse, presumably at the highest possible speeds. The various validations we performed suggest that this is not a major problem. At the same time, our reported values should be taken as maximal mobility estimates, due to this issue. Native (non-tagged) proteins have not been investigated often, with only a handful of studies available. Several such studies were reproduced well by our data (Appendix Fig S6). At the same time, a FRAP measurement of knock-in Munc13 provided a substantially lower mobility (Kalla *et al*, 2006), with the shortest time constant measured in cultured mouse cortical neurons being around ~3 min, as opposed to a few seconds in our measurements. This difference probably has both technical and biological grounds. The previous work imaged the synapses at intervals of a few minutes, to avoid photobleaching. Analyzing our Munc13 data at 20–30 s of intervals (as opposed to two times per second, as in our original data) raised the time constant from ~4 to ~30 s. Analyzing such data every few minutes would presumably result in an even longer time constant. Also, the previous work bleached multiple boutons in the same area, which probably resulted in bleaching a considerable proportion of the fast-moving molecules in the respective axons, which will reduce the fluorescence recovery. Nevertheless, it is still possible that Munc13 mobility is particularly sensitive to overexpression.

In spite of these caveats, several conclusions could nevertheless be drawn. First, synaptic protein mobility seems to be influenced by the interaction of the proteins with the vesicles. For soluble proteins, it has been hypothesized that strong interactions to the vesicle cluster cause their enrichment in synapses (Shupliakov, 2009; Denker *et al*, 2011a; Milovanovic & Camilli, 2017). This was observed especially for synapsin (Benfenati *et al*, 1989; Takamori *et al*, 2006; Milovanovic *et al*, 2018), whose slow movement in synapses was paralleled by strong binding to vesicles. This effect was even more strongly visible for membrane proteins (Appendix Fig S7) and is mostly explained by the fact that molecules that are more highly enriched in synaptic vesicles are present at lower levels on the plasma membrane. This implies that large fractions of these proteins will recover slowly during FRAP, through the infrequent active transport of synaptic vesicles (Fig 5). This will result in large time constants for the respective proteins. However, this is not the only explanation for this observation. The time constants of *bona fide* synaptic vesicle proteins are also higher in the axon, when compared to non-vesicular proteins (Appendix Fig S8). As all of these molecules are found in axons mainly as molecules fused to the plasma membrane, an explanation based on the transport of synaptic vesicles seems unlikely. A potential solution to this question is that synaptic vesicle proteins may diffuse in the axon in the form of assemblies composed of multiple molecules. This issue has been discussed for several decades (see e.g., Ceccarelli & Hurlbut, 1980; Haucke *et al*, 2011; Rizzoli, 2014), and it is still open for further interpretation. However, a series of recent observations, made mainly through super-resolution imaging of fused synaptic vesicles, suggested that such assemblies are indeed present in the axon, and may even be the dominant form in which vesicle proteins are found in the axonal compartment (Richter *et al*, 2018; Truckenbrodt *et al*, 2018; Seitz & Rizzoli, 2019).

Second, soluble unstructured proteins also appeared to move more slowly in synapses. This observation is especially interesting in the context of a recently proposed mechanism of synaptic vesicle cluster segregation. It has been suggested that synaptic vesicles, together with synaptic vesicle binding proteins, form a distinct liquid phase via liquid–liquid phase separation within the synapses (Milovanovic & Camilli, 2017; Milovanovic *et al*, 2018). By definition, material exchange between liquid phases is slower than free diffusion; therefore, it is expected that soluble proteins of synaptic vesicle cluster would have slower recovery rates. Since the presence of multiple disordered coils is one of the main structural characteristics of proteins known to take part in liquid phase separation, our observations fit very well with this model.

Third, several correlations could be found to the presence of different amino acids in the protein sequence, or to the presence of particular nucleotides in the mRNA sequence. While the correlations to specific amino acids were relatively easy to interpret, as mentioned in Results, the links to mRNA composition are less obvious. Different parameters of protein homeostasis have been linked to the mRNA composition in mammalian cells, and especially to the mRNA secondary structure (Kudla *et al*, 2009) or to the GC contents (Kudla *et al*, 2006). At the same time, the mRNA composition has been suggested to control the folding conformation of specific proteins (Zhou *et al*, 2013; Fu *et al*, 2016). It is still unclear whether the relations between mRNA composition and cell biology parameters are causative in nature (Arhondakis *et al*, 2008), but they are sufficiently strong to enable reasonable predictions of protein abundance, lifetime, and translation rate (Mandad *et al*, 2018). Overall, it is therefore not entirely surprising that protein mobility also correlates with mRNA composition, albeit it is difficult to explain why a high percentage of adenine correlates with higher mobility. One hypothesis could be based on the observation that proteins related to specialized function, including synapse formation, are encoded by GC-rich genes (Gingold *et al*, 2014; Fornasiero & Rizzoli, 2019). In contrast, proteins involved in cell proliferation and in general cellular metabolism are encoded by AU-rich genes. This implies that "less synaptic" proteins would have mRNAs containing higher adenine percentages than *bona fide* synaptic proteins. The former would interact less with synaptic vesicles or other synaptic components, and would therefore be more mobile than true synaptic proteins. This hypothesis is supported by the fact that the top adenine-containing targets, which influence mostly these correlations, are SNAP23, Rab5, VAMP4, and SNAP29, trafficking molecules that are not specific to synapses in any fashion. At the opposite end, the top adenine-lacking proteins are the synaptic vesicle markers synaptophysin, synaptogyrin, and vGlut (glutamate transporter), along with the endocytosis cofactor epsin, further confirming this hypothesis.

Finally, we analyzed thoroughly the FRAP data, to provide diffusion coefficients for the different proteins. These coefficients were validated by several types of measurements, as described above, and should provide a good starting point for models of synaptic physiology. We are confident that laboratories specialized in neuronal and synaptic modeling could exploit our entire dataset by introducing the different protein amounts and mobilities in multireaction synaptic models (as, e.g., in Gallimore *et al*, 2018). Importantly, our data could be compared and combined with any dataset on hippocampal cultured synapses, which are a commonly used experimental model, for which large numbers of functional datasets are available.

We conclude that our work provides a novel resource for the analysis of synaptic function, which should enable synaptic modeling with substantially higher precision than in the past.

Materials and Methods

Cell culture and transfections

Primary hippocampal neuronal cultures were obtained from newborn (P1-P3) rats as previously described (Banker & Cowan, 1977; Kaech & Banker, 2006). Cells were grown in 12-well plates on glass coverslips in Neurobasal-A medium (Gibco, Paisley, Scotland), pH 7.5, at 37°C in 5% CO_2.

Cells were transfected using either calcium phosphate or lipofectamine transfection. Transfections with calcium phosphate were performed after 7–8 days *in vitro*, using the ProFection® Mammalian Transfection System Calcium Phosphate Kit following a protocol according to the manufacturer's recommendations with slight modifications described previously (Truckenbrodt *et al*, 2018).

Lipofection was performed after 2–6 days *in vitro*. Coverslips with cells were placed into 400 µl of DMEM (BioWhittaker, Lonza, Verviers, Belgium) complemented with 10 mM $MgCl_2$ and incubated for 30 min at 37°C in 5% CO_2. 50 µl of a transfection mix containing 2 µl of Lipofectamine® 2000 reagent (Invitrogen, Carlsbad, CA, USA) and 1 µg of plasmid DNA in Opti-MEM® (Gibco, Paisley, Scotland) medium were added per coverslip. After 20-min incubation at 37°C in 5% CO_2, cells were washed three times with DMEM (BioWhittaker, Lonza, Verviers, Belgium) complemented with 10 mM $MgCl_2$ and placed into original wells with Neurobasal-A medium (Gibco, Paisley, Scotland).

DNA plasmids

For ectopic expression of fluorescently labeled proteins, plasmids coding for proteins of interest fused to a monomeric variant of enhanced GFP (A206K mutant, mEGFP) or EGFP were used. See Table 1 for mRNA reference sequences, backbones used, and sequences of linkers between the fluorescent tag and the proteins of interest of the plasmids used in the FRAP experiments. Information on the chimeric proteins is also shown in Appendix Fig S3.

Synthesis and cloning of sequences coding for mEGFP-beta-Actin, mEGFP-alpha-SNAP, Amphiphysin-mEGFP, mEGFP-AP180, mEGFP-AP2 alpha-C, Calmodulin1-mEGFP, Clathrin light chain b-mEGFP, Complexin 1-mEGFP, Complexin 2-mEGFP, mEGFP-CSP, Dynamin-mEGFP, EndophilinA1-mEGFP, Epsin-mEGFP, mEGFP-Hsc70, mEGFP-Intersectin 1-L, Munc13-mEGFP, NSF-mEGFP, Rab3a-mEGFP, Rab7a-mEGFP, mEGFP-SCAMP1, mEGFP-Septin5, SNAP23-mEGFP, SNAP29-mEGFP, SV2B-mEGFP, Synaptogyrin-mEGFP, Synaptotagmin 1-mEGFP, Synaptotagmin7-mEGFP, Syndapin1-mEGFP, mEGFP-Syntaxin16, VAMP1-mEGFP, VAMP4-mEGFP, vDlut1-mEGFP, and vATPaseV0A1-mEGFP into a mammalian expression vector pcDNA3.1 were ordered at GenScript® (Piscataway, NJ, USA). N- or C-terminal position of fluorescent tag was chosen based on information available on influence of, respectively, positioned tag on protein localization or function favoring that with minimal reported effect. Plasmids coding

for Munc18-EGFP, Syntaxin 1-mEGFP, and VAMP2-EGFP were previously described (Vreja *et al*, 2015). Plasmids coding for Doc2a-EGFP, Rab5-EGFP, mEGFP-SNAP25, and Synaptophysin-EGFP were produced by eliminating stop codons from previously described plasmids (Vreja *et al*, 2015). For this, primers listed in Table 2 were used. Primers were designed to anneal to coding sequences and contain overlapping regions to be used in the Gibson Assembly reaction. In case of Doc2a, Rab5, and Synaptophysin, only one pair of primers was used to amplify the region of interest (entire plasmid except for stop codon containing linker) with overlapping regions coding for new linkers. For SNAP25, three pairs of primers were synthesized to amplify the vector, mEGFP, and SNAP25-coding sequences. Plasmid coding for Vti1a-β-mEGFP was made by cloning the Vti1a-β-coding sequence from a previously described plasmid (Vreja *et al*, 2015) into an mEGFP-containing vector purchased from GenScript (Piscataway, NJ, USA).

PCR amplification was done using Phusion polymerase (New England Biolabs, Ipswich, MA, USA) according to recommendations of the manufacturer. Amplified fragments were used for assembly of the plasmids in the Gibson Assembly (New England Biolabs, Ipswich, MA, USA) reaction, performed according to recommendations of the manufacturer.

For expression of a control protein mEGFP, an empty pmEGFP-N1 vector was used, which was a gift from Prof. Dr. Reinhard Jahn (Max Planck Institute for Biophysical Chemistry, Göttingen, Germany). As a control for membrane proteins, a plasmid coding for mEGFP fused to palmitoylation sites of SNAP25 (amino acids 1–14, 80–142, and 203–206) was used. Plasmids coding for EGFP-Tubulin and EGFP-PIP5KIgamma were obtained through Addgene (plasmid numbers 30487 and 22299, respectively); EGFP-Synapsin and mCherry-Synapsin were gifts from Prof. Dr. Flavia Valtorta (San Raffaele Vita-Salute University, Milan, Italy) and have been previously described (Pennuto *et al*, 2002; Verstegen *et al*, 2014); alpha-Synuclein-EGFP was a gift from Prof. Dr. Tiago F. Outeiro (University Medical Center Göttingen, Germany).

FRAP experiments

A TCS SP5 confocal microscope (Leica, Wetzlar, Germany) equipped with an HCX Plan Apochromat 100× 1.40 oil immersion objective was used for the imaging. The 488 nm line of an Argon laser was used for imaging of EGFP. Neurons were used for the FRAP experiments 3–7 days after calcium phosphate transfection or 6–14 days after lipofection (at least 11–14 days in culture). The culture medium was replaced by pre-warmed Tyrode's solution (124 mM NaCl, 2.7 mM KCl, 10 mM Na_2HPO_4, 2 mM KH_2PO_4, pH 7.3). The temperature of the imaging chamber system was maintained at 37°C. Synapses were located manually based on their morphology, preferably distal synapses, and axonal segments were used in FRAP experiments. For imaging of single synapses, 48× zoom and a 128 × 128 pixel resolution were used; same settings were used for imaging of axonal segments. Before bleaching, 4 control images were taken, and then, the region of interest was bleached for 80 ms with laser intensity of 50 μW at 488 nm, 14 μW at 496 nm, and 15 μW at 476 nm. After bleaching, 24 images were taken every 0.5 s, then 24 images every 1 s, and 24 images every 2 s. Additionally, images with the same time settings, but using 0% laser intensity for bleaching, were acquired to be used for acquisition bleaching correction.

FRAP image analysis

The FRAP movies were analyzed automatically using custom-written MATLAB (The MathWorks Inc, Natick, MA, USA) routines. After loading all frames, the FRAP region was automatically determined, by comparing the last pre-FRAP frame to the first post-FRAP frame. The region whose intensity changed substantially was determined and was set as the FRAP region of interest (ROI). The intensity in this ROI was then determined for all frames and was corrected for background by subtracting the intensity in the non-cellular areas (which was virtually equal to 0 arbitrary units, AU). To correct for bleaching induced during image acquisition, we produced a number of identical image series for each coverslip (typically 5), in which the exact same imaging procedure was followed, but without applying any laser intensity for the FRAP step. The decrease in fluorescence intensity during these series was measured, thereby providing the imaging-induced bleaching curve. The FRAP curves were corrected using the average bleaching curve for the respective protein (the bleaching curve was normalized by dividing it by the first point, and the FRAP curve was divided by the normalized bleaching curve). The FRAP curves were then fitted with single exponentials automatically, producing the results presented in Fig 2 and Appendix Fig S3. All curves were additionally plotted and were visually inspected by an experienced investigator, to avoid employing results from unusual or badly fitted curves.

FCS experiments

For fluorescence correlation spectroscopy experiments (FCS), a home-built setup, integrated with an inverted microscope body (Olympus IX73, Olympus, Hamburg, Germany) was used. The experiments were performed using a diode-pumped laser with a wavelength of 491 nm (Cobolt Calypso Cobolt AB, Solna, Sweden). After exiting from the optical fiber, the laser light passed a clean-up filter (HC Laser Clean-Up MaxLine 491/1.9, AHF Analysentechnik, Tübingen, Germany) and was reflected by a dichroic mirror (Dual-Line zt488/532rpc, AHF Analysentechnik) into the microscope body. The light was focused onto the sample using a 60× water-immersion objective (UPlanApo, NA 1.2, Olympus). After passing an emission filter (488 LP Edge Basic Longpass filter, AHF Analysentechnik) and a pinhole (diameter 50 μm, Qioptiq Photonics Gmbh & Co. KG, Göttingen, Germany), the fluorescence light emitted by the sample was focused on two avalanche photodiodes (τ-SPAD, Picoquant GmbH, Berlin, Germany). The τ-SPADs were connected to a digital correlator card (ALV-7004 USB, ALV, Langen, Germany) used for autocorrelation measurements.

In order to identify measurement positions within the neuron, epifluorescence images were taken using a mercury arc lamp (X-Cite 120 PC Q, Excelitas Technologies, Uckfield, United Kingdom) as excitation light and a GFP fluorescence filter set (GFP HC BrightLine Basic Filter Set, AHF Analysentechnik). Images were acquired using a CCD-camera (Hamamatsu Orca R-2, Hamamatsu Photonics, Herrsching am Ammersee, Germany) controlled by Micro-Manager (Edelstein *et al*, 2010). An automated sample stage (Prior Scientific, Inc., Rockland, MA, USA) was used to access the different positions within the neurons. Before each experiment, a calibration measurement was performed using the fluorescent dye Atto488 (ATTO-TEC GmbH Siegen, Germany), which has a known diffusion coefficient

Table 1. List of constructs, vectors, reference sequences, and linker sequences.

Protein of interest	Vector	RefSeq	Linker sequence
beta-Actin	pcDNA3.1	NM_031144.3	TGGGSGGGSGGGSAAA
alpha-SNAP	pcDNA3.1	NM_080585.1	TGGGSGGGSGGGSAAA
alpha-Synuclein	pEGFP-N1	NM_001009158.3	GTAGPGSIAT
Amphiphysin	pcDNA3.1	NM_022217.1	TGGGSGGGSGGGSAAA
AP180	pcDNA3.1	×68877.1	TGGGSGGGSGGGSAAA
AP2 alpha-C	pcDNA3.1	×53773.1	TGGGSGGGSGGGSAAA
Calmodulin 1	pcDNA3.1	NM_031969.2	TGGGSGGGSGGGSAAA
Clathrin light chain	pcDNA3.1	NM_053835.1	TGGGSGGGSGGGSAAA
Complexin 1	pcDNA3.1	U35098.1	TGGGSGGGSGGGSAAA
Complexin 2	pcDNA3.1	NM_053878.1	TGGGSGGGSGGGSAAA
CSP	pcDNA3.1	NM_024161.2	TGGGSGGGSGGGSAAA
Doc2a	pEGFP-N1	NM_022937.2	GSTVPSARDPPVAT
Dynamin 1	pcDNA3.1	NM_080689.4	TGGGSGGGSGGGSAAA
EndophilinA1	pcDNA3.1	NM_053935.1	TGGGSGGGSGGGSAAA
Epsin	pcDNA3.1	NM_057136.1	TGGGSGGGSGGGSAAA
Hsc70	pcDNA3.1	NM_024351.2	TGGGSGGGSGGGSAAA
Intersectin 1-L	pcDNA3.1	NM_001136096.1	TGGGSGGGSGGGSAAA
Munc13	pcDNA3.1	NM_022861.1	TGGGSGGGSGGGSAAA
Munc18	pEGFP-N1	L26087.1	GSTPGG
NSF	pcDNA3.1	NM_021748.1	TGGGSGGGSGGGSAAA
PIP5KIgamma	pEGFP-C2	NM_012398.2	RPDSDLELKLRI
Rab3a	pcDNA3.1	NM_013018.2	TGGGSGGGSGGGSAAA
Rab5a	pEGFP-N1	BC161848.1	GSTPGG
Rab7a	pcDNA3.1	NM_023950.3	TGGGSGGGSGGGSAAA
SCAMP1	pcDNA3.1	NM_001100636.1	TGGGSGGGSGGGSAAA
Septin 5	pcDNA3.1	NM_053931.4	TGGGSGGGSGGGSAAA
SNAP23	pcDNA3.1	NM_022689.2	TGGGSGGGSGGGSAAA
SNAP25	pEGFP-N1	NM_011428.3	GSTPGG
SNAP29	pcDNA3.1	NM_011428.3	TGGGSGGGSGGGSAAA
SV2B	pcDNA3.1	AF372834.2	TGGGSGGGSGGGSAAA
Synapsin 1	pEGFP-N1	NM_019133.2	SGLRSREAAT
Synaptogyrin	pcDNA3.1	NM_019166.2	TGGGSGGGSGGGSAAA
Synaptophysin	pEGFP-N1	NM_012664.3	GSTPGG
Synaptotagmin 1	pcDNA3.1	NM_001033680.2	TGGGSGGGSGGGSAAA
Synaptotagmin 7	pcDNA3.1	NM_021659.1	TGGGSGGGSGGGSAAA
Syndapin 1	pcDNA3.1	NM_017294.1	TGGGSGGGSGGGSAAA
Syntaxin1A	pEGFP-N1	NM_053788.2	LVSRARDPPVAT
Syntaxin 16	pcDNA3.1	NM_001108610.1	TGGGSGGGSGGGSAAA
alpha-tubulin	pcDNA3.1	NM_006082.2	SGLRSR
VAMP1	pcDNA3.1	NM_013090.2	TGGGSGGGSGGGSAAA
VAMP2	pEGFP-N1	NM_009497.3	RILQSTVPRARDPPVAT
VAMP4	pcDNA3.1	NM_001108856.1	TGGGSGGGSGGGSAAA
vATPase V0A1	pcDNA3.1	NM_031604.2	TGGGSGGGSGGGnSAAA
vGluT1	pcDNA3.1	U07609.1	TGGGSGGGSGGGSAAA
Vti1a-β	pEGFP-N1	AF262222.1	TGGGSGGGSAAA

Table 2. List of primers used for molecular cloning.

Protein coded	Primers' sequences
Doc2a	5′ GGTACCATCAGCTAGGGATCCACCGGTCGCCACC 3′ 5′ CCTAGCTGATGGTACCGTCGACccGGCCAAC 3′
Rab5	5′ GGATCTACACCTGGAGGAATGGTGAGCAAGGGCGAGGA 3′ 5′ TCCTCCAGGTGTAGATCCGTTACTACAACACTGGCTTCTGGC 3′
SNAP25	Vector: 5′ TAATCTGCAGATTAATCTAGATAACTGATCATAATCAGCCATACCAC 3′ 5′ GGTGGCTCGAGGCTAGCGGATCTGACGGTTCACTAAACCA 3′ mEGFP: 5′ CTAGCCTCGAGCCACCATGGTGAGCAAGGGCGAGG 3′ 5′ TCCTCCAGGTGTAGATCCCTTGTACAGCTCGTCCATGCCG 3′ SNAP25: 5′ GGATCTACACCTGGAGGAATGGCCGAGGACGCAGAC 3′ 5′ ATCTAGATTAATCTGCAGATTAACCACTTCCCAGCATCTTTGTTGC 3′
Synaptophysin	5′ GGATCTACACCTGGAGGAATGGTGAGCAAGGGCGAGGA 3′ 5′ TCCTCCAGGTGTAGATCCCATCTGATTGGAGAAGGAGGTAGG 3′
Vti1a-β	Vector-mEGFP: 5′ AGGACACACCGGCGGAGGAAGCGGC 3′ 5′ CGGCCGCTTTACTTGTACAGCTCGTCCATGCCGTGAG 3′ Vti1a: 5′ CAAGTAAAGCGGCCGCGACTCTAGATCATAATCAGCC 3′ 5′ GCCGGTGTGTCCTCTGACAAAAAAAGTGATGGCCGTCAG 3′

(400 μm^2/s at 25°C) (Kapusta). The coverslips were mounted on the sample holder, in Tyrode's solution. For each protein analyzed, we acquired data from different positions in the axons of the neurons. Each position was measured at least 20 times, with acquisition times between 10 and 30 s for each round of acquisition. All data were then fitted with a Levenberg–Marquardt nonlinear least-square routine using a self-written Python code (Python Software Foundation, https://www.python.org/). Data in which large fluorescence peaks were observed, or with pronounced photobleaching, were excluded from the analysis.

Organelle tracking analysis

For organelle tracking, neurons were transfected following the lipofection procedure described above. Neurons were imaged 6–10 days after lipofection. The culture medium was replaced by pre-warmed Tyrode's solution (124 mM NaCl, 2.7 mM KCl, 10 mM Na_2HPO_4, 2 mM KH_2PO_4, pH 7.3). The temperature of the imaging chamber system was maintained at 37°C. Axons of transfected cells were then imaged using a Nikon Ti-E epifluorescence microscope (Nikon Corporation, Chiyoda, Tokyo, Japan) equipped with a 100 × 1.4 NA oil-immersion Plan Apochromat objective (Nikon Corporation, Chiyoda, Tokyo, Japan). Cells were imaged for up to 3 min with a picture taken every 500 ms. For a control experiment, cells were fixed with 4% PFA in PBS, quenched with 100 mM NH_4Cl and imaged following the same procedure as done for live cell imaging.

The images were processed by a bandpass procedure (using a freely available MATLAB code, copyright 1997 by John C. Crocker and David G. Grier). This removes background and enables the observation of individual spots. This was followed by a particle finding and tracking routine (performed again using a freely available MATLAB code, copyright February 4, 2005, by Eric R. Dufresne, Yale University). The codes are available at: http://site.physics.georgetown.edu/matlab/code.html. The particle tracks were then analyzed for speed.

Overexpression analysis

Overexpressing cells were immunostained for synaptophysin (as a synapse marker) and for the protein of interest (the overexpressed protein). The levels of the proteins of interest were measured by immunostaining in the transfected boutons, as well as in the non-transfected boutons. All analyzed boutons were selected by the synaptophysin immunostaining. They were then separated into overexpressing and non-overexpressing populations, based on the GFP signal. The overexpression levels were then derived by dividing the immunostaining intensity in the overexpressing boutons by that in the non-overexpressing boutons, both normalized to the respective synaptophysin levels, to account for differences in synapse size [see also (Truckenbrodt *et al*, 2018), for further examples of this procedure].

Immunostainings and confocal and STED microscopy

The cultures were immunostained for the proteins of interest, and for the synaptic vesicle marker synaptophysin (using a guinea pig antibody from Synaptic Systems; catalogue number 101 004) and the active zone marker bassoon (using antibodies from StressGene, catalogue number ADI-VAM-PS003-D, or from Synaptic Systems, catalogue number 141 002). The primary antibodies used for the proteins of interest are all noted in Appendix Fig S2. We used the following secondary antibodies: Cy2-conjugated goat anti-mouse or anti-rabbit antibodies for bassoon (Dianova); Cy3-conjugated goat anti-guinea pig antibodies for synaptophysin (Dianova); and Atto647N-conjugated goat anti-mouse or anti-rabbit antibodies for the proteins of interest (Synaptic Systems or Rockland). The cultures were fixed using 4% PFA in PBS for 45 min, were quenched using 100 mM

NH_4Cl in PBS for 15 min, and were then permeabilized using 0.1% Triton X-100 in PBS, in the presence of 1.5% BSA. The same medium was then used for incubations with primary and secondary antibodies. The samples were then washed several times with PBS and high-salt PBS (containing 500 mM NaCl) and were embedded in Mowiol or in 2,2′-thiodiethanol (TDE), as described (Wilhelm *et al*, 2014). The samples were imaged using a Leica TCS SP5 STED microscope, with a 100× oil-immersion objective (1.4 NA; HCX PL APO CS, Leica).

Confocal excitation was obtained with the 488-nm line of an Argon laser (green channel, for Cy2). Similarly, we used the 543-nm line of a Helium Neon laser for the orange (Cy3) channel. STED imaging was performed (for Atto647N) using a pulsed diode laser, at 635 nm, for the excitation channel, and a Spectra-Physics MaiTai tunable laser (Newport Spectra-Physics, Irvine, CA) for depletion at 750 nm. We set the AOTF filter of the system to the appropriate emission intervals for confocal imaging; an avalanche photodiode was used for the STED imaging. The AOTF filter of the microscope was used to select appropriate emission intervals for the different dyes. Signal detection was performed either by a photomultiplier (confocal mode) or by an avalanche photodiode (STED mode).

Electron microscopy and reconstruction of synapses

Neuronal cultures were fixed and processed for electron microscopy as follows: Entire coverslips with neurons were immersed into 2.5% glutaraldehyde buffered with 150 mM sodium cacodylate containing 2 mM $CaCl_2$ at pH 7.4 for 30 min. Samples were washed with sodium cacodylate and postfixed with 1% osmium tetroxide in 150 mM sodium cacodylate and 1.5% potassium ferrocyanide at room temperature for 30 min. After washing, samples were again postfixed in 1% osmium tetroxide in sodium cacodylate for another 30 min. Samples were thoroughly washed in distilled water and block contrasted in 2% uranyl acetate at room temperature for 60 min. Next, specimens were *en bloc* contrasted with lead (33 mg lead nitrate in 10 ml of 30 mM aspartic acid; modification of (Walton, 1979) at 60°C for 60 min. After washing in water, specimens were dehydrated in an ascending acetone series (50, 70, and 90%) followed by two steps in dry 100% ethanol for 20 min each. A mixture of Epon and Spurr's resin (1 + 1) was used to infiltrate the cells, and blocks were polymerized at 60°C for 2 days. Cultures were then thin-sectioned in the plane of the coverslips with a UC6 ultramicrotome (Leica Microsystems, Wetzlar, Germany). Serial sections were imaged with a JEOL 100CX microscope equipped with a mid-mount 4MP Hamamatsu camera controlled by AMT software (Advanced Microscopy Techniques, Woburn, MA).

For synapse reconstructions, we relied on serial sections which we aligned manually in Photoshop (Adobe Systems, San Jose, CA). The different elements of the synapse (active zone, membrane, vacuoles, mitochondria, and vesicles) were marked manually on each consecutive frame, and the values were compiled using a self-written MATLAB routine, as described (Rizzoli & Betz, 2004; Denker *et al*, 2011b).

Modeling analysis I: Generation of the 3D synapse

We first determined different parameters from 30 different 3D synapse models. We then selected one synapse whose various parameters (active zone surface, volume, vacuole volume and number, synaptic vesicle volume and number, mitochondria volume) were close to the average of all synapses (difference from the average of all 30 synapses of only 26.9%, over all measured parameters). As the 3D measurements were performed from chemically fixed samples, we accounted for their shrinkage during fixation and plastic-embedding (Gaffield *et al*, 2006).

To obtain a widely applicable model, we then prolonged the axonal connections of this synapse for several micrometers, as shown in the 3D view of the model (Appendix Fig S17), relying on published super-resolution axon diameter and shape measurements (Xu *et al*, 2013). The model, initially obtained at an approximately 3 nm X-Y plane resolution, and a 70 nm axial resolution, was then modified to obtain 25 × 25 × 25 nm voxels, as presented in Appendix Fig S17, in which the different organelles were placed according to the measured positions from the original EM images. The 25 × 25 nm size was chosen as this is also the value used in the live FRAP movies. Synaptic vesicles were placed in multiple pixels, since the vesicle volume [for a 42 nm diameter (Takamori *et al*, 2006)] is approximately 2.5-fold larger than the voxel volume. As we planned to model protein binding on vesicles and/or on components of the vesicle cluster, we increased the number of voxels allotted to synaptic vesicles approximately 2-fold, to account for large molecules being able to bind vesicles from a distance of a few nanometers, or for molecules binding other elements that are themselves bound to vesicles, but not directly to vesicles (as, e.g., would be the case for actin, which is likely to bind to actin strands or to synapsin in the vesicle cluster, but probably not to the vesicle surfaces).

Modeling analysis II: moving particles in the 3D synapse

We placed particles in the 3D synapse model and allowed them to move randomly. The particles either moved only in the plasma membrane, or in the cytosol. The movement in the plasma membrane was modeled in a simple fashion, with the particles always moving at a specified single-step velocity. This approximated a Gaussian distribution, with a width of ~25 nm; the following displacements were modeled: 25, 50, 75, 100, 125, 150, and 200 nm as well as several intermediate displacements.

The same type of motion was also induced in the cytosol. In addition, the particles that reached synaptic vesicle pixels also remained bound to them for defined time periods, ranging from 1 movement steps (no binding to vesicles) to 200 movement steps. Up to 1000 particle tracks were generated for every movement model.

Modeling analysis III: placing fluorophores on the particle tracks

To use them for further analysis, the movement tracks for one model (for every single-step velocity and for every vesicle binding capacity) were combined, and fluorophores were placed on their various particle positions. For this, we convoluted the particle positions with a confocal point-spread-function (PSF), measured exactly as in the actual FRAP movies. The actual PSF is shown in Fig 6. This results in fluorescence movies for the different movement models, in which the fluorophores corresponding to the different particle positions overlap, creating a realistic synapse image, as shown in Fig 6.

Modeling analysis IV: generating *in silico* FRAP movies

To mimic FRAP situations, we eliminated (bleached) the fluorophores from regions identical in size to those observed in the actual FRAP movies, and we then allowed the particles to move, to induce the signal recovery. The particles continued to move along their tracks, and some that were not bleached entered the FRAP zone, generating a recovery signal. To account for the diffusion of particles to and from neighboring axonal regions, we forced particles that exited on either open side of the axon to return through the opposite side, thereby generating an equilibrium movement situation. Bleached particles that exited the axon became fluorescent again upon re-entry, to mimic the exchange of such particles for fluorescent ones from the neighboring areas, which is known to happen *in vivo* (Darcy *et al*, 2006).

We generated, in independent *in silico* experiments, FRAP data for both the synapse and for the axon, by choosing appropriate FRAP regions in the 3D model.

Modeling analysis V: the analysis of the *in silico* FRAP movies

The resulting artificial FRAP movies were fitted with single exponential curves exactly as performed for the biological FRAP movies. As for each model, we generated both axon and synapse FRAP data, the fits resulted in two parameters: (i) Synapse FRAP τ (time constant) values and (ii) Axon FRAP τ (time constant) values.

For the membrane movement models, the time constants for the axonal and synapse FRAP correlated linearly to each other, and occupied a line that overlapped broadly with the measured values for the proteins that we expect to diffuse as single molecules in the plasma membrane. The real data were best reproduced when the length of the model time step (the interval between movement steps) was chosen as 5.7 ms.

For the cytosolic proteins, we obtained the synapse and axon FRAP time constants for different single-step velocities (from 25 to 250 nm), combined with different periods of binding synaptic vesicles (from 1 movement step to 200 movement steps). Placing a 3 ms value for the length of the model time step resulted in a good correlation between the models and all of the measured data.

Modeling analysis VI: determining the models that best fit the real data

Each real experiment provides two values: the synapse FRAP τ and the axon FRAP τ. Similarly, each model also provides a synapse FRAP τ and an axon FRAP τ. One can thus calculate the two-dimensional distance between each experimental pair of values, and each model pair of values. For each protein, we determined the 3–5 models (with different single-step velocities and/or different vesicle binding) that were closest to the respective experimental synapse and axon τ values. The diffusion coefficients reported for the proteins correspond to the single closest model, with the errors corresponding to the range of values of the 3-5 models.

Modeling analysis VII: determining the diffusion coefficients

We then determined the diffusion coefficients of the different models by determining their mean square displacements (Qian *et al*, 1991), relying on the Einstein–Smoluchowski equation (Islam, 2004). The diffusion coefficients were determined at different positions within the synapse or in the axon, and, for the soluble proteins, also in the vesicle cluster.

Modeling analysis VIII: the case of bona fide synaptic vesicle or endosome proteins

For proteins found mainly in synaptic vesicles or in endosomes, the procedure outlined above cannot reproduce the synapse time constants (for proteins found mainly in the synapse) or the axonal tau constants (for VAMP4, which tends to be found in axonal endosomes). For these proteins, we extracted the model diffusion values that fitted the movement of the molecules in the compartment in which they would move as single proteins (in the axon, for most of these proteins, or in the synapse, for VAMP4). We then extrapolated the diffusion of the free molecules in the other compartment (synapse or axon, respectively) from the models. For proteins such as synaptogyrin, vGlut, and SCAMP, which have only been measured in the synapse, we assigned diffusion coefficients by analogy to the most similar vesicle molecules (synaptophysin for the first two, vATPase and VAMP1 for SCAMP).

To validate this procedure, we determined the average diffusion coefficient of the synaptic vesicles. The procedure explained above provides the diffusion coefficient of free molecules in the synapse (D_{free}). Applying the diffusion models to the time constant obtained in real experiments in the synapses provides a diffusion coefficient for a mixture of molecules found in vesicles and free molecules ($D_{free + vesicles}$). At the same time, the proportion of molecules found in vesicles is identical to the fraction of immobile molecules in the synapse, since very little vesicle exchange can take place during our short FRAP procedure. Thus, knowing the two diffusion coefficients, as well as the proportions of the molecules involved, one can extract the diffusion coefficient for the vesicle-bound proteins. The average value obtained over all vesicle proteins is ~0.0102 $\mu m^2/s$, similar to what has been reported in the literature (see main text).

Analyzing the proportion of molecules in the axon or in the synapse

To determine the proportion of molecules in the axon and in the synapse (Fig 7A–C), we turned to the *in silico* FRAP movies, and simply counted particles found in the axon or in the synapse at the FRAP time point. The respective values were compared to results obtained by measuring the intensity in manually measured ROIs in synapses and in neighboring areas, from immunostaining experiments (the synapse positions were determined by immunostaining for synaptophysin and the active zone protein bassoon, as indicated in the Materials and Methods section on immunostaining procedures).

Generating and analyzing artificial STED images

To obtain and analyze artificial STED images, we first noted the number of antibodies that would be expected to bind within one synapse, for each protein (Richter *et al*, 2018). We then selected randomly a number of protein positions (taken from the positions

behind the artificial FRAP movies) corresponding to the number of antibodies, and convoluted these positions with a measured STED point-spread-function, measured exactly as in the STED immunostainings for the respective proteins. The remaining pixels in the resulting 2D images were covered with a measured STED background, containing measured salt-and-pepper-like noise. 100 simulated STED images were generated for every protein, and the STED spots were automatically detected, by first filtering the images using a bandpass filter, and then selecting as regions-of-interest all spots that were above a user-defined threshold (same for all images, for all proteins; chosen so as to eliminate salt-and-pepper noise). The full width at half maximum (FWHM) and the intensity of the spots were then determined from Lorentzian fits to the spots (Willig *et al*, 2006; Maidorn *et al*, 2018). Real STED immunostaining images were then analyzed in a similar fashion. The regions of interest were first selected in the synaptophysin channel, to restrict the analysis to synapses. This type of analysis has also been recently discussed in (Maidorn *et al*, 2018). For display purposes, we deconvolved the STED images using Huygens Essential software (Scientific Volume Imaging, Hilversum, The Netherlands), based on the inbuilt routines generated by the company.

Construction of the dynamic graphical model

The individual protein views were constructed using custom-written plug-ins and scripts in the 3D software Autodesk Maya (Autodesk Inc., San Rafael, CA). Protein structure information was derived from the UniProt database. The same individual protein view models were used as in Wilhelm *et al* (2014), and the references used are presented in the particular paper. When available, we used protein database (PDB) coordinates in order to reconstruct proteins. If not available, we relied on structure information provided by a number of prediction servers. We used the following types of information: secondary structure information (http://bioinf.cs.ucl.ac.uk/psipred/); disorder calculations (http://mbs.cbrc.jp/poodle/poodle-s.html; http://mbs.cbrc.jp/poodle/poodle-w.html; alignment (http://web.expasy.org/sim/); predictions of coiled coil regions (http://toolkit.tuebingen.mpg.de/pcoils; http://mbs.cbrc.jp/poodle/poodle-l.html), information on transmembrane domains (http://www.ch.embnet.org/software/TMPRED_form.html); information on glycosylation domains (http://www.glycosciences.de/modeling/glyprot/php/main.php); domain identification (http://smart.embl-heidelberg.de/index2.cgi); and the presence of homologue proteins (http://web.expasy.org/blast/).

As mentioned in the main text, simulated different particle motion behaviors, with different movement speeds, in order to find the behaviors that most closely reproduced the FRAP results. We transformed the particle motion in artificial FRAP movies by applying fluorophore point-spread-functions onto the tracks. We then compared the results to the original FRAP data, in order to find the models that best reproduced the biological time constants in the axons and in the synapses. We then placed the protein structures in the 3D space of the model synapse, relying on the same movement tracks we used in the rest of this work. For each protein type, we used for the graphical models a number of protein tracks from the model that had reproduced best the FRAP behavior of the respective protein. The number of tracks was chosen as equal to the expected protein copy number for the respective protein (Richter *et al*, 2018). The protein views were then placed on every pixel of the tracks and were also allowed to turn around their own axis. Synaptic vesicles were presented according to their known composition (Takamori *et al*, 2006), relying on previously generated models (Wilhelm *et al*, 2014). The vesicles are typically shown in grayscale. To avoid confusing the viewer, no vesicle motion is shown (or only a rotational/vibrational motion); this is a reasonable procedure, since the net diffusive vesicle motion is expected to be extremely limited for the time interval we show.

Statistical analysis

All FRAP data are presented in detail in the extensive Appendix Fig S3. Other figures may also present data subsets as means ± SEM, or means ± SD, as indicated in the respective figure legends. All statistical comparisons are presented in detail in the respective figure legends. For comparisons of synaptic datasets, we relied on Kruskal–Wallis tests, followed by Mann–Whitney comparisons, and, where necessary, additional corrections for multiple testing, using the Bonferroni or Benjamini-Hochberg procedures, as indicated in the respective figure legends.

Code and materials availability

All routines are available upon request to S.O.R., and all requests for materials and correspondence should be directed to S.O.R. (srizzol@gwdg.de).

Expanded View for this article is available online.

Acknowledgements
We thank Reinhard Jahn (Max Planck Institute for Biophysical Chemistry, Göttingen, Germany) for helpful comments on the manuscript. We thank Oleh Rymarenko (Max Planck Institute for Biophysical Chemistry, Göttingen, Germany) for helping with data plotting automation. We thank Reinhard Jahn (Max Planck Institute for Biophysical Chemistry, Göttingen, Germany), Flavia Valtorta (San Raffaele Vita-Salute University, Milan, Italy), and Tiago F. Outeiro (University Medical Center Göttingen, Germany) for providing several plasmids used in this work. The work was supported by grants to S.O.R. from the European Research Council (ERC-2013-CoG NeuroMolAnatomy) and from the Deutsche Forschungsgemeinschaft (SFB1190/P09, SFB 1286/B02). We acknowledge the support of project SFB 1286/Z02, led by Stefan Bonn (University Hospital Hamburg-Eppendorf (UKE), Germany). Also supported by the DFG under Germany's Excellence Strategy—EXC 2067/1- 390729940.

Author contributions
SR performed all fluorescence imaging experiments. J-EU and TS performed the electron microscopy experiments. EP and SR performed and analyzed the FCS measurements under the supervision of SK. EFF participated in the refinement of experimental conditions. SR, ST, and SOR analyzed the data. BR and SOR produced the 3D visualization. SR and SOR wrote the initial draft of the manuscript, which was then refined by all other authors.

Conflict of interest
The authors declare that they have no conflict of interest.

References

Albrecht D, Winterflood CM, Sadeghi M, Tschager T, Noé F, Ewers H (2016) Nanoscopic compartmentalization of membrane protein motion at the axon initial segment. *J Cell Biol* 215: 37 – 46

Arhondakis S, Clay O, Bernardi G (2008) GC level and expression of human coding sequences. *Biochem Biophys Res Commun* 367: 542 – 545

Axelrod D, Koppel DE, Schlessinger J, Elson E, Webb WW (1976) Mobility measurement by analysis of fluorescence photobleaching recovery kinetics. *Biophys J* 16: 1055 – 1069

Bademosi AT, Lauwers E, Padmanabhan P, Odierna L, Chai YJ, Papadopulos A, Goodhill GJ, Verstreken P, van Swinderen B, Meunier FA (2017) *In vivo* single-molecule imaging of syntaxin1A reveals polyphosphoinositide- and activity-dependent trapping in presynaptic nanoclusters. *Nat Commun* 8: 13660

Banker GA, Cowan WM (1977) Rat hippocampal neurons in dispersed cell culture. *Brain Res* 126: 397 – 425

Benfenati F, Bähler M, Jahn R, Greengard P (1989) Interactions of synapsin I with small synaptic vesicles: distinct sites in synapsin I bind to vesicle phospholipids and vesicle proteins. *J Cell Biol* 108: 1863 – 1872

Bläßle A, Soh G, Braun T, Mörsdorf D, Preiß H, Jordan BM, Müller P (2018) Quantitative diffusion measurements using the open-source software PyFRAP. *Nat Commun* 9: 1582

Blumenthal D, Goldstien L, Edidin M, Gheber LA (2015) Universal approach to FRAP analysis of arbitrary bleaching patterns. *Sci Rep* 5: 11655

Ceccarelli B, Hurlbut WP (1980) Vesicle hypothesis of the release of quanta of acetylcholine. *Physiol Rev* 60: 396 – 441

Cesca F, Baldelli P, Valtorta F, Benfenati F (2010) The synapsins: key actors of synapse function and plasticity. *Prog Neurobiol* 91: 313 – 348

Chou PY, Fasman GD (1974) Prediction of protein conformation. *Biochemistry* 13: 222 – 245

Darcy KJ, Staras K, Collinson LM, Goda Y (2006) Constitutive sharing of recycling synaptic vesicles between presynaptic boutons. *Nat Neurosci* 9: 315 – 321

Denker A, Bethani I, Kröhnert K, Körber C, Horstmann H, Wilhelm BG, Barysch SV, Kuner T, Neher E, Rizzoli SO (2011b) A small pool of vesicles maintains synaptic activity *in vivo*. *Proc Natl Acad Sci USA* 108: 17177 – 17182

Denker A, Kröhnert K, Bückers J, Neher E, Rizzoli SO (2011a) The reserve pool of synaptic vesicles acts as a buffer for proteins involved in synaptic vesicle recycling. *Proc Natl Acad Sci USA* 108: 17183 – 17188

Dörrbaum AR, Kochen L, Langer JD, Schuman EM (2018) Local and global influences on protein turnover in neurons and glia. *Elife* 7: e34202

Edelstein A, Amodaj N, Hoover K, Vale R, Stuurman N (2010) Computer control of microscopes using μManager. *Curr Protoc Mol Biol* 92: 14.20.1-14.20.17

Fornasiero EF, Raimondi A, Guarnieri FC, Orlando M, Fesce R, Benfenati F, Valtorta F (2012) Synapsins contribute to the dynamic spatial organization of synaptic vesicles in an activity-dependent manner. *J Neurosci* 32: 12214 – 12227

Fornasiero EF, Mandad S, Wildhagen H, Alevra M, Rammner B, Keihani S, Opazo F, Urban I, Ischebeck T, Sakib MS *et al* (2018) Precisely measured protein lifetimes in the mouse brain reveal differences across tissues and subcellular fractions. *Nat Commun* 9: 4230

Fornasiero EF, Rizzoli SO (2019) Pathological changes are associated with shifts in the employment of synonymous codons at the transcriptome level. *BMC Genom* 20: 566

Freeman SA, Vega A, Riedl M, Collins RF, Ostrowski PP, Woods EC, Bertozzi CR, Tammi MI, Lidke DS, Johnson P *et al* (2018) Transmembrane pickets connect cyto- and pericellular skeletons forming barriers to receptor engagement. *Cell* 172: 305 – 317.e10

Fu J, Murphy KA, Zhou M, Li YH, Lam VH, Tabuloc CA, Chiu JC, Liu Y (2016) Codon usage affects the structure and function of the *Drosophila* circadian clock protein PERIOD. *Genes Dev* 30: 1761 – 1775

Gaffield MA, Rizzoli SO, Betz WJ (2006) Mobility of synaptic vesicles in different pools in resting and stimulated frog motor nerve terminals. *Neuron* 51: 317 – 325

Gallimore AR, Kim T, Tanaka-Yamamoto K, Schutter ED (2018) Switching on depression and potentiation in the cerebellum. *Cell Rep* 22: 722 – 733

Gingold H, Tehler D, Christoffersen NR, Nielsen MM, Asmar F, Kooistra SM, Christophersen NS, Christensen LL, Borre M, Sørensen KD *et al* (2014) A dual program for translation regulation in cellular proliferation and differentiation. *Cell* 158: 1281 – 1292

Haucke V, Neher E, Sigrist SJ (2011) Protein scaffolds in the coupling of synaptic exocytosis and endocytosis. *Nat Rev Neurosci* 12: 127 – 138

Herzog E, Nadrigny F, Silm K, Biesemann C, Helling I, Bersot T, Steffens H, Schwartzmann R, Nägerl UV, Mestikawy SE *et al* (2011) *In vivo* imaging of intersynaptic vesicle exchange using VGLUT1Venus knock-in mice. *J Neurosci* 31: 15544 – 15559

Hirokawa N, Niwa S, Tanaka Y (2010) Molecular motors in neurons: transport mechanisms and roles in brain function, development, and disease. *Neuron* 68: 610 – 638

Islam MA (2004) Einstein-smoluchowski diffusion equation: a discussion. *Phys Scr* 70: 120

Jordan R, Lemke EA, Klingauf J (2005) Visualization of synaptic vesicle movement in intact synaptic boutons using fluorescence fluctuation spectroscopy. *Biophys J* 89: 2091 – 2102

Kaech S, Banker G (2006) Culturing hippocampal neurons. *Nat Protoc* 1: 2406 – 2415

Kalla S, Stern M, Basu J, Varoqueaux F, Reim K, Rosenmund C, Ziv NE, Brose N (2006) Molecular dynamics of a presynaptic active zone protein studied in Munc13-1–enhanced yellow fluorescent protein knock-in mutant mice. *J Neurosci* 26: 13054 – 13066

Kamin D, Lauterbach MA, Westphal V, Keller J, Schönle A, Hell SW, Rizzoli SO (2010) High- and low-mobility stages in the synaptic vesicle cycle. *Biophys J* 99: 675 – 684

Kang M, Day CA, Kenworthy AK, DiBenedetto E (2012) Simplified equation to extract diffusion coefficients from confocal FRAP data. *Traffic* 13: 1589 – 1600

Koopmans F, van Nierop P, Andres-Alonso M, Byrnes A, Cijsouw T, Coba MP, Cornelisse LN, Farrell RJ, Goldschmidt HL, Howrigan DP *et al* (2019) SynGO: an evidence-based, expert-curated knowledge base for the synapse. *Neuron* 103: 217 – 234.e4

Kudla G, Lipinski L, Caffin F, Helwak A, Zylicz M (2006) High guanine and cytosine content increases mRNA levels in mammalian cells. *PLoS Biol* 4: e180

Kudla G, Murray AW, Tollervey D, Plotkin JB (2009) Coding-sequence determinants of gene expression in *Escherichia coli*. *Science* 324: 255 – 258

Kumar M, Mommer MS, Sourjik V (2010) Mobility of cytoplasmic, membrane, and DNA-binding proteins in *Escherichia coli*. *Biophys J* 98: 552 – 559

Lee S, Jung KJ, Jung HS, Chang S (2012) Dynamics of multiple trafficking behaviors of individual synaptic vesicles revealed by quantum-dot based presynaptic probe. *PLoS ONE* 7: e38045

Lee SH, Jin C, Cai E, Ge P, Ishitsuka Y, Teng KW, de Thomaz AA, Nall D, Baday M, Jeyifous O *et al* (2017) Super-resolution imaging of synaptic and Extra-synaptic AMPA receptors with different-sized fluorescent probes. *Elife* 6: e27744

Maidorn M, Olichon A, Rizzoli SO, Opazo F (2018) Nanobodies reveal an extra-synaptic population of SNAP-25 and Syntaxin 1A in hippocampal neurons. MAbs

Mandad S, Rahman R-U, Centeno TP, Vidal RO, Wildhagen H, Rammner B, Keihani S, Opazo F, Urban I, Ischebeck T *et al* (2018) The codon sequences predict protein lifetimes and other parameters of the protein life cycle in the mouse brain. *Sci Rep* 8: 1 – 19

Milovanovic D, Camilli PD (2017) Synaptic vesicle clusters at synapses: a distinct liquid phase? *Neuron* 93: 995 – 1002

Milovanovic D, Wu Y, Bian X, Camilli PD (2018) A liquid phase of synapsin and lipid vesicles. *Science* 361: 604 – 607

Pennuto M, Dunlap D, Contestabile A, Benfenati F, Valtorta F (2002) Fluorescence resonance energy transfer detection of synaptophysin I and vesicle-associated membrane protein 2 interactions during exocytosis from single live synapses. *Mol Biol Cell* 13: 2706 – 2717

Qian H, Sheetz MP, Elson EL (1991) Single particle tracking. Analysis of diffusion and flow in two-dimensional systems. *Biophys J* 60: 910 – 921

Ribrault C, Reingruber J, Petković M, Galli T, Ziv NE, Holcman D, Triller A (2011) Syntaxin1A lateral diffusion reveals transient and local SNARE interactions. *J Neurosci* 31: 17590 – 17602

Richter KN, Wildhagen H, Helm MS, Ußling J-E, Schikorski T, Rizzoli SO (2018) Comparative synaptosome imaging: a semi-quantitative method to obtain copy numbers for synaptic and neuronal proteins. *Sci Rep* 8: 14838

Rizzoli SO, Betz WJ (2004) The structural organization of the readily releasable pool of synaptic vesicles. *Science* 303: 2037 – 2039

Rizzoli SO (2014) Synaptic vesicle recycling: steps and principles. *EMBO J* 33: 788 – 822

Rothman JS, Kocsis L, Herzog E, Nusser Z, Silver RA (2016) Physical determinants of vesicle mobility and supply at a central synapse. *Elife* 5: e15133

Roy S (2014) Seeing the unseen: the hidden world of slow axonal transport. *Neurosci Rev J Bringing Neurobiol Neurol Psychiatry* 20: 71 – 81

Sadovsky RG, Brielle S, Kaganovich D, England JL (2017) Measurement of rapid protein diffusion in the cytoplasm by photo-converted intensity profile expansion. *Cell Rep* 18: 2795 – 2806

Salvatico C, Specht CG, Triller A (2015) Synaptic receptor dynamics: from theoretical concepts to deep quantification and chemistry in cellulo. *Neuropharmacology* 88: 2 – 9

Schanzenbächer CT, Sambandan S, Langer JD, Schuman EM (2016) Nascent proteome remodeling following homeostatic scaling at hippocampal synapses. *Neuron* 92: 358 – 371

Schikorski T, Stevens CF (1997) Quantitative ultrastructural analysis of hippocampal excitatory synapses. *J Neurosci Off J Soc Neurosci* 17: 5858 – 5867

Schikorski T, Stevens CF (2001) Morphological correlates of functionally defined synaptic vesicle populations. *Nat Neurosci* 4: 391 – 395

Seitz KJ, Rizzoli SO (2019) GFP nanobodies reveal recently-exocytosed pHluorin molecules. *Sci Rep* 9: 1 – 10

Shtrahman M, Yeung C, Nauen DW, Bi G, Wu X (2005) Probing vesicle dynamics in single hippocampal synapses. *Biophys J* 89: 3615 – 3627

Shupliakov O (2009) The synaptic vesicle cluster: a source of endocytic proteins during neurotransmitter release. *Neuroscience* 158: 04 – 210

Spinelli KJ, Taylor JK, Osterberg VR, Churchill MJ, Pollock E, Moore C, Meshul CK, Unni VK (2014) Presynaptic alpha-synuclein aggregation in a mouse model of Parkinson's disease. *J Neurosci Off J Soc Neurosci* 34: 2037 – 2050

Sudhof TC (2004) The synaptic vesicle cycle. *Annu Rev Neurosci* 27: 509 – 547

Takamori S, Holt M, Stenius K, Lemke EA, Grønborg M, Riedel D, Urlaub H, Schenck S, Brügger B, Ringler P *et al* (2006) Molecular anatomy of a trafficking organelle. *Cell* 127: 831 – 846

Truckenbrodt S, Viplav A, Jähne S, Vogts A, Denker A, Wildhagen H, Fornasiero EF, Rizzoli SO (2018) Newly produced synaptic vesicle proteins are preferentially used in synaptic transmission. *EMBO J* 37: e98044

Verstegen AMJ, Tagliatti E, Lignani G, Marte A, Stolero T, Atias M, Corradi A, Valtorta F, Gitler D, Onofri F *et al* (2014) Phosphorylation of synapsin I by cyclin-dependent kinase-5 sets the ratio between the resting and recycling pools of synaptic vesicles at hippocampal synapses. *J Neurosci Off J Soc Neurosci* 34: 7266 – 7280

Vreja IC, Nikić I, Göttfert F, Bates M, Kröhnert K, Outeiro TF, Hell SW, Lemke EA, Rizzoli SO (2015) Super-resolution microscopy of clickable amino acids reveals the effects of fluorescent protein tagging on protein assemblies. *ACS Nano* 9: 11034 – 11041

Walton J (1979) Lead aspartate, an en bloc contrast stain particularly useful for ultrastructural enzymology. *J Histochem Cytochem Off J Histochem Soc* 27: 1337 – 1342

Westphal V, Rizzoli SO, Lauterbach MA, Kamin D, Jahn R, Hell SW (2008) Video-rate far-field optical nanoscopy dissects synaptic vesicle movement. *Science* 320: 246 – 249

Wilhelm BG, Mandad S, Truckenbrodt S, Kröhnert K, Schäfer C, Rammner B, Koo SJ, Claßen GA, Krauss M, Haucke V *et al* (2014) Composition of isolated synaptic boutons reveals the amounts of vesicle trafficking proteins. *Science* 344: 1023 – 1028

Willig KI, Kellner RR, Medda R, Hein B, Jakobs S, Hell SW (2006) Nanoscale resolution in GFP-based microscopy. *Nat Methods* 3: 721 – 723

Xu K, Zhong G, Zhuang X (2013) Actin, spectrin, and associated proteins form a periodic cytoskeletal structure in axons. *Science* 339: 452 – 456

Yeung C, Shtrahman M, Wu X (2007) Stick-and-diffuse and caged diffusion: a comparison of two models of synaptic vesicle dynamics. *Biophys J* 92: 2271 – 2280

Zhou M, Guo J, Cha J, Chae M, Chen S, Barral JM, Sachs MS, Liu Y (2013) Non-optimal codon usage affects expression, structure and function of clock protein FRQ. *Nature* 495: 111 – 115

Table of Contents

Table of Contents

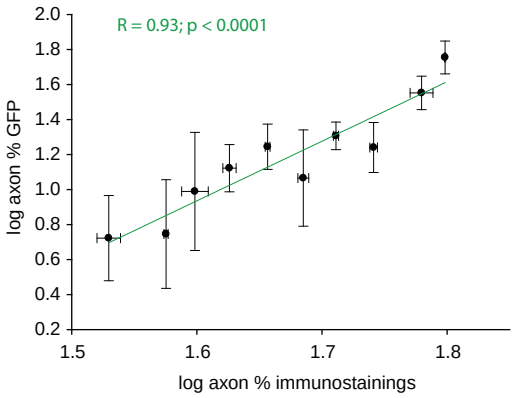

Appendix Fig. S1. Correlation between the synapto-axonal distribution of proteins in FRAP experiments and in immunostainings. We determined the fraction of each GFP-tagged protein that is found in the axon, as % of the amount found in the synapse, in every FRAP movie we performed. In separate experiments, we immunostained neurons for the proteins of interest and for synaptophysin, as a marker for the vesicle cluster, and for bassoon, as a marker for the active zone. These immunostainings (shown in Appendix Fig. S2) enabled us to determine the same parameter, the fraction of the protein found in the axon, as % of the intensity in the nearest synapses. We then compared the two measurements, in the form of a two-dimensional scatter plot. The symbols indicate the different proteins analyzed (binned, for clarity; each symbol represents the mean of 2-8 proteins, ± SEM or ± range of values).

Multi-page figure

Appendix Fig. S2. Typical super-resolution images for the different proteins analyzed here. Neurons were immunostained for the protein of interest (red), and for synaptophysin (green), as a marker for the vesicle cluster, and bassoon (blue), as a marker for the active zone (using the antibodies indicated in methods). Images were then obtained in STED mode (protein of interest) or in confocal mode (synaptophysin and bassoon). Scale bar, 5 µm.

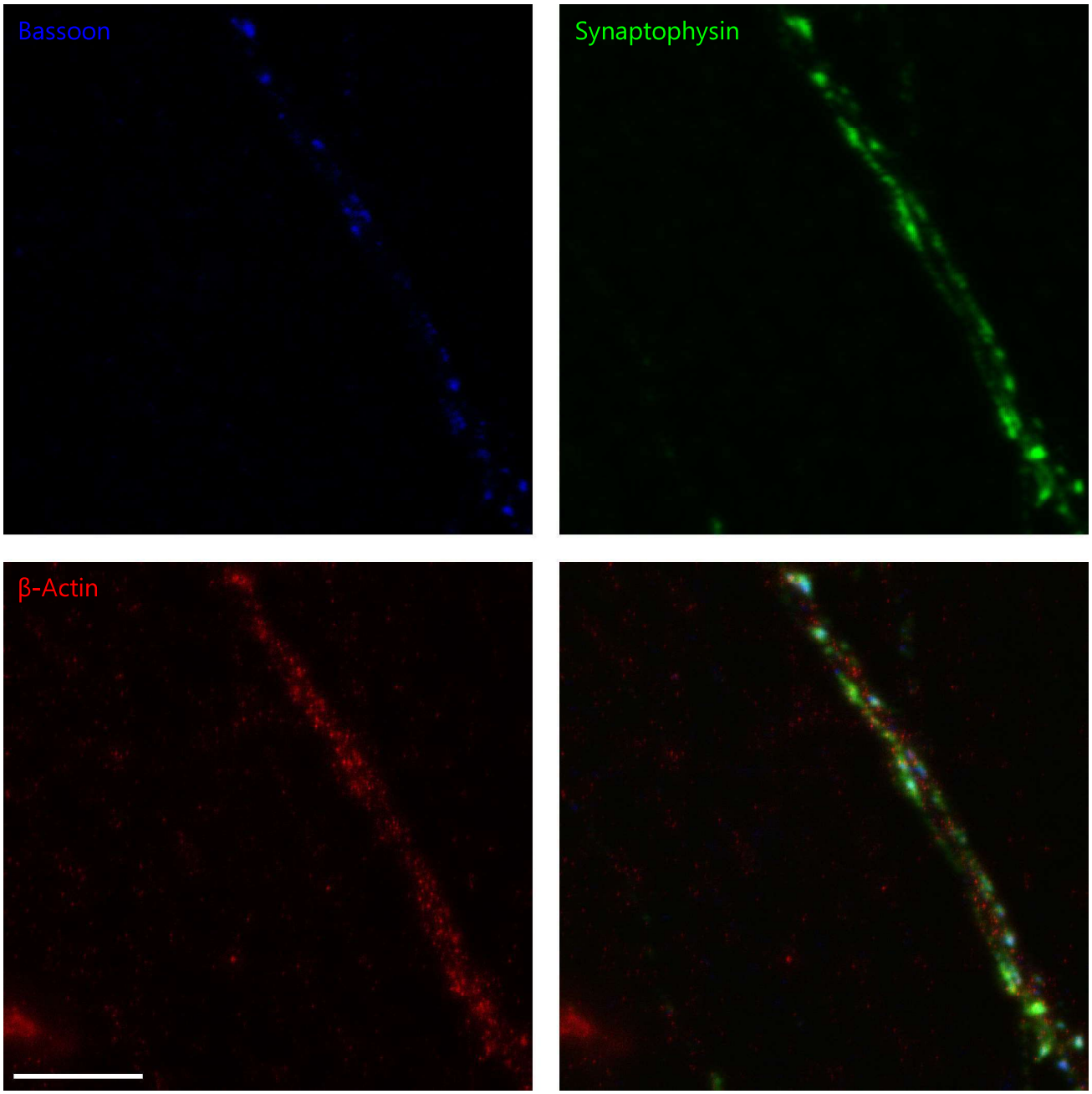

Scale bar: 5 µm

Antibodies used:
Bassoon - Synaptic Systems (Göttingen, Germany), 141 021
Synaptophysin - Synaptic Systems (Göttingen, Germany), 101 011
β-Actin - Sigma (Taufkirchen, Germany), A1978

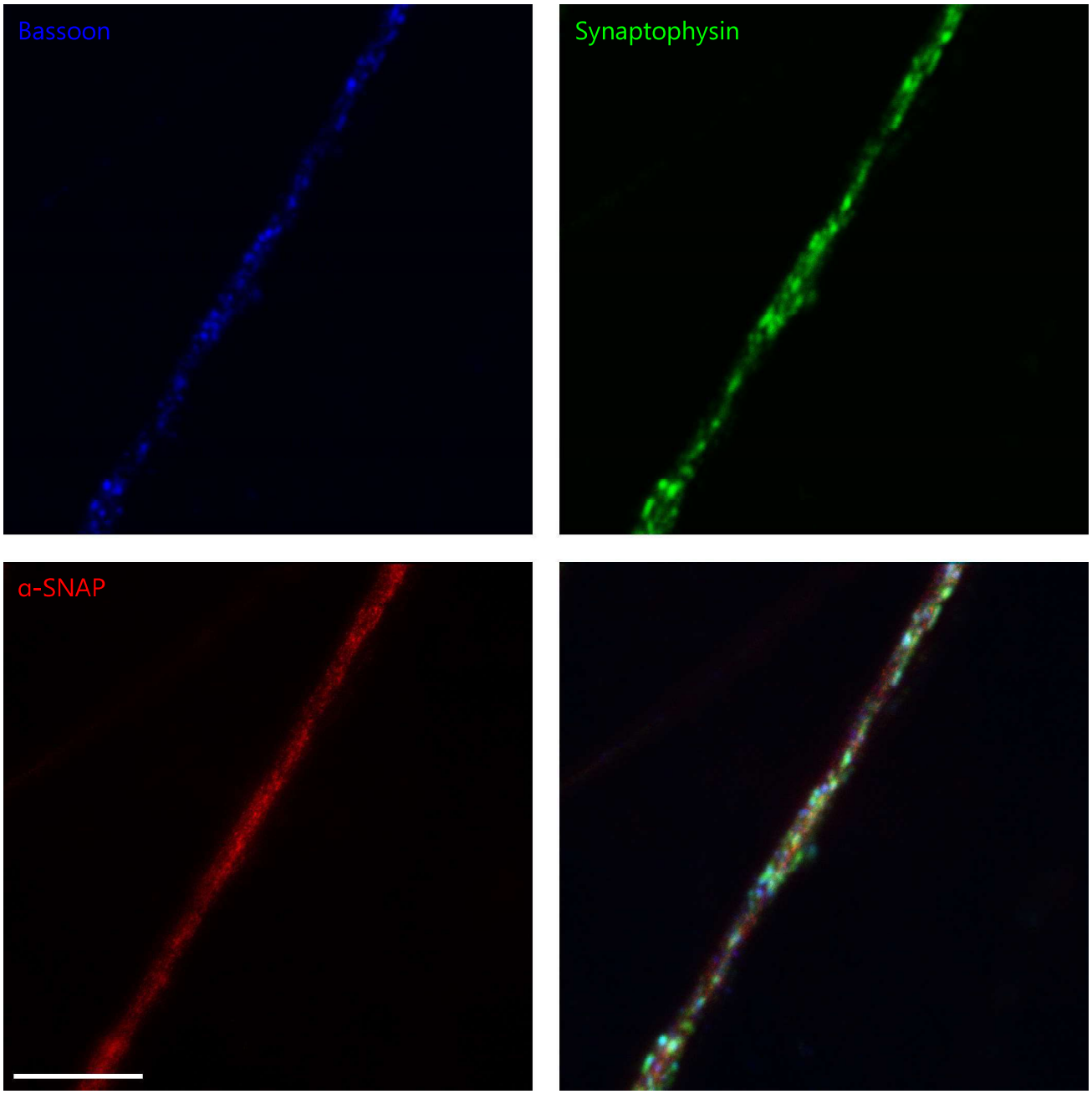

Scale bar: 5 µm

Antibodies used:
Bassoon - Synaptic Systems (Göttingen, Germany), 141 021
Synaptophysin - Synaptic Systems (Göttingen, Germany), 101 011
α-SNAP - Synaptic Systems (Göttingen, Germany), 112 111

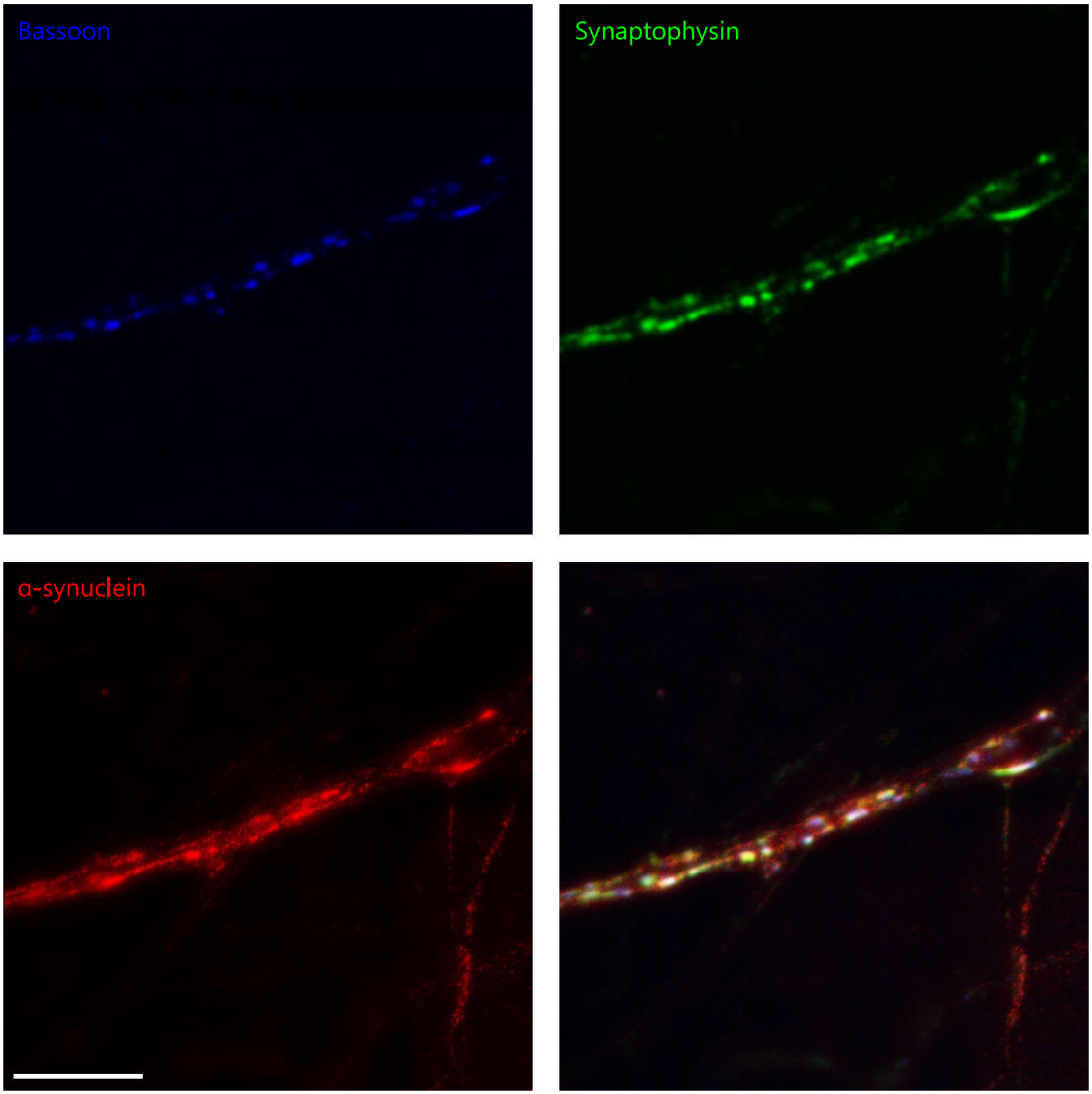

Scale bar: 5 µm

Antibodies used:
Bassoon - Synaptic Systems (Göttingen, Germany), 141 021
Synaptophysin - Synaptic Systems (Göttingen, Germany), 101 011
α-synuclein - Synaptic Systems (Göttingen, Germany), 128 002

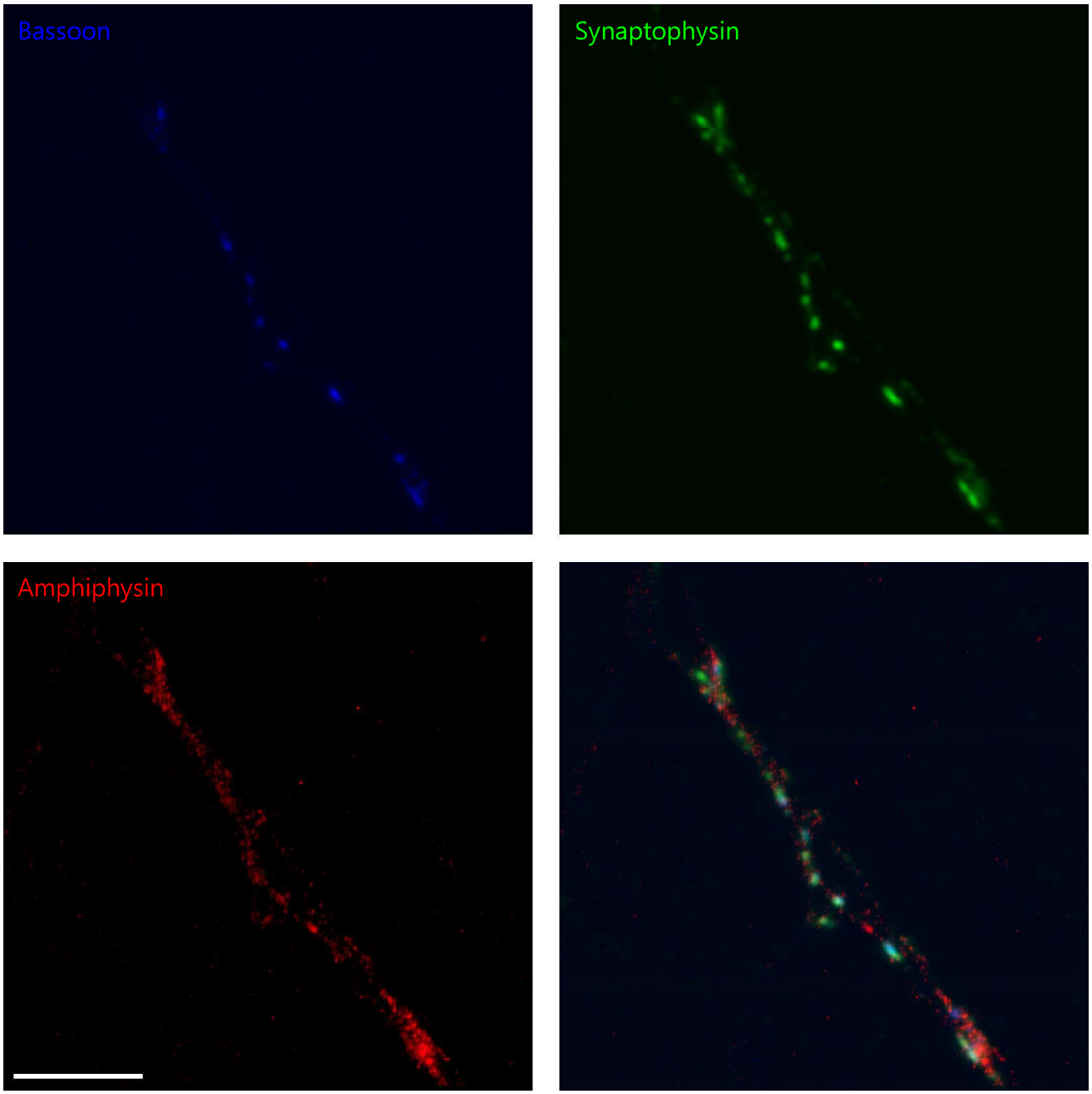

Scale bar: 5 µm

Antibodies used:
Bassoon - Synaptic Systems (Göttingen, Germany), 141 021
Synaptophysin - Synaptic Systems (Göttingen, Germany), 101 011
Amphiphysin - Synaptic Systems (Göttingen, Germany), 120 002

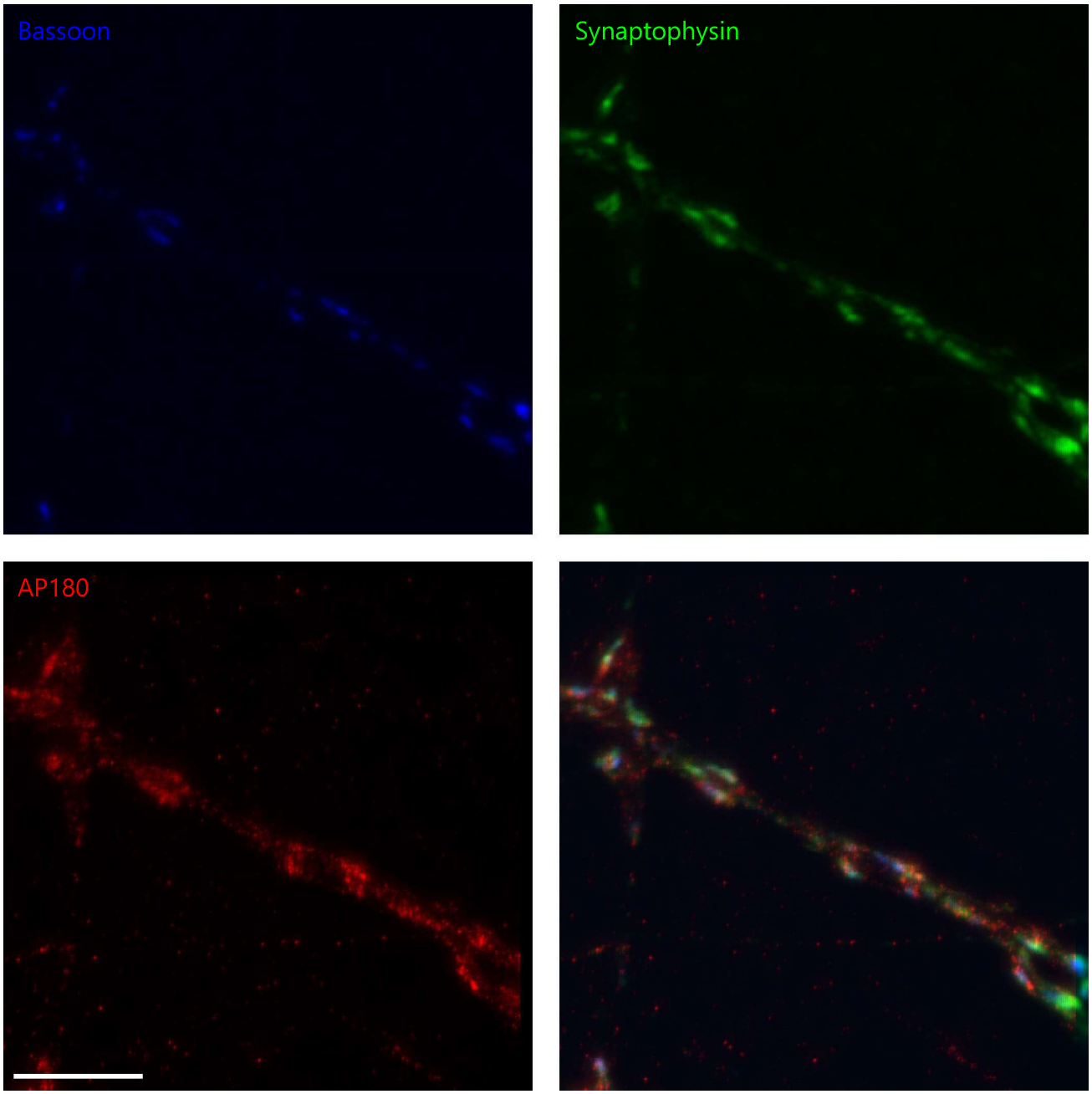

Scale bar: 5 µm

Antibodies used:
Bassoon - Synaptic Systems (Göttingen, Germany), 141 021
Synaptophysin - Synaptic Systems (Göttingen, Germany), 101 011
AP180 - Synaptic Systems (Göttingen, Germany), 155 003

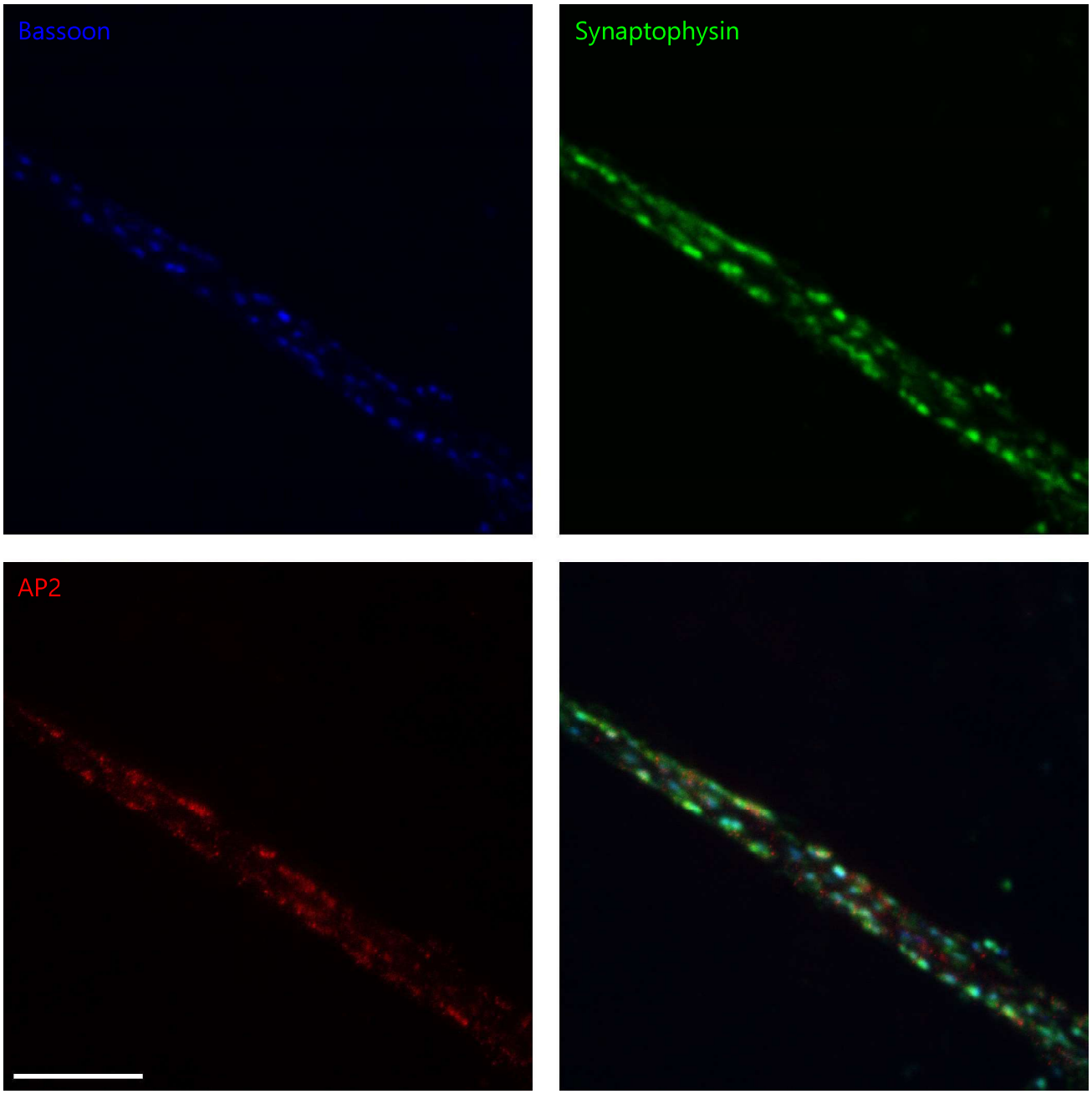

Scale bar: 5 µm

Antibodies used:
Bassoon - Synaptic Systems (Göttingen, Germany), 141 021
Synaptophysin - Synaptic Systems (Göttingen, Germany), 101 011
AP2 - Santa Cruz (Heidelberg, Germany), sc-99026

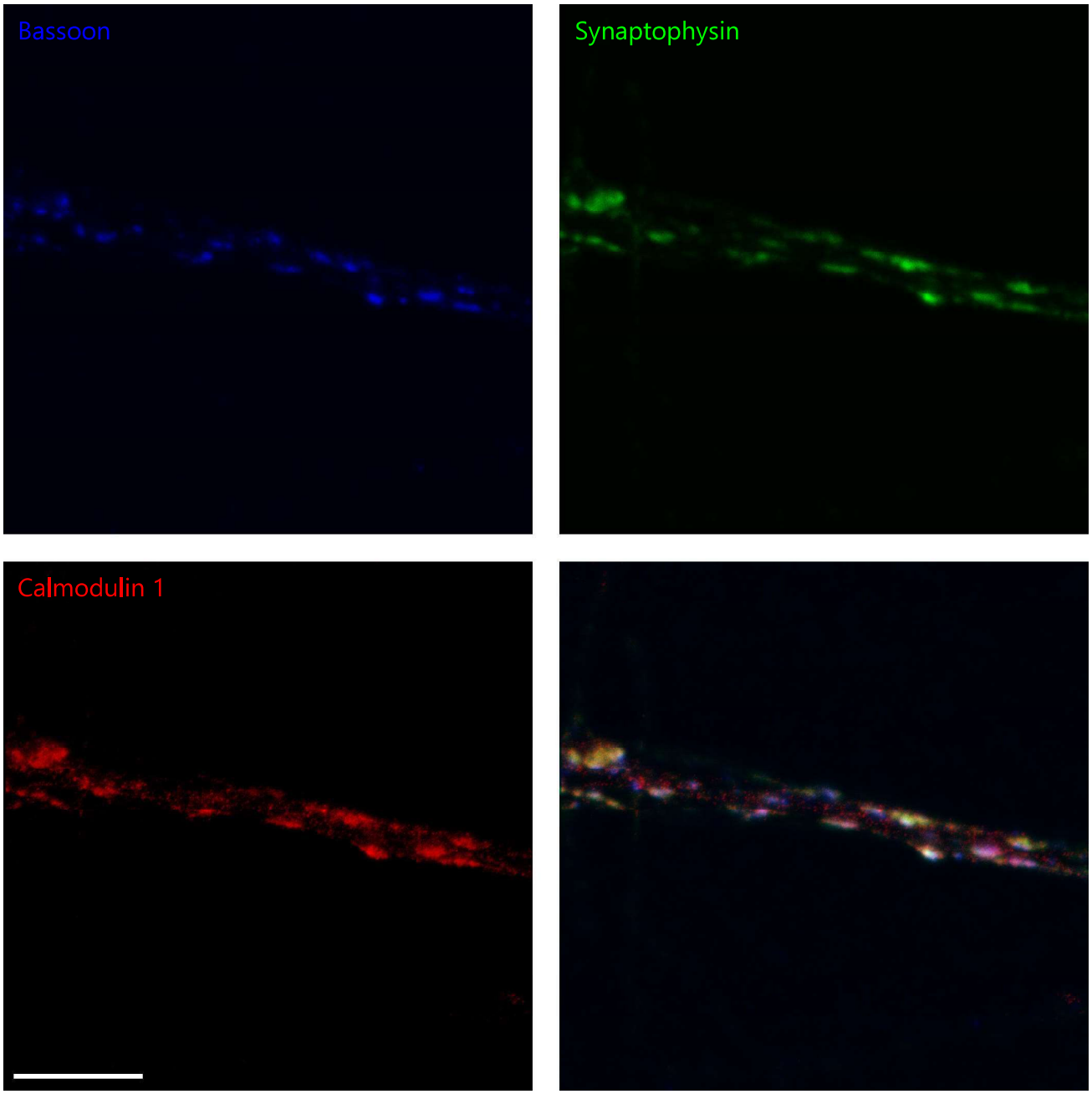

Scale bar: 5 µm

Antibodies used:
Bassoon - Synaptic Systems (Göttingen, Germany), 141 021
Synaptophysin - Synaptic Systems (Göttingen, Germany), 101 011
Calmodulin 1 - Novus Biologicals (Littleton, Colorado, USA), NB110-55649

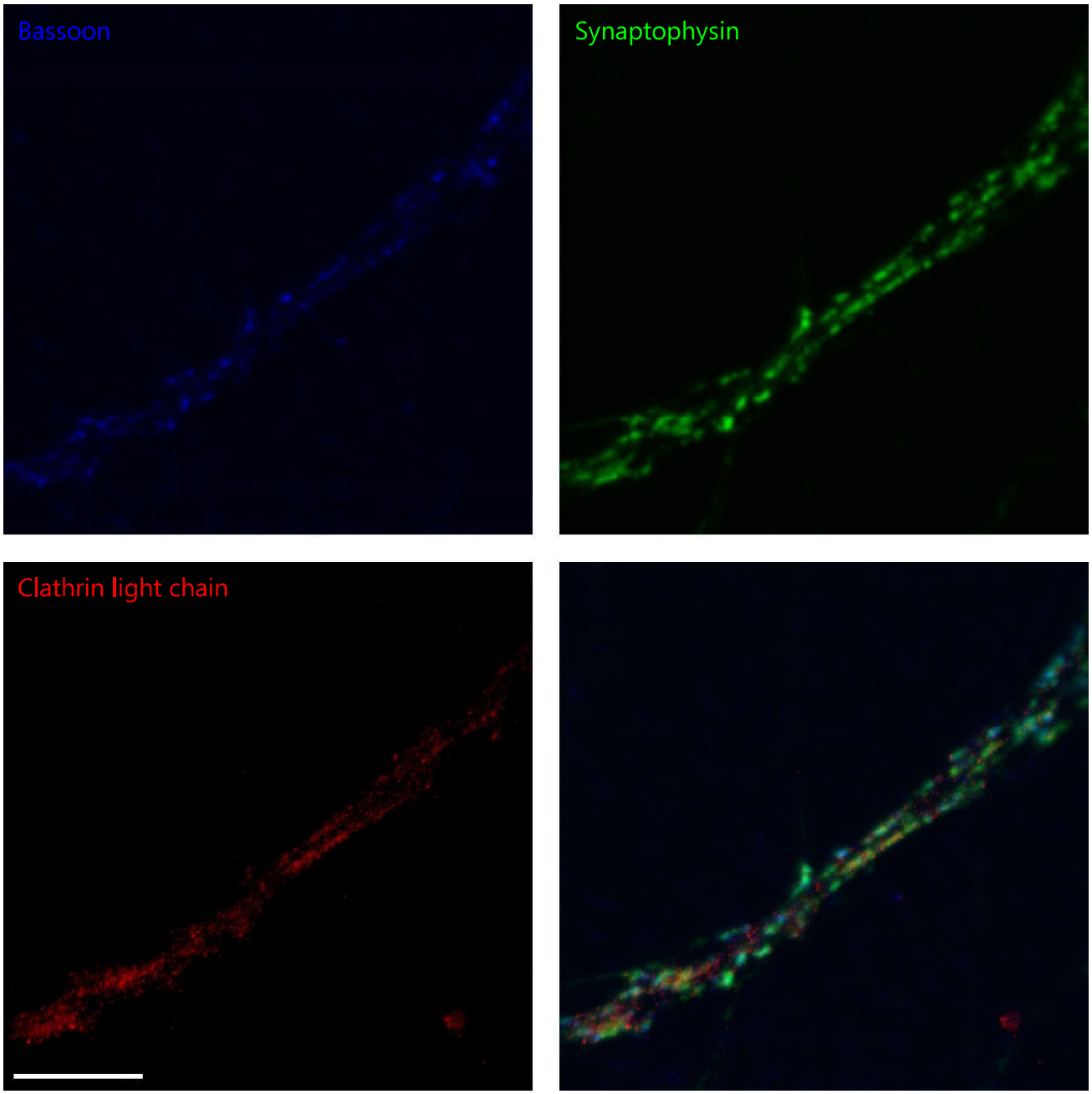

Scale bar: 5 µm

Antibodies used:
Bassoon - Synaptic Systems (Göttingen, Germany), 141 021
Synaptophysin - Synaptic Systems (Göttingen, Germany), 101 011
Clathrin light chain - Synaptic Systems (Göttingen, Germany), 113 001

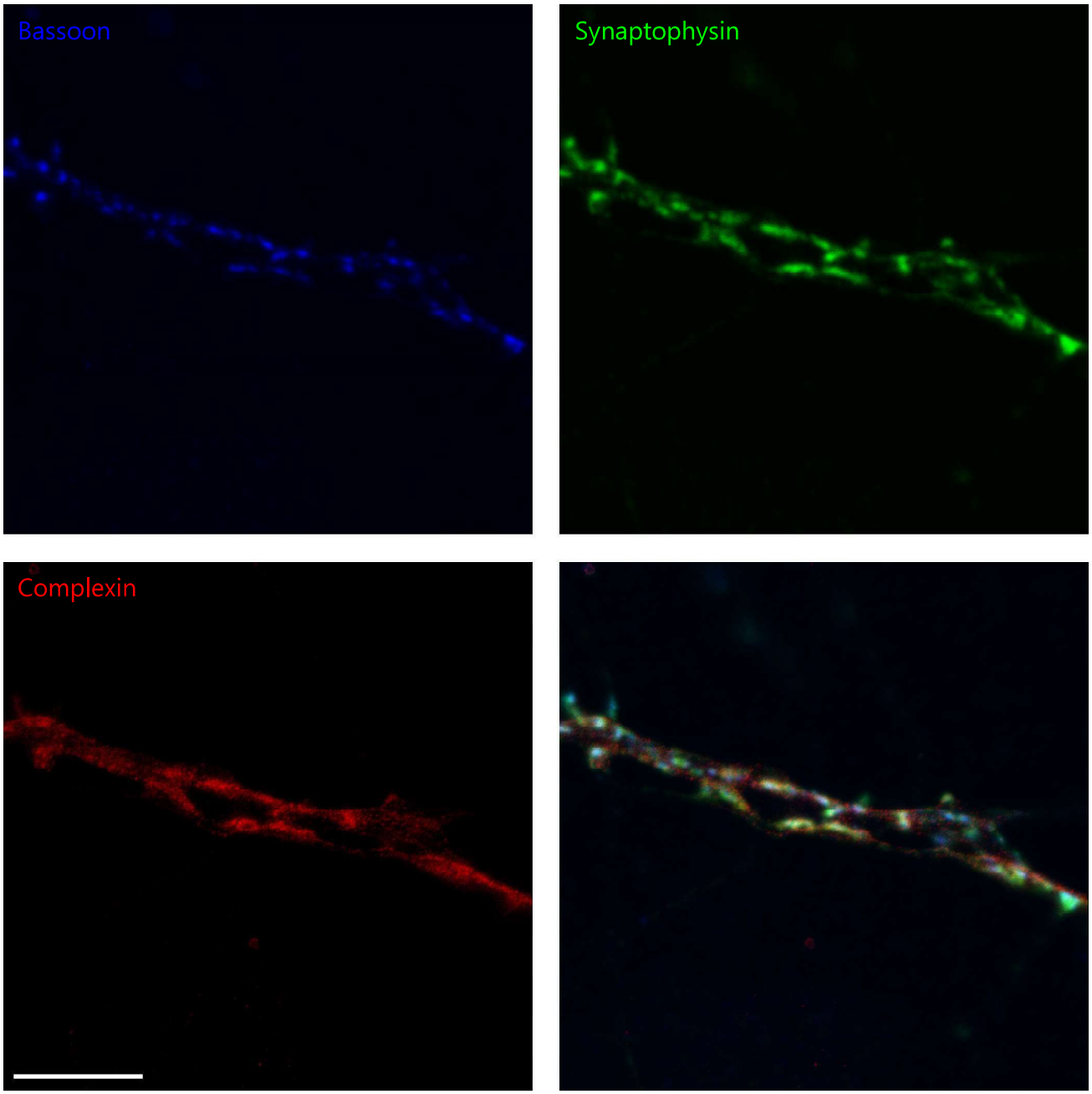

Scale bar: 5 µm

Antibodies used:
Bassoon - Synaptic Systems (Göttingen, Germany), 141 021
Synaptophysin - Synaptic Systems (Göttingen, Germany), 101 011
Complexin - Synaptic Systems (Göttingen, Germany), 122 002

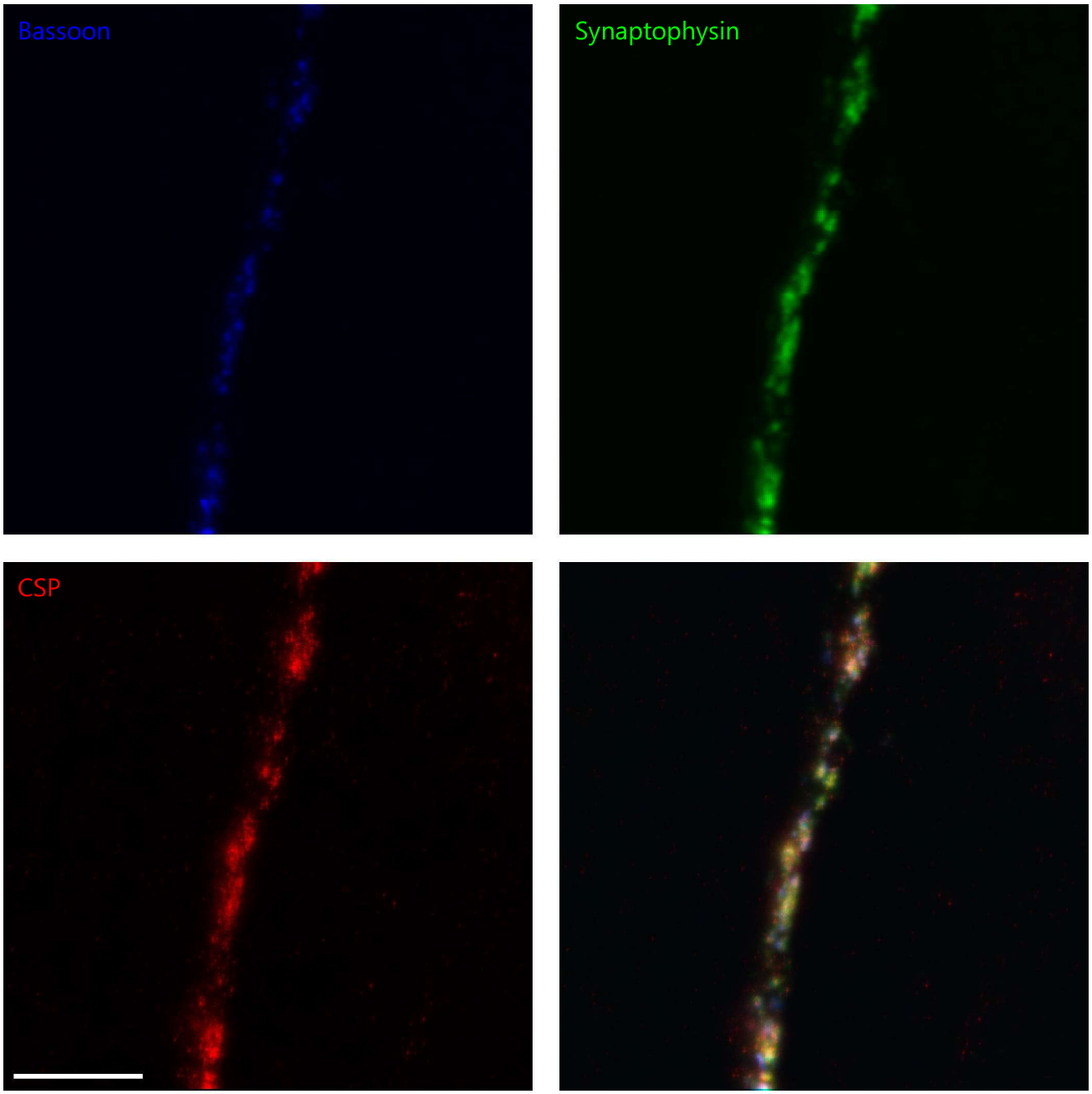

Scale bar: 5 µm

Antibodies used:
Bassoon - Synaptic Systems (Göttingen, Germany), 141 021
Synaptophysin - Synaptic Systems (Göttingen, Germany), 101 011
CSP - Synaptic Systems (Göttingen, Germany), 154 003

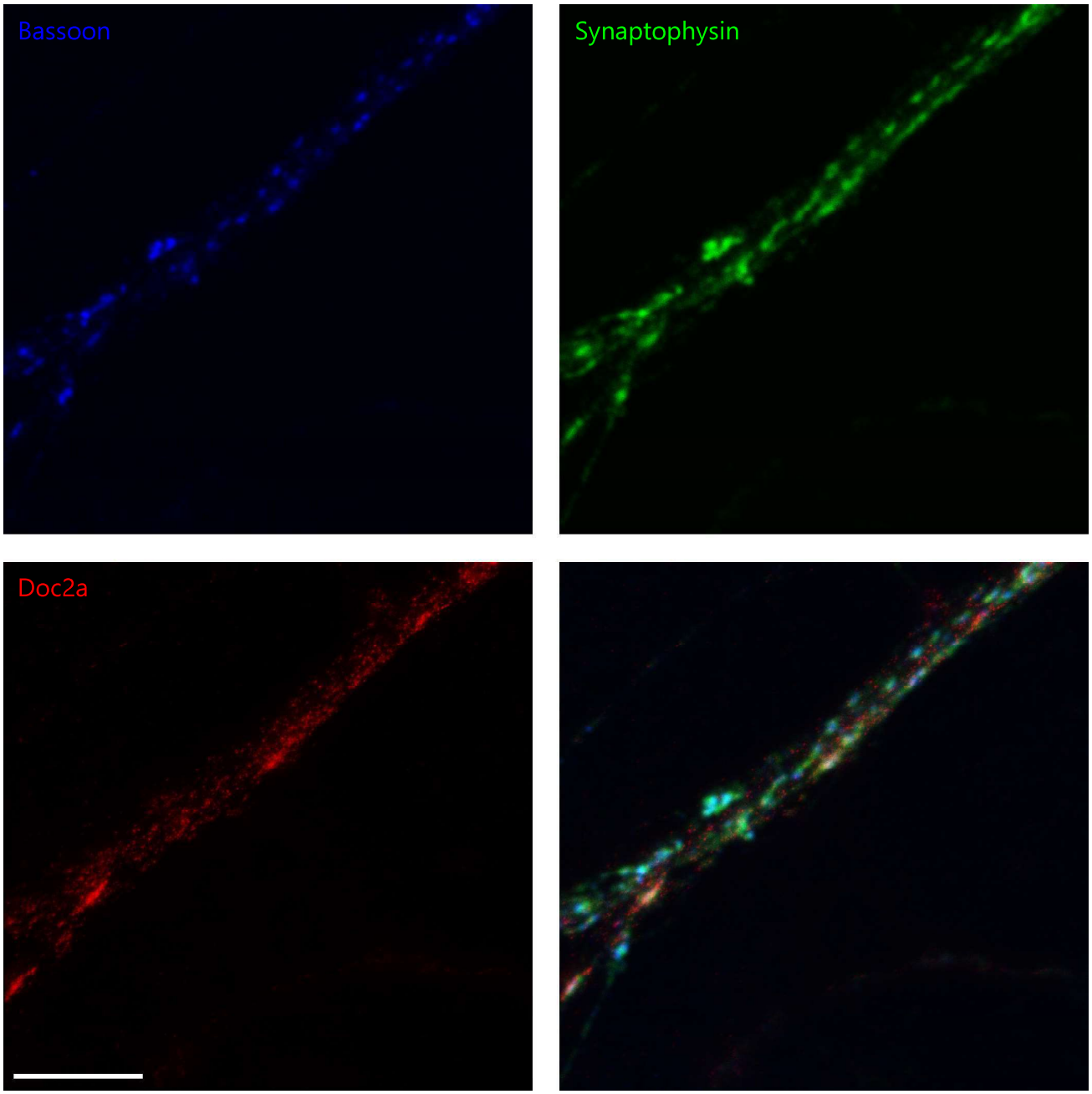

Scale bar: 5 µm

Antibodies used:
Bassoon - Synaptic Systems (Göttingen, Germany), 141 021
Synaptophysin - Synaptic Systems (Göttingen, Germany), 101 011
Doc2a - Synaptic Systems (Göttingen, Germany), 174 203

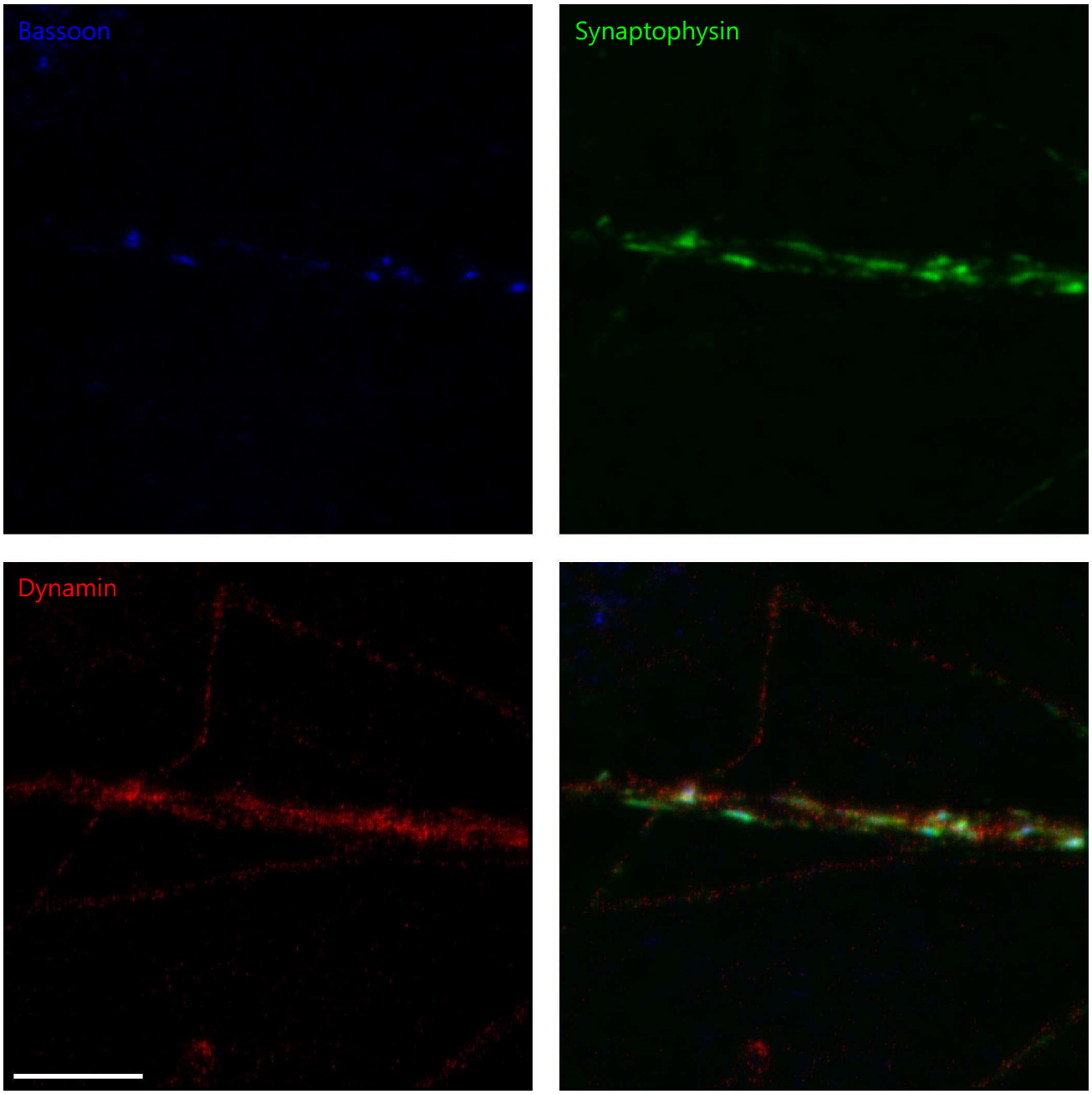

Scale bar: 5 µm

Antibodies used:
Bassoon - Synaptic Systems (Göttingen, Germany), 141 021
Synaptophysin - Synaptic Systems (Göttingen, Germany), 101 011
Dynamin - BD Biosciences (Heidelberg, Germany), 610245

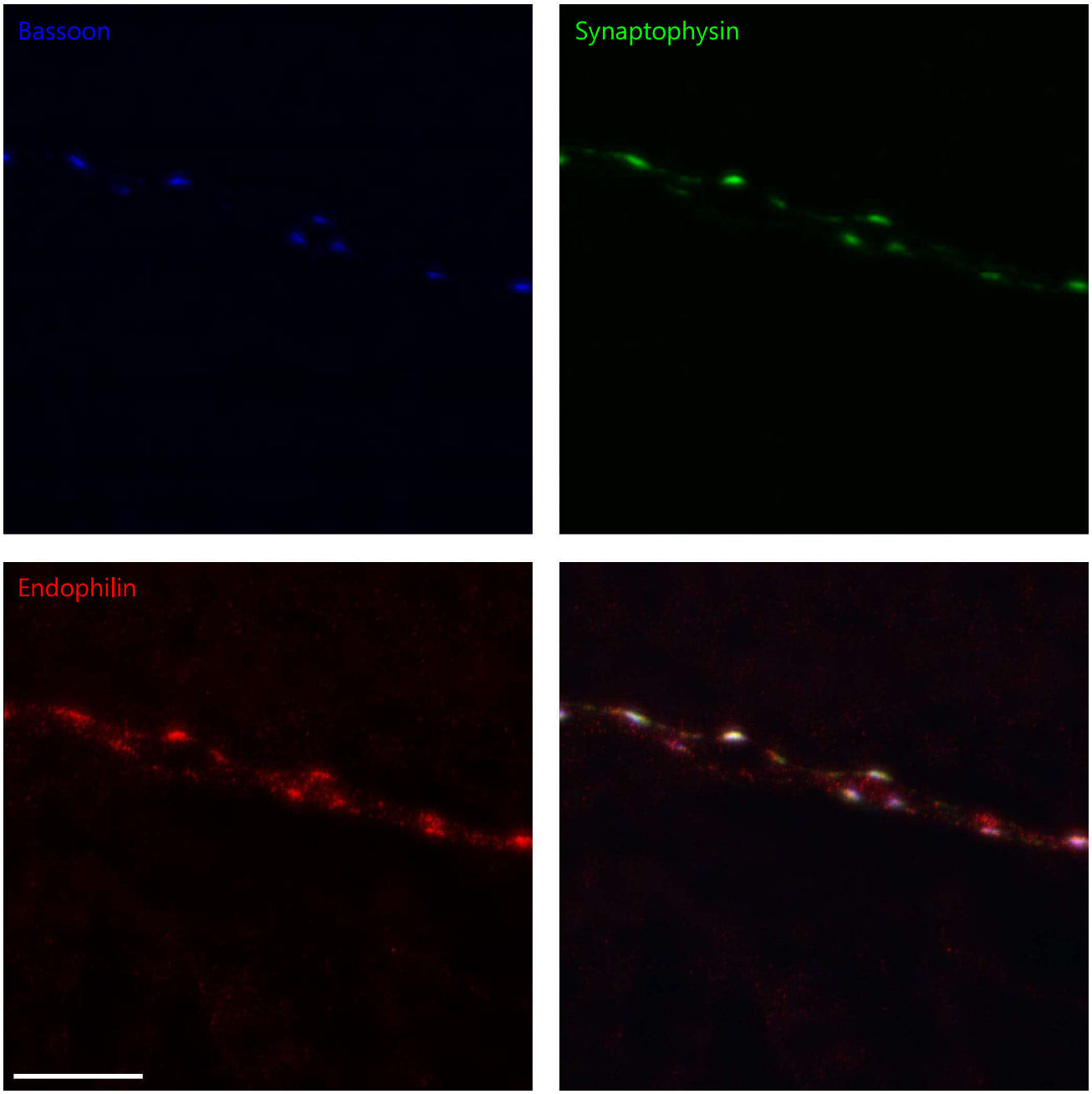

Scale bar: 5 µm

Antibodies used:
Bassoon - Synaptic Systems (Göttingen, Germany), 141 021
Synaptophysin - Synaptic Systems (Göttingen, Germany), 101 011
Endophilin - Synaptic Systems (Göttingen, Germany), 159 002

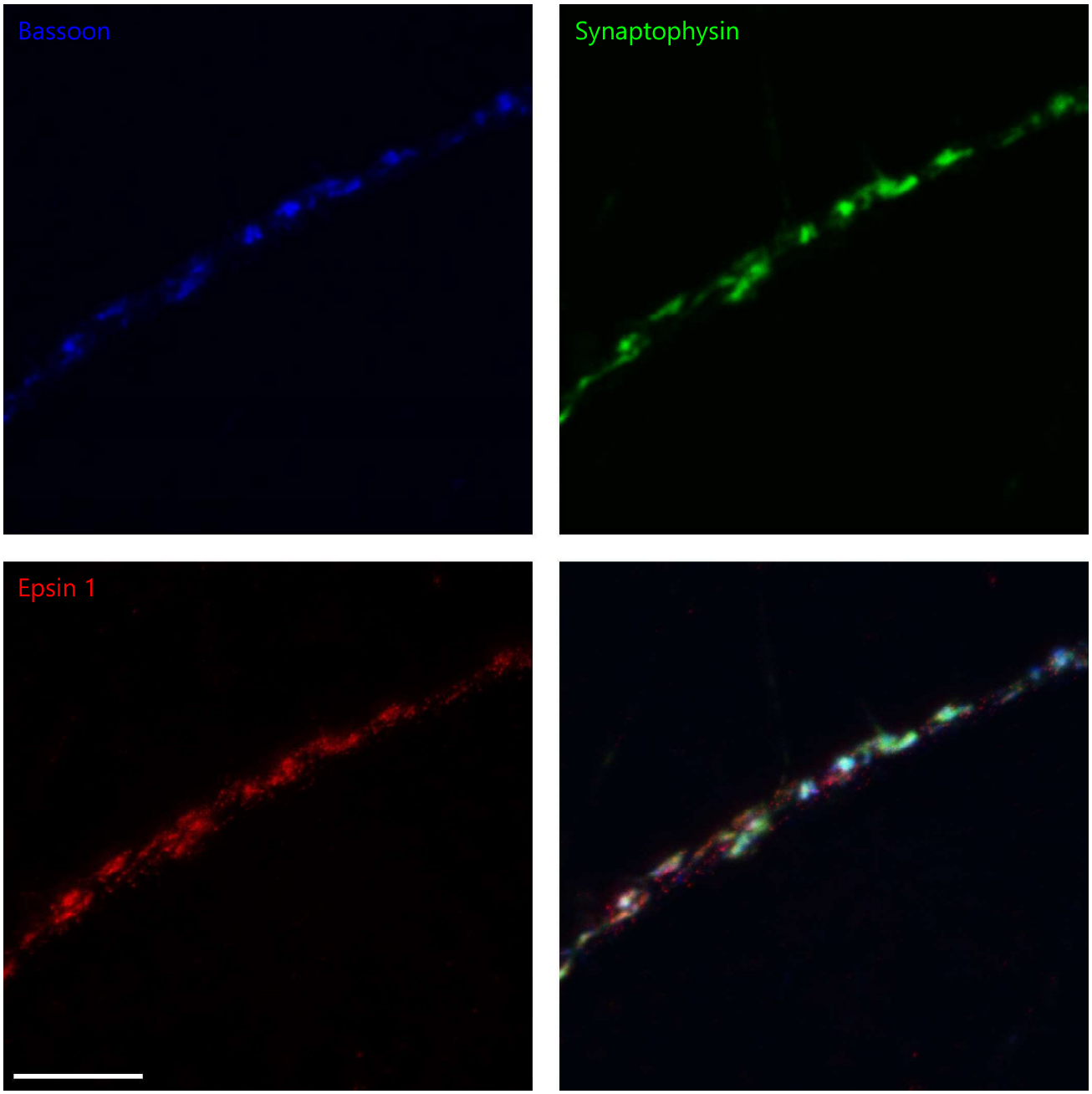

Scale bar: 5 µm

Antibodies used:
Bassoon - Synaptic Systems (Göttingen, Germany), 141 021
Synaptophysin - Synaptic Systems (Göttingen, Germany), 101 011
Epsin 1 - Novus Biologicals (Littleton, Colorado, USA), NBP1-40602

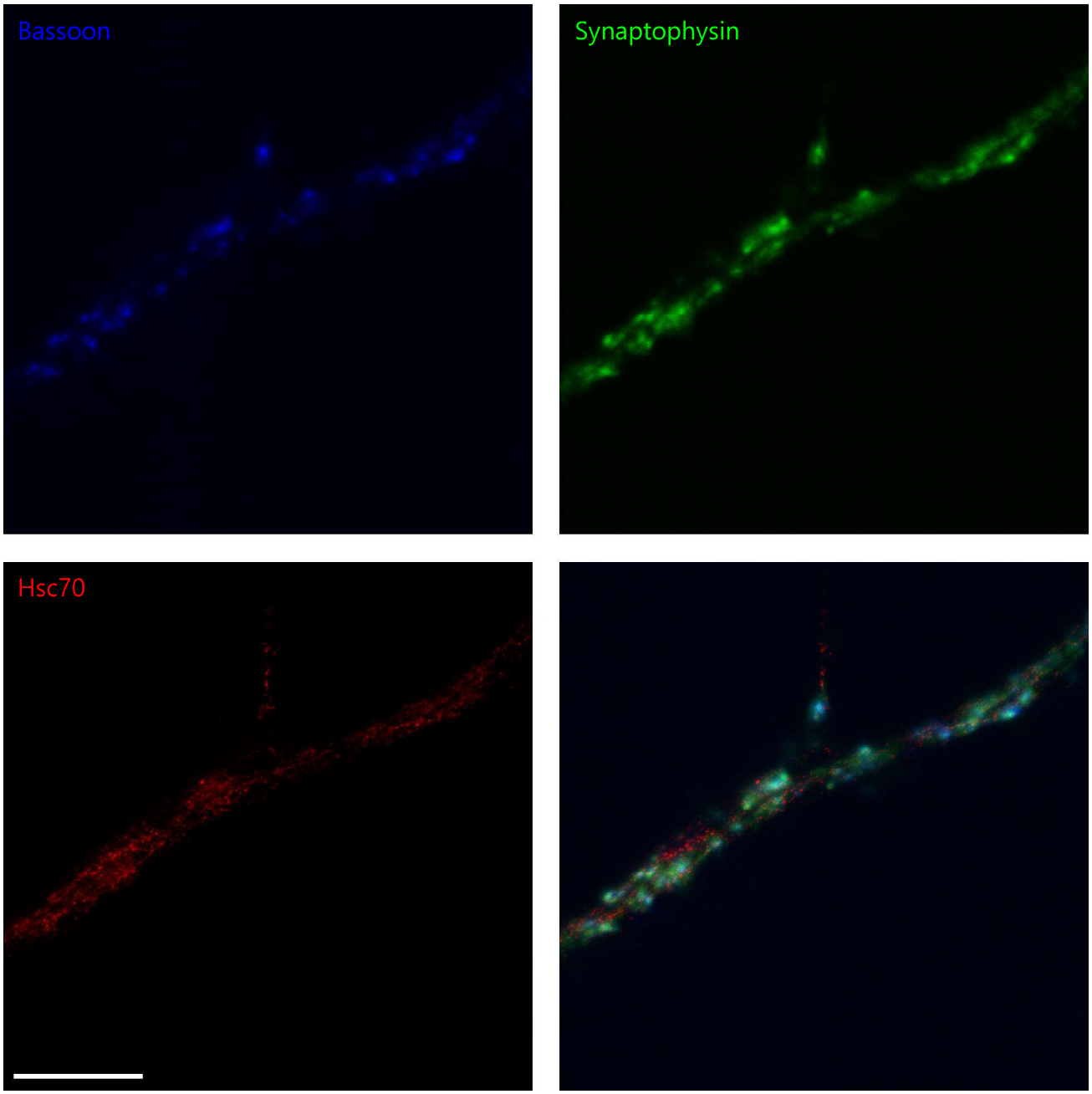

Scale bar: 5 µm

Antibodies used:
Bassoon - Synaptic Systems (Göttingen, Germany), 141 021
Synaptophysin - Synaptic Systems (Göttingen, Germany), 101 011
Hsc70 - Santa Cruz (Heidelberg, Germany), sc-7298

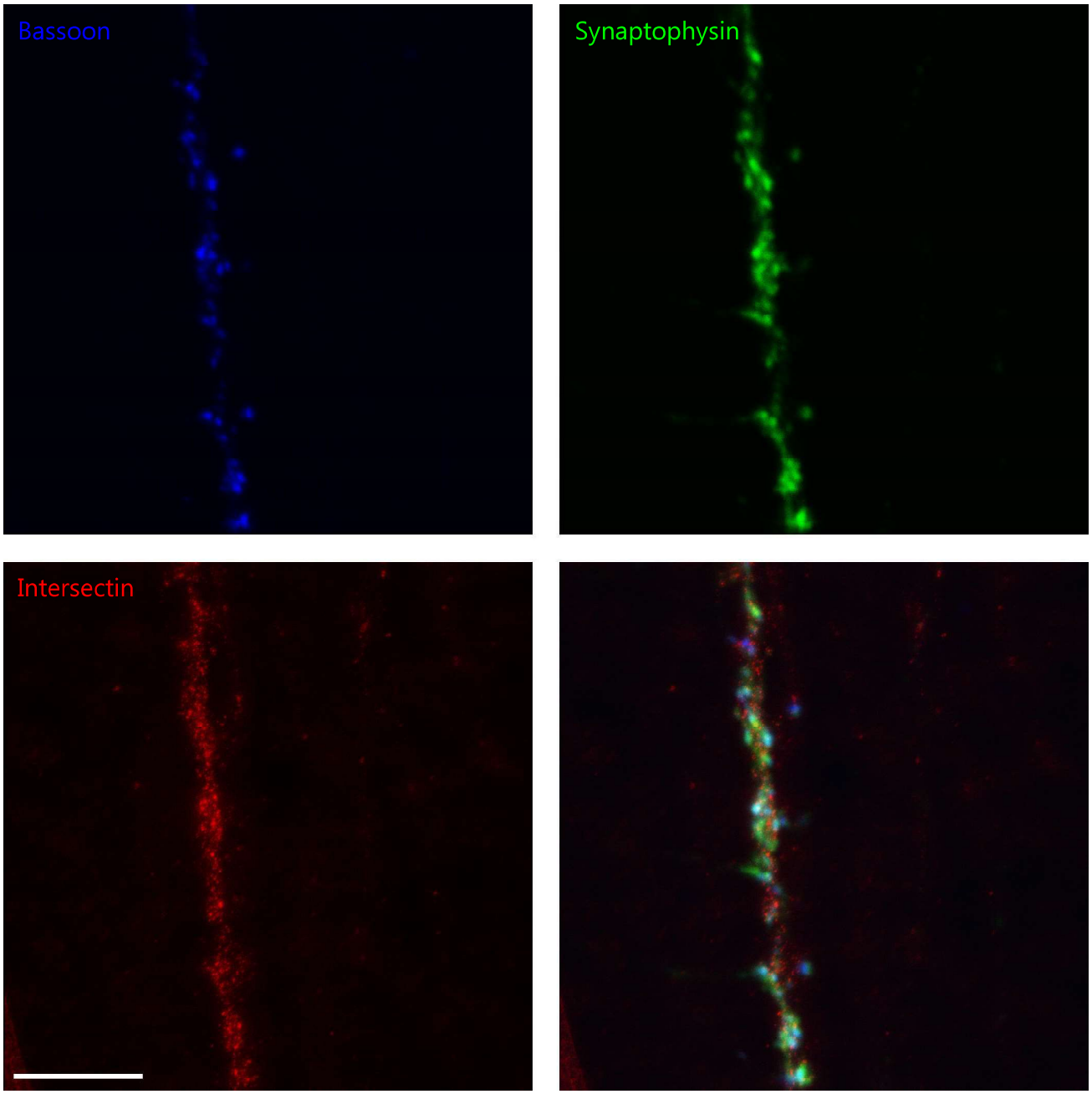

Scale bar: 5 µm

Antibodies used:
Bassoon - Synaptic Systems (Göttingen, Germany), 141 021
Synaptophysin - Synaptic Systems (Göttingen, Germany), 101 011
Intersectin - Volker Haucke (FMP, Berlin, Germany)

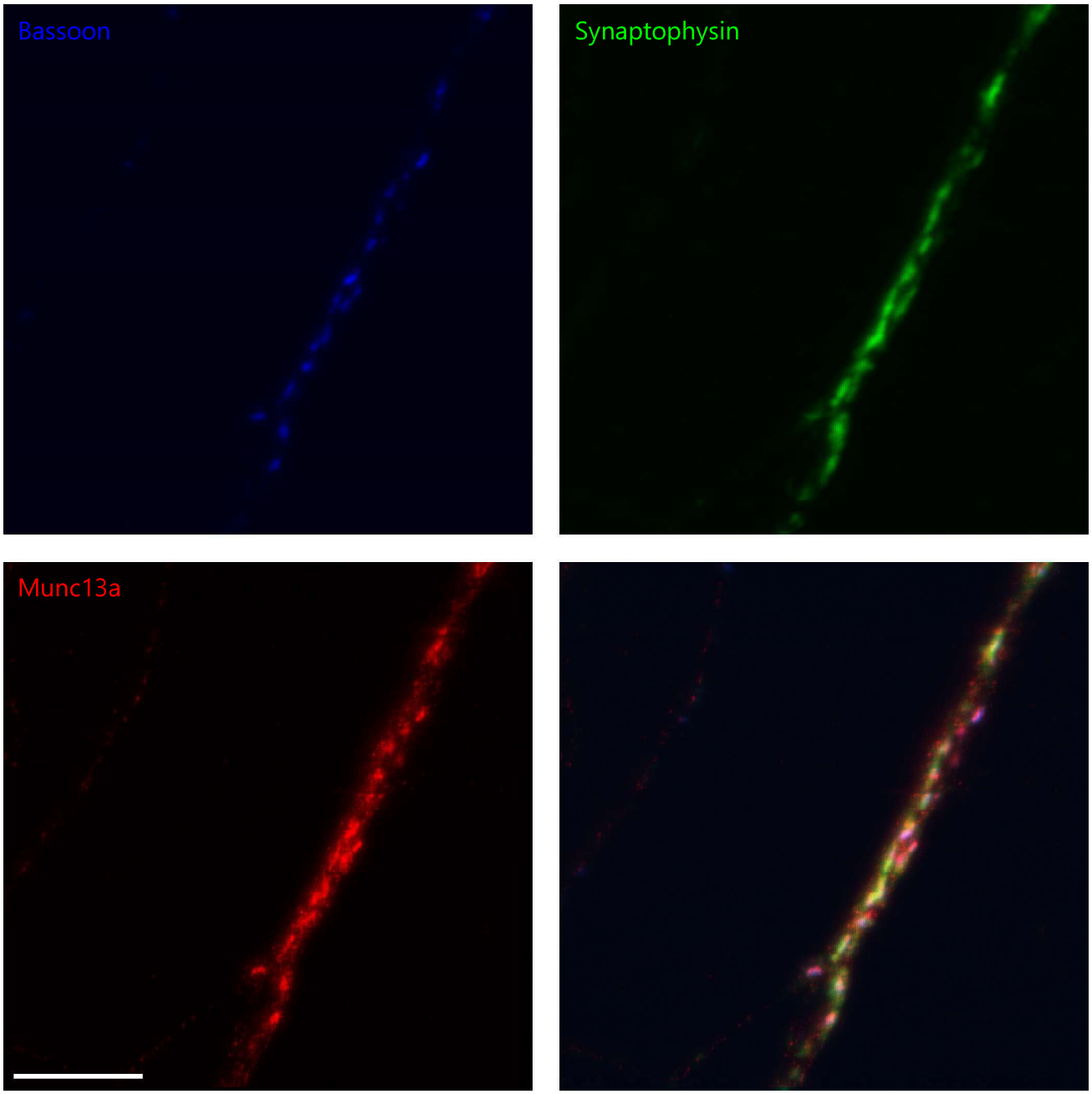

Scale bar: 5 µm

Antibodies used:
Bassoon - Synaptic Systems (Göttingen, Germany), 141 021
Synaptophysin - Synaptic Systems (Göttingen, Germany), 101 011
Munc13a - Antibodies-Online (Aachen, Germany), ABIN571921

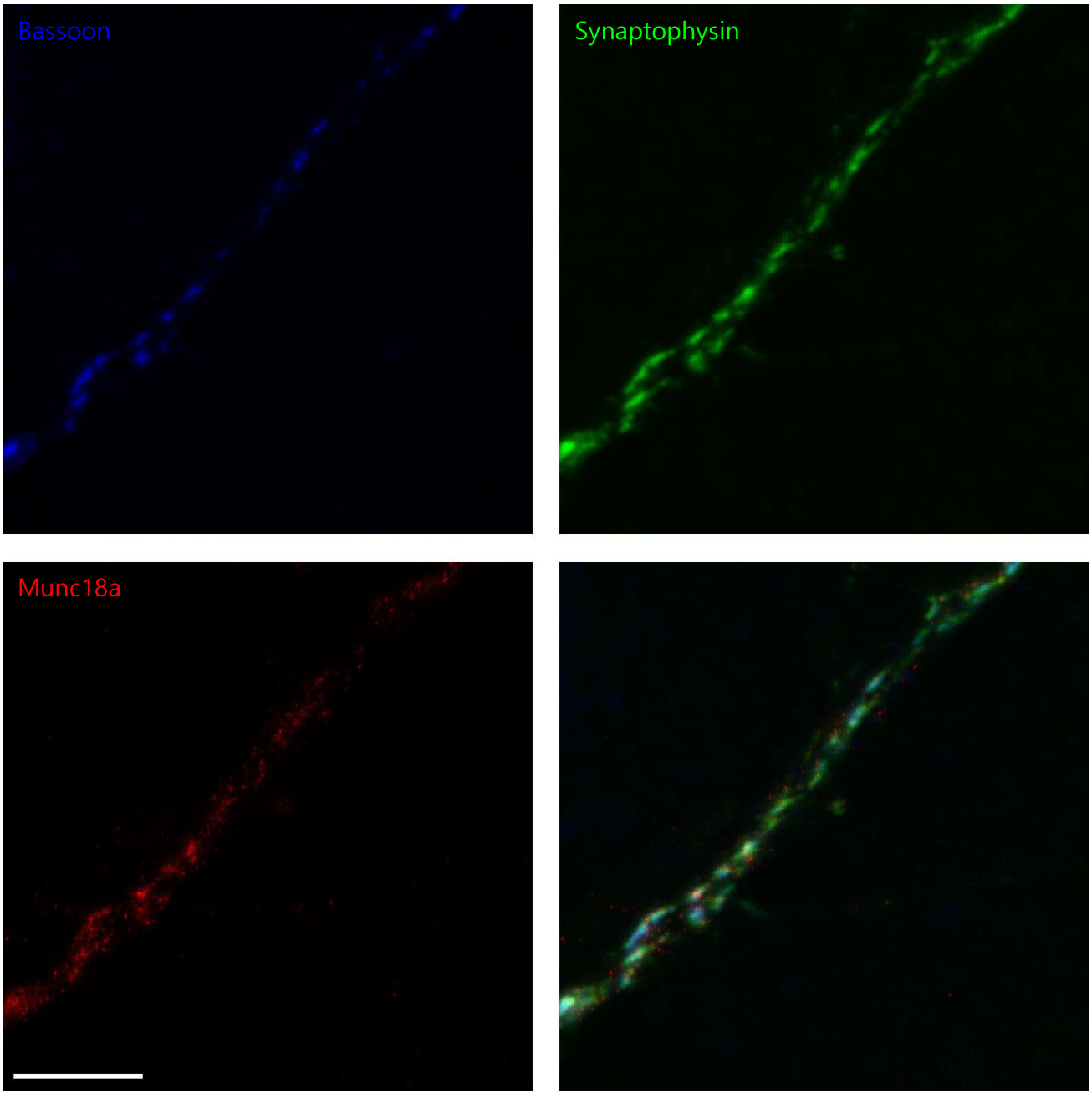

Scale bar: 5 µm

Antibodies used:
Bassoon - Synaptic Systems (Göttingen, Germany), 141 021
Synaptophysin - Synaptic Systems (Göttingen, Germany), 101 011
Munc18a - BD Biosciences (Heidelberg, Germany), 610336

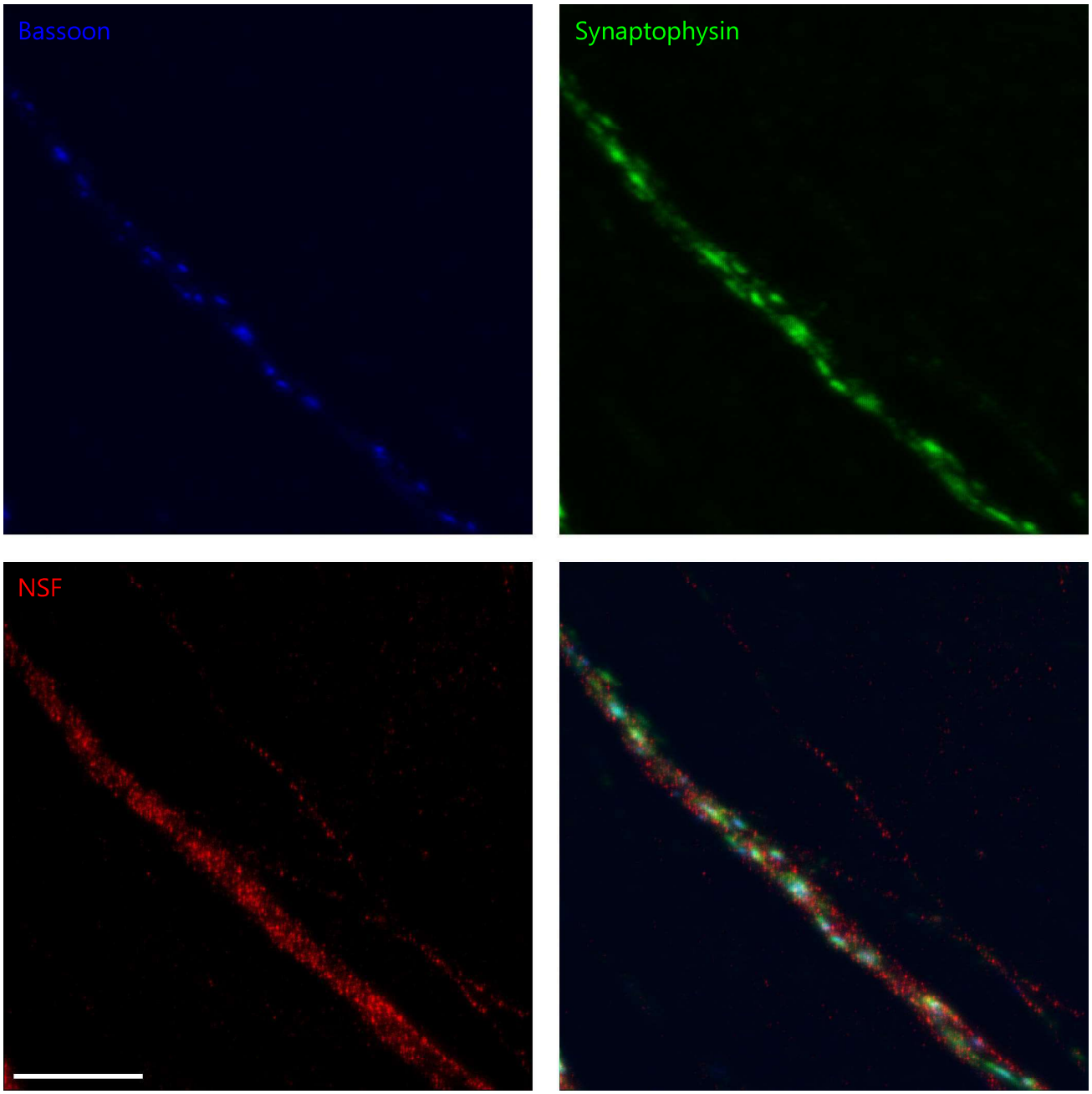

Scale bar: 5 µm

Antibodies used:
Bassoon - Synaptic Systems (Göttingen, Germany), 141 021
Synaptophysin - Synaptic Systems (Göttingen, Germany), 101 011
NSF - Synaptic Systems (Göttingen, Germany), 123 002

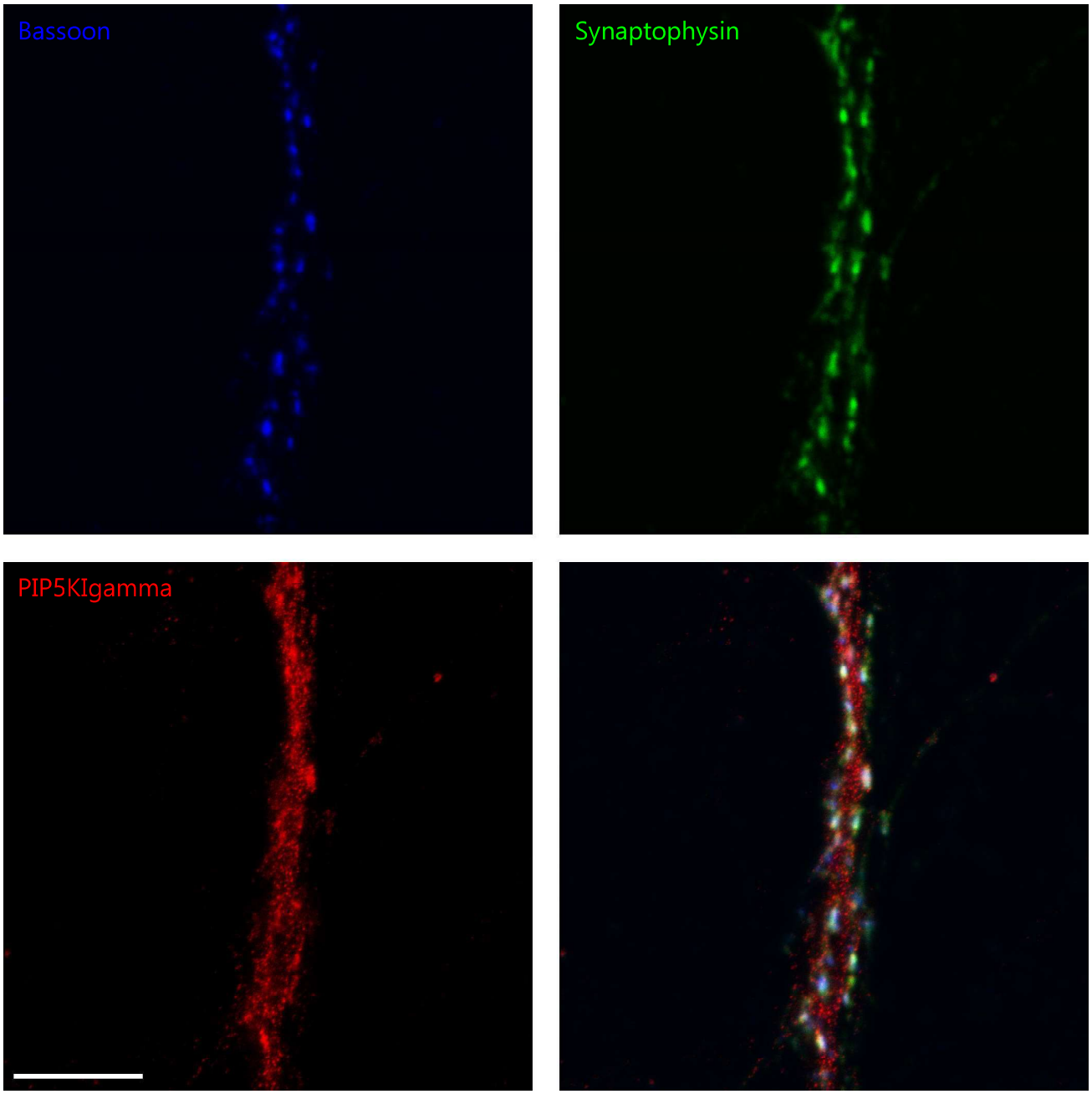

Scale bar: 5 µm

Antibodies used:
Bassoon - Synaptic Systems (Göttingen, Germany), 141 021
Synaptophysin - Synaptic Systems (Göttingen, Germany), 101 011
PIP5KIgamma - Volker Haucke (FMP, Berlin, Germany)

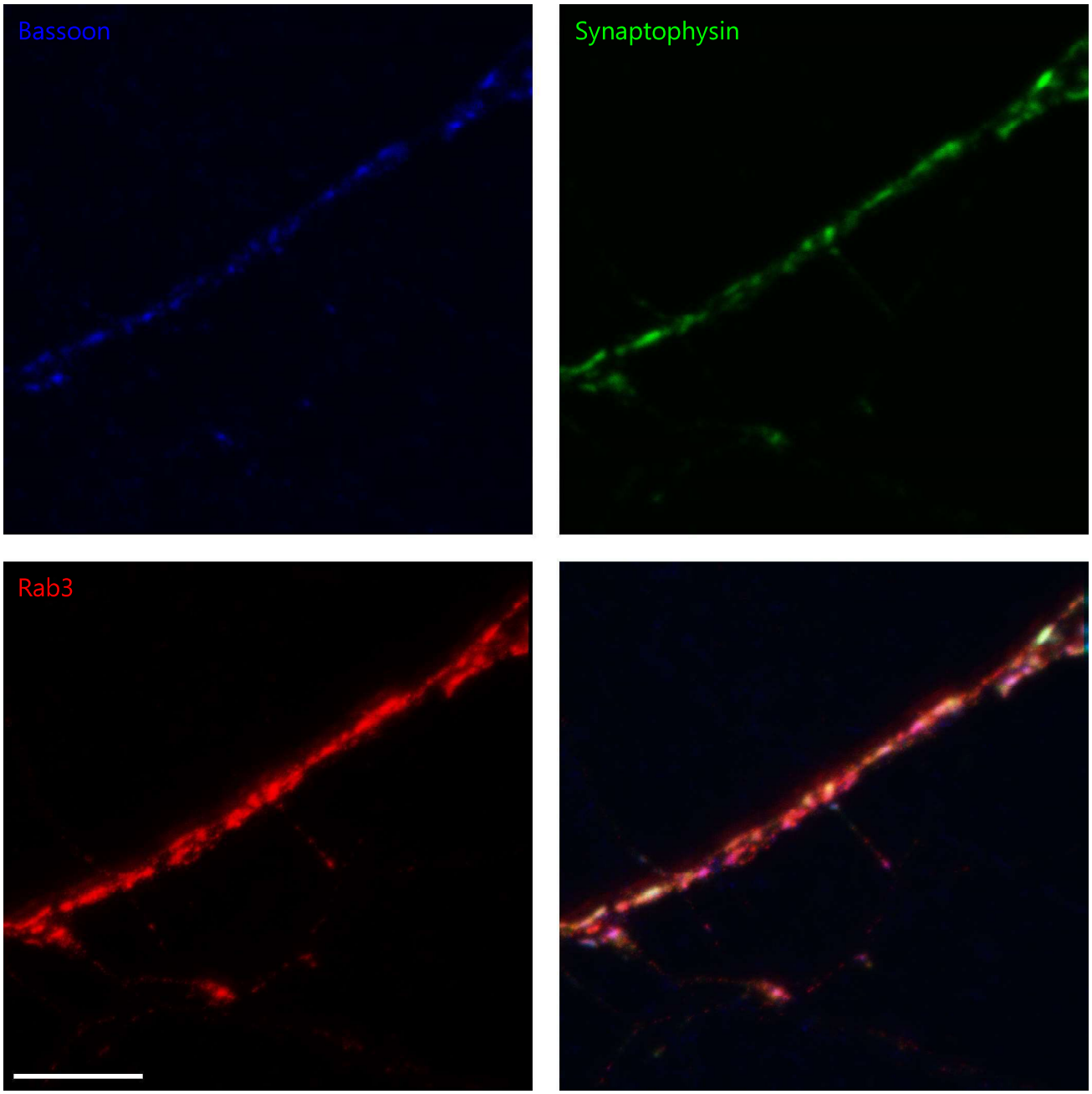

Scale bar: 5 µm

Antibodies used:
Bassoon - Synaptic Systems (Göttingen, Germany), 141 021
Synaptophysin - Synaptic Systems (Göttingen, Germany), 101 011
Rab3 - BD Biosciences (Heidelberg, Germany), 610379

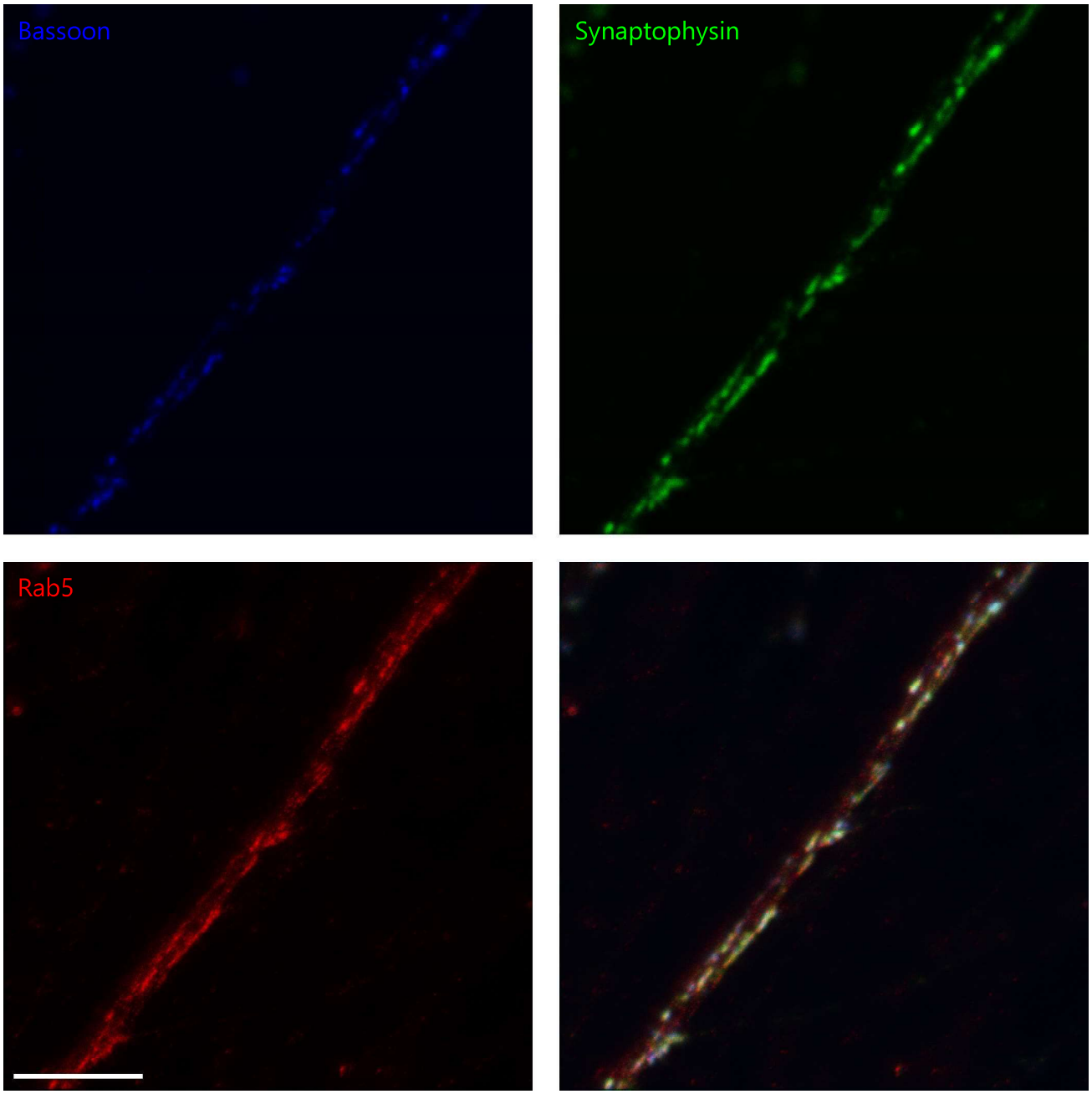

Scale bar: 5 µm

Antibodies used:
Bassoon - Synaptic Systems (Göttingen, Germany), 141 021
Synaptophysin - Synaptic Systems (Göttingen, Germany), 101 011
Rab5 - Cell Signaling Technology (Beverly, Massachusetts, USA), 3547

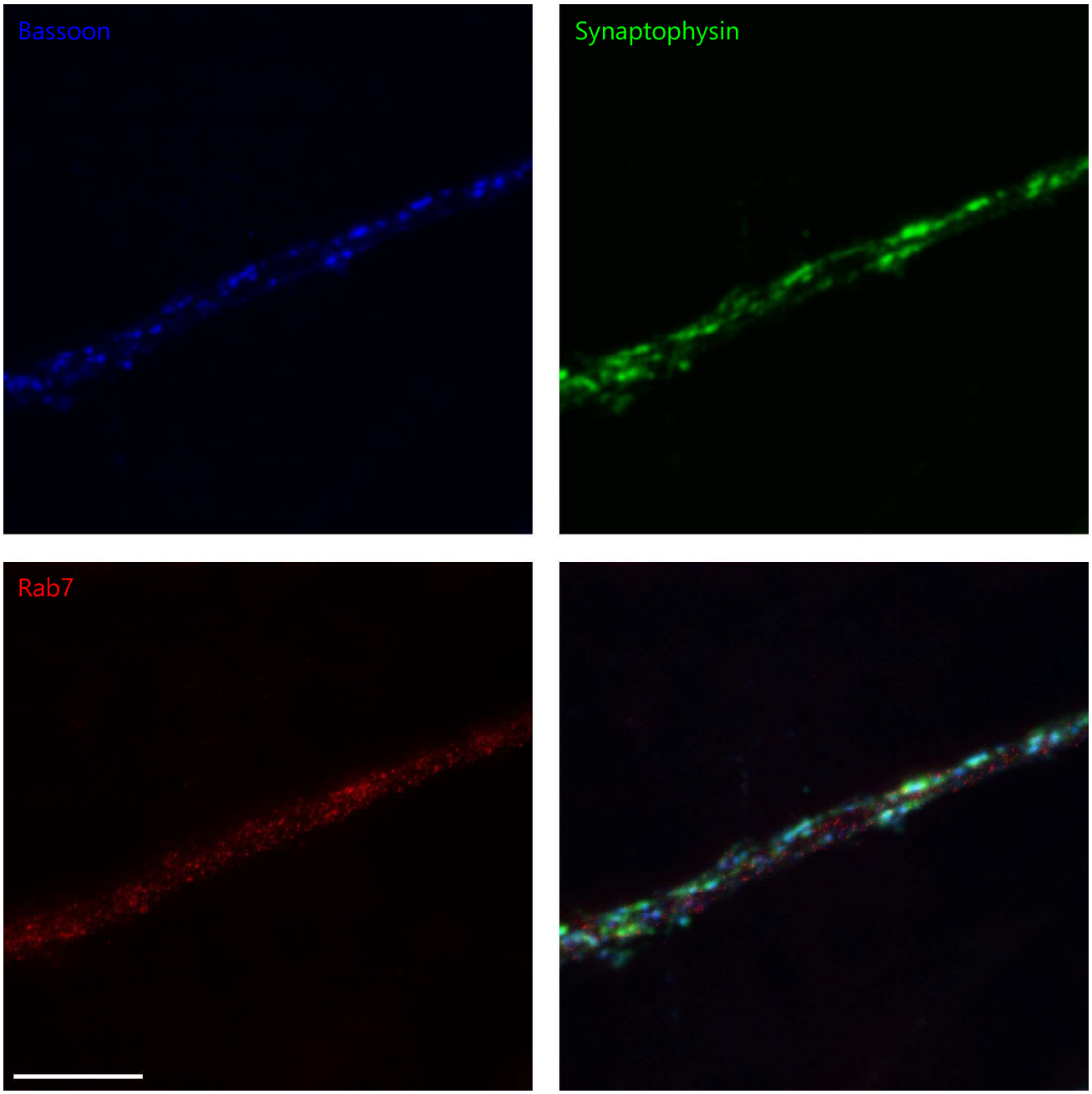

Scale bar: 5 µm

Antibodies used:
Bassoon - Synaptic Systems (Göttingen, Germany), 141 021
Synaptophysin - Synaptic Systems (Göttingen, Germany), 101 011
Rab7 - Novus Biologicals (Littleton, Colorado, USA), NBP1-05048

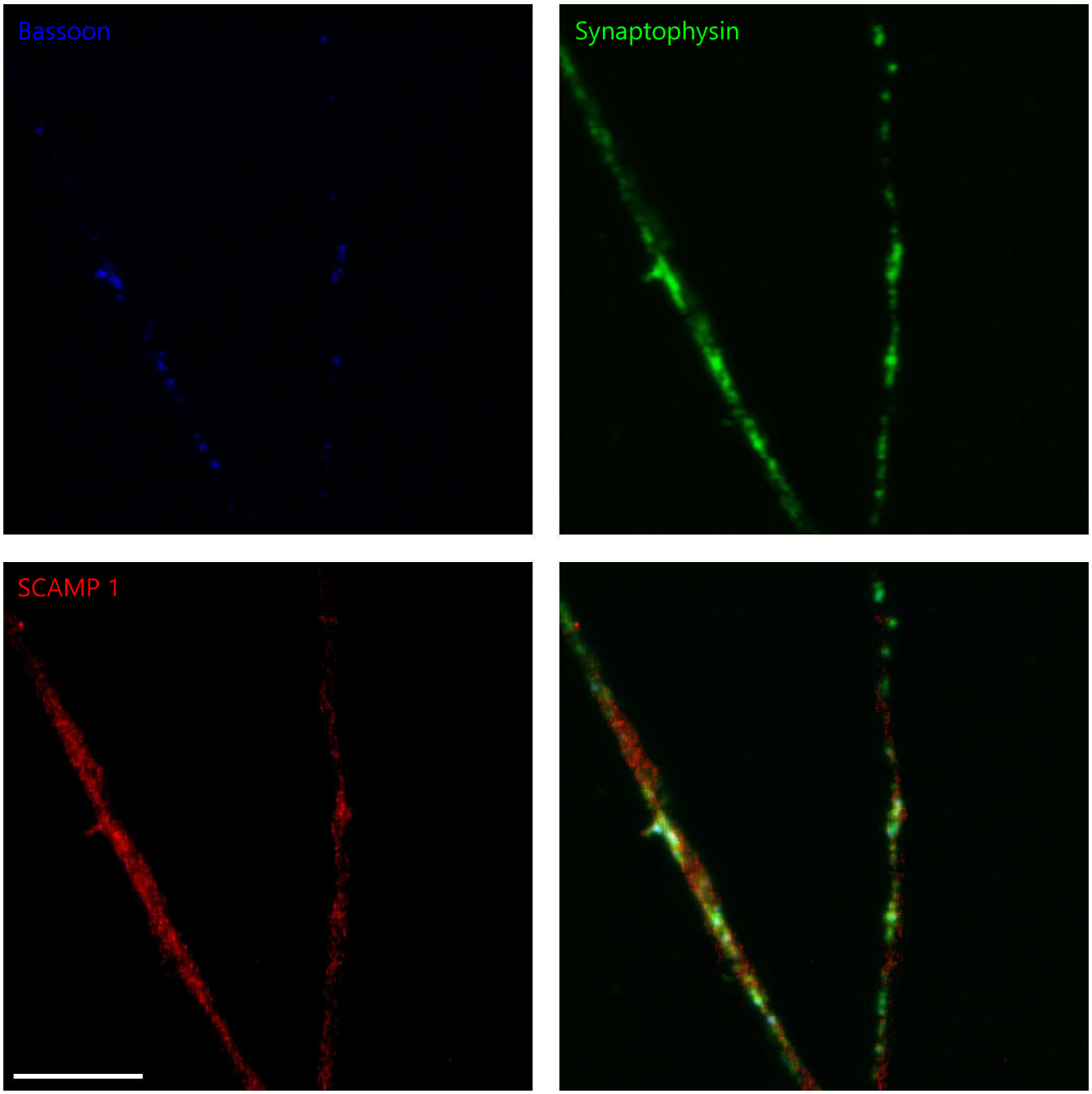

Scale bar: 5 µm

Antibodies used:
Bassoon - Synaptic Systems (Göttingen, Germany), 141 021
Synaptophysin - Synaptic Systems (Göttingen, Germany), 101 011
SCAMP 1 - Synaptic Systems (Göttingen, Germany), 121 001

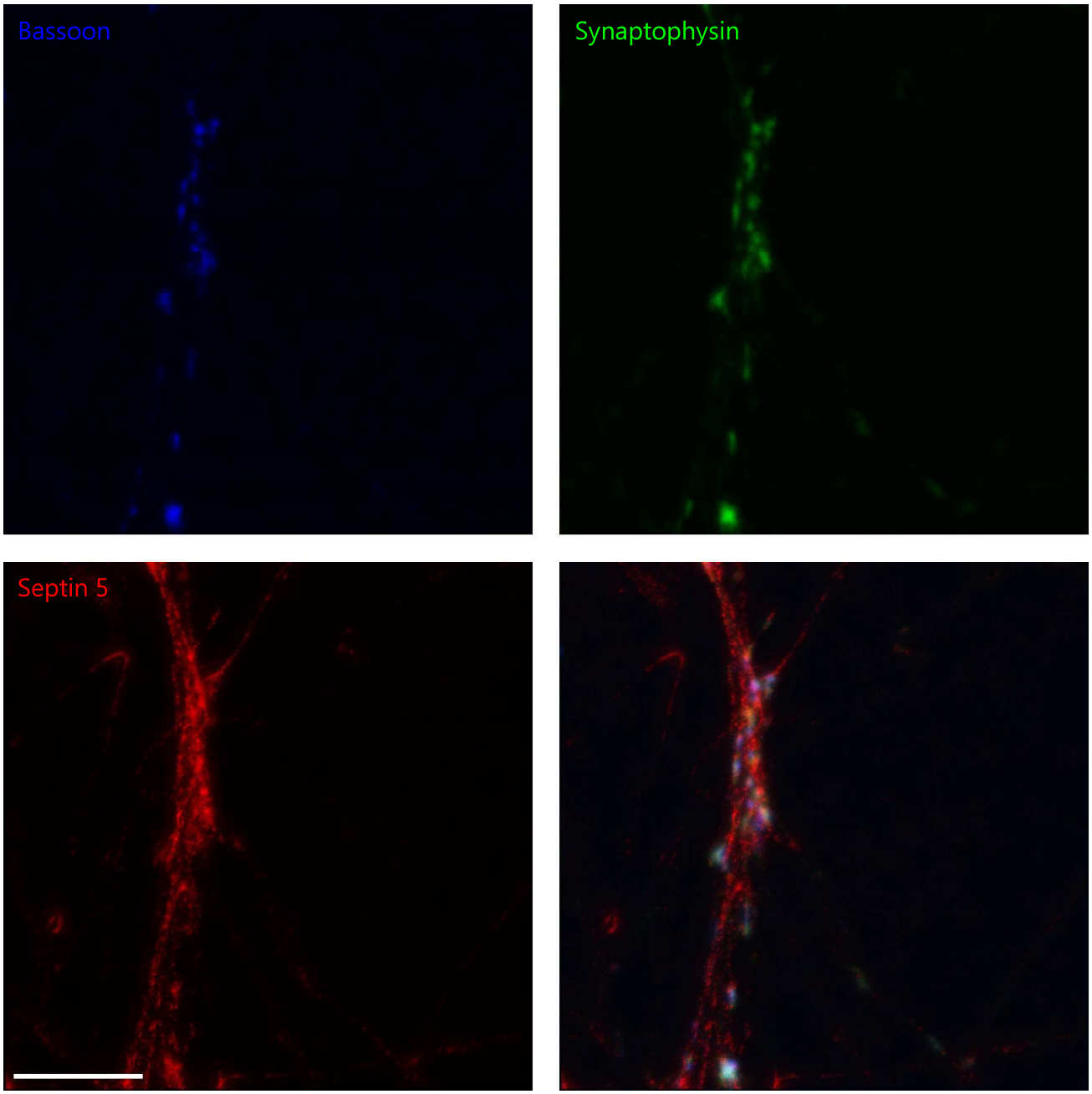

Scale bar: 5 µm

Antibodies used:
Bassoon - Synaptic Systems (Göttingen, Germany), 141 021
Synaptophysin - Synaptic Systems (Göttingen, Germany), 101 011
Septin 5 - Volker Haucke (FMP, Berlin, Germany)

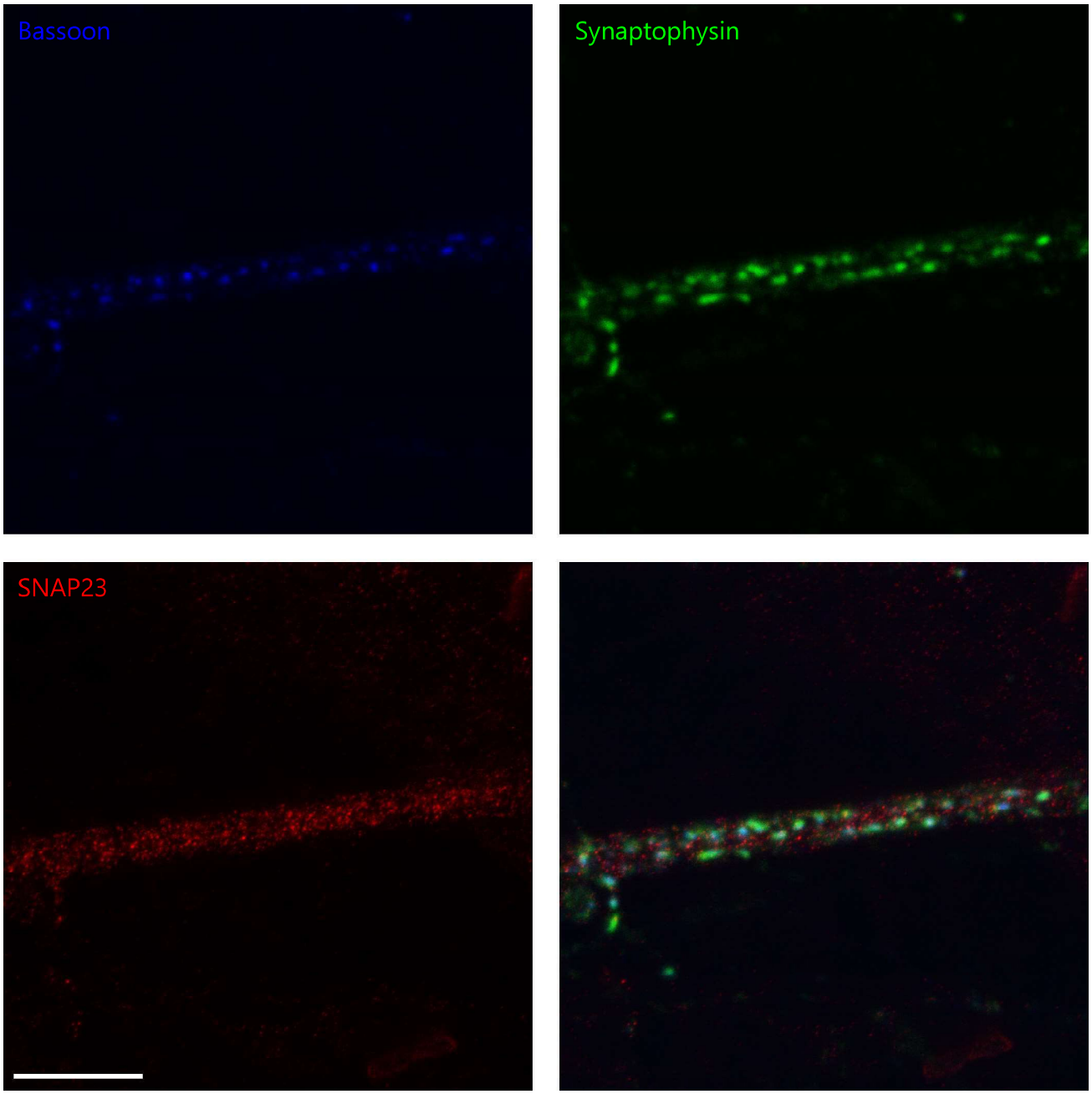

Scale bar: 5 µm

Antibodies used:
Bassoon - Synaptic Systems (Göttingen, Germany), 141 021
Synaptophysin - Synaptic Systems (Göttingen, Germany), 101 011
SNAP23 - Synaptic Systems (Göttingen, Germany), 111 202

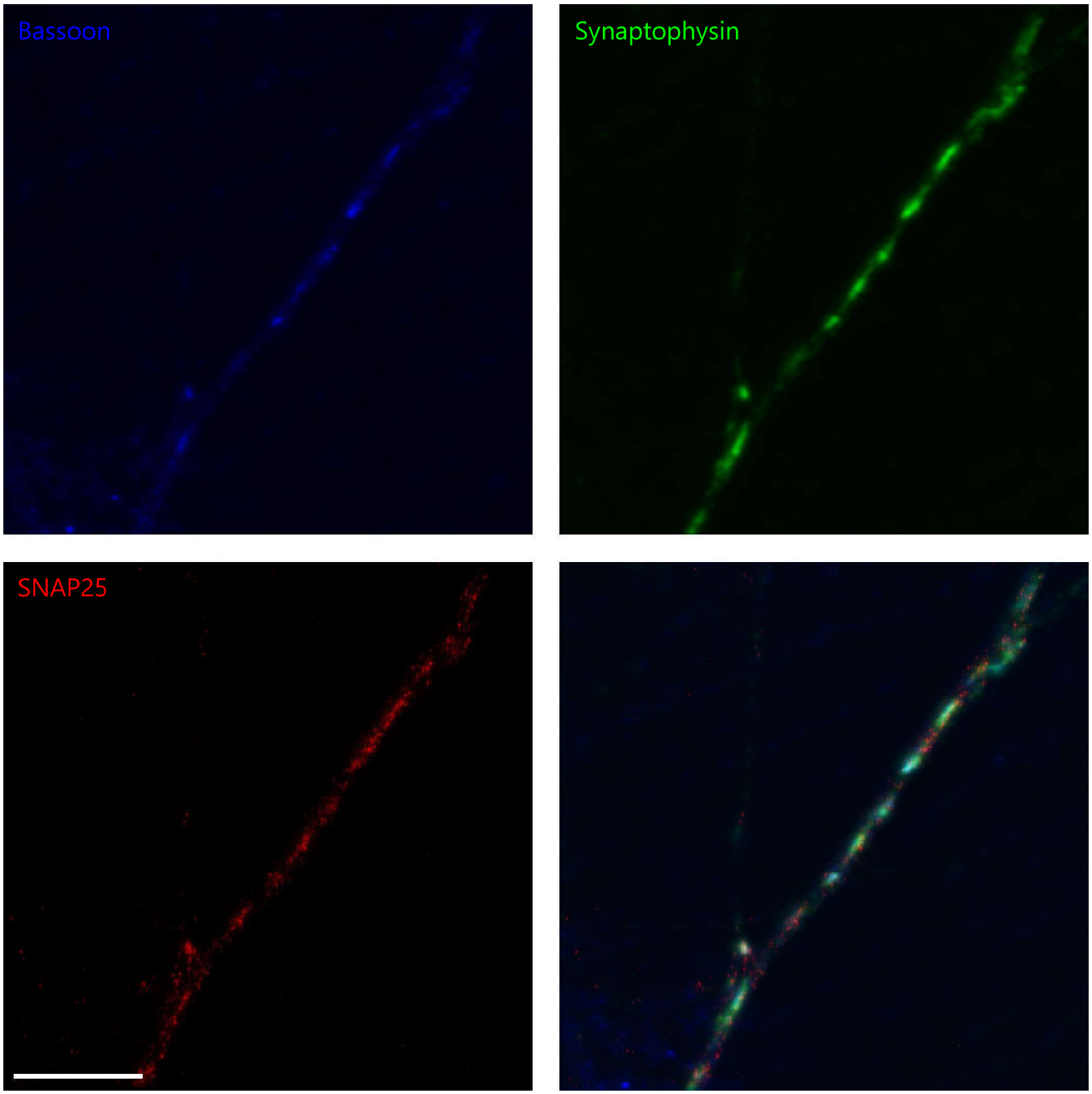

Scale bar: 5 µm

Antibodies used:
Bassoon - Synaptic Systems (Göttingen, Germany), 141 021
Synaptophysin - Synaptic Systems (Göttingen, Germany), 101 011
SNAP25 - Synaptic Systems (Göttingen, Germany), 111 011

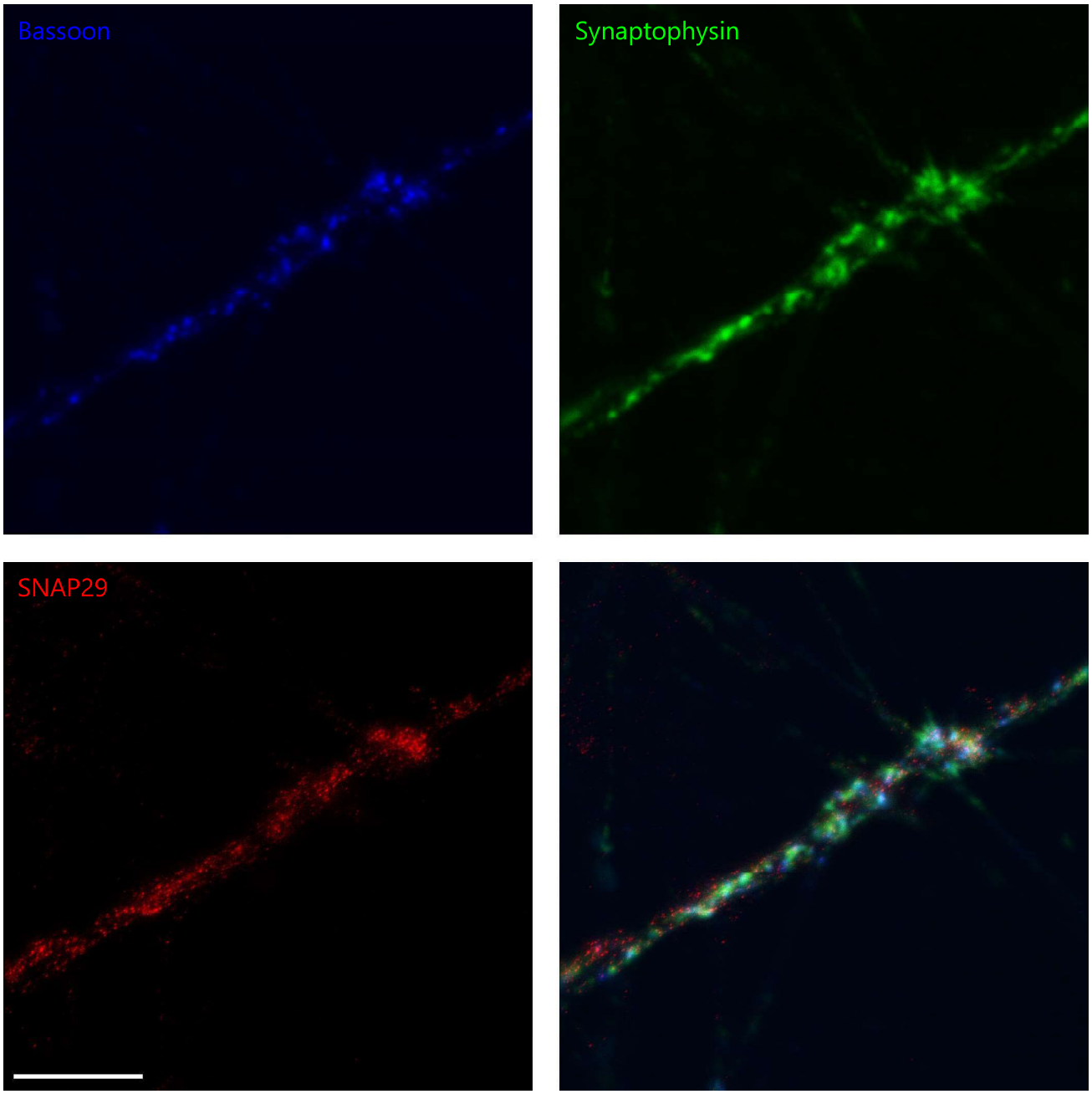

Scale bar: 5 µm

Antibodies used:
Bassoon - Synaptic Systems (Göttingen, Germany), 141 021
Synaptophysin - Synaptic Systems (Göttingen, Germany), 101 011
SNAP29 - Abcam (Cambridge, England), ab68824

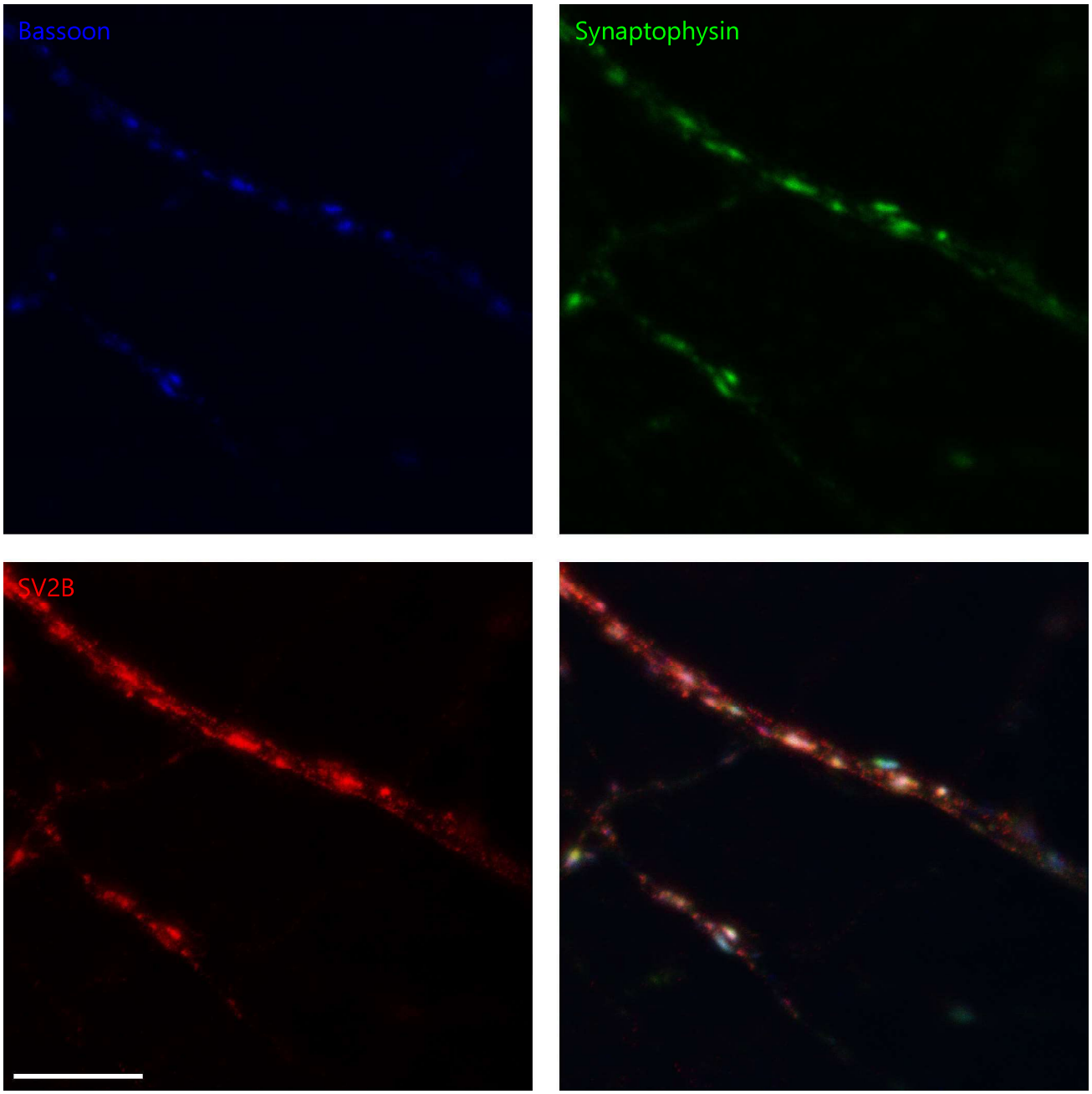

Scale bar: 5 µm

Antibodies used:
Bassoon - Synaptic Systems (Göttingen, Germany), 141 021
Synaptophysin - Synaptic Systems (Göttingen, Germany), 101 011
SV2B - Reinhard Jahn (MPI-BPC, Göttingen, Germany)

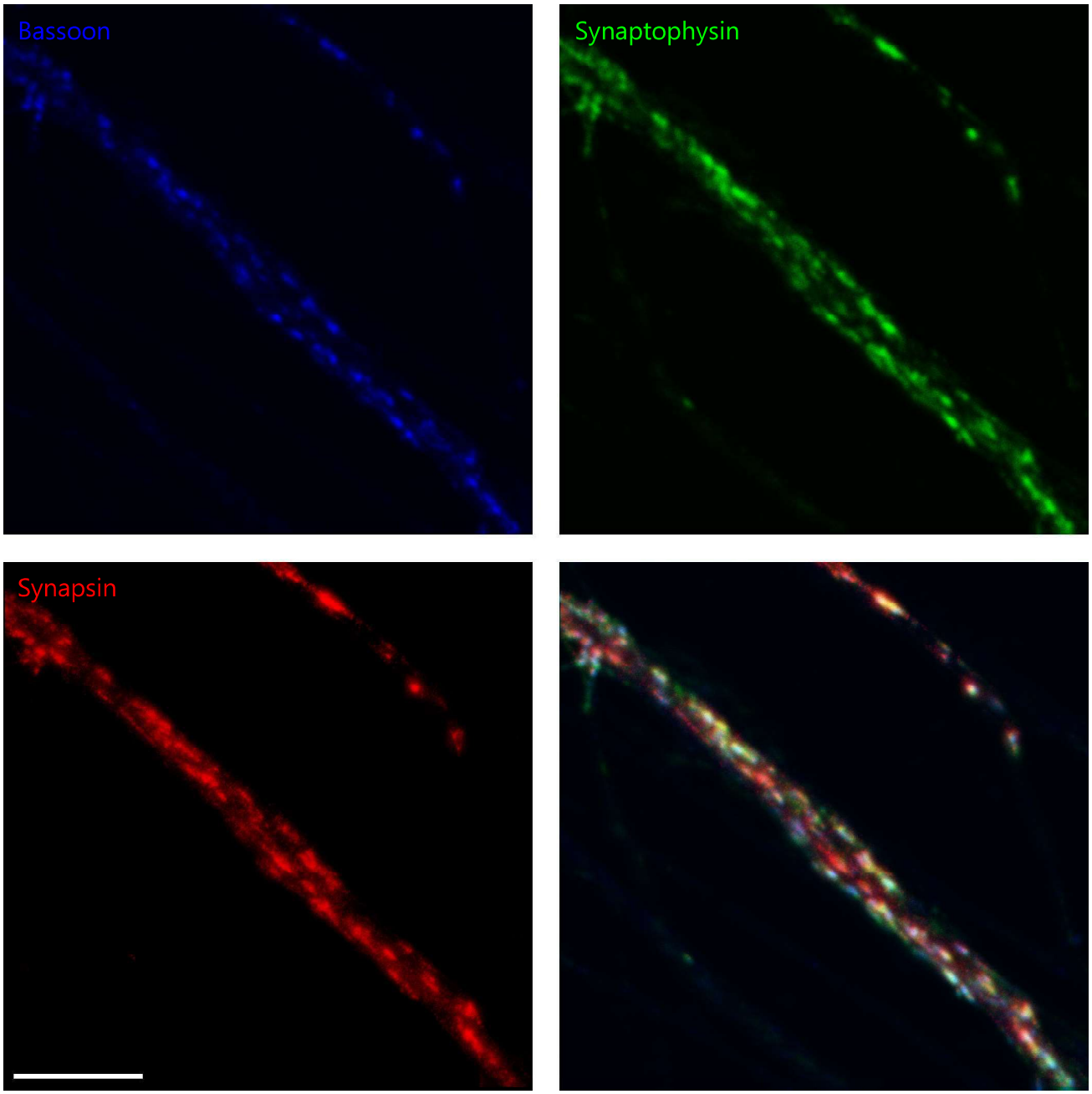

Scale bar: 5 µm

Antibodies used:
Bassoon - Synaptic Systems (Göttingen, Germany), 141 021
Synaptophysin - Synaptic Systems (Göttingen, Germany), 101 011
Synapsin - Reinhard Jahn (MPI-BPC, Göttingen, Germany)

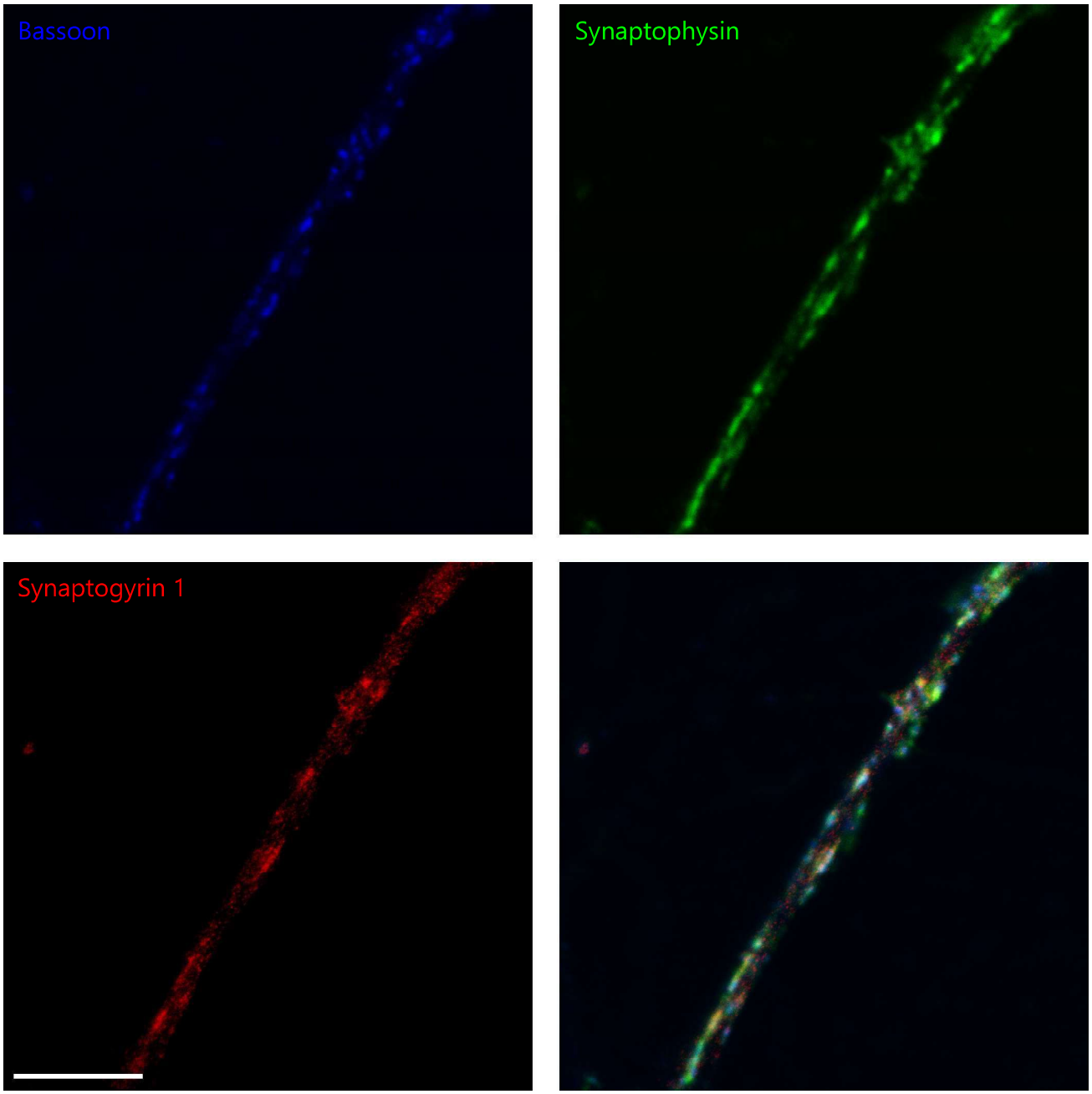

Scale bar: 5 µm

Antibodies used:
Bassoon - Synaptic Systems (Göttingen, Germany), 141 021
Synaptophysin - Synaptic Systems (Göttingen, Germany), 101 011
Synaptogyrin 1 - Synaptic Systems (Göttingen, Germany), 103 002

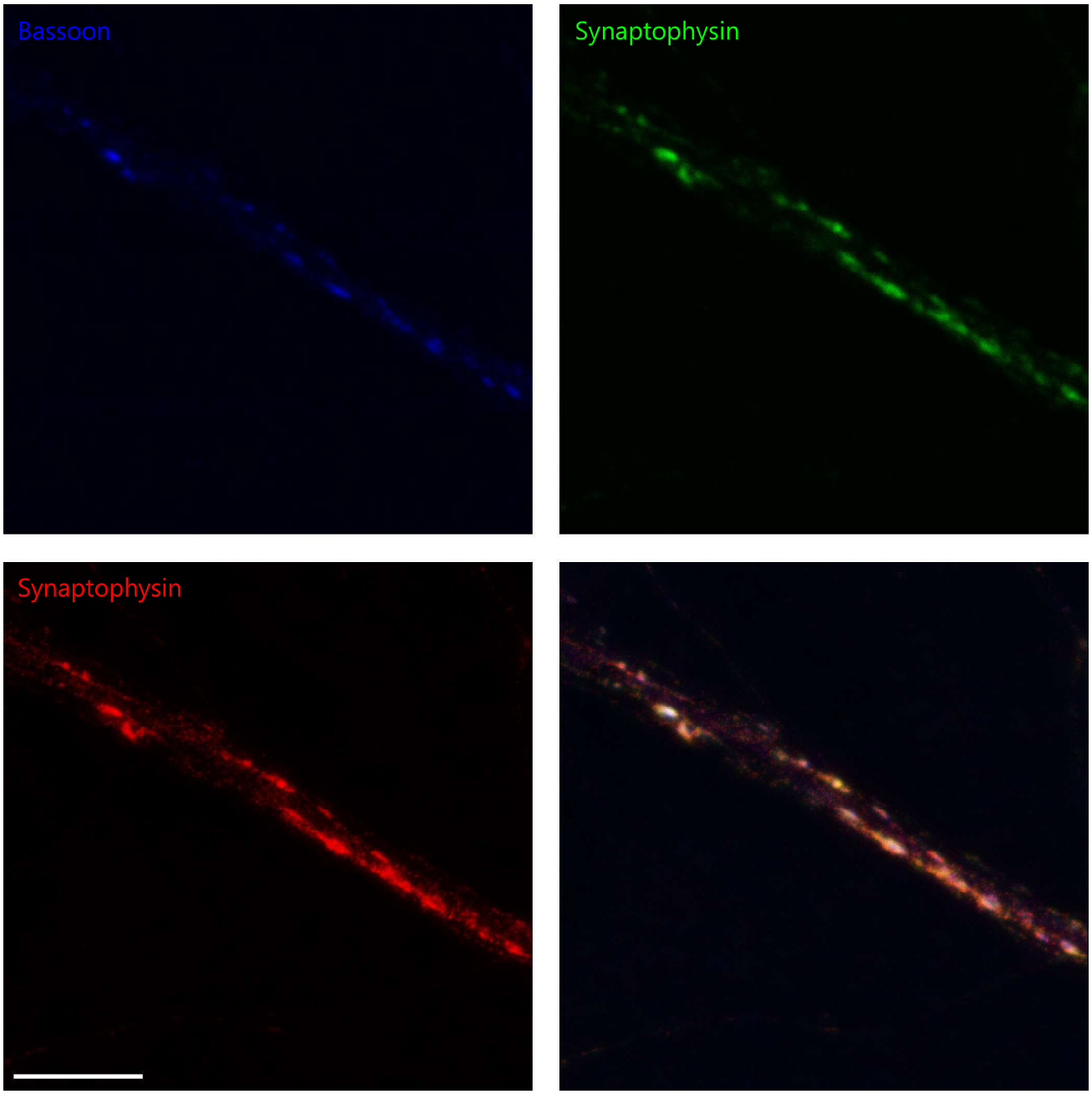

Scale bar: 5 µm

Antibodies used:
Bassoon - Synaptic Systems (Göttingen, Germany), 141 021
Synaptophysin - Synaptic Systems (Göttingen, Germany), 101 011
Synaptophysin - Synaptic Systems (Göttingen, Germany), 101 011

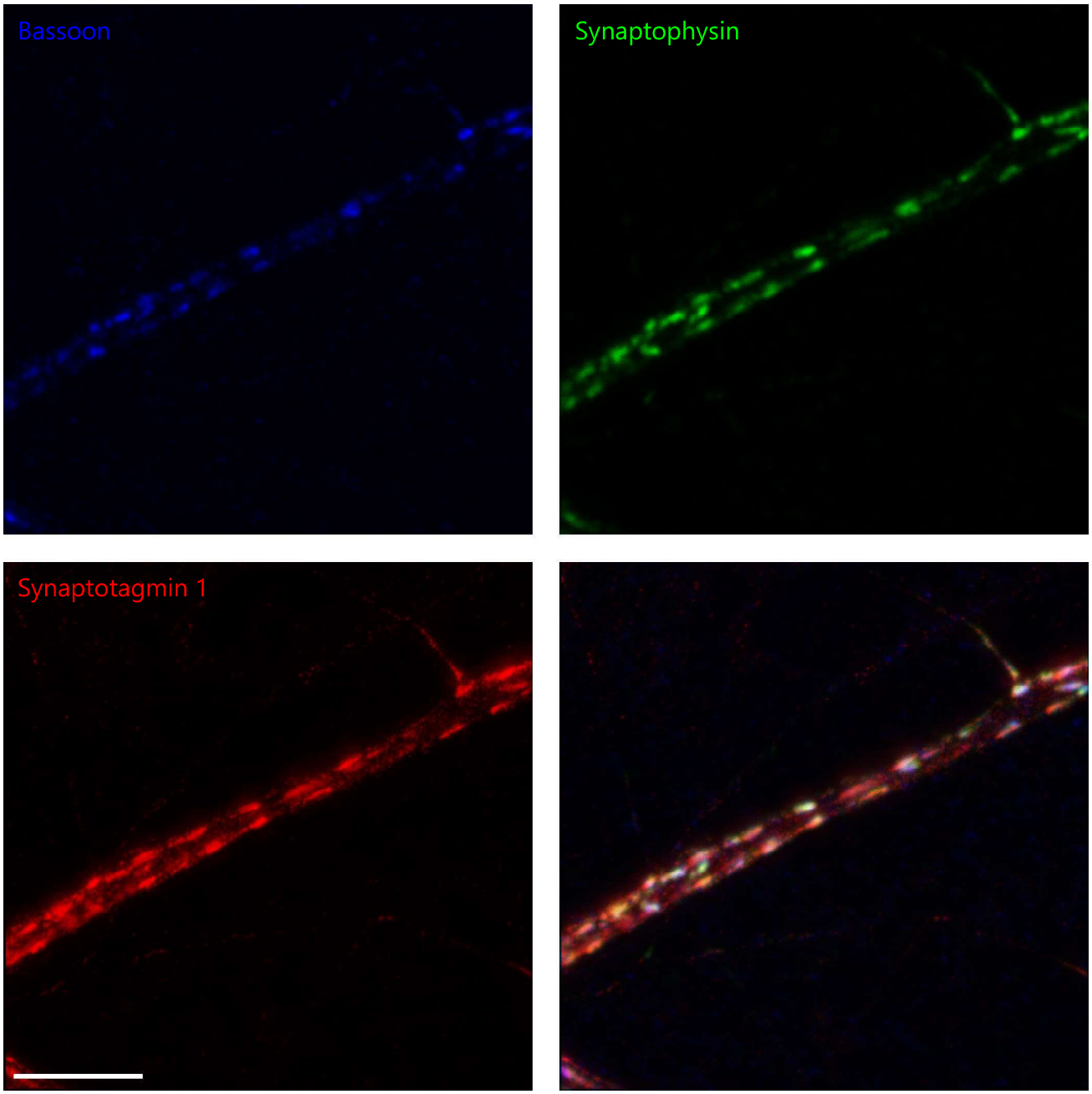

Scale bar: 5 µm

Antibodies used:
Bassoon - Synaptic Systems (Göttingen, Germany), 141 021
Synaptophysin - Synaptic Systems (Göttingen, Germany), 101 011
Synaptotagmin 1 - Synaptic Systems (Göttingen, Germany), 105 311AT1

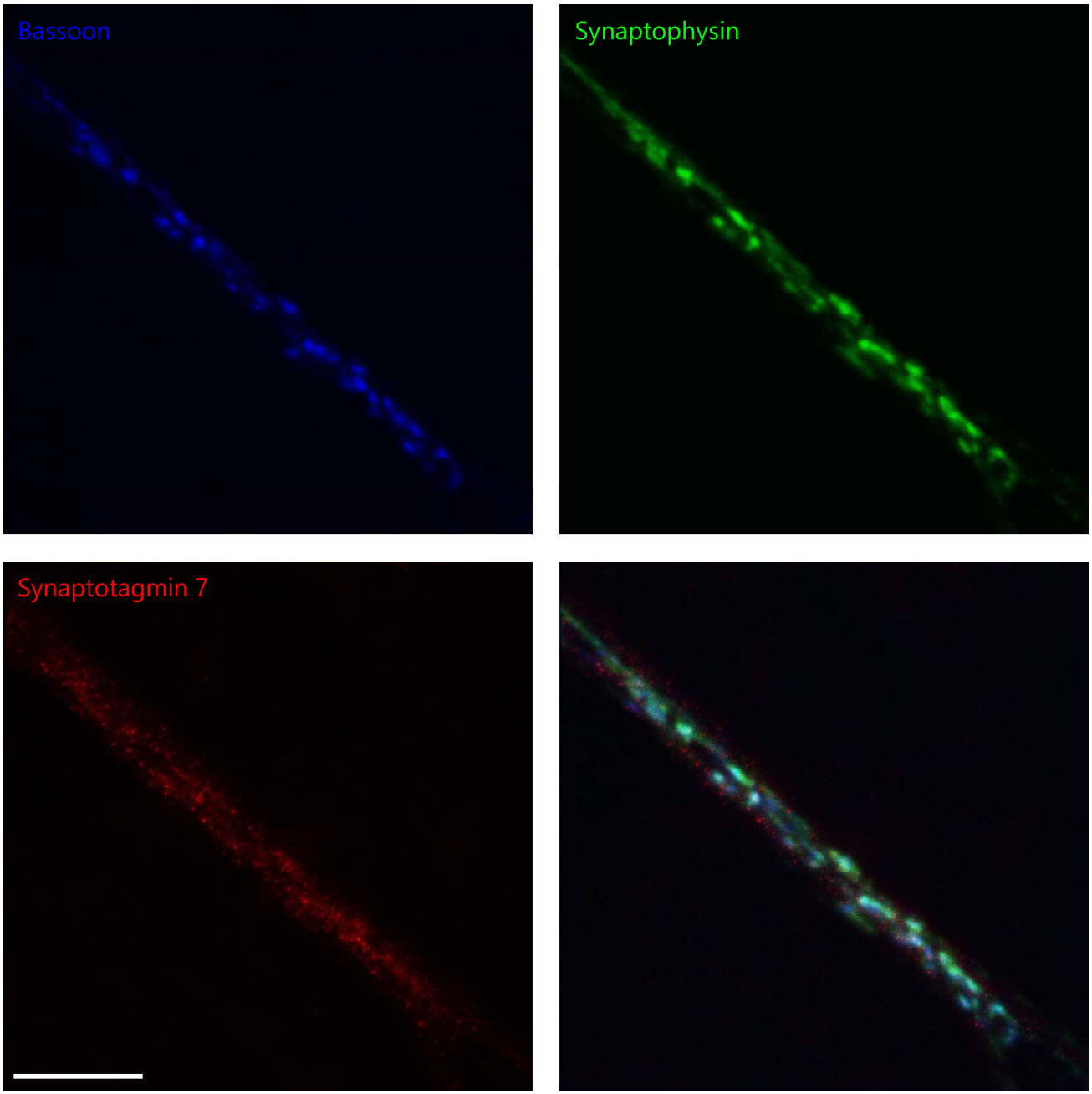

Scale bar: 5 µm

Antibodies used:
Bassoon - Synaptic Systems (Göttingen, Germany), 141 021
Synaptophysin - Synaptic Systems (Göttingen, Germany), 101 011
Synaptotagmin 7 - Synaptic Systems (Göttingen, Germany), 105 173

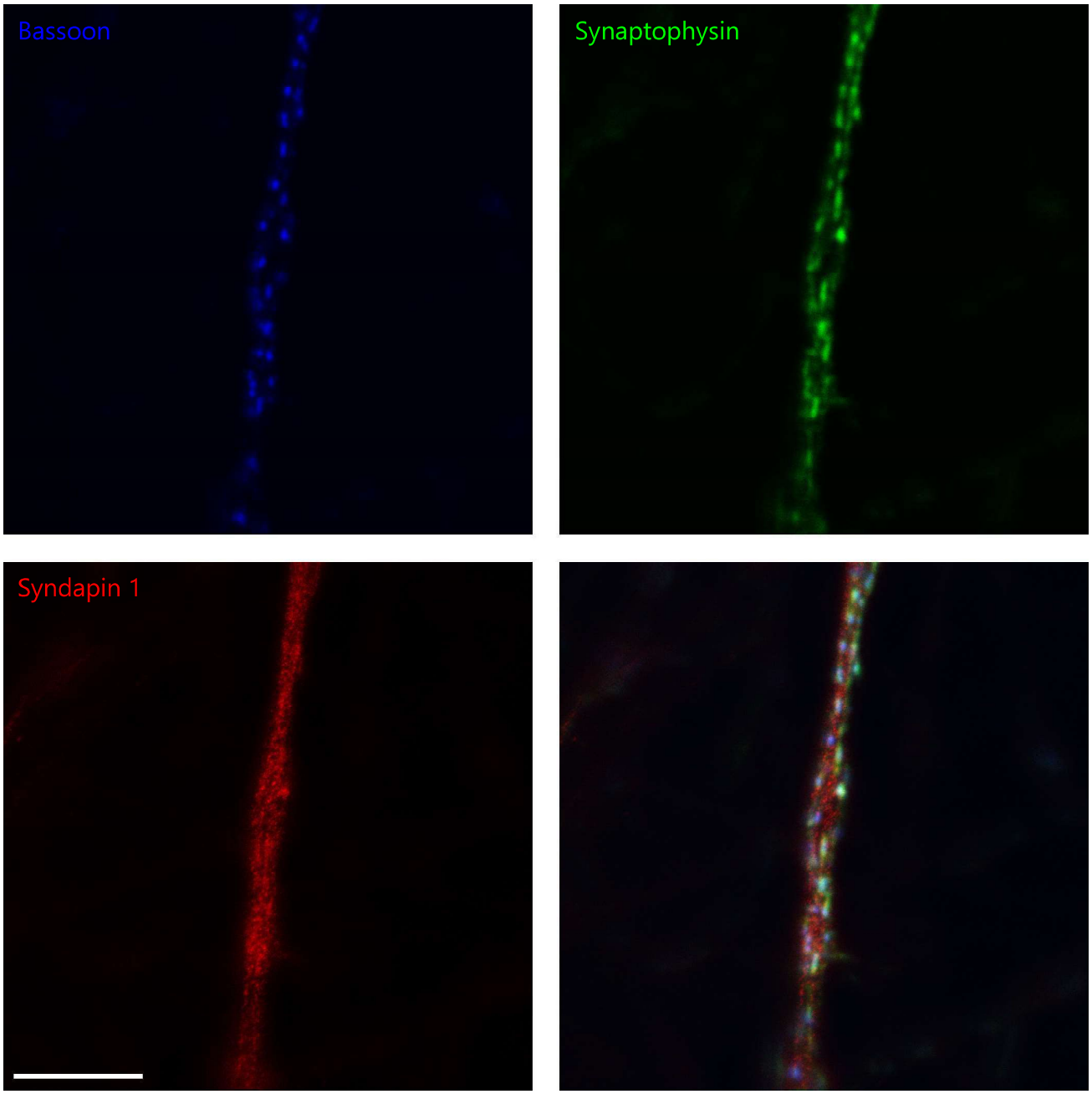

Scale bar: 5 µm

Antibodies used:
Bassoon - Synaptic Systems (Göttingen, Germany), 141 021
Synaptophysin - Synaptic Systems (Göttingen, Germany), 101 011
Syndapin 1 - Novus Biologicals (Littleton, Colorado, USA), H00029993-B01

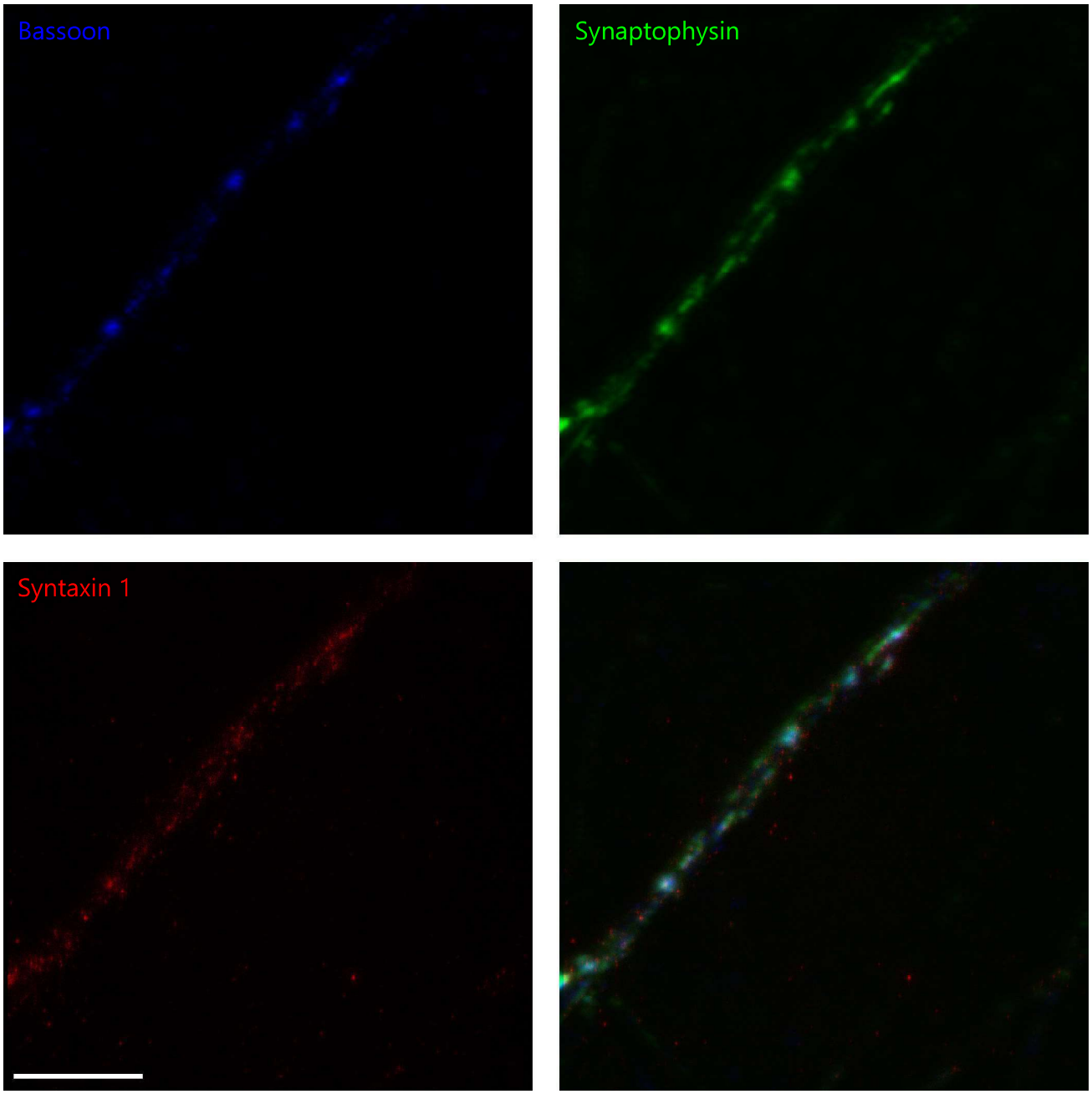

Scale bar: 5 µm

Antibodies used:
Bassoon - Synaptic Systems (Göttingen, Germany), 141 021
Synaptophysin - Synaptic Systems (Göttingen, Germany), 101 011
Syntaxin 1 - Reinhard Jahn (MPI-BPC, Göttingen, Germany)

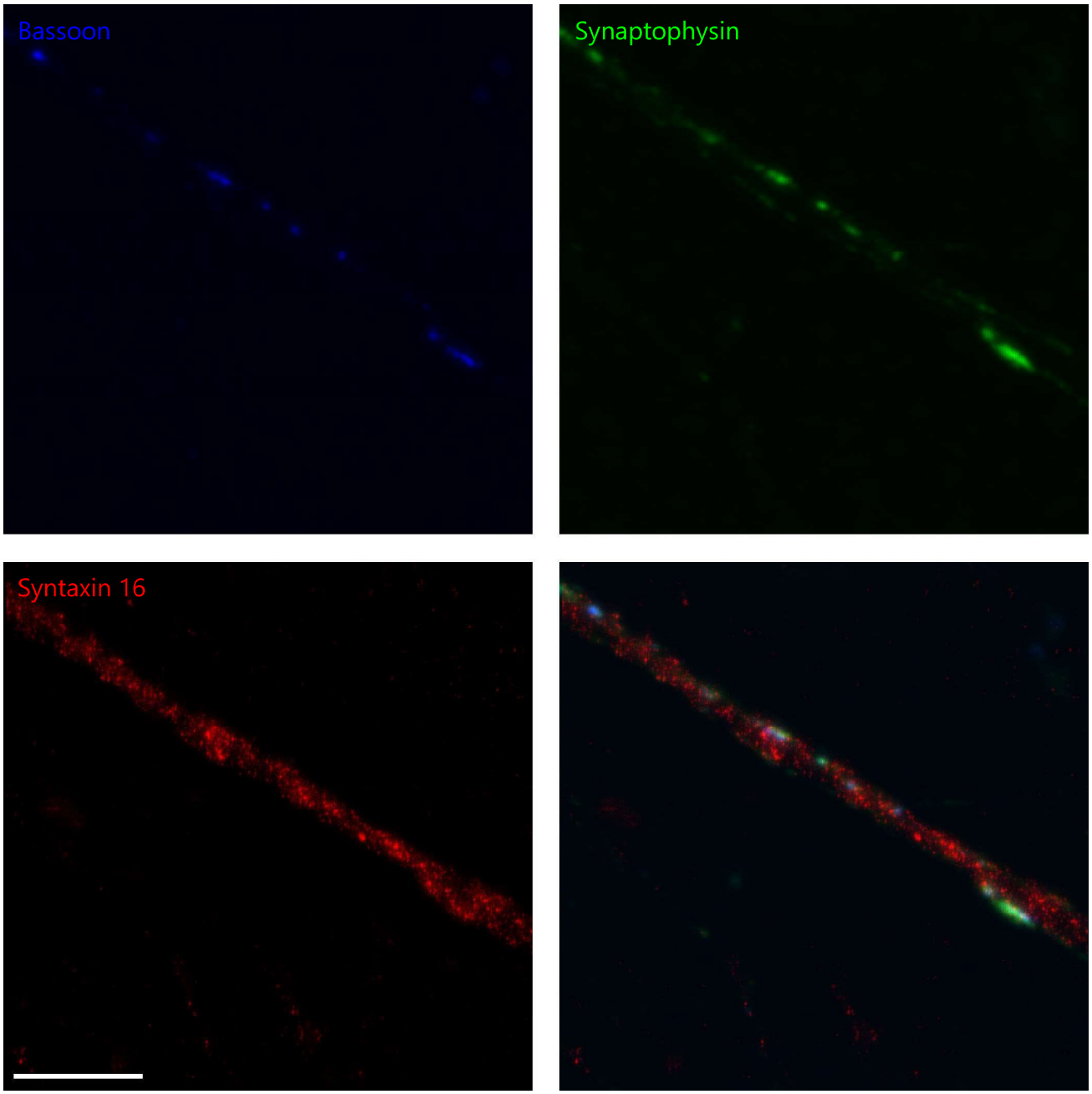

Scale bar: 5 µm

Antibodies used:
Bassoon - Synaptic Systems (Göttingen, Germany), 141 021
Synaptophysin - Synaptic Systems (Göttingen, Germany), 101 011
Syntaxin 16 - Synaptic Systems (Göttingen, Germany), 110 162

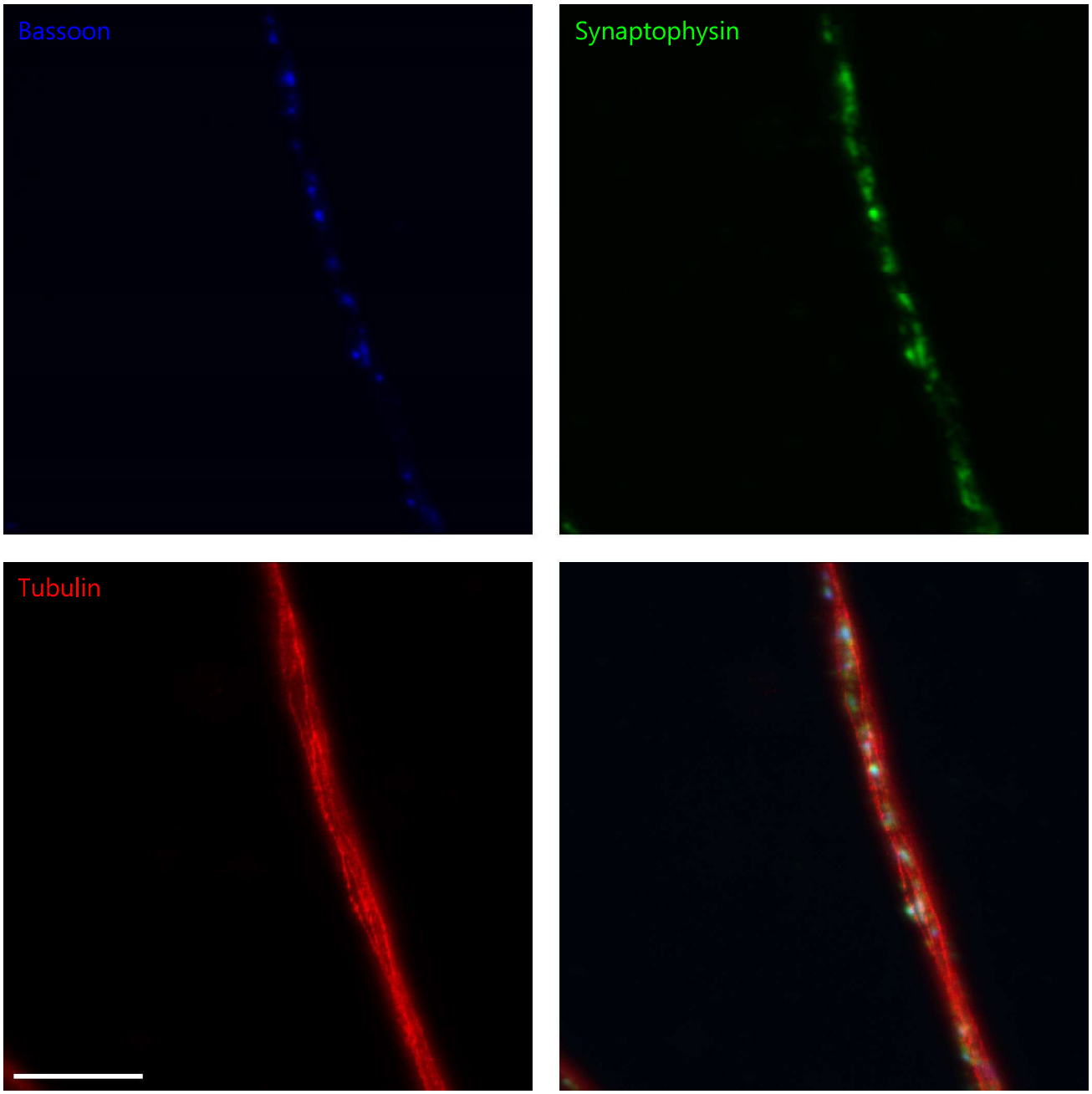

Scale bar: 5 µm

Antibodies used:
Bassoon - Synaptic Systems (Göttingen, Germany), 141 021
Synaptophysin - Synaptic Systems (Göttingen, Germany), 101 011
Tubulin - Synaptic Systems (Göttingen, Germany), 302 203

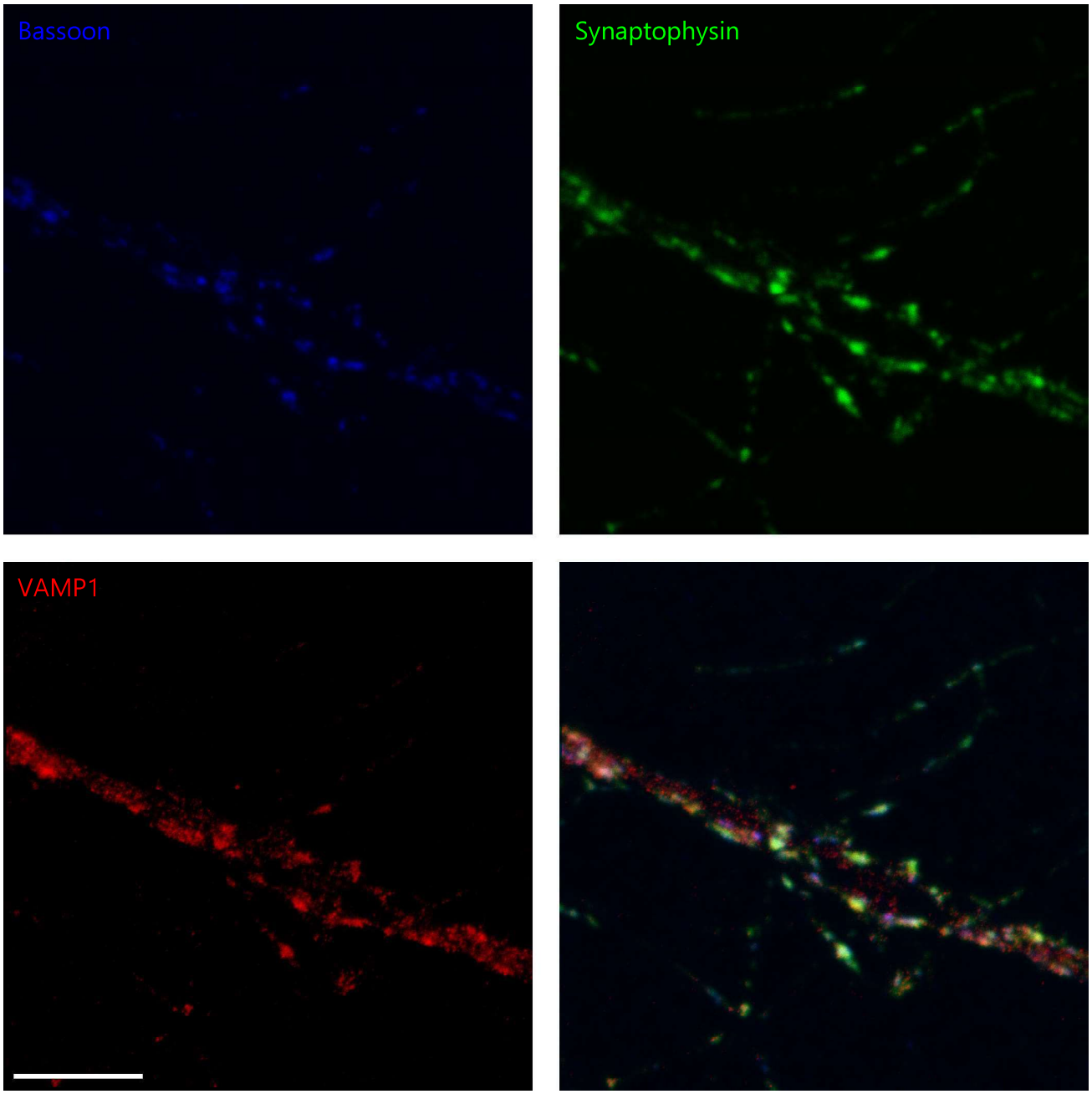

Scale bar: 5 µm

Antibodies used:
Bassoon - Synaptic Systems (Göttingen, Germany), 141 021
Synaptophysin - Synaptic Systems (Göttingen, Germany), 101 011
VAMP1 - Synaptic Systems (Göttingen, Germany), 104 002

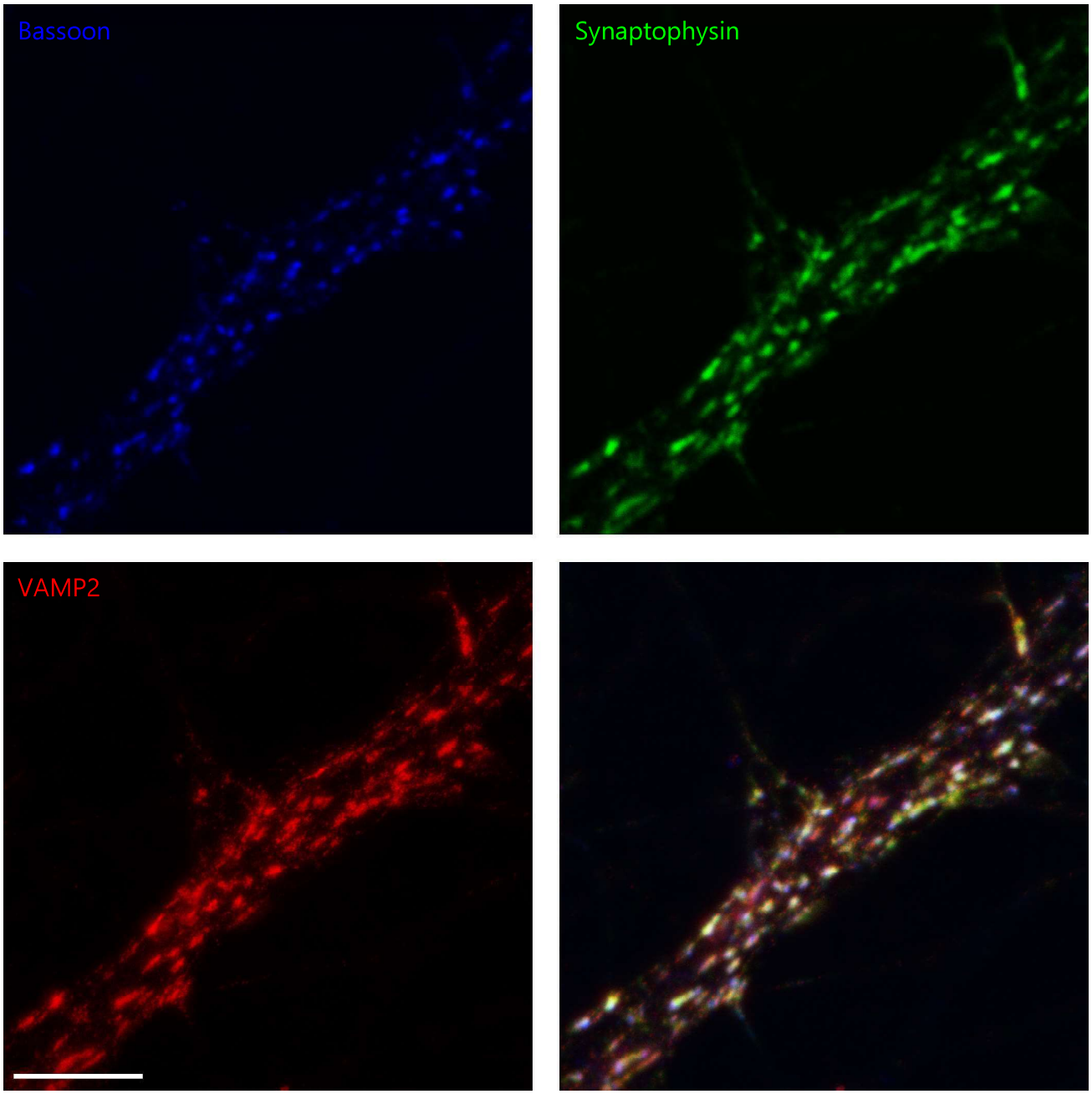

Scale bar: 5 µm

Antibodies used:
Bassoon - Synaptic Systems (Göttingen, Germany), 141 021
Synaptophysin - Synaptic Systems (Göttingen, Germany), 101 011
VAMP2 - Synaptic Systems (Göttingen, Germany), 104 211

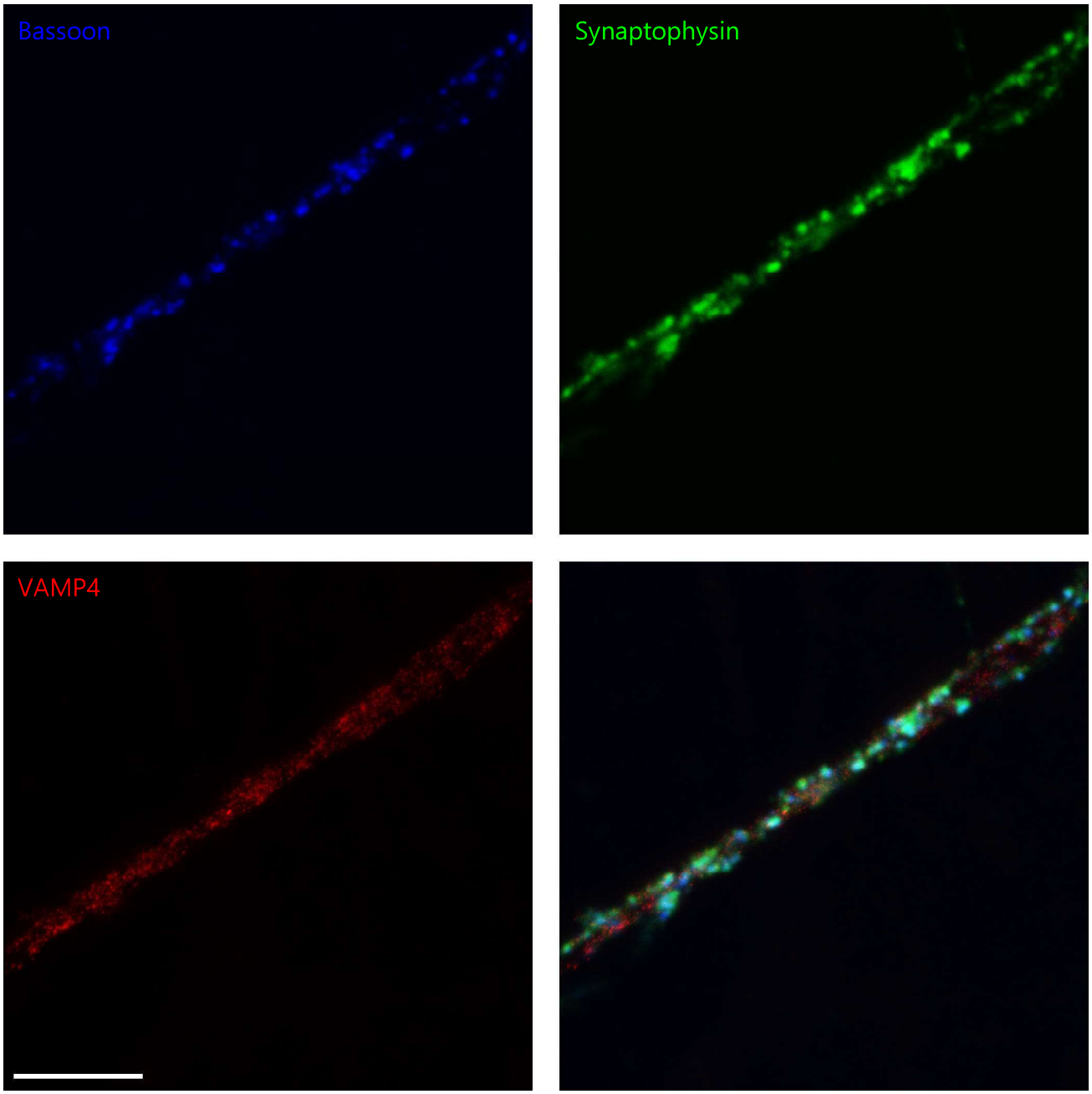

Scale bar: 5 µm

Antibodies used:
Bassoon - Synaptic Systems (Göttingen, Germany), 141 021
Synaptophysin - Synaptic Systems (Göttingen, Germany), 101 011
VAMP4 - Synaptic Systems (Göttingen, Germany), 136 002

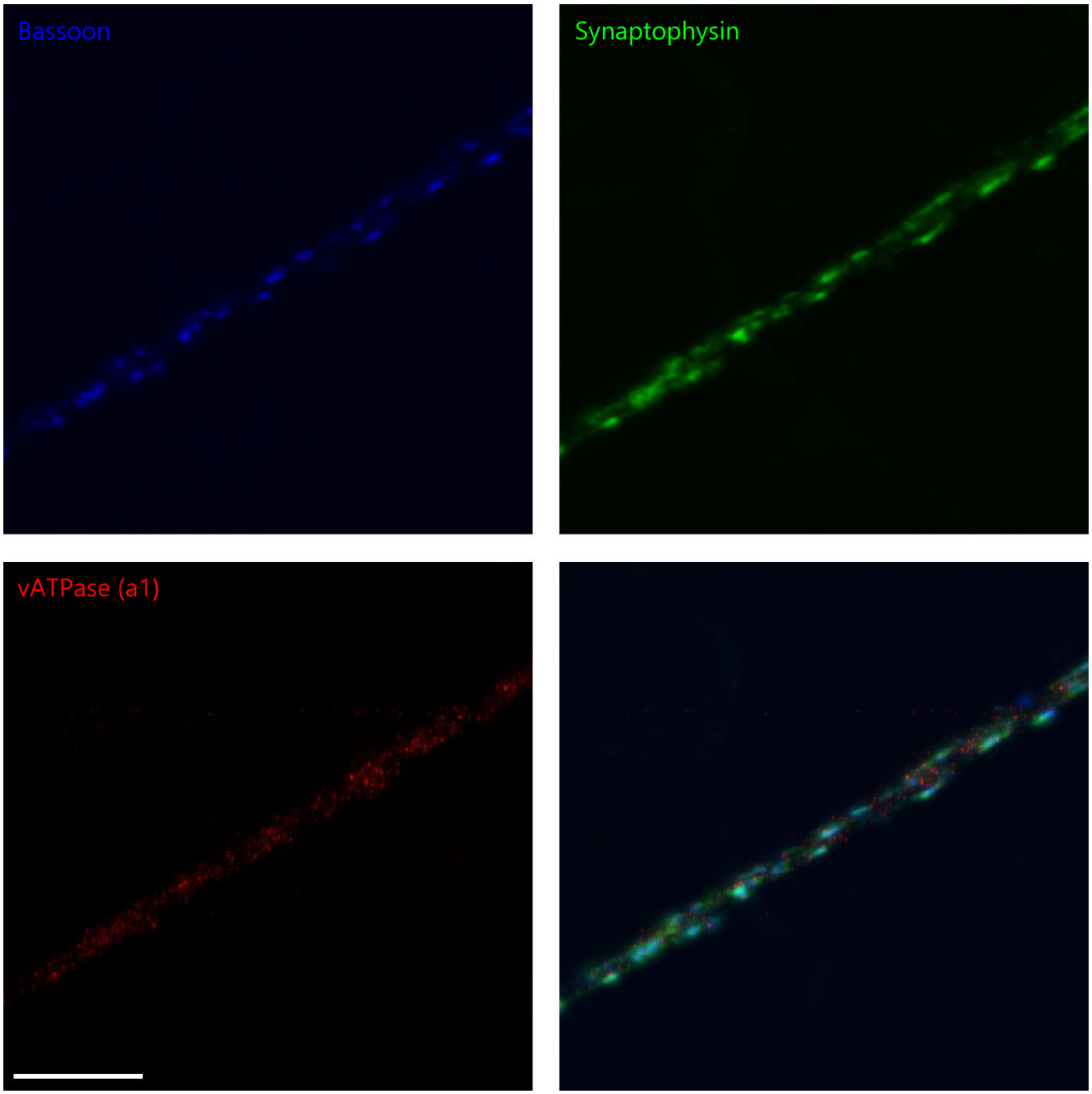

Scale bar: 5 µm

Antibodies used:
Bassoon - Synaptic Systems (Göttingen, Germany), 141 021
Synaptophysin - Synaptic Systems (Göttingen, Germany), 101 011
vATPase (a1) - Synaptic Systems (Göttingen, Germany), 109 002

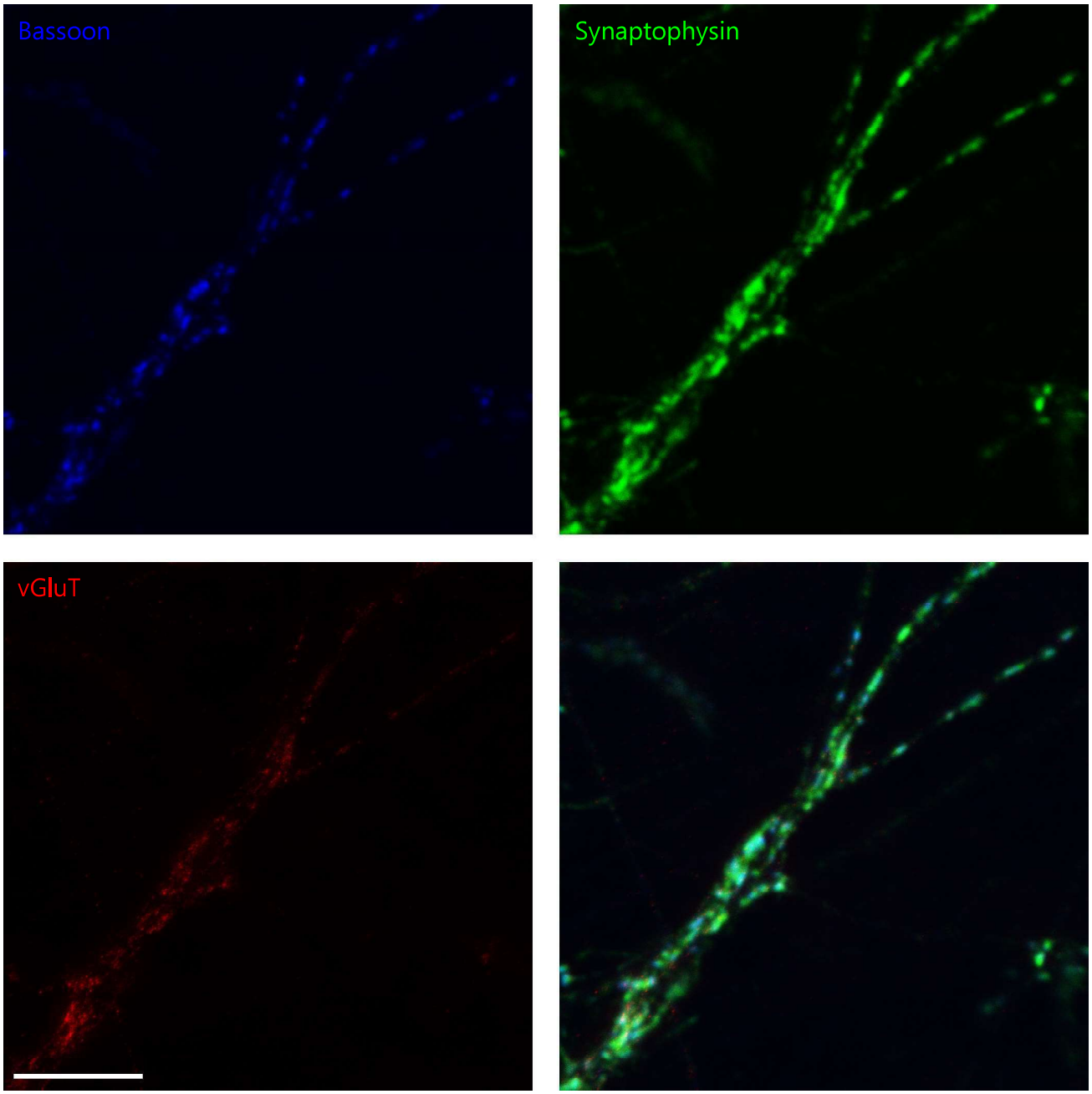

Scale bar: 5 µm

Antibodies used:
Bassoon - Synaptic Systems (Göttingen, Germany), 141 021
Synaptophysin - Synaptic Systems (Göttingen, Germany), 101 011
vGluT - Synaptic Systems (Göttingen, Germany), 135 503

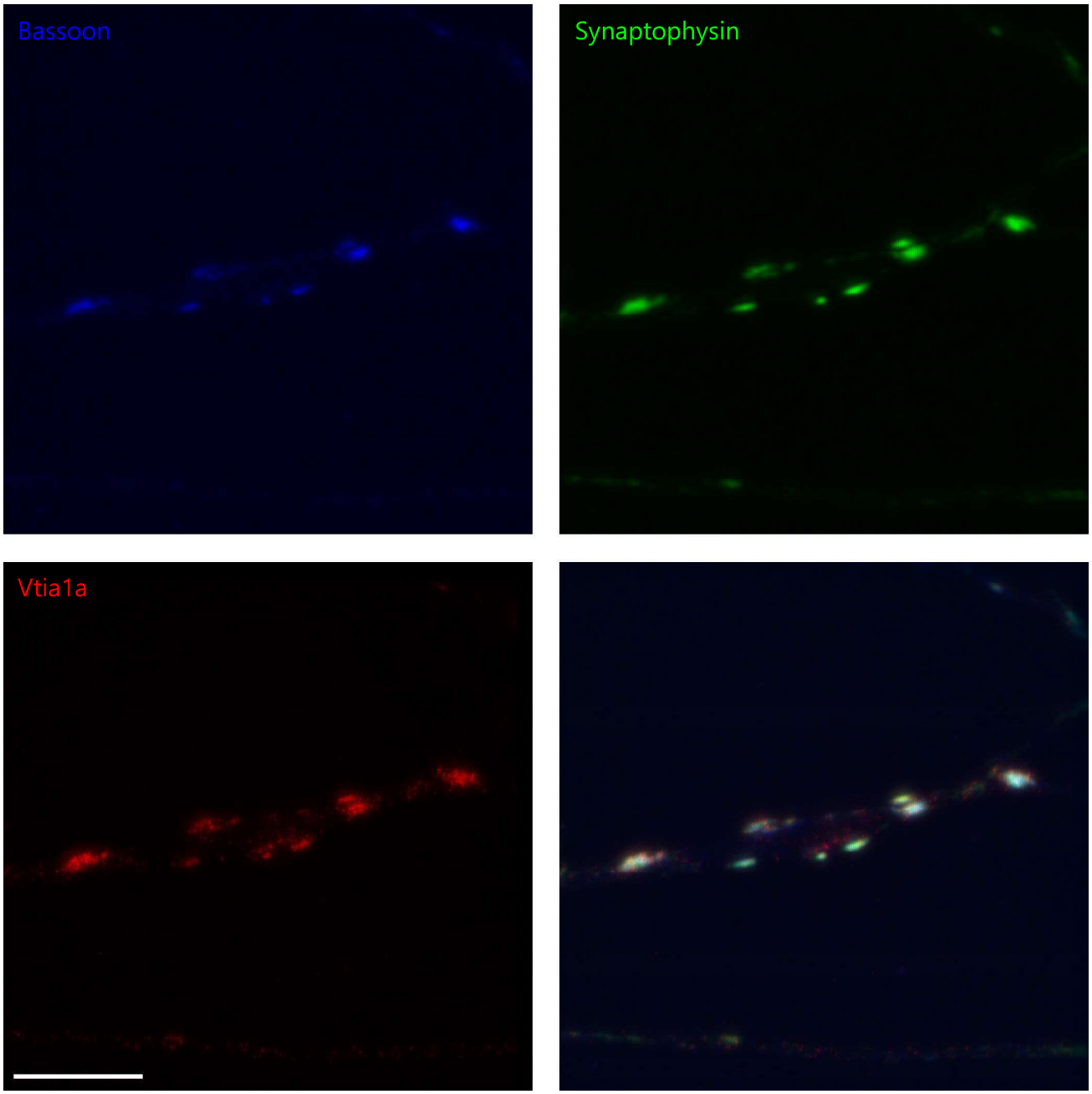

Scale bar: 5 µm

Antibodies used:
Bassoon - Synaptic Systems (Göttingen, Germany), 141 021
Synaptophysin - Synaptic Systems (Göttingen, Germany), 101 011
Vtia1a - BD Biosciences (Heidelberg, Germany), 611220

Multi-page figure

Appendix Fig. S3. Measured FRAP parameters for each individual protein. Please follow the graphical legend presented on the first page of this figure. The box plots are organized as follows: the middle line shows the median; the box edges indicate the 25th percentile; the error bars show the 75th percentile; the symbols show the 90th percentile.

protein name

MW (kDa)	Category	τ_{axon} (s)	$\tau_{synapse}$ (s)	IF_{axon} (%)	$IF_{synapse}$ (%)
molecular weight	category according to localization and function	mean time constant in axon ± SEM	mean time constant in synapse ± SEM	mean immobile fraction in axon ± SEM	mean immobile fraction in synapse ± SEM

-1.7 s 0.5 s 1 s 3 s 10 s 20 s 40 s 82 s

Axon

Examplary frames from a typical FRAP experiment in axonal regions. First post-bleach frame is labeled 0.5 s. 8 frames of a total of 76 frames taken in each experiment are shown. Scale bar, 500 nm. The panel is empty if the protein cannot be found in axons.

Synapse

Examplary frames from a typical FRAP experiment in synapses. First post-bleach frame is labeled 0.5 s. 8 frames of a total of 76 frames taken in each experiment are shown. Scale bar, 500 nm.

Average FRAP curves recorded in axons (blue) and synapses (green). Shaded area represents SEM.

Box plot of time constants in axons and synapses. Asterisks denote significant differences.

Box plot of immobile fractions in axons and synapses. Asterisks denote significant differences.

Number of FRAP experiments done in axonal regions and synapses. P-values are shown when the difference is significant for FDR = 0.05, using the Benjamini-Hochberg procedure for multiple testing correction.

Tagged protein outline:

Schematic representation of the expressed protein. The relative sizes of the fluorescent tag, linker region and the protein of interest are preserved. The sequence of linker region is shown in one-letter amino acid code. The reference number of the mRNA sequence is shown below the protein of interest.

List of proteins with significantly different values for the time constants or immobile fractions in axons or synapses, in comparison to the protein of interest. Kruskal-Wallis tests were followed by Wilcoxon rank-sum tests, with a Bonferroni multiple test correction; corrected p-values are shown.

References

β-Actin

MW (kDa)	Category	τ_{axon} (s)	$\tau_{synapse}$ (s)	IF_{axon} (%)	$IF_{synapse}$ (%)
41.7	cytoskeletal	1.37 ± 0.11	6.35 ± 0.79	28.40 ± 4.59	13.19 ± 8.88

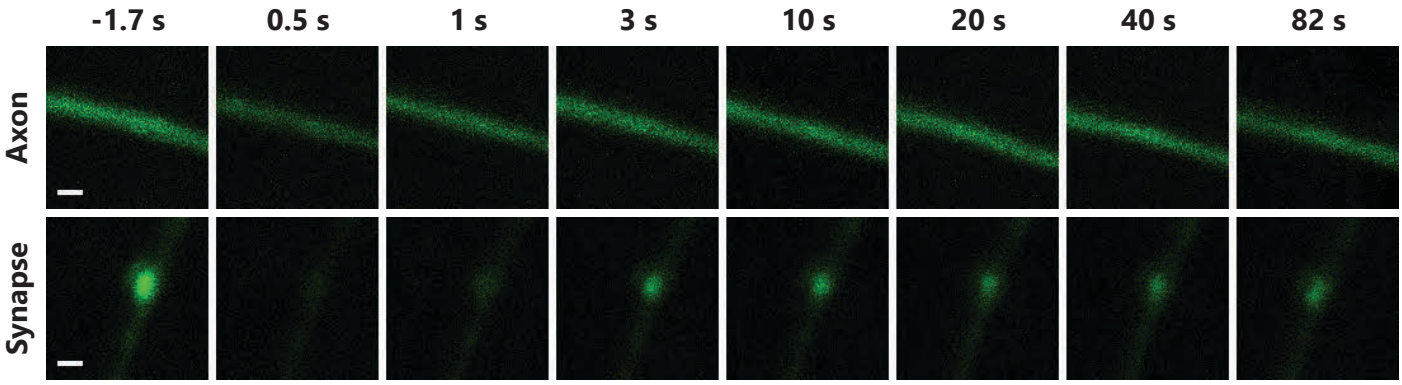

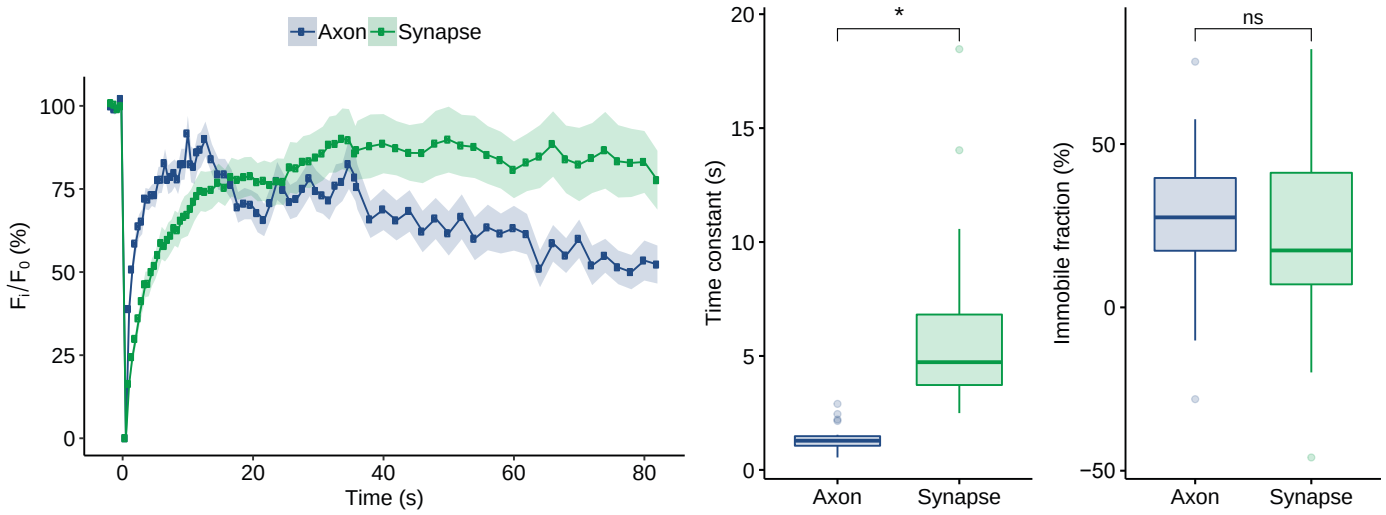

N (axons) = 24, N (synapses) = 26; p (time constant) = 3.03E-09.

Tagged protein outline:

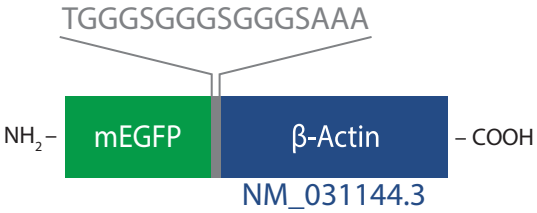

Time constant (axon) is significantly different from time constant (axon) of: Amphiphysin (p = 2.47E-04), Complexin 2 (p = 2.23E-02), Endophilin (p = 1.44E-02), PIPKgamma (p = 2.75E-02), Rab3 (p = 3.28E-03), SNAP23 (p = 6.86E-03), SNAP29 (p = 4.97E-05), Synapsin (p = 2.82E-02), Synaptotagmin 1 (p = 1.97E-03), Synaptotagmin 7 (p = 9.12E-03), Syntaxin 1 (p = 3.88E-04), Syntaxin 16 (p = 4.95E-05), VAMP 1 (p = 1.96E-04).
Immobile fraction (axon) is not significantly different from immobile fraction (axon) of any other proteins.
Time constant (synapse) is significantly different from time constant (synapse) of: Calmodulin (p = 4.78E-02), Hsc70 (p = 1.82E-02), Synapsin (p = 1.04E-02), Synaptogyrin (p = 1.08E-04), Synaptophysin (p = 1.04E-05), Synaptotagmin 1 (p = 4.59E-06), Syntaxin 16 (p = 2.66E-02), VAMP 1 (p = 2.70E-03), mEGFP (p = 5.73E-09), vGlut (p = 6.74E-05).
Immobile fraction (synapse) is significantly different from immobile fraction (synapse) of: SV2B (p = 7.07E-06), Synaptogyrin (p = 3.08E-02), Synaptophysin (p = 1.04E-05), vATPase (p = 4.02E-02), vGlut (p = 1.54E-03).

References

Sankaranarayanan, S., et al. (2003). Nat Neurosci 6, 127-35

α-SNAP

MW (kDa)	Category	τ_{axon} (s)	$\tau_{synapse}$ (s)	IF_{axon} (%)	$IF_{synapse}$ (%)
33.2	soluble, SNARE co-factor	2.40 ± 0.46	5.25 ± 0.47	9.71 ± 5.66	26.74 ± 4.27

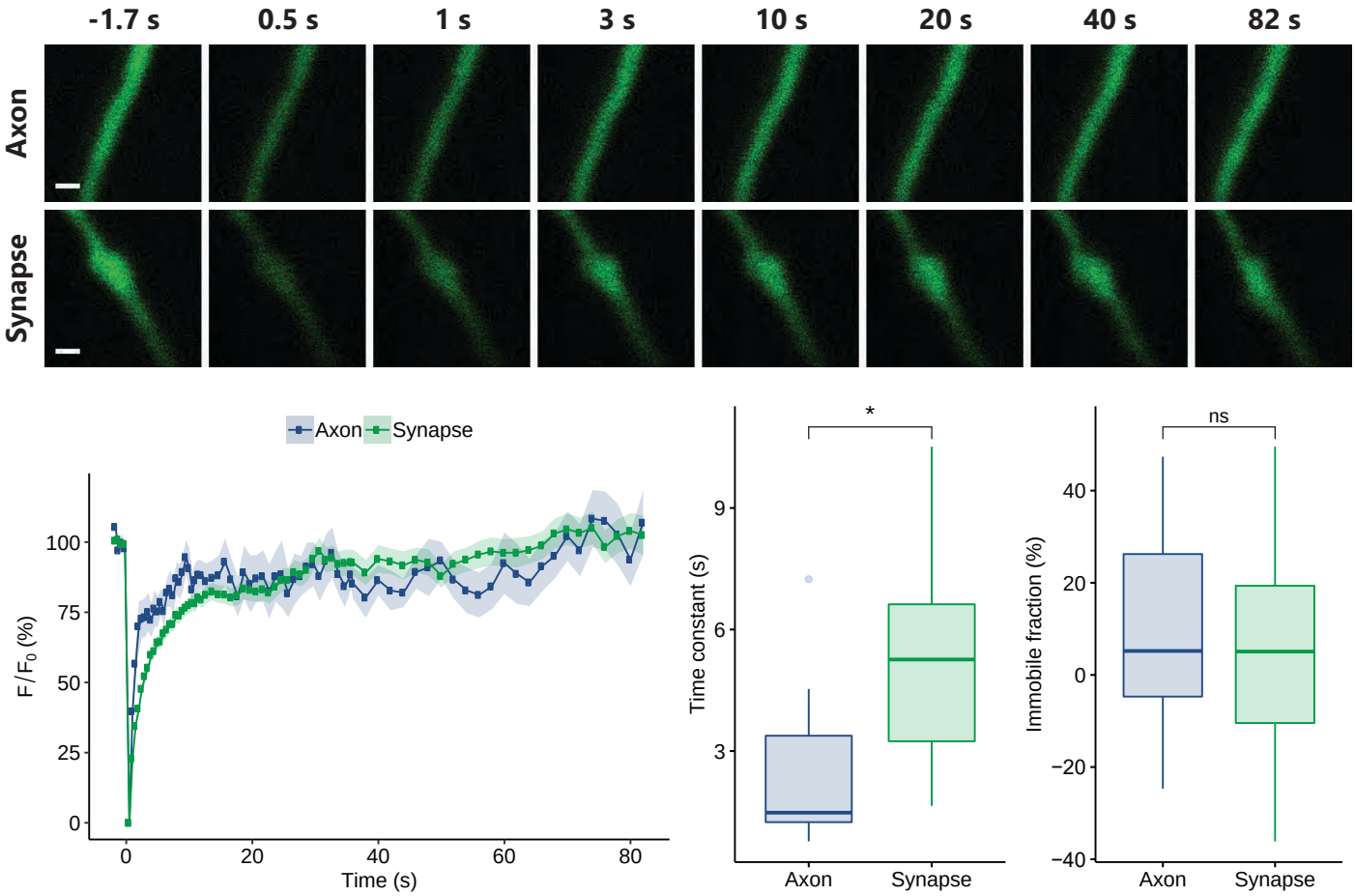

N (axons) = 15, N (synapses) = 25; p (time constant) = 2.26E-04.

Tagged protein outline:

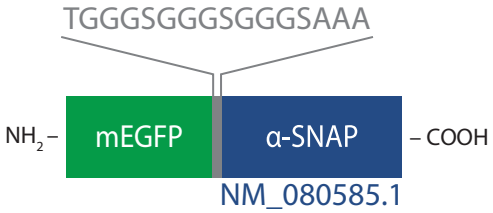

Time constant (axon) is not significantly different from time constant (axon) of any other proteins.
Immobile fraction (axon) is not significantly different from immobile fraction (axon) of any other proteins.
Time constant (synapse) is significantly different from time constant (synapse) of: mEGFP (p = 1.12E-06), SCAMP1 (p = 1.16E-02), Synapsin 1A (p = 4.39E-04), Synaptogyrin (p = 4.97E-05), Synaptophysin (p = 1.47E-06), Synaptotagmin 1 (p = 3.37E-07), Syntaxin 16 (p = 2.97E-03), alpha-Tubulin 1b (p = 3.00E-02), VAMP1 (p = 5.23E-05), vGluT1 (p = 5.86E-06).
Immobile fraction (synapse) is significantly different from immobile fraction (synapse) of: NSF (p = 1.23E-03), SCAMP1 (p = 8.31E-03), SV2B (p = 5.49E-07), Synaptogyrin (p = 7.39E-04), Synaptophysin (p = 2.06E-07), Synaptotagmin 1 (p = 4.68E-04), VAMP2 (p = 3.23E-03), VAMP4 (p = 2.25E-03), vATPase V0a1 (p = 7.38E-05), vGluT1 (p = 1.35E-05).

References

Söllner, T. (1993b). Nature 362, 318-24.
Jahn, R., and Scheller, R.H. (2006). Nat Rev Mol Cell Biol 7, 631-43.

α-synuclein

MW (kDa)	Category	τ_{axon} (s)	$\tau_{synapse}$ (s)	IF_{axon} (%)	$IF_{synapse}$ (%)
14.5	soluble, vesicle tethering	2.41 ± 0.41	6.07 ± 0.72	18.91 ± 4.30	26.74 ± 4.27

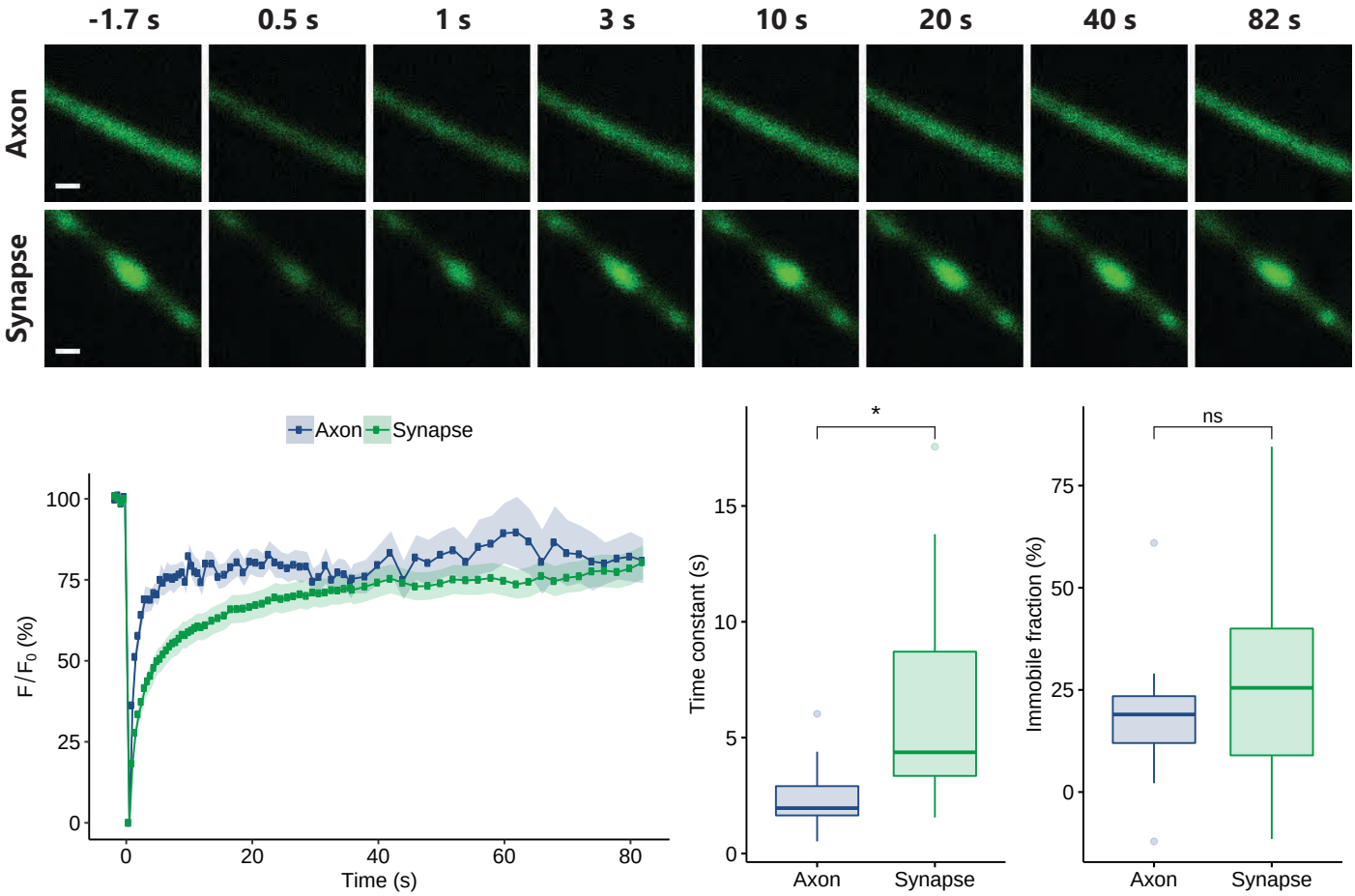

N (axons) = 14, N (synapses) = 31; p (time constant) = 3.28E-04.

Tagged protein outline:

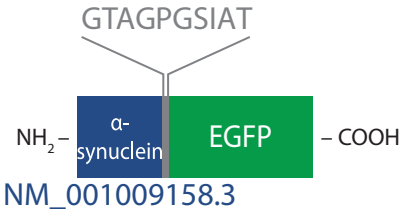

NM_001009158.3

Time constant (axon) is not significantly different from time constant (axon) of any other proteins.
Immobile fraction (axon) is not significantly different from immobile fraction (axon) of any other proteins.
Time constant (synapse) is significantly different from time constant (synapse) of: mEGFP (p = 3.02E-08), Synapsin 1A (p = 4.14E-03), Synaptogyrin (p = 1.85E-05), Synaptophysin (p = 1.13E-06), Synaptotagmin 1 (p = 1.00E-06), Syntaxin 16 (p = 1.06E-02), VAMP1 (p = 1.08E-03), vGluT1 (p = 2.02E-05).
Immobile fraction (synapse) is significantly different from immobile fraction (synapse) of: SV2B (p = 2.43E-06), Synaptogyrin (p = 2.02E-02), Synaptophysin (p = 3.63E-06), vGluT1 (p = 1.69E-03).

References

Scott, D., and Roy, S. (2012). J Neurosci 32, 10129-35.
Marques, O., and Outeiro, T.F. (2012). Cell Death Dis 2, 140-51.

Amphiphysin

MW (kDa)	Category	τ_{axon} (s)	$\tau_{synapse}$ (s)	IF_{axon} (%)	$IF_{synapse}$ (%)
74.88	soluble, endocytic	3.22 ± 0.27	6.77 ± 0.43	18.62 ± 5.77	22.93 ± 6.18

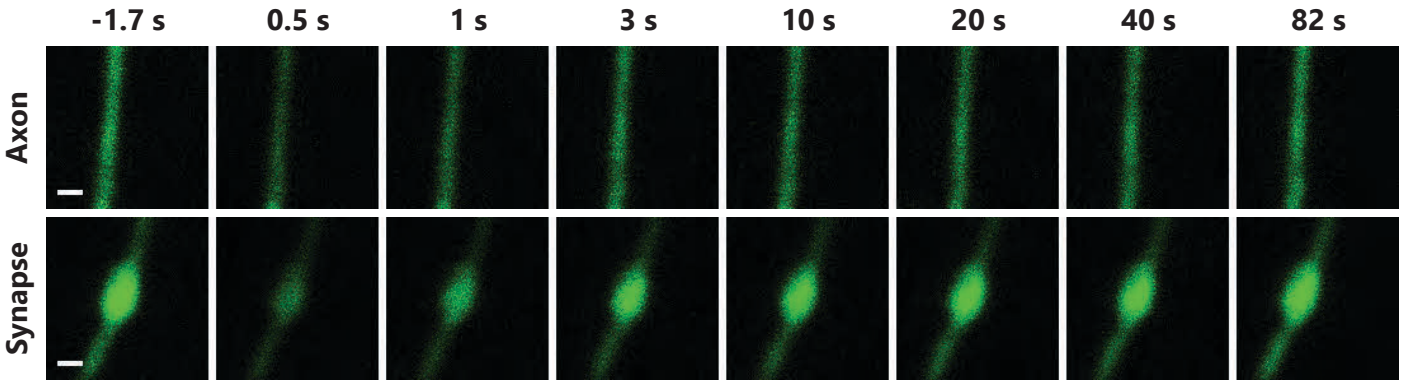

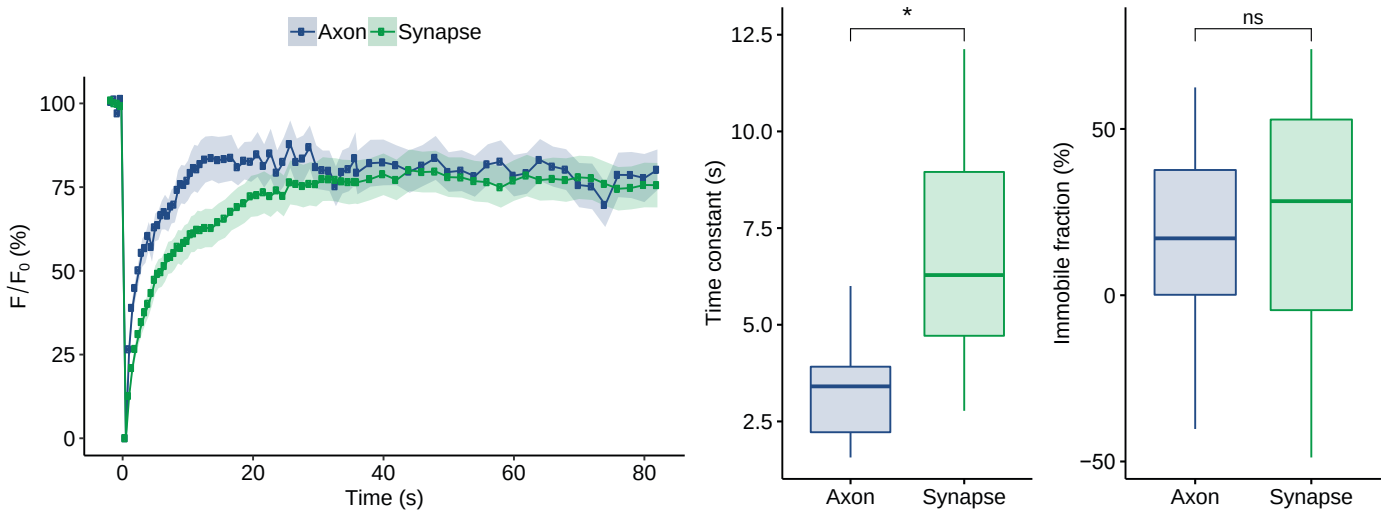

N (axons) = 22, N (synapses) = 35; p (time constant) = 1.49E-07.

Tagged protein outline:

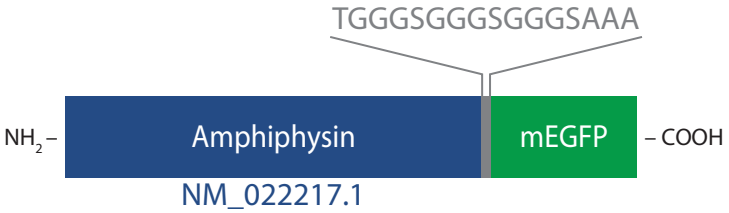

Time constant (axon) is significantly different from time constant (axon) of: Actin (p = 2.47E-04), Clathrin light chain B (p = 4.64E-02), Doc2a (p = 1.16E-02), Munc13 (p = 2.42E-04), Rab5a (p = 1.32E-02), Rab7a (p = 2.79E-02).
Immobile fraction (axon) is not significantly different from immobile fraction (axon) of any other proteins.
Time constant (synapse) is significantly different from time constant (synapse) of: AP2 (p = 2.45E-04), Calmodulin 1 (p = 9.23E-06), Clathrin light chain B (p = 5.44E-05), Complexin 1 (p = 3.63E-03), Endophilin A1 (p = 3.36E-02), Hsc70 (p = 9.52E-07), mEGFP (p = 4.74E-13), Munc13 (p = 1.07E-03), NSF (p = 1.15E-03), Rab3a (p = 3.21E-02), Rab5a (p = 3.19E-04), Rab7a (p = 1.60E-02), Septin 5 (p = 2.64E-02), SNAP23 (p = 2.71E-04), SNAP25 (p = 2.71E-03), Synapsin 1A (p = 1.34E-03), Synaptogyrin (p = 1.88E-05), Synaptophysin (p = 1.85E-07), Synaptotagmin 1 (p = 7.09E-08), VAMP1 (p = 2.45E-04), vGluT1 (p = 6.32E-06).
Immobile fraction (synapse) is significantly different from immobile fraction (synapse) of: SV2B (p = 1.24E-06), Synaptogyrin (p = 2.05E-02), Synaptophysin (p = 1.92E-06), vGluT1 (p = 2.46E-03).

References

Wigge, P., et al. (1997). Mol Biol Cell 8, 2003-15.
Shupliakov, O., et al. (1997). Science 276, 259-63.

AP180

MW (kDa)	Category	τ_{axon} (s)	$\tau_{synapse}$ (s)	IF_{axon} (%)	$IF_{synapse}$ (%)
93.52	soluble, endocytic	1.81 ± 0.21	4.51 ± 0.35	29.24 ± 4.81	7.06 ± 3.69

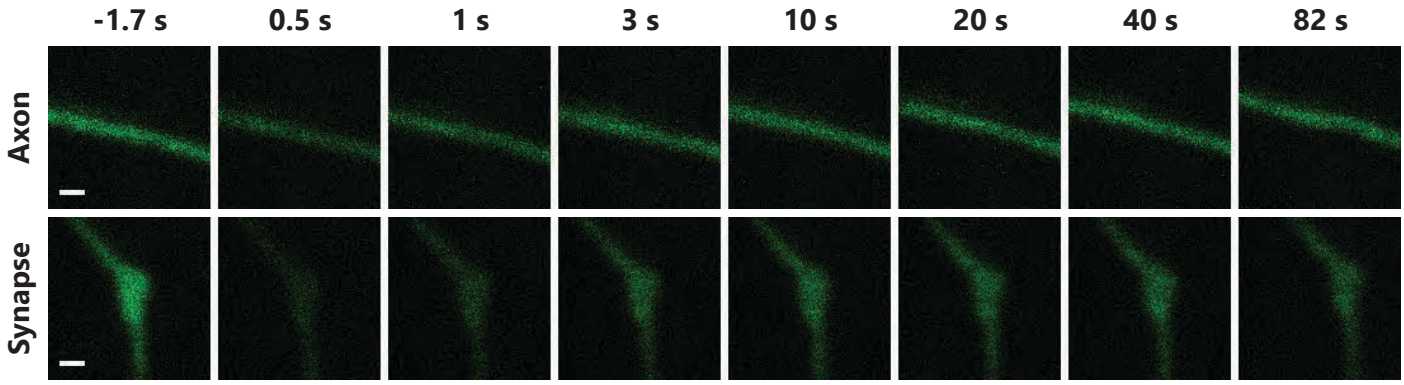

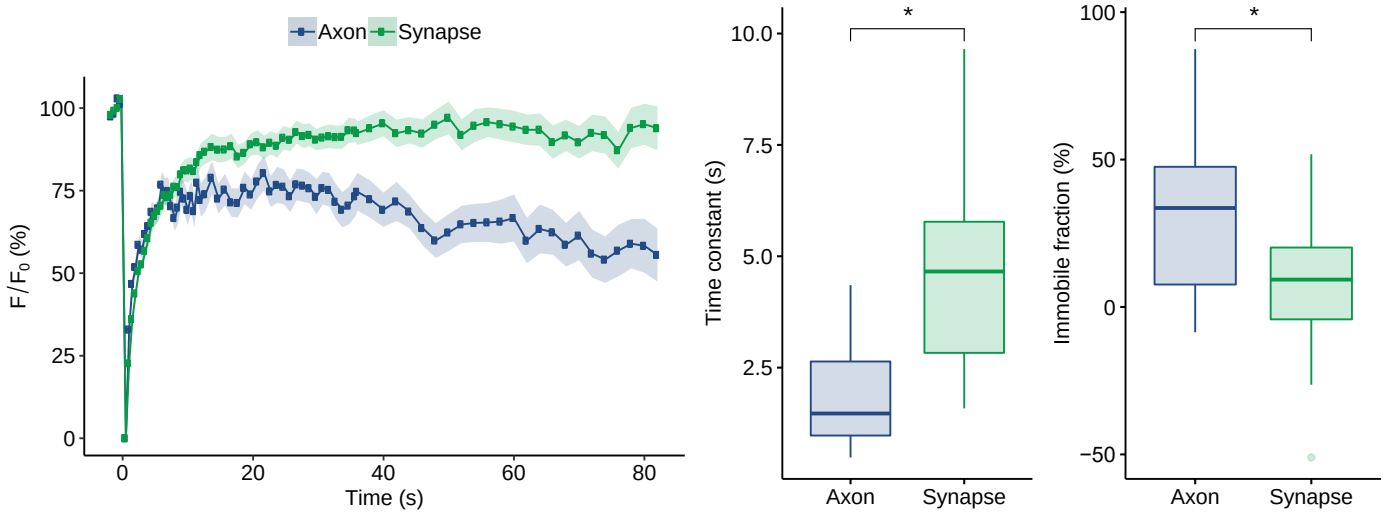

N (axons) = 27, N (synapses) = 33; p (time constant) = 1.83E-07, p (immobile fraction) = 2.44E-03.

Tagged protein outline:

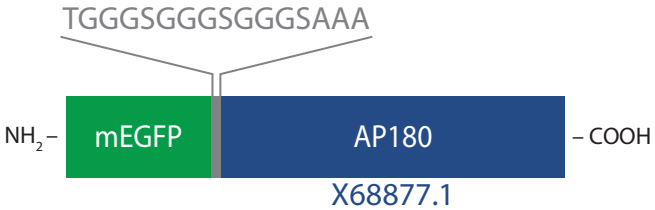

Time constant (axon) is significantly different from time constant (axon) of: SNAP29 (p = 3.55E-02), Synaptotagmin 1 (p = 1.78E-03).
Immobile fraction (axon) is not significantly different from immobile fraction (axon) of any other proteins.
Time constant (synapse) is significantly different from time constant (synapse) of: Dynamin 1 (p = 3.44E-03), mEGFP (p = 5.24E-06), SCAMP1 (p = 1.91E-04), SV2B (p = 9.12E-03), Synapsin 1A (p = 2.84E-05), Synaptogyrin (p = 3.84E-06), Synaptophysin (p = 2.55E-08), Synaptotagmin 1 (p = 6.50E-09), Syntaxin 16 (p = 1.31E-05), alpha-Tubulin 1b (p = 5.43E-04), VAMP1 (p = 1.28E-06), vATPase V0a1 (p = 2.44E-02), vGluT1 (p = 3.07E-08), Vti1a-beta (p = 4.68E-03).
Immobile fraction (synapse) is significantly different from immobile fraction (synapse) of: NSF (p = 1.21E-04), SCAMP1 (p = 3.25E-03), SV2B (p = 1.74E-08), Synaptogyrin (p = 2.45E-04), Synaptophysin (p = 4.81E-09), Synaptotagmin 1 (p = 4.74E-05), VAMP2 (p = 3.40E-04), VAMP4 (p = 6.80E-04), vATPase V0a1 (p = 5.64E-06), vGluT1 (p = 7.37E-07).

References

Morgan, J.R., et al. (2000). J Neurosci 20, 8667-76.
Nonet, M.L., et al. (1999). Mol Biol Cell 10, 2343-60.

AP2

MW (kDa)	Category	τ_{axon} (s)	$\tau_{synapse}$ (s)	IF_{axon} (%)	$IF_{synapse}$ (%)
104.05	soluble, endocytic	2.17 ± 0.17	3.56 ± 0.25	16.49 ± 3.86	7.99 ± 6.05

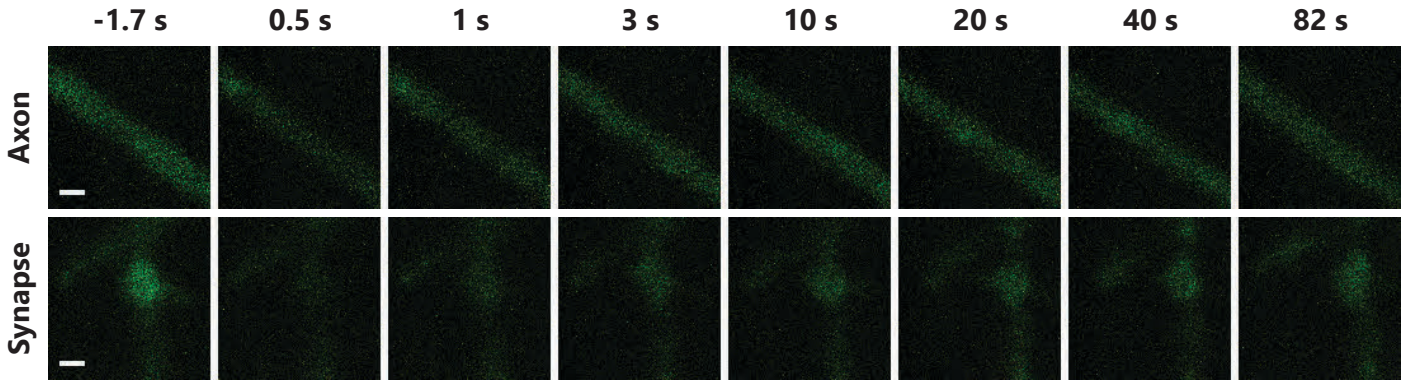

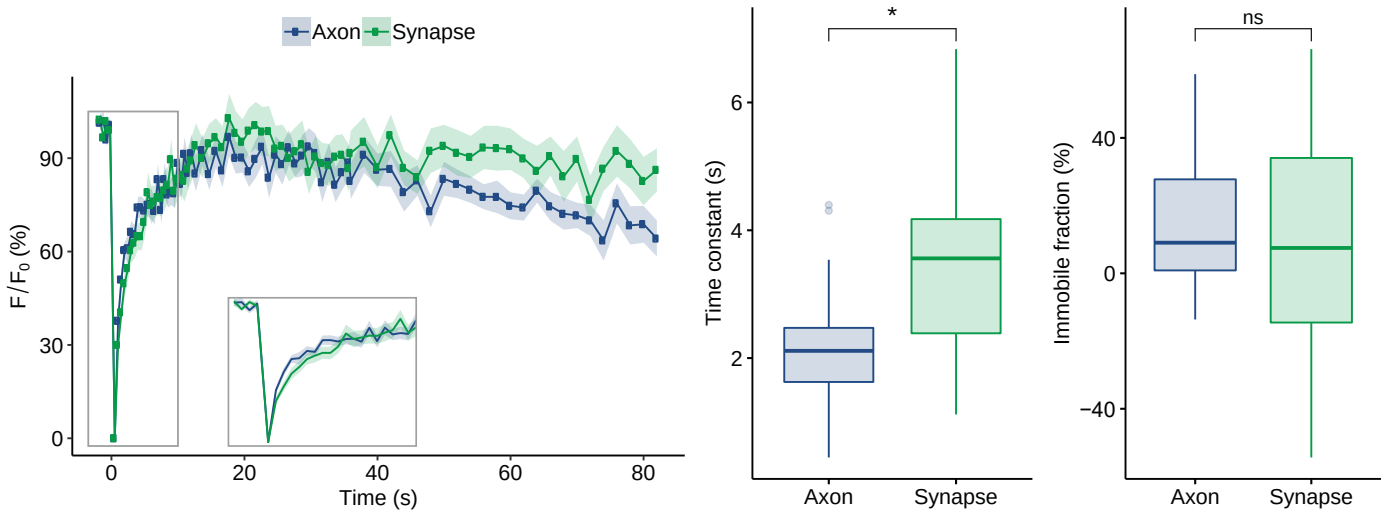

N (axons) = 28, N (synapses) = 28; p (time constant) = 1.49E-04.

Time constant (axon) is significantly different from time constant (axon) of: Synaptotagmin 1 (p = 2.10E-03).
Immobile fraction (axon) is not significantly different from immobile fraction (axon) of any other proteins.
Time constant (synapse) is significantly different from time constant (synapse) of: Amphiphysin (p = 2.45E-04), Dynamin 1 (p = 3.03E-04), Epsin (p = 1.12E-03), , ITSN 1-L (p = 1.56E-03), mEGFP (p = 2.68E-04), PIP5KI-gamma (p = 1.77E-04), SCAMP1 (p = 2.62E-05), SV2B (p = 6.85E-03), Synapsin 1A (p = 1.07E-05), Synaptogyrin (p = 2.85E-06), Synaptophysin (p = 7.96E-08), Synaptotagmin 1 (p = 3.69E-08), Synaptotagmin 7 (p = 4.55E-03), Syntaxin 1A (p = 4.35E-04), Syntaxin 16 (p = 2.81E-07), alpha-Tubulin 1b (p = 9.69E-05), VAMP1 (p = 1.14E-06), vATPase V0a1 (p = 6.28E-03), vGluT1 (p = 5.50E-08), Vti1a-beta (p = 1.78E-03).
Immobile fraction (synapse) is significantly different from immobile fraction (synapse) of: SCAMP1 (p = 2.74E-02), SV2B (p = 6.71E-07), Synaptogyrin (p = 1.46E-03), Synaptophysin (p = 2.53E-07), Synaptotagmin 1 (p = 2.81E-03), VAMP4 (p = 4.17E-02), vATPase V0a1 (p = 4.23E-04), vGluT1 (p = 6.70E-05).

References

Honing, S., et al. (2005). Mol Cell 18, 519-31. Collins, B.M., et al. (2002). Cell 109, 523-35. Takamori, S., et al. (2006). Cell 127, 831-46.

Calmodulin 1

MW (kDa)	Category	τ_{axon} (s)	$\tau_{synapse}$ (s)	IF_{axon} (%)	$IF_{synapse}$ (%)
16.84	soluble, calcium sensor	2.68 ± 0.25	3.04 ± 0.23	13.43 ± 2.77	20.43 ± 4.83

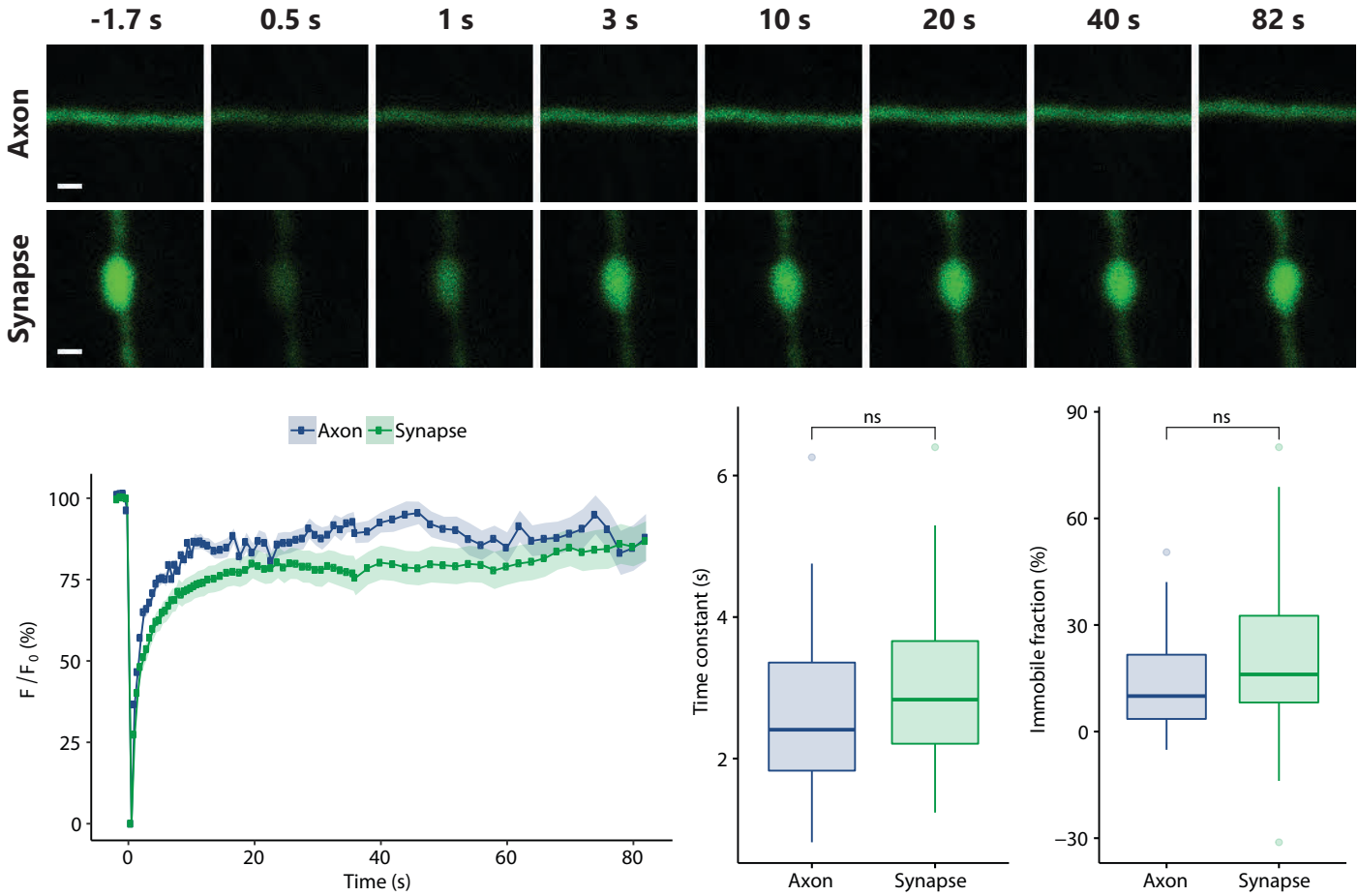

N (axons)=28, N (synapses)=28.

Tagged protein outline:

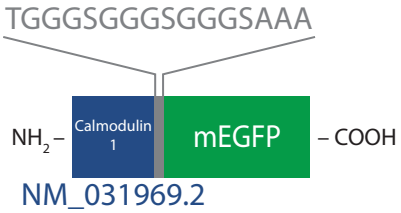

Time constant (axon) is signifi cantly different from time constant (axon) of: Synaptotagmin 1 (p = 2.13E-02). Immobile fraction (axon) is not signifi cantly different from immobile fraction (axon) of any other proteins. Time constant (synapse) is signifi cantly different from time constant (synapse) of: Actin (p = 4.78E-02), Amphiphysin (p = 9.23E06), CSP (p = 6.93E-03), Dynamin 1 (p = 1.55E-04), Epsin (p = 2.58E-04), ITSN 1-L (p = 3.96E-04), PIP5KI-gamma (p = 2.80E-05), SCAMP1 (p = 1.59E-05), SNAP29 (p = 1.67E-03), SV2B (p = 8.46E-04), Synapsin 1A (p = 4.45E-06), Synaptogyrin (p = 1.62E-06), Synaptophysin (p = 4.21E-08), Synaptotagmin 1 (p = 3.69E-08), Synaptotagmin 7 (p = 1.59E-04), Syndapin 1 (p = 1.06E-02), Syntaxin 1A (p = 2.00E-05), Syntaxin 16 (p = 4.02E-08), alpha-Tubulin 1b (p = 3.52E-05), VAMP1 (p = 4.98E-07), vATPase V0a1 (p = 1.96E-03), vGluT1 (p = 4.23E-08), Vti1a-beta (p = 5.24E-04). Immobile fraction (synapse) is signifi cantly different from immobile fraction (synapse) of: SV2B (p = 1.94E-06), Synaptogyrin (p = 1.32E-02), Synaptophysin (p = 1.98E-06), vATPase V0a1 (p = 1.37E-02), vGluT1 (p = 5.13E-04).

References

Chin, D., and Means, A.R. (2000). Trends Cell Biol 10, 322-28.
Quetglas, S., et al. (2002). EMBO J 21, 3970-9.
Igarashi, M., and Watanabe, M. (2007). Neurosci Res 58, 226-33.

Clathrin light chain

MW (kDa)	Category	τ_{axon} (s)	$\tau_{synapse}$ (s)	IF_{axon} (%)	$IF_{synapse}$ (%)
26.98	soluble, endocytic	1.61 ± 0.17	3.39 ± 0.26	23.69 ± 5.29	16.42 ± 6.71

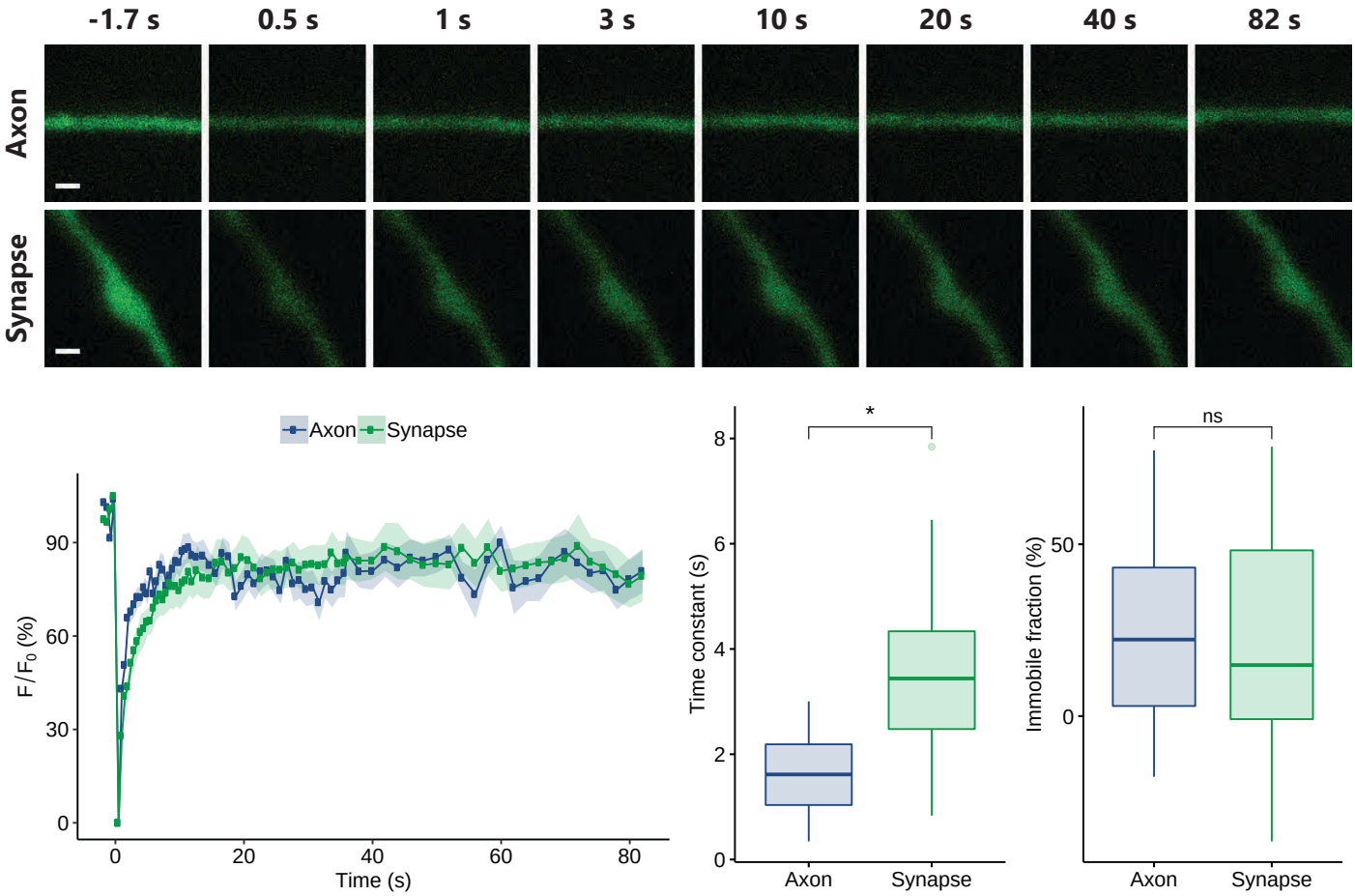

N (axons) = 22, N (synapses) = 33; p (time constant) = 6.86E-06.

Tagged protein outline:

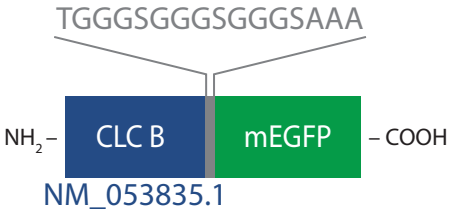

Time constant (axon) is significantly different from time constant (axon) of: Amphiphysin (p = 4.64E-02), SNAP29 (p = 5.30E-03), Synaptotagmin 1 (p = 2.01E-03), Syntaxin 1A (p = 3.07E-03), Syntaxin 16 (p = 1.74E-02), VAMP1 (p = 9.12E-03).
Immobile fraction (axon) is not significantly different from immobile fraction (axon) of any other proteins.
Time constant (synapse) is significantly different from time constant (synapse) of: Amphiphysin (p = 5.44E-05), CSP (p = 3.32E-02), Dynamin 1 (p = 2.81E-04), Epsin (p = 1.29E-03), ITSN 1-L (p = 2.89E-04), mEGFP (p = 4.03E-03), PIP5KI-gamma (p = 4.91E-05), SCAMP1 (p = 1.33E-05), SNAP29 (p = 1.62E-02), SV2B (p = 1.32E-03), Synapsin 1A (p = 3.95E-06), Synaptogyrin (p = 1.05E-06), Synaptophysin (p = 1.15E-08), Synaptotagmin 1 (p = 7.19E-09), Synaptotagmin 7 (p = 2.48E-03), Syntaxin 1A (p = 2.10E-04), Syntaxin 16 (p = 6.33E-08), alpha-Tubulin 1b (p = 3.75E-05), VAMP1 (p = 2.63E-07), vATPase V0a1 (p = 2.62E-03), vGluT1 (p = 2.09E-08), Vti1a-beta (p = 8.35E-04).
Immobile fraction (synapse) is significantly different from immobile fraction (synapse) of: SV2B (p = 6.61E-07), Synaptogyrin (p = 8.30E-03), Synaptophysin (p = 3.64E-06), vATPase V0a1 (p = 4.20E-02), vGluT1 (p = 1.13E-03).

References

Royle, S.J., Lagnado, L. (2010). Traffic 11, 1489-97.
Cheng, Y., et al. (2007). J Mol Biol 365, 892-9.
Wigge, P., et al. (1997). Mol Biol Cell 8, 2003-15.
Musacchio, A., et al. (1999). Mol Cell 3, 761-70.

Complexin 1

MW (kDa)	Category	τ_{axon} (s)	$\tau_{synapse}$ (s)	IF_{axon} (%)	$IF_{synapse}$ (%)
15.12	soluble, SNARE co-factor	2.64 ± 0.39	3.70 ± 0.40	19.24 ± 5.96	23.57 ± 2.89

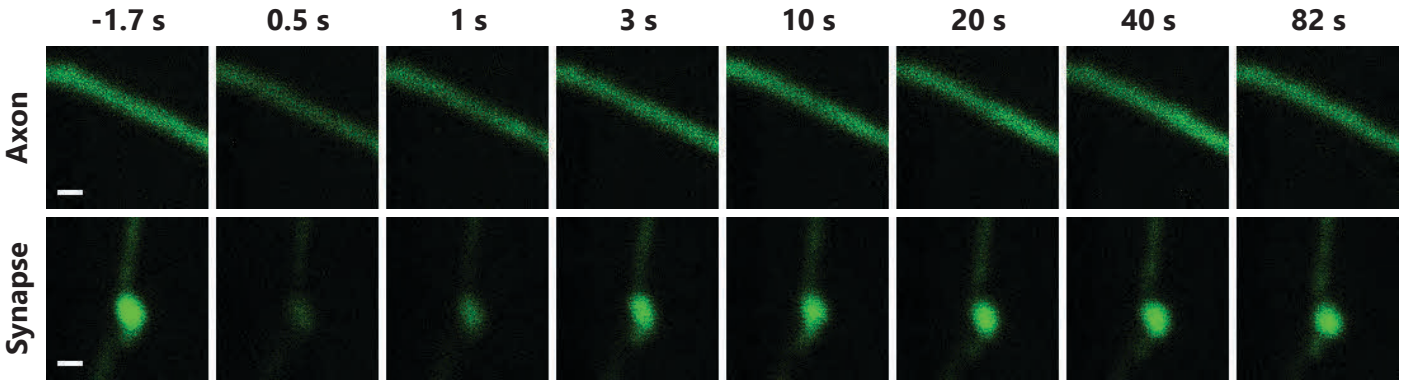

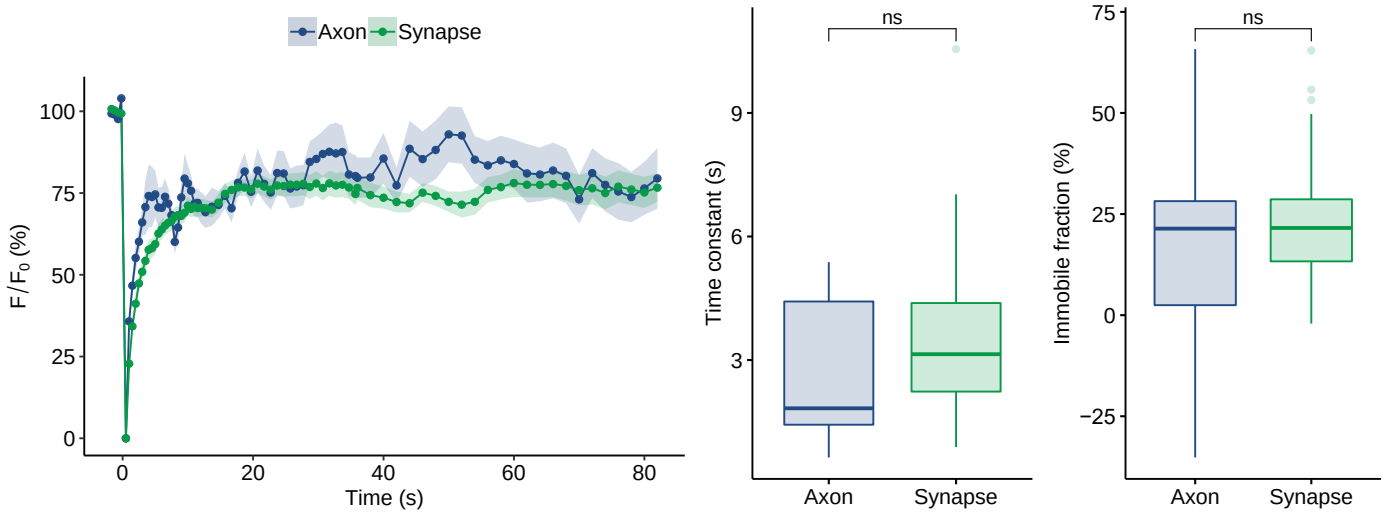

N (axons) = 18, N (synapses) = 30.

Tagged protein outline:

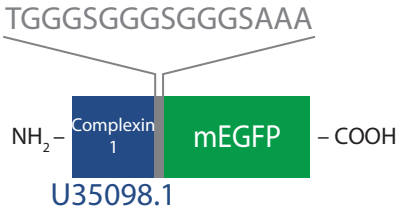

Time constant (axon) is not significantly different from time constant (axon) of any other proteins.
Immobile fraction (axon) is not significantly different from immobile fraction (axon) of any other proteins.
Time constant (synapse) is significantly different from time constant (synapse) of: Amphiphysin (p = 3.63E-03), Dynamin 1 (p = 1.00E-03), Epsin (p = 2.08E-02), ITSN 1-L (p = 4.09E-03), mEGFP (p = 2.66E-02), PIP5KI-gamma (p = 7.51E-03), SCAMP1 (p = 1.25E-04), SV2B (p = 2.04E-03), Synapsin 1A (p = 1.19E-05), Synaptogyrin (p = 2.22E-06), Synaptophysin (p = 3.82E-08), Synaptotagmin 1 (p = 2.12E-08), Syntaxin 1A (p = 1.22E-02), Syntaxin 16 (p = 5.21E-07), alpha-Tubulin 1b (p = 2.33E-04), VAMP1 (p = 1.12E-06), vATPase V0a1 (p = 6.55E-03), vGluT1 (p = 4.48E-08), Vti1a-beta (p = 1.20E-03).
Immobile fraction (synapse) is significantly different from immobile fraction (synapse) of: SV2B (p = 5.41E-07), Synaptogyrin (p = 8.84E-03), Synaptophysin (p = 1.64E-07), Synaptotagmin 1 (p = 9.74E-03), vATPase V0a1 (p = 4.99E-03), vGluT1 (p = 9.48E-05).

References

Chen, X., et al. (2002). Neuron 33, 397-409.
Bracher, A., et al. (2002). J Biol Chem 277, 26517-23.
Denker, A., et al. (2011). Proc Natl Acad Sci U S A 108, 17183-8.
Wragg, R.T., et al. (2013). Neuron 77, 323-34.

Complexin 2

MW (kDa)	Category	τ_{axon} (s)	$\tau_{synapse}$ (s)	IF_{axon} (%)	$IF_{synapse}$ (%)
15.39	soluble, SNARE co-factor	4.03 ± 0.53	5.01 ± 0.39	0.88 ± 6.23	15.44 ± 3.26

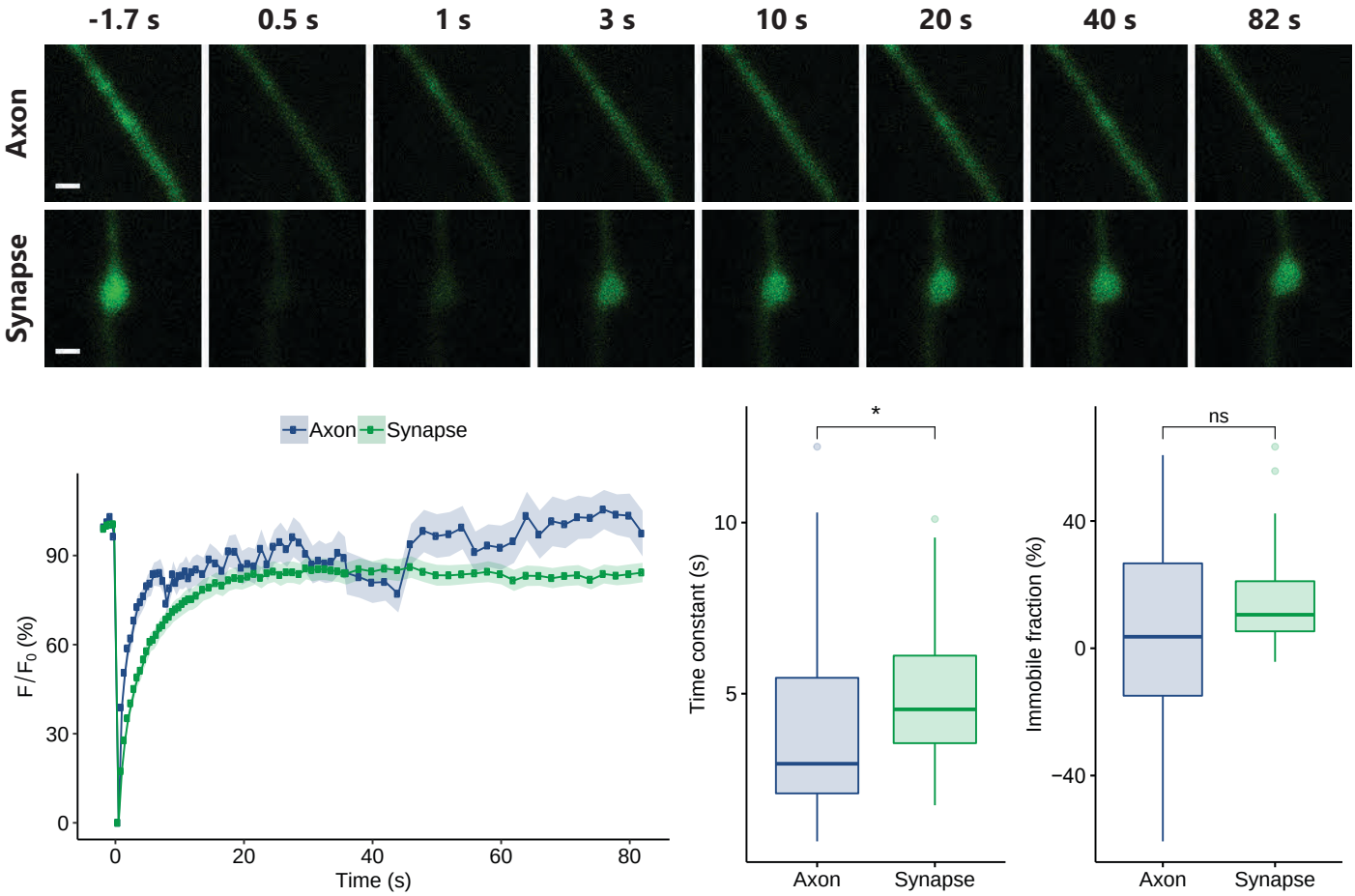

N (axons) = 27, N (synapses) = 28; p (time constant) = 3.54E-02.

Tagged protein outline:

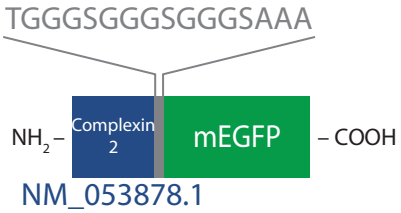

Time constant (axon) is significantly different from time constant (axon) of: Actin (p = 2.23E-02), Doc2a (p = 2.97E-02), Munc13 (p = 2.22E-03).
Immobile fraction (axon) is not significantly different from immobile fraction (axon) of any other proteins.
Time constant (synapse) is significantly different from time constant (synapse) of: Hsc70 (p = 4.69E-02), mEGFP (p = 1.05E-08), SCAMP1 (p = 2.16E-03), Synapsin 1A (p = 1.45E-04), Synaptogyrin (p = 1.48E-05), Synaptophysin (p = 3.29E-07), Synaptotagmin 1 (p = 6.71E-08), Syntaxin 16 (p = 2.41E-04), alpha-Tubulin 1b (p = 6.48E-03), VAMP1 (p = 1.66E-05), vGluT1 (p = 8.22E-07), Vti1a-beta (p = 2.87E-02).
Immobile fraction (synapse) is significantly different from immobile fraction (synapse) of: NSF (p = 5.14E-03), SCAMP1 (p = 3.02E-02), SV2B (p = 2.47E-07), Synaptogyrin (p = 1.60E-03), Synaptophysin (p = 1.04E-07), Synaptotagmin 1 (p = 1.07E-03), VAMP2 (p = 9.68E-03), VAMP4 (p = 2.79E-02), vATPase V0a1 (p = 5.79E-04), vGluT1 (p = 4.02E-05).

References

Chen, X., et al. (2002). Neuron 33, 397-409.
Bracher, A., et al. (2002). J Biol Chem 277, 26517-23.
Denker, A., et al. (2011). Proc Natl Acad Sci U S A 108, 17183-8.
Wragg, R.T., et al. (2013). Neuron 77, 323-34.

CSP

MW (kDa)	Category	τ_{axon} (s)	$\tau_{synapse}$ (s)	IF_{axon} (%)	$IF_{synapse}$ (%)
22.10	membrane-associated, SNARE co-factor	2.87 ± 0.33	8.45 ± 0.90	23.00 ± 4.60	22.05 ± 12.68

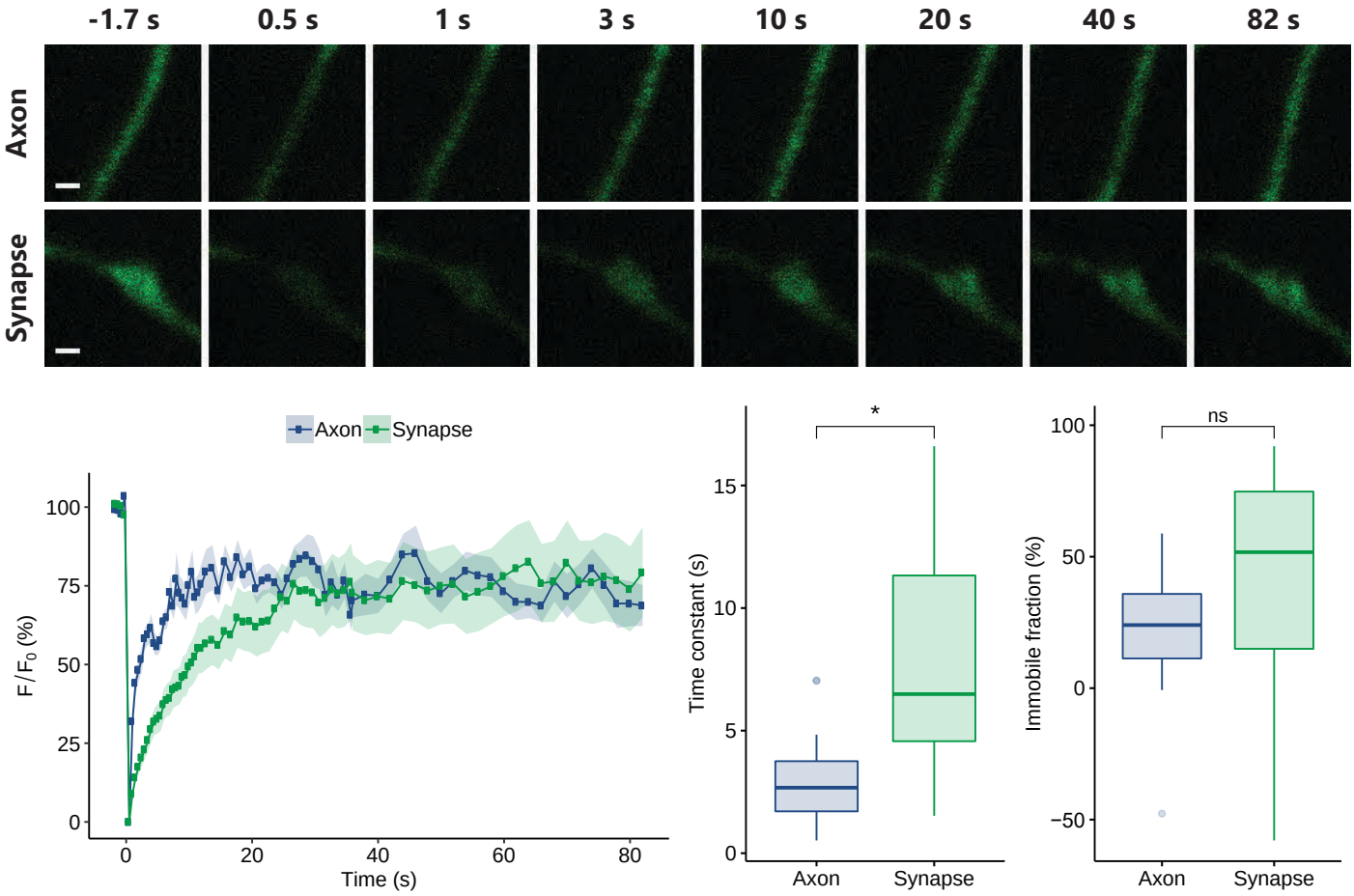

N (axons) = 25, N (synapses) = 28; p (time constant) = 1.06E-05.

Tagged protein outline:

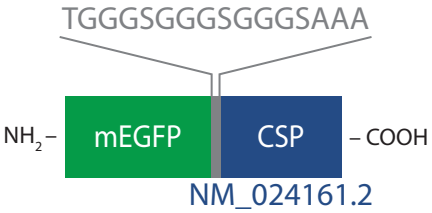

Time constant (axon) is not significantly different from time constant (axon) of any other proteins.
Immobile fraction (axon) is not significantly different from immobile fraction (axon) of any other proteins.
Time constant (synapse) is significantly different from time constant (synapse) of: Calmodulin 1 (p = 6.93E-03), Clathrin light chain B (p = 3.32E-02), Hsc70 (p = 1.48E-03), mEGFP (p = 6.02E-08), Synaptogyrin (p = 6.67E-04), Synaptophysin (p = 1.49E-04), Synaptotagmin 1 (p = 8.25E-05), vGluT1 (p = 4.34E-03).
Immobile fraction (synapse) is not significantly different from immobile fraction (synapse) of ny other proteins.

References

Fernandez-Chacon, R., et al. (2004). Neuron 42, 237-51.
Sharma, M., et al. (2011). Nat Cell Biol 13, 30-9.
Sharma, M., et al. (2011). EMBO J 31, 829-41.
Takamori, S., et al. (2006). Cell 127, 831-46.

Doc2a

MW (kDa)	Category	τ_{axon} (s)	$\tau_{synapse}$ (s)	IF_{axon} (%)	$IF_{synapse}$ (%)
44.59	soluble, calcium sensor	1.64 ± 0.09	5.47 ± 0.53	21.93 ± 2.92	21.00 ± 2.55

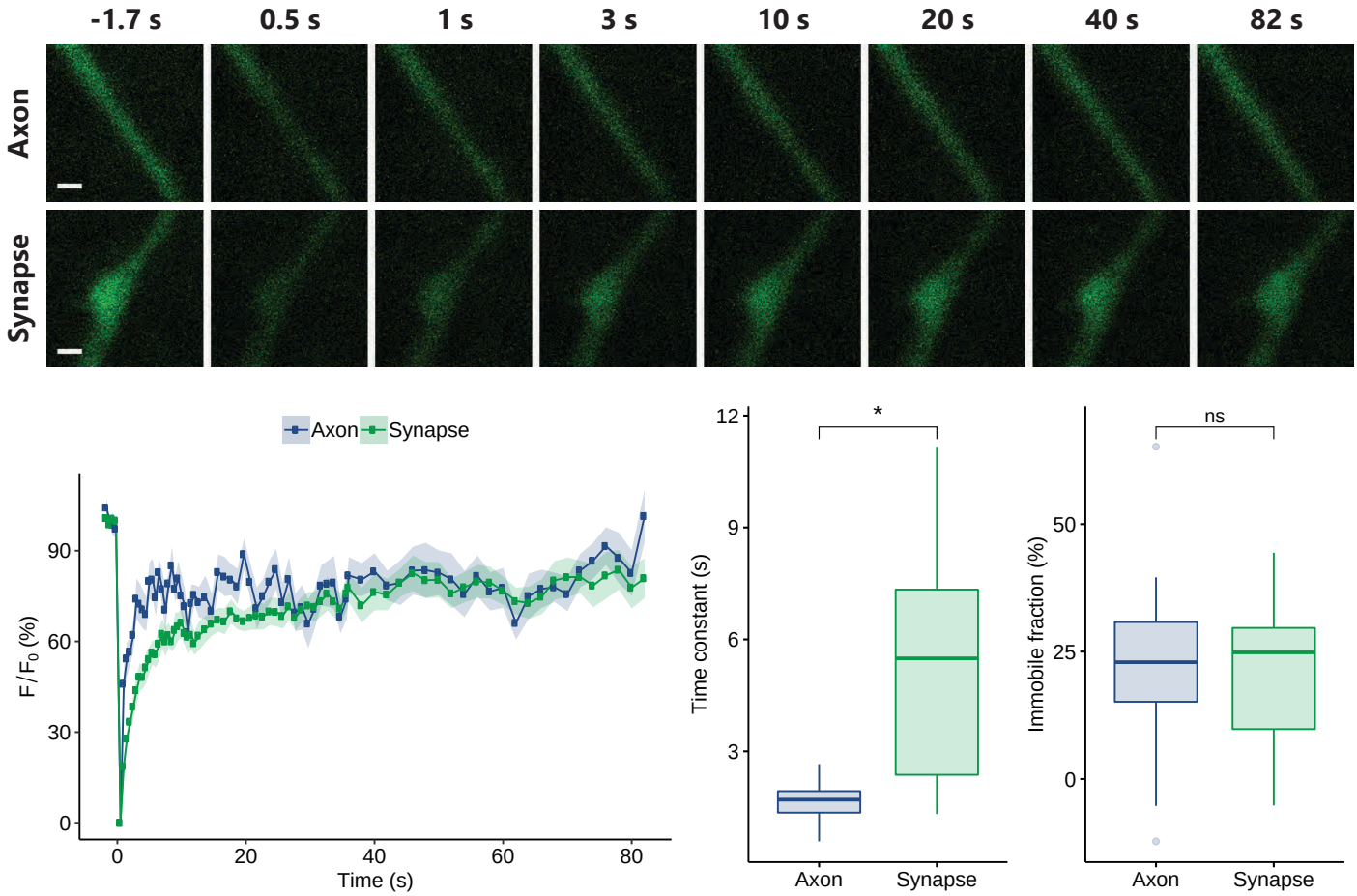

N (axons) = 29, N (synapses) = 30; p (time constant) = 2.91E-08.

Tagged protein outline:

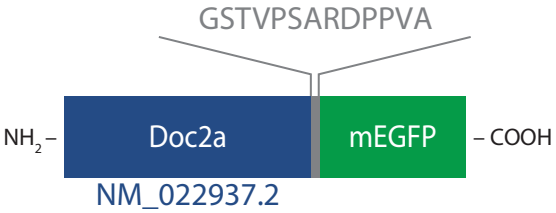

Time constant (axon) is significantly different from time constant (axon) of: Amphiphysin (p = 1.16E-02), Complexin 2 (p = 2.97E-02), SNAP29 (p = 4.27E-05), Synaptotagmin 1 (p = 9.18E-04), Syntaxin 1A (p = 8.24E-05), Syntaxin 16 (p = 5.13E-04), VAMP1 (p = 1.75E-04), Immobile fraction (axon) is not significantly different from immobile fraction (axon) of any other proteins.
Time constant (synapse) is significantly different from time constant (synapse) of: mEGFP (p = 4.57E-05), SV2B (p = 4.00E-02), Synapsin 1A (p = 3.38E-04), Synaptogyrin (p = 3.19E-05), Synaptophysin (p = 3.26E-07), Synaptotagmin 1 (p = 1.03E-07), Syntaxin 16 (p = 2.21E-03), VAMP1 (p = 5.52E-05), vGluT1 (p = 1.67E-06), Vti1a-beta (p = 4.45E-02).
Immobile fraction (synapse) is significantly different from immobile fraction (synapse) of: , SCAMP1 (p = 4.35E-02), SV2B (p = 8.17E-07), Synaptogyrin (p = 5.99E-03), Synaptophysin (p = 1.06E-07), Synaptotagmin 1 (p = 5.01E-03), VAMP4 (p = 3.60E-02), vATPase V0a1 (p = 8.52E-04), vGluT1 (p = 2.37E-05).

References

Groffen, A.J., et al. (2006). J Neurochem 97, 818-33.
Verhage et al. (1997). Neuron 18, 453-61.
Groffen, A.J., et al. (2010). Science 327, 1614-18.
Takamori, S., et al. (2006). Cell 127, 831-46.

Dynamin 1

MW (kDa)	Category	τ_{axon} (s)	$\tau_{synapse}$ (s)	IF_{axon} (%)	$IF_{synapse}$ (%)
97.29	soluble, endocytic	2.51 ± 0.33	10.75 ± 1.20	2.33 ± 5.34	21.01 ± 10.15

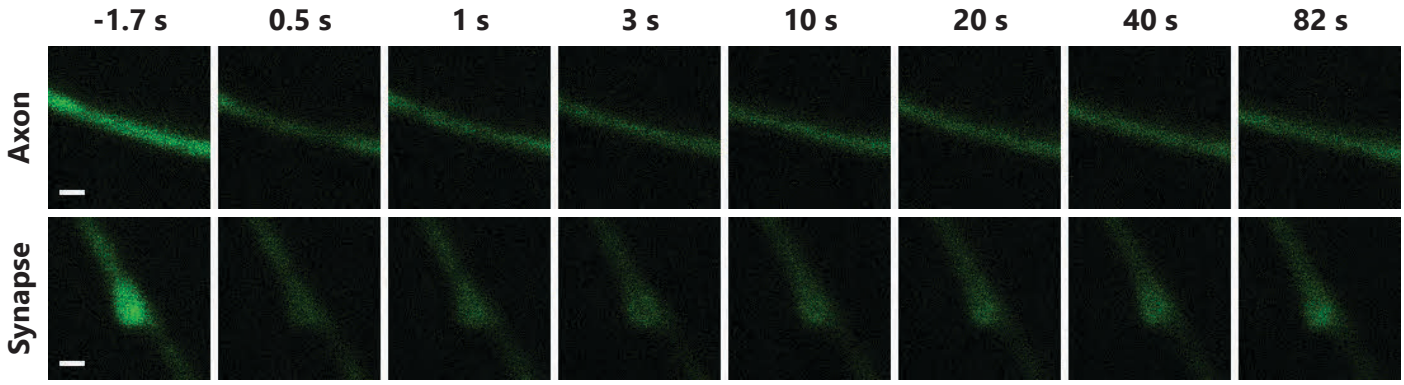

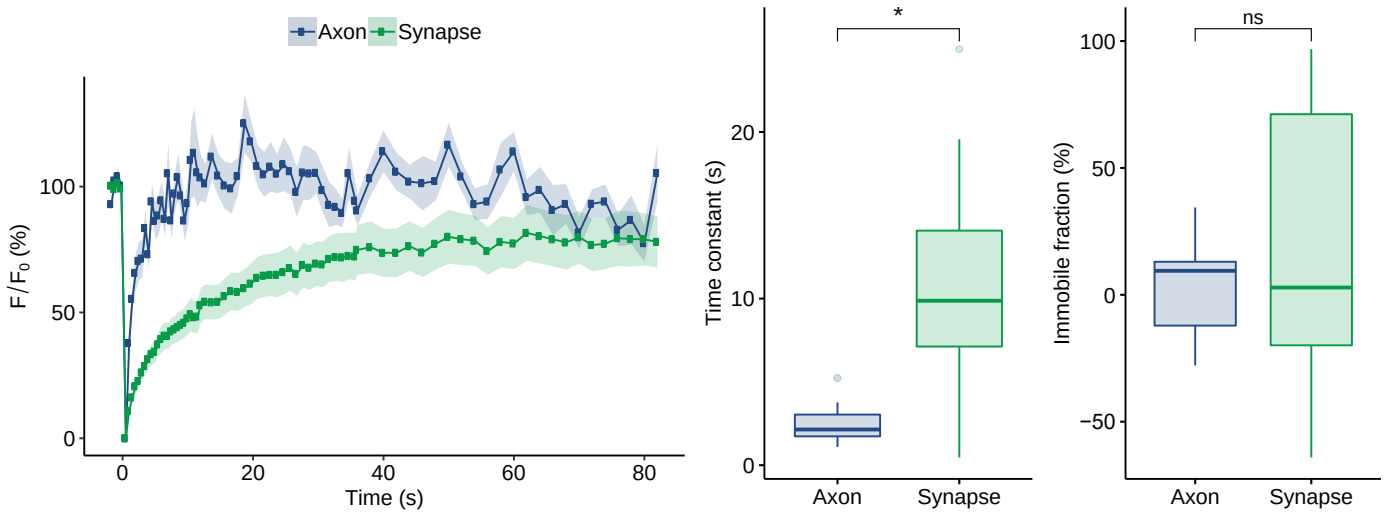

N (axons) = 12, N (synapses) = 25; p (time constant) = 1.99E-05.

NM_080689.4

Time constant (axon) is not significantly different from time constant (axon) of any other proteins.
Immobile fraction (axon) is not significantly different from immobile fraction (axon) of any other proteins.
Time constant (synapse) is significantly different from time constant (synapse) of: AP180 (p = 3.44E-03), AP2 (p = 3.03E-04), Calmodulin 1 (p = 1.55E-04), Clathrin light chain B (p = 2.81E-04), Complexin 1 (p = 1.00E-03), Endophilin A1 (p = 3.50E-03), Hsc70 (p = 1.46E-05), mEGFP (p = 4.72E-08), membrane mEGFP (p = 2.18E-02), Munc13 (p = 1.96E-04), Munc18 (p = 3.53E-04), NSF (p = 1.01E-03), Rab3a (p = 1.31E-03), Rab5a (p = 7.14E-05), Rab7a (p = 2.07E-03), Septin 5 (p = 4.22E-03), SNAP23 (p = 1.01E-03), SNAP25 (p = 1.44E-04), Synaptogyrin (p = 7.16E-03), Synaptophysin (p = 2.57E-02), Synaptotagmin 1 (p = 4.71E-02).
Immobile fraction (synapse) is significantly different from immobile fraction (synapse) of: SV2B (p = 4.80E-03).

References

Ferguson, S.M., and De Camili, P. (2012). Nat Rev Mol Cell Biol 13, 75-88.
Roux, A., et al. (2006). Nature 441, 528-31.
Koenig, J.H., and Ikeda, K. (1989). J Neurosci 9, 3844-60.
Takamori, S., et al. (2006). Cell 127, 831-46.

Endophilin

MW (kDa)	Category	τ_{axon} (s)	$\tau_{synapse}$ (s)	IF_{axon} (%)	$IF_{synapse}$ (%)
39.90	soluble, endocytic	2.52 ± 0.21	4.28 ± 0.28	9.87 ± 2.53	17.98 ± 3.68

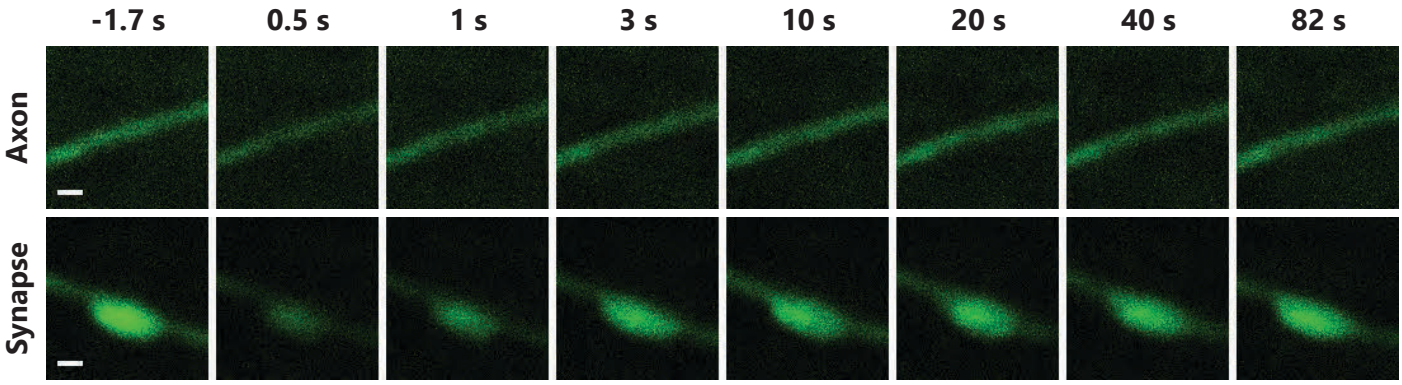

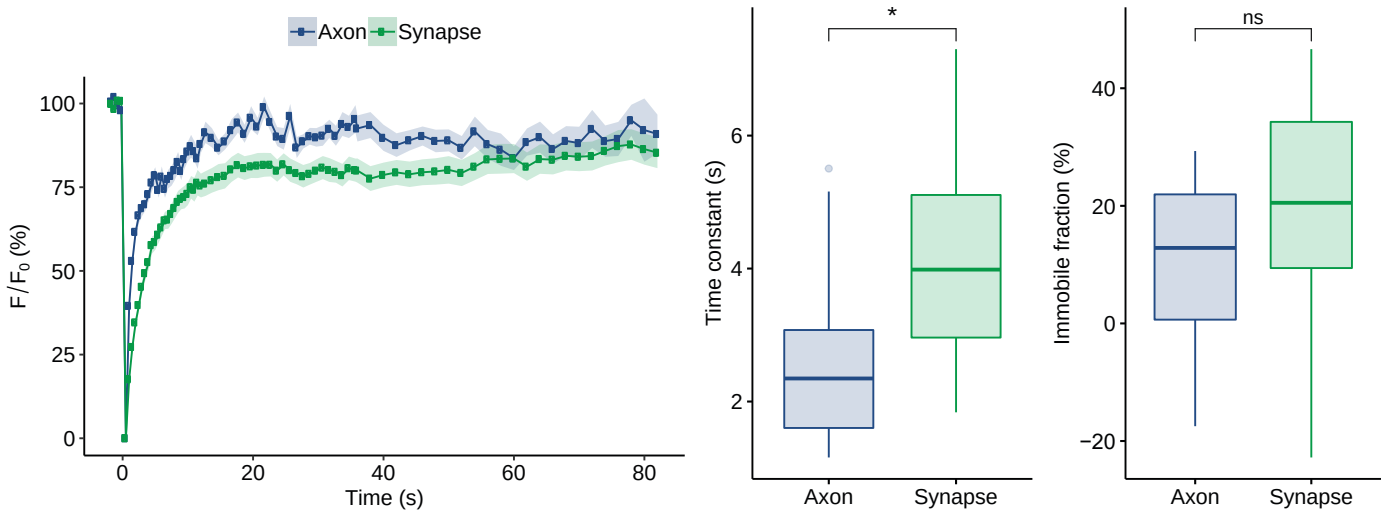

N (axons) = 28 N (synapses) = 28; p (time constant) = 1.26E-05.

Tagged protein outline:

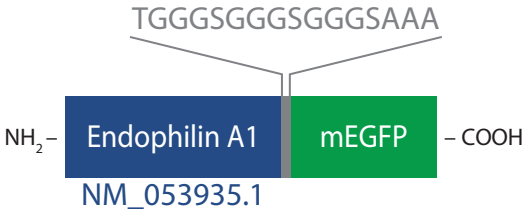

Time constant (axon) is significantly different from time constant (axon) of: Actin (p = 1.44E-02), Munc13 (p = 2.19E-02), Synaptotagmin 1 (p = 8.12E-03).
Immobile fraction (axon) is significantly different from immobile fraction (axon) of: Syndapin 1 (p = 1.12E-02).
Time constant (synapse) is significantly different from time constant (synapse) of: Amphiphysin (p = 3.36E-02), Dynamin 1 (p = 3.50E-03), ITSN 1-L (p = 1.32E-02), mEGFP (p = 9.94E-09), PIP5KI-gamma (p = 2.37E-02), SCAMP1 (p = 1.28E-04), Synapsin 1A (p = 3.45E-05), Synaptogyrin (p = 5.55E-06), Synaptophysin (p = 1.78E-07), Synaptotagmin 1 (p = 3.69E-08), Syntaxin 16 (p = 4.96E-06), alpha-Tubulin 1b (p = 9.35E-04), VAMP1 (p = 2.84E-06), vATPase V0a1 (p = 4.01E-02), vGluT1 (p = 1.42E-07), Vti1a-beta (p = 9.68E-03).
Immobile fraction (synapse) is significantly different from immobile fraction (synapse) of: SCAMP1 (p = 2.49E-02), SV2B (p = 9.59E-07), Synaptogyrin (p = 5.14E-03), Synaptophysin (p = 1.94E-07), Synaptotagmin 1 (p = 4.33E-03), VAMP4 (p = 3.02E-02), vATPase V0a1 (p = 6.16E-04), vGluT1 (p = 3.73E-05).

References

Schuske, K.R., et al. (2003). Nauron 40, 749-62.
Sundborger, A., et al. (2011). J Cell Sci 124, 133-43.
Kjaerulff, O., et al. (2010). Cell Biochem Biophys 60, 137-54.

Epsin

MW (kDa)	Category	τ_{axon} (s)	$\tau_{synapse}$ (s)	IF_{axon} (%)	$IF_{synapse}$ (%)
60.16	soluble, endocytic	2.63 ± 0.32	6.78 ± 0.53	24.51 ± 4.89	17.65 ± 5.35

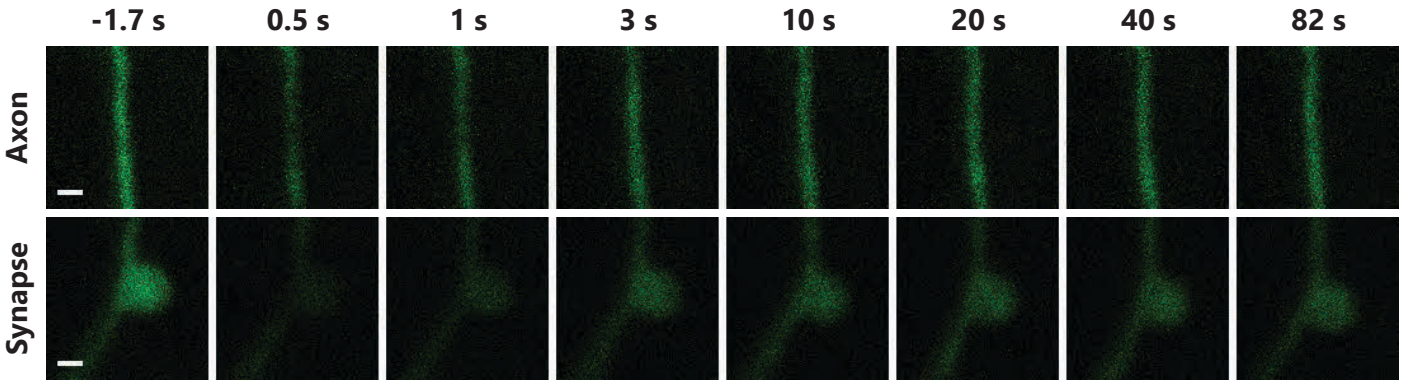

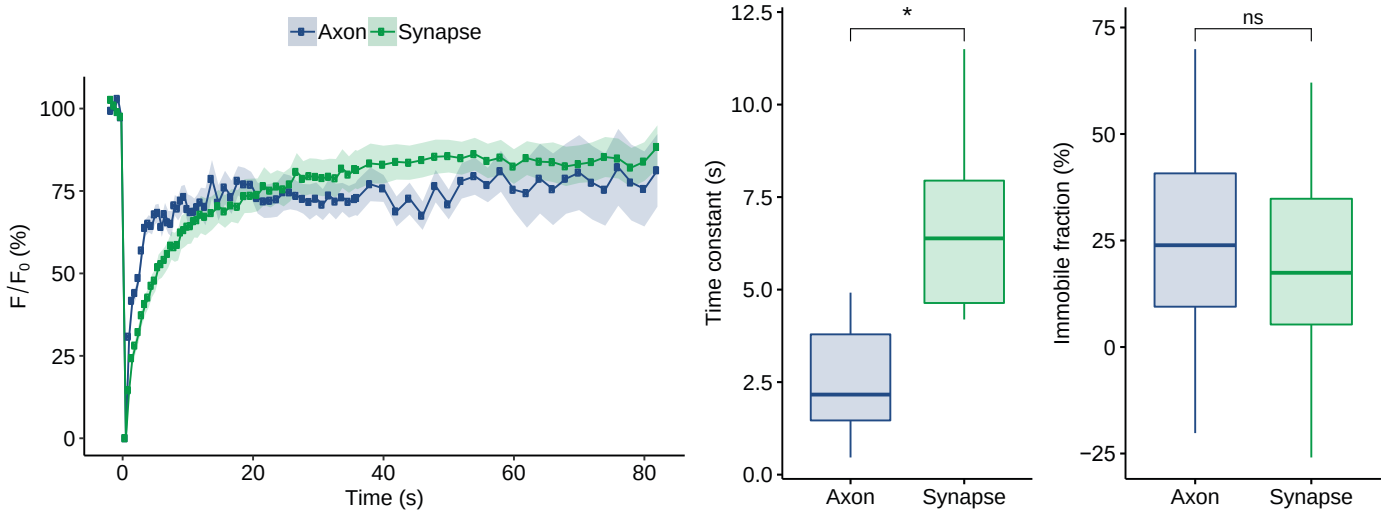

N (axons) = 19, N (synapses) = 19; p (time constant) = 5.97E-07.

Tagged protein outline:

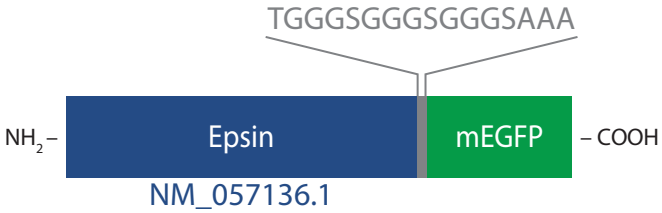

Time constant (axon) is not significantly different from time constant (axon) of any other proteins.
Immobile fraction (axon) is not significantly different from immobile fraction (axon) of any other proteins.
Time constant (synapse) is significantly different from time constant (synapse) of: AP2 (p = 1.12E-03), Calmodulin 1 (p = 2.58E-04), Clathrin light chain B (p = 1.29E-03), Complexin 1 (p = 2.08E-02), Hsc70 (p = 1.19E-04), mEGFP (p = 4.64E-08), Munc13 (p = 1.32E-02), NSF (p = 1.57E-02), Rab5a (p = 5.39E-03), SNAP23 (p = 1.70E-03), Synapsin 1A (p = 3.75E-02), Synaptogyrin (p = 2.17E-03), Synaptophysin (p = 1.15E-04), Synaptotagmin 1 (p = 2.10E-05), VAMP1 (p = 6.83E-03), vGluT1 (p = 8.87E-04).
Immobile fraction (synapse) is significantly different from immobile fraction (synapse) of: SV2B (p = 4.21E-05), Synaptogyrin (p = 3.02E-02), Synaptophysin (p = 2.59E-05), vATPase V0a1 (p = 2.98E-02), vGluT1 (p = 2.68E-03).

References

Horvath, C.A., et al. (2007). Int J Biochem Cell Biol 39, 1765-70.
Ford, M.G., et al. (2002). Nature 419, 361-6.

Hsc70

MW (kDa)	Category	τ_{axon} (s)	$\tau_{synapse}$ (s)	IF_{axon} (%)	$IF_{synapse}$ (%)
70.87	soluble, endocytic	2.63 ± 0.28	2.92 ± 0.24	14.69 ± 4.30	24.41 ± 3.00

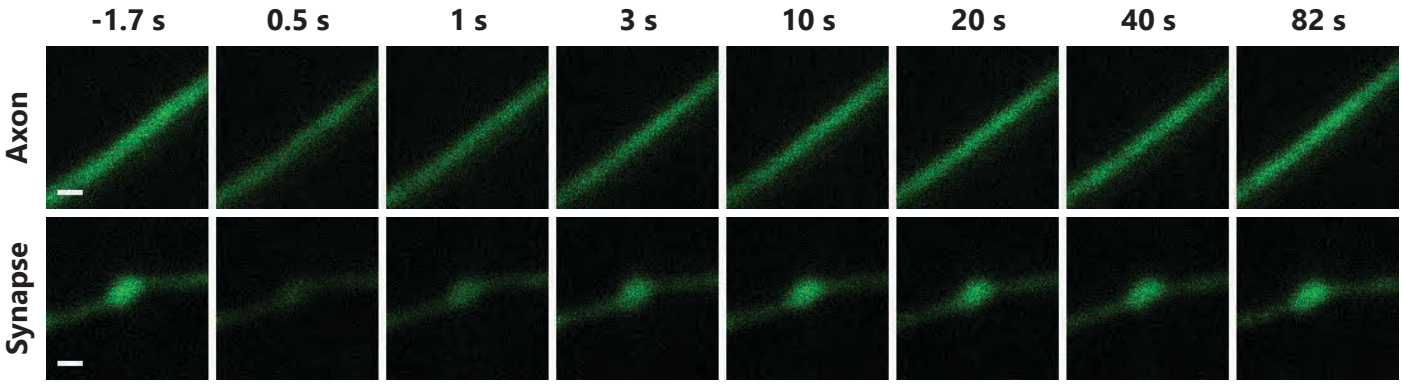

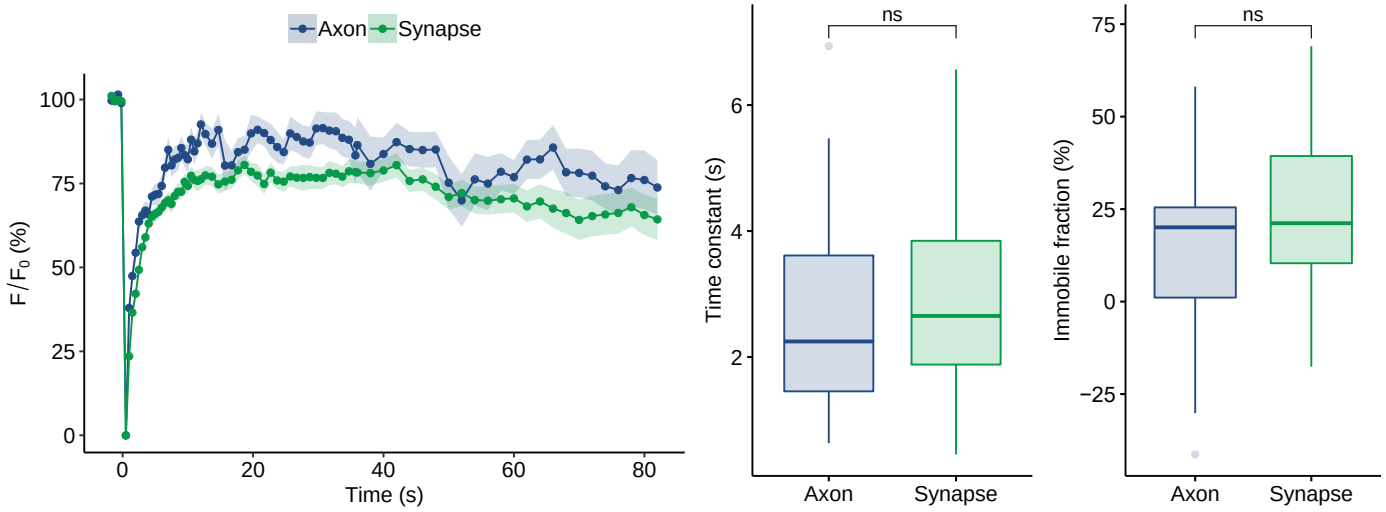

N (axons) = 29, N (synapses) = 40.

Tagged protein outline:

NM_024351.2

Time constant (axon) is significantly different from time constant (axon) of: Synaptotagmin 1 (p = 3.80E-02).
Immobile fraction (axon) is not significantly different from immobile fraction (axon) of any other proteins.
Time constant (synapse) is significantly different from time constant (synapse) of: Actin (p = 1.82E-02), Amphiphysin (p = 9.52E-07), Complexin 2 (p = 4.69E-02), CSP (p = 1.48E-03), Dynamin 1 (p = 1.46E-05), Epsin (p = 1.19E-04), ITSN 1-L (p = 2.81E-05), Munc18 (p = 1.49E-02), PIP5KI-gamma (p = 7.79E-06), SCAMP1 (p = 1.51E-06), SNAP29 (p = 5.47E-04), SV2B (p = 1.82E-05), Synapsin 1A (p = 3.53E-07), Synaptogyrin (p = 9.92E-08), Synaptophysin (p = 4.40E-10), Synaptotagmin 1 (p = 4.70E-10), Synaptotagmin 7 (p = 7.21E-05), Syndapin 1 (p = 2.09E-03), Syntaxin 1A (p = 5.02E-06), Syntaxin 16 (p = 7.36E-10), alpha-Tubulin 1b (p = 1.60E-06), VAMP1 (p = 1.40E-08), VAMP2 (p = 1.71E-02), vATPase V0a1 (p = 5.56E-05), vGluT1 (p = 3.36E-10), Vti1a-beta (p = 3.39E-05).
Immobile fraction (synapse) is significantly different from immobile fraction (synapse) of: , Rab5a (p = 4.95E-02), SV2B (p = 5.25E-08), Synaptogyrin (p = 2.96E-03), Synaptophysin (p = 1.25E-08), Synaptotagmin 1 (p = 1.12E-02), vATPase V0a1 (p = 2.10E-03), vGluT1 (p = 3.28E-05).

References

Schlossman, D.M., et al. (1984). J Cell Biol 99, 723-33.
Rothnie, A., et al. (2011). Proc Natl Acad Sci U S A 108, 6927-32.
Cremona, O., et al. (1999). Cell 99, 179-88.

Intersectin 1-L

MW (kDa)	Category	τ_{axon} (s)	$\tau_{synapse}$ (s)	IF_{axon} (%)	$IF_{synapse}$ (%)
194.20	soluble, endocytic	1.89 ± 0.23	9.52 ± 0.88	26.14 ± 7.26	40.73 ± 7.23

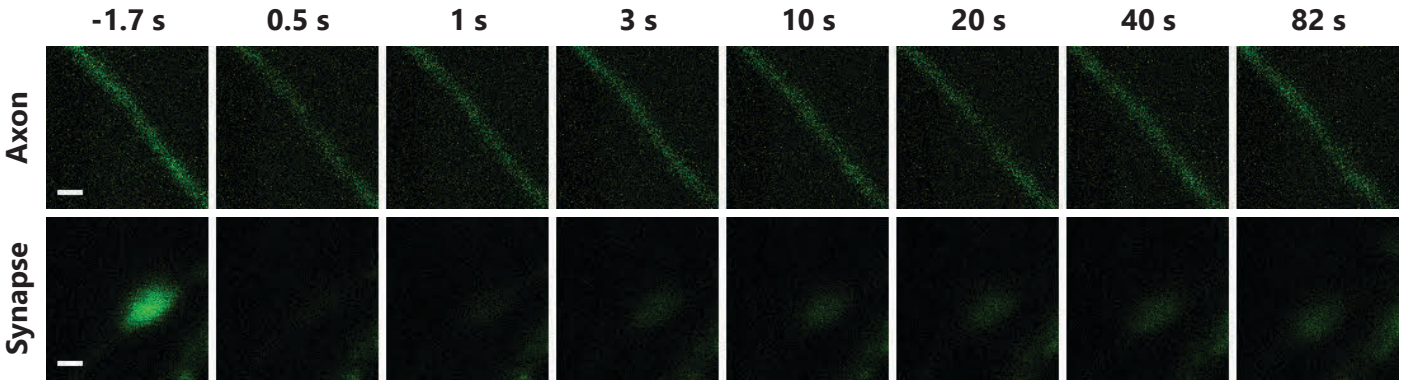

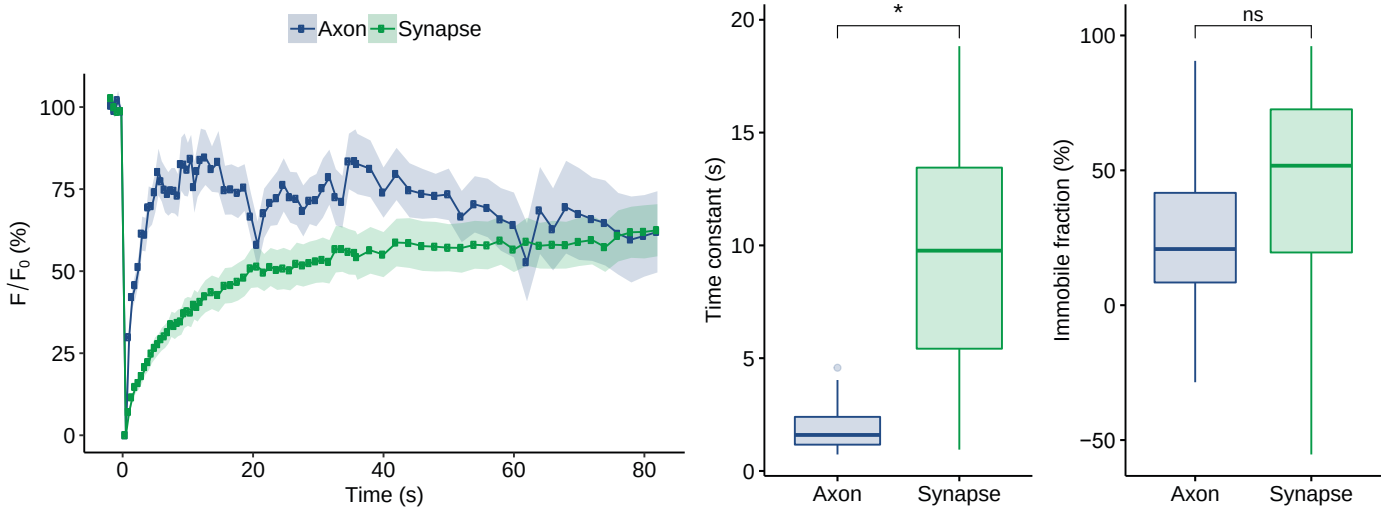

N (axons) = 20, N (synapses) = 32; p (time constant) = 2.97E-07.

NM_001136096.1

Time constant (axon) is significantly different from time constant (axon) of: SNAP29 (p = 4.56E-02), Synaptotagmin 1 (p = 1.35E-02).
Immobile fraction (axon) is not significantly different from immobile fraction (axon) of any other proteins.
Time constant (synapse) is significantly different from time constant (synapse) of: AP2 (p = 1.56E-03), Calmodulin 1 (p = 3.96E-04), Clathrin light chain B (p = 2.89E-04), Complexin 1 (p = 4.09E-03), Endophilin A1 (p = 1.32E-02), Hsc70 (p = 2.81E-05), mEGFP (p = 4.96E-08), Munc13 (p = 6.76E-04), Munc18 (p = 1.13E-03), NSF (p = 6.07E-03), Rab3a (p = 9.89E-03), Rab5a (p = 3.17E-04), Rab7a (p = 9.36E-03), Septin 5 (p = 6.14E-03), SNAP23 (p = 3.48E-03), SNAP25 (p = 3.49E-04), Synaptogyrin (p = 7.83E-04), Synaptophysin (p = 6.11E-04), Synaptotagmin 1 (p = 1.75E-03).
Immobile fraction (synapse) is significantly different from immobile fraction (synapse) of: Rab5a (p = 3.67E-02), SV2B (p = 1.03E-02).

References

Pechstein, A., et al. (2010a). Proc Natl Acad Sci U S A 107, 4206-11.
Pechstein, A., et al. (2010b). Biochem Soc Trans 38, 181-6.
Gerth, F. et al. Proc. Natl. Acad. Sci. U.S.A. 114, 12057–12062 (2017).

mEGFP

MW (kDa)	Category	τ_{axon} (s)	$\tau_{synapse}$ (s)	IF_{axon} (%)	$IF_{synapse}$ (%)
26.92	soluble, control	1.94 ± 0.12	2.08 ± 0.08	20.47 ± 2.32	18.15 ± 1.65

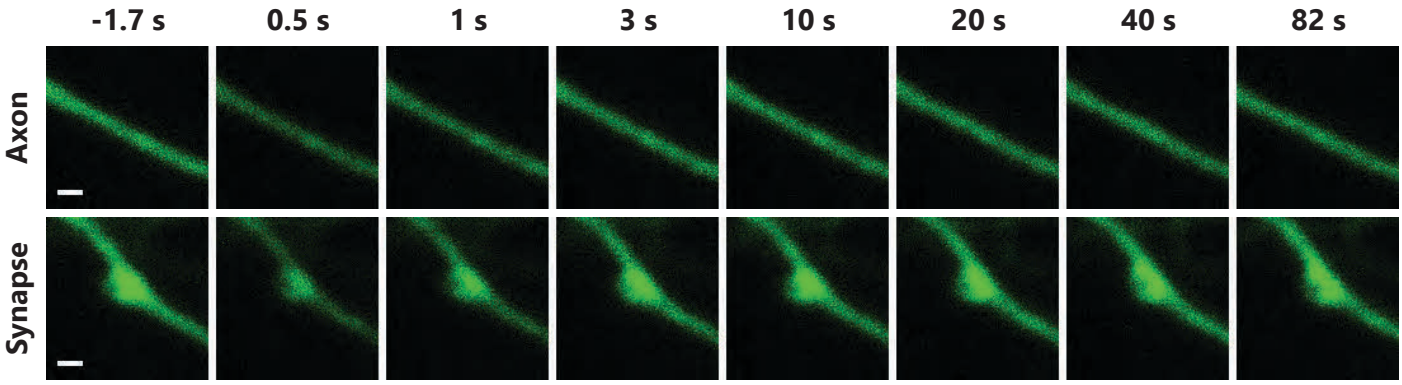

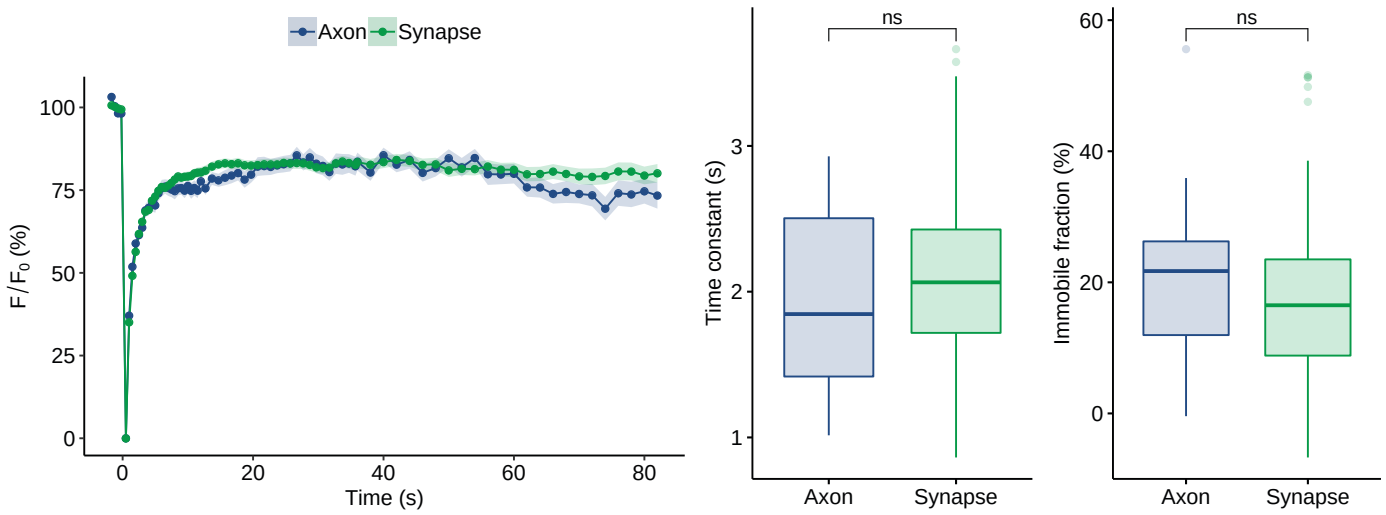

N (axons) = 26, N (synapses) = 65.

Tagged protein outline: mEGFP

Time constant (axon) is significantly different from time constant (axon) of: SNAP29 (p = 5.91E-03), Synaptotagmin 1 (p = 1.50E-03), Syntaxin 1A (p = 1.50E-03), VAMP1 (p = 1.21E-02).
Immobile fraction (axon) is not significantly different from immobile fraction (axon) of any other proteins.
Time constant (synapse) is significantly different from time constant (synapse) of: Actin (p = 5.73E-09), alpha-SNAP (p = 1.12E-06), alpha-synuclein (p = 3.02E-08), Amphiphysin (p = 4.74E-13), AP180 (p = 5.24E-06), AP2 (p = 2.68E-04), Clathrin light chain B (p = 4.03E-03), Complexin 1 (p = 2.66E-02), Complexin 2 (p = 1.05E-08), CSP (p = 6.02E-08), Doc2a (p = 4.57E-05), Dynamin 1 (p = 4.72E-08), Endophilin A1 (p = 9.94E-09), Epsin (p = 4.64E-08), ITSN 1-L (p = 4.96E-08), membrane mEGFP (p = 3.77E-06), Munc13 (p = 3.52E-06), Munc18 (p = 1.96E-12), PIP5KI-gamma (p = 1.63E-09), Rab3a (p = 2.54E-04), Rab5a (p = 2.42E-07), Rab7a (p = 2.24E-04), SCAMP1 (p = 4.64E-08), Septin 5 (p = 1.05E-08), SNAP23 (p = 7.99E-05), SNAP25 (p = 8.10E-13), SNAP29 (p = 8.59E-10), SV2B (p = 2.00E-09), Synapsin 1A (p = 7.77E-10), Synaptogyrin (p = 6.34E-10), Synaptophysin (p = 2.09E-13), Synaptotagmin 1 (p = 1.67E-12), Synaptotagmin 7 (p = 5.55E-11), Syndapin 1 (p = 2.70E-10), Syntaxin 1A (p = 3.71E-11), Syntaxin 16 (p = 2.52E-15), alpha-Tubulin 1b (p = 3.06E-09), VAMP1 (p = 3.48E-11), VAMP2 (p = 2.58E-06), VAMP4 (p = 7.08E-04), vATPase V0a1 (p = 3.66E-08), vGluT1 (p = 9.06E-14), Vti1a-beta (p = 8.41E-08).
Immobile fraction (synapse) is significantly different from immobile fraction (synapse) of: NSF (p = 5.86E-05), SCAMP1 (p = 2.16E-03), SV2B (p = 1.94E-11), Synaptogyrin (p = 3.29E-05), Synaptophysin (p = 2.69E-12), Synaptotagmin 1 (p = 7.13E-06), VAMP2 (p = 1.51E-04), VAMP4 (p = 1.73E-03), vATPase V0a1 (p = 9.46E-07), vGluT1 (p = 7.67E-09).

References

Zacharias D., et al. (2002). Science 296, 913–916.

membrane mEGFP

MW (kDa)	Category	τ_{axon} (s)	$\tau_{synapse}$ (s)	IF_{axon} (%)	$IF_{synapse}$ (%)
36.29	PM-associated, control	2.30 ± 0.29	4.84 ± 0.41	33.99 ± 3.89	26.86 ± 4.53

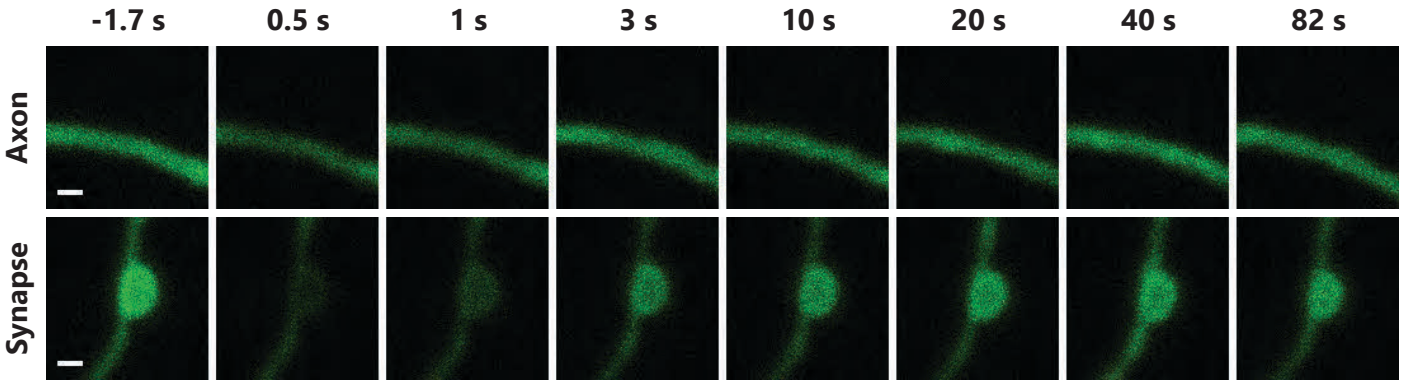

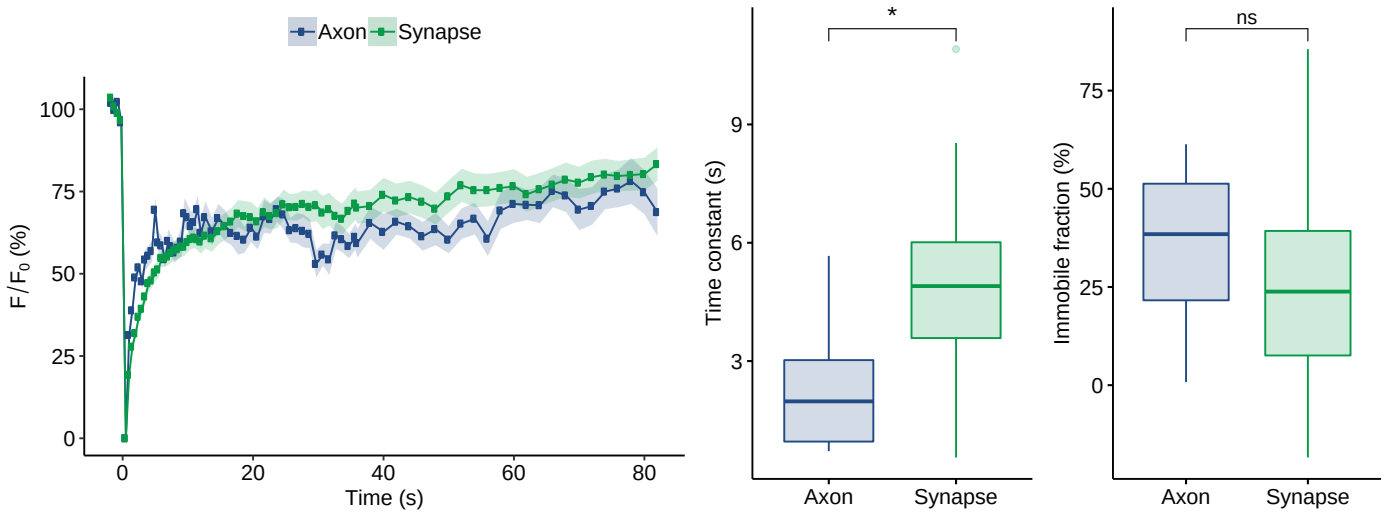

N (axons) = 22, N (synapses) = 29; p (time constant) = 5.31E-05.

Tagged protein outline:

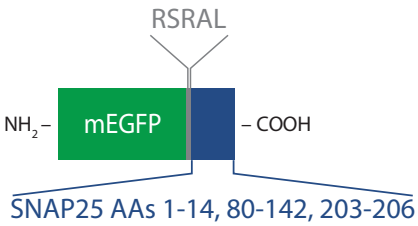

Time constant (axon) is significantly different from time constant (axon) of: Synaptotagmin 1 (p = 2.87E-02).
Immobile fraction (axon) is significantly different from immobile fraction (axon) of: VAMP2 (p = 4.07E-02).
Time constant (synapse) is significantly different from time constant (synapse) of: Dynamin 1 (p = 2.18E-02), mEGFP (p = 3.77E-06), SCAMP1 (p = 1.23E-03), SV2B (p = 4.51E-02), Synapsin 1A (p = 1.91E-04), Synaptogyrin (p = 1.90E-05), Synaptophysin (p = 1.79E-07), Synaptotagmin 1 (p = 3.92E-08), Syntaxin 16 (p = 2.19E-04), alpha-Tubulin 1b (p = 4.21E-03), VAMP1 (p = 6.56E-06), vGluT1 (p = 3.98E-07), Vti1a-beta (p = 2.09E-02).
Immobile fraction (synapse) is significantly different from immobile fraction (synapse) of: SV2B (p = 5.76E-06), Synaptogyrin (p = 4.54E-02), Synaptophysin (p = 8.57E-06), vGluT1 (p = 3.44E-03).

Munc13

MW (kDa)	Category	τ_{axon} (s)	$\tau_{synapse}$ (s)	IF_{axon} (%)	$IF_{synapse}$ (%)
19.64	soluble, SNARE co-factor	1.53 ± 0.12	3.95 ± 0.27	21.91 ± 2.41	4.64 ± 4.88

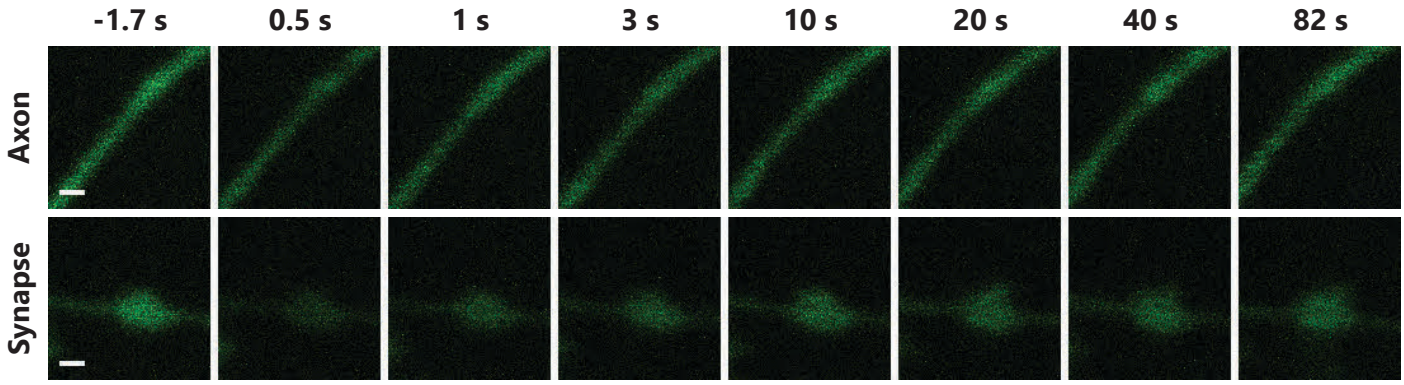

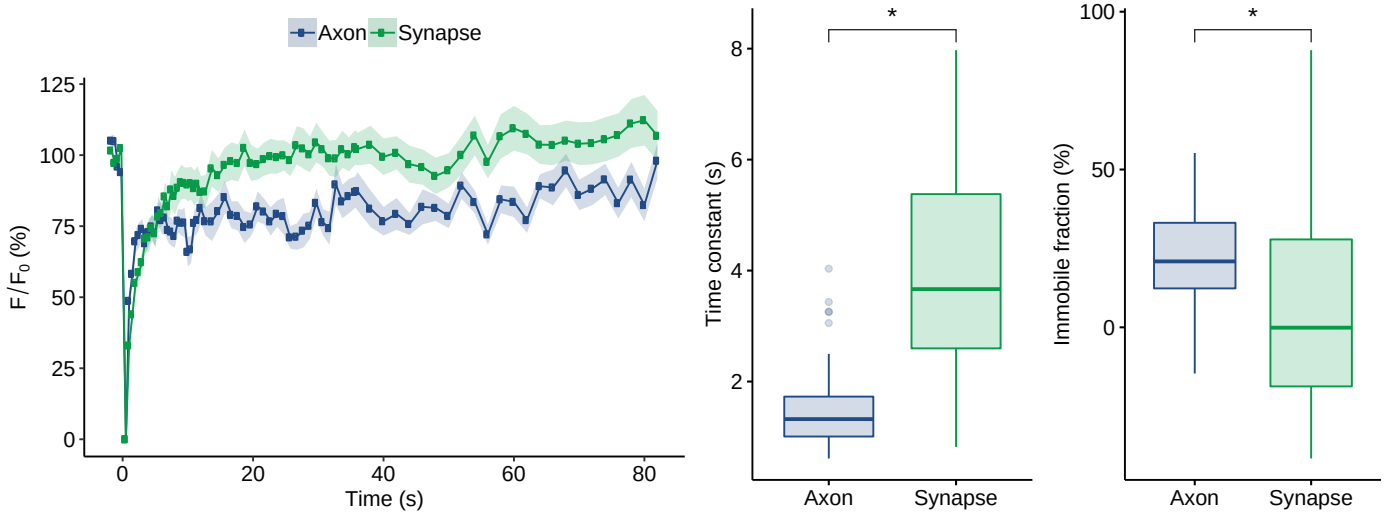

N (axons) = 47, N (synapses) = 45; p (time constant) = 9.18E-12, p (immobile fraction) = 1.10E-03.

NM_022861.1

Time constant (axon) is significantly different from time constant (axon) of: Amphiphysin (p = 2.42E-04), Complexin 2 (p = 2.22E-03), Endophilin A1 (p = 2.19E-02), PIP5KI-gamma (p = 2.96E-02), Rab3a (p = 1.48E-03), SNAP23 (p = 5.20E-03), SNAP29 (p = 8.64E-06), Synapsin 1A (p = 2.47E-02), Synaptotagmin 1 (p = 8.17E-05), Synaptotagmin 7 (p = 8.65E-03), Syntaxin 1A (p = 2.36E-04), Syntaxin 16 (p = 4.07E-06), VAMP1 (p = 4.30E-05), VAMP2 (p = 4.64E-02).
Immobile fraction (axon) is not significantly different from immobile fraction (axon) of any other proteins.
Time constant (synapse) is significantly different from time constant (synapse) of: Amphiphysin (p = 1.07E-03), Dynamin 1 (p = 1.96E-04), Epsin (p = 1.32E-02), ITSN 1-L (p = 6.76E-04), mEGFP (p = 3.52E-06), PIP5KI-gamma (p = 1.92E-03), SCAMP1 (p = 1.20E-05), SV2B (p = 7.96E-04), Synapsin 1A (p = 9.74E-07), Synaptogyrin (p = 1.09E-07), Synaptophysin (p = 4.08E-10), Synaptotagmin 1 (p = 1.14E-10), Syntaxin 1A (p = 7.17E-03), Syntaxin 16 (p = 1.42E-08), alpha-Tubulin 1b (p = 1.50E-05), VAMP1 (p = 2.71E-08), vATPase V0a1 (p = 9.04E-04), vGluT1 (p = 3.44E-10), Vti1a-beta (p = 3.07E-04).
Immobile fraction (synapse) is significantly different from immobile fraction (synapse) of: , NSF (p = 1.05E-02), SCAMP1 (p = 2.46E-03), SV2B (p = 5.12E-09), Synaptogyrin (p = 8.53E-05), Synaptophysin (p = 6.77E-09), Synaptotagmin 1 (p = 1.72E-04), VAMP2 (p = 1.01E-02), VAMP4 (p = 1.02E-03), vATPase V0a1 (p = 4.95E-06), vGluT1 (p = 5.82E-07).

References

Deng, L., et al. (2011). Neuron 69, 317-31.
Betz, A., et al. (1997). J Biol Chem 272, 2520-6.
Varoqueaux, F., et al. (2002). Proc Natl Acad Sci U S A 99, 9037-42.

Munc18

MW (kDa)	Category	τ_{axon} (s)	$\tau_{synapse}$ (s)	IF_{axon} (%)	$IF_{synapse}$ (%)
67.57	soluble, SNARE co-factor	2.37 ± 0.33	4.66 ± 0.25	21.50 ± 4.41	18.24 ± 1.55

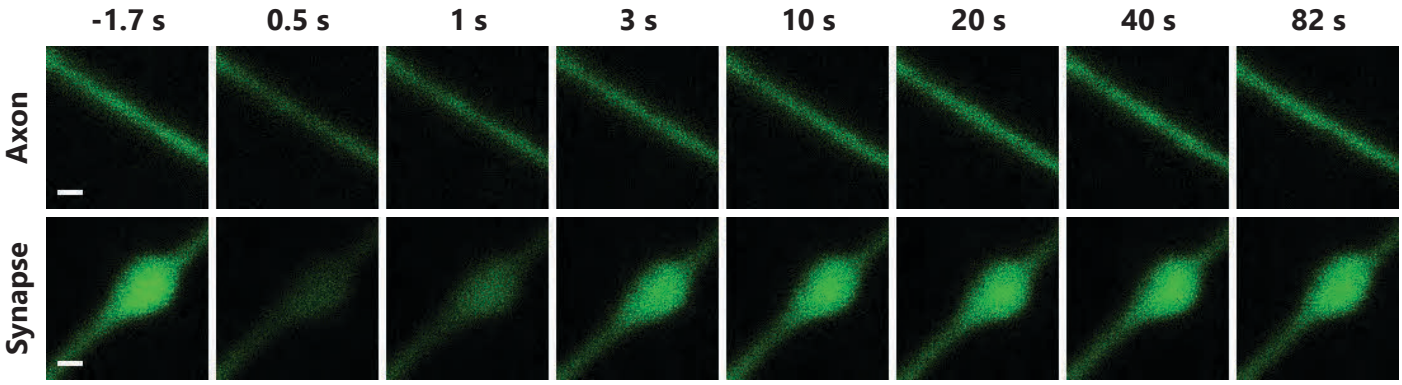

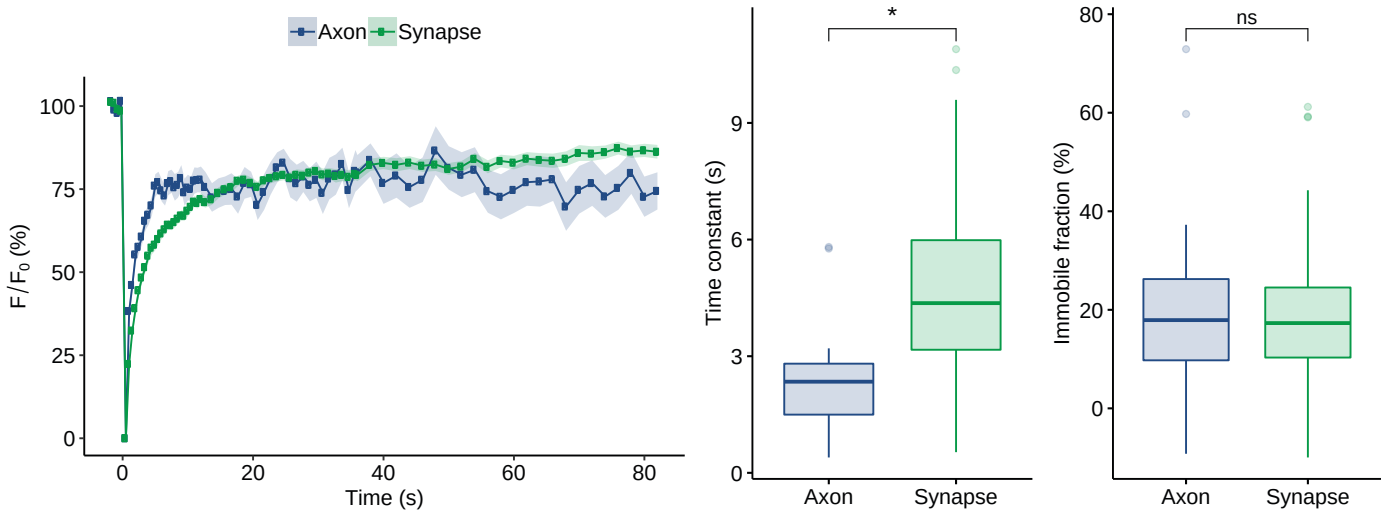

N (axons) = 19, N (synapses) = 78; p (time constant) = 1.02E-05.

Tagged protein outline:

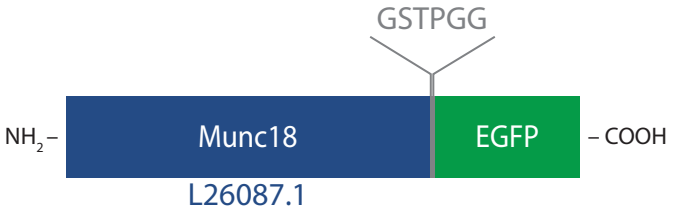

Time constant (axon) is not significantly different from time constant (axon) of any other proteins.
Immobile fraction (axon) is not significantly different from immobile fraction (axon) of any other proteins.
Time constant (synapse) is significantly different from time constant (synapse) of: , Dynamin 1 (p = 3.53E-04), Hsc70 (p = 1.49E-02), ITSN 1-L (p = 1.13E-03), mEGFP (p = 1.96E-12), PIP5KI-gamma (p = 4.29E-02), SCAMP1 (p = 1.29E-05), SV2B (p = 3.27E-04), Synapsin 1A (p = 1.88E-07), Synaptogyrin (p = 1.01E-08), Synaptophysin (p = 1.66E-12), Synaptotagmin 1 (p = 4.96E-13), Syntaxin 16 (p = 7.39E-09), alpha-Tubulin 1b (p = 1.70E-05), VAMP1 (p = 2.01E-09), vATPase V0a1 (p = 5.85E-04), vGluT1 (p = 4.59E-12), Vti1a-beta (p = 1.22E-04).
Immobile fraction (synapse) is significantly different from immobile fraction (synapse) of: , NSF (p = 2.30E-05), SCAMP1 (p = 2.58E-03), SV2B (p = 3.07E-12), Synaptogyrin (p = 2.52E-05), Synaptophysin (p = 1.92E-13), Synaptotagmin 1 (p = 2.69E-06), VAMP2 (p = 7.20E-05), VAMP4 (p = 9.24E-04), vATPase V0a1 (p = 1.89E-07), vGluT1 (p = 2.15E-09).

References

Burgoyne, R.D., et al. (2009). Ann N Y Acad Sci 1152, 76-86.
Takamori, S., et al. (2006). Cell 127, 831-46.
Verhage, M., et al. (2000). Science 287, 864-69.

NSF

MW (kDa)	Category	τ_{axon} (s)	$\tau_{synapse}$ (s)	IF_{axon} (%)	$IF_{synapse}$ (%)
82.65	soluble, SNARE co-factor	1.69 ± 0.24	3.40 ± 0.34	27.68 ± 5.49	42.49 ± 4.00

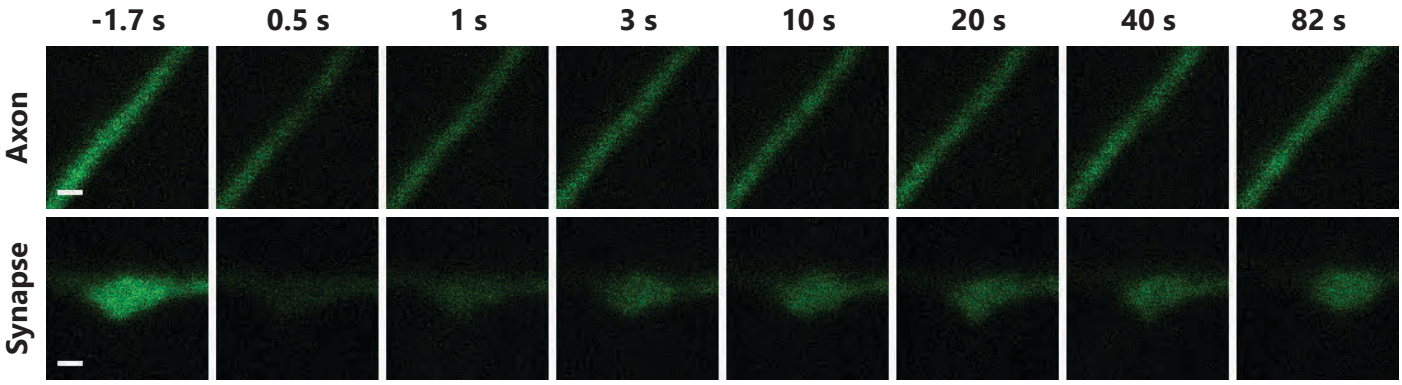

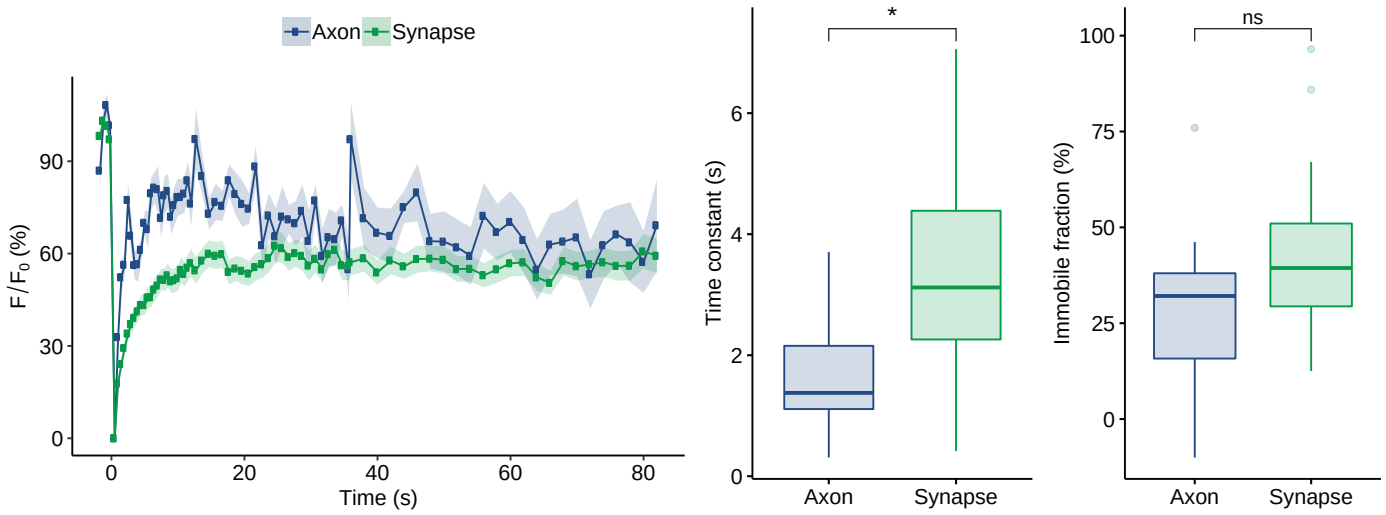

N (axons) = 15, N (synapses) = 24; p (time constant) = 5.04E-04.

Tagged protein outline:

Time constant (axon) is significantly different from time constant (axon) of: Synaptotagmin 1 (p = 2.19E-02).
Immobile fraction (axon) is not significantly different from immobile fraction (axon) of any other proteins.
Time constant (synapse) is significantly different from time constant (synapse) of: Amphiphysin (p = 1.15E-03), Dynamin 1 (p = 1.01E-03), Epsin (p = 1.57E-02), ITSN 1-L (p = 6.07E-03), PIP5KI-gamma (p = 1.63E-03), SCAMP1 (p = 1.15E-04), SV2B (p = 5.79E-03), Synapsin 1A (p = 3.83E-05), Synaptogyrin (p = 1.16E-05), Synaptophysin (p = 4.40E-07), Synaptotagmin 1 (p = 2.39E-07), Synaptotagmin 7 (p = 2.43E-02), Syntaxin 1A (p = 2.52E-03), Syntaxin 16 (p = 2.63E-06), alpha-Tubulin 1b (p = 3.19E-04), VAMP1 (p = 4.45E-06), vATPase V0a1 (p = 1.49E-02), vGluT1 (p = 4.12E-07), Vti1a-beta (p = 3.58E-03).
Immobile fraction (synapse) is significantly different from immobile fraction (synapse) of: alpha-SNAP (p = 1.23E-03), AP180 (p = 1.21E-04), Complexin 2 (p = 5.14E-03), mEGFP (p = 5.86E-05), Munc13 (p = 1.05E-02), Munc18 (p = 2.30E-05), Rab3a (p = 1.62E-02), Rab5a (p = 1.44E-06), Rab7a (p = 1.00E-03), Munc13 (p = 1.05E-02), SNAP29 (p = 1.46E-03), SV2B (p = 5.79E-03), Synaptophysin (p = 6.85E-03), Synaptotagmin 7 (p = 1.27E-02), Syndapin 1 (p = 1.82E-02), Syntaxin 1A (p = 3.28E-02).

References

Söllner, T., et al. (1997a). Cell 75, 409-18.
Jahn, R., and Scheller, R.H. (2006) Nat Rev Mol Cell Biol 7, 631-43.
Takamori, S., et al. (2006). Cell 127, 831-46.

PIP5KIγ

MW (kDa)	Category	τ_{axon} (s)	$\tau_{synapse}$ (s)	IF_{axon} (%)	$IF_{synapse}$ (%)
75.60	soluble, endocytic	3.77 ± 0.64	7.16 ± 0.56	32.76 ± 5.13	16.15 ± 5.98

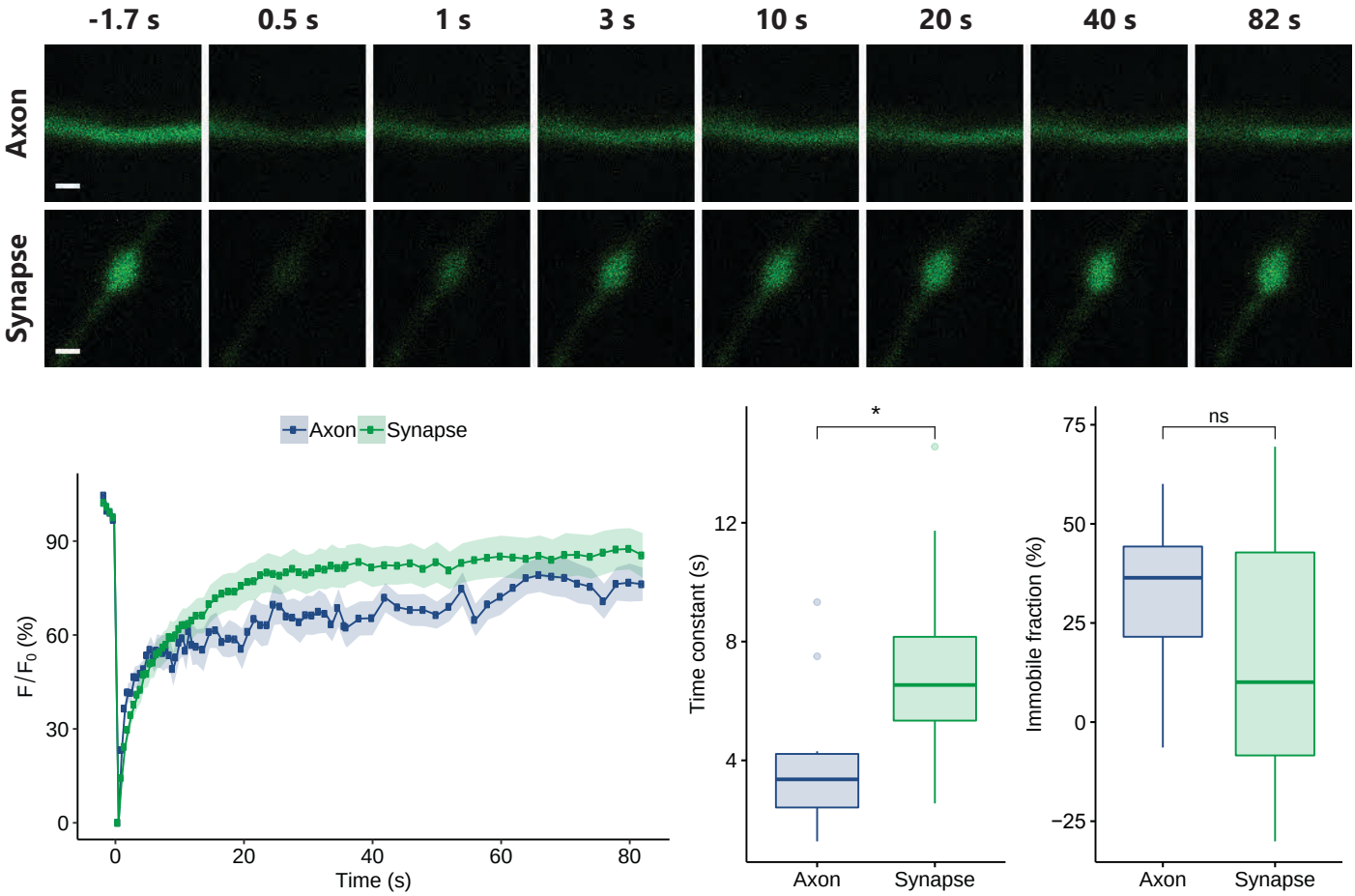

N (axons) = 13, N (synapses) = 24; p (time constant) = 3.45E-04.

Tagged protein outline:

Time constant (axon) is significantly different from time constant (axon) of: Actin (p = 2.75E-02), Munc13 (p = 2.96E-02).
Immobile fraction (axon) is not significantly different from immobile fraction (axon) of any other proteins.
Time constant (synapse) is significantly different from time constant (synapse) of: AP2 (p = 1.77E-04), Calmodulin 1 (p = 2.80E-05), Clathrin light chain B (p = 4.91E-05), Complexin 1 (p = 7.51E-03), Endophilin A1 (p = 2.37E-02), Hsc70 (p = 7.79E-06), mEGFP (p = 1.63E-09), Munc13 (p = 1.92E-03), Munc18 (p = 4.29E-02), NSF (p = 1.63E-03), Rab3a (p = 1.27E-02), Rab5a (p = 4.09E-04), Rab7a (p = 1.57E-02), SNAP23 (p = 5.10E-04), SNAP25 (p = 1.57E-03), Synapsin 1A (p = 4.70E-02), Synaptogyrin (p = 6.32E-04), Synaptophysin (p = 2.97E-05), Synaptotagmin 1 (p = 5.34E-06), VAMP1 (p = 4.31E-03), vGluT1 (p = 4.85E-04).
Immobile fraction (synapse) is significantly different from immobile fraction (synapse) of: SV2B (p = 9.59E-06), Synaptogyrin (p = 1.18E-02), Synaptophysin (p = 6.05E-06), vATPase V0a1 (p = 9.68E-03), vGluT1 (p = 1.28E-03).

References

Giudici, M.L., et al. (2004). Biochem J 379, 489-96.
Krauss, M., et al. (2003). J Cell Biol 162, 113-24.

Rab3a

MW (kDa)	Category	τ_{axon} (s)	$\tau_{synapse}$ (s)	IF_{axon} (%)	$IF_{synapse}$ (%)
24.97	vesicle-associated, SNARE co-factor	3.24 ± 0.33	4.00 ± 0.32	8.31 ± 3.79	14.31 ± 3.58

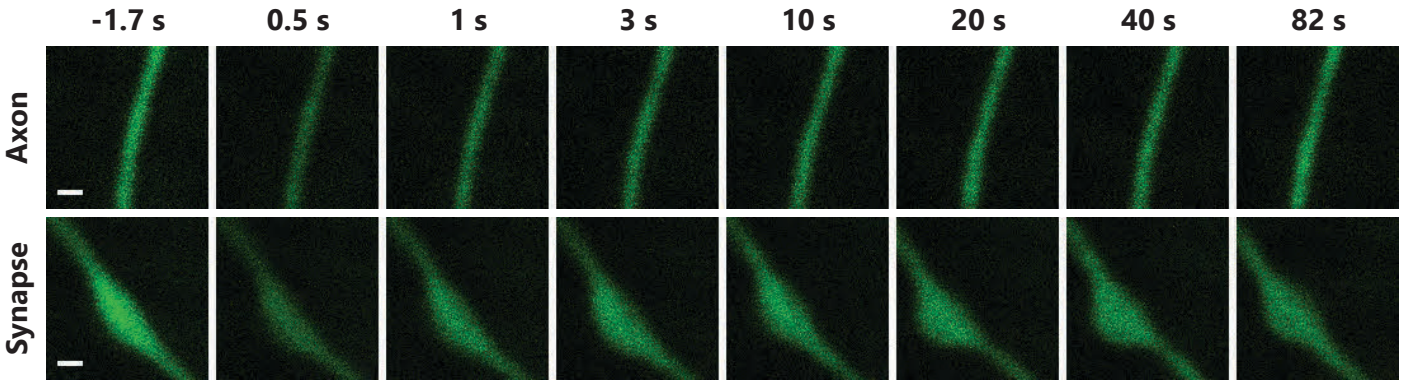

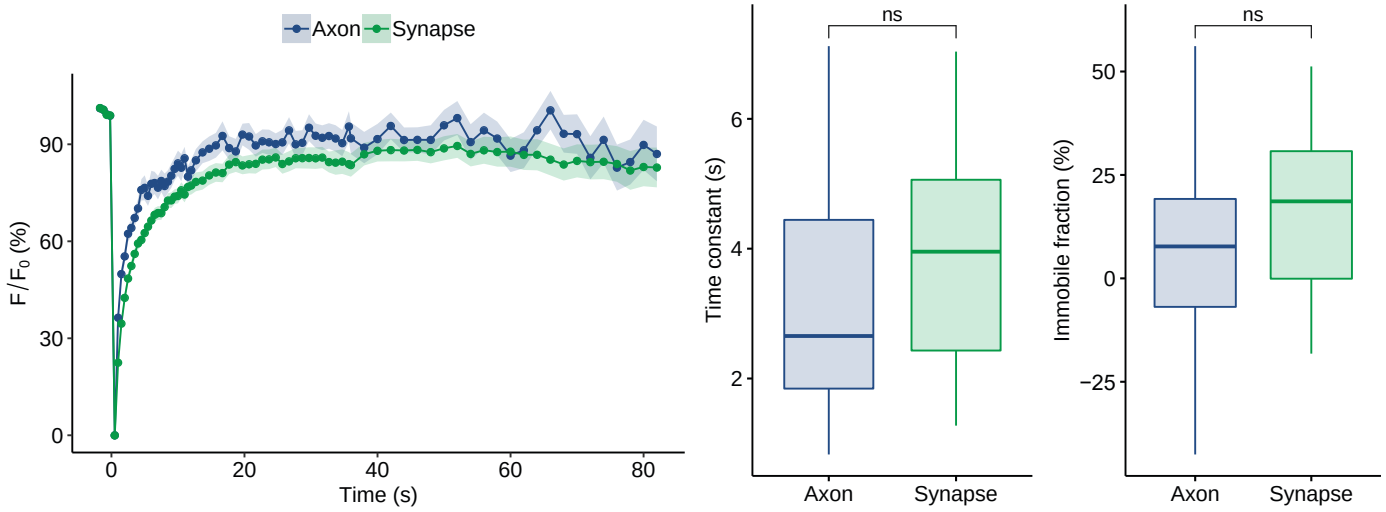

N (axons) = 29, N (synapses) = 29.

Tagged protein outline:

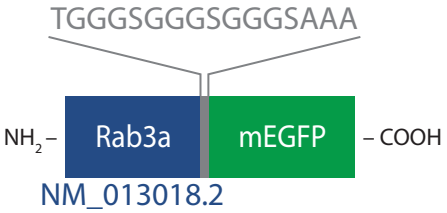

Time constant (axon) is significantly different from time constant (axon) of: Actin (p = 3.28E-03), Munc13 (p = 1.48E-03).
Immobile fraction (axon) is not significantly different from immobile fraction (axon) of any other proteins.
Time constant (synapse) is significantly different from time constant (synapse) of: Amphiphysin (p = 3.21E-02), Dynamin 1 (p = 1.31E-03), ITSN 1-L (p = 9.89E-03), mEGFP (p = 2.54E-04), PIP5KI-gamma (p = 1.27E-02), SCAMP1 (p = 6.65E-05), SV2B (p = 6.95E-03), Synapsin 1A (p = 3.19E-05), Synaptogyrin (p = 5.36E-06), Synaptophysin (p = 6.84E-08), Synaptotagmin 1 (p = 2.40E-08), Syntaxin 1A (p = 2.49E-02), Syntaxin 16 (p = 5.62E-06), alpha-Tubulin 1b (p = 3.45E-04), VAMP1 (p = 1.02E-06), vATPase V0a1 (p = 1.62E-02), vGluT1 (p = 7.59E-08), Vti1a-beta (p = 3.67E-03).
Immobile fraction (synapse) is significantly different from immobile fraction (synapse) of: NSF (p = 1.62E-02), SCAMP1 (p = 1.16E-02), SV2B (p = 4.42E-07), Synaptogyrin (p = 1.62E-03), Synaptophysin (p = 8.15E-08), Synaptotagmin 1 (p = 1.21E-03), VAMP2 (p = 2.18E-02), VAMP4 (p = 5.05E-03), vATPase V0a1 (p = 2.83E-04), vGluT1 (p = 9.77E-06).

References

Schlüter, O.M., et al. (2004). J Biol Chem 277, 40919-29.
Fische von Mollard, G., et al. (1991), Nature 349, 79-81.
Takamori, S., et al. (2006). Cell 127, 831-46.

Rab5a

MW (kDa)	Category	τ_{axon} (s)	$\tau_{synapse}$ (s)	IF_{axon} (%)	$IF_{synapse}$ (%)
23.62	endosome-associated	1.54 ± 0.13	3.82 ± 0.23	21.48 ± 3.46	8.23 ± 2.31

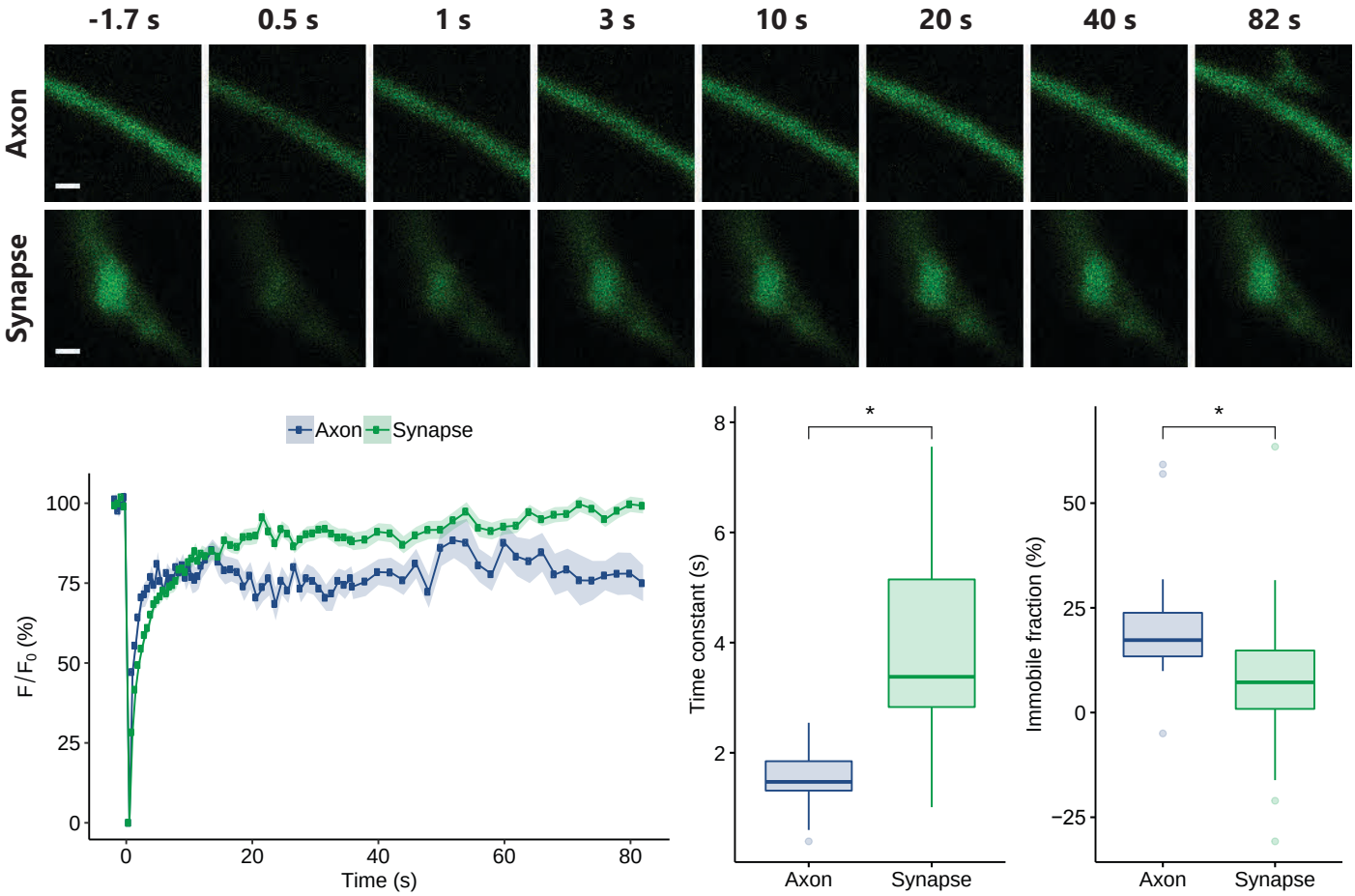

N (axons) = 19, N (synapses) = 45; p (time constant) = 3.58E-08, p (immobile fraction) = 6.52E-04.

Tagged protein outline:

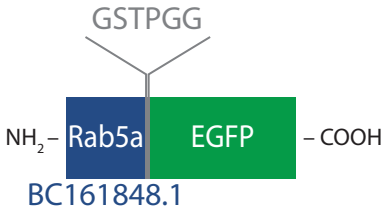

Time constant (axon) is significantly different from time constant (axon) of: Amphiphysin (p = 1.32E-02), SNAP29 (p = 8.11E-04), Synaptotagmin 1 (p = 5.57E-03), Syntaxin 1A (p = 1.15E-03), Syntaxin 16 (p = 3.71E-03), VAMP1 (p = 2.70E-03).
Immobile fraction (axon) is not significantly different from immobile fraction (axon) of any other proteins.
Time constant (synapse) is significantly different from time constant (synapse) of: Amphiphysin (p = 3.19E-04), Dynamin 1 (p = 7.14E-05), Epsin (p = 5.39E-03), ITSN 1-L (p = 3.17E-04), mEGFP (p = 2.42E-07), PIP5KI-gamma (p = 4.09E-04), SCAMP1 (p = 3.21E-06), SV2B (p = 7.56E-04), Synapsin 1A (p = 8.31E-07), Synaptogyrin (p = 1.28E-07), Synaptophysin (p = 3.31E-10), Synaptotagmin 1 (p = 1.14E-10), Synaptotagmin 7 (p = 3.81E-02), Syntaxin 1A (p = 6.81E-04), Syntaxin 16 (p = 4.98E-09), alpha-Tubulin 1b (p = 6.29E-06), VAMP1 (p = 1.15E-08), vATPase V0a1 (p = 7.59E-04), vGluT1 (p = 2.45E-10), Vti1a-beta (p = 1.80E-04).
Immobile fraction (synapse) is significantly different from immobile fraction (synapse) of: Hsc70 (p = 4.95E-02), ITSN 1-L (p = 3.67E-02), NSF (p = 1.44E-06), SCAMP1 (p = 1.27E-03), SNAP23 (p = 2.47E-02), SV2B (p = 1.73E-10), Synaptogyrin (p = 1.64E-05), Synaptophysin (p = 5.12E-11), Synaptotagmin 1 (p = 1.58E-06), VAMP1 (p = 2.04E-02), VAMP2 (p = 9.24E-06), VAMP4 (p = 7.42E-05), vATPase V0a1 (p = 3.70E-07), vGluT1 (p = 2.10E-08), Vti1a-beta (p = 2.58E-02).

References

Stenmark, H., et al. (1994). EMBO J 13, 1287-96.
Stenmark, H., et al. (1995). Cell 83, 423-32.
Takamori, S., et al. (2006). Cell 127, 831-46.

Rab7a

MW (kDa)	Category	τ_{axon} (s)	$\tau_{synapse}$ (s)	IF_{axon} (%)	$IF_{synapse}$ (%)
23.50	endosome-associated	1.74 ± 0.18	3.91 ± 0.34	24.83 ± 3.71	3.26 ± 4.68

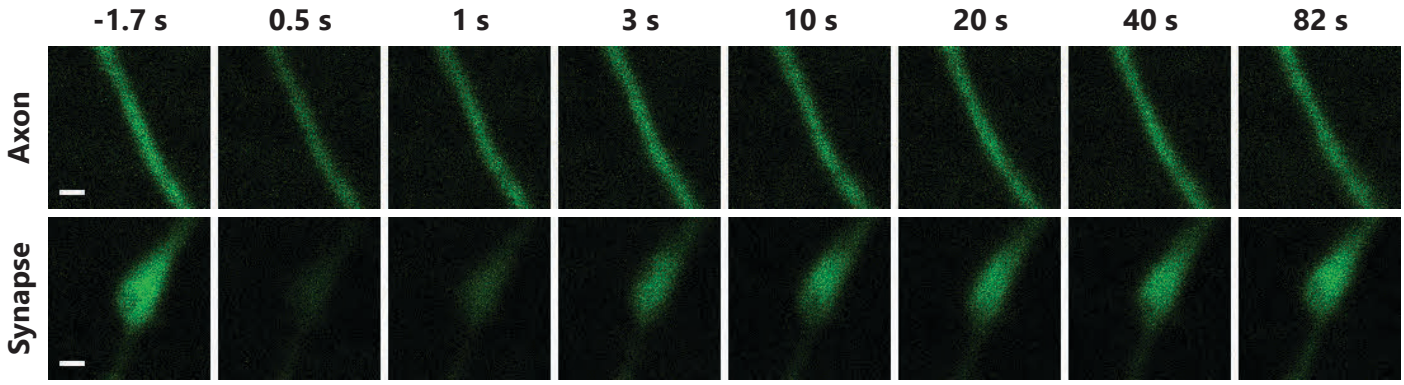

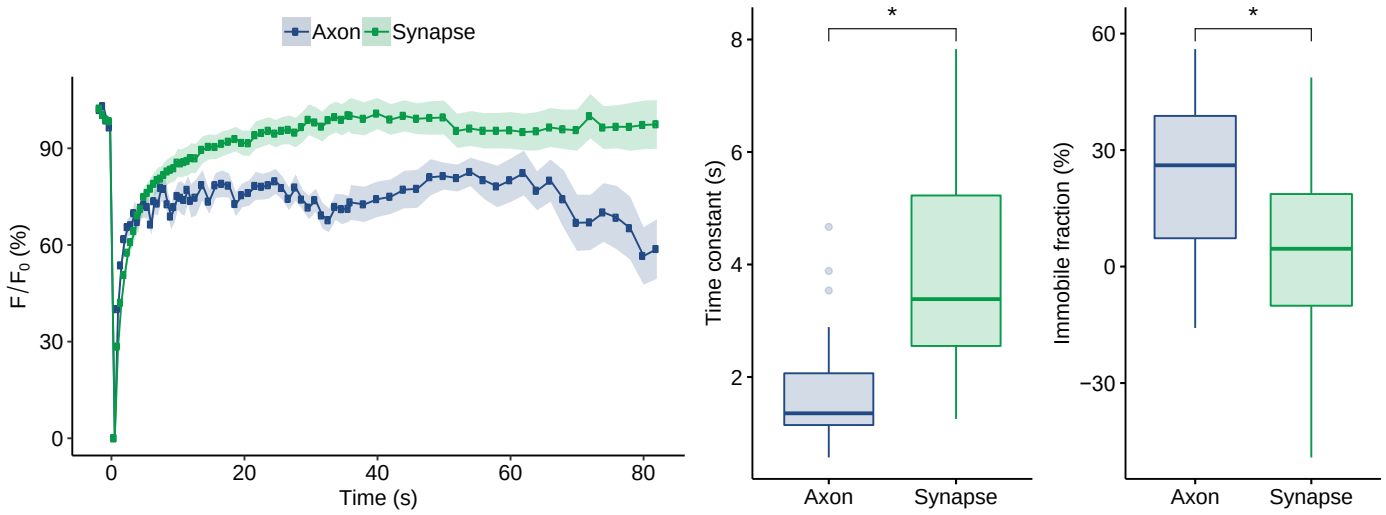

N (axons) = 29, N (synapses) = 28; p (time constant) = 4.37E-07, p (immobile fraction) = 1.71E-03.

Tagged protein outline:

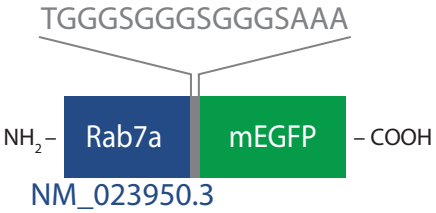

Time constant (axon) is significantly different from time constant (axon) of: Amphiphysin (p = 2.79E-02), SNAP29 (p = 1.56E-03), Synaptotagmin 1 (p = 1.74E-03), Syntaxin 1A (p = 7.74E-03), Syntaxin 16 (p = 5.21E-03), VAMP1 (p = 6.19E-03).
Immobile fraction (axon) is not significantly different from immobile fraction (axon) of any other proteins.
Time constant (synapse) is significantly different from time constant (synapse) of: Amphiphysin (p = 1.60E-02), Dynamin 1 (p = 2.07E-03), ITSN 1-L (p = 9.36E-03), mEGFP (p = 2.24E-04), PIP5KI-gamma (p = 1.57E-02), SCAMP1 (p = 1.44E-04), SV2B (p = 6.85E-03), Synapsin 1A (p = 2.26E-05), Synaptogyrin (p = 5.55E-06), Synaptophysin (p = 1.04E-07), Synaptotagmin 1 (p = 3.69E-08), Syntaxin 1A (p = 2.34E-02), Syntaxin 16 (p = 3.01E-06), alpha-Tubulin 1b (p = 2.58E-04), VAMP1 (p = 1.40E-06), vATPase V0a1 (p = 1.53E-02), vGluT1 (p = 1.30E-07), Vti1a-beta (p = 3.61E-03).
Immobile fraction (synapse) is significantly different from immobile fraction (synapse) of: NSF (p = 1.00E-03), SCAMP1 (p = 2.97E-03), SV2B (p = 1.56E-07), Synaptogyrin (p = 2.16E-04), Synaptophysin (p = 5.06E-08), Synaptotagmin 1 (p = 1.65E-04), VAMP2 (p = 1.33E-03), VAMP4 (p = 1.21E-03), vATPase V0a1 (p = 1.75E-05), vGluT1 (p = 4.09E-06).

References

Takamori, S., et al. (2006). Cell 127, 831-86.
Bucci, C., et al. (2000). Mol Biol Cell 11, 467-80.

SCAMP1

MW (kDa)	Category	τ_{axon} (s)	$\tau_{synapse}$ (s)	IF_{axon} (%)	$IF_{synapse}$ (%)
37.99	plasma membrane	-	12.57 ± 1.77	-	57.63 ± 6.92

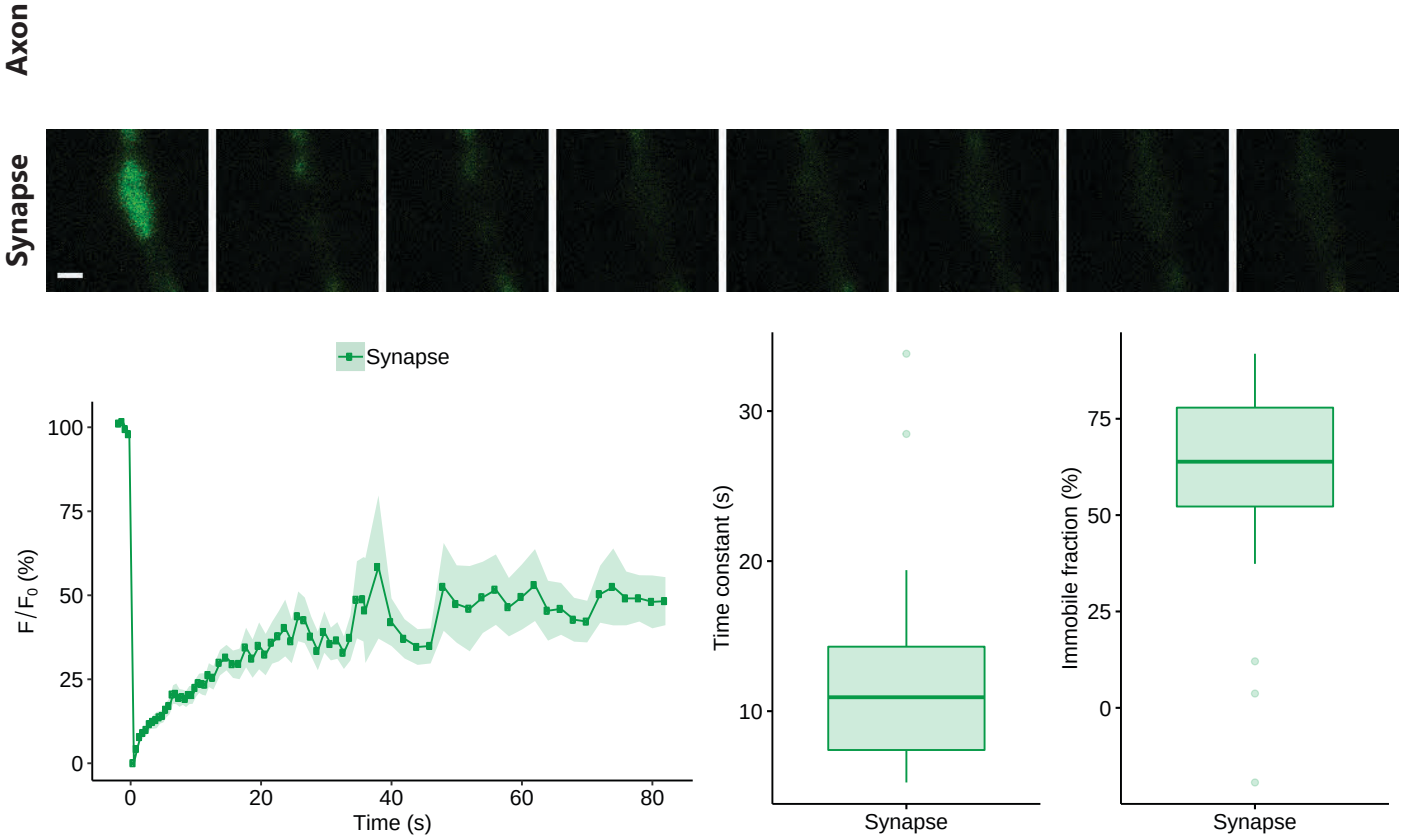

N (axons) = 0, N (synapses) = 19.

Tagged protein outline:

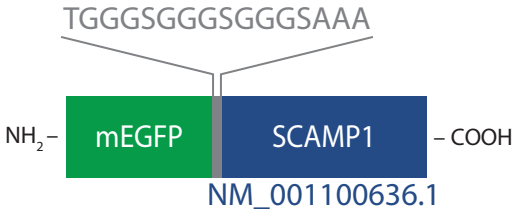

Time constant (synapse) is significantly different from time constant (synapse) of: alpha-SNAP (p = 1.16E-02), AP180 (p = 1.91E-04), AP2 (p = 2.62E-05), Calmodulin 1 (p = 1.59E-05), Clathrin light chain B (p = 1.33E-05), Complexin 1 (p = 1.25E-04), Complexin 2 (p = 2.16E-03), Endophilin A1 (p = 1.28E-04), Hsc70 (p = 1.51E-06), mEGFP (p = 4.64E-08), membrane mEGFP (p = 1.23E-03), Munc13 (p = 1.20E-05), Munc18 (p = 1.29E-05), NSF (p = 1.15E-04), Rab3a (p = 6.65E-05), Rab5a (p = 3.21E-06), Rab7a (p = 1.44E-04), Septin 5 (p = 1.91E-04), SNAP23 (p = 4.43E-05), SNAP25 (p = 3.72E-06), SNAP29 (p = 4.07E-03), Synaptotagmin 7 (p = 1.71E-02), Syndapin 1 (p = 4.52E-03), VAMP2 (p = 3.73E-02), VAMP4 (p = 7.09E-03).
Immobile fraction (synapse) is significantly different from immobile fraction (synapse) of: , alpha-SNAP (p = 8.31E-03), AP180 (p = 3.25E-03), AP2 (p = 2.74E-02), Complexin 2 (p = 3.02E-02), Doc2a (p = 4.35E-02), Endophilin A1 (p = 2.49E-02), mEGFP (p = 2.16E-03), Munc13 (p = 2.46E-03), Munc18 (p = 2.58E-03), Rab3a (p = 1.16E-02), Rab5a (p = 1.27E-03), Rab7a (p = 2.97E-03), Munc13 (p = 2.46E-03), SNAP29 (p = 6.83E-03), Synaptotagmin 7 (p = 7.84E-03), Syndapin 1 (p = 1.90E-02), Syntaxin 1A (p = 1.38E-02), Syntaxin 16 (p = 1.97E-02).

References

Castle, A., and Castle, D. (2005). J Cell Sci 118, 3769-80.
Takamori, S., et al. (2006). Cell 127, 831-846.

Septin 5

MW (kDa)	Category	τ_{axon} (s)	$\tau_{synapse}$ (s)	IF_{axon} (%)	$IF_{synapse}$ (%)
42.85	cytoskeletal	2.72 ± 0.35	4.40 ± 0.33	21.18 ± 4.78	21.23 ± 4.87

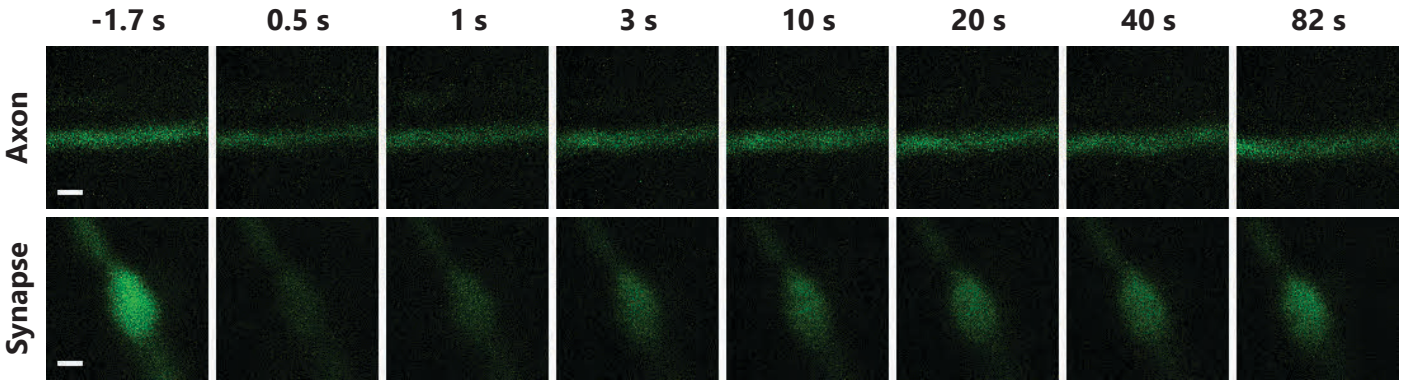

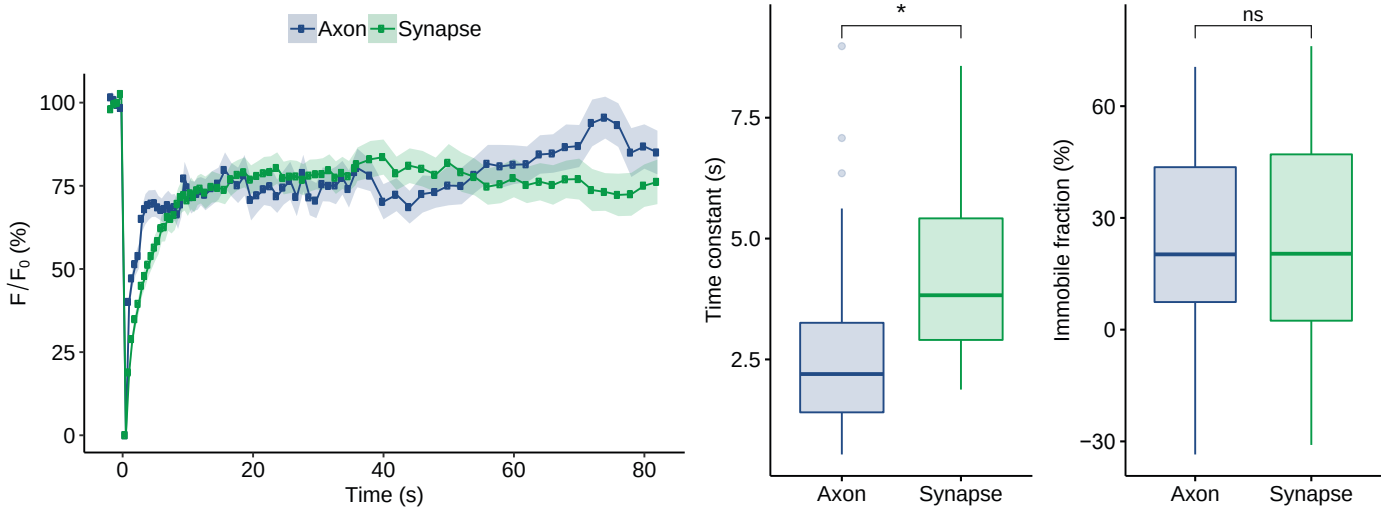

N (axons) = 32, N (synapses) = 37; p (time constant) = 8.98E-05.

Tagged protein outline:

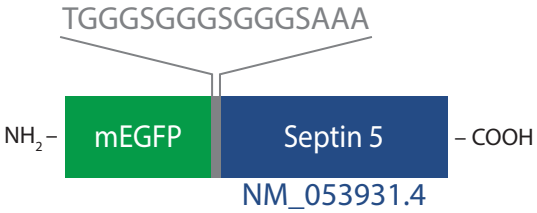

Time constant (axon) is not significantly different from time constant (axon) of any other proteins.
Immobile fraction (axon) is not significantly different from immobile fraction (axon) of any other proteins.
Time constant (synapse) is significantly different from time constant (synapse) of: Amphiphysin (p = 2.64E-02), Dynamin 1 (p = 4.22E-03), ITSN 1-L (p = 6.14E-03), mEGFP (p = 1.05E-08), SCAMP1 (p = 1.91E-04), SV2B (p = 9.04E-03), Synapsin 1A (p = 4.86E-06), Synaptogyrin (p = 6.51E-07), Synaptophysin (p = 8.36E-09), Synaptotagmin 1 (p = 1.72E-09), Syntaxin 16 (p = 8.21E-07), alpha-Tubulin 1b (p = 3.37E-04), VAMP1 (p = 2.55E-07), vATPase V0a1 (p = 1.99E-02), vGluT1 (p = 2.10E-08), Vti1a-beta (p = 1.93E-03).
Immobile fraction (synapse) is significantly different from immobile fraction (synapse) of: SV2B (p = 1.66E-07), Synaptogyrin (p = 4.69E-03), Synaptophysin (p = 1.54E-07), Synaptotagmin 1 (p = 4.16E-02), vATPase V0a1 (p = 7.34E-03), vGluT1 (p = 2.36E-04).

References

Mostowy, S., and Cossart, P. (2012). Nat Rev Mol Cell Biol 13, 183-94.
Beites, C.L., et al. (1999). Nat Neurosci 2, 434-9.
Amin, N.D., et al. (2008). J Neurosci 28, 3631-43.

SNAP23

MW (kDa)	Category	τ_{axon} (s)	$\tau_{synapse}$ (s)	IF_{axon} (%)	$IF_{synapse}$ (%)
23.23	plasma membrane-associated	2.79 ± 0.22	2.54 ± 0.23	16.58 ± 4.48	25.56 ± 3.09

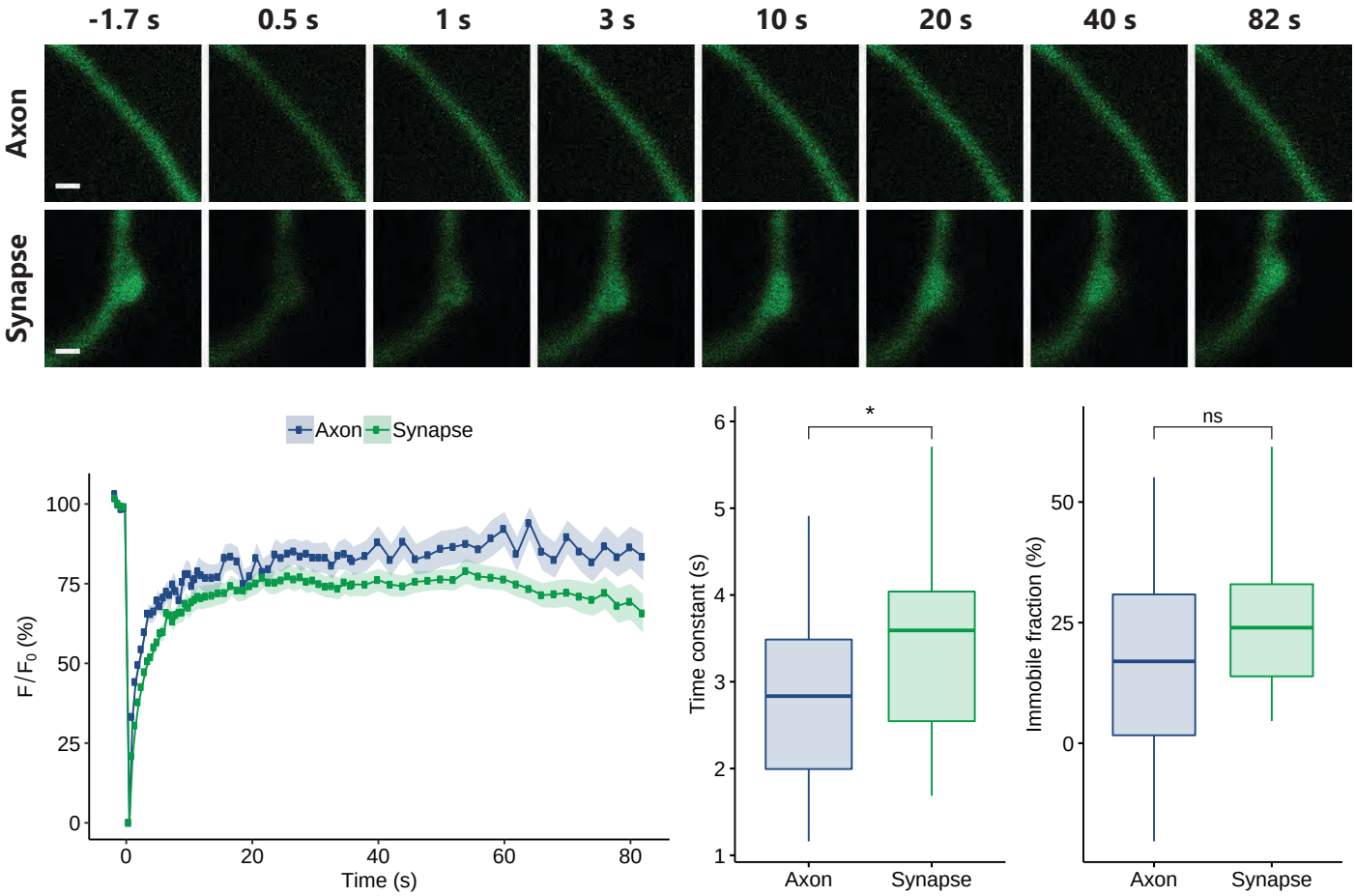

N (axons) = 22, N (synapses) = 24; p (time constant) = 2.56E-02.

Tagged protein outline:

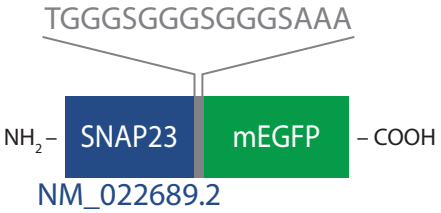

Time constant (axon) is significantly different from time constant (axon) of: Actin (p = 6.86E-03), Munc13 (p = 5.20E-03), Synaptotagmin 1 (p = 2.87E-02).
Immobile fraction (axon) is not significantly different from immobile fraction (axon) of any other proteins.
Time constant (synapse) is significantly different from time constant (synapse) of: Amphiphysin (p = 2.71E-04), Dynamin 1 (p = 1.01E-03), Epsin (p = 1.70E-03), ITSN 1-L (p = 3.48E-03), mEGFP (p = 7.99E-05), PIP5KI-gamma (p = 5.10E-04), SCAMP1 (p = 4.43E-05), SV2B (p = 2.15E-02), Synapsin 1A (p = 4.31E-05), Synaptogyrin (p = 8.06E-06), Synaptophysin (p = 4.85E-07), Synaptotagmin 1 (p = 2.39E-07), Synaptotagmin 7 (p = 7.72E-03), Syntaxin 1A (p = 1.00E-03), Syntaxin 16 (p = 1.38E-06), alpha-Tubulin 1b (p = 1.95E-04), VAMP1 (p = 3.98E-06), vATPase V0a1 (p = 2.01E-02), vGluT1 (p = 5.44E-07), Vti1a-beta (p = 4.64E-03).
Immobile fraction (synapse) is significantly different from immobile fraction (synapse) of: Rab5a (p = 2.47E-02), SV2B (p = 9.59E-06), Synaptogyrin (p = 2.74E-02), Synaptophysin (p = 2.91E-06), vATPase V0a1 (p = 3.05E-02), vGluT1 (p = 8.84E-04).

References

Jahn, R., and Scheller, R.H. (2006). Nat Rev Mol Cell Biol 7, 631-43.
Takamori, S., et al. (2006). Cell 127, 831-46.
Sorensen, J.B., et al. (2003). Cell 114, 75-86.

SNAP25

MW (kDa)	Category	τ_{axon} (s)	$\tau_{synapse}$ (s)	IF_{axon} (%)	$IF_{synapse}$ (%)
23.31	plasma membrane-associated	1.89 ± 0.17	4.38 ± 0.24	17.90 ± 3.31	19.49 ± 3.39

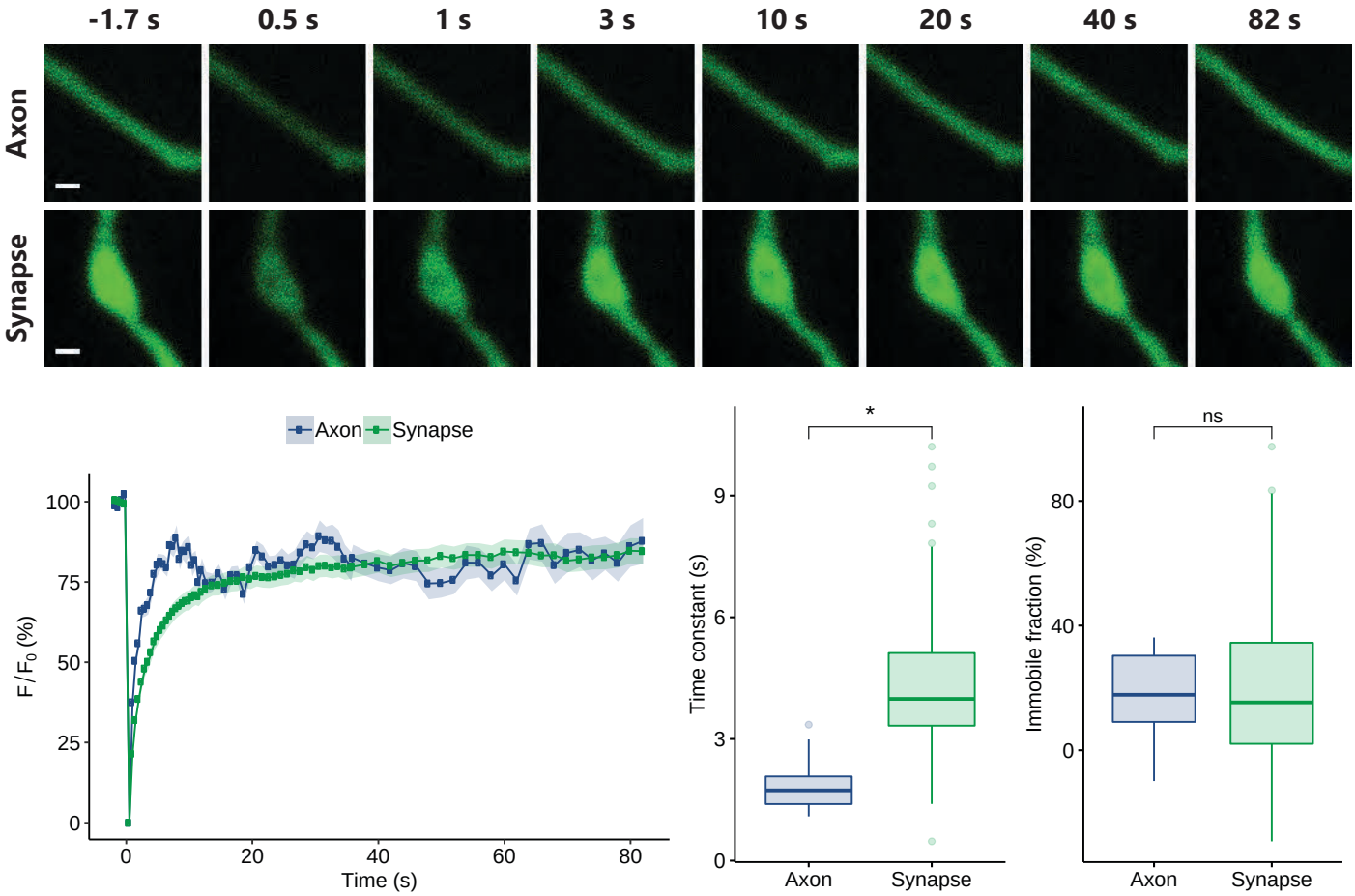

N (axons) = 16 N (synapses) = 65; p (time constant) = 1.18E-07.

Tagged protein outline:

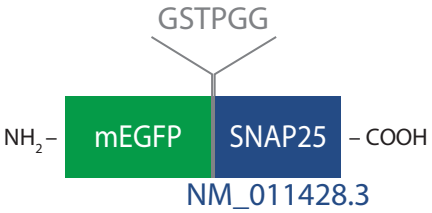

NM_011428.3

Time constant (axon) is significantly different from time constant (axon) of: , Synaptotagmin 1 (p = 2.17E-02), Syntaxin 1A (p = 4.78E-02).
Immobile fraction (axon) is not significantly different from immobile fraction (axon) of any other proteins.
Time constant (synapse) is significantly different from time constant (synapse) of: Amphiphysin (p = 2.71E-03), Dynamin 1 (p = 1.44E-04), ITSN 1-L (p = 3.49E-04), mEGFP (p = 8.10E-13), PIP5KI-gamma (p = 1.57E-03), SCAMP1 (p = 3.72E-06), SV2B (p = 6.10E-04), Synapsin 1A (p = 2.03E-07), Synaptogyrin (p = 1.16E-08), Synaptophysin (p = 6.30E-12), Synaptotagmin 1 (p = 3.10E-12), Syntaxin 1A (p = 4.43E-03), Syntaxin 16 (p = 4.90E-09), alpha-Tubulin 1b (p = 5.16E-06), VAMP1 (p = 3.44E-09), vATPase V0a1 (p = 7.65E-04), vGluT1 (p = 2.19E-11), Vti1a-beta (p = 9.96E-05).
Immobile fraction (synapse) is significantly different from immobile fraction (synapse) of: , SCAMP1 (p = 3.21E-02), SV2B (p = 1.17E-09), Synaptogyrin (p = 5.57E-04), Synaptophysin (p = 1.44E-09), Synaptotagmin 1 (p = 1.29E-03), VAMP4 (p = 2.92E-02), vATPase V0a1 (p = 9.08E-05), vGluT1 (p = 2.12E-06).

References

Walch-Solimena C., et. al. (1995). J Cell Biol 128, 637-45.
Takamori, S., et al. (2006). Cell 127, 831-46.
Bar-On, D., et. al. (2012). J Biol Chem 287, 27158-67.

SNAP29

MW (kDa)	Category	τ_{axon} (s)	$\tau_{synapse}$ (s)	IF_{axon} (%)	$IF_{synapse}$ (%)
29.07	plasma membrane-associated	3.65 ± 0.31	5.41 ± 0.32	6.58 ± 4.51	10.64 ± 3.28

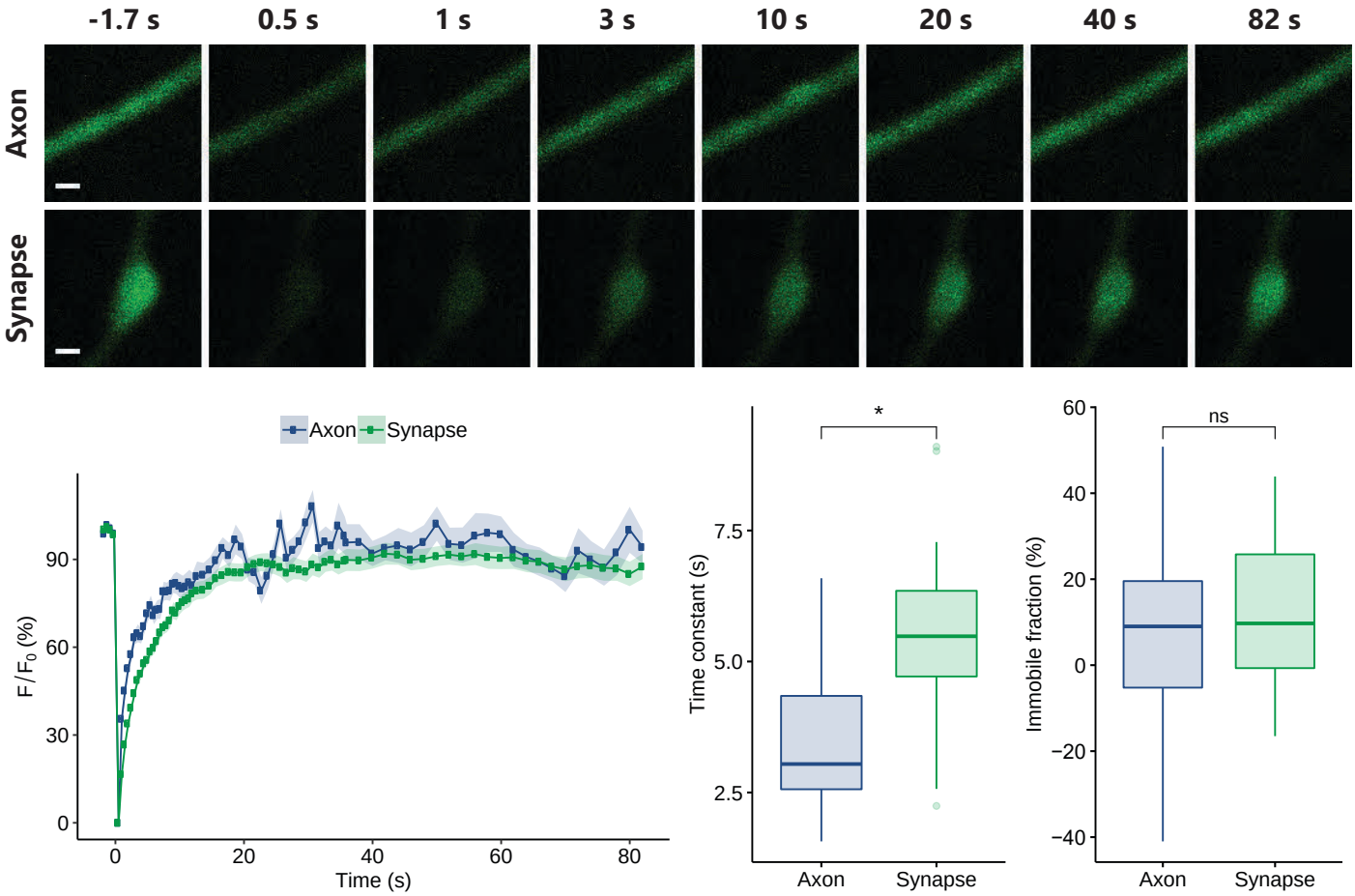

N (axons) = 25, N (synapses) = 35; p (time constant) = 5.29E-04.

Tagged protein outline:

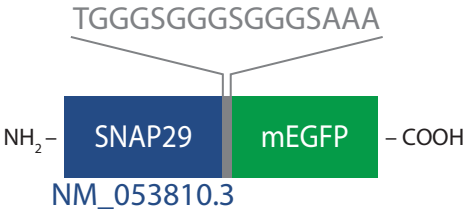

Time constant (axon) is significantly different from time constant (axon) of: Actin (p = 4.97E-05), AP180 (p = 3.55E-02), Clathrin light chain B (p = 5.30E-03), Doc2a (p = 4.27E-05), ITSN 1-L (p = 4.56E-02), mEGFP (p = 5.91E-03), Munc13 (p = 8.64E-06), Rab5a (p = 8.11E-04), Rab7a (p = 1.56E-03), Syndapin 1 (p = 1.16E-02).
Immobile fraction (axon) is not significantly different from immobile fraction (axon) of any other proteins.
Time constant (synapse) is significantly different from time constant (synapse) of: Calmodulin 1 (p = 1.67E-03), Clathrin light chain B (p = 1.62E-02), Hsc70 (p = 5.47E-04), mEGFP (p = 8.59E-10), SCAMP1 (p = 4.07E-03), Synapsin 1A (p = 6.27E-04), Synaptogyrin (p = 5.23E-05), Synaptophysin (p = 3.92E-07), Synaptotagmin 1 (p = 6.71E-08), Syntaxin 16 (p = 2.55E-03), alpha-Tubulin 1b (p = 1.74E-02), VAMP1 (p = 1.37E-05), vGluT1 (p = 9.68E-07).
Immobile fraction (synapse) is significantly different from immobile fraction (synapse) of: NSF (p = 1.46E-03), SCAMP1 (p = 6.83E-03), SV2B (p = 2.25E-07), Synaptogyrin (p = 6.89E-04), Synaptophysin (p = 5.06E-08), Synaptotagmin 1 (p = 3.38E-04), VAMP2 (p = 2.47E-03), VAMP4 (p = 1.46E-03), vATPase V0a1 (p = 6.41E-05), vGluT1 (p = 7.63E-06).

References

Peng, J., et al. (2004). J Biol Chem 279, 21003-11.
Takamori, S., et al. (2006). Cell 127, 831-846.

SV2B

MW (kDa)	Category	τ_{axon} (s)	$\tau_{synapse}$ (s)	IF_{axon} (%)	$IF_{synapse}$ (%)
77.50	vesicular	6.85 ± 1.45	17.35 ± 2.88	28.68 ± 10.33	75.35 ± 5.19

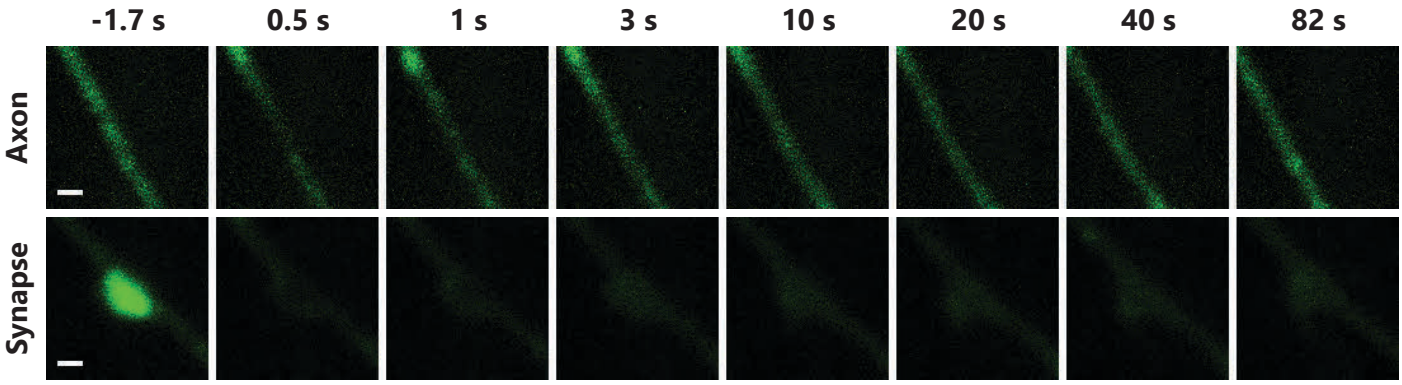

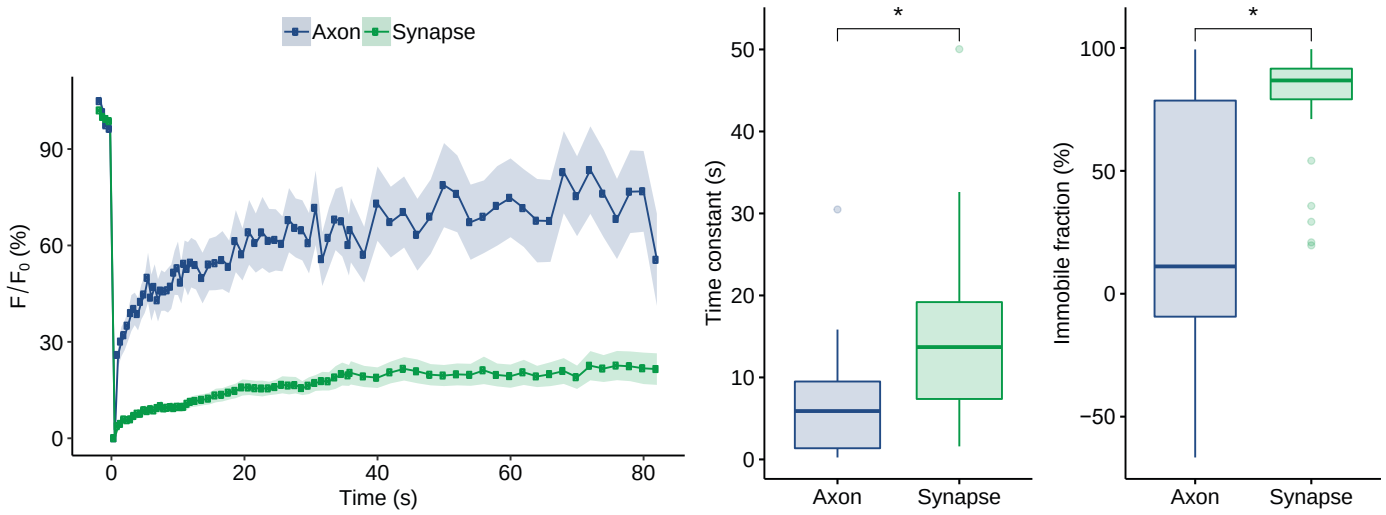

N (axons) = 23, N (synapses) = 35; p (time constant) = 7.83E-04, p (immobile fraction) = 1.66E-04.

Tagged protein outline:

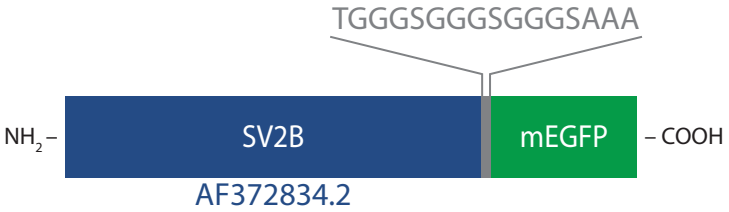

Time constant (axon) is not significantly different from time constant (axon) of any other proteins.
Immobile fraction (axon) is not significantly different from immobile fraction (axon) of any other proteins.
Time constant (synapse) is significantly different from time constant (synapse) of: AP180 (p = 9.12E-03), AP2 (p = 6.85E-03), Calmodulin 1 (p = 8.46E-04), Clathrin light chain B (p = 1.32E-03), Complexin 1 (p = 2.04E-03), Doc2a (p = 4.00E-02), Hsc70 (p = 1.82E-05), mEGFP (p = 2.00E-09), membrane mEGFP (p = 4.51E-02), Munc13 (p = 7.96E-04), Munc18 (p = 3.27E-04), NSF (p = 5.79E-03), Rab3a (p = 6.95E-03), Rab5a (p = 7.56E-04), Rab7a (p = 6.85E-03), Septin 5 (p = 9.04E-03), SNAP23 (p = 2.15E-02), SNAP25 (p = 6.10E-04).
Immobile fraction (synapse) is significantly different from immobile fraction (synapse) of: Actin (p = 7.07E-06), alpha-SNAP (p = 5.49E-07), alpha-synuclein (p = 2.43E-06), Amphiphysin (p = 1.24E-06), AP180 (p = 1.74E-08), AP2 (p = 6.71E-07), Calmodulin 1 (p = 1.94E-06), Clathrin light chain B (p = 6.61E-07), Complexin 1 (p = 5.41E-07), Complexin 2 (p = 2.47E-07), Doc2a (p = 8.17E-07), Dynamin 1 (p = 4.80E-03), Endophilin A1 (p = 9.59E-07), Epsin (p = 4.21E-05), Hsc70 (p = 5.25E-08), ITSN 1-L (p = 1.03E-02), mEGFP (p = 1.94E-11), membrane mEGFP (p = 5.76E-06), Munc13 (p = 5.12E-09), Munc18 (p = 3.07E-12), NSF (p = 5.79E-03), PIP5KI-gamma (p = 9.59E-06), Rab3a (p = 4.42E-07), Rab5a (p = 1.73E-10), Rab7a (p = 1.56E-07), Septin 5 (p = 1.66E-07), SNAP23 (p = 9.59E-06), Munc13 (p = 5.12E-09), SNAP29 (p = 2.25E-07), Synapsin 1A (p = 9.19E-05), Synaptotagmin 1 (p = 2.35E-03), Synaptotagmin 7 (p = 4.05E-07), Syndapin 1 (p = 3.22E-07), Syntaxin 1A (p = 3.90E-07), Syntaxin 16 (p = 5.17E-08), alpha-Tubulin 1b (p = 4.89E-03), VAMP1 (p = 2.88E-05), VAMP2 (p = 3.74E-04), Vti1a-beta (p = 2.40E-03).

References

Buckley, K., and Kelly, R.B. (1985). J Cell Biol 100, 1284-94.
Bajjalieh, S.M., et al. (1992). Science 257, 1271-3.
Takamori, S., et al. (2006). Cell 127, 831-46.

Synapsin 1A

MW (kDa)	Category	τ_{axon} (s)	$\tau_{synapse}$ (s)	IF_{axon} (%)	$IF_{synapse}$ (%)
73.99	soluble, vesicle tethering	5.84 ± 1.03	13.38 ± 1.19	19.74 ± 8.70	23.51 ± 8.84

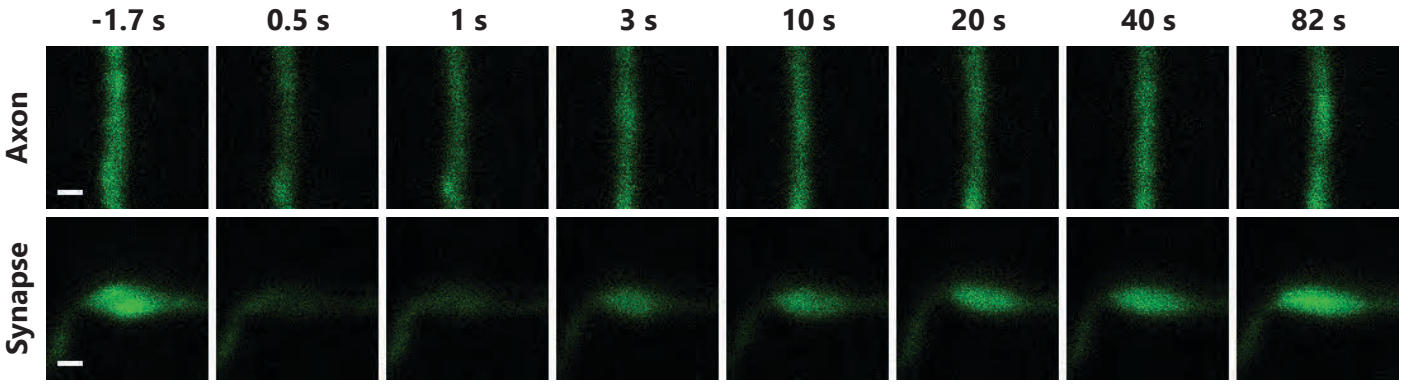

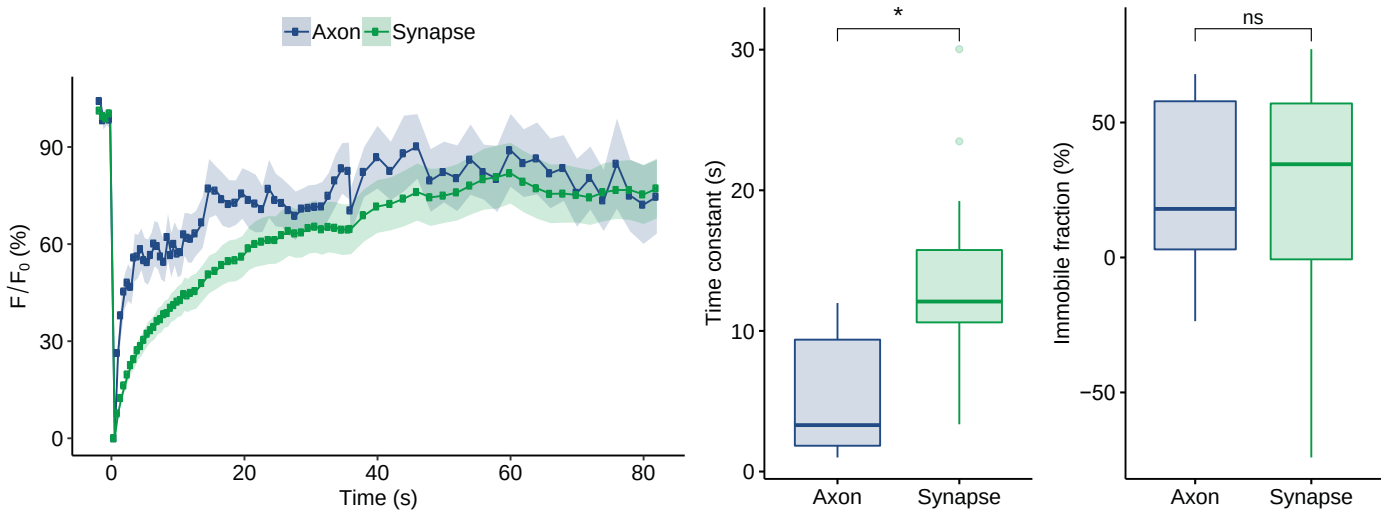

N (axons) = 17, N (synapses) = 24; p (time constant) = 4.66E-05.

Tagged protein outline:

Time constant (axon) is significantly different from time constant (axon) of: Actin (p = 2.82E-02), Munc13 (p = 2.47E-02).
Immobile fraction (axon) is not significantly different from immobile fraction (axon) of any other proteins.
Time constant (synapse) is significantly different from time constant (synapse) of: Actin (p = 1.04E-02), alpha-SNAP (p = 4.39E-04), alpha-synuclein (p = 4.14E-03), Amphiphysin (p = 1.34E-03), AP180 (p = 2.84E-05), AP2 (p = 1.07E-05), Calmodulin 1 (p = 4.45E-06), Clathrin light chain B (p = 3.95E-06), Complexin 1 (p = 1.19E-05), Complexin 2 (p = 1.45E-04), Doc2a (p = 3.38E-04), Endophilin A1 (p = 3.45E-05), Epsin (p = 3.75E-02), Hsc70 (p = 3.53E-07), mEGFP (p = 7.77E-10), membrane mEGFP (p = 1.91E-04), Munc13 (p = 9.74E-07), Munc18 (p = 1.88E-07), NSF (p = 3.83E-05), PIP5KI-gamma (p = 4.70E-02), Rab3a (p = 3.19E-05), Rab5a (p = 8.31E-07), Rab7a (p = 2.26E-05), Septin 5 (p = 4.86E-06), SNAP23 (p = 4.31E-05), SNAP25 (p = 2.03E-07), SNAP29 (p = 6.27E-04), Synaptotagmin 7 (p = 1.48E-03), Syndapin 1 (p = 1.54E-04), Syntaxin 1A (p = 2.76E-03), VAMP2 (p = 8.19E-04), VAMP4 (p = 3.30E-04).
Immobile fraction (synapse) is significantly different from immobile fraction (synapse) of: SV2B (p = 9.19E-05), Synaptophysin (p = 4.95E-04).

References

Cesca, F., et al. (2010). Prog Neurobiol 91, 313-48.
Siksou, L., et al. (2007). J Neurosci 27, 6868-77.
Hirokawa, N., et al. (1989). J Cell Biol 108, 111-26.
Takamori, S., et al. (2006). Cell 127, 831-46.

Synaptogyrin

MW (kDa)	Category	τ_{axon} (s)	$\tau_{synapse}$ (s)	IF_{axon} (%)	$IF_{synapse}$ (%)
25.67	vesicular	-	33.65 ± 4.19	-	65.35 ± 6.54

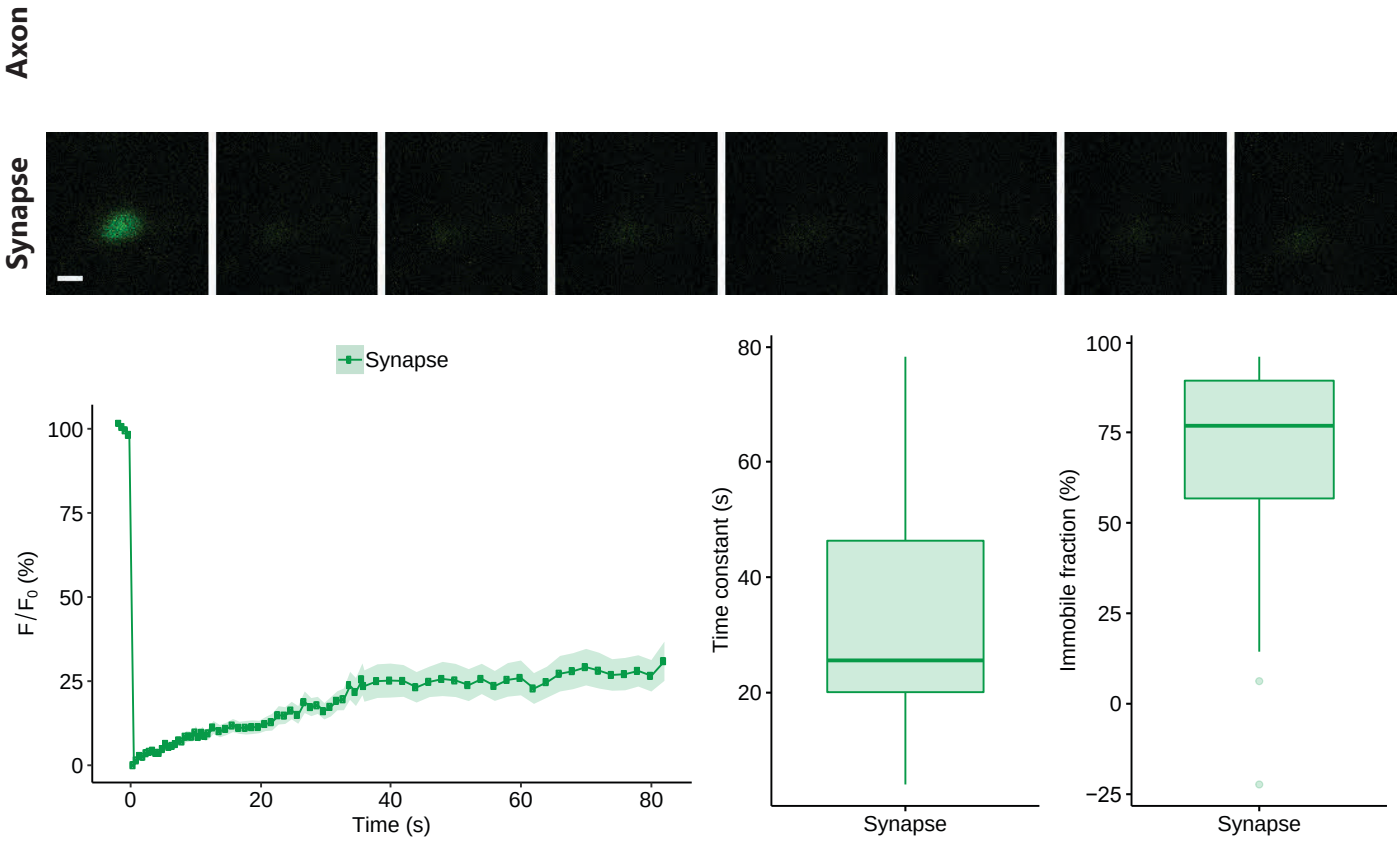

N (axons) = 0, N (synapses) = 24.

Tagged protein outline:

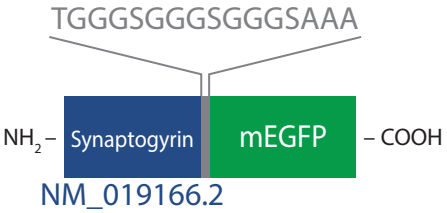

Time constant (synapse) is significantly different from time constant (synapse) of: Actin (p = 1.08E-04), alpha-SNAP (p = 4.97E-05), alpha-synuclein (p = 1.85E-05), Amphiphysin (p = 1.88E-05), AP180 (p = 3.84E-06), AP2 (p = 2.85E-06), Calmodulin 1 (p = 1.62E-06), Clathrin light chain B (p = 1.05E-06), Complexin 1 (p = 2.22E-06), Complexin 2 (p = 1.48E-05), CSP (p = 6.67E-04), Doc2a (p = 3.19E-05), Dynamin 1 (p = 7.16E-03), Endophilin A1 (p = 5.55E-06), Epsin (p = 2.17E-03), Hsc70 (p = 9.92E-08), ITSN 1-L (p = 7.83E-04), mEGFP (p = 6.34E-10), membrane mEGFP (p = 1.90E-05), Munc13 (p = 1.09E-07), Munc18 (p = 1.01E-08), NSF (p = 1.16E-05), PIP5KI-gamma (p = 6.32E-04), Rab3a (p = 5.36E-06), Rab5a (p = 1.28E-07), Rab7a (p = 5.55E-06), Septin 5 (p = 6.51E-07), SNAP23 (p = 8.06E-06), SNAP25 (p = 1.16E-08), SNAP29 (p = 5.23E-05), Synaptotagmin 7 (p = 4.32E-05), Syndapin 1 (p = 2.18E-05), Syntaxin 1A (p = 8.74E-05), Syntaxin 16 (p = 5.38E-03), alpha-Tubulin 1b (p = 4.71E-03), VAMP2 (p = 1.08E-04), VAMP4 (p = 6.11E-05), vATPase V0a1 (p = 1.58E-02).
Immobile fraction (synapse) is significantly different from immobile fraction (synapse) of: Actin (p = 3.08E-02), alpha-SNAP (p = 7.39E-04), alpha-synuclein (p = 2.02E-02), Amphiphysin (p = 2.05E-02), AP180 (p = 2.45E-04), AP2 (p = 1.46E-03), Calmodulin 1 (p = 1.32E-02), Clathrin light chain B (p = 8.30E-03), Complexin 1 (p = 8.84E-03), Complexin 2 (p = 1.60E-03), Doc2a (p = 5.99E-03), Endophilin A1 (p = 5.14E-03), Epsin (p = 3.02E-02), Hsc70 (p = 2.96E-03), mEGFP (p = 3.29E-05), membrane mEGFP (p = 4.54E-02), Munc13 (p = 8.53E-05), Munc18 (p = 2.52E-05), PIP5KI-gamma (p = 1.18E-02), Rab3a (p = 1.62E-03), Rab5a (p = 1.64E-05), Rab7a (p = 2.16E-04), Septin 5 (p = 4.69E-03), SNAP23 (p = 2.74E-02), Munc13 (p = 8.53E-05), SNAP29 (p = 6.89E-04), Synaptotagmin 7 (p = 7.84E-04), Syndapin 1 (p = 2.13E-03), Syntaxin 1A (p = 1.10E-03), Syntaxin 16 (p = 6.27E-04),

References

Baumert, M., et al. (1990). J Cell Biol 110, 1285-94.
Jahn, R., et al. (1985). Proc Natl Acad Sci U S A 82, 4127-41.
Takamori, S., et al. (2006). Cell 127, 831-46.

Synaptophysin

MW (kDa)	Category	τ_{axon} (s)	$\tau_{synapse}$ (s)	IF_{axon} (%)	$IF_{synapse}$ (%)
33.31	vesicular	3.08 ± 0.64	24.60 ± 3.53	22.26 ± 7.20	72.59 ± 2.99

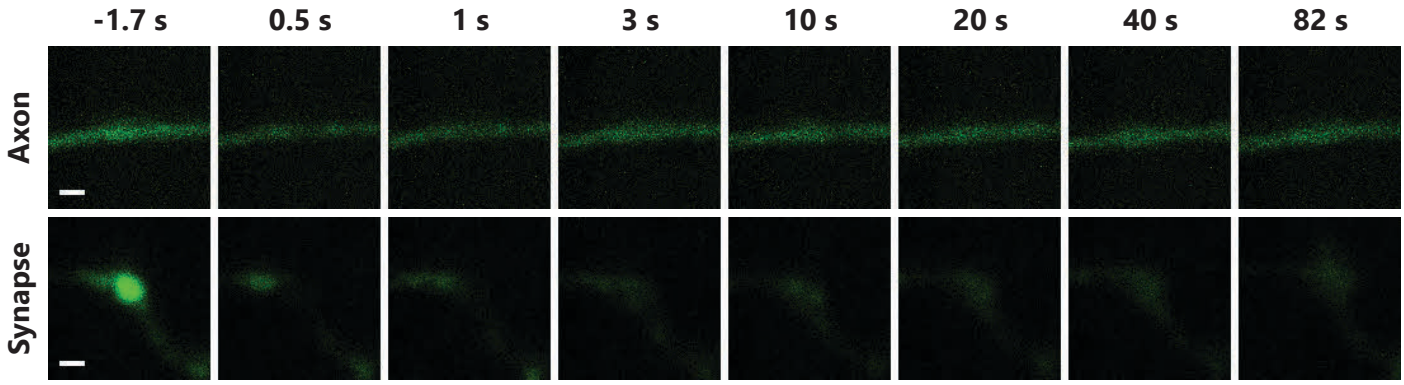

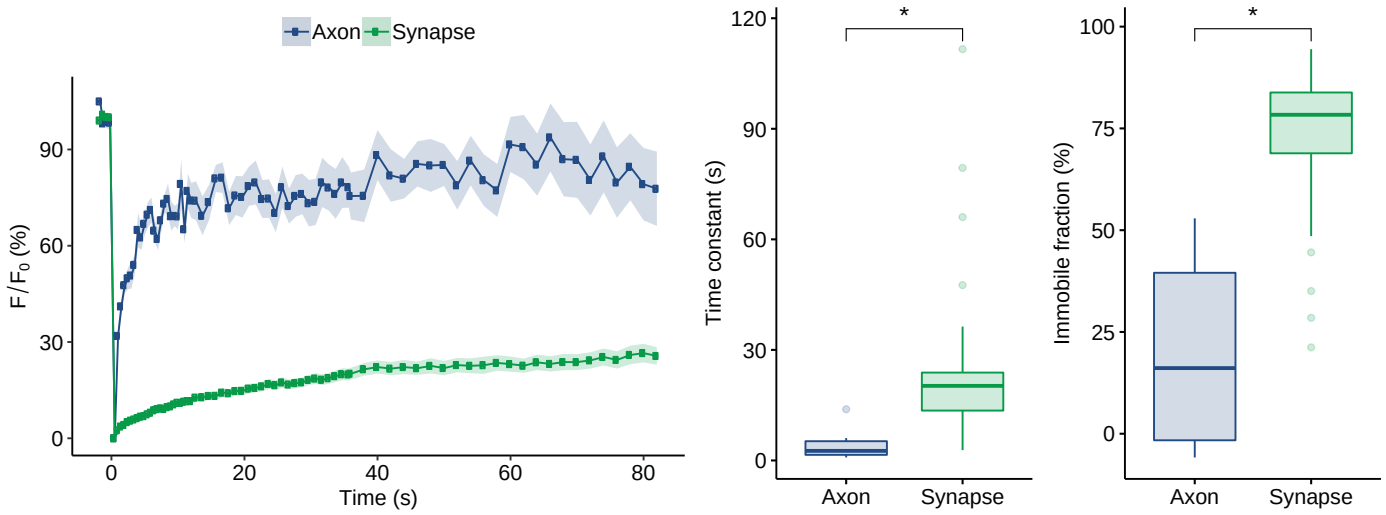

N (axons) = 10, N (synapses) = 36; p (time constant) = 4.53E-06, p (immobile fraction) = 7.29E-06.

Tagged protein outline:

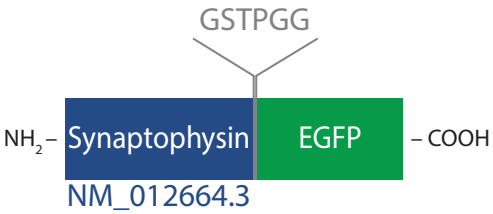

Time constant (axon) is not significantly different from time constant (axon) of any other proteins.
Immobile fraction (axon) is not significantly different from immobile fraction (axon) of any other proteins.
Time constant (synapse) is significantly different from time constant (synapse) of: Actin (p = 1.04E-05), alpha-SNAP (p = 1.47E-06), alpha-synuclein (p = 1.13E-06), Amphiphysin (p = 1.85E-07), AP180 (p = 2.55E-08), AP2 (p = 7.96E-08), Calmodulin 1 (p = 4.21E-08), Clathrin light chain B (p = 1.15E-08), Complexin 1 (p = 3.82E-08), Complexin 2 (p = 3.29E-07), CSP (p = 1.49E-04), Doc2a (p = 3.26E-07), Dynamin 1 (p = 2.57E-02), Endophilin A1 (p = 1.78E-07), Epsin (p = 1.15E-04), Hsc70 (p = 4.40E-10), ITSN 1-L (p = 6.11E-04), mEGFP (p = 2.09E-13), membrane mEGFP (p = 1.79E-07), Munc13 (p = 4.08E-10), Munc18 (p = 1.66E-12), NSF (p = 4.40E-07), PIP5KI-gamma (p = 2.97E-05), Rab3a (p = 6.84E-08), Rab5a (p = 3.31E-10), Rab7a (p = 1.04E-07), Septin 5 (p = 8.36E-09), SNAP23 (p = 4.85E-07), SNAP25 (p = 6.30E-12), SNAP29 (p = 3.92E-07), Synaptotagmin 7 (p = 5.41E-07), Syndapin 1 (p = 2.11E-07), Syntaxin 1A (p = 1.30E-06), alpha-Tubulin 1b (p = 1.10E-02), VAMP2 (p = 2.76E-06), VAMP4 (p = 1.83E-06).
Immobile fraction (synapse) is significantly different from immobile fraction (synapse) of: Actin (p = 1.04E-05), alpha-SNAP (p = 2.06E-07), alpha-synuclein (p = 3.63E-06), Amphiphysin (p = 1.92E-06), AP180 (p = 4.81E-09), AP2 (p = 2.53E-07), Calmodulin 1 (p = 1.98E-06), Clathrin light chain B (p = 3.64E-06), Complexin 1 (p = 1.64E-07), Complexin 2 (p = 1.04E-07), Doc2a (p = 1.06E-07), Endophilin A1 (p = 1.94E-07), Epsin (p = 2.59E-05), Hsc70 (p = 1.25E-08), mEGFP (p = 2.69E-12), membrane mEGFP (p = 8.57E-06), Munc13 (p = 6.77E-09), Munc18 (p = 1.92E-13), NSF (p = 6.85E-03), PIP5KI-gamma (p = 6.05E-06), Rab3a (p = 8.15E-08), Rab5a (p = 5.12E-11), Rab7a (p = 5.06E-08), Septin 5 (p = 1.54E-07), SNAP23 (p = 2.91E-06), Munc13 (p = 6.77E-09), SNAP29 (p = 5.06E-08), Synapsin 1A (p = 4.95E-04), Synaptotagmin 7 (p = 7.47E-08), Syndapin 1 (p = 5.89E-08), Syntaxin 1A (p = 1.14E-07), Syntaxin 16 (p = 3.97E-08), alpha-Tubulin 1b (p = 2.16E-02), VAMP1 (p = 3.85E-05), VAMP2 (p = 3.03E-04), Vti1a-beta (p = 3.66E-02).

References

Jahn, R., et al. (1985). Proc Natl Acad Sci U S A 82, 4137-41.
Reisinger, C., et al. (2004). J Neurochem 90, 1-8.
Takamori, S., et al. (2006). Cell 127, 831-846.

Synaptotagmin 1

MW (kDa)	Category	τ_{axon} (s)	$\tau_{synapse}$ (s)	IF_{axon} (%)	$IF_{synapse}$ (%)
47.40	vesicular	6.48 ± 0.96	25.36 ± 3.28	6.77 ± 7.34	26.66 ± 13.46

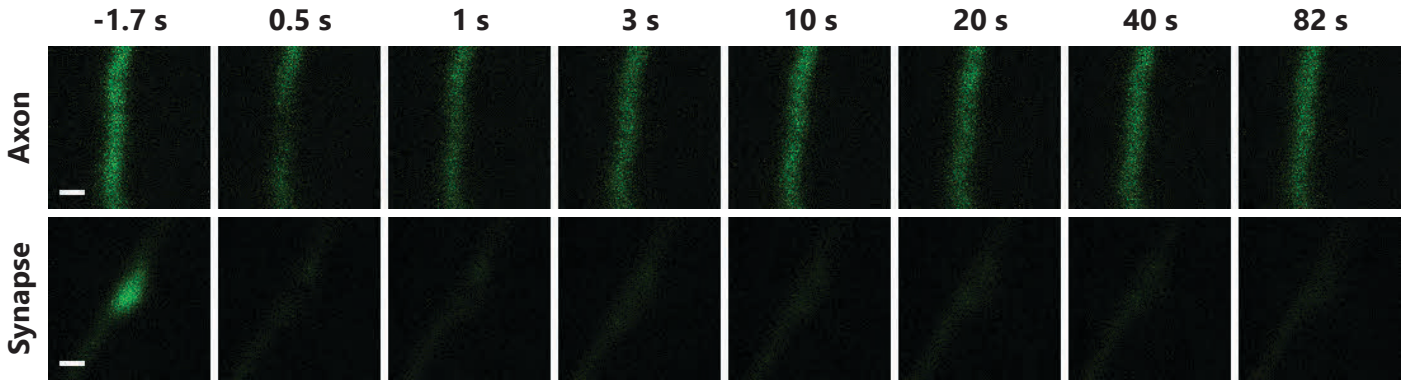

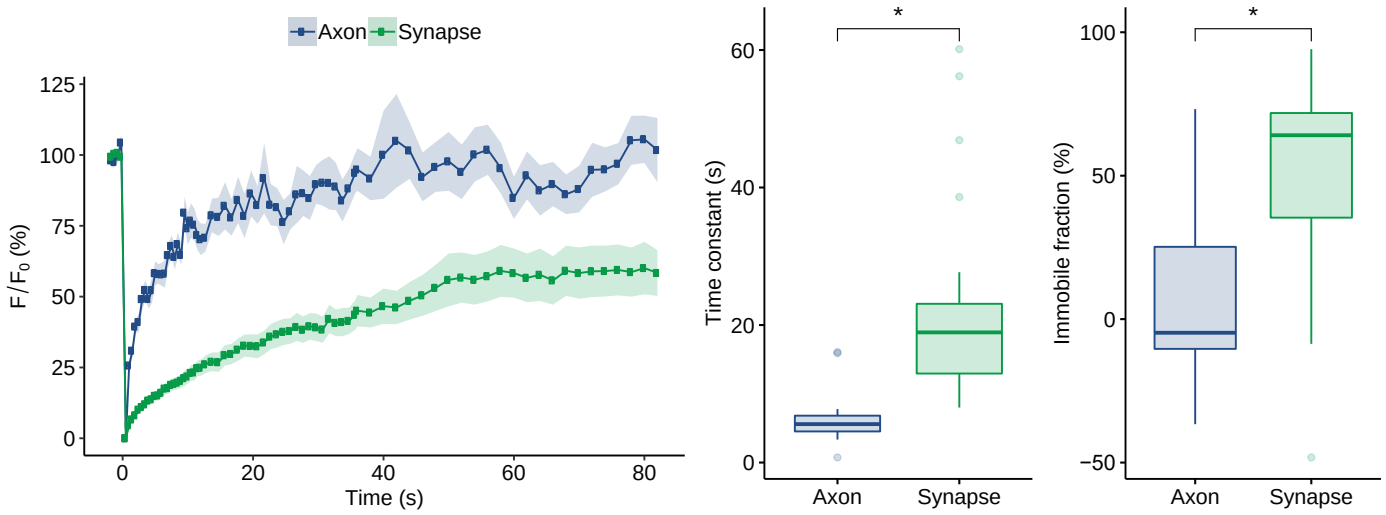

N (axons) = 17, N (synapses) = 35; p (time constant) = 2.52E-07, p (immobile fraction) = 6.88E-05.

Tagged protein outline:

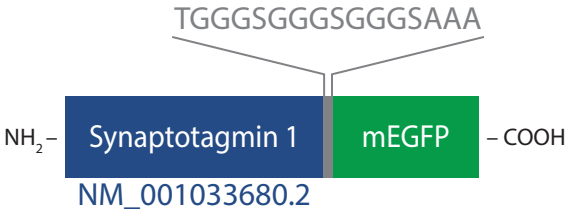

Time constant (axon) is significantly different from time constant (axon) of: Actin (p = 1.97E-03), AP180 (p = 1.78E-03), AP2 (p = 2.10E-03), Calmodulin 1 (p = 2.13E-02), Clathrin light chain B (p = 2.01E-03), Doc2a (p = 9.18E-04), Endophilin A1 (p = 8.12E-03), Hsc70 (p = 3.80E-02), ITSN 1-L (p = 1.35E-02), mEGFP (p = 1.50E-03), membrane mEGFP (p = 2.87E-02), Munc13 (p = 8.17E-05), NSF (p = 2.19E-02), Rab5a (p = 5.57E-03), Rab7a (p = 1.74E-03), SNAP23 (p = 2.87E-02), SNAP25 (p = 2.17E-02), Synaptotagmin 7 (p = 2.82E-02), Syndapin 1 (p = 1.38E-03).
Immobile fraction (axon) is not significantly different from immobile fraction (axon) of any other proteins.
Time constant (synapse) is significantly different from time constant (synapse) of: Actin (p = 4.59E-06), alpha-SNAP (p = 3.37E-07), alpha-synuclein (p = 1.00E-06), Amphiphysin (p = 7.09E-08), AP180 (p = 6.50E-09), AP2 (p = 3.69E-08), Calmodulin 1 (p = 3.69E-08), Clathrin light chain B (p = 7.19E-09), Complexin 1 (p = 2.12E-08), Complexin 2 (p = 6.71E-08), CSP (p = 8.25E-05), Doc2a (p = 1.03E-07), Dynamin 1 (p = 4.71E-02), Endophilin A1 (p = 3.69E-08), Epsin (p = 2.10E-05), Hsc70 (p = 4.70E-10), ITSN 1-L (p = 1.75E-03), mEGFP (p = 1.67E-12), membrane mEGFP (p = 3.92E-08), Munc13 (p = 1.14E-10), Munc18 (p = 4.96E-13), NSF (p = 2.39E-07), PIP5KI-gamma (p = 5.34E-06), Rab3a (p = 2.40E-08), Rab5a (p = 1.14E-10), Rab7a (p = 3.69E-08), Septin 5 (p = 1.72E-09), SNAP23 (p = 2.39E-07), SNAP25 (p = 3.10E-12), SNAP29 (p = 6.71E-08), Synaptotagmin 7 (p = 7.74E-08), Syndapin 1 (p = 3.43E-08), Syntaxin 1A (p = 2.39E-07), alpha-Tubulin 1b (p = 2.41E-02), VAMP2 (p = 2.74E-07), VAMP4 (p = 3.29E-07).
Immobile fraction (synapse) is significantly different from immobile fraction (synapse) of: alpha-SNAP (p = 4.68E-04), AP180 (p = 4.74E-05), AP2 (p = 2.81E-03), Complexin 1 (p = 9.74E-03), Complexin 2 (p = 1.07E-03), Doc2a (p = 5.01E-03), Endophilin A1 (p = 4.33E-03), Hsc70 (p = 1.12E-02), mEGFP (p = 7.13E-06), Munc13 (p = 1.72E-04), Munc18 (p = 2.69E-06), Rab3a (p = 1.21E-03), Rab5a (p = 1.58E-06), Rab7a (p = 1.65E-04), Septin 5 (p = 4.16E-02), Munc13 (p = 1.72E-04), SNAP29 (p = 3.38E-04), SV2B (p = 2.35E-03), Synaptotagmin 7 (p = 7.20E-04), Syndapin 1 (p = 2.05E-03), Syntaxin 1A (p = 1.25E-03), Syntaxin 16 (p = 1.70E-02),

References

Opazo, F., et al. (2010). Traffic 11, 800-12.
Takamori, S., et al. (2006). Cell 127, 831-46.

Synaptotagmin 7

MW (kDa)	Category	τ_{axon} (s)	$\tau_{synapse}$ (s)	IF_{axon} (%)	$IF_{synapse}$ (%)
45.48	vesicular	2.66 ± 0.29	5.90 ± 0.39	19.51 ± 2.66	8.21 ± 5.15

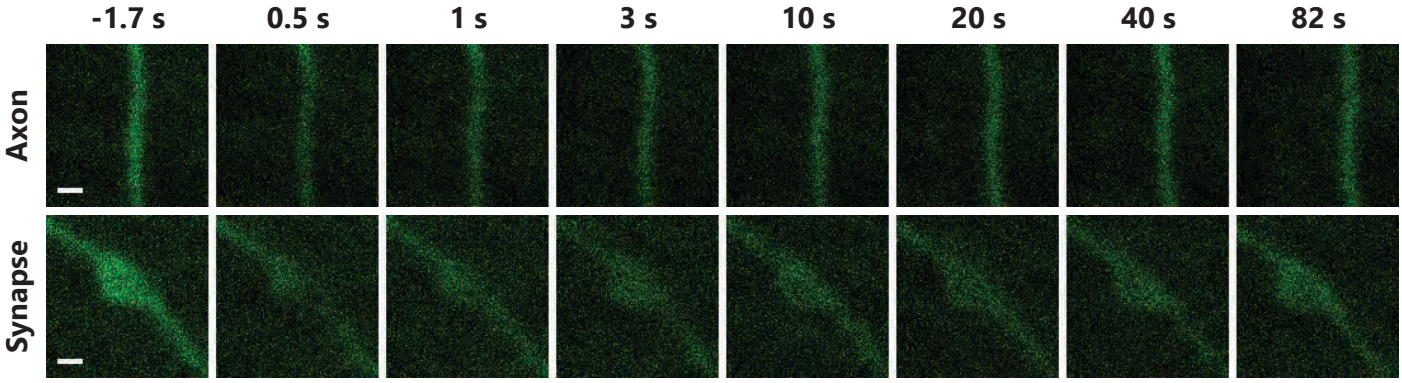

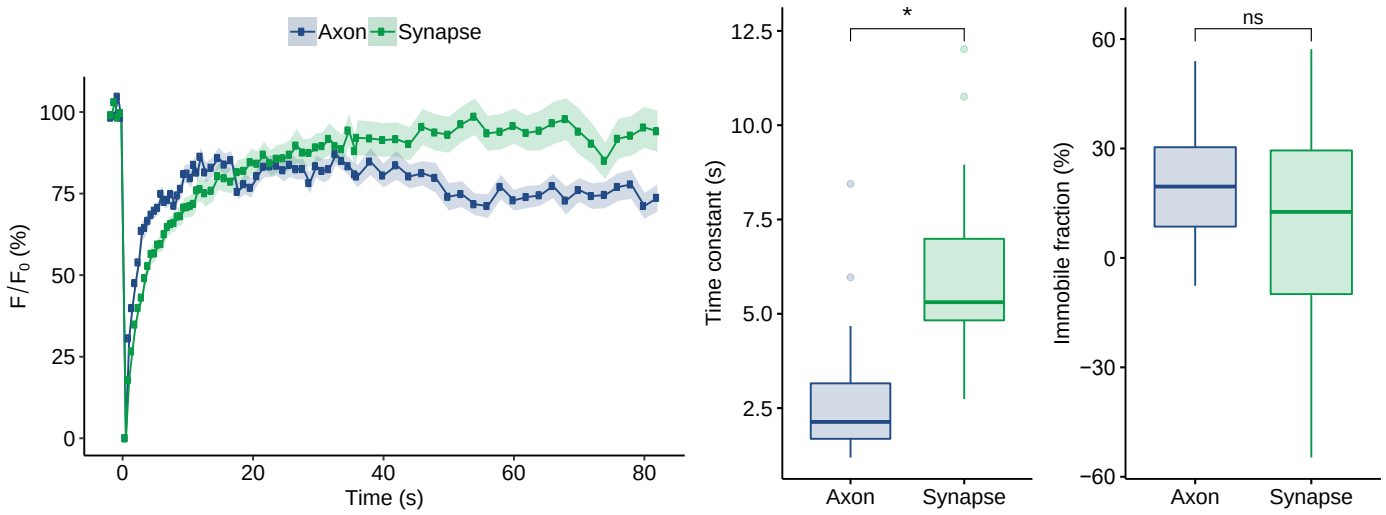

N (axons) = 29, N (synapses) = 29; p (time constant) = 3.09E-08.

Tagged protein outline:

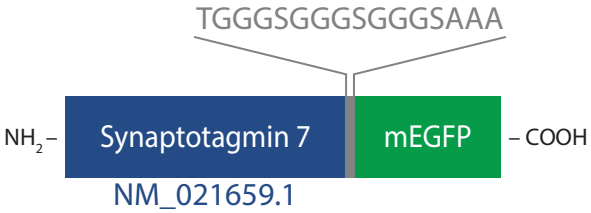

Time constant (axon) is significantly different from time constant (axon) of: Actin (p = 9.12E-03), Munc13 (p = 8.65E-03), Synaptotagmin 1 (p = 2.82E-02).
Immobile fraction (axon) is not significantly different from immobile fraction (axon) of any other proteins.
Time constant (synapse) is significantly different from time constant (synapse) of: AP2 (p = 4.55E-03), Calmodulin 1 (p = 1.59E-04), Clathrin light chain B (p = 2.48E-03), Hsc70 (p = 7.21E-05), mEGFP (p = 5.55E-11), NSF (p = 2.43E-02), Rab5a (p = 3.81E-02), SCAMP1 (p = 1.71E-02), SNAP23 (p = 7.72E-03), Synapsin 1A (p = 1.48E-03), Synaptogyrin (p = 4.32E-05), Synaptophysin (p = 5.41E-07), Synaptotagmin 1 (p = 7.74E-08), Syntaxin 16 (p = 9.27E-03), VAMP1 (p = 4.22E-05), vGluT1 (p = 2.47E-06).
Immobile fraction (synapse) is significantly different from immobile fraction (synapse) of: NSF (p = 1.27E-02), SCAMP1 (p = 7.84E-03), SV2B (p = 4.05E-07), Synaptogyrin (p = 7.84E-04), Synaptophysin (p = 7.47E-08), Synaptotagmin 1 (p = 7.20E-04), VAMP2 (p = 1.16E-02), VAMP4 (p = 5.50E-03), vATPase V0a1 (p = 9.62E-05), vGluT1 (p = 7.23E-06).

References

Fernandez, I., et al. (2001). Neuron 32, 1057-69.
Takamori, S., et al. (2006). Cell 127, 831-46.

Syndapin 1

MW (kDa)	Category	τ_{axon} (s)	$\tau_{synapse}$ (s)	IF_{axon} (%)	$IF_{synapse}$ (%)
50.45	soluble, endocytic	2.00 ± 0.14	5.30 ± 0.36	28.10 ± 2.78	16.17 ± 3.59

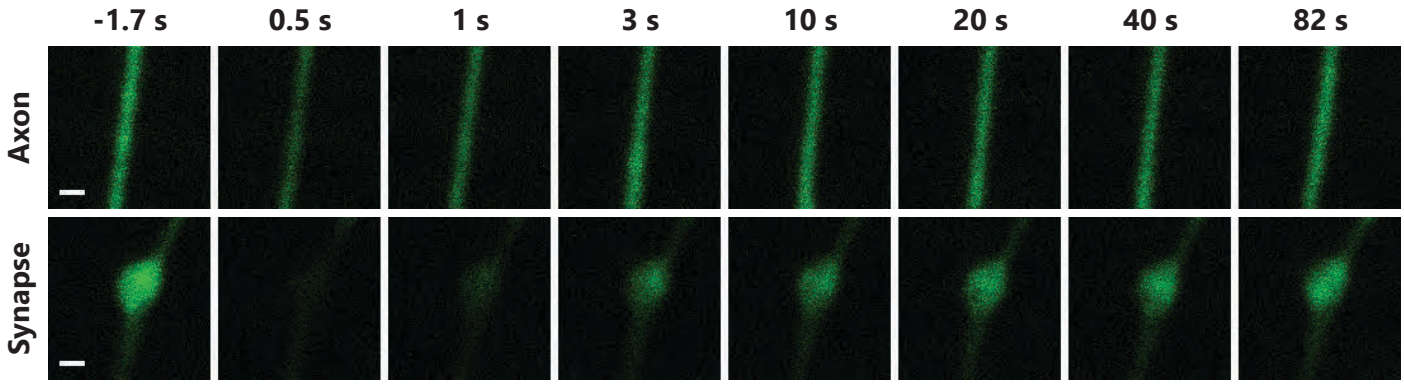

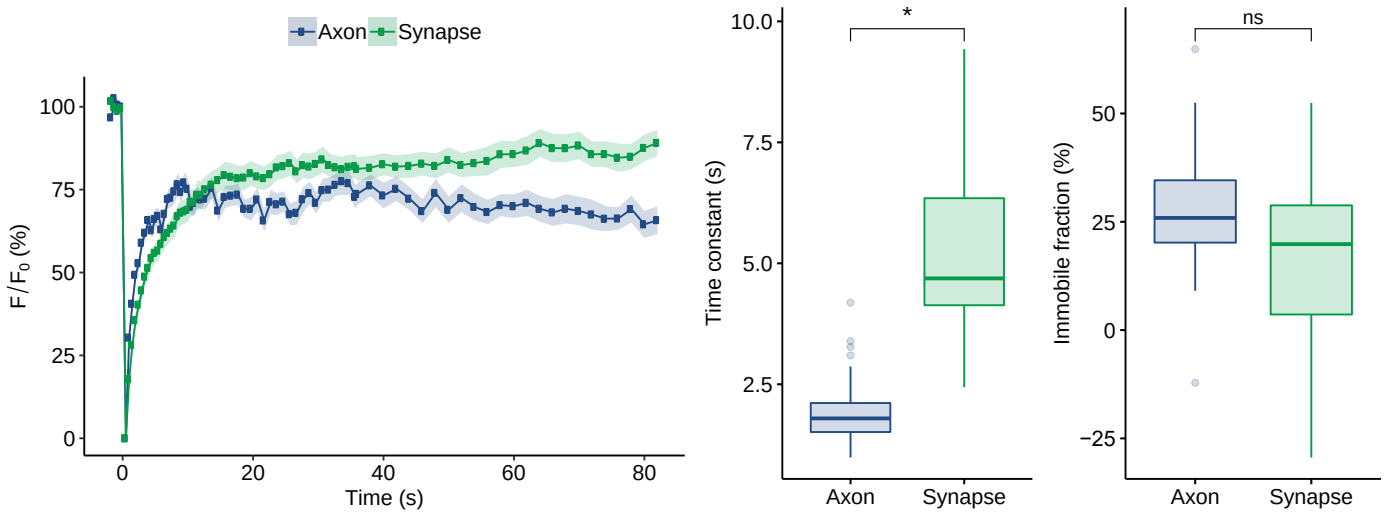

N (axons) = 29, N (synapses) = 30; p (time constant) = 7.84E-10.

Tagged protein outline:

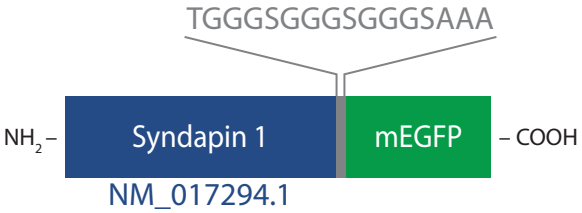

Time constant (axon) is significantly different from time constant (axon) of: SNAP29 (p = 1.16E-02), Synaptotagmin 1 (p = 1.38E-03), Syntaxin 1A (p = 9.67E-03), VAMP1 (p = 2.41E-02).
Immobile fraction (axon) is significantly different from immobile fraction (axon) of: Endophilin A1 (p = 1.12E-02), VAMP2 (p = 4.91E-02).
Time constant (synapse) is significantly different from time constant (synapse) of: Calmodulin 1 (p = 1.06E-02), Hsc70 (p = 2.09E-03), mEGFP (p = 2.70E-10), SCAMP1 (p = 4.52E-03), Synapsin 1A (p = 1.54E-04), Synaptogyrin (p = 2.18E-05), Synaptophysin (p = 2.11E-07), Synaptotagmin 1 (p = 3.43E-08), Syntaxin 16 (p = 5.78E-04), alpha-Tubulin 1b (p = 9.82E-03), VAMP1 (p = 1.42E-05), vGluT1 (p = 5.53E-07), Vti1a-beta (p = 4.84E-02).
Immobile fraction (synapse) is significantly different from immobile fraction (synapse) of: NSF (p = 1.82E-02), SCAMP1 (p = 1.90E-02), SV2B (p = 3.22E-07), Synaptogyrin (p = 2.13E-03), Synaptophysin (p = 5.89E-08), Synaptotagmin 1 (p = 2.05E-03), VAMP2 (p = 1.73E-02), VAMP4 (p = 1.82E-02), vATPase V0a1 (p = 2.77E-04), vGluT1 (p = 1.42E-05).

References

Kessels, M.M., and Qualmann, B. (2004). J Cell Sci 117, 3077-86.
Anggono, V., et al. (2006). Nat Neurosci 9, 752-60.
Kessels, M.M., and Qualmann, B. (2006). J Biol Chem 281. 13285-99.

Syntaxin 1A

MW (kDa)	Category	τ_{axon} (s)	$\tau_{synapse}$ (s)	IF_{axon} (%)	$IF_{synapse}$ (%)
33.07	plasma membrane	3.42 ± 0.20	6.56 ± 0.42	11.94 ± 4.61	12.66 ± 4.08

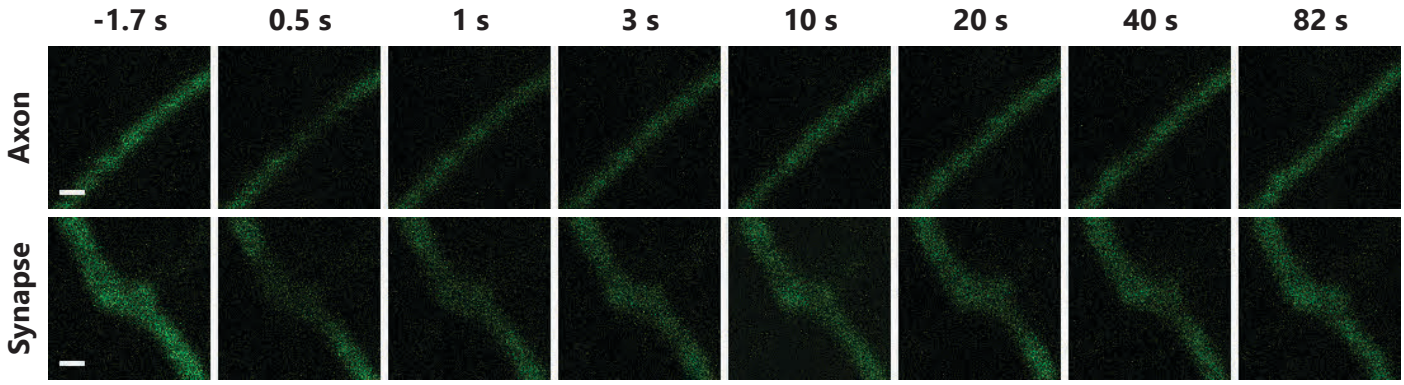

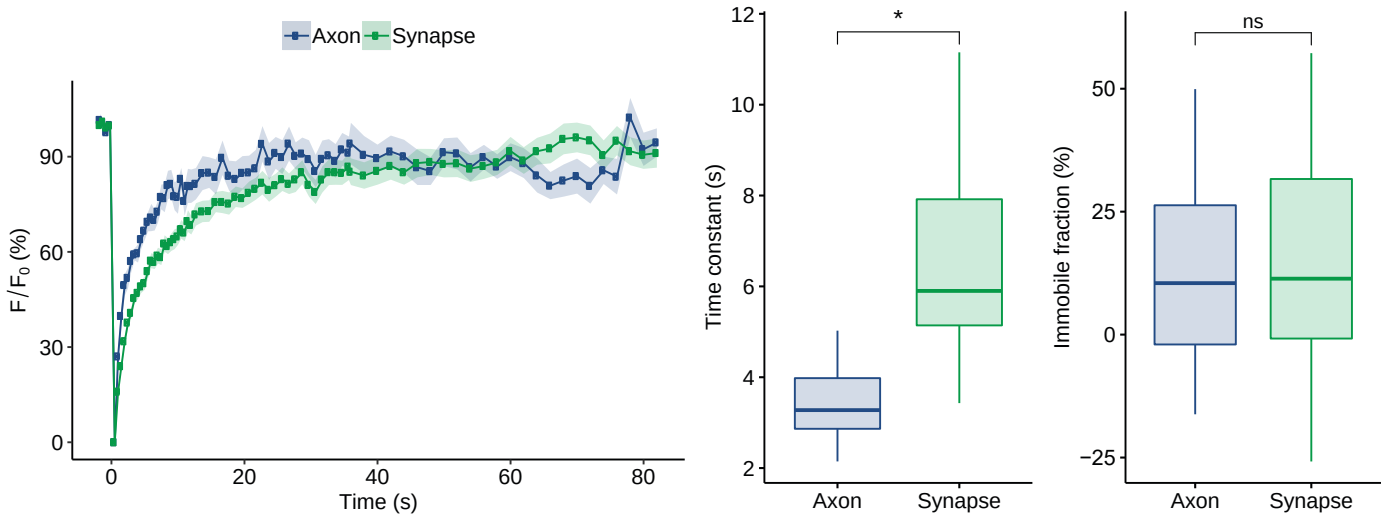

N (axons) = 16, N (synapses) = 28; p (time constant) = 1.13E-06.

Tagged protein outline:

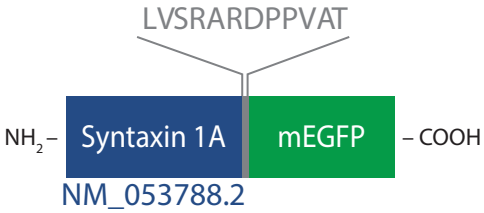

Time constant (axon) is significantly different from time constant (axon) of: Actin (p = 3.88E-04), Clathrin light chain B (p = 3.07E-03), Doc2a (p = 8.24E-05), mEGFP (p = 1.50E-03), Munc13 (p = 2.36E-04), Rab5a (p = 1.15E-03), Rab7a (p = 7.74E-03), SNAP25 (p = 4.78E-02), Syndapin 1 (p = 9.67E-03).
Immobile fraction (axon) is not significantly different from immobile fraction (axon) of any other proteins.
Time constant (synapse) is significantly different from time constant (synapse) of: AP2 (p = 4.35E-04), Calmodulin 1 (p = 2.00E-05), Clathrin light chain B (p = 2.10E-04), Complexin 1 (p = 1.22E-02), Hsc70 (p = 5.02E-06), mEGFP (p = 3.71E-11), Munc13 (p = 7.17E-03), NSF (p = 2.52E-03), Rab3a (p = 2.49E-02), Rab5a (p = 6.81E-04), Rab7a (p = 2.34E-02), SNAP23 (p = 1.00E-03), SNAP25 (p = 4.43E-03), Synapsin 1A (p = 2.76E-03), Synaptogyrin (p = 8.74E-05), Synaptophysin (p = 1.30E-06), Synaptotagmin 1 (p = 2.39E-07), VAMP1 (p = 3.99E-04), vGluT1 (p = 1.52E-05).
Immobile fraction (synapse) is significantly different from immobile fraction (synapse) of: NSF (p = 3.28E-02), SCAMP1 (p = 1.38E-02), SV2B (p = 3.90E-07), Synaptogyrin (p = 1.10E-03), Synaptophysin (p = 1.14E-07), Synaptotagmin 1 (p = 1.25E-03), VAMP2 (p = 2.02E-02), VAMP4 (p = 1.22E-02), vATPase V0a1 (p = 2.54E-04), vGluT1 (p = 2.39E-05).

References

Bennett, M.K., et al. (2004). Neuron 41, 495-511.
Sieber, J.J., et al. (2007). Science 317, 1072-6.
Takamori, S., et al. (2006). Cell 127, 831-46.

Syntaxin 16

MW (kDa)	Category	τ_{axon} (s)	$\tau_{synapse}$ (s)	IF_{axon} (%)	$IF_{synapse}$ (%)
35.44	endosomal	3.42 ± 0.26	12.63 ± 1.08	2.40 ± 5.16	9.14 ± 6.72

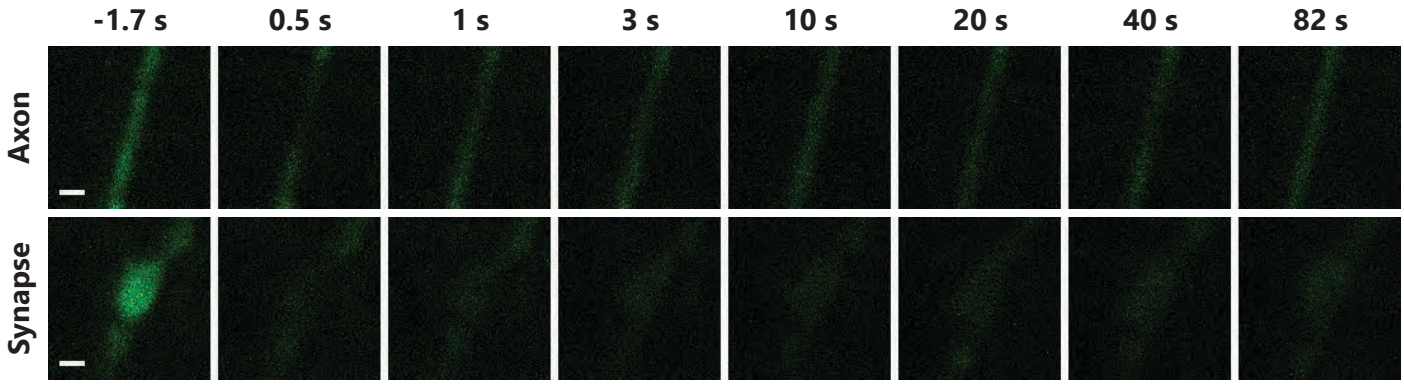

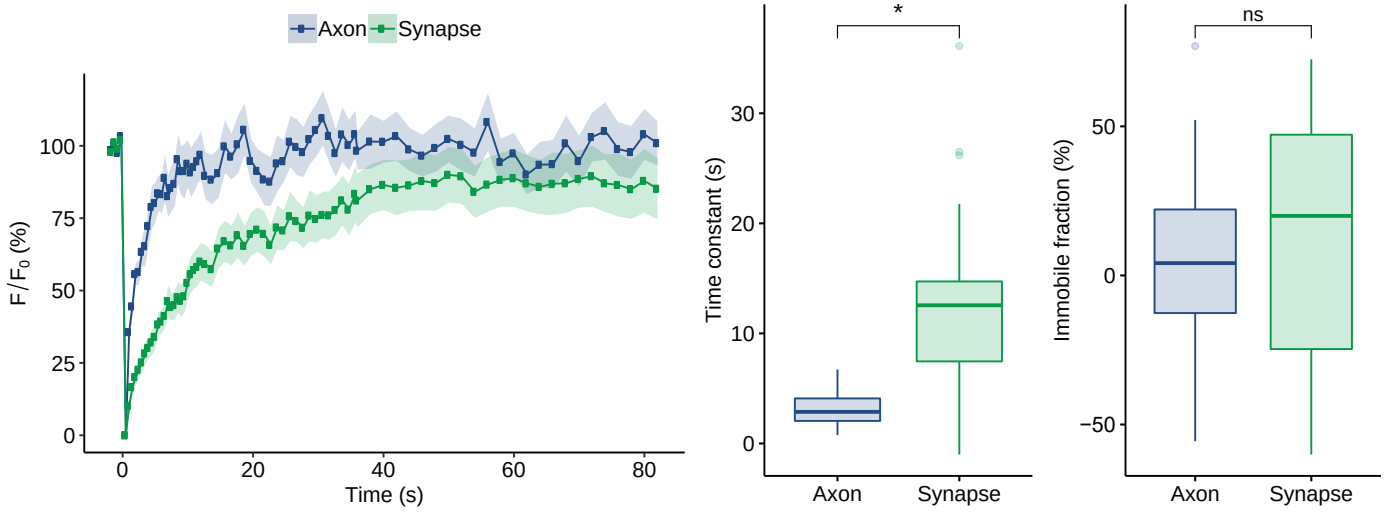

N (axons) = 42, N (synapses) = 44; p (time constant) = 1.29E-12.

Tagged protein outline:

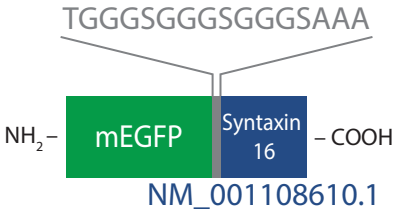

Time constant (axon) is significantly different from time constant (axon) of: Actin (p = 4.95E-05), Clathrin light chain B (p = 1.74E-02), Doc2a (p = 5.13E-04), Munc13 (p = 4.07E-06), Rab5a (p = 3.71E-03), Rab7a (p = 5.21E-03).
Immobile fraction (axon) is not significantly different from immobile fraction (axon) of any other proteins.
Time constant (synapse) is significantly different from time constant (synapse) of: Actin (p = 2.66E-02), alpha-SNAP (p = 2.97E-03), alpha-synuclein (p = 1.06E-02), AP180 (p = 1.31E-05), AP2 (p = 2.81E-07), Calmodulin 1 (p = 4.02E-08), Clathrin light chain B (p = 6.33E-08), Complexin 1 (p = 5.21E-07), Complexin 2 (p = 2.41E-04), Doc2a (p = 2.21E-03), Endophilin A1 (p = 4.96E-06), Hsc70 (p = 7.36E-10), mEGFP (p = 2.52E-15), membrane mEGFP (p = 2.19E-04), Munc13 (p = 1.42E-08), Munc18 (p = 7.39E-09), NSF (p = 2.63E-06), Rab3a (p = 5.62E-06), Rab5a (p = 4.98E-09), Rab7a (p = 3.01E-06), Septin 5 (p = 8.21E-07), SNAP23 (p = 1.38E-06), SNAP25 (p = 4.90E-09), SNAP29 (p = 2.55E-03), Synaptogyrin (p = 5.38E-03), Synaptotagmin 7 (p = 9.27E-03), Syndapin 1 (p = 5.78E-04), VAMP2 (p = 4.85E-03), VAMP4 (p = 6.27E-04).
Immobile fraction (synapse) is significantly different from immobile fraction (synapse) of: , SCAMP1 (p = 1.97E-02), SV2B (p = 5.17E-08), Synaptogyrin (p = 6.27E-04), Synaptophysin (p = 3.97E-08), Synaptotagmin 1 (p = 1.70E-02), vATPase V0a1 (p = 1.65E-03), vGluT1 (p = 4.59E-05).

References

Simonsen, A., et al. (1998). Eur J Cell Biol 75, 223-31.
Chen, Y., et al. (2010). J Cell Physiol 225, 326-32.
Takamori, S., et al. (2006). Cell 127, 831-46.

α-Tubulin

MW (kDa)	Category	τ_{axon} (s)	$\tau_{synapse}$ (s)	IF_{axon} (%)	$IF_{synapse}$ (%)
50.15	cytoskeletal	7.04 ± 1.89	10.61 ± 0.93	45.48 ± 11.49	35.23 ± 6.40

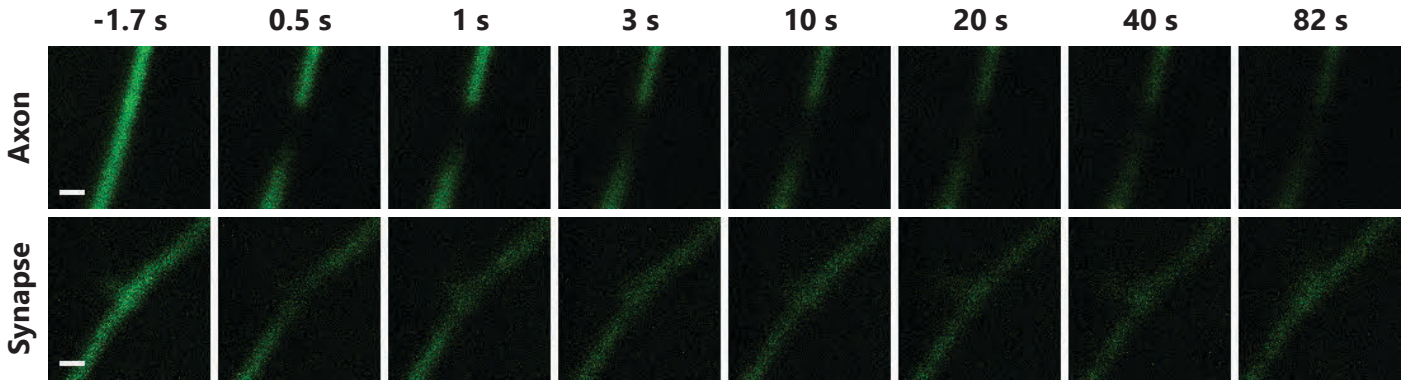

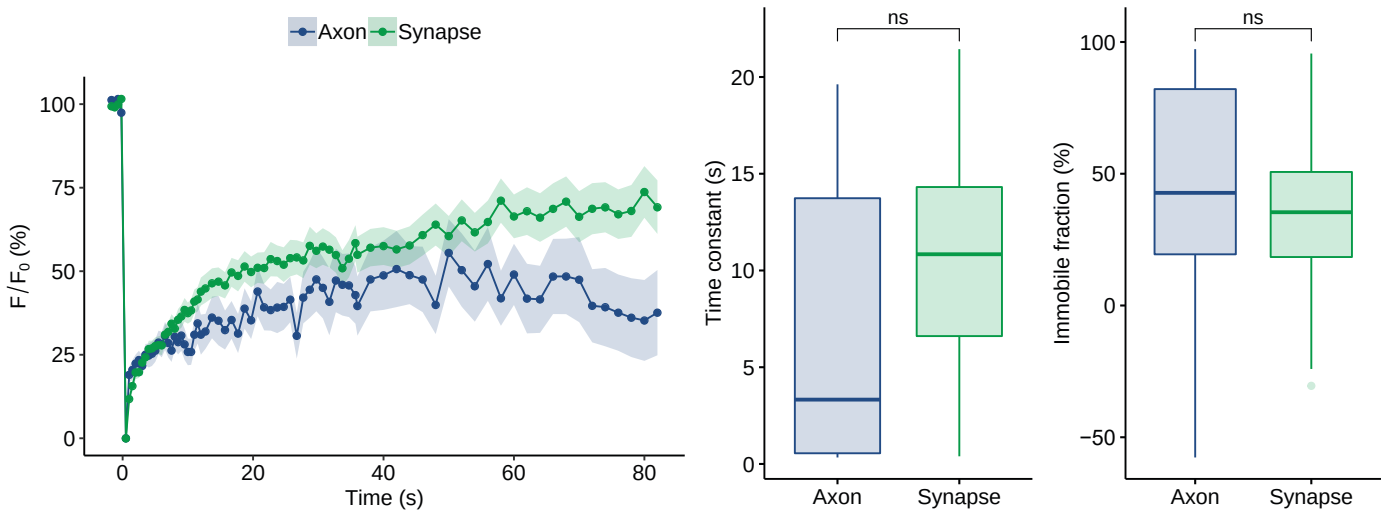

N (axons) = 15, N (synapses) = 28.

Tagged protein outline:

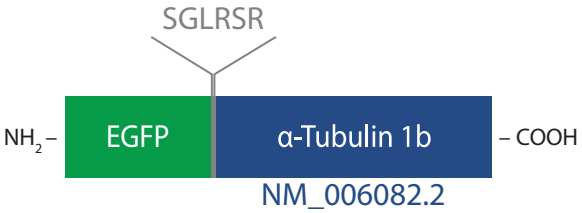

Time constant (axon) is not significantly different from time constant (axon) of any other proteins.
Immobile fraction (axon) is not significantly different from immobile fraction (axon) of any other proteins.
Time constant (synapse) is significantly different from time constant (synapse) of: alpha-SNAP (p = 3.00E-02), AP180 (p = 5.43E-04), AP2 (p = 9.69E-05), Calmodulin 1 (p = 3.52E-05), Clathrin light chain B (p = 3.75E-05), Complexin 1 (p = 2.33E-04), Complexin 2 (p = 6.48E-03), Endophilin A1 (p = 9.35E-04), Hsc70 (p = 1.60E-06), mEGFP (p = 3.06E-09), membrane mEGFP (p = 4.21E-03), Munc13 (p = 1.50E-05), Munc18 (p = 1.70E-05), NSF (p = 3.19E-04), Rab3a (p = 3.45E-04), Rab5a (p = 6.29E-06), Rab7a (p = 2.58E-04), Septin 5 (p = 3.37E-04), SNAP23 (p = 1.95E-04), SNAP25 (p = 5.16E-06), SNAP29 (p = 1.74E-02), Synaptogyrin (p = 4.71E-03), Synaptophysin (p = 1.10E-02), Synaptotagmin 1 (p = 2.41E-02), Syndapin 1 (p = 9.82E-03), VAMP4 (p = 1.32E-02).
Immobile fraction (synapse) is significantly different from immobile fraction (synapse) of: , SV2B (p = 4.89E-03), Synaptophysin (p = 2.16E-02).

References

Hirokawa, N., et al. (1989). J Cell Biol 108, 111-26.
Conde, C. and Caceres, A. (2009). Nat Rev Neurosci 10, 319-32.

VAMP1

MW (kDa)	Category	τ_{axon} (s)	$\tau_{synapse}$ (s)	IF_{axon} (%)	$IF_{synapse}$ (%)
12.80	vesicular	3.38 ± 0.25	13.64 ± 1.01	9.68 ± 3.65	32.25 ± 4.39

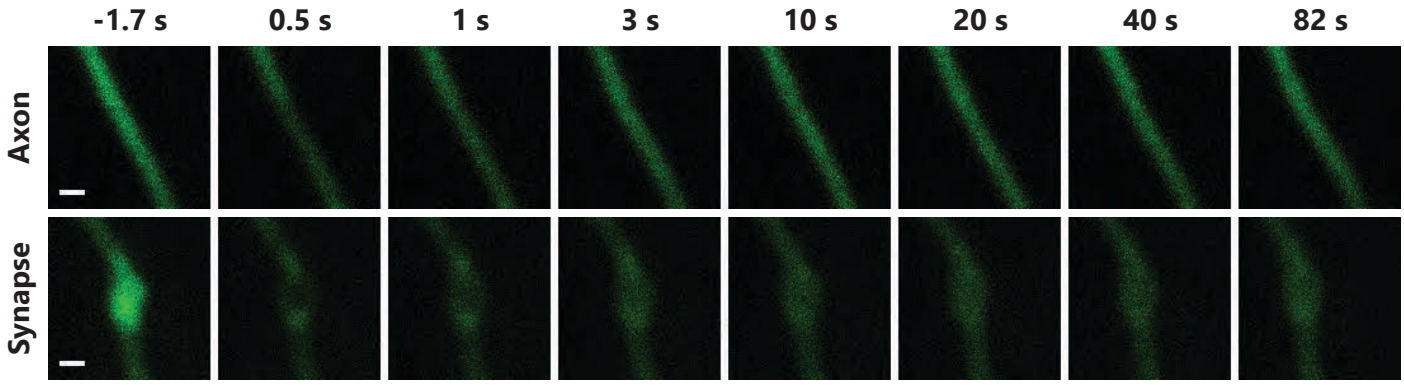

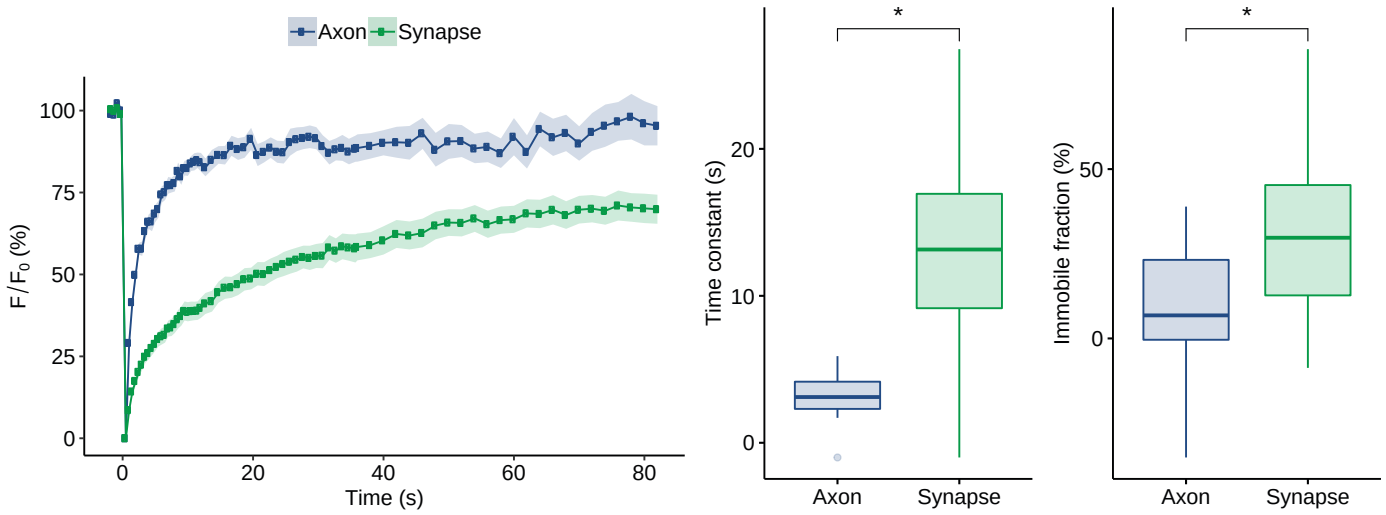

N (axons) = 21, N (synapses) = 28; p (time constant) = 1.15E-08, p (immobile fraction) = 1.10E-03.

Tagged protein outline:

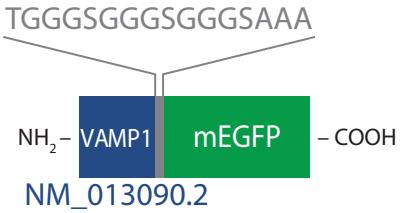

Time constant (axon) is significantly different from time constant (axon) of: Actin (p = 1.96E-04), Clathrin light chain B (p = 9.12E-03), Doc2a (p = 1.75E-04), mEGFP (p = 1.21E-02), Munc13 (p = 4.30E-05), Rab5a (p = 2.70E-03), Rab7a (p = 6.19E-03), Syndapin 1 (p = 2.41E-02).
Immobile fraction (axon) is not significantly different from immobile fraction (axon) of any other proteins.
Time constant (synapse) is significantly different from time constant (synapse) of: Actin (p = 2.70E-03), alpha-SNAP (p = 5.23E-05), alpha-synuclein (p = 1.08E-03), Amphiphysin (p = 2.45E-04), AP180 (p = 1.28E-06), AP2 (p = 1.14E-06), Calmodulin 1 (p = 4.98E-07), Clathrin light chain B (p = 2.63E-07), Complexin 1 (p = 1.12E-06), Complexin 2 (p = 1.66E-05), Doc2a (p = 5.52E-05), Endophilin A1 (p = 2.84E-06), Epsin (p = 6.83E-03), Hsc70 (p = 1.40E-08), mEGFP (p = 3.48E-11), membrane mEGFP (p = 6.56E-06), Munc13 (p = 2.71E-08), Munc18 (p = 2.01E-09), NSF (p = 4.45E-06), PIP5KI-gamma (p = 4.31E-03), Rab3a (p = 1.02E-06), Rab5a (p = 1.15E-08), Rab7a (p = 1.40E-06), Septin 5 (p = 2.55E-07), SNAP23 (p = 3.98E-06), SNAP25 (p = 3.44E-09), SNAP29 (p = 1.37E-05), Synaptotagmin 7 (p = 4.22E-05), Syndapin 1 (p = 1.42E-05), Syntaxin 1A (p = 3.99E-04), VAMP2 (p = 1.16E-04), VAMP4 (p = 2.80E-05).
Immobile fraction (synapse) is significantly different from immobile fraction (synapse) of: Rab5a (p = 2.04E-02), SV2B (p = 2.88E-05), Synaptophysin (p = 3.85E-05), vGluT1 (p = 1.48E-02).

References

Trimble, W.S., et al. (1998). Proc Natl Acad Sci U S A 85, 4528-42.
Raptis, A., et al. (2005). J Chem Neuroanat 30, 201-11.
Takamori, S., et al. (2006). Cell 127, 831-46.

VAMP2

MW (kDa)	Category	τ_{axon} (s)	$\tau_{synapse}$ (s)	IF_{axon} (%)	$IF_{synapse}$ (%)
12.69	vesicular	2.64 ± 0.20	5.53 ± 0.45	-11.95 ± 7.29	41.67 ± 4.07

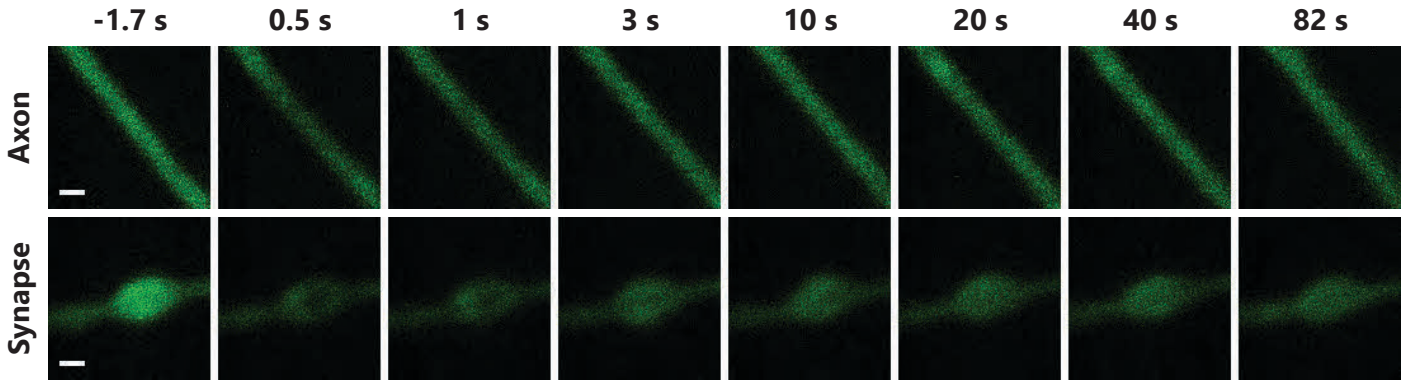

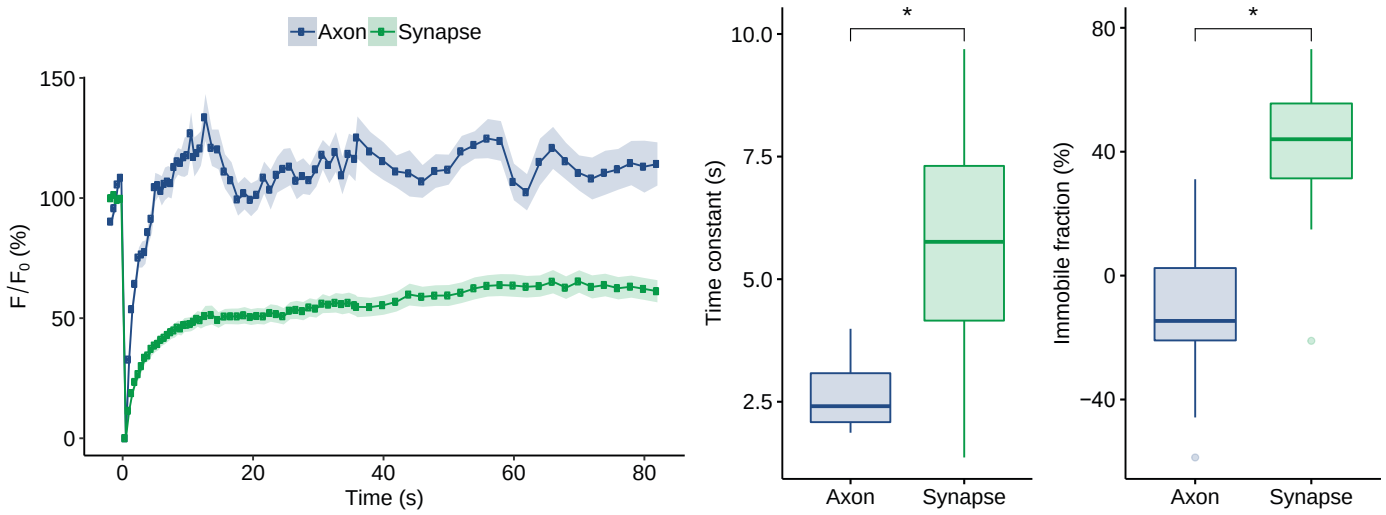

N (axons) = 12, N (synapses) = 25; p (time constant) = 5.50E-04, p (immobile fraction) = 1.28E-05.

Tagged protein outline:

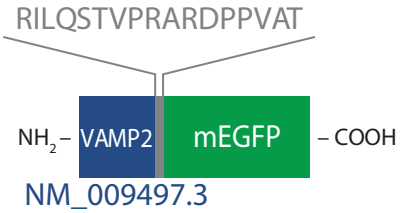

Time constant (axon) is significantly different from time constant (axon) of: Munc13 (p = 4.64E-02).
Immobile fraction (axon) is significantly different from immobile fraction (axon) of: membrane mEGFP (p = 4.07E-02), Syndapin 1 (p = 4.91E-02).
Time constant (synapse) is significantly different from time constant (synapse) of: Hsc70 (p = 1.71E-02), mEGFP (p = 2.58E-06), SCAMP1 (p = 3.73E-02), Synapsin 1A (p = 8.19E-04), Synaptogyrin (p = 1.08E-04), Synaptophysin (p = 2.76E-06), Synaptotagmin 1 (p = 2.74E-07), Syntaxin 16 (p = 4.85E-03), VAMP1 (p = 1.16E-04), vGluT1 (p = 3.23E-06).
Immobile fraction (synapse) is significantly different from immobile fraction (synapse) of: alpha-SNAP (p = 3.23E-03), AP180 (p = 3.40E-04), Complexin 2 (p = 9.68E-03), mEGFP (p = 1.51E-04), Munc13 (p = 1.01E-02), Munc18 (p = 7.20E-05), Rab3a (p = 2.18E-02), Rab5a (p = 9.24E-06), Rab7a (p = 1.33E-03), Munc13 (p = 1.01E-02), SNAP29 (p = 2.47E-03), SV2B (p = 3.74E-04), Synaptophysin (p = 3.03E-04), Synaptotagmin 7 (p = 1.16E-02), Syndapin 1 (p = 1.73E-02), Syntaxin 1A (p = 2.02E-02).

References

Baumert, M., et al. (1989). J Cell Biol 110, 1285-94.
Takamori, S., et al. (2006). Cell 127, 831-46.

VAMP4

MW (kDa)	Category	τ_{axon} (s)	$\tau_{synapse}$ (s)	IF_{axon} (%)	$IF_{synapse}$ (%)
16.35	endosomal	14.74 ± 3.91	4.71 ± 0.47	1.61 ± 16.31	51.38 ± 5.68

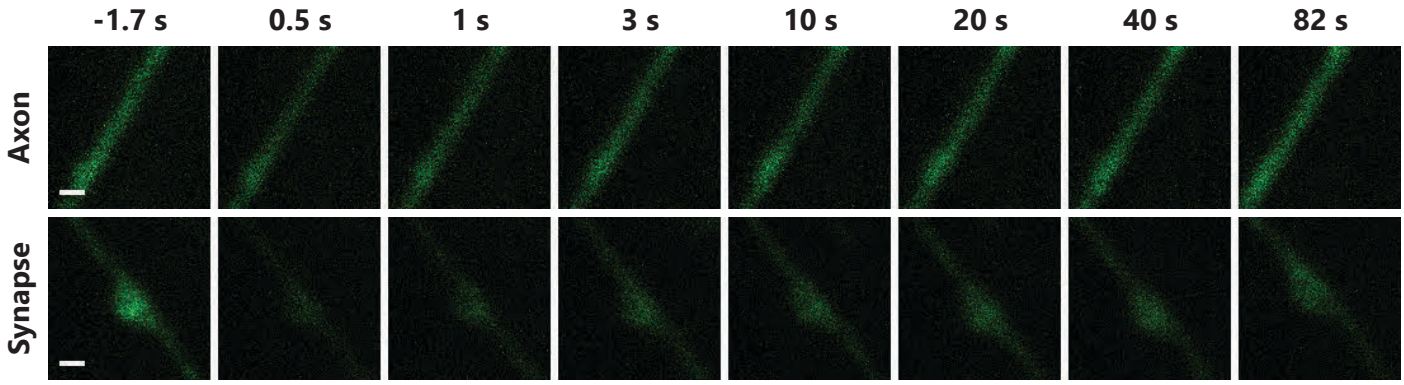

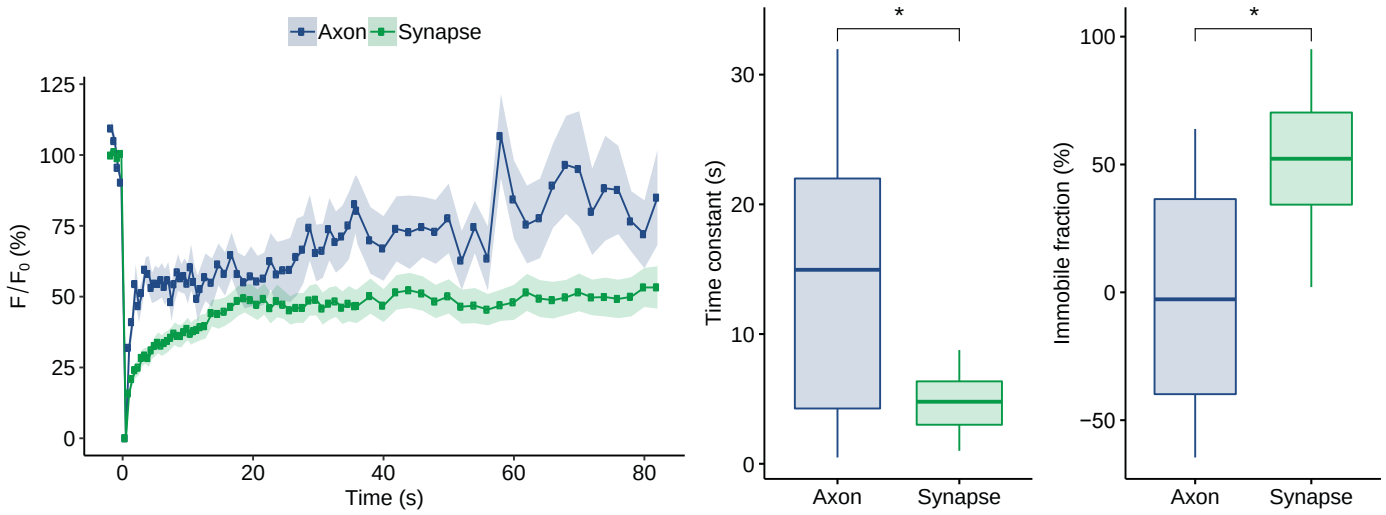

N (axons) = 9, N (synapses) = 24; p (time constant) = 4.99E-02, p (immobile fraction) = 1.03E-02.

Tagged protein outline:

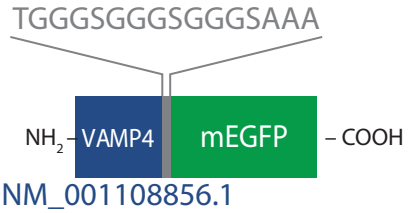

NM_001108856.1

Time constant (axon) is not significantly different from time constant (axon) of any other proteins.
Immobile fraction (axon) is not significantly different from immobile fraction (axon) of any other proteins.
Time constant (synapse) is significantly different from time constant (synapse) of: mEGFP (p = 7.08E-04), SCAMP1 (p = 7.09E-03), Synapsin 1A (p = 3.30E-04), Synaptogyrin (p = 6.11E-05), Synaptophysin (p = 1.83E-06), Synaptotagmin 1 (p = 3.29E-07), Syntaxin 16 (p = 6.27E-04), alpha-Tubulin 1b (p = 1.32E-02), VAMP1 (p = 2.80E-05), vGluT1 (p = 3.29E-06), Vti1a-beta (p = 4.91E-02).
Immobile fraction (synapse) is significantly different from immobile fraction (synapse) of: alpha-SNAP (p = 2.25E-03), AP180 (p = 6.80E-04), AP2 (p = 4.17E-02), Complexin 2 (p = 2.79E-02), Doc2a (p = 3.60E-02), Endophilin A1 (p = 3.02E-02), mEGFP (p = 1.73E-03), Munc13 (p = 1.02E-03), Munc18 (p = 9.24E-04), Rab3a (p = 5.05E-03), Rab5a (p = 7.42E-05), Rab7a (p = 1.21E-03), Munc13 (p = 1.02E-03), SNAP29 (p = 1.46E-03), Synaptotagmin 7 (p = 5.50E-03), Syndapin 1 (p = 1.82E-02), Syntaxin 1A (p = 1.22E-02).

References

Steegmaier, M., et al. (1999). Mol Biol Cell 10, 1957-72.
Mallard, F., et al. (2002). J Cell Biol 156, 653-64.
Raingo, J., et al. (2012). Nat Neurosci 15, 738-45.
Takamori, S., et al. (2006). Cell 127, 831-46.

vATPase

MW (kDa)	Category	τ_{axon} (s)	$\tau_{synapse}$ (s)	IF_{axon} (%)	$IF_{synapse}$ (%)
95.66	vesicular	3.13 ± 0.71	13.56 ± 1.99	20.97 ± 5.90	54.99 ± 4.56

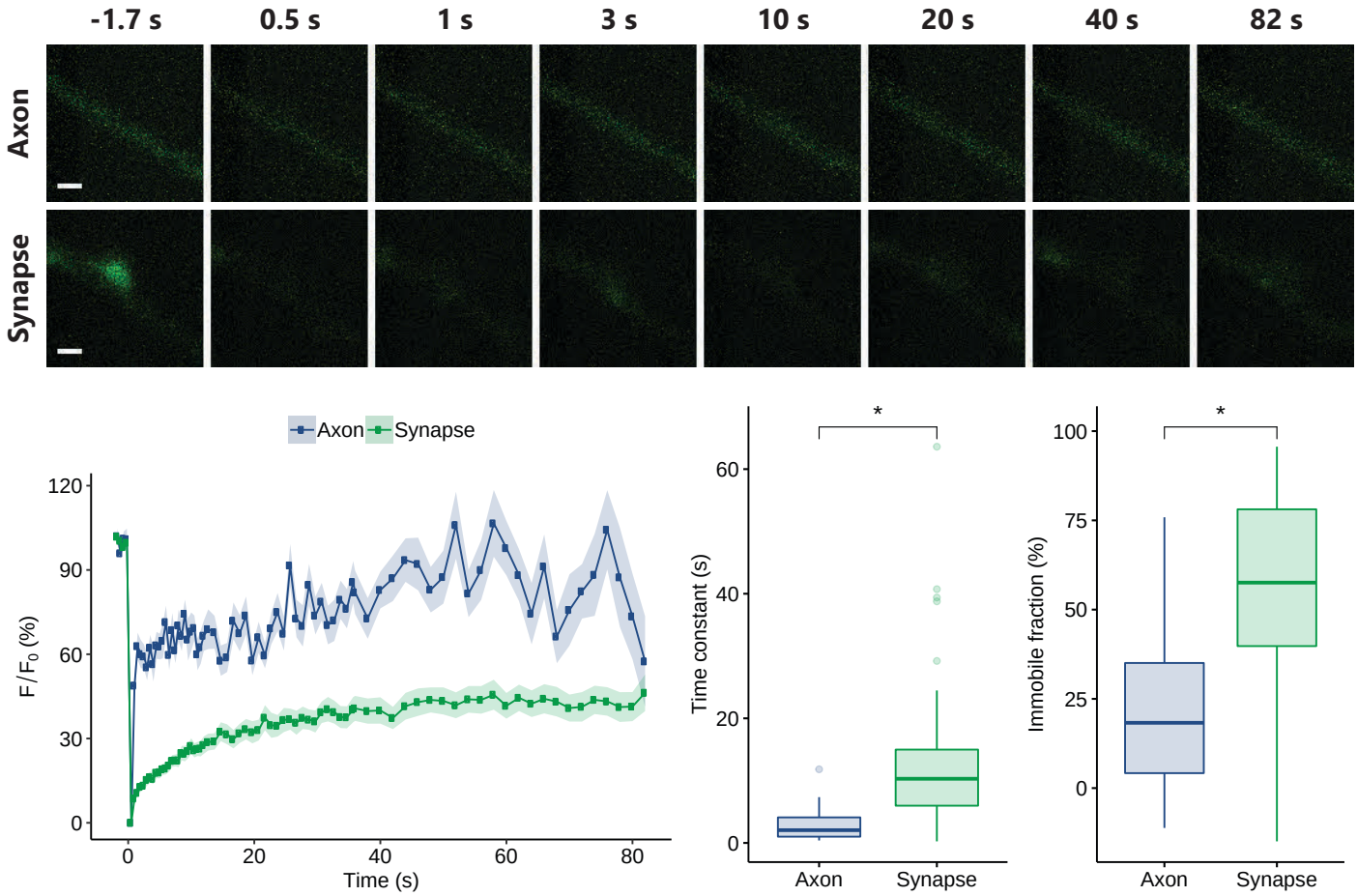

N (axons) = 18, N (synapses) = 42; p (time constant) = 1.98E-05, p (immobile fraction) = 1.28E-04.

Time constant (axon) is not significantly different from time constant (axon) of any other proteins.
Immobile fraction (axon) is not significantly different from immobile fraction (axon) of any other proteins.
Time constant (synapse) is significantly different from time constant (synapse) of: AP180 (p = 2.44E-02), AP2 (p = 6.28E-03), Calmodulin 1 (p = 1.96E-03), Clathrin light chain B (p = 2.62E-03), Complexin 1 (p = 6.55E-03), Endophilin A1 (p = 4.01E-02), Hsc70 (p = 5.56E-05), mEGFP (p = 3.66E-08), Munc13 (p = 9.04E-04), Munc18 (p = 5.85E-04), NSF (p = 1.49E-02), Rab3a (p = 1.62E-02), Rab5a (p = 7.59E-04), Rab7a (p = 1.53E-02), Septin 5 (p = 1.99E-02), SNAP23 (p = 2.01E-02), SNAP25 (p = 7.65E-04), Synaptogyrin (p = 1.58E-02).
Immobile fraction (synapse) is significantly different from immobile fraction (synapse) of: Actin (p = 4.02E-02), alpha-SNAP (p = 7.38E-05), AP180 (p = 5.64E-06), AP2 (p = 4.23E-04), Calmodulin 1 (p = 1.37E-02), Clathrin light chain B (p = 4.20E-02), Complexin 1 (p = 4.99E-03), Complexin 2 (p = 5.79E-04), Doc2a (p = 8.52E-04), Endophilin A1 (p = 6.16E-04), Epsin (p = 2.98E-02), Hsc70 (p = 2.10E-03), mEGFP (p = 9.46E-07), Munc13 (p = 4.95E-06), Munc18 (p = 1.89E-07), PIP5KI-gamma (p = 9.68E-03), Rab3a (p = 2.83E-04), Rab5a (p = 3.70E-07), Rab7a (p = 1.75E-05), Septin 5 (p = 7.34E-03), SNAP23 (p = 3.05E-02), Munc13 (p = 4.95E-06), SNAP29 (p = 6.41E-05), Synaptotagmin 7 (p = 9.62E-05), Syndapin 1 (p = 2.77E-04), Syntaxin 1A (p = 2.54E-04), Syntaxin 16 (p = 1.65E-03).

References

Perin, M.S., et al. (1991). J Biol Chem 266, 3877-81.
Takamori, S., et al. (2006). Cell 127, 831-46.
Oot, R.A., et al. (2012). Structure 20, 1881-92.
Kitagawa, N., et al. (2008). J Biol Chem 283, 3329-37.

vGluT1

MW (kDa)	Category	τ_{axon} (s)	$\tau_{synapse}$ (s)	IF_{axon} (%)	$IF_{synapse}$ (%)
61.66	vesicular	-	23.53 ± 3.20	-	63.24 ± 4.86

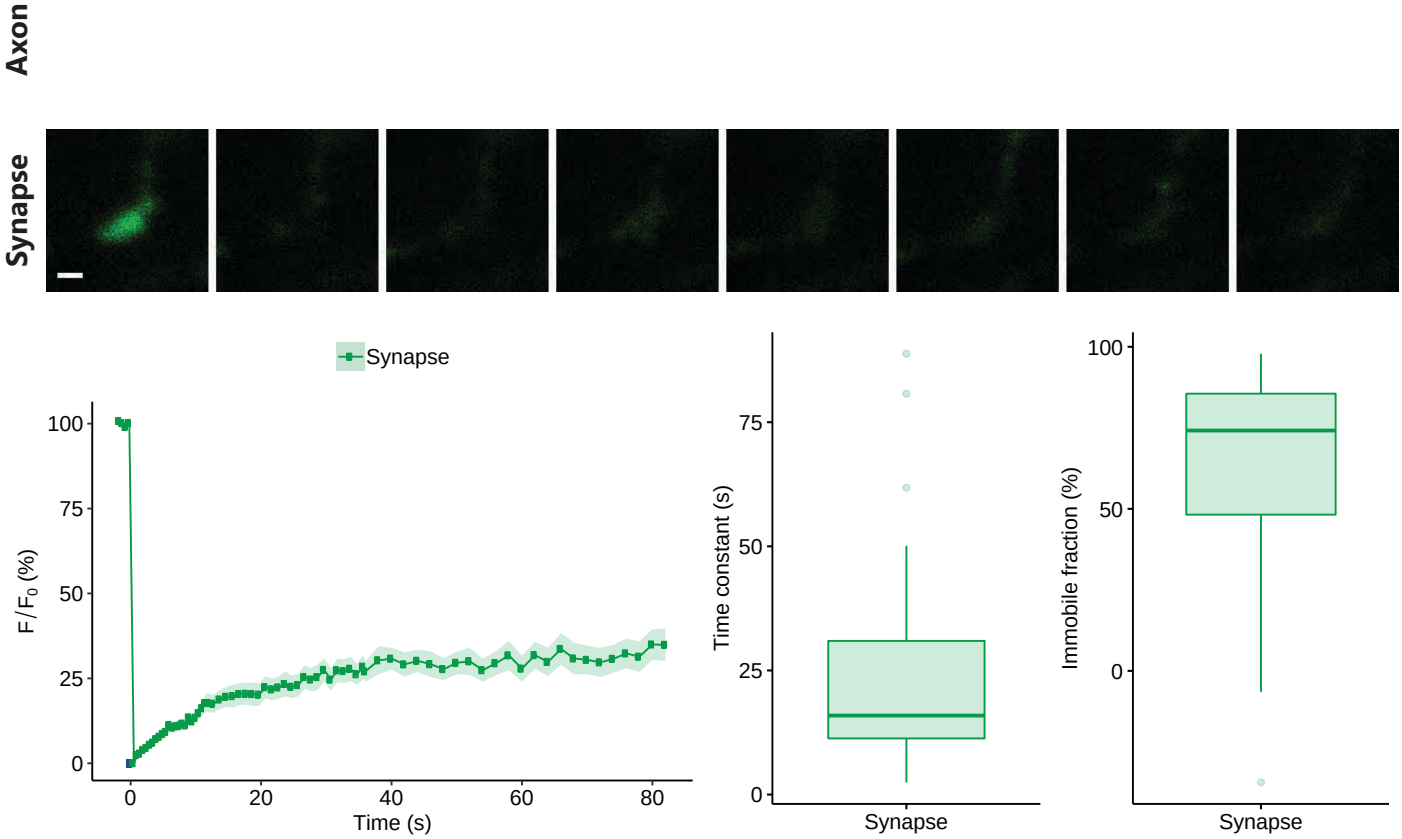

N (synapses) = 38.

Tagged protein outline:

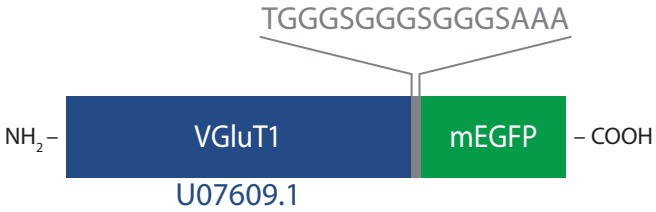

Time constant (synapse) is significantly different from time constant (synapse) of: Actin (p = 6.74E-05), alpha-SNAP (p = 5.86E-06), alpha-synuclein (p = 2.02E-05), Amphiphysin (p = 6.32E-06), AP180 (p = 3.07E-08), AP2 (p = 5.50E-08), Calmodulin 1 (p = 4.23E-08), Clathrin light chain B (p = 2.09E-08), Complexin 1 (p = 4.48E-08), Complexin 2 (p = 8.22E-07), CSP (p = 4.34E-03), Doc2a (p = 1.67E-06), Endophilin A1 (p = 1.42E-07), Epsin (p = 8.87E-04), Hsc70 (p = 3.36E-10), mEGFP (p = 9.06E-14), membrane mEGFP (p = 3.98E-07), Munc13 (p = 3.44E-10), Munc18 (p = 4.59E-12), NSF (p = 4.12E-07), PIP5KI-gamma (p = 4.85E-04), Rab3a (p = 7.59E-08), Rab5a (p = 2.45E-10), Rab7a (p = 1.30E-07), Septin 5 (p = 2.10E-08), SNAP23 (p = 5.44E-07), SNAP25 (p = 2.19E-11), SNAP29 (p = 9.68E-07), Synaptotagmin 7 (p = 2.47E-06), Syndapin 1 (p = 5.53E-07), Syntaxin 1A (p = 1.52E-05), VAMP2 (p = 3.23E-06), VAMP4 (p = 3.29E-06),.Immobile fraction (synapse) is significantly different from immobile fraction (synapse) of: Actin (p = 1.54E-03), alpha-SNAP (p = 1.35E-05), alpha-synuclein (p = 1.69E-03), Amphiphysin (p = 2.46E-03), AP180 (p = 7.37E-07), AP2 (p = 6.70E-05), Calmodulin 1 (p = 5.13E-04), Clathrin light chain B (p = 1.13E-03), Complexin 1 (p = 9.48E-05), Complexin 2 (p = 4.02E-05), Doc2a (p = 2.37E-05), Endophilin A1 (p = 3.73E-05), Epsin (p = 2.68E-03), Hsc70 (p = 3.28E-05), mEGFP (p = 7.67E-09), membrane mEGFP (p = 3.44E-03), Munc13 (p = 5.82E-07), Munc18 (p = 2.15E-09), PIP5KI-gamma (p = 1.28E-03), Rab3a (p = 9.77E-06), Rab5a (p = 2.10E-08), Rab7a (p = 4.09E-06), Septin 5 (p = 2.36E-04), SNAP23 (p = 8.84E-04), Munc13 (p = 5.82E-07), SNAP29 (p = 7.63E-06), Synaptotagmin 7 (p = 7.23E-06), Syndapin 1 (p = 1.42E-05), Syntaxin 1A (p = 2.39E-05), Syntaxin 16 (p = 4.59E-05), VAMP1 (p = 1.48E-02),

References

Bellocchio, F., et al. (2000). Science 289, 957-60.
Takamori, S., et al. (2006). Cell 127, 831-46.

Vti1a-β

MW (kDa)	Category	τ_{axon} (s)	$\tau_{synapse}$ (s)	IF_{axon} (%)	$IF_{synapse}$ (%)
26.04	endosomal	4.53 ± 0.95	21.24 ± 4.33	11.82 ± 8.78	38.28 ± 7.12

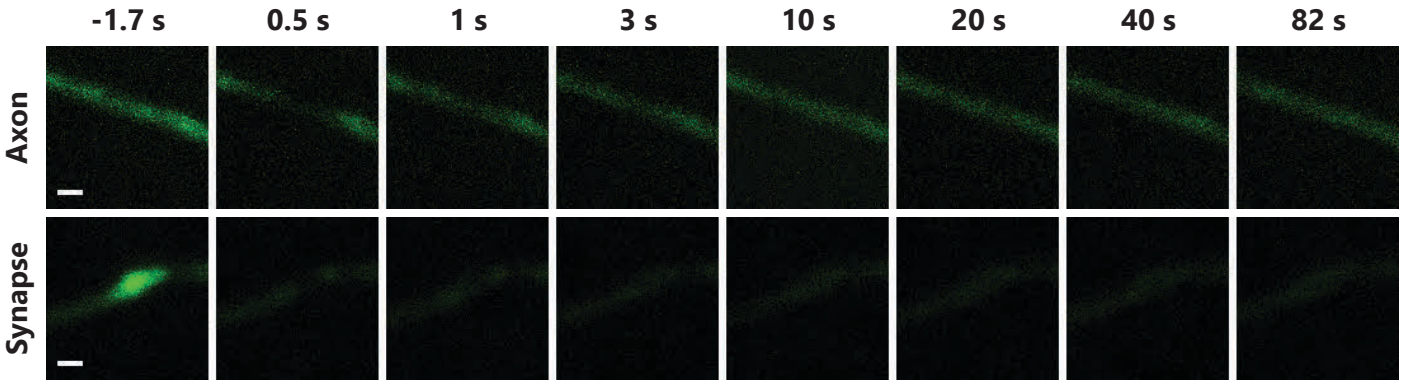

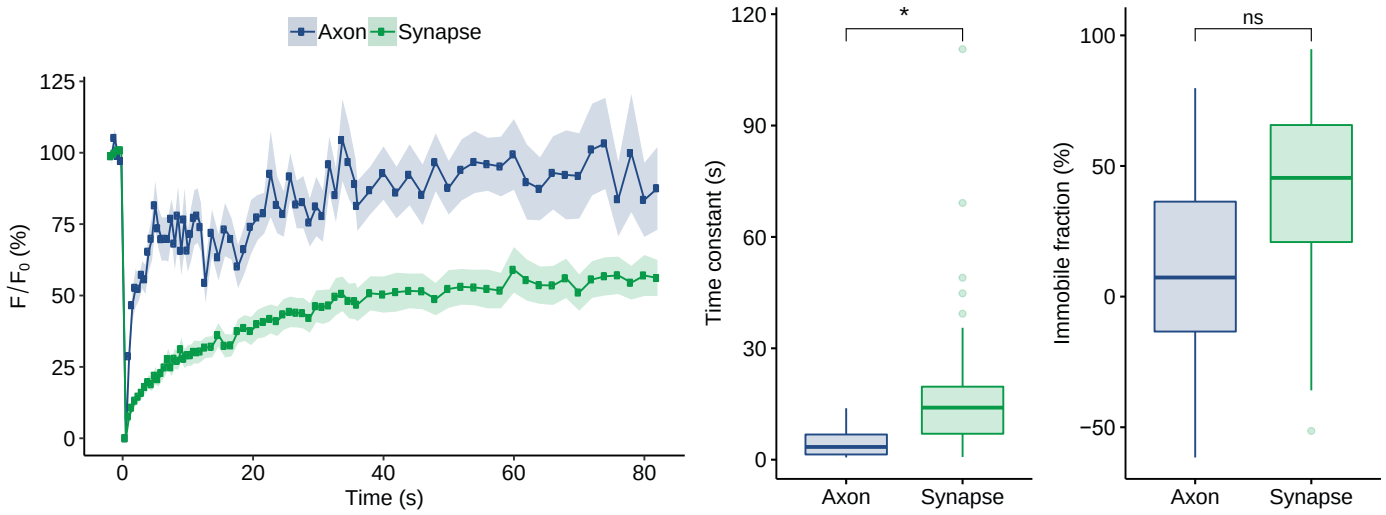

N (axons) = 18, N (synapses) = 29; p (time constant) = 1.03E-04.

Tagged protein outline:

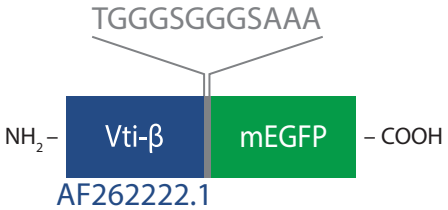

Time constant (axon) is not significantly different from time constant (axon) of any other proteins.
Immobile fraction (axon) is not significantly different from immobile fraction (axon) of any other proteins.
Time constant (synapse) is significantly different from time constant (synapse) of: , AP180 (p = 4.68E-03), AP2 (p = 1.78E-03), Calmodulin 1 (p = 5.24E-04), Clathrin light chain B (p = 8.35E-04), Complexin 1 (p = 1.20E-03), Complexin 2 (p = 2.87E-02), Doc2a (p = 4.45E-02), Endophilin A1 (p = 9.68E-03), Hsc70 (p = 3.39E-05), mEGFP (p = 8.41E-08), membrane mEGFP (p = 2.09E-02), Munc13 (p = 3.07E-04), Munc18 (p = 1.22E-04), NSF (p = 3.58E-03), Rab3a (p = 3.67E-03), Rab5a (p = 1.80E-04), Rab7a (p = 3.61E-03), Septin 5 (p = 1.93E-03), SNAP23 (p = 4.64E-03), SNAP25 (p = 9.96E-05), Syndapin 1 (p = 4.84E-02), VAMP4 (p = 4.91E-02).
Immobile fraction (synapse) is significantly different from immobile fraction (synapse) of: , Rab5a (p = 2.58E-02), SV2B (p = 2.40E-03), Synaptophysin (p = 3.66E-02).

References

Mallard, F., et al. (2002). J Cell Biol 156, 653-64.
Kreykenbohm, V., et al. (2002). Eur J Cell Biol 81, 273-80.
Takamori, S., et al. (2006). Cell 127, 831-846.

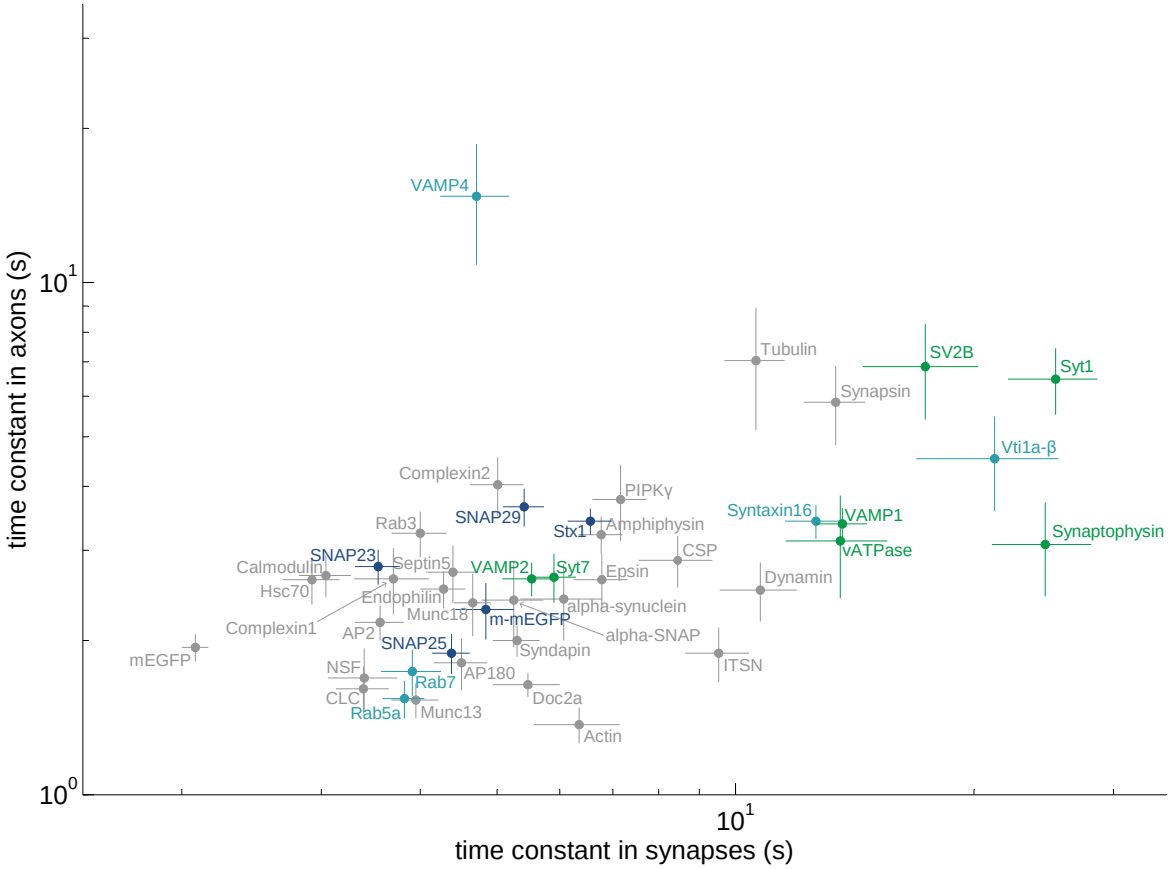

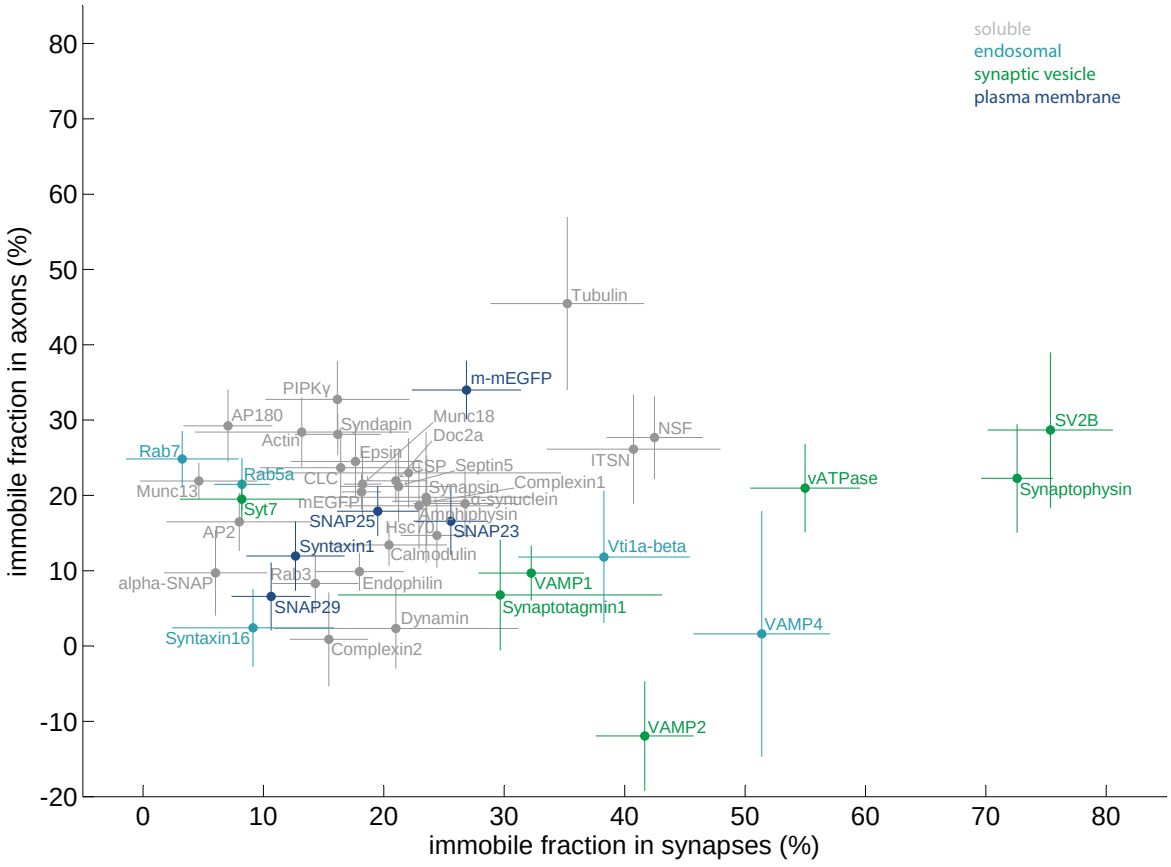

Appendix Fig. S4. Time constants and immobile fractions of analyzed proteins in axons and synapses. Symbols indicate means ± SEM; all data are shown as box plots in Appendix Fig. S3.

Multi-page figure

	axon		synapse	
protein	correlation coefficient	P value	correlation coefficient	P value
Actin	0.248	0.232	0.1558	0.4285
alpha-SNAP	0.1965	0.4657	0.082	0.6842
alpha-synuclein	0.1356	0.6298	0.3254	0.0604
Amphiphysin	0.0184	0.9321	0.2103	0.2116
AP180	0.2327	0.2335	0.1434	0.4112
AP2	0.1697	0.3789	0.1729	0.361
Calmodulin	0.1152	0.5445	0.1848	0.3284
Clathrin light chain	0.0407	0.8503	0.1165	0.5187
Complexin1	0.0214	0.9327	0.2452	0.2084
Complexin2	0.0511	0.7887	0.2544	0.175
CSP	0.1384	0.5003	0.2334	0.2958
Doc2a	0.0563	0.8136	0.5967	0.0055
Dynamin	0.2943	0.307	0.1019	0.628
Endophilin	0.3345	0.0708	0.1974	0.2957
Epsin	0.1276	0.5918	0.4722	0.0355
Hsc70	0.1229	0.5102	0.0099	0.9522
Intersectin 1-L	0.1207	0.6122	0.0359	0.848
mEGFP	0.0472	0.815	0.3224	0.0069
membrane mEGFP	0.4647	0.0255	0.3038	0.116
Munc13	0.26	0.1732	0.1578	0.4224
Munc18	0.2849	0.2107	0.1608	0.1569
NSF	0.0576	0.8383	0.1176	0.5754
PIP5KIgamma	0.0579	0.8441	0.0869	0.6729
Rab3a	0.3085	0.0972	0.1938	0.2963
Rab5a	0.123	0.5953	0.1128	0.4554
Rab7a	0.2886	0.122	0.149	0.4319
SCAMP1	n/a		0.2141	0.3388
Septin5	0.0643	0.7221	0.0474	0.7775
SNAP23	0.2536	0.2317	0.1341	0.5229
SNAP25	0.1183	0.6512	0.1965	0.1055
SNAP29	0.0932	0.6576	0.0565	0.7709
SV2B	0.2168	0.3874	0.1606	0.4534
Synapsin	0.0505	0.8475	0.075	0.7158
Synaptogyrin	n/a		0.5142	0.0722
Synaptophysin	0.4044	0.2173	0.1048	0.7334
Synaptotagmin1	0.3878	0.1119	0.3719	0.0331
Synaptotagmin7	0.2132	0.2761	0.0805	0.6781
Syndapin	0.1585	0.3944	0.4153	0.0202
Syntaxin1	0.2573	0.3189	0.479	0.0099
Syntaxin16	0.0758	0.7072	0.1993	0.2999
Tubulin	0.2352	0.5423	0.1208	0.6441
VAMP1	0.1877	0.3911	0.3558	0.0582
VAMP2	0.3157	0.2715	0.1144	0.5621
VAMP4	0.1008	0.7681	0.0888	0.68
vATPase	0.1657	0.4979	0.1831	0.3242
vGluT	n/a		0.0606	0.8369
Vti1a-beta	0.129	0.6216	0.1206	0.6227

Appendix Fig. S5. An analysis of the correlation between overexpression levels and mobility rates. Protein overexpression was quantified as the fluorescence intensity in the analyzed regions, and was compared with the time constants obtained from the respective regions. This page: table showing correlation coefficients and P values of all analyzed proteins. SCAMP1, Synaptogyrin, and vGluT were not detected in axons and therefore no time constants were obtained for these proteins in axons. No correlation was significant, when corrected for multiple testing (Benjamini-Hochberg procedure, with a false discovery rate as high as 0.2, meaning 20%). Following pages: scatter plots showing the relation between fluorescence intensity and time constants of all proteins. Each point represents one synapse/axonal region.

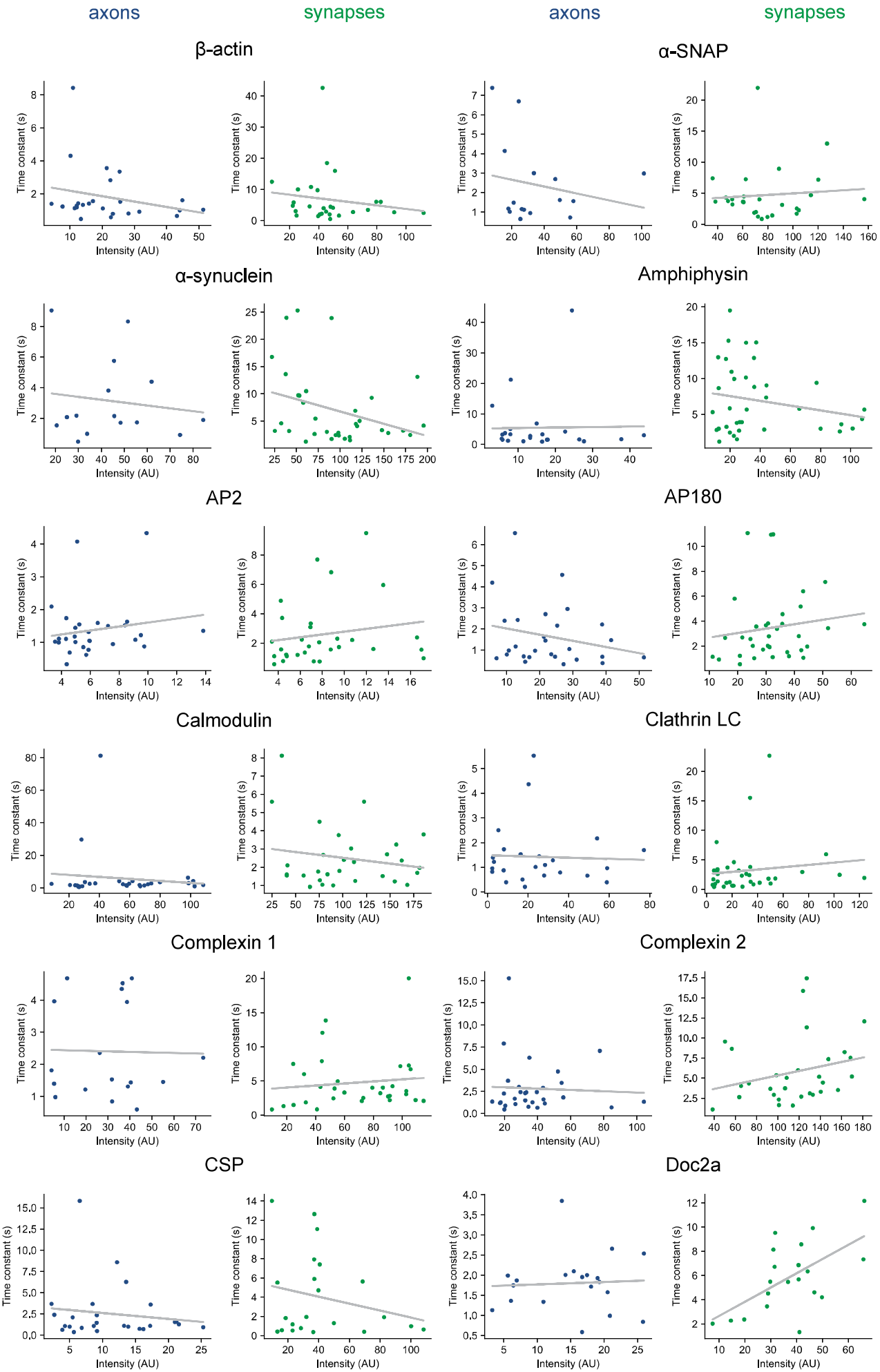
axons
synapses
axons
synapses
β-actin
α-SNAP
α-synuclein
Amphiphysin
AP2
AP180
Calmodulin
Clathrin LC
Complexin 1
Complexin 2
CSP
Doc2a
Time constant (s)
Intensity (AU)

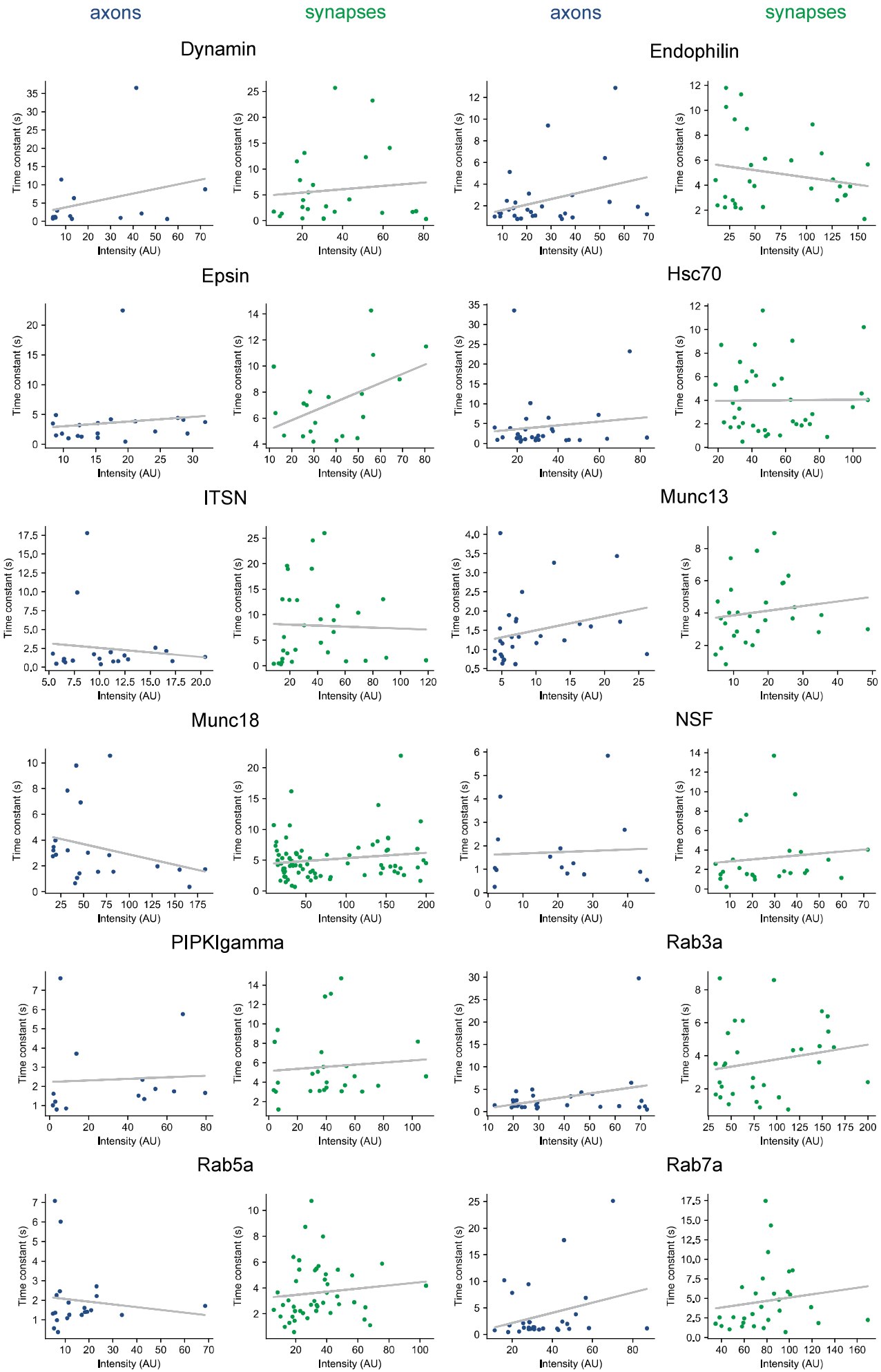
axons
synapses
axons
synapses
Dynamin
Endophilin
Epsin
Hsc70
ITSN
Munc13
Munc18
NSF
PIPKIgamma
Rab3a
Rab5a
Rab7a
Time constant (s)
Intensity (AU)

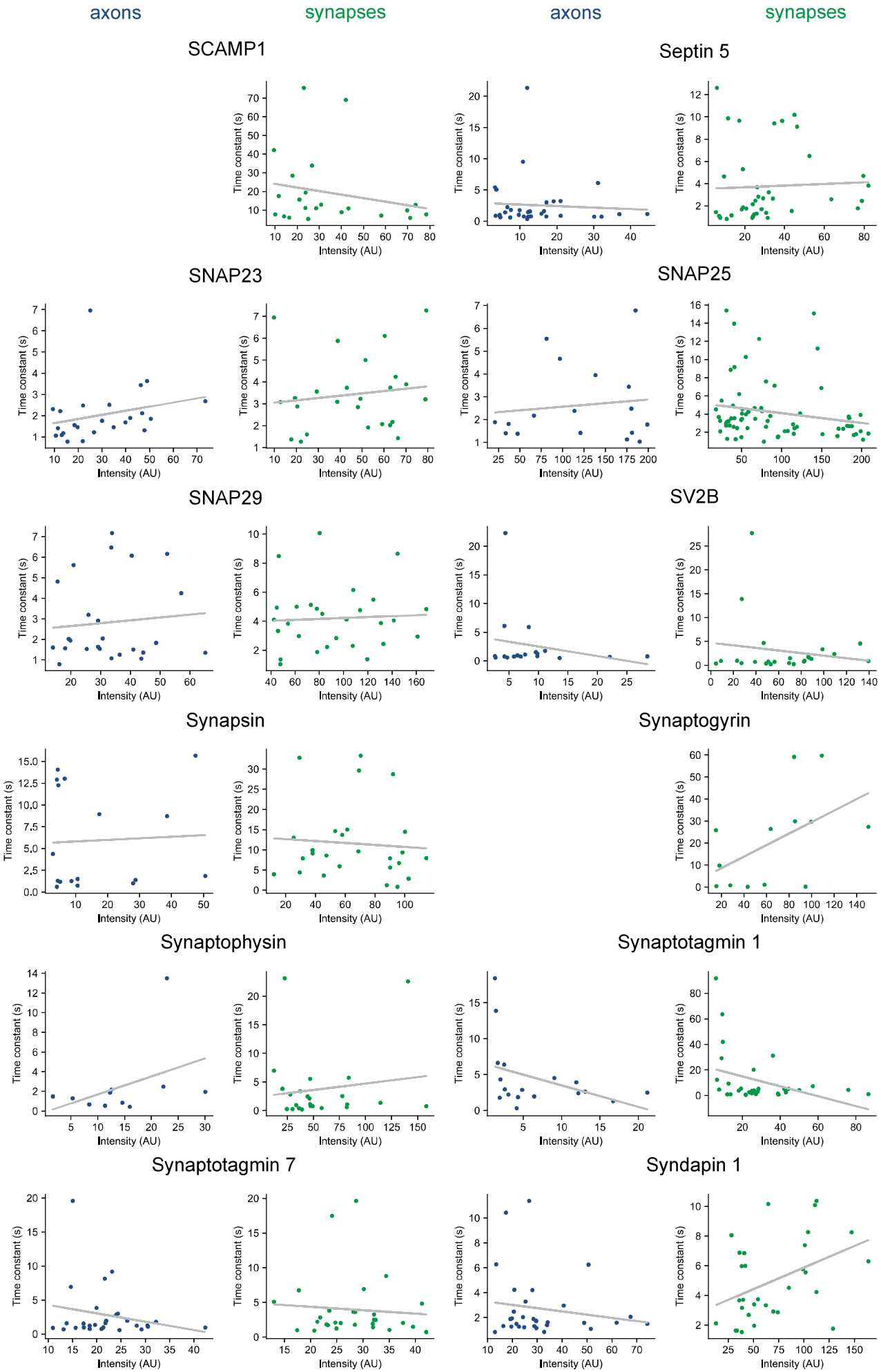
axons
synapses
axons
synapses
SCAMP1
Septin 5
SNAP23
SNAP25
SNAP29
SV2B
Synapsin
Synaptogyrin
Synaptophysin
Synaptotagmin 1
Synaptotagmin 7
Syndapin 1
Time constant (s)
Intensity (AU)

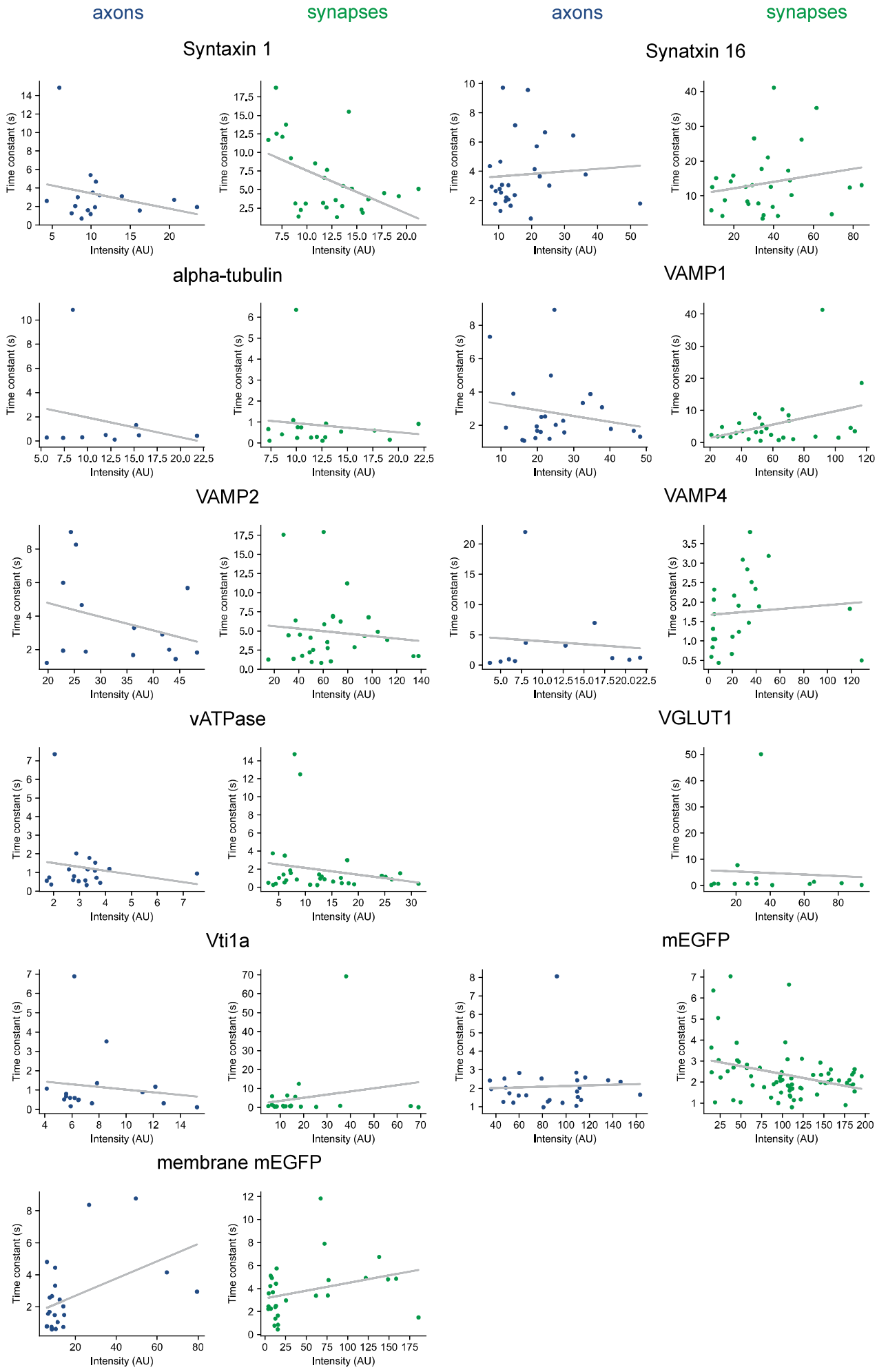
axons
synapses
axons
synapses
Syntaxin 1
Synatxin 16
alpha-tubulin
VAMP1
VAMP2
VAMP4
vATPase
VGLUT1
Vti1a
mEGFP
membrane mEGFP
Time constant (s)
Intensity (AU)

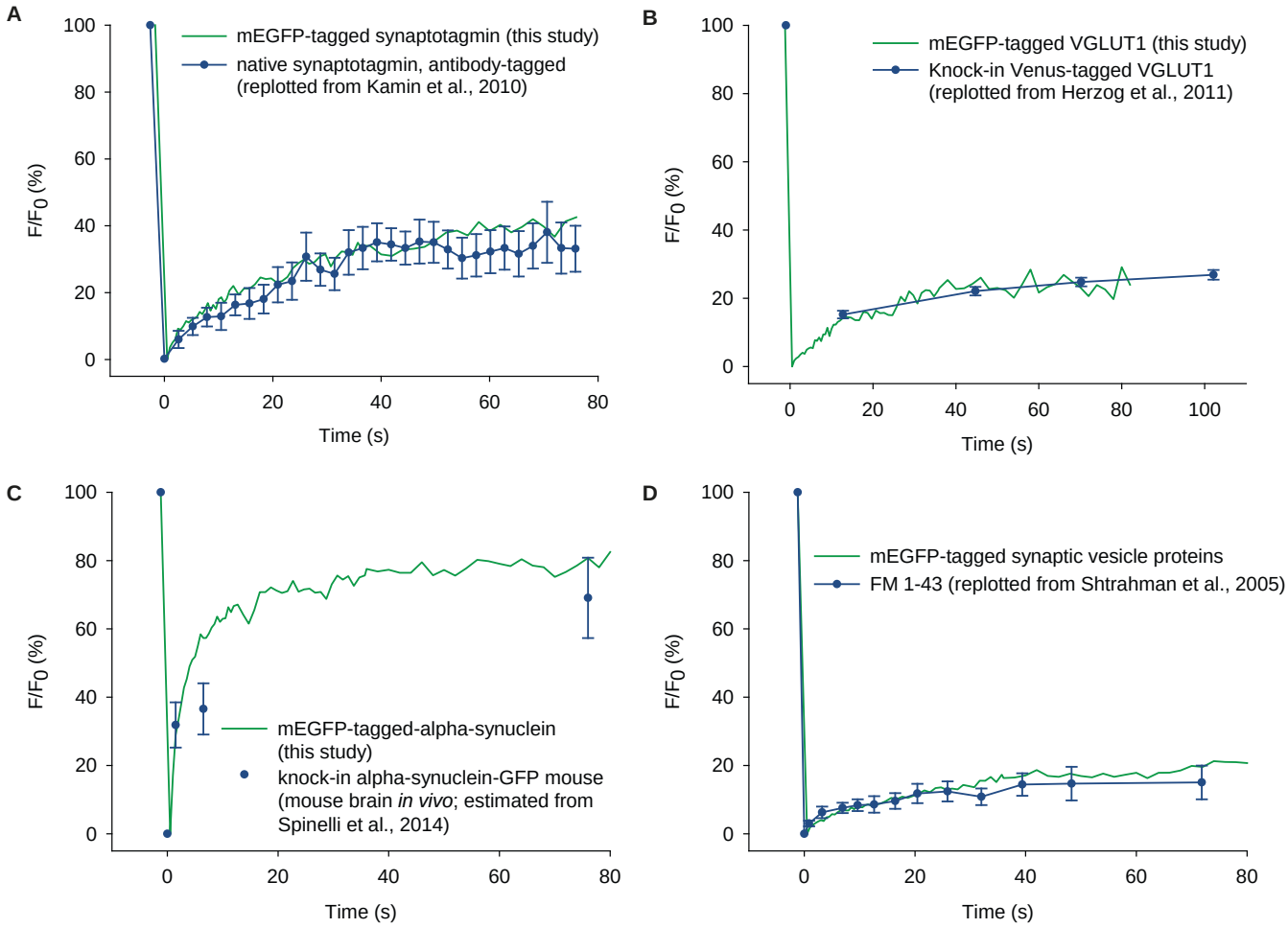

Appendix Fig. S6. Our FRAP results reproduce previous results obtained on knock-in tagged proteins or on endogenous proteins labeled with fluorescent tags. A, We compared our results with previously published FRAP experiments performed on endogenous synaptotagmin 1 visualized by the use of antibodies (Kamin et al., 2010). **B**, A similar comparison to VGLUT1, measured in cultures from mice tagged in-locus with a fluorescent version of the protein (Herzog et al., 2011). No intensity of VGLUT1Venus is shown at 0 s, since the first measurement came at ~12 seconds in the original publication. **C**, We obtained similar results to the ones measured in live brains of knock-in Syn-GFP mice (minimal expression, mimicking human disease; estimated from Spinelli et al., 2014); **D**, The average FRAP curve of several SV proteins (relying on the most vesicle-enriched proteins, as known from the literature: Synaptogyrin, Synaptophysin, SV2, VGLUT) measured here overlaps closely with the recovery of FM 1-43 labeled synaptic vesicles (measured in Shtrahman et al., 2005). All green traces indicate the median values of the respective FRAP distributions from our measurements, shown here without error bars, to avoid obscuring the other measurements shown. -The errors represent the error measurements from the original publications.

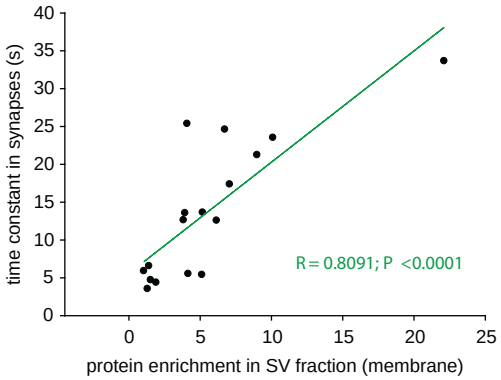

Appendix Fig. S7. Protein mobility is affected by association with synaptic vesicles. We compared the time constants in synapses to the enrichment of the proteins in synaptic vesicles, obtained from biochemical experiments (Takamori et al., 2006). Significant correlations were observed for membrane proteins.

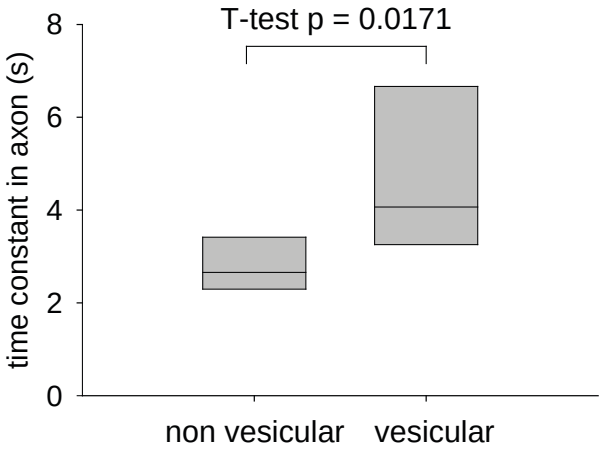

Appendix Fig. S8. Comparison of the axonal time constants of vesicular and non-vesicular proteins. True vesicular proteins move significantly slower in the axonal plasma membrane compared to other membrane proteins.

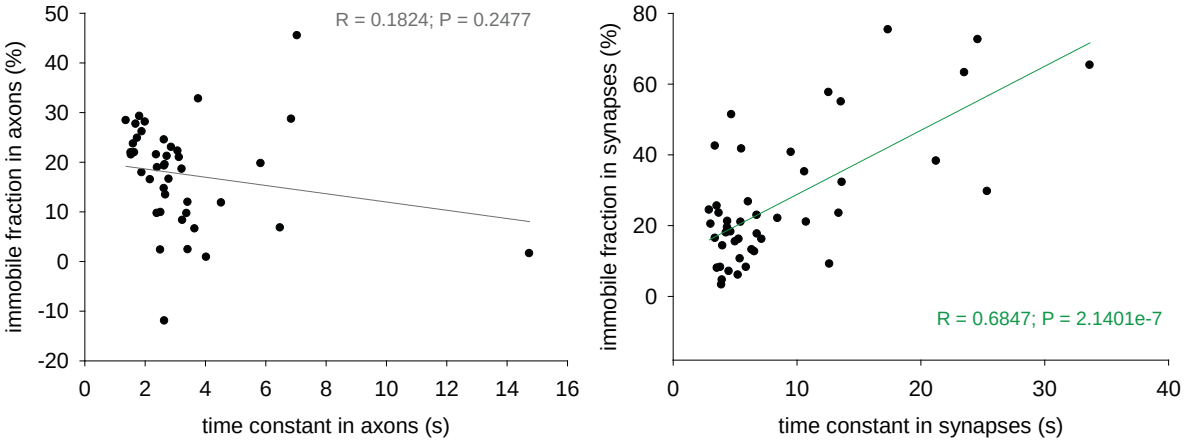

Appendix Fig. S9. Correlation between the time constants and the immobile fractions in axons (left) and synapses (right). A significant correlation is observed in synapses, but not in axons. Similar results were observed when analyzing the soluble or membrane proteins separately.

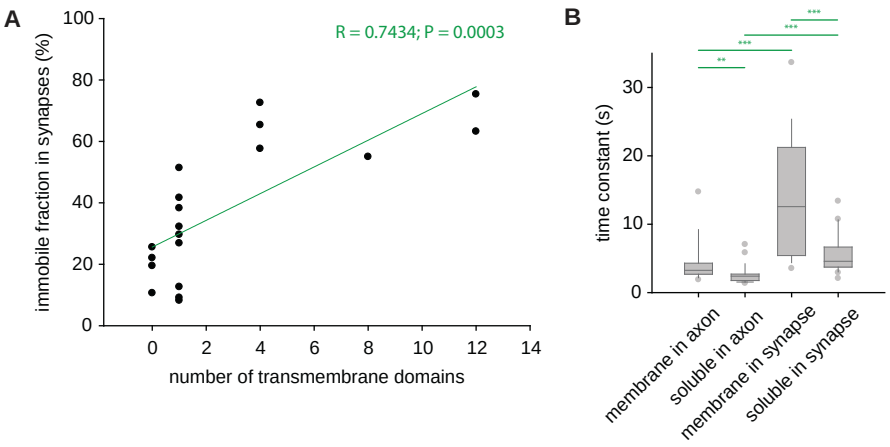

Appendix Fig. S10. An analysis of basic movement parameters of the proteins. A, Correlation of synaptic immobile fractions with the number of transmembrane domains, for the different membrane proteins. Significant correlation can be observed, which agrees with the previous literature, and with the expectation that proteins with large numbers of membrane domains diffuse more slowly. Similar trends were observed for the axonal measurements. **B**, A comparison of time constants in different compartments shows differences between soluble and membrane proteins, as well as differences between axons and synapse for both protein categories. Wilcoxon rank-sum test, ** $P < 0.01$, *** $P < 0.001$.

	correlation coefficients (all proteins)																			
	%Ala	%Arg	%Asn	%Asp	%Cys	%Gln	%Glu	%Gly	%His	%Ile	%Leu	%Lys	%Met	%Phe	%Pro	%Ser	%Thr	%Trp	%Tyr	%Val
time constant (axon)	-0.2315	0.2361	-0.021	0.1318	-0.0858	-0.0959	-0.058	-0.0662	0.173	0.1588	0.1211	0.0165	0.0389	0.1638	-0.0407	-0.0305	-0.1738	0.0392	-0.1676	0.0711
immobile fraction (axon)	0.1919	-0.3364	-0.0339	-0.2722	0.2314	-0.307	-0.2546	0.3133	0.1215	-0.145	-0.1037	-0.3514	-0.2161	0.2179	0.2263	0.1955	0.2606	0.333	0.3387	0.0479
time constant (synapse)	0.0147	-0.1917	-0.0449	-0.4928	0.0444	-0.0803	-0.3212	0.2717	0.1994	-0.1362	0.1738	-0.3449	-0.1316	0.4891	0.1386	0.0702	-0.113	0.3353	0.4329	0.2829
immobile fraction (synapse)	-0.0571	-0.1539	0.0391	-0.3972	0.0411	-0.1205	-0.2769	0.3473	0.0895	0.0918	0.1223	-0.3725	0.1089	0.5618	0.058	-0.1224	-0.1717	0.4274	0.2278	0.196

	P values (all proteins)																			
	%Ala	%Arg	%Asn	%Asp	%Cys	%Gln	%Glu	%Gly	%His	%Ile	%Leu	%Lys	%Met	%Phe	%Pro	%Ser	%Thr	%Trp	%Tyr	%Val
time constant (axon)	0.1402	0.1322	0.8951	0.4054	0.5891	0.5456	0.715	0.6772	0.2733	0.3152	0.445	0.9172	0.8066	0.2999	0.798	0.848	0.2709	0.8055	0.2889	0.6545
immobile fraction (axon)	0.2293	0.0315	0.8332	0.0852	0.1455	0.0509	0.1082	0.0461	0.4491	0.3656	0.5188	0.0243	0.1747	0.1711	0.1548	0.2207	0.0999	0.0334	0.0303	0.766
time constant (synapse)	0.9237	0.2071	0.7694	5.84E-04	0.7719	0.6001	0.0315	0.071	0.189	0.3722	0.2537	0.0203	0.3888	6.51E-04	0.3639	0.6468	0.4598	0.0243	2.97E-03	0.0597
immobile fraction (synapse)	0.7095	0.3128	0.799	6.90E-03	0.7886	0.4304	0.0655	0.0194	0.5586	0.5488	0.4235	0.0117	0.4766	5.92E-05	0.705	0.4232	0.2595	3.41E-03	0.1323	0.1969

	correlation coefficients (soluble proteins)																			
	%Ala	%Arg	%Asn	%Asp	%Cys	%Gln	%Glu	%Gly	%His	%Ile	%Leu	%Lys	%Met	%Phe	%Pro	%Ser	%Thr	%Trp	%Tyr	%Val
time constant (axon)	-0.0258	0.0342	-0.2812	-0.0371	0.0236	0.161	0.0179	0.2308	0.2455	-0.1125	-0.1977	-0.1169	-0.0688	-0.0428	0.1963	-0.0462	0.0201	-0.2626	0.0994	-2.96E-03
immobile fraction (axon)	0.0919	-0.142	0.0506	-0.1787	0.1398	-0.3319	-0.3209	0.0972	0.2289	-0.0221	0.0659	-0.4187	-0.3365	0.0672	0.2076	0.3243	0.256	0.3344	0.1728	0.2185
time constant (synapse)	-0.0234	0.0646	-0.1527	-0.38	0.0964	0.1844	-0.2691	0.1874	0.4066	-0.2199	0.0856	-0.33	-0.3177	-0.2397	0.4968	0.2609	0.0945	0.0648	0.0938	0.0378
immobile fraction (synapse)	-0.2415	0.058	-0.181	-0.0556	-0.0939	0.0733	0.1136	0.3233	0.1866	0.076	0.1358	9.04E-03	-0.0206	-0.2933	0.1078	-0.2645	-5.57E-03	-0.1759	-0.1933	0.1152

	P values (soluble proteins)																			
	%Ala	%Arg	%Asn	%Asp	%Cys	%Gln	%Glu	%Gly	%His	%Ile	%Leu	%Lys	%Met	%Phe	%Pro	%Ser	%Thr	%Trp	%Tyr	%Val
time constant (axon)	0.8963	0.8627	0.1472	0.8513	0.9051	0.4132	0.928	0.2374	0.2079	0.5688	0.3133	0.5536	0.7281	0.8287	0.3169	0.8153	0.9191	0.177	0.6147	0.9881
immobile fraction (axon)	0.6419	0.471	0.7983	0.3628	0.478	0.0845	0.0959	0.6228	0.2414	0.911	0.7391	0.0266	0.0799	0.7342	0.2892	0.0922	0.1885	0.0819	0.3791	0.264
time constant (synapse)	0.9059	0.7442	0.4379	4.61E-02	0.6256	0.3477	0.1662	0.3397	0.0318	0.2609	0.6651	0.0864	0.0995	2.19E-01	7.16E-03	0.1799	0.6323	0.7431	6.35E-01	0.8485
immobile fraction (synapse)	0.2158	0.7692	0.3567	7.79E-01	0.6345	0.7109	0.5649	0.0933	0.3417	0.7005	0.4908	0.9636	0.9172	1.30E-01	0.5849	0.1739	0.9776	3.71E-01	0.3244	0.5595

	correlation coefficients (membrane proteins)																			
	%Ala	%Arg	%Asn	%Asp	%Cys	%Gln	%Glu	%Gly	%His	%Ile	%Leu	%Lys	%Met	%Phe	%Pro	%Ser	%Thr	%Trp	%Tyr	%Val
time constant (axon)	-0.2891	0.1989	-0.0694	0.2542	-0.2201	-0.3643	-0.037	-0.1717	0.1871	0.1232	0.1358	0.2299	-0.0628	0.2731	-0.0929	-0.0469	-0.4022	0.1853	-0.2418	7.08E-02
immobile fraction (axon)	0.0312	-0.47	0.1424	-0.4894	0.6138	-0.3071	-0.2817	0.7148	-0.0411	-0.0693	-0.1246	-0.384	0.364	0.5023	-0.048	-0.1209	0.2124	0.4839	0.5625	-0.2911
time constant (synapse)	0.3376	-0.5524	-0.3517	-0.6418	0.1587	-0.2442	-0.3701	0.5763	0.201	-0.5671	0.0472	-0.3229	-0.3757	0.636	0.2818	-0.0915	-0.1714	0.3832	0.7897	0.4095
immobile fraction (synapse)	0.3472	-0.5082	-0.1242	-0.6124	0.3779	-0.3034	-0.5924	0.637	0.0557	-0.2284	-0.0848	-5.88E-01	0.036	0.8235	0.3058	-0.1813	-2.79E-01	0.7279	0.5804	0.1564

	P values (membrane proteins)																			
	%Ala	%Arg	%Asn	%Asp	%Cys	%Gln	%Glu	%Gly	%His	%Ile	%Leu	%Lys	%Met	%Phe	%Pro	%Ser	%Thr	%Trp	%Tyr	%Val
time constant (axon)	0.3162	0.4955	0.8136	0.3804	0.4497	0.2004	0.9	0.5572	0.5219	0.6748	0.6435	0.4292	0.8311	0.3448	0.752	0.8736	0.154	0.5258	0.405	0.81
immobile fraction (axon)	0.9194	0.1051	0.6427	0.0896	0.0257	0.3075	0.3511	6.03E-03	0.8941	0.822	0.6851	0.1952	0.2215	0.0802	0.8762	0.694	0.486	0.0938	0.0454	0.3346
time constant (synapse)	0.185	0.0215	0.1663	5.48E-03	0.5431	0.345	0.1437	0.0155	0.4391	0.0176	0.8572	0.2062	0.1373	6.06E-03	2.73E-01	0.7269	0.5108	0.129	1.63E-04	0.1026
immobile fraction (synapse)	0.1722	0.0373	0.6349	8.97E-03	0.1348	0.2365	0.0122	5.96E-03	0.8319	0.3779	0.7463	0.0131	0.8909	4.86E-05	0.2326	0.4862	0.2788	9.25E-04	0.0146	0.5489

Appendix Fig. S11. Correlations between FRAP parameters and the amino acid composition of the proteins. Correlation coefficients and P values for mobility parameters versus the % of each amino acid in the protein sequences are shown. Statistically significant correlations (after correction for multiple testing) are underlined.

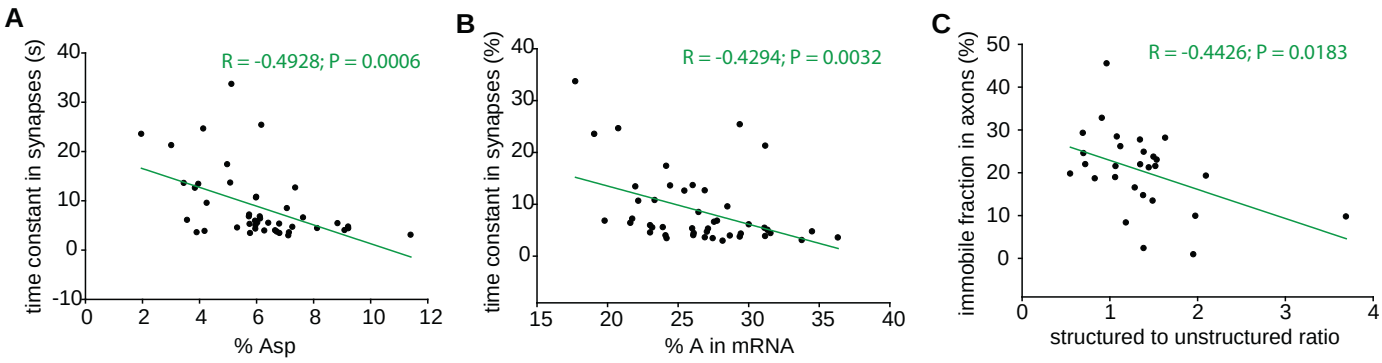

Appendix Fig. S12. Correlation of protein mobility parameters to different cell biology parameters. A, correlation between time constants in synapses (all proteins) and the percentage of aspartate residues in the protein sequence. **B**, correlation between time constants in synapses and the percentage of adenine in the mRNA sequences. **C**, correlations the immobile fraction in axons and structured-to-unstructured ratio (indicating the fraction of each protein sequence that is predicted to be structured, divided by the fraction that is predicted to be organized as random coils). The structural parameters were determined in Mandad et al., 2018.

	correlation coefficients (all proteins)			
	time constant (axon)	immobile fraction (axon)	time constant (synapse)	immobile fraction (synapse)
%A	0.2017	-5.05E-01	-4.29E-01	-0.2503
%C	-0.2156	4.14E-01	0.2356	0.0383
%G	-0.2056	-0.0926	-0.021	-0.1132
%U	0.241	0.1908	0.2827	3.93E-01

	P values (all proteins)			
	time constant (axon)	immobile fraction (axon)	time constant (synapse)	immobile fraction (synapse)
%A	0.2003	7.68E-04	3.25E-03	0.0973
%C	0.1703	7.08E-03	0.1193	0.8027
%G	0.1915	0.5646	0.891	0.459
%U	0.1242	0.2321	0.0599	7.52E-03

	correlation coefficients (soluble proteins)			
	time constant (axon)	immobile fraction (axon)	time constant (synapse)	immobile fraction (synapse)
%A	-0.2067	-0.4562	-0.4774	0.0485
%C	0.2265	0.2947	0.5332	-0.0606
%G	0.014	-0.1951	-0.1356	0.0549
%U	-0.0727	0.3509	0.0105	-0.0398

	P values (soluble proteins)			
	time constant (axon)	immobile fraction (axon)	time constant (synapse)	immobile fraction (synapse)
%A	0.2914	1.47E-02	1.02E-02	0.8062
%C	0.2465	1.28E-01	3.48E-03	0.7593
%G	0.9435	0.3197	0.4916	0.7813
%U	0.7132	0.0671	0.9578	8.41E-01

	correlation coefficients (membrane proteins)			
	time constant (axon)	immobile fraction (axon)	time constant (synapse)	immobile fraction (synapse)
%A	0.359	-0.5079	-0.6115	-0.5055
%C	-0.4523	0.4972	0.3974	0.2829
%G	-0.439	-0.0483	0.3256	-0.1117
%U	0.4198	0.1852	0.258	0.6008

	P values (membrane proteins)			
	time constant (axon)	immobile fraction (axon)	time constant (synapse)	immobile fraction (synapse)
%A	0.2075	0.0764	9.09E-03	0.0384
%C	0.1044	0.0838	0.1142	0.2713
%G	0.1163	0.8754	0.2021	0.6695
%U	0.1351	0.5448	0.3174	0.0108

Appendix Fig. S13. Correlations between FRAP parameters and nucleotide composition of proteins' mRNAs. Correlation coefficients and P values for mobility parameters versus the % percentage of each nucleotide in the mRNA sequences are shown. Statistically significant correlations (after correction for multiple testing) are underlined.

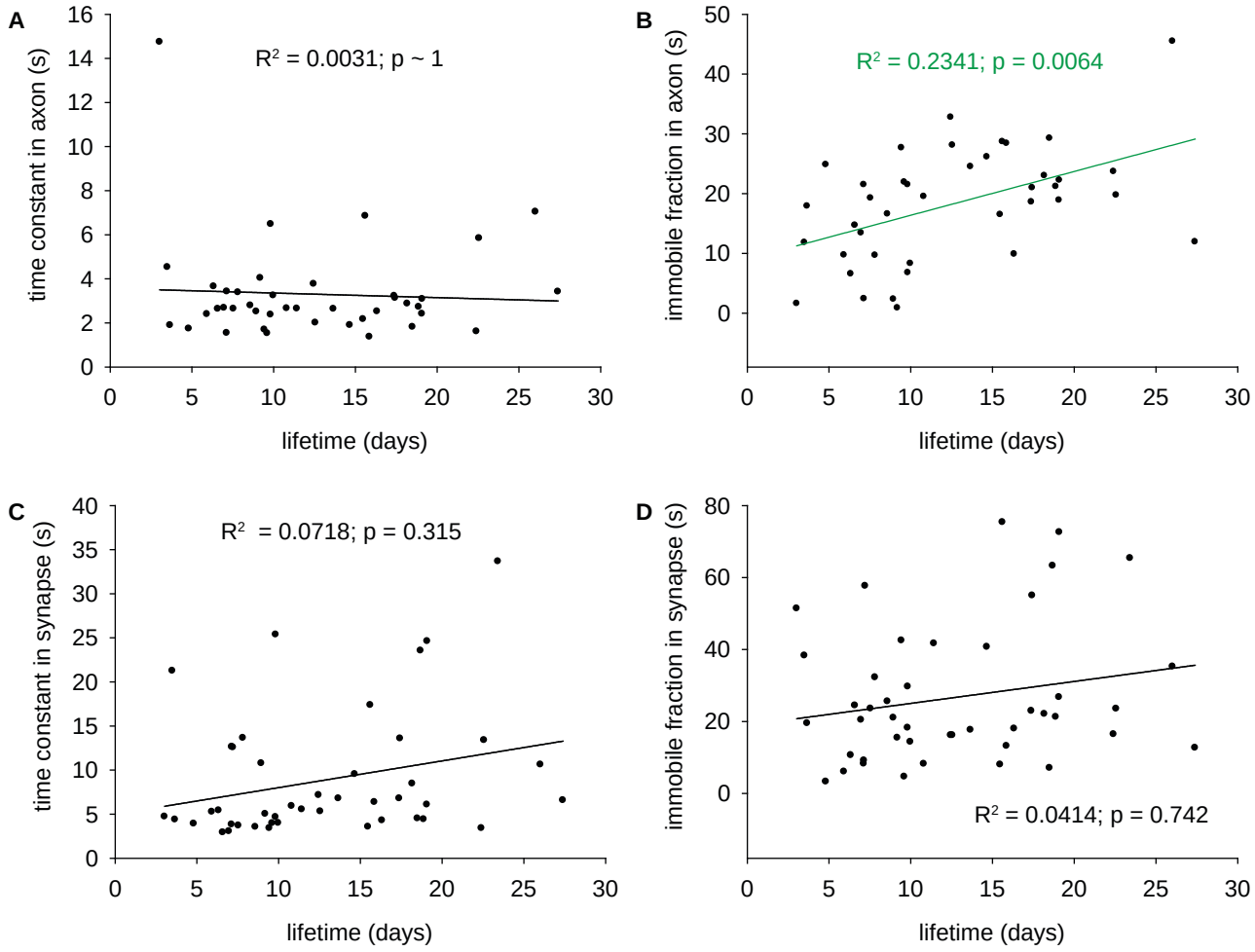

Appendix Fig. S14. A comparison of protein movement parameters to protein lifetimes. We plotted here the lifetimes of the proteins we analyzed (measured in vivo by Fornasiero et al., 2018) against the FRAP time constants and the immobile fractions measured in axons and synapses. A significant correlation was found between the axonal immobile fraction and the protein lifetime ($P < 0.01$, after a Bonferroni correction for multiple testing). Panel B is also shown in Fig. 4 F.

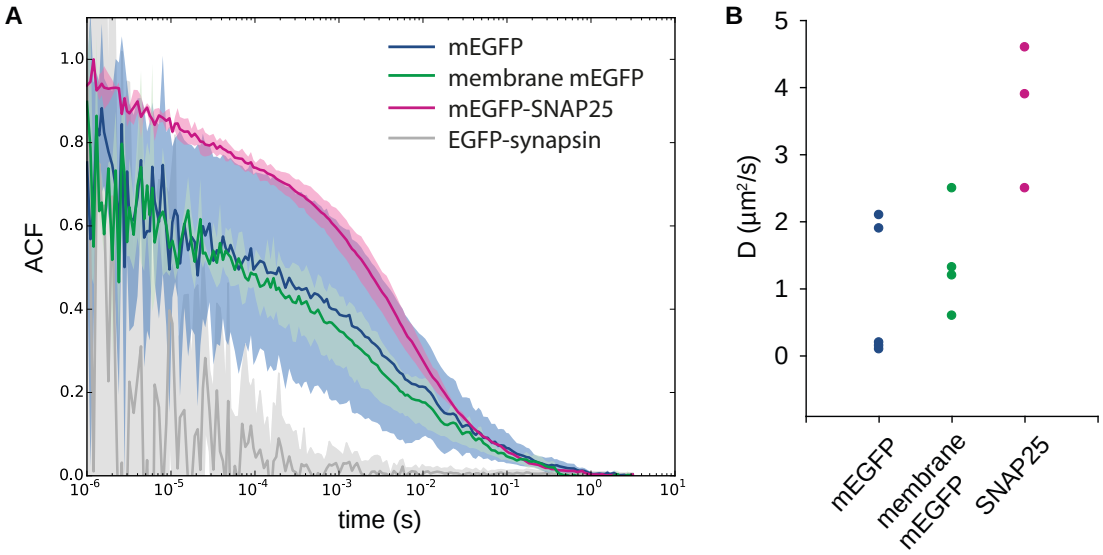

Appendix Fig. S15. FCS experiments for determining protein mobility in synapses and axons. FCS experiments were conducted on neurons expressing mEGFP-SNAP25, EGFP-synapsin, soluble mEGFP or membrane-anchored mEGFP. The acquired autocorrelation curves were fitted using a single- or a dual-component model for particles diffusing in 2D (Lakowicz, 2006). **A,** the normalized average curves for each of the four expressed proteins. **B**, average diffusion coefficients determined at each measurement position for each protein. Diffusion was measured at 5, 4, and 3 different positions inside axons for mEGFP, membrane mEGFP and SNAP25 respectively. Each position was measured at least 20 times, with acquisition times between 10 and 30 s for each round of acquisition. For EGFP-synapsin the effects of bleaching and high density of the molecules dominate the measurement, implying that a reasonable correlation of the data is impossible. For membrane EGFP the measured diffusion coefficient is slightly higher than free mEGFP, 1.4 ± 0.4 $\mu m^2/s$ (the coefficient for free mEGFP was 0.9 ± 0.4 $\mu m^2/s$). For mEGFP-SNAP25 we measured a diffusion coefficient of 3.7 ± 0.6 $\mu m^2/s$. These values are surprising, since the membrane-attached mEGFP-SNAP25 as well as membrane mEGFP are expected to diffuse considerably slower than free mEGFP in the cytosol. At the same time, SNAP25 value is ~15-fold higher than expected from previous measurements, at ~0.24 $\mu m^2/s$ (for measurements in neuroendocrine PC12 cells (Knowles et al., 2010)).

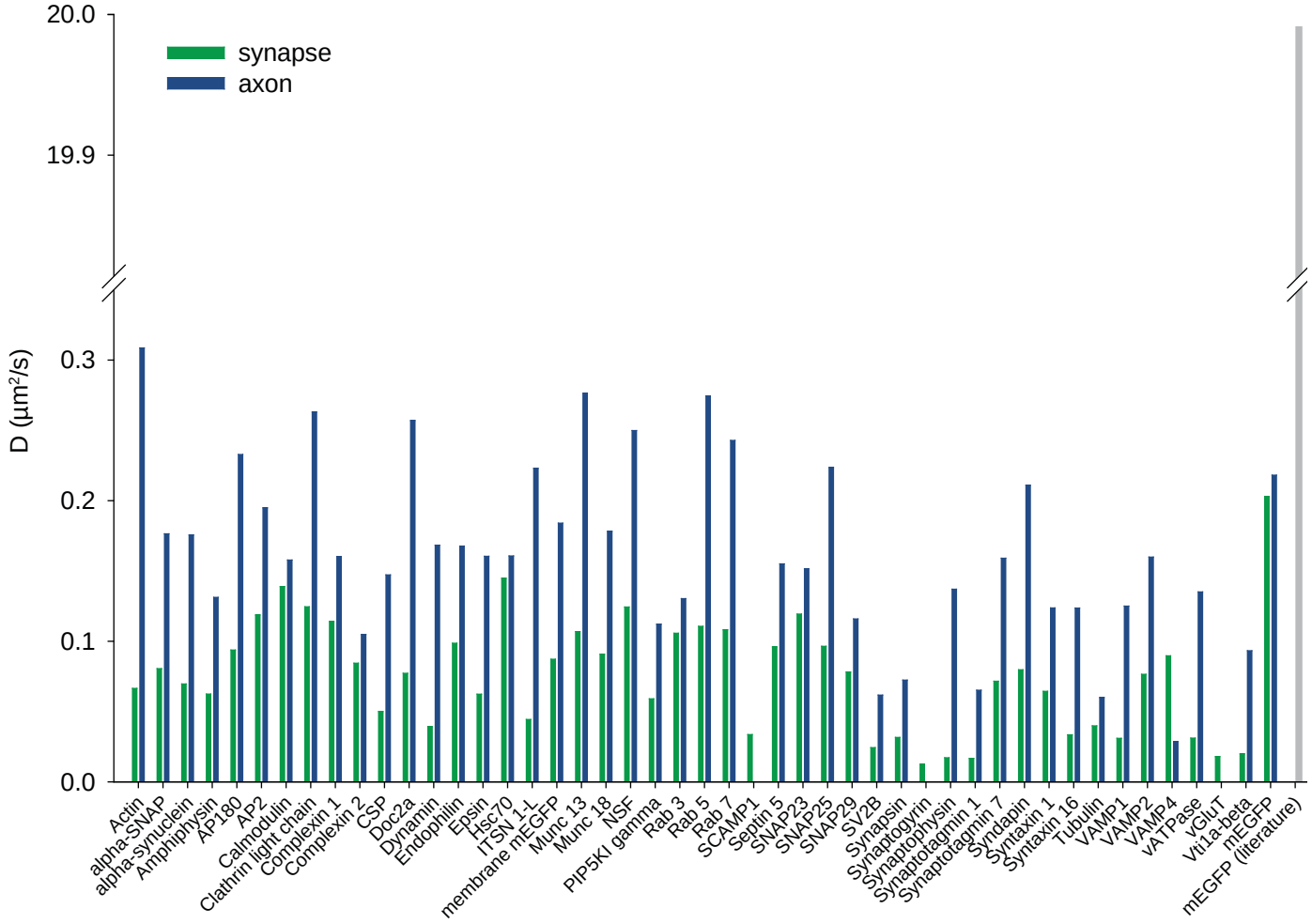

Appendix Fig. S16. Calculation of protein diffusion coefficients using a simple FRAP interpretation model. We applied a previously published equation dedicated to FRAP interpretation (Kang et al., 2012) to our dataset. The diffusion coefficients are shown here. A number of problems are evident. For example, the equation underestimates the diffusion coefficient of mEGFP by ~100 fold compared to the diffusion coefficient measured in eukaryotic cells (Sadovsky et al., 2017). Also, there is no evident difference between soluble and membrane proteins. Finally, free mEGFP is expected to be the fastest-moving molecule, but this does not seem to be the case when using this interpretation model.

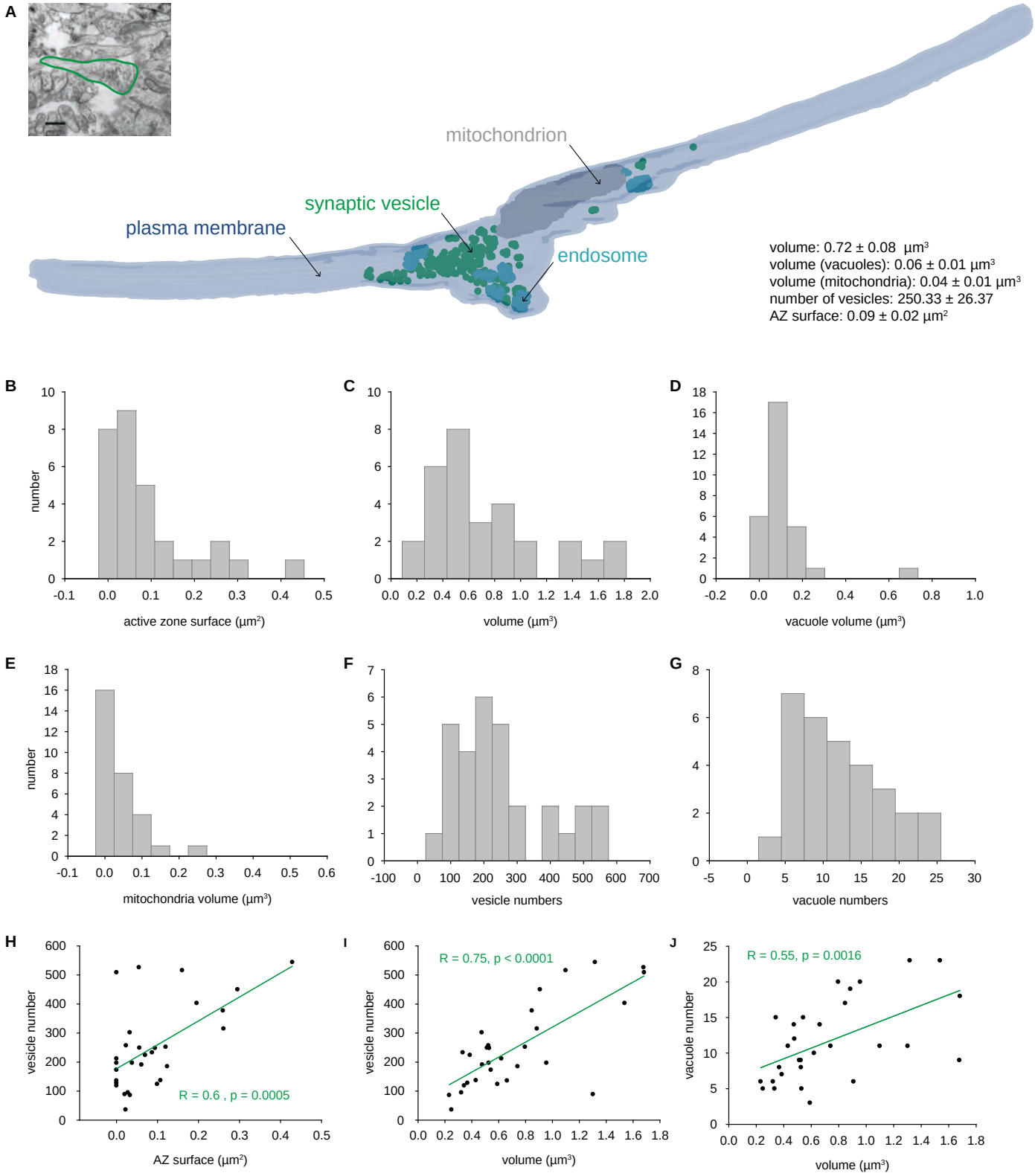

Appendix Fig. S17. 3D model of a synapse, and synaptic parameters measured from serial-section electron microscopy. A, A view of the 3D synapse used in this work. The inset shows one EM section of the selected synapse. Scale bar, 500 nm. Average measured parameters ± SEM shown in the right lower corner of the panel. We reconstructed 30 synapses from series of 70 nm-thick sections. Their various parameters, including active zone surface area, total volume, vacuole (endosome) total volume, mitochondria volume, vesicle numbers, and vacuole (endosome) numbers are indicated in the form of histograms (**B**-**G**), or as scatter plots (**H**-**J**). As expected from the previous literature (Murthy et al., 2001; Schikorski and Stevens, 1997, 2001), the different parameters correlate to each other. For example, the vesicle numbers correlate to the active zone surface area (**H**), and the synaptic volume also correlates to the vacuole and vesicle numbers (**I**-**J**).

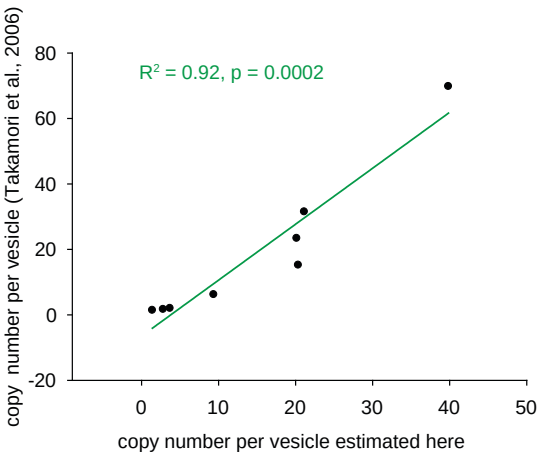

Appendix Fig. S18. The *in silico* models, in combination with the available literature, suggest accurate numbers of synaptic vesicle proteins per vesicle. The copy numbers of synaptic vesicle proteins have been estimated in a seminal paper in 2006 (Takamori et al., 2006) , and have been later confirmed in a further quantitative study (Wilhelm et al., 2014). To test whether our in silico models confirm these measured values, we proceeded as follows. We first estimated the numbers of proteins present in the synapto-axonal compartment, relying on values published in Wilhelm et al., 2014, adjusted to hippocampus neurons following the method of Richter et al., 2018. We then extracted from the models the fraction of proteins that is predicted to be present in the synapses. This parameter was already used in Fig. 4A-C. We then proceeded for *bona fide* synaptic vesicle proteins as follows. The fraction of each protein found on the synaptic plasma membrane or in vesicles can be obtained from the literature (Bodzęta et al., 2017; Granseth et al., 2006; Hoopmann et al., 2010; Voglmaier et al., 2006), which enables us to easily correct the previous parameter to determine the total copy numbers present in the vesicle population in the model synapse. Finally, these numbers can be divided by the number of vesicles in the model, to obtain a predicted copy number per synaptic vesicle. This value correlates excellently with the value from Takamori et al., 2006 ($R^2 > 0.9$)

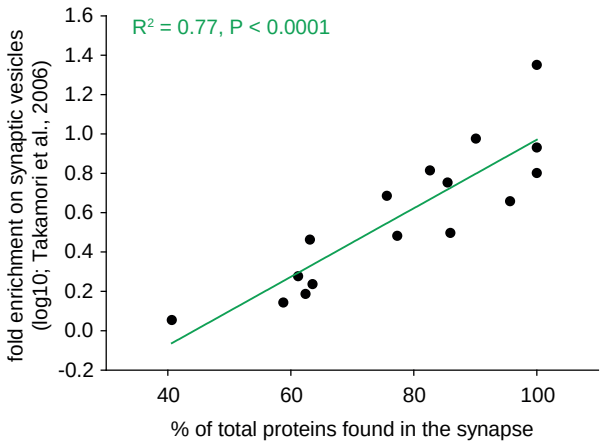

Appendix Fig. S19. The *in silico* models suggest accurate enrichment of the proteins in the vesicles. Our movement models enabled us to calculate easily the fraction of proteins found in the synapse, in comparison to the axon regions near the synapse, for all membrane proteins. We plotted this on the X axis, and compared it to the enrichment of the respective proteins in synaptic vesicles vs. the brain homogenate fraction as measured by Takamori et al., 2006.

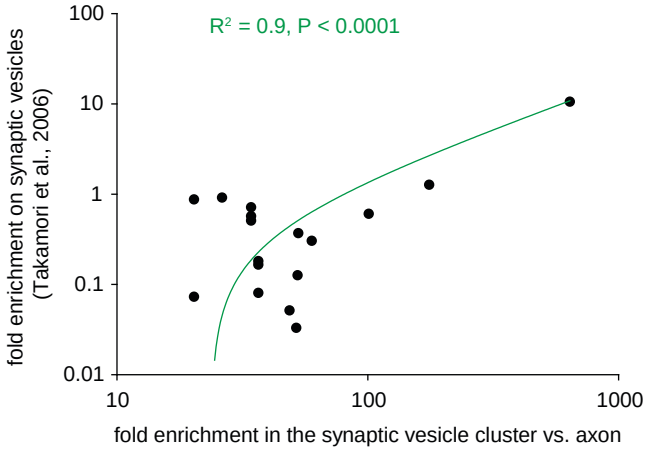

Appendix Fig. S20. The *in silico* models suggest accurate enrichment of soluble proteins in the synaptic vesicle cluster. We calculated the enrichment of soluble proteins in the vesicle cluster compared to the axon as predicted by our model. The values correlate well with the enrichment on synaptic vesicles vs. the brain homogenate fraction as measured by Takamori et al., 2006.

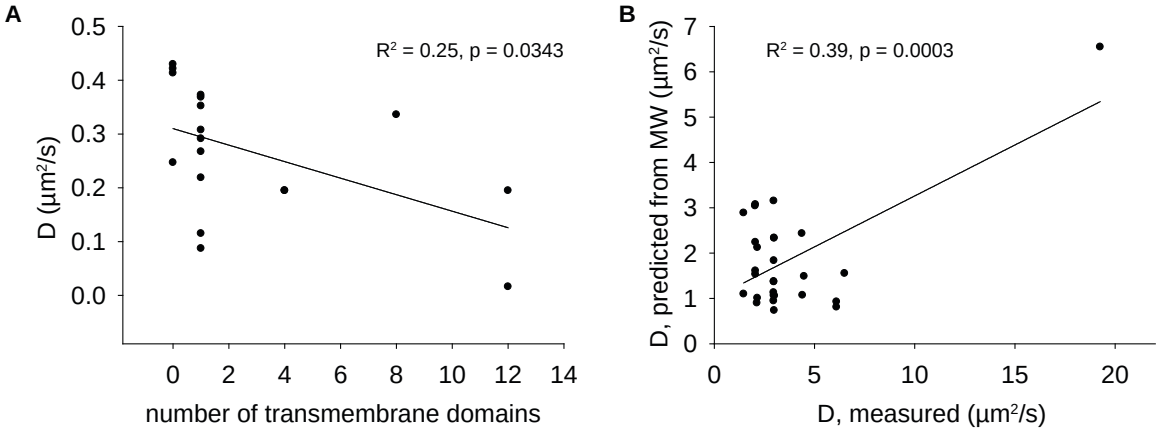

Appendix Fig. S21. An analysis of basic movement parameters of the proteins. A, We compared the diffusion coefficients obtained in the axons with the number of transmembrane domains, for the different membrane proteins. A significant, albeit not very strong, correlation can be observed, which agrees with the previous literature, and with the expectation that proteins with large numbers of membrane domains diffuse more slowly. **B**, We compared the diffusion coefficients obtained in the axons for soluble proteins with the ideal diffusion coefficients for the respective proteins, predicted from their molecular weights (according to Kumar et al., 2010). A significant correlation was obtained, which is again in agreement with the previous literature. If soluble EGFP is removed (upper right spot), the correlation loses significance, implying that the soluble proteins do not, in general, move according to their mass in the synaptic system.

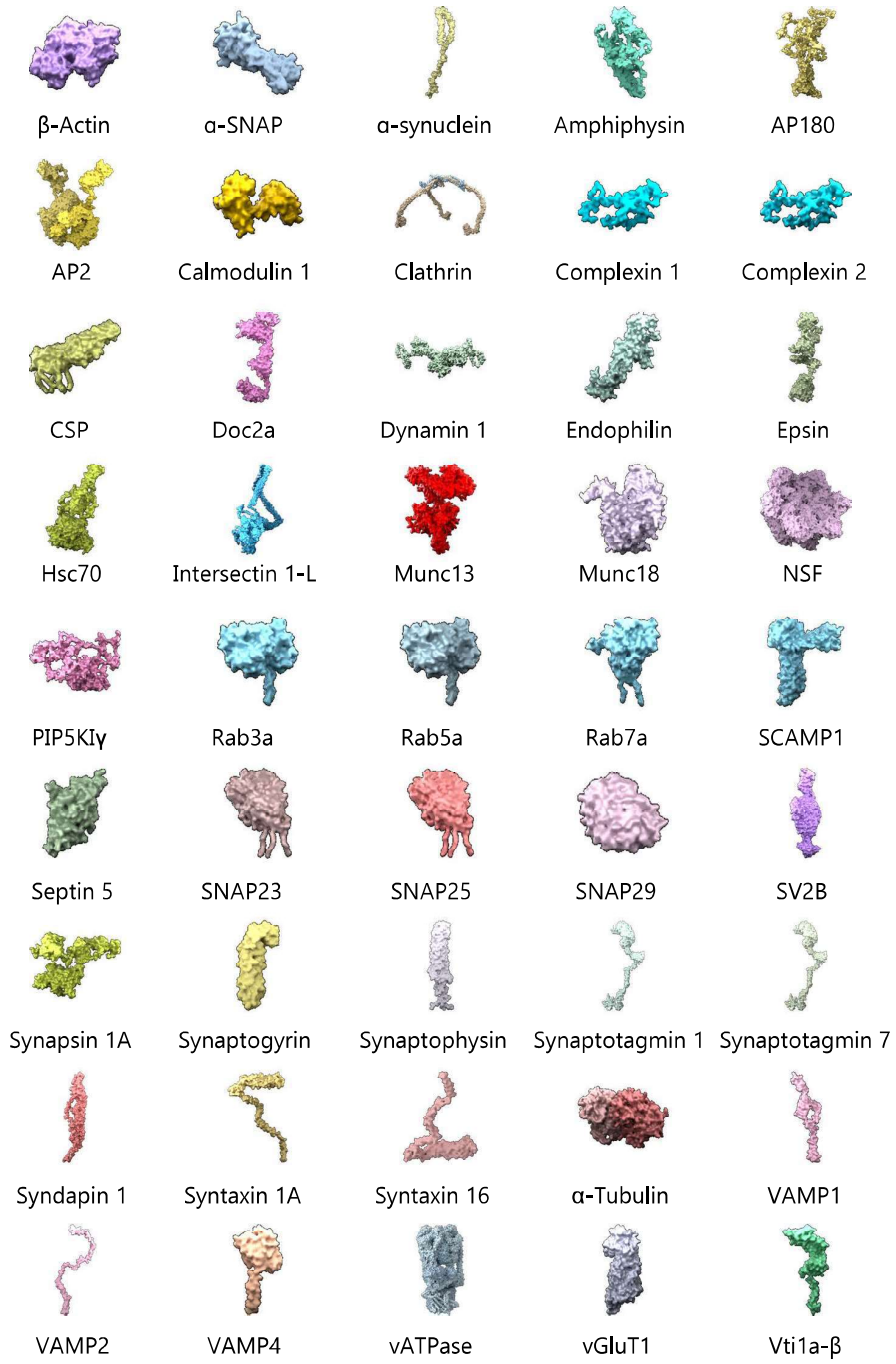

Appendix Fig. S22. The shapes and colors of the proteins shown in the Movies EV1-4. The proteins are not show to scale (the sizes are automatically scaled for all).

Table EV1. A summary of previously published verifications of localizations and functional involvement of proteins used in this study fused to fluorescent reporters.

Tagged protein	Score*	Example publications	Comments
β-actin	3	Ballestrem et al., 1998; Choidas et al., 1998; Sankaranarayanan et al., 2003	Localization and functional incorporation in actin structures has been verified in mammalian cell cultures; validation in synapses as well.
α-SNAP	3	Barszczewski et al., 2008; Miao et al., 2013	Functional recruitment verified in living neuroendocrine cell line (PC12).
α-synuclein	3	Hansen et al., 2013; McLean et al., 2001; Price et al., 2016; Spinelli et al., 2014	Numerous cell models, and also mouse models expressing GFP-tagged α-synuclein. They reproduce the expected behavior of the protein.
Amphiphysin	3	Hayer et al., 2016; Meier et al., 2005; Nakanishi et al., 2008	Accumulation of the tagged protein was observed at endocytosis sites, suggesting normal function. Curvature sensing is apparent also in tagged BAR domains.
AP180	2	Stavrou and O'Halloran, 2006; Zhao et al., 2010	Recruitment to endocytotic structures in various cell types.
AP2a	4	Motley et al., 2006; Rappoport and Simon, 2008; Rappoport et al., 2003	GFP-tagging at the C-terminus blocks endocytosis. The N-terminus tagging is not deleterious to function, and can rescue endocytosis in cells in which the wild-type protein is depleted.
Calmodulin	4	Partridge, 2015; Truong et al., 2001	Protein resistant to tagging, and which has been used as a basis for genetically-encoded calcium indicators for many years. Multiple in vivo tagged models also exist.
Clathrin light chain	3	Mueller et al., 2004; Hoffmann et al., 2010 and further references therein	Verification of both clathrin coat formation and endocytosis in mammalian cells. GFP-tagged clathrin light chain (albeit typically the light chain A) has been used for more than a decade in synaptic work, showing the expected dynamics.
Complexin 1	5	Snead et al., 2014; Wragg et al., 2015	GFP-complexin rescues complexin deletion in C. elegans. Complexin 1-GFP behaves as expected in neuronal cell cultures (dispersion upon heavy synaptic release, and no dispersion if release is blocked).
Complexin 2	5	An et al., 2010; Snead et al., 2014	GFP-complexin rescues complexin deletion in C. elegans. Complexin 2-GFP shows the expected dynamics at the sites of single dense-core vesicle fusion in a neuroendocrine cell line (PC12).
CSP	2	Greaves and Chamberlain, 2006; Greaves et al., 2012	Localization to dense-core vesicles in a neuroendocrine cell line (PC12), as expected.
Doc2a	2	Groffen et al., 2006	Localization in relation to calcium and neuronal stimulation demonstrated in neurons.
Dynamin 1	2	Song et al., 2004; Taylor et al., 2011	Both GFP-dynamin and mCherry-dynamin shown to be recruited correctly to endocytosis sites.
Endophilin A1	3	Murdoch et al., 2016; Schuske et al., 2003; Yang et al., 2015	Localization of tagged molecules (mCherry, EGFP) verified in neurons, non-neuronal cells, and C. elegans.
Epsin1	2	Chen and Zhuang, 2008; Kyung et al., 2016	Localization to endocytotic structures demonstrated in mammalian cell cultures; normal expression and distribution in neurons also demonstrated with Epsin1-mKate2.
Hsc70	2	Dastoor and Dreyer, 2000	Demonstration of active changes in localization, upon cell stress, mimicking the changes in normal protein, in mammalian cell culture.
Intersectin 1-L	2	Henne et al., 2010; Makhoul et al., 2019	Localization to endocytotic structures demonstrated in mammalian cell cultures

Tagged protein	Score*	Example publications	Comments
Munc13	5	Ashery et al., 1999; Kalla et al., 2006	Multiple articles on cell cultures, and normal mice expressing Munc13-1-EYFP in the locus of the protein.
Munc18	4	Kasula et al., 2016; Martin et al., 2013	Munc18-GFP rescues function in neuroendocrine cell line (PC12) depleted of the wild-type protein. Other constructs (for example with mEos) are also functional.
NSF	3	Dalal et al., 2004; Zhao et al., 2010a	Localization and activity (versus dominant negative effects of mutants) verified in non-neuronal cells.
PIP5KIγ	4	Wang et al., 2008, 2013	Functional rescue of knock-out cells via GFP-tagged protein, in mammalian cell culture
Rab3a	2	Encarnação et al., 2016; Pavlos et al., 2010	Functional localization on vesicular structures and in cultures verified in neurons and other mammalian cells.
Rab5a	3	Bethani et al., 2007; Hoopmann et al., 2010; Pavlos et al., 2010	Functional localization and dysfunction, using specific mutations, have been verified over multiple publications, typically in mammalian cell cultures. Localization has been analyzed in neurons as well.
Rab7a	2	Choudhury et al., 2002; Rowland et al., 2014	Localization and presence on active organelles verified in non-neuronal cells.
SCAMP1	1	Castle and Castle, 2005; The present work	Localization and presence on the appropriate organelles verified in non-neuronal cells; synaptic presence verified in the present work.
Septin5	2	Dagdas et al., 2012; O'Neill and Clark, 2016; Su et al., 2013	Localization of GFP-tagged variant apparently normal from plants to Drosophila. As it is a cytoskeletal element, the localization implies at least a good degree of function.
SNAP23	1	Takuma et al., 2002; Weber et al., 2017	Normal targeting to the plasma membrane in mammalian cell cultures, including a neuroendocrine cell line (PC12).
SNAP25	3	An and Almers, 2004; Halemani et al., 2010; Rickman et al., 2010	Normal targeting and function tested mainly in neuroendocrine cell lines (PC12).
SNAP29	1	Itakura et al., 2012; Wesolowski et al., 2012	Normal targeting to the plasma membrane in mammalian cell cultures
SV2B	4	Nowack et al., 2010	GFP-tagged proteins rescue the functional phenotype of knock-out neurons
Synapsin1A	3	Gitler et al., 2004; Orenbuch et al., 2012	Normal targeting to synaptic vesicle clusters, and the expected functional effects in synapsin knock-out neurons.
Synaptogyrin	2	Stevens et al., 2012; Zhao and Nonet, 2001; the present work	Normal targeting in cultured neurons, in C. elegans, and in Drosophila.
Synaptophysin	2	Granseth et al., 2006; Truckenbrodt et al., 2018	Normal targeting in cultured neurons, and extensive use as a sensor for neuronal and synaptic function. Other tagging possibilities, including SNAP25 segments attached to the protein, still allow it to target properly.
Synaptotagmin1	2	Dean et al., 2012; Opazo et al., 2010	Normal targeting to synaptic vesicles, and use as a sensor for synaptic function. Overexpression induces increased expression on the plasma membrane, same as for other such constructs (e.g. synaptophysin, synaptobrevin).
Synaptotagmin7	2	Dean et al., 2012	Normal targeting to axons, where it reveals exocytosis.
Syndapin1	5	Dharmalingam et al., 2009; Quan et al., 2012; Sherlekar and Rikhy, 2016	Normal targeting in neurons, and clear functional effects upon overexpression. GFP-tagged variant rescues knock-out function in Drosophila.

Tagged protein	Score*	Example publications	Comments
Syntaxin1A	3	Barg et al., 2010; Knowles et al., 2010; Ribrault et al., 2011	Normal targeting and functional organization tested mainly in neuroendocrine cell lines (PC12), but also in neurons and synapses.
Syntaxin16	2	Chun et al., 2008; Garafalo et al., 2015	Normal targeting in C. elegans, where it is used as a compartment marker. Endosomal targeting in axons shown in the current study.
α-Tubulin	3	Samora and McAinsh, 2011; Tulu et al., 2003	Integration in normal tubulin filaments. Also used as a tool to study dynamics, using photo-activatable GFP.
VAMP1	3	Meng et al., 2016; Rodepeter et al., 2017	Normal targeting and function tested in neurons, and also in non-neuronal cells.
VAMP2	4	Miesenböck et al., 1998; Sinha et al., 2011	Normal targeting in neurons, and rescue of function in knock-out neurons.
VAMP4	1	Nicholson-Fish et al., 2015; Tran et al., 2007	Normal targeting tested in neurons, and also in non-neuronal cells.
vATPase	2	Bodzęta et al., 2017	Normal targeting to synaptic boutons tested in neurons.
vGlut1	5	Herzog et al., 2011; Wilson et al., 2005; the present work	Normal targeting to synaptic boutons tested in culture. Replacement of the endogenous protein in living mice.
Vti1a-β	3	Hoopmann et al., 2010; Ramirez et al., 2012	Normal targeting and function in neurons, including use as a sensor for exocytosis.

* Verification score based on published data on GFP-tagged protein localization and function. The score is assigned as follows, from 0 (no previous tests) to 5 (the tagged protein can replace functionally the endogenous protein in vivo):

0) The tagged protein has not been tested before. Does not apply to any of the proteins we used.

1) The correct protein localization upon tagging is verified, but the function was not tested.

2) The correct protein localization upon tagging is verified, but function was difficult to test, due to the presence of the un-tagged protein. The appropriate function-related changes take place upon manipulations.

3) The appropriate protein function was verified for the tagged protein, typically in cell cultures (for example primary neuronal cultures).

4) The endogenous protein can be replaced by the tagged protein in cells in culture, with appropriate functional replacement.

5) The endogenous protein can be replaced by the tagged protein in living animals, with appropriate functional replacement.

Most of the analyzed proteins have a score of 2 and more, meaning the correct localization and function of the tagged proteins have been shown previously. In detail: 4 proteins have a score of 1; 16 proteins have a score of 2; 14 proteins have a score of 3; 6 proteins have a score of 4; 5 proteins have a score of 5. The average score is 2.82.

Only fusions to GFP family proteins, and not other fluorescent proteins were considered in this analysis.

Table EV2. The table summarizes the FRAP parameters presented in Appendix Fig. S3, in the form of means ± SEM and various values estimated from simulations.

Protein	MW, kDa	membrane	Time constant in axon ± SEM (s)	Immobile fraction in axon ± SEM (%)	Time constant in synapse ± SEM (s)	Immobile fraction in synapse ± SEM (%)	Diffusion coefficient in axon ± SEM (um^2/s)	Diffusion coefficient in synapse ± SEM (um^2/s)	Diffusion coefficient in SV cluster ± SEM (um^2/s)	Concentration in axon (uM)	Concentration in synapse, outsice the vesicle cluster (uM)	Concentrtion in the synaptic vesicle cluster (uM)	Fold enrichment in the synapse over the axon	Fold enrichment in the SV cluster over the axon	Fold enrichment in the SV cluster over the rest of the synapse
Actin	42.00	0	1.36 ± 0.11	28.39 ± 4.59	6.35 ± 0.78	13.19 ± 8.88	6.5 ± 0.605	3.35 ± 0.2081	0.5 ± 0.0286	2.4321	6.5423	319.9106	2.6899	131.5368	48.8991
alpha-SNAP	33.19	0	2.39 ± 0.45	9.71 ± 5.66	5.24 ± 0.47	6.02 ± 4.26	2.97 ± 0.0029	2.19 ± 0.0041	0.44 ± 0.0231	0.2939	0.439	15.5198	1.4935	52.8064	35.3538
alpha-synuclein	14.46	0	2.4 ± 0.41	18.9 ± 4.3	6.06 ± 0.72	26.74 ± 4.27	2.96 ± 0.0014	2.18 ± 0.0047	0.37 ± 0.0164	0.8428	1.1896	44.2194	1.4115	52.4673	37.1708
Amphiphysin	74.88	0	3.21 ± 0.26	18.62 ± 5.76	6.76 ± 0.42	22.93 ± 6.17	2.97 ± 0.0014	2.16 ± 0.0047	0.32 ± 0.0164	0.2748	0.4133	16.4272	1.5039	59.7787	39.7483
AP180	93.52	0	1.81 ± 0.21	29.24 ± 4.81	4.5 ± 0.34	7.06 ± 3.68	2.96 ± 0.0087	2.23 ± 0.0146	0.53 ± 0.0502	1.7446	1.7118	45.7765	0.9812	26.239	26.7419
AP2	104.05	0	2.16 ± 0.17	16.48 ± 3.86	3.55 ± 0.25	7.98 ± 6.05	2.13 ± 0.0076	2.28 ± 0.0008	2.02 ± 0.002	0.8118	1.8175	26.1955	2.2387	32.2684	14.413
Calmodulin	16.84	0	2.67 ± 0.25	13.42 ± 2.76	3.04 ± 0.23	20.42 ± 4.82	1.46 ± 0.0077	1.64 ± 0.0004	1.47 ± 0.0019	6.4083	9.1578	72.1691	1.4291	11.2618	7.8806
Clathrin light chain	26.98	0	1.6 ± 0.16	23.68 ± 5.29	3.39 ± 0.26	16.41 ± 6.7	2.15 ± 0.3833	2.27 ± 0.2133	2.02 ± 0.1852	2.2688	4.0912	46.015	1.8032	20.2816	11.2473
Complexin1	15.12	0	2.63 ± 0.39	19.24 ± 5.95	3.7 ± 0.39	23.56 ± 2.89	2.05 ± 0.0246	1.77 ± 0.1673	0.54 ± 0.4927	0.4435	0.8454	16.2338	1.9062	36.6038	19.2016
Complexin2	15.39	0	4.03 ± 0.53	0.88 ± 6.22	5 ± 0.39	15.44 ± 3.25	2.04 ± 0.0169	1.71 ± 0.0035	0.34 ± 0.0172	0.2949	0.4548	15.2908	1.5422	51.8508	33.6245
CSP	22.10	0	2.86 ± 0.33	22.99 ± 4.59	8.44 ± 0.9	22.05 ± 12.67	4.37 ± 0.4558	2.69 ± 0.1889	0.29 ± 0.021	0.0934	0.2431	13.8461	2.6026	148.2452	56.9559
Doc2a	44.59	0	1.64 ± 0.08	21.92 ± 2.91	5.47 ± 0.52	21 ± 2.55	4.48 ± 0.0245	2.81 ± 0.0146	0.56 ± 0.0272	0.996	1.6468	48.5574	1.6535	48.7524	29.4854
Dynamin	97.30	0	2.5 ± 0.33	2.32 ± 5.34	10.75 ± 1.2	21.01 ± 10.14	6.09 ± 0.4445	3.24 ± 0.1896	0.24 ± 0.0125	0.2007	0.4107	35.2974	2.0469	175.8714	85.9398
Endophilin	39.90	0	2.51 ± 0.21	9.87 ± 2.53	4.28 ± 0.28	17.97 ± 3.68	2.05 ± 0.302	1.77 ± 0.1522	0.54 ± 0.001	0.8313	1.5845	30.4262	1.9061	36.6007	19.2023
Epsin	60.16	0	2.63 ± 0.31	24.51 ± 4.89	6.77 ± 0.52	17.65 ± 5.35	2.97 ± 0.0014	2.16 ± 0.0047	0.32 ± 0.0164	0.0134	0.03	1.3127	2.2386	97.9627	43.8152
Hsc70	70.87	0	2.62 ± 0.28	14.69 ± 4.29	2.91 ± 0.24	24.41 ± 3	1.46 ± 0.0059	1.64 ± 0.0014	1.47 ± 0.0005	6.0839	8.6947	68.5166	1.4291	11.262	7.8803
Intersectin 1-L	194.20	0	1.89 ± 0.22	26.13 ± 7.25	9.52 ± 0.88	40.72 ± 7.23	6.09 ± 0.6474	3.24 ± 0.2055	0.24 ± 0.0141	0.2671	0.5228	46.9818	1.9573	175.8959	89.8729
mEGFP	27.00	0	1.93 ± 0.11	20.46 ± 2.31	2.08 ± 0.07	18.14 ± 1.64	19.25 ± 4.7687	9.31 ± 1.7503	9.14 ± 1.7257						
membrane mEGFP	27.00	1	2.29 ± 0.29	33.98 ± 3.88	4.84 ± 0.41	26.86 ± 4.53	0.41 ± 0.0387	0.47 ± 0.0511							
Munc13	196.36	0	1.52 ± 0.11	21.9 ± 2.4	3.95 ± 0.27	4.64 ± 4.88	2.98 ± 0.0087	2.27 ± 0.0146	0.68 ± 0.0502	0.5431	0.9667	18.5927	1.7802	34.2344	19.2328
Munc18	67.57	0	2.37 ± 0.33	21.49 ± 4.41	4.65 ± 0.24	18.23 ± 1.54	2.96 ± 0.0047	2.23 ± 0.0133	0.53 ± 0.0305	1.986	1.9487	52.1105	0.9812	26.2389	26.7418
NSF	82.65	0	1.69 ± 0.24	27.67 ± 5.49	3.39 ± 0.33	42.48 ± 3.99	2.15 ± 0.0076	2.27 ± 0.0008	2.02 ± 0.002	2.025	3.6516	41.0705	1.8032	20.2817	11.2473
PIP5KIgamma	75.59	0	3.76 ± 0.63	32.75 ± 5.12	7.15 ± 0.55	16.15 ± 5.97	3 ± 0.0111	2.12 ± 0.013	0.23 ± 0.0308	0.0739	0.1459	6.6167	1.975	89.5359	45.3367

Protein	MW, kDa	membrane	Time constant in axon ± SEM (s)	Immobile fraction in axon ± SEM (%)	Time constant in synapse ± SEM (s)	Immobile fraction in synapse ± SEM (%)	Diffusion coefficient in axon ± SEM (um^2/s)	Diffusion coefficient in synapse ± SEM (um^2/s)	Diffusion coefficient in SV cluster ± SEM (um^2/s)	Concentration in axon (uM)	Concentration in synapse, outsice the vesicle cluster (uM)	Concentrtion in the synaptic vesicle cluster (uM)	Fold enrichment in the synapse over the axon	Fold enrichment in the SV cluster over the axon	Fold enrichment in the SV cluster over the rest of the synapse
Rab3a	24.97	0	3.24 ± 0.32	8.3 ± 3.78	3.99 ± 0.31	14.3 ± 3.58	2.05 ± 0.0266	1.77 ± 0.0128	0.54 ± 0.0399	6.2062	11.8298	227.1552	1.9061	36.6013	19.202
Rab5a	23.63	0	1.53 ± 0.12	21.48 ± 3.45	3.81 ± 0.23	8.22 ± 2.3	2.98 ± 0.1048	2.27 ± 0.213	0.68 ± 0.6308	0.2218	0.3948	7.5941	1.7801	34.2385	19.233
Rab7a	23.50	0	1.73 ± 0.17	24.82 ± 3.71	3.9 ± 0.33	3.26 ± 4.67	2.98 ± 0.2862	2.27 ± 0.0005	0.68 ± 0.4435	1.5603	2.7776	53.4207	1.7801	34.2375	19.233
SCAMP1	38.00	1			12.56 ± 1.76	57.62 ± 6.92	0.3 ± 0.012	0.34 ± 0.0141							
Septin5	42.85	0	2.72 ± 0.34	21.18 ± 4.77	4.39 ± 0.33	21.22 ± 4.87	2.05 ± 0.0266	1.77 ± 0.0128	0.54 ± 0.0399	0.5684	1.0835	20.8057	1.9061	36.604	19.2022
SNAP23	23.24	1	2.78 ± 0.22	16.57 ± 4.47	3.53 ± 0.23	25.56 ± 3.09	0.42 ± 0.0442	0.49 ± 0.0606							
SNAP25	23.32	1	1.88 ± 0.16	17.89 ± 3.31	4.38 ± 0.23	19.48 ± 3.39	0.42 ± 0.0285	0.5 ± 0.0413							
SNAP29	29.07	1	3.64 ± 0.31	6.57 ± 4.5	5.4 ± 0.31	10.63 ± 3.28	0.24 ± 0.0264	0.27 ± 0.0285							
SV2B	77.50	1	6.84 ± 1.44	28.67 ± 10.32	17.35 ± 2.88	75.35 ± 5.18	0.01 ± 0.0414	0.05 ± 0.0341							
Synapsin	73.99	0	5.83 ± 1.02	19.74 ± 8.69	13.37 ± 1.19	23.5 ± 8.83	4.4 ± 0.4837	2.65 ± 0.1855	0.15 ± 0.0103	0.5739	2.7405	367.1104	4.7752	639.6766	133.9563
Synaptogyrin	25.67	1			33.65 ± 4.19	65.35 ± 6.54	0.19 ± 0.0145	0.21 ± 0.0152							
Synaptophysin	33.31	1	3.08 ± 0.63	22.25 ± 7.2	24.6 ± 3.53	72.58 ± 2.98	0.19 ± 0.0145	0.21 ± 0.0152							
Synaptotagmin1	47.40	1	6.47 ± 0.96	6.77 ± 7.34	25.36 ± 3.27	29.66 ± 13.46	0.08 ± 0.021	0.11 ± 0.0194							
Synaptotagmin7	45.48	1	2.65 ± 0.29	19.51 ± 2.66	5.9 ± 0.39	8.21 ± 5.15	0.35 ± 0.069	0.39 ± 0.0834							
Syndapin	50.45	0	2 ± 0.13	28.1 ± 2.77	5.3 ± 0.35	16.16 ± 3.59	2.97 ± 0.5268	2.19 ± 0.1903	0.44 ± 0.0104	0.8176	1.2211	43.1729	1.4935	52.8044	35.3544
Syntaxin1	33.07	1	3.41 ± 0.2	11.94 ± 4.61	6.56 ± 0.42	12.65 ± 4.07	0.21 ± 0.0145	0.24 ± 0.0152							
Syntaxin16	35.44	1	3.41 ± 0.26	2.39 ± 5.15	12.62 ± 1.07	9.14 ± 6.72	0.26 ± 0.012	0.29 ± 0.0141							
Tubulin	50.00	0	7.04 ± 1.89	45.47 ± 11.49	10.61 ± 0.93	35.22 ± 6.39	2.97 ± 0.3002	2.09 ± 0.1445	0.16 ± 0.0076	1.7606	2.5278	177.6266	1.4358	100.8898	70.2692
VAMP1	12.80	1	3.38 ± 0.25	9.68 ± 3.64	13.63 ± 1	32.24 ± 4.38	0.29 ± 0.012	0.32 ± 0.0141							
VAMP2	12.69	1	2.64 ± 0.2	-11.94 ± 7.29	5.52 ± 0.45	41.67 ± 4.06	0.37 ± 0.0649	0.42 ± 0.0783							
VAMP4	16.35	1	14.74 ± 3.9	1.61 ± 16.3	4.71 ± 0.46	51.37 ± 5.67	0.36 ± 0.0442	0.41 ± 0.0606							
vATPase	95.66	1	3.12 ± 0.7	20.97 ± 5.89	13.56 ± 1.98	54.98 ± 4.55	0.33 ± 0.0442	0.37 ± 0.0606							
vGluT	61.67	1			23.52 ± 3.19	63.24 ± 4.86	0.19 ± 0.0145	0.21 ± 0.0152							
Vti1a-beta	26.04	1	4.52 ± 0.95	11.82 ± 8.77	21.24 ± 4.32	38.27 ± 7.11	0.11 ± 0.021	0.13 ± 0.0194							

CHAPTER 2. A MINIMALIST MODEL TO MEASURE INTERACTIONS BETWEEN PROTEINS AND SYNAPTIC VESICLES

Eleonora Perego*, Sofiia Reshetniak*, Charlotta Lorenz, Christian Hoffmann, Dragomir Milovanović, Silvio O. Rizzoli & Sarah Köster

* These authors contributed equally to this work.

Published in *Scientific Reports*, vol. 10, no. 1, p. 21086, Dec. 2020, doi: 10.1038/s41598-020-77887-1.

Author contribution of Sofiia Reshetniak:

- design (together with SOR, SK, and EP), performance (together with EP), and analysis (together with EP and SR) of the experiments shown in Figs. 1, 2, 4, 5, 6a, 6b, 6c,6 e, Figs. S1, S3;
- design, performance and analysis of experiments shown in Fig. 3, Fig. S2;
- design (together with SOR) and performance of experiments shown in Fig. S6;
- data visualization, figure design, layout and generation: Figs. 1b, 1c, 3, S2, S6;
- manuscript writing: initial draft and refinements with all other authors.

Rights and permissions:

Formatting and contents:

The paper format is preserved from the journal it is published in. Page numbers conforming to this thesis page numbering have been added at the bottom of the pages.

www.nature.com/scientificreports

scientific reports

Check for updates

OPEN

A minimalist model to measure interactions between proteins and synaptic vesicles

Eleonora Perego[1,5], Sofiia Reshetniak[2,5], Charlotta Lorenz[1], Christian Hoffmann[3], Dragomir Milovanović[3], Silvio O. Rizzoli[2,4] & Sarah Köster[1,4]✉

Protein dynamics in the synaptic bouton are still not well understood, despite many quantitative studies of synaptic structure and function. The complexity of the synaptic environment makes investigations of presynaptic protein mobility challenging. Here, we present an in vitro approach to create a minimalist model of the synaptic environment by patterning synaptic vesicles (SVs) on glass coverslips. We employed fluorescence correlation spectroscopy (FCS) to measure the mobility of monomeric enhanced green fluorescent protein (mEGFP)-tagged proteins in the presence of the vesicle patterns. We observed that the mobility of all eleven measured proteins is strongly reduced in the presence of the SVs, suggesting that they all bind to the SVs. The mobility observed in these conditions is within the range of corresponding measurements in synapses of living cells. Overall, our simple, but robust, approach should enable numerous future studies of organelle-protein interactions in general.

Information processing in the brain depends on the transmission of information at the level of inter-neuronal synapses. The large majority of the brain synapses base their activity on the release of neurotransmitters from the presynaptic side (the so-called synaptic bouton) onto receptors on the plasma membrane of the postsynaptic cells. This process takes place through the fusion of neurotransmitter-filled synaptic vesicles (SVs) with the presynaptic plasma membrane (exocytosis), followed by the retrieval of SV proteins from the membrane (endocytosis), and the formation of new SVs, which are ready for function[1,2]. The composition of the synaptic bouton reflects the importance of neurotransmitter release, as much of its space is taken up by the SVs, organized in a dense cluster[3]. Exo- and endocytosis cofactor proteins are also prominent in the bouton, where they tend to be strongly enriched[4].

Synaptic transmission has been the subject of many quantitative studies, which have established, for example, the copy numbers of many of the vesicular[5] or presynaptic proteins[4]. The spatial distribution of the proteins has also been analyzed[4], and recently the average mobility of multiple synaptic proteins has been estimated[6]. However, in spite of the rich quantitative information available on synaptic transmission, the true molecular organization of the presynaptic bouton is still unclear. Importantly, it is still unresolved, why the soluble synaptic proteins are enriched in the bouton. They must be retained locally by mechanisms that apply to most or all of the exo- and endocytosis cofactors, as otherwise they would be lost in the axon, which can be many orders of magnitude larger in volume than the synapse[7]. The nature of these mechanisms is not yet understood, despite more than a decade of research on this subject. As many presynaptic proteins colocalize well with the SVs, it has been proposed that the vesicles bind them, thereby serving as a form of storage container for such proteins[7,8]. This concept has more recently been extended to include the hypothesis that the clustered SVs form a distinct liquid phase, together with some of the presynaptic proteins[9,10]. While this hypothesis is highly attractive, a formal demonstration of its main assumption, namely that multiple exo- and endocytosis cofactors interact strongly with the SVs, is still missing. Biochemical experiments have suggested that isolated SVs can collect soluble proteins on their surfaces[5,7], but the interpretation of such experiments is difficult, since most of the tested proteins failed to enrich on purified SVs[5].

To test the interaction of presynaptic proteins with the SVs in a more direct and controlled fashion, it is necessary to analyze the behavior of individual proteins in a highly defined system, in which both the vesicles and the

[1]Institute for X-Ray Physics, University of Göttingen, 37077 Göttingen, Germany. [2]Institute for Neuro- and Sensory Physiology, Center for Biostructural Imaging of Neurodegeneration, University Medical Center Göttingen, 37075 Göttingen, Germany. [3]Laboratory of Molecular Neuroscience, German Center for Neurodegenerative Diseases (DZNE), 10117 Berlin, Germany. [4]Cluster of Excellence "Multiscale Bioimaging: from Molecular Machines to Networks of Excitable Cells" (MBExC), University of Göttingen, 37073 Göttingen, Germany. [5]These authors contributed equally: Eleonora Perego and Sofiia Reshetniak. ✉email: sarah.koester@phys.uni-goettingen.de

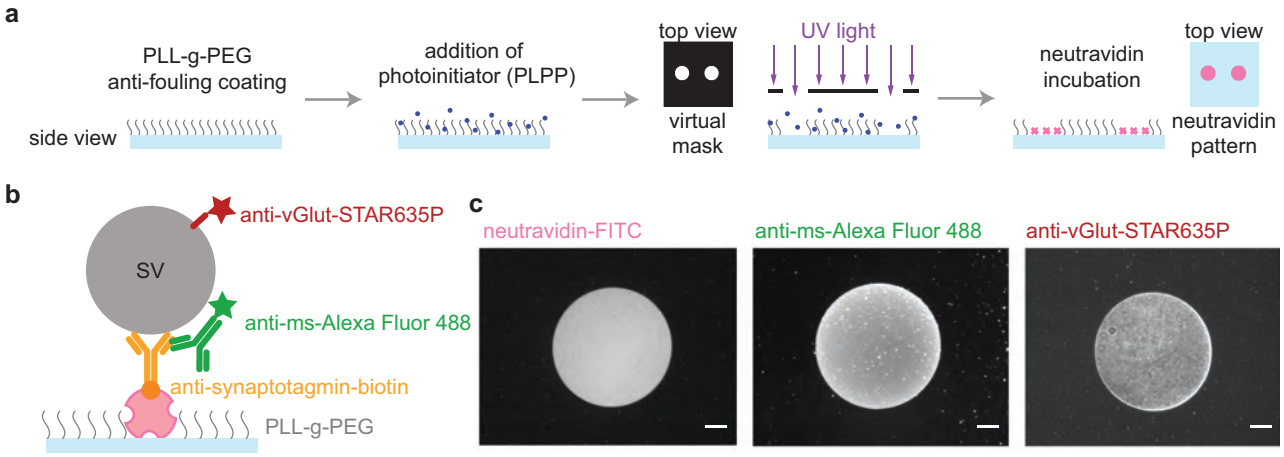

Figure 1. Patterning strategy and SV immobilization. (**a**) Schematic representation of photopatterning of neutravidin on a glass coverslip. The glass coverslip was uniformly coated with an anti-fouling layer of PLL-g-PEG. The photoinitiator (PLPP) was added on top of the PLL-g-PEG layer and the substrate was exposed to UV light through a virtual photomask to activate the PLPP. Under UV light, the PLPP degraded the PLL-PEG layer, leaving accessible regions for neutravidin to attach. (**b**) Schematic of our strategy to attach the SVs to the substrate. The purified SVs (gray) were attached to the neutravidin (pink) functionalized glass coverslips via a biotinylated mouse anti-synaptotagmin antibody (orange). The attachment of antibodies was controlled by a secondary anti-mouse antibody labeled with Alexa Fluor 488 (green). To image the SVs, a single-domain antibody against vGLUT1, labeled with STAR635P (red) was employed. (**c**) Fluorescence micrographs of the individual steps of the vesicle immobilization strategy. The neutravidin functionalization step was assessed by fluorescently labeled neutravidin (neutravidin-FITC, left), the attachment of the biotinylated mouse anti-synaptotagmin antibody was tested with a secondary anti-mouse antibody labeled with Alexa Fluor 488 (center), and the SV attachment was tested with a single-domain antibody against vGLUT1 labeled with STAR635P (right). Note that the uniform fluorescence in the right image shows the bound SVs, whereas the small bright spots are aggregates. The images of neutravidin-FITC and anti-ms-Alexa488 were taken on two different glass coverslips. In the actual experiments, we used unlabeled neutravidin, so as to not interfere with the fluorescence of the mEGFP-tagged proteins. The scale bars are 25 µm.

proteins can be introduced in standardized conditions, and in the absence of most cellular components. Here, we present a minimalist in vitro model of the synaptic environment that enables such controlled measurements. Using a micro-patterning strategy, SVs were immobilized on glass coverslips, creating a 2D vesicle cluster, where protein dynamics could be investigated in a straightforward manner. We employed fluorescence correlation spectroscopy (FCS) to quantify the mobility of eleven different synaptic proteins in this system, and we found a dramatic decrease of the protein mobility in the presence of the SVs, confirming an effective interaction between each of the proteins and the SVs. Importantly, we found a strong agreement of the in vitro diffusion coefficients and corresponding values measured in living cells[6,11–13]. This result implies not only that such proteins interact with the vesicles, but also that their mobility is governed by this interaction, confirming the hypothesis that the SV cluster is a major factor in the organization of presynaptic proteins[7–9].

Results and discussion

An in vitro replica of the synapse. Measuring protein diffusion and interaction directly in the synapse is challenging, owing to the complex and crowded environment[4]. Therefore, we designed a minimalist in vitro version of the synapse, composed of two-dimensional SV arrays adhered to a glass surface, with which we studied protein mobility in a highly controlled manner. To attach SVs to glass coverslips, we first functionalized the substrates with patterns of neutravidin. The size and the shape of the patterns are of little relevance for the present study, albeit the method can be adapted to many other research questions, where these parameters may play a role. In the present case, we chose to pattern the surface instead of uniformly coating it, because it provides a straightforward way of controlling the success of the subsequent steps by comparing the pattern to the uncoated regions nearby. The process, as well as the quality control, is shown in Fig. 1. A passivated glass coverslip was exposed to UV light through a virtual photomask, which projects the pattern onto the substrate employing digital micromirror devices (DMD), thus avoiding the use of a real mask. For more details on this procedure, see Ref.14. The photo-initiator (4-benzoylbenzyl-trimethylammonium chloride, sold as PLPP (Product of Liaison for Protein Patterning) by Alvéole, Paris, France) degraded the anti-fouling layer of poly(L-lysine)-graft-poly(ethylene glycol) (PLL-PEG) upon exposure, making the exposed area accessible to neutravidin (pink in Fig. 1a,b). The reliable attachment of neutravidin was tested using a fluorescently labeled variant, see Fig. 1c, left. The SVs (gray in Fig. 1b) were attached via a biotinylated anti-synaptotagmin antibody (orange in Fig. 1b). Synaptotagmin is an abundant vesicle protein, which is essential for both exo- and endocytosis, and which is presumably present in all functional vesicles, thereby rendering it a convenient tool for anchoring the SVs to the neutravidin. The proper attachment of the biotinylated anti-synaptotagmin antibodies was tested via a secondary anti-mouse-

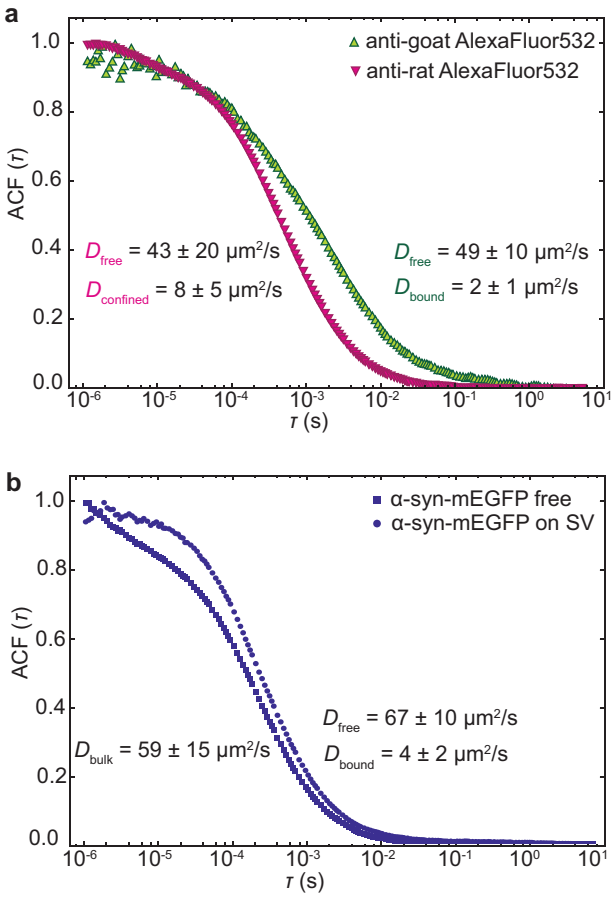

Figure 2. Control measurements for the newly developed assay. (**a**) ACF curves (averaged data from 25 single curves) of anti-goat-Alexa Fluor 532 (green upright triangles) and anti-rat-Alexa Fluor 532 (magenta inverted triangles) in the presence of SV patterns. For both antibodies, two diffusion coefficients were retrieved from the fits. The values are reported in the graph (color coded). The anti-goat-Alexa Fluor 532 interacted with the patterned SVs; the diffusion coefficient D_{bound} corresponds to interacting antibodies and D_{free} to non-interacting, i.e. freely diffusing antibodies. Although anti-rat-Alexa Fluor 532 is not expected to interact with the vesicles, we observed two diffusion coefficients; D_{free} corresponds to freely diffusing antibodies, whereas $D_{confined}$, corresponds to a slower component, which we attribute to the crowded environment in the vesicle layer. (**b**) ACF curves (averaged data from 20 single curves) of α-synuclein-mEGFP in the presence of SVs (blue squares) and for comparison without the vesicle pattern (blue circles). As expected, without the vesicle pattern, we obtained the bulk diffusion coefficient of α-synuclein-mEGFP, D_{bulk}; by contrast, in presence of the SV pattern, we observed two diffusion coefficients; D_{free} is very similar to the bulk diffusion coefficient, D_{bound} is much smaller and corresponds to α-synuclein-mEGFP interacting with the SVs.

Alexa Fluor 488 antibody (green in Fig. 1b). As shown in Fig. 1c, center, the antibody attachment is well defined and with a low background. To check for unspecific interactions to the patterned neutravidin, a secondary antibody (anti-ms-STAR635) was incubated on the neutravidin pattern without the biotinylated anti-synaptotagmin antibody added. As shown in Fig. S1a, no signal was obtained from the secondary antibody. Finally, to assess the attached SVs, a single-domain antibody against vGLUT1 labeled with STAR635P was employed (red in Fig. 1b). vGLUT1 is a major neurotransmitter transporter and can therefore be used to detect the vesicles. As shown in Fig. 1c, right, the signal stemming form the vesicle pattern was well confined to the circle region and displayed low background. As a negative control, the single domain antibody against vGLUT1 labeled with STAR635P was incubated on functionalized coverslips without SVs. As shown in Fig. S1b, no unspecific interaction was found.

To verify our approach of measuring protein mobility in the presence of a 2D SV array, we performed two control experiments. We targeted the abundant vesicular glycoprotein synaptophysin with primary rabbit anti-synaptophysin antibodies and secondary goat anti-rabbit antibodies, and thereby visualized the vesicles. The first control was provided by the use of diffusing anti-goat-Alexa Fluor 532 antibodies, which interact with the antibody complex on the SVs, whereas as a second control we used diffusing anti-rat-Alexa Fluor 532 antibodies, which are not expected to bind to the system. Figure 2a shows the average normalized autocorrelation function (ACF) (average data from 25 ACFs each) for both control antibodies, measured in the presence of SVs. We focused on the surface of our substrate with the SVs attached and thus ensured that the measured diffusion took

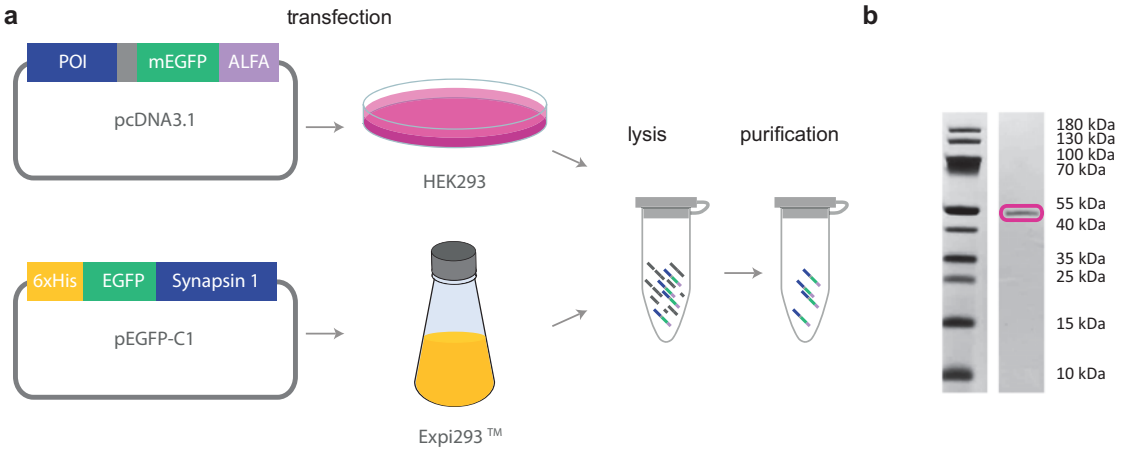

Figure 3. Protein purification strategy. (**a**) The protein of interest (POI, blue) fused to mEGFP (green) and ALFA-tag (purple) or His tag (orange) in the case of synapsin was expressed in HEK293 or Expi293 cells, which were then lysed. The protein was then purified using an ALFA-tag purification system[21] or Ni-NTA purification with consecutive size exclusion chromatography. (**b**) Example of a coomassie stained polyacrylamide gel showing, as an example, purified α-synuclein. The magenta box indicates the main band, which runs at the expected molecular weight. The full-length coomassie stained polyacrylamide gel for the remaining proteins is shown in Supplementary Fig. S2.

place in the crowded environment of the layer of SVs to which the proteins and antibodies can bind. For the interacting antibody, anti-goat-Alexa Fluor 532 (green upright triangles in Fig. 2a), two diffusion coefficients were retrieved from fitting the data. The first diffusion coefficient, D_{free}, reflects the non-interacting component, i.e. the freely diffusing antibodies, with a value of (49 ± 10) μm²/s. This value is similar to other measurements of freely diffusing antibodies[15] and to a value of D_{bulk} = (55 ± 20) μm²/s which we obtained for the same antibody measured in bulk, i.e. without the SV pattern. The second diffusion coefficient D_{bound} is much smaller, (2 ± 1) μm²/s, and we interpret it as stemming from antibodies interacting with the SVs. Note that the two separate "ensembles" of freely diffusing and interacting, or bound, antibodies, respectively, correspond to average amounts of time for each antibody spent in "bound" and in "free" states. Interestingly, although anti-rat antibodies are not supposed to bind to anything in the SV array, two diffusion coefficients were also retrieved from the analysis of the corresponding data (magenta inverted triangles in Fig. 2a). Again, we observed one diffusion coefficient of D_{free} = (43 ± 20) μm²/s that we attribute to the freely diffusing component as verified by a bulk measurement without an SV pattern (D_{bulk} = (47 ± 29) μm²/s). A more slowly diffusing component was additionally measured, with $D_{confined}$ = (8 ± 5) μm²/s. We speculate that this component describes confinement effects caused by the dense 2D vesicle pattern. Such confinement may slow down the mobility of the antibody[16–18].

As an additional test for our newly developed assay, we compared the diffusion of purified α-synuclein-mEGFP (monomeric enhanced green fluorescent protein) with and without the SV pattern, as shown in Fig. 2b. α-synuclein is a SV-binding protein particularly important in Parkinson's disease. When α-synuclein-mEGFP was measured in bulk, without the SV pattern present (blue circles in Fig. 2b), a diffusion coefficient of D_{bulk} = (59 ± 15) μm²/s was obtained. This diffusion coefficient is smaller than the ones found in literature[19,20] and by us (for α-synuclein-Alexa Fluor 532, D = (102 ± 20) μm²/s) when the protein is labeled with chemical dyes.

We attribute this difference to the heavy fluorescent tag (mEGFP) employed here. When α-synuclein-mEGFP was measured in the presence of the SVs, two diffusing components were retrieved from the analysis of the ACF (blue squares in Fig. 2b). The first diffusion coefficient, D_{free}, again corresponds to the non-interacting component, i.e. freely diffusing protein, with a value of (67 ± 10) μm²/s. The second diffusion coefficient, D_2, is much smaller, D_{bound} = (4 ± 2) μm²/s, which we attribute to α-synuclein interacting with the SVs.

Mobility and binding efficiency of synaptic proteins. To test the interaction of SVs and different proteins, we relied on several synaptic proteins, which are known to be involved in synaptic transmission. All synaptic proteins considered here were expressed in HEK293 cells, except synapsin and EGFP, which were expressed in Expi293 cells. The cells were lysed and the lysate was either used as is or further purified. For purification, an ALFA-tag system[21] was employed, as described in the Materials and Methods section. Synapsin and EGFP were purified via NiNTA columns and size exclusion chromatography. A schematic representation of the protein production and purification process is shown in Fig. 3a, and the resulting purified fraction of α-synuclein is shown in Fig. 3b. The coomassie stained polyacrylamide gel for the remaining proteins is shown in Supplementary Fig. S2.

We characterized the diffusion properties of cell lysate containing α-synuclein-mEGFP by FCS (see Fig. 4a, open blue squares), and compared it to α-synuclein-mEGFP purified from cell lysate (closed blue squares). The ACFs as well as the diffusion coefficients derived from the fits, (63 ± 20) μm²/s and (59 ± 15) μm²/s, respectively, are in very good agreement, suggesting that the mobility of α-synuclein-mEGFP is identical before and after purification. In a next step, we investigated the ability of both versions of α-synuclein-mEGFP to interact with a

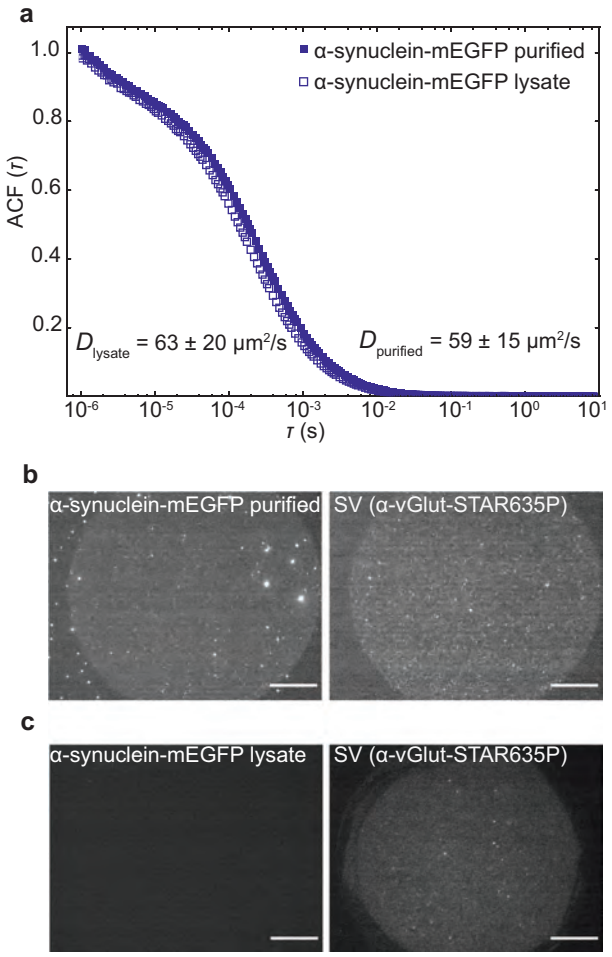

Figure 4. Comparison of cell lysate and purified α-synuclein-mEGFP. (**a**) Average normalized ACF of purified α-synuclein-mEGFP (closed squares, $N = 30$) and α-synuclein-mEGFP from HEK cell lysate (open squares, $N = 30$); there was no SV pattern present in these experiments; both protein preparations show the same diffusion behavior. (**b**) The purified α-synuclein-mEGFP interacted with the SV pattern (left hand side), as shown by the fluorescence signal (right; SV pattern visualized by anti-vGlut-STAR635P). (**c**) By contrast, α-synuclein-mEGFP from the cell lysate (left) did not bind to the SV pattern (right). The images in (**b**) and (**c**) were recorded after 2 hours of incubation of the SV layer with α-synuclein-mEGFP. The scale bars are 25 μm. Note that the uniform fluorescence in the right images in (**b**) and (**c**) shows the bound SVs, whereas the small bright spots are aggregates.

SV pattern. We incubated the preparation in the presence of the SV pattern for two hours, and took fluorescence images of the mEGFP signal. For the purified α-synuclein, a fluorescent pattern (see Fig. 4b, left) similar to the SV signal (right) was visible in the GFP channel, indicating binding of the protein to the SVs. Using the non-purified cell lysate, as shown in Fig. 4c, the fluorescent pattern was not detectable in the GFP channel (left), although the SV pattern was present (right), indicating a reduced or null binding. We speculate that additional components in the cell lysate unspecifically bind to the SVs, thus blocking the binding sites for the proteins under investigation. Based on these results, we performed all remaining experiments with purified proteins, which simplified the assay, enabling us to concentrate solely on the interaction of one protein with the SVs, without the conflicting presence of all other proteins from the lysate.

Synaptic protein mobility in the presence of SVs. After evaluating our in vitro model of a synapse using purified α-synuclein-mEGFP, we investigated ten additional soluble proteins. All these soluble proteins are known to be present in the synaptic bouton, and are important for different synaptic processes[1,2,22]. In brief, Rab3 is thought to be involved in the so-called priming process, preparing vesicles for exocytosis. Complexin 1 and α-synuclein are involved in the late stages of exocytosis by interacting with the molecules fusing the vesicle to the plasma membrane (SNAREs). Clathrin, epsin, endophilin, amphiphysin and clathrin assembly lymphoid myeloid leukemia (CALM) are involved in endocytosis, from initializing membrane curvature to coating the forming vesicle. Rab7 is involved in SV sorting after endocytosis, whereas calmodulin acts as a general regula-

Protein	D_{bulk} ± SD (μm²/s)	D_{bound} ± SD (μm²/s)	% bound ± SD	M_W (kDa)
Amphiphysin-mEGFP	72 ± 31	2.2 ± 2.4	24 ± 13	105
α-Synuclein-mEGFP	60 ± 16	1.8 ± 2.0	15 ± 12	44
CALM-mEGFP	28 ± 13	2.8 ± 2.5	10 ± 10	99
Calmodulin1-mEGFP	79 ± 13	2.3 ± 2.5	10 ± 11	47
Clathrin-LC-B-mEGFP	64 ± 13	3.3 ± 2.7	22 ± 18	55
Complexin1-mEGFP	50 ± 11	1.6 ± 1.6	17 ± 14	45
EGFP	85 ± 6	–	–	28
EndophilinA1-mEGFP	50 ± 12	2.4 ± 2.3	14 ± 14	70
Epsin-mEGFP	15 ± 10	2.4 ± 2.7	16 ± 11	90
Rab3a-mEGFP	55 ± 14	3.2 ± 2.9	15 ± 12	55
Rab7a-mEGFP	32 ± 23	2.8 ± 3.1	17 ± 14	53
Synapsin-EGFP	33 ± 3	3.3 ± 2.6	30 ± 18	102

Table 1. Summary of the diffusion coefficients measured in the absence (bulk) and presence (bound) of SVs. The % bound shown in the fourth column corresponds to the percentage of protein that interacts at any given moment, or the time-share the protein spends in bound state. As EGFP does not interact with the vesicles, the percentage of protein bound to the SVs is zero. Values are mean ± standard deviation of at least 12 different SV patterns per protein. The last column shows the molecular weight of the respective mEGFP-fusion protein.

tor of calcium signaling, thereby affecting both exo- and endocytosis. Finally, we also included in this analysis synapsin I, a neuronal phosphoprotein that interacts with SVs and the actin cytoskeleton, and has recently been shown to form a liquid phase with lipid vesicles[10].

Initially, the proteins were measured in bulk, i.e. without the SVs, to quantify the free diffusion. The averages of the ACFs for each protein (N varies between 18 and 70 single ACFs, 30 s of acquisition each) are reported in Fig. 5a, where each ACF was normalized to the maximum value, see legend for the color code. The distributions of the diffusion coefficients D_{bulk} retrieved from the single ACF curves are shown in Fig. 5c, and Table 1 summarizes the average diffusion coefficients.

The large and heavy fluorescent EGFP-tag (27 kDa) decreases the diffusion coefficient of all proteins compared to the unlabeled case or the use of chemical labels, as the diffusion coefficient is proportional to the molecular weight of the diffusing molecule[23]. Relatively, this effect is more pronounced for the lighter proteins, such as α-synuclein (14 kDa) or calmodulin (16 kDa)[11]. In the case of calmodulin-mEGFP we obtained an average diffusion coefficient of D_{bulk} = (79 ± 13) μm²/s, and for α-synuclein we obtained D_{bulk} = (60 ± 16) μm²/s, which both are only slightly lower than the diffusion coefficient for EGFP measured to be D = (85 ± 6) μm²/s. The rigid barrel-like shape of mEGFP might indeed influence and dominate the mobility of the mEGFP-fusion protein in the case of lighter proteins[11]. However, for the larger proteins, such as epsin (63 kDa), CALM (72 kDa) and synapsin (74 kDa), a clear difference between the protein diffusion coefficients and the EGFP diffusion coefficient was observed. For endophilin A1 (43 kDa), which has a size in-between the smallest and the largest examples considered here, the measured bulk diffusion coefficient was, as expected, smaller compared to the theoretical value for the protein without mEGFP, D = 97 μm²/s, calculated using the Stokes-Einstein law[23] and considering a radius of gyration of 48 Å[24], and comparable, within one standard deviation, to fluorescence recovery after photobleaching (FRAP) measurements on EGFP-fused endophilin A1[25].

When measured in the presence of SVs (Fig. 5b), the average ACFs (N varies between 20 and 90 single ACFs, 30 s acquisition each) were more noisy for small τ, i.e. fast time scales, as shown in Figure 5b. The interaction with the SVs may lead to variations in the protein concentration in the observation volume, affecting the low-τ ACFs. Furthermore, as these measurements took place very close to the glass surface, artefacts like scattered photons or bleaching of the dye may be more pronounced[26]. In this case, we analyzed the ACFs using a two-component FCS model [Eq. (3)]. For all proteins, apart from EGFP, we found one diffusion coefficient, D_{free}, in the same range as the bulk values, and a second, much lower one, D_{bound}. For a comparison of the bulk diffusion coefficients D_{bulk} and D_{free}, see Supplementary Fig. S3. The ACFs of EGFP can be fully described with one component only, confirming that EGFP does not interact with the SVs. In fact, the average diffusion coefficient measured on the SV patterns, D = (81 ± 30) μm²/s is comparable to the value measured in bulk. For all proteins D_{bulk} and D_{free} are very similar, however, in some cases D_{free} is decreased to some extent in comparison to the bulk diffusion. We can only speculate about the reason for this behavior. Possibly the diffusing proteins are binding interaction partners from the vesicle surfaces, making them slightly heavier, or their mobility is decreased because of the confinement effects caused by the 2D vesicle pattern. By contrast, we attribute D_{bound} to the bound component. The corresponding distributions of the diffusion coefficients D_{bound} are shown as box plots in Fig. 5d, and in Table 1, the average values are reported.

The diffusion coefficients for the bound component are statistically different (Mann–Whitney test, p-values are presented in Table S1) from the diffusion coefficients measured without the SVs, indicating a clearly different mobility in the two cases. The decrease in mobility of synaptic proteins in the presence of SVs, between 7-fold (epsin) and 40-fold (amphiphysin), is shown by the ratio between the bulk diffusion coefficient D_{bulk} and the bound diffusion coefficient D_{bound}, see Fig. 6a. This decrease in mobility differs between different proteins. It reflects the diffusion coefficient D_{free} of the proteins, since D_{bound} is very similar in all cases. In particular, the

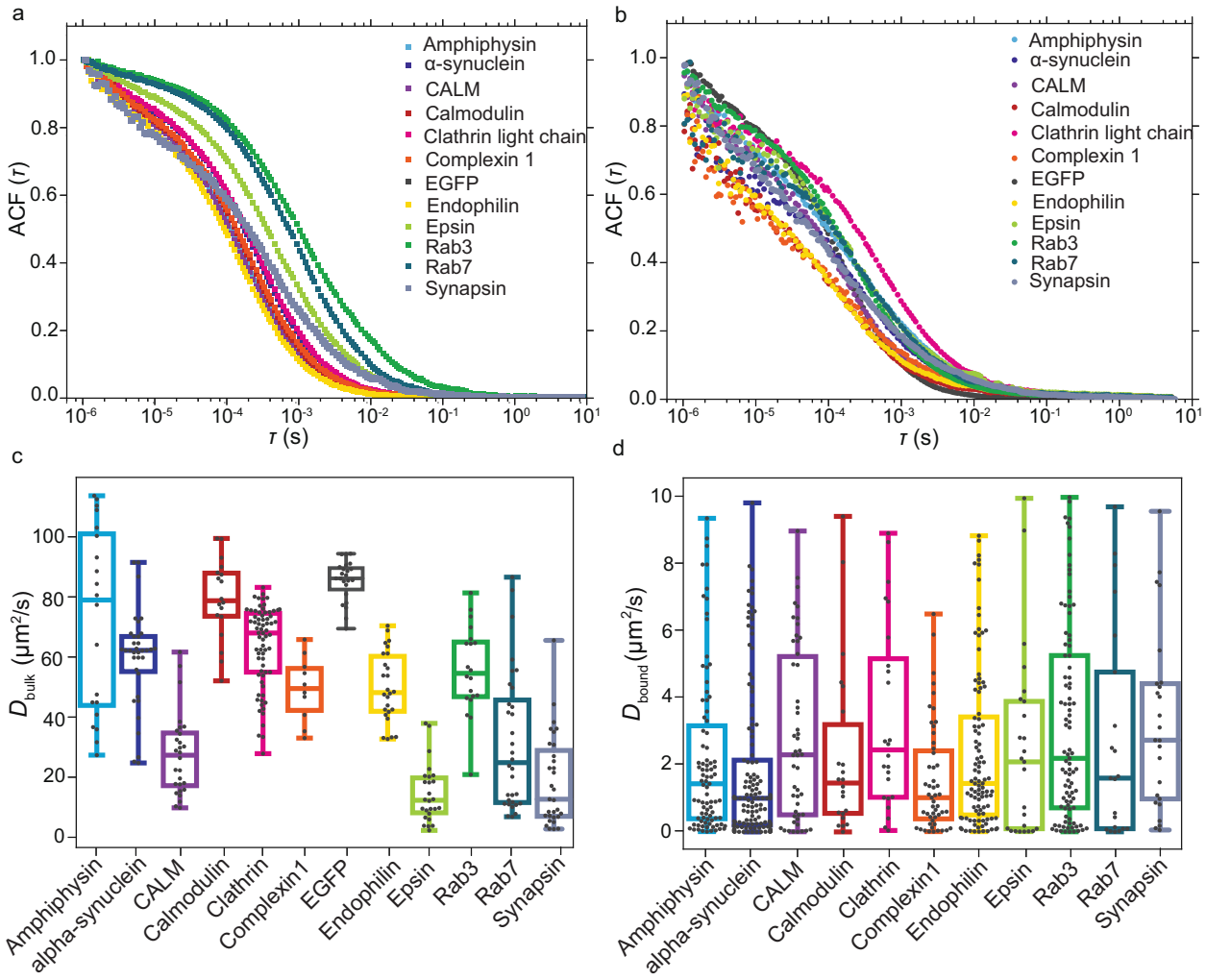

Figure 5. FCS measurements of all purified synaptic proteins considered here. (**a**) Average normalized FCS curves of synaptic proteins diffusing in bulk, i.e. in the absence of SVs; see legend for color code. (**b**) Average normalized FCS curves of synaptic proteins diffusing in the presence of the SVs. (**c**) Diffusion coefficients D_{bulk} obtained from the fit of the FCS functions in (**a**). These diffusion coefficients reflect the 3D mobility of the proteins tagged with mEGFP in bulk. (**d**) Diffusion coefficients D_{bound} obtained from fitting the FCS functions in (**b**) (excluding EGFP which did not show a bound diffusion coefficient). In this case, two diffusion coefficients were found and we show only the bound component here. Supplementary Fig. S3 shows the free component in comparison to the bulk diffusion without SVs. In (**c**) and (**d**) the boxes extend from the lower quartile to the upper quartile of the data, the middle line in each box plot represents the median, the whiskers extend from the minimum to the maximum data point. The data were plotted using Python (Python Software Foundation, Python Language Reference, version 3.7 Available at http://www.python.org).

decrease in mobility is less pronounced for the heaviest proteins, CALM, epsin and synapsin, which naturally already show a lower mobility without the SVs. Interestingly, the average diffusion coefficients of the bound component D_{bound} for the measured proteins do not depend on the molecular weight of the mEGFP-fusion proteins, as shown in Fig. 6b, but are all found to be on the order of 2 μm²/s. These results show that the decreased mobility in the presence of SVs is a property of binding and confinement effects, rather than a property of protein size. All measured proteins do, on average, interact with the SVs for at least 10 % of the time, as shown in Table 1, where the average percentages of the bound component are reported for all proteins.

We calculated the energy difference between the free and the bound state, taking advantage of Boltzmann statistics. The percentage of the bound component, shown in Fig. 6c, reflects the probability, or time-share, p_b that a protein interacts with the SVs. Since we observe $p_b < 0.5$ for all proteins, the interacting state has an average higher energy than the free state. In fact, the average energy difference ΔE derived from the average probability values (Table 1) is negative for all proteins, see Fig. 6d, left hand side axis. Note that these quantities were directly derived from the data plotted in Fig. 6c and are thus not independent. The energy difference is the energy necessary to overcome entropy, which favors free diffusion. The energy difference and the ratio of transition rates for all single data points are shown in Supplementary Fig. S4. Neither quantity depends on the molecular weight

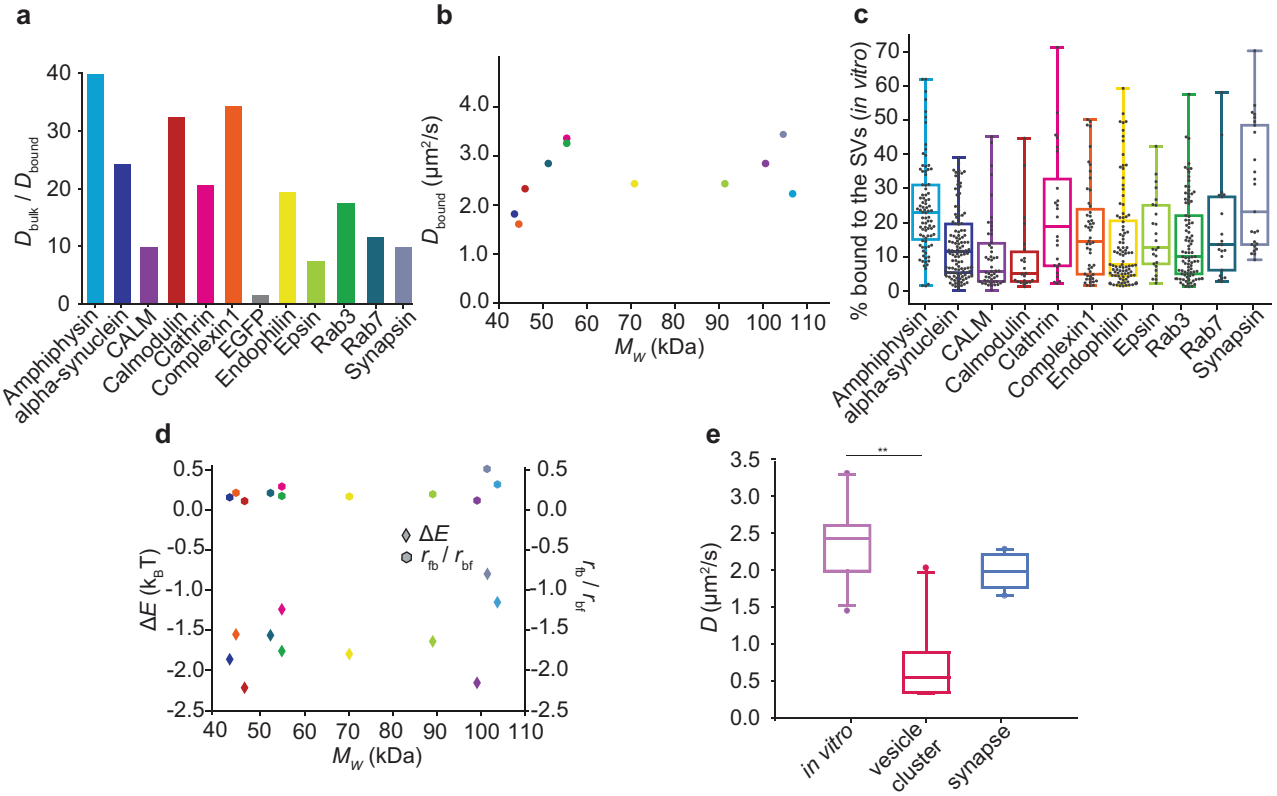

Figure 6. Interpretation of the diffusion coefficients measured in the presence of SVs. (**a**) Ratio between the diffusion coefficients for the non-interacting component D_{bulk} and for the interacting component D_{bound} for all synaptic proteins considered here. The protein mobility was considerably slowed down by interaction with the vesicles. (**b**) The average diffusion coefficients D_{bound} of the bound fraction do not correlate with the molecular weights of the mEGFP-fusion proteins. The colors represent the proteins, color coded as in (**a**). (**c**) Percentage of the time that each protein remains bound. (**d**) Energy difference between the free and the bound state (left hand side axis, diamonds) measured in units of k_BT and ratio between the transition rate from free to bound state, r_{fb}, and transition rate from bound to free state, r_{bf} (right hand side axis, circles). The colors represent the proteins, color coded as in (**a**) and (**c**). (**e**) The median diffusion coefficients D_{bound} of the interacting components (purple) are similar to the values obtained in synapses in living cells (blue), and are considerably higher than those obtained in the vesicle cluster in living cells (magenta)[6]. We performed a Kruskal-Wallis test followed by Tukey's post-hoc test, and obtained $p = 0.003$ (significance level 0.05), confirming the statistical difference between D_{bound} and the values obtained in vesicle clusters, and no significant difference for D_{bound} and the values obtained in the synapse ($p = 0.08$). In (**c**) and (**e**) the boxes extend from the lower quartile to the upper quartile of the data, the middle line in each box plot represents the median, the whiskers extend from the minimum to the maximum data point. The data were plotted using Python (Python Software Foundation, Python Language Reference, version 3.7 Available at http://www.python.org).

of the protein-mEGFP-construct, supporting the idea that the measured interaction is governed by the binding properties of each single protein instead of the protein size. For all proteins, the average ratio of the transition rates from free to bound, r_{fb}, and from bound to free, r_{bf}, is lower than 1, as shown in Fig. 6d, right hand side axis, suggesting that the transition from the bound state to the free state is more likely than vice versa. Thus, as expected from the average percentage of the bound pool, the proteins prefer the free state over the bound state. If the energy of the free state is influenced only by thermal energy, the energy of the bound state can be obtained in units of k_BT using Eq. (7), see Supplementary Fig. S5. As expected, it is lowest for synapsin ($E_b = (2.5 \pm 0.9)$ k_BT) and amphiphysin ($E_b = (2.8 \pm 0.8)$ k_BT), the proteins that interact the most, and highest for calmodulin ($E_b = (4.2 \pm 1.0)$ k_BT), the protein that interacts the least.

Our in vitro results for D_{bound} are in agreement with literature values in living cells. For example, for calmodulin in HEK cells[11,13] a range from 0.01 up to 10 μm²/s, depending on the measuring conditions and the type of fluorescent label used, i.e. EGFP[11] or chemical dyes[13], was reported. This wide range of diffusion coefficients found in HEK cells also reflects different experimental techniques employed, i.e. correlation spectroscopy versus single-molecule tracking. Additionally, calmodulin is found in different cellular compartments, and is involved in different transport mechanisms. Another example is complexin 1, for which a diffusion coefficient of 2 μm²/s, similar to our value, was measured in synapses of living *C. elegans*[12]. Additionally, we compared our in vitro data with our recent data measured by FRAP in living neurons[6]. To do so, we show the median diffusion coefficients

of the bound component D_{bound} together with median values derived from living neurons, see Fig. 6e. For the living neurons, we distinguished between values measured for the whole synapse (blue box plot) and for the vesicle cluster (magenta box plot). A Kruskal-Wallis test, followed by Tukey's post-hoc test, confirmed the significant difference (p-value = 0.003, α-level = 0.05, N = 9, CALM is excluded here as it was not measured in living cells) between the mobility measured in vitro in the presence of the SV pattern and in the dense vesicle cluster in living neurons. This difference may be due to the geometry of our in vitro synapse model, which constitutes a 2D layer of vesicles that is in contrast to the dense 3D cluster of vesicles found in cells, which might further reduce protein mobility. When quantifying the vesicle density on our 2D patterns using STED microscopy (see Supplementary Fig. S6), we find about 15 vesicles per μm^2, with a distance of about 177 nm between vesicle centers. In real synapses, the density in a plane taken through the vesicle cluster is higher, around 37 vesicles per μm^2, and 93 nm between vesicle centers. This may at least to some extent explain, why we do not reproduce the values found deep in the vesicle cluster.

By contrast, when comparing our in vitro results, averaged over all proteins, to data from living cells for the whole synapse, they are very similar. Indeed, a Kruskal-Wallis test confirmed the non-significant difference, with a p-value of 0.08 (α-level = 0.05, N = 9, CALM is excluded here as it was not measured in living cells), between the mobility measured in the in vitro vesicle pattern and in the overall synapse in living neurons. We speculate that our in vitro results reproduce the situation in cell compartments, where the protein mobility is mostly Brownian, complemented by vesicle interaction. By contrast, if active transport or extreme confinement affected the protein mobility in the synaptic bouton, the diffusion coefficients of the proteins would differ substantially.

In summary, all eleven proteins, excluding EGFP, bind to the patterned SVs, and a clear decrease of mobility was measured in all cases (see Fig. 6a). We did not find a correlation between the average time spent bound (see Table 1) and the diffusion coefficients of the bound fraction, D_{bound}. However, for some of the proteins, we can speculate about their binding behavior as measured here and their biological role and function.

Amphiphysin (light blue in Figs. 5 and 6) is known to directly interact with the lipids in the SVs[27], rather than binding protein partners as is the case for most other proteins. This aspect is reflected in our finding that amphiphysin is slowed down the most, spends the highest percentage of time bound to the SVs and consequently the binding energy E_b is lowest. Proteins that require protein partners, and especially soluble co-factors, to bind to the vesicles, would in contrast be at a disadvantage, as our purified vesicles are mostly devoid of soluble co-factors. Calmodulin (red in Figs. 5 and 6) spends the least time bound to the vesicles and thus has the highest binding energy E_b compared to the other proteins, which is to some extent expected, as this molecule is less strongly connected to presynaptic function than all others. Calmodulin is a general signaling component that is also involved in many vesicle-unrelated processes, such as postsynaptic dynamics[28]. Similarly, CALM (purple in Figs. 5 and 6) shows a low percentage of time it spends bound and therefore has a high binding energy E_b. It is known to bind the SV SNAREs directly. However, the interaction is dependent on the presence of phosphatidylinositol 4,5-bisphosphate (PIP_2), which is present in the SVs[29], but not enriched as in the plasma membrane[30]. α-synuclein (dark blue in Figs. 5 and 6) is known to bind SNAREs[31] and may attach to them on the SVs, thus being slowed down resulting in a low value for D_{bound} than the other proteins. We found synapsin to be the molecule that interacted most with the SVs. This molecule is capable of binding both SV proteins and SV lipids[32] and its main function seems to be the tethering of vesicles to each other and to the actin cytoskeleton, being a main contributor to vesicle clustering[33]. It is therefore not surprising that it also displays a strong interaction in our assay.

Conclusion

We established a minimalist in vitro model of the synaptic environment, designed by patterning SVs on glass coverslips. We employed FCS on fluorescently tagged synaptic proteins to quantify their mobility in the presence of SVs. Our approach is able to mimic the situation in the cell very closely and offers the additional advantage of high controllability and flexibility. For example, in future experiments, the design could be combined with microfluidic channels to add or wash-out reagents in a highly defined manner. The system further allows to quantitatively assess how the addition of kinases and phosphatases affects the kinetics of protein binding to SVs. We observed a clear decrease in mobility for proteins in the presence of the SVs, which we attribute to interaction events between the vesicles and the synaptic proteins. Overall, these data demonstrate that eleven different synaptic proteins, involved in different steps of SV exo- and endocytosis, can bind to SVs, which strongly reduces their mobility. Interestingly, the simple interaction to a monolayer of vesicles reduced the protein mobility to the values observed in living neurons to the level of the whole synapse[6], thereby implying that SV interaction is a major controller of synaptic protein mobility. These experiments therefore provide an answer to the question of whether the SV cluster acts as a determinant of protein organization in the synapse, as described in the introduction, and provide further support to the hypothesis that the SV cluster forms a distinct phase in the synapse, which locally concentrates a plethora of proteins important for synaptic transmission[9].

Methods

Glass coverslip functionalization. Glass coverslips (number 1, Thermo Scientific Technologies Inc., Wilmington, USA) were functionalized with neutravidin (Thermo Fisher Scientific, Waltham, MA, USA) to allow for the immobilization of SVs. The neutravidin was patterned on the glass coverslips using a photopatterning system (PRIMO, Alvéole, Paris, France), mounted on top of an inverted microscope (Olympus IX83, Olympus Europa SE & CO. KG, Hamburg, Germany). The photopatterning system was calibrated in the beginning of each patterning day, following the manufacturer's instructions. Glass coverslips were cleaned by rinsing them with isopropanol. After drying the coverslips with dry N_2, they were treated with air plasma (ZEPTO, plasma cleaner, Diener Electronics GmbH, KG Ebhausen, Germany) for 3 minutes at 40 W. After the plasma treatment, a polydimethylsiloxane (PDMS) stencil creating a circular chamber (diameter 3.5 mm) designed to enclose the

patterns, was applied to the surface, and 20 µL of PLL-g-PEG (0.1 mg/mL, PLL(20)-g[3.5]-PEG(2 kDa), SuSoS AG, Dübendorf, Switzerland) diluted in phosphate buffered saline (PBS) were added into the PDMS well and incubated for 1 h.

Figure 1a summarizes the main steps of the functionalization of the glass coverslips. The PLL-g-PEG coating provided the coverslips with anti-fouling properties, preventing unspecific protein adsorption. After rinsing three times with PBS, 8–10 µL of UV-sensitive photoinitiator (PLPP, Alvéole) were added into the PDMS well. To create the virtual mask with the pattern (in our case circular dots with 130 or 170 µm diameter), the open source software Inkscape (Inkscape Project, https://inkscape.org) was used. The pattern was loaded into the photopatterning software, Leonardo (Alvéole), and a 20 × objective (Olympus LUCPLFLN 20X, NA = 0.45) projected the UV light through the virtual mask. The PLPP, once activated by UV light, degraded the anti-fouling layer of PLL-g-PEG, leaving the exposed regions available for the attachment of neutravidin. A dose between 1800 and 2000 mJ/mm^2 was used. After patterning, the PLPP was removed by washing three times with PBS, and neutravidin (concentration of 0.05 mg/mL) was added to the pattern in the PDMS well. We used fluorescently labeled neutavidin-FITC (concentration of 0.05 mg/mL) to check the quality of the patterned substrate. However, in the actual experiments, unlabeled neutravidin was used. The protein was incubated overnight at 4 °C, and, after washing off the remaining protein with PBS, the functionalized glass coverslips were ready to be used.

Vesicle immobilization. Biotinylated mouse anti-synaptotagmin monoclonal antibodies (Synaptic Systems GmbH, Göttingen, Germany), were added to neutravidin-functionalized coverslips (concentration of 0.01 mg/mL) and incubated for 1 hour. SVs were purified from rat brain as previously described[5] and incubated with anti-vGLUT1 single-domain antibodies (concentration of 0.05 mg/mL) labeled with STAR635P (Nanotag, Göttingen, Germany) for 1 hour. Subsequently, the pattern was washed with PBS 3 times and the labeled SVs were incubated on the pattern for 1 hour. The coverslips were then washed 3 times with PBS to remove unbound vesicles. A schematic representation of the resulting assembly is shown in Fig. 1b.

STED imaging and vesicle density quantification. For quantification of the SV density, vesicles were immobilized on FITC-conjugated neutravidin patterns, as described above, and were stained with primary anti-synaptophysin and secondary anti-guinea pig antibodies conjugated to STAR635P. Imaging was performed using an Abberior easy3D STED microscope (Abberior GmbH, Göttingen, Germany) equipped with a UPlanSApo 100 ×, 1.4 NA oil immersion objective (Olympus) and an EMCCD iXon Ultra camera (Andor, Belfast, Northern Ireland, UK). A pulsed 640 nm laser was used for excitation, and an easy3D module 775 nm laser was used for depletion. Images were analyzed using a custom written Matlab script. In brief, the STED images were filtered using a bandpass filter to eliminate background noise and the spots above an empirically-defined threshold were identified. Their number was used to determine the vesicle densities, while their positions were used to measure the inter-vesicular distance. The example STED image presented in Supplementary Fig. S6 was processed by deconvolution, using in-built algorithms in Huygens Essential 4.4 (Scientific Volume Imaging, Hilversum, The Netherlands).

Protein purification. The following proteins (with the respective mRNA reference sequence numbers indicated in parentheses) were simultaneously tagged with mEGFP for FCS measurements and ALFA-tag for affinity purification[21]: α-synuclein (NM_001009158.3), amphiphysin (NM_022217.1), clathrin assembly lymphoid myeloid leukemia (CALM) (AF_041374.1), calmodulin 1 (NM_031969.2), clathrin light chain B (NM_053835.1), complexin 1 (U35098.1), endophilin A1 (NM_053935.1), epsin (NM_057136.1), Rab3a (NM_013018.2), and Rab7a (NM_023950.3). HEK293 cells were transfected with the coding plasmids using Lipofectamine 2000 reagent (Invitrogen, Carlsbad, CA, USA) following the manufacturer's recommendations. The proteins were expressed for approximately 24 hours and then purified using ALFA Selector PE-based chromatography. In brief, the cells were lysed with lysis buffer (1 % triton, 2 mM EDTA, protease inhibitor cocktail in PBS), the cell debris was pelleted by centrifugation and the supernatant was applied to the ALFA Selector PE resin. The ALFA-tagged proteins were allowed to bind to the resin for 1 h at 4 °C, while rotating, and all non-bound components were washed away twice with lysis buffer and once with ice-cold PBS. The bound proteins were then eluted with ALFA elution peptide. The presence of the protein of interest was confirmed by observing mEGFP fluorescence at every purification step and the resulting purified fractions were analyzed on a coomassie stained polyacrylamide gel (Supplementary Fig. S2). EGFP-Synapsin 1 and EGFP were expressed in Expi293F cells (Thermo Fisher Scientific) for three days following enhancement. Cells were harvested and lysed in buffer that contained 25 mM Tris-HCl (pH 7.4), 300 mM NaCl, 0.5 mM TCEP (buffer A), and protease inhibitor (cOmplete Protease Inhibitor Cocktail, EDTA-free, Roche, Penzberg, Germany). The lysates were centrifuged for 1h at 20,000×*g*, followed by a two-step purification. The first step was affinity purification on an Ni-NTA column (HisTrap HP, GE Healthcare Life Sciences, Freiburg, Germany) with binding at 20 mM, wash at 40 mM, and elution with 400 mM Imidazole in buffer A. The second step was size exclusion chromatography (Superdex 200 Increase 10/300, GE Healthcare) in 25 mM Tris-HCl (pH 7.4), 150 mM NaCl, 0.5 mM TCEP.

Optical setup. The setup used was based on an inverted microscope (Olympus IX73, Olympus). The excitation light was provided by two pulsed diode lasers (Cobolt Samba-532 100 mW and Cobolt Calypso-491 25 mW, Cobolt AB, Solna, Sweden) inserted into a laser combiner box (C-Flex, Cobolt AB). After exiting the optical fiber, the laser light passed through a clean-up filter (HC Laser Clean-Up MaxLine 491/1.9 or HC Laser Clean-up MaxLine 532/2, AHF Analysentechnik AG, Tübingen, Germany). The laser beam was expanded by a factor of 10 in order to illuminate the full back aperture of the microscope objective. The laser intensity was attenuated with a neutral density filter (OD = 6, Qioptiq Photonics, Göttingen, Germany) before being deflected by a dichroic mir-

ror (DualLine zt488/532rpc, AHF Analysentechnik AG) into the microscope. The laser beam was focused onto the sample using a 60× water immersion objective (UPlanApo, NA = 1.2, Olympus). The fluorescence light was then focused using an $f = 200$ mm lens onto the confocal pinhole (diameter 50 µm, Qioptiq Photonics). After the emission filter (Razor Edge Long Pass Filter 488 or RazorEdge LP Edge Filter 532, AHF Analysentechnik AG) the light was collimated using an $f = 50$ mm lens and directed to the avalanche photo diode (τ-SPAD, Picoquant GmbH, Berlin, Germany). The τ-SPADs were connected to a digital correlator card (ALV-7004 USB, ALV-Laser Vertriebsgesellschaft mbH, Langen, Germany). The digital correlator card was directly connected to the PC to store the data and then analyze them using Python (Python Software Foundation, https://www.python.org).

The same microscope was also used for epi-fluorescence microscopy. A mirror in the second deck of the microscope body enabled us to switch between the two microscope configurations. The excitation light came from a mercury arc lamp (X-Cite 120 PC Q, Excelitas Technologies, Waltham, USA) and was guided onto a fluorescence filter cube (filter sets available: DAPI, GFP, Cy3, TxRed and Cy5, all from AHF Analysentechnik AG). Images were acquired using a CCD-camera (Hamamatsu Orca R-2, Hamamatsu Photonics Deutschland GmbH, Herrsching am Ammersee, Germany) controlled by Micro-Manager[34]. To access different positions in the sample, an automated sample stage (Prior Scientific, Inc., Rockland, MA, USA) was used.

Single-point FCS measurements. FCS measurements without the SVs were performed using about 250 µL of sample placed in an eight-well chamber slide (Nunc, Thermo Fisher Scientific). In the beginning of every measurement day, the setup was aligned and the observation volume was determined. The diameter of the observation volume, w_0, was calculated measuring the ACF of a well-characterized dye, Atto 488 (AttoTech GmbH, Siegen, Germany , $D = (400 \pm 10)$ µm^2/s at 25 °C[35]) or Rhodamine 6G (Thermo Fisher, $D = (414 \pm 5)$ µm^2/s at 25 °C[36]), at a concentration of 10 nM. The ACF, was fitted using a single-component model for diffusion[23]:

$$\mathrm{ACF}(\tau) = \frac{\gamma}{N}\frac{1}{1+\frac{\tau}{\tau_D}}\frac{1}{\sqrt{1+\frac{\tau}{\tau_D}(\frac{w_0}{z_0})^2}}, \tag{1}$$

where τ is the correlation time, N is the average number of fluorescently labeled objects in the observation volume, w_0 and z_0 are the beam profile parameters of the observation volume, $\tau_D = w_0/4D$ is the diffusion time with D as the diffusion coefficient, and γ is the illumination profile factor, which in our case is 0.35. The one-component ACF can also be rewritten as:

$$\mathrm{ACF}(\tau) = \frac{\gamma}{N}G(\tau) = G(0)G(\tau), \tag{2}$$

where $G(0)$ is the amplitude of the ACF at $\tau = 0$, which contains information about the concentration of the sample. The measurements were performed at 22 °C. Typically, the diameter of the observation volume was $w_0 = (310 \pm 10)$ nm. Each protein was investigated using multiple samples with SV patterns. For each pattern, about 30 ACFs were recorded with an acquisition time of 30 s each.

For the measurements, where we detected two diffusing components, a two-component model[23] was employed to describe the data:

$$\mathrm{ACF}_2(\tau) = \frac{\gamma}{N^2}\big(N_1G_1(\tau) + N_2G_2(\tau)\big), \tag{3}$$

where N_1 and N_2 are the average numbers of fluorescently labeled objects of each species, $N = N_1 + N_2$ is the total number of diffusing objects and $G_1(\tau)$ and $G_2(\tau)$ correspond to the single species, see Eq. (2). The data were analyzed using a self-written fitting routine employing Python code. Measurements, where strong fluorescence peaks caused by aggregates affect the correlation curves, were excluded from the analysis. All correlation curves were fitted with a Levenberg-Marquardt nonlinear least-square routine.

Evaluation of interaction energy. To describe the behavior of synaptic proteins in the presence of SVs, we assumed two states, a bound state b with an average energy E_b and an unbound, or free, state f with an average energy E_f. We assumed that both states are always available to each copy of the proteins, i.e. no state is saturated or blocked by steric effects. The probability that a protein binds to an SV is p_b and the probability that it freely diffuses is p_f. Since we allowed for enough time for the system to equilibrate before the measurement, we assumed a steady state distribution between the bound and the unbound state and free state. The partition function Z of the two states is

$$Z = \exp(-E_b/k_BT) + \exp(-E_f/k_BT), \tag{4}$$

with the thermal energy of the system k_BT. The ratio of the probabilities to find the protein in the bound state p_b or the free state p_f is obtained via Boltzmann distributions

$$\frac{p_b}{p_f} = \frac{\frac{1}{Z}\exp(-E_b/k_BT)}{\frac{1}{Z}\exp(-E_f/k_BT)} = \exp((E_f - E_b)/k_BT). \tag{5}$$

Thus, the energy difference between the two states can be expressed as

$$E_f - E_b = k_BT\ln(p_b/p_i) = k_BT\ln(p_b/(1-p_b)). \tag{6}$$

In first approximation, for the free state, we assumed three degrees of freedom, $f = 3$, per protein, i.e. only translational kinetic energy, and thus assigned the energy $E_f = f/2 \cdot k_B T = 3/2 \cdot k_B T$. Thus, for the energy of the bound state, we obtain

$$E_b = \frac{3}{2} k_B T - k_B T \ln(p_b/(1 - p_b)). \tag{7}$$

As we assume the system to be in equilibrium, the ratio of the transition rates r_{fb} from the free state to the bound state and r_{bf} from the bound state to the free state directly follows from Eq. (5):

$$\frac{r_{fb}}{r_{bf}} = \frac{p_b}{p_f} = \exp\left((E_f - E_b)/k_B T\right), \tag{8}$$

and consequently,

$$r_{fb} = r_{bf} \cdot p_b/p_f. \tag{9}$$

Thus, the transition from the free to the bound state is p_b/p_f times slower than the reverse transition.

Data availability

The datasets generated and/or analyzed during the current study are available from the corresponding author on reasonable request.

Code availability

The codes generated for the analysis in the current study are available from the corresponding author on request.

Received: 21 July 2020; Accepted: 17 November 2020
Published online: 03 December 2020

References

1. Südhof, T. C. The synaptic vesicle cycle. *Annu. Rev. Neurosci.* **27**, 509–547. https://doi.org/10.1146/annurev.neuro.26.041002.131412 (2004).
2. Rizzoli, S. O. Synaptic vesicle recycling: steps and principles. *EMBO J.* **33**, 788–822. https://doi.org/10.1002/embj.201386357 (2014).
3. Birks, R., Huxley, H. E. & Katz, B. The fine structure of the neuromuscular junction of the frog. *J. Physiol.* **150**, 134–144. https://doi.org/10.1113/jphysiol.1960.sp006378 (1960).
4. Wilhelm, B. G. *et al.* Composition of isolated synaptic boutons reveals the amounts of vesicle trafficking proteins. *Science* **344**, 1023–1028. https://doi.org/10.1126/science.1252884 (2014).
5. Takamori, S. *et al.* Molecular anatomy of a trafficking organelle. *Cell* **127**, 831–846. https://doi.org/10.1016/j.cell.2006.10.030 (2006).
6. Reshetniak, S. *et al.* A comparative analysis of the mobility of 45 proteins in the synaptic bouton. *EMBO J.* e104596, https://doi.org/10.15252/embj.2020104596 (2020).
7. Denker, A., Krohnert, K., Buckers, J., Neher, E. & Rizzoli, S. O. The reserve pool of synaptic vesicles acts as a buffer for proteins involved in synaptic vesicle recycling. *Proc. Natl. Acad. Sci. USA* **108**, 17183–17188. https://doi.org/10.1073/pnas.1112690108 (2011).
8. Shupliakov, O. The synaptic vesicle cluster: a source of endocytic proteins during neurotransmitter release. *Neuroscience* **158**, 204–210. https://doi.org/10.1016/j.neuroscience.2008.03.035 (2009).
9. Milovanovic, D. & Camilli, P. D. Synaptic vesicle clusters at synapses: a distinct liquid phase?. *Neuron* **93**, 995–1002. https://doi.org/10.1016/j.neuron.2017.02.013 (2017).
10. Milovanovic, D., Wu, Y., Bian, X. & Camilli, P. D. A liquid phase of synapsin and lipid vesicles. *Science* **361**, 604–607. https://doi.org/10.1126/science.aat5671 (2018).
11. Sanabria, H., Digman, M. A., Gratton, E. & Waxham, M. N. Spatial diffusivity and availability of intracellular calmodulin. *Biophys. J.* **95**, 6002–6015. https://doi.org/10.1529/biophysj.108.138974 (2008).
12. Wragg, R. T. *et al.* Synaptic activity regulates the abundance and binding of complexin. *Biophys. J.* **108**, 1318–1329. https://doi.org/10.1016/j.bpj.2014.12.057 (2015).
13. Johnson, C. K. & Harms, G. S. Tracking and localization of calmodulin in live cells. *Biochim. Biophys. Acta* **2017–2026**, 2016. https://doi.org/10.1016/j.bbamcr.2016.04.021 (1863).
14. Strale, P.-O. *et al.* Multiprotein printing by light-induced molecular adsorption. *Adv. Mater.* **28**, 2024–2029. https://doi.org/10.1002/adma.201504154 (2015).
15. Saltzman, W., Radomsky, M., Whaley, K. & Cone, R. Antibody diffusion in human cervical mucus. *Biophys. J.* **66**, 508–515. https://doi.org/10.1016/s0006-3495(94)80802-1 (1994).
16. Dauty, E. & Verkman, A. S. Molecular crowding reduces to a similar extent the diffusion of small solutes and macromolecules: measurement by fluorescence correlation spectroscopy. *J. Mol. Recognit.* **17**, 441–447. https://doi.org/10.1002/jmr.709 (2004).
17. Weiss, M., Elsner, M., Kartberg, F. & Nilsson, T. Anomalous subdiffusion is a measure for cytoplasmic crowding in living cells. *Biophys. J.* **87**, 3518–3524. https://doi.org/10.1529/biophysj.104.044263 (2004).
18. Fujiwara, T. K. *et al.* Confined diffusion of transmembrane proteins and lipids induced by the same actin meshwork lining the plasma membrane. *Mol. Biol. Cell* **27**, 1101–1119. https://doi.org/10.1091/mbc.e15-04-0186 (2016).
19. Rhoades, E., Ramlall, T. F., Webb, W. W. & Eliezer, D. Quantification of α-synuclein binding to lipid vesicles using fluorescence correlation spectroscopy. *Biophys. J.* **90**, 4692–4700. https://doi.org/10.1529/biophysj.105.079251 (2006).
20. Nath, S., Meuvis, J., Hendrix, J., Carl, S. A. & Engelborghs, Y. Early aggregation steps in α-synuclein as measured by FCS and FRET: evidence for a contagious conformational change. *Biophys. J.* **98**, 1302–1311. https://doi.org/10.1016/j.bpj.2009.12.4290 (2010).
21. Götzke, H. *et al.* The ALFA-tag is a highly versatile tool for nanobody-based bioscience applications. *Nat. Commun.* **10**. https://doi.org/10.1038/s41467-019-12301-7 (2019).
22. Haucke, V., Neher, E. & Sigrist, S. J. Protein scaffolds in the coupling of synaptic exocytosis and endocytosis. *Nat. Rev. Neurosci.* **12**, 127–138. https://doi.org/10.1038/nrn2948 (2011).
23. Lakowicz, J. R. *Principles of Fluorescence Spectroscopy*, 3 edn (Springer, New York, 2006).
24. Wang, Q., Kaan, H. Y. K., Hooda, R. N., Goh, S. L. & Sondermann, H. Structure and plasticity of endophilin and sorting nexin 9. *Structure* **16**, 1574–1587. https://doi.org/10.1016/j.str.2008.07.016 (2008).

25. Ross, J. A. *et al.* Dimeric endophilin a2 stimulates assembly and GTPase activity of dynamin 2. *Biophys. J.* **100**, 729–737. https://doi.org/10.1016/j.bpj.2010.12.3717 (2011).
26. Ries, J. & Schwille, P. New concepts for fluorescence correlation spectroscopy on membranes. *Phys. Chem. Chem. Phys.* **10**, 3487. https://doi.org/10.1039/b718132a (2008).
27. Salzer, U., Kostan, J. & Djinović-Carugo, K. Deciphering the BAR code of membrane modulators. *Cell. Mol. Life Sci.* **74**, 2413–2438. https://doi.org/10.1007/s00018-017-2478-0 (2017).
28. Xia, Z. & Storm, D. R. The role of calmodulin as a signal integrator for synaptic plasticity. *Nat. Rev. Neurosci.* **6**, 267–276. https://doi.org/10.1038/nrn1647 (2005).
29. Paolo, G. D. & Camilli, P. D. Phosphoinositides in cell regulation and membrane dynamics. *Nature* **443**, 651–657. https://doi.org/10.1038/nature05185 (2006).
30. Miller, S. E. *et al.* The molecular basis for the endocytosis of small r-SNAREs by the clathrin adaptor CALM. *Cell* **147**, 1118–1131. https://doi.org/10.1016/j.cell.2011.10.038 (2011).
31. Tang, Y., Das, U., Scott, D. A. & Roy, S. The slow axonal transport of alpha-synuclein-mechanistic commonalities amongst diverse cytosolic cargoes. *Cytoskeleton* **69**, 506–513. https://doi.org/10.1002/cm.21019 (2012).
32. Cesca, F., Baldelli, P., Valtorta, F. & Benfenati, F. The synapsins: Key actors of synapse function and plasticity. *Progress Neurobiol.* **91**, 313–348. https://doi.org/10.1016/j.pneurobio.2010.04.006 (2010).
33. Pechstein, A. *et al.* Vesicle clustering in a living synapse depends on a synapsin region that mediates phase separation. *Cell Rep.* **30**, 2594–2602. https://doi.org/10.1016/j.celrep.2020.01.092 (2020).
34. Edelstein, A., Amodaj, N., Hoover, K., Vale, R. & Stuurman, N. Computer control of microscopes using μmanager. *Curr. Protoc. Mol. Biol.* **92**. https://doi.org/10.1002/0471142727.mb1420s92 (2010).
35. Kapusta, P. Absolute diffusion coefficients: Compilation of reference data for fcs calibration. *PicoQuant GmbH*https://www.picoquant.com/scientific/technical-and-application-notes/category/technical_notes_techniques_and_methods *(2010).*
36. Müller, C. B. *et al.* Precise measurement of diffusion by multi-color dual-focus fluorescence correlation spectroscopy. *Europhys. Lett.* **83**, 46001. https://doi.org/10.1209/0295-5075/83/46001 (2008).

Acknowledgements

This work was supported by the German Research Foundation (DFG) in the framework of SFB 1286 "Quantitative Synaptology", project B02, and under Germany's Excellence Strategy - EXC 2067/1- 390729940. Further funding was provided by the European Research Council (ERC, Grant No. CoG 724932) and the Studienstiftung des deutschen Volkes e.V.

Author contributions

S.K. and S.O.R. conceived the project and supervised the experiments, E.P. and S.R. conducted the experiments, CH and DM purified synapsin and EGFP. , E.P., S.R., S.O.R. and C.L. analyzed the data. All authors wrote the manuscript.

Funding

Open Access funding enabled and organized by Projekt DEAL.

Competing interests

SOR is a shareholder of NanoTag Biotechnologies and received compensation as consultant of NanoTag Biotechnologies. There are no conflicts of interest for any of the other authors.

Additional information

Supplementary information is available for this paper at https://doi.org/10.1038/s41598-020-77887-1.

Correspondence and requests for materials should be addressed to S.K.

Reprints and permissions information is available at www.nature.com/reprints.

Publisher's note Springer Nature remains neutral with regard to jurisdictional claims in published maps and institutional affiliations.

A minimalist model to measure interactions between proteins and synaptic vesicles

Eleonora Perego[1,+], Sofiia Reshetniak[2,+], Charlotta Lorenz[1], Christian Hoffmann[3], Dragomir Milovanović[3], Silvio Rizzoli[2,4], and Sarah Köster[1,4,*]

[1]Institute for X-Ray Physics, University of Göttingen, Göttingen, 37077, Germany
[2]Institute for Neuro- and Sensory Physiology, Center for Biostructural Imaging of Neurodegeneration, University Medical Center Göttingen, Göttingen, 37075, Germany
[4]Cluster of Excellence "Multiscale Bioimaging: from Molecular Machines to Networks of Excitable Cells" (MBExC), University of Göttingen, Göttingen, 37075, Germany
[3]Laboratory of Molecular Neuroscience, German Center for Neurodegenerative Diseases (DZNE), 10117 Berlin, Germany
[*]sarah.koester@phys.uni-goettingen.de
[+]these authors contributed equally to this work

Additional control measurements on patterned glass coverslips

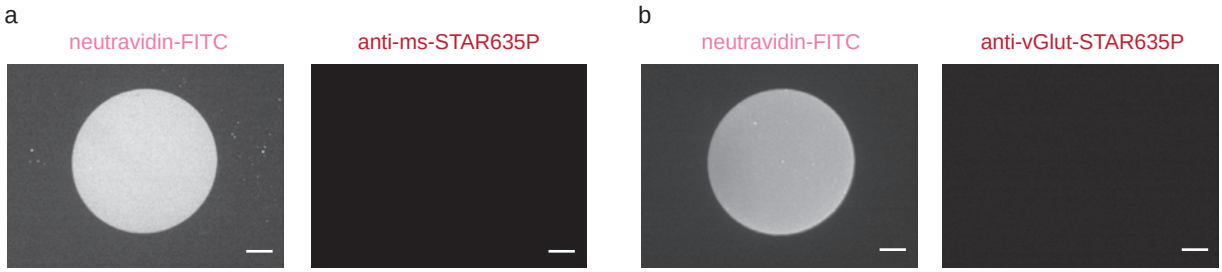

Figure S1. Negative controls on patterned glass coverslips without added SVs. a) After the neutravidin functionalization (neutravidin-FITC, left), the patterns were directly incubated with a secondary anti-mouse antibody labeled with STAR635P (right). b) After the neutravidin functionalization (neutravidin-FITC, left) and the incubation with biotinylated mouse anti-synaptotagmin antibody, a single-domain antibody against vGLUT1 labeled with STAR635P was added (without addition of SVs, right). Non-specific interactions are not observed in either case. The scale bars are 25 μm.

Coomassie stained polyacrylamide gel for the purified proteins

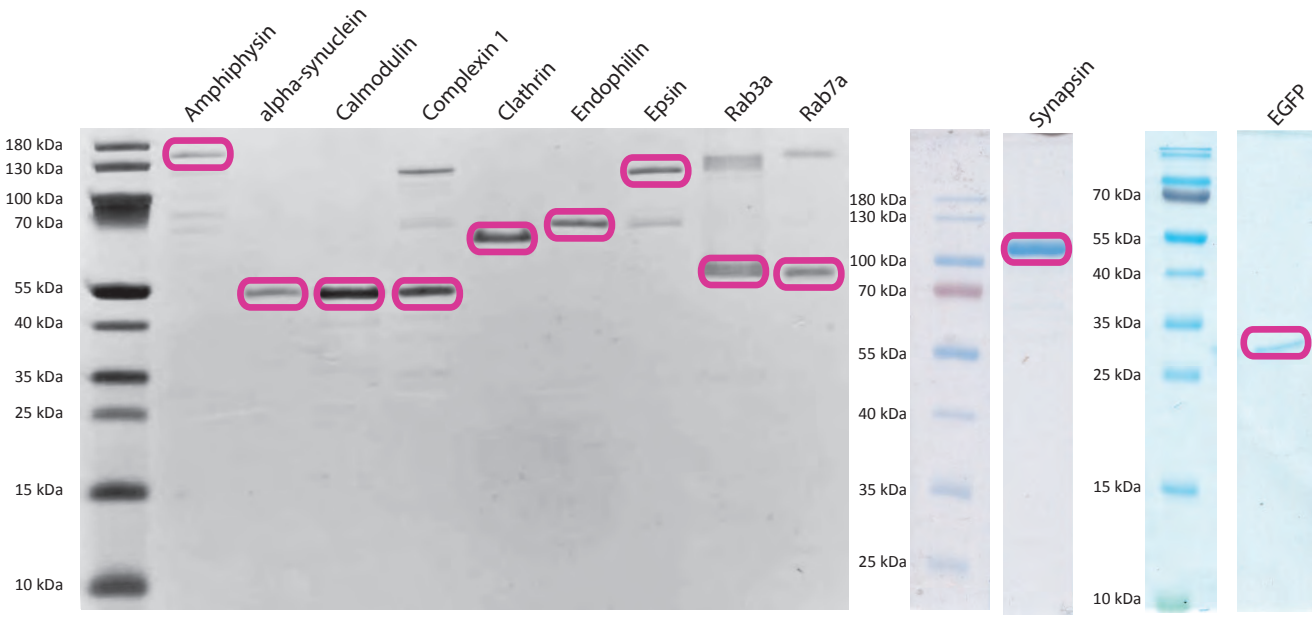

Figure S2. Coomassie stained polyacrylamide gel for all purified proteins tested in this study. Approximately 1 μg of protein was run on each lane, after protein purification (performed as shown in Fig. 3a). The behavior of the proteins is consistent with literature. Most proteins show one clear main band (indicated by the magenta boxes), found at the expected molecular weight. Synapsin and EGFP were run on separate polyacrylamide gels. Amphiphysin and epsin, and, to a lower extent, clathrin, run at higher molecular weights than their nominal values, as previously reported in the literature[1–3]. Some protein show secondary bands are that account for, on average, (11 ± 13) % of the total protein amounts. CALM was not analyzed in the same fashion, because this protein purifies to very low levels and is difficult to visualize by coomassie stained polyacrylamide gels. Additionally, CALM is known to display an unusual behavior during SDS-PAGE, separating into multiple bands of different molecular weights[4,5].

S2/S7

Comparison of the bulk diffusion coefficient and the free diffusion coefficient in the presence of SVs

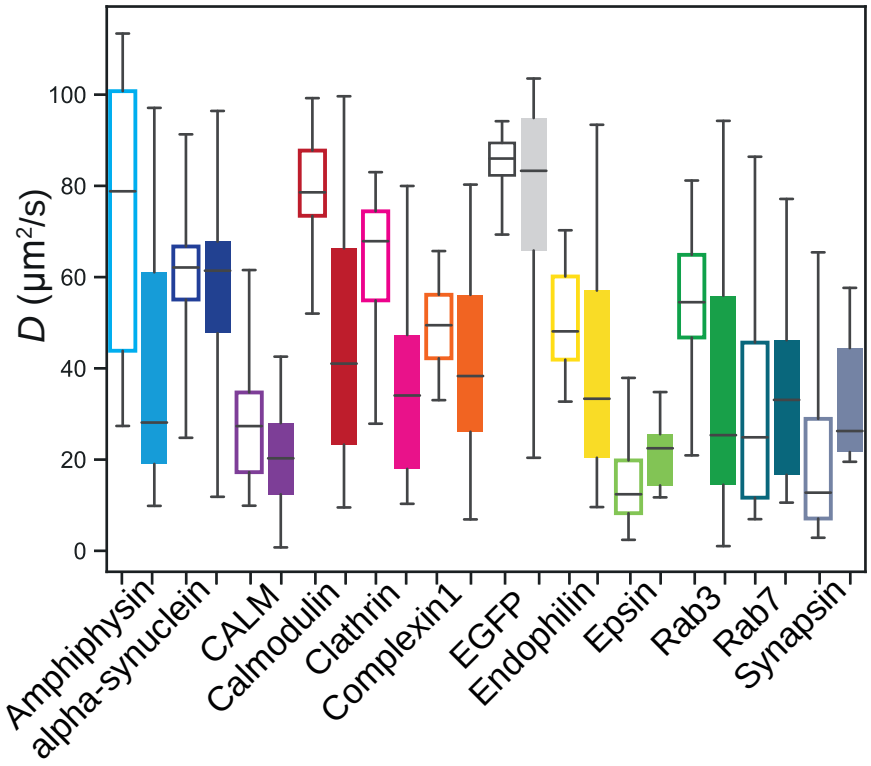

Figure S3. Diffusion coefficients of the proteins freely diffusing in bulk (D_{bulk}, empty boxes) and of the freely diffusing component in the SV patterns (D_{free}, filled boxes). The boxes extend from the lower quartile to upper quartile of the data, the middle lines in the box plots represent the median, the whiskers extend from the minimum to the maximum data point. The colors code represents the proteins as in the main text.

Results of the Mann-Whitney test to compare D_{bulk} and D_{bound}

Protein	p-value
Amphiphysin-mEGFP	2×10^{-12}
α-synuclein-mEGFP	5×10^{-20}
CALM-mEGFP	2×10^{-13}
Calmodulin-mEGFP	4×10^{-8}
Clathrin-mEGFP	2×10^{-13}
Complexin1-mEGFP	3×10^{-7}
Endophilin-mEGFP	2×10^{-15}
Epsin-mEGFP	2×10^{-8}
Rab3-mEGFP	1×10^{-12}
Rab7-mEGFP	1×10^{-9}
Synapsin-mEGFP	5×10^{-8}

Table S1. p-values for a Mann-Whitney statistical test, chosen because of the non-normality of the data, performed to compare the diffusion coefficients for proteins in bulk, D_{bulk}, and for the bound diffusing component in the SVs patterns, D_{bound}. All tested pairs show a p-value below the tolerance level of 0.05; thus we observe a significant difference for each protein. N varies between 20 and 90 data points depending on the protein.

Energy differences and transition rate ratios

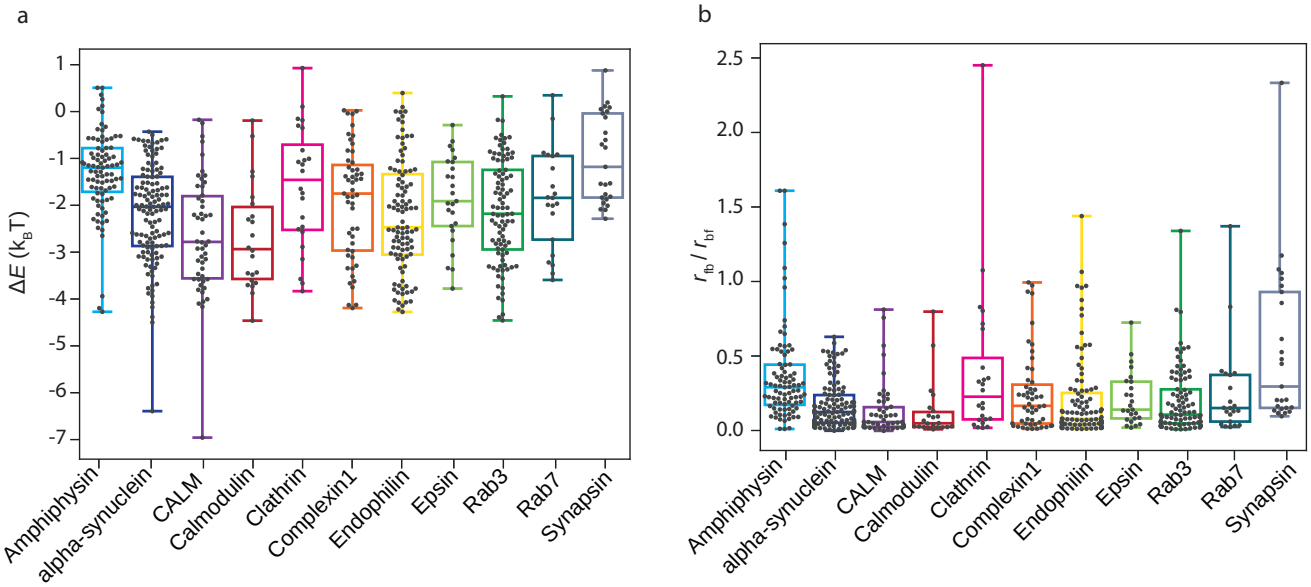

Figure S4. a) Energy difference between the free state and the bound state for all proteins. b) Ratio between the transition rate from the free state to the bound state and from the bound state to the free state. The boxes extend from the lower quartile to upper quartile of the data, the middle lines in the box plots represent the median, the whiskers extend from the minimum to the maximum data point.

Energies of the interaction state

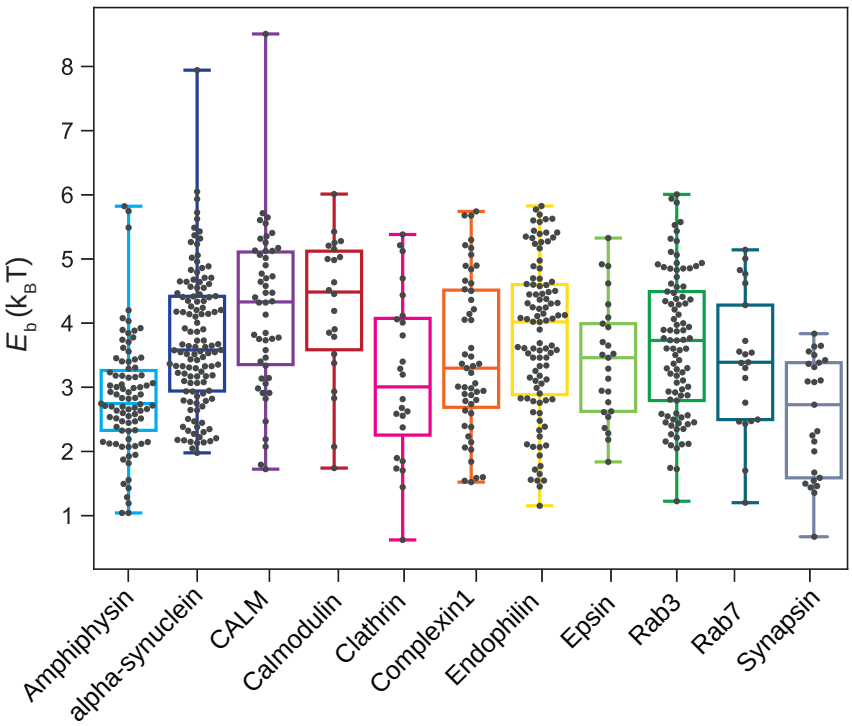

Figure S5. Estimated energy for the bound state for all measured proteins. The boxes extend from the lower quartile to upper quartile of the data, the middle lines in the box plots represent the median, the whiskers extend from the minimum to the maximum data point.

STED imaging of vesicle density

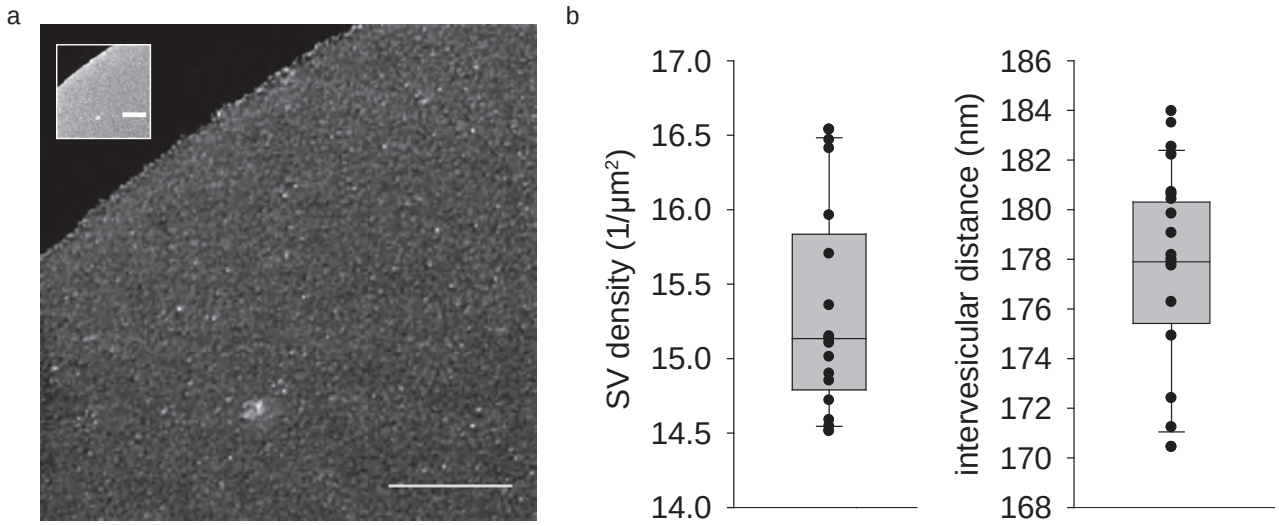

Figure S6. STED imaging of the patterned SVs to quantify the vesicle density. a) Representative STED image of labeled SVs attached to a neutravidin pattern. Inset: the respective confocal image of the underlying neutravidin-FITC pattern. Scale bars: 5 μm. b) Box plots of calculated vesicle densities (left) and distances between vesicle centers (right). 17 distinct pattern regions were analyzed, from one representative experiment (3 independent experiments in total. The middle line shows the median, the box edges indicate the 25th percentile, the error bars show the 75th percentile.).

References

1. Chen, H. *et al.* Epsin is an EH-domain-binding protein implicated in clathrin-mediated endocytosis. *Nature* **394**, 793–797, DOI: 10.1038/29555 (1998).
2. Laporte, S. A., Oakley, R. H., Holt, J. A., Barak, L. S. & Caron, M. G. The interaction of β-arrestin with the AP-2 adaptor is required for the clustering of β2-adrenergic receptor into clathrin-coated pits. *J. Biol. Chem.* **275**, 23120–23126, DOI: 10.1074/jbc.m002581200 (2000).
3. Slepnev, V. I., Ochoa, G.-C., Butler, M. H. & Camilli, P. D. Tandem arrangement of the clathrin and AP-2 binding domains in amphiphysin 1 and disruption of clathrin coat function by amphiphysin fragments comprising these sites. *J. Biol. Chem.* **275**, 17583–17589, DOI: 10.1074/jbc.m910430199 (2000).
4. Kim, J.-A. *et al.* Properties of GST-CALM expressed in e. coli. *Exp. Mol. Med.* **32**, 93–99, DOI: 10.1038/emm.2000.17 (2000).
5. Kim, J.-A. & Kim, H.-L. Cell-free expression and functional reconstitution of CALM in clathrin assembly. *Exp. Mol. Med.* **33**, 89–94, DOI: 10.1038/emm.2001.16 (2001).

DISCUSSION AND CONCLUSIONS

Synaptic protein mobility rates

This work comprises the first large-scale comparison of the synaptic protein mobility and provides the diffusion coefficients for a variety of proteins, in different locations. This now enables us to approach the questions posed in the Introduction.

One fundamental question relates to the overall protein mobility in the synapse. Macromolecular crowding caused by high protein concentrations and the presence of synaptic vesicles in the synapse was suggested to impede protein mobility in this compartment (Wilhelm et al., 2014). Indeed, the current work shows that on average, protein diffusion rates are 1.4 times lower in the synapse compared to the axon, and in the synaptic vesicle cluster the diffusion of soluble proteins is 3.8 times slower than in the axon. These differences arise not only due to the geometrical constrains of the vesicle-rich cluster, but also due to specific interaction between the proteins and the vesicles, which were demonstrated before (Shupliakov, 2009; Takamori et al., 2006).

To maintain synaptic activity, these effects might need to be counteracted, to allow for efficient protein delivery to the active zone. One way in which the cell might compensate for the hindered mobility rates is by adjusting the protein copy numbers present in the synapse. For example, a set number of molecules of a highly abundant protein with a particularly low diffusion speed would be statistically as likely to pass by the active zone within a certain time frame, as the same number of molecules of a protein that is present in much lower quantities but has a higher mobility rate. I have not observed any considerable correlation between the known protein copy numbers and their diffusion rates in the synapse measured here. On the contrary, some proteins present in the synapse in roughly the same quantities have drastically different diffusion rates (e. g. dynamin and endophilin), while some that have approximately the same mobility rates may be present in very different quantities (e. g. epsin and amphiphysin). However, the absence of a direct correlation between the two values does not mean that no such relation exists. To efficiently fulfill their functions, proteins are needed in different copy numbers and without knowing the copy number requirements for all the analyzed proteins it is impossible to truly assess whether the total copy numbers are linked with the protein mobility.

An alternative mechanism to ensure efficient protein delivery to the active zone, despite vesicle binding and crowding constrains, is employment of active directed delivery routes. Such a delivery, dependent on actomyosin-based transport, has been suggested for the synaptic vesicles (Chenouard et al., 2020; Evans et al., 1998; Prekeris and Terrian, 1997; Shupliakov et al., 2002), which might act as carriers of the bound soluble proteins. It is questionable, however, that the amount of proteins bound to a single vesicle would be sufficient for the fusion of the said vesicle, and delivery of additional soluble proteins is likely to be required. So far, there are no known motors that function in the synapse and can bind soluble proteins directly, and the experiments reported here demonstrate that no such active transport is required. Free diffusion alone, while being slower than the transport in axons, provides a high rate of protein mobility,

which can be appreciated from the Figure 4. To make the measured protein diffusion speeds easier to perceive, one can use the generated trajectories to estimate the time that it would take any protein molecule to reach the active zone. Such estimation shows that within 6 seconds virtually every (of more than a million, considering only protein species analyzed in this work) soluble protein molecule will pass by the active zone at least once and can potentially be involved in its respective functional processes. To put this number in a physiological context, one should consider the normal activity rates of a synapse. In the span of 6 seconds a synapse of the cultured neurons used in this study would release only ~3.6 vesicles on average (Truckenbrodt et al., 2018). Delivery of every protein molecule present in the synapse within this time via simple diffusion seems to be more than sufficient to maintain endo- and exocytosis required during the normal network activity.

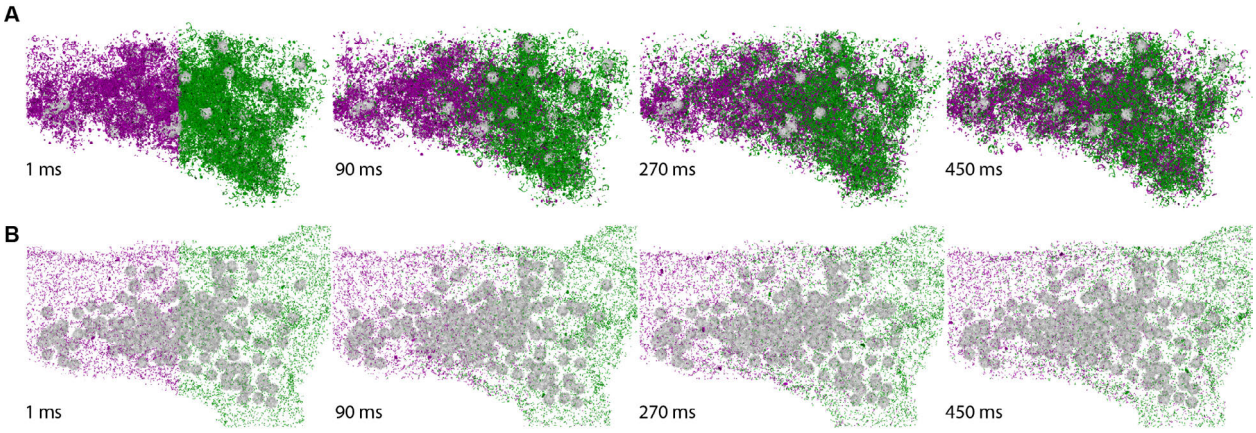

Figure 4. Visualization of the overall protein mobility rates in the synapse. All analyzed proteins (A – soluble, B - membrane) represented in their respective shape models and copy numbers were color-coded at time 0 and were allowed to intermix following the trajectories and diffusion rates generated by their respective models for up to 450 ms.

Another issue this work aimed to investigate is the differences in protein mobilities in different parts of the axon and between different proteins. As mentioned above, proteins generally move faster in axons than in synapses, and the mechanisms behind this will be discussed in more detail in later sections. One observation on the numbers themselves that is particularly interesting is how different the distribution of protein mobility rates in axons and synapses is. With the exception for VAMP4, all proteins have very similar time constants in the axons, while they vary significantly in the synapse. This indicates that the regulatory mechanisms that exist to control protein mobility in the synapse affect different proteins to a different extent. It appears that less specialized proteins, whose functions are not limited to the synapses, have the smallest difference in their time constants and diffusion coefficients between the axons and the synapses (e. g. Hsc70, calmodulin). Similarly, such proteins are also equally mobile within the synaptic vesicle cluster (e. g. AP2, clathrin). This observation supports the conclusion that association with the SVs is the key regulator of protein mobility in the synapses. The fact that the molecular weight does not correlate with any of the mobility parameters also supports the idea that even in the axons, in the absence of the SVs, specific interactions and functional engagements are more important than physical properties of the soluble proteins.

As is shown in Chapter 1 and illustrated in the Figure 4, membrane proteins are generally less mobile compared to the soluble ones. The likely reason for this are differences in viscosity between the lipid membrane and the aqueous cytosol. Also, unlike for the soluble proteins, whose molecular weight did not influence mobility, the mobility of membrane proteins negatively correlates with the number of their transmembrane domains. This further confirms the assumption of the mechanical nature of the cause of their slower mobilities. Various specific protein-protein interactions are likely to also play a role in defining membrane protein diffusion rates, but it is important to note that no such interactions were considered in the computational simulations presented here. These simulations, nonetheless, were able to accurately reproduce protein behavior, leading to a conclusion that the synaptic geometry is a key factor that affects mobility of membrane proteins.

Mechanisms regulating protein mobility

Technical considerations

The experiments presented in the Chapter 1 and Chapter 2 indicate that protein mobility in the synapse is regulated by simple and robust mechanisms based on cellular geometry and interactions with the SVs. To make interpretation of these observations clearer, I will start by discussing several aspects of the methods used to obtain this information.

A large portion of the data presented in the Chapter 1 is based on computational simulations of particle movement in the synapse. These were used to extract diffusion coefficients from the FRAP data, since the approaches commonly used for other systems (Axelrod et al., 1976; Blumenthal et al., 2015; Kang et al., 2012) failed to reproduce the real behavior of analyzed proteins. The complexity of the synapse requires dedicated models and not just the use of generic mathematical formulas. Despite the frequent use of the word “model”, it is important to keep in mind that the simulations used here were not generated using mathematical modeling that relies on governing equations. Instead, a Monte Carlo simulation approach was used. I provide a schematic explanation of the simulation procedure in the Figure 5.

Using such a simulation we generated a set of possible particle trajectories within the *in silico* reconstructed synapse space that differed in their movement speed, or their propensity to bind to a vesicle. Both parameters are set as simple numeric values for each model (“move X pixels in one step” or “upon reaching a vesicle do not change coordinates for X steps”) and the models do not have any relation to the proteins when they are generated. At no point the simulated particles alter their behavior based on the variables in their surroundings. For example, the Model 3 in the Figure 5 codes the particle to bind to the curved surface on the left in the event of reaching it. This is set in the model by specific coordinates of this surface, rather than its characteristics. The simulation does not execute any calculations to check if the surface is curved or to estimate its position relative to other borders. Instead, it relies on the descriptive variable “curved part of the left border”, whose value (“true” or “false”) is assigned by the experimenter to each coordinate in the spatial model.

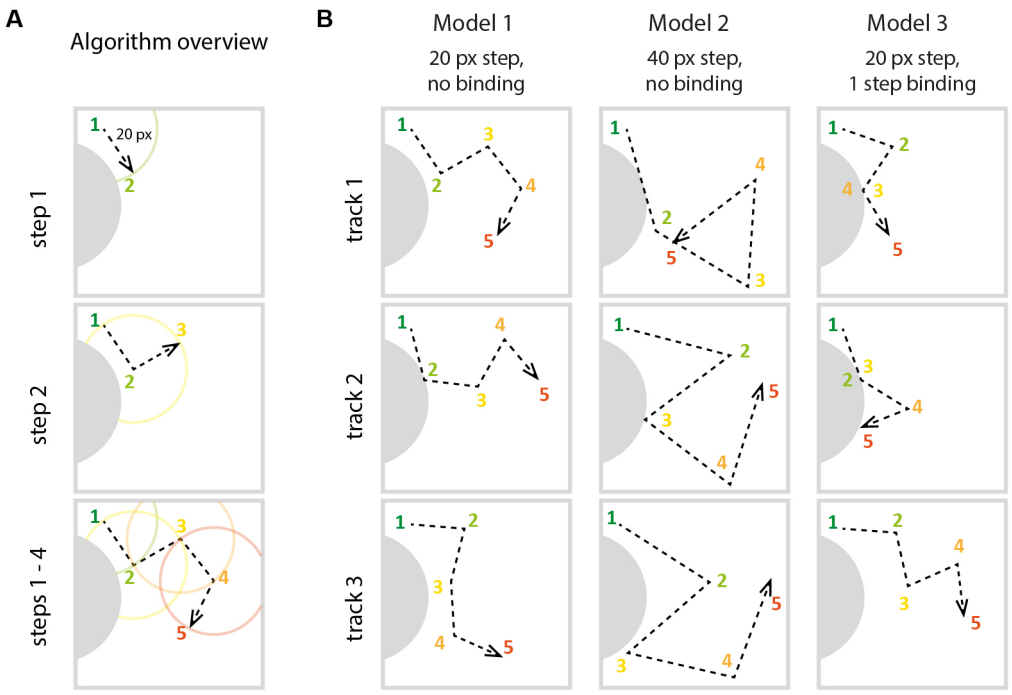

Figure 5. A schematic representation of the principles of the particle movement simulations used in the Chapter 1. A, the general algorithm used for the generation of the tracks. In this example a particle is moving in the white space bounded by the grey outline and the only parameter set by the experimeter affecting the particle's behaviour is the distance the particle can travel in one step: 20 px. Starting at the position 1, the particle has an equal chance to move to any position on the green curve, which is a segment of a circle with a radius of 20 px, centered at the position 1. The boundaries of the movement space do not allow the particle to move outside of this shape. In the case of the synaptic space, such boundaries would also prevent the particle from crossig the membranes of organelles. After moving to the position 2, the particle now has an equal chance to relocate to any position on the yellow curve, following the same spatial restrictions and the set step size. The process continues for a set amount of steps, generating a random track. **B,** the possible resulting tracks. For each model a number of random tracks is generated, all having different trajectories, despite following the same set of rules. In our simulations, models differed by two parameters: single step displacement, and vesicle binding. Model 2 illustrated here shows how the size of the step affects the particle movement. In the Model 3 a second parameter is introduced, that forses the particle to "bind" to the curved part of the left border. Note how in the track 1 both positions 3 and 4 are labeled at the same location: upon reaching the border, the particle remained bound to it for one step, and did not change its coordinates. Compare this to the Model 1, which has the same single step size, but no binding parameter: in the track 2, upon reaching the position 2, which is located on the curved border, the particle was not retained and changed its coordinates in the next step.

Such an approach allows to introduce minimal assumptions on biological processes we do not have sufficient information on, and to avoid artifacts introduced by suboptimal governing equations. The models themselves serve descriptive rather than analytical purpose and the reasons for a certain mobility behavior of each protein can then be deduced based on the experimental evidence. This must be kept in mind when interpreting the results presented here. For example, the "binding to the vesicles" parameter does not directly represent protein interactions with the synaptic vesicle membranes. Instead, it can indicate association with other components of the vesicle cluster. The numerous validations performed confirm that the simulations truthfully reproduce the behavior of the proteins in the cells, but they cannot provide information on the binding sites or the specific partners. Similarly, the simulations used to quantify the movement of the membrane proteins do not take specific interactions into account at all.

These interactions might play a role in defining the mobility of membrane proteins, but in the presented simulations they appear to be accounted for by the values of the single step displacements. The averaging nature of the analysis is another important feature. While we do have individual movement tracks that we use to illustrate the movement of individual protein molecules, they only represent the average movement pattern of this protein species and are not equal to tracks obtained by single molecule tracking experiments.

The Chapter 2 describes a use of a simplified *in vitro* imitation of the synaptic vesicle cluster to confirm the observation of the effect of the synaptic vesicles on protein mobility made in the Chapter 1. While it detects the same pattern and the values obtained by this *in vitro* approach correlate with the ones calculated form the live imaging experiments, the absolute values of the diffusion coefficients are not the same in the two. This can be explained by the difference in the concentration of the vesicles found in the *in vitro* experiments and living synapse, but also by the differences in their spatial organization. In the generated *in vitro* system, the SVs were patterned on a solid surface as a single layer. In the synapses, in comparison, vesicles exist as a three-dimensional cluster. The geometric constrictions would be expected to affect mobility of an inert protein that does not bind to the vesicles (as is also demonstrated for the negative control antibodies in the Chapter 2), but in the combination with the vesicle binding, the spatial organization of the synaptic vesicle cluster would have even larger influence on the protein mobility. This serves as an additional evidence in favor of the conclusion that both synaptic geometry and synaptic vesicle binding affect synaptic protein mobility.

Synaptic geometry

Three basic observations from the data presented in the Chapter 1 and Chapter 2 indicate that the synaptic geometry alone can affect protein mobility, without the need of specific regulatory mechanisms.

First, in the FRAP experiments free mEGFP showed slower recovery and diffusion in the synapses compared to the axons. This protein is not supposed to specifically bind to any cellular components and therefore differences in protein composition between the axons and synapses should not affect its mobility. Indeed, unlike synapse-specific proteins, mEGFP shows no differences in its diffusion rates within the synaptic vesicle cluster and the whole synapse. Its behavior is described by a model that does not include any binding to the SVs. The nearly two-fold difference in its diffusion rate between the axons and the synapses can only be explained by the differences in the geometry of the two compartments. If the geometry had a substantial effect on the mobility of an inert protein, it is safe to assume that it would also affect the behavior of the endogenous proteins.

Second, our simulations show that the mobility of membrane proteins is mainly affected by the synaptic geometry without any specific regulatory mechanisms involved. As described above, these simulations only took the geometry of an axon or a synapse into account and introduced no other variables between the two, but were able to accurately reproduce protein behavior in the respective compartments. This observation is not completely expected, as specific mechanisms to restrict membrane protein diffusion were identified in other parts of the neuron (Albrecht et al., 2016; Ewers et al., 2014), and implies an absence of specific nanoscopic morphological features of the presynaptic neck.

Third, the presence of the synaptic vesicles affected the mobility of inert proteins in the *in vitro* model, which is likely explained by the confining effects. At the same time, the presence of the SVs was not sufficient to reproduce the same exact diffusion rates as seen in the synapses. This might be partially attributed to the impact of other cellular components, but a more likely explanation is the difference in the spatial organization of the synaptic vesicle cluster and the vesicle cluster generated artificially. The influence of the cluster geometry and organization can be unequivocally identified in further experiments based on immobilized vesicles, using different approaches to reproduce the three-dimensionality of the synaptic vesicle cluster and varying the number and density of the vesicles in the artificial cluster.

It does not come as a surprise that the available space and its shape can affect movement possibilities. The question is whether this effect is coincidental or has any functional relevance. Above I discussed how the mobility rates reported here can be used to estimate the time it would take any molecule to reach the active zone. Interestingly, these calculations also hint at a possible functional role of the effects of the synaptic geometry on the protein mobility, and I would like to discuss these considerations in more detail. For the sake of simplicity and easier perception, let us take a look at the protein mobility reconstruction generated in Chapter 1, but modified in a way to "fix" molecules in place when they reach the active zone. A few frames from such a modified mobility visualization are shown in Figure 6A. Over time, proteins would accumulate at the active zone, and one can measure the fraction of proteins accumulated there at any given time point. One can then do the same kind of quantification, but instead force the proteins to accumulate in any other location in the synapse. In Figure 6B I show 4 regions that are of similar size and shape to the active zone, but surprisingly have a different pattern of protein accumulation. In the case of the real active zone there is a good agreement between the percentage of the protein molecules accumulated at the active zone and an experimentally measured parameter indicating their correlation to the active zone (Wilhelm et al., 2014), but no such agreement is observed for the "fake" active zones.

This observation itself is remarkable since the location of the active zone was not introduced in the models when the tracks were generated and no interactions with active zone proteins were considered. Faster accumulation of the proteins that correlate to the active zone is maintained exclusively by random diffusion and this further reinforces the conclusion made before: directed transport of proteins to the active zone is not required. Furthermore, when the accumulation in other regions of the synapse is measured, no relation with the protein's correlation to the active zone is found (Figure 6B). This indicates that even when specific interactions with the adaptors of the active some are neglected, the proteins that are supposed to be located at the active zone do not only find their way there faster than others, but also do this in a specific manner, not showing this behavior in other parts of the synapse. This might be achieved by the relative position and density of the synaptic vesicles close to the active zone, which would not be the same in other parts of the synapse. If this assumption is correct, it would mean that the effects of the synaptic geometry on protein mobility play an important role in maintaining synaptic activity. In this case, the overall shape of the synapse and the positions and sizes of the organelles within might have specifically evolved to sustain the correct flow of the proteins to the functionally relevant sites without the need of energy consuming processes.

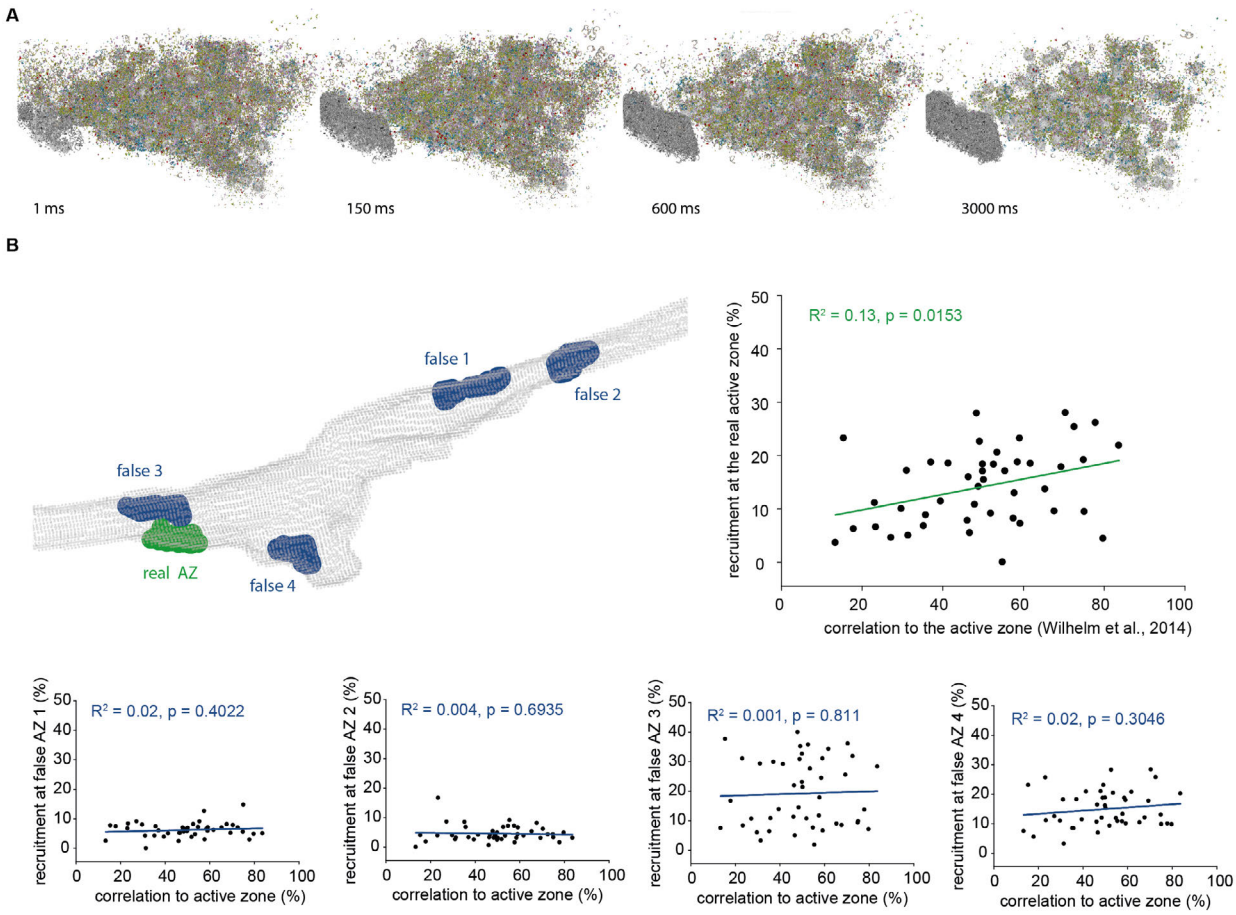

Figure 6. Analysis of protein passage through an active zone. A, in a putative experiment proteins diffusing close to the active zone (within 100 nm of it) were recruited there, to measure the rates and amounts of proteins that could reach the active zone by diffusion. The accumulated proteins are shown in gray (only soluble proteins). **B**, the protein accumulation can be measured at the real active zone (green) or at four equivalently sized and -shaped false active zones (blue), in independent *in silico* experiments. The amounts recruited after a set amount of time (as % of all proteins of the respective type) can then be compared to the correlation of these proteins to the active zones measured experimentally (Wilhelm et al., 2014).

Binding to the synaptic vesicles

The second key parameter that affects protein mobility identified in this work is the binding to the synaptic vesicles. This is only relevant for soluble proteins and this section will only discuss these proteins.

It has been established for many years that the synaptic vesicle cluster binds multiple endocytosis and exocytosis cofactors, as well as other soluble proteins. The current work for the first time provides a large-scale quantification of this binding's effects on the dynamic organization of the synapses and opens an opportunity to explore the role of this binding beyond the previously suggested protein buffering. The Figure 7 summarizes the soluble proteins binding to the SVs, relying on the quantifications from the Chapter 1.

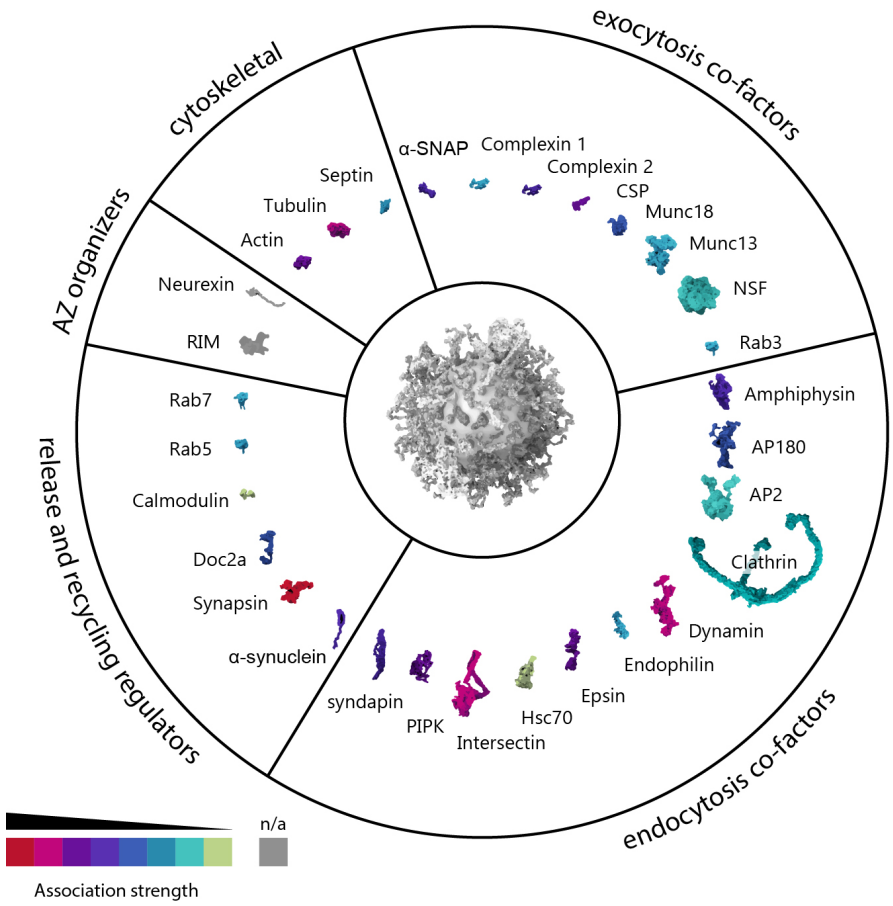

Figure 7. Overview of the soluble proteins' association with the synaptic vesicles. The proteins are colored according to their fold enrichments in the synaptic vesicle cluster, quantified in the Chapter 1, and are grouped according to their functional categories (figure reproduced from Reshetniak and Rizzoli, 2021).

While there are differences in the strength of association with the vesicles between the different proteins, no clear pattern can be identified in relation to their functional categories. Instead, many proteins whose function is not limited to the synapses seem to be less affected by the vesicle binding. In this context, a particular case of intersectin is interesting. Intersectin is well known for its synaptic functions related to synaptic vesicle recycling (Gerth et al., 2017; Jäpel et al., 2020; Pechstein et al., 2010), but it is also an important adaptor protein involved in the early stages of endocytosis in all cells (Henne et al., 2010; Okamoto et al., 1999; Predescu et al., 2003; Sengar et al., 1999). Despite having such a fundamental role in other cells, its association with the SVs is on the opposite side of the spectrum compared to many other endocytic proteins. While this might seem illogical, it is easily explained by a technical detail that is often not discussed when the neuronal functions of intersectin are investigated. In my experiments I used a neuron-specific long isoform of intersectin 1, while endocytosis in other cells relies on a more abundant short isoform. The short isoform is also present in the neurons and is probably involved in the endocytic events outside of the synapse. Based on the functional distinction itself, I would expect the short isoform to be less affected by the vesicle binding and behave similarly to Hsc70, endophilin and AP2. In this case, interaction with the SVs is the mechanism that allows the synapse to

distinguish between very similar proteins of which one has a more important role in the synapses than the other.

The available data suggests that vesicle binding is the mechanism that ensures that the proteins required for synaptic function are delivered and kept in the synapse, while proteins required to fulfill their functions elsewhere are not as strongly confined to this compartment. This, in turn, helps to answer further questions. First, it can be assumed that this is not another manifestation of the geometry effects. One can argue that the bare presence of the SVs in the synapse changes the geometry of the space available for diffusion, which affects protein mobility and, as a result, distribution. However, the fact that these effects are protein-specific indicates that this is not the case, and other organelles should then not have the same effects as the SVs do. Second, this provides a possible mechanism for a targeted protein delivery to the synapse and to the active zone. While there are known mechanisms that restrict protein entry to the axon or the dendrite, it was not clear how the protein composition of the synapse is regulated. The data presented here demonstrates that the interaction with the SVs is a possible protein "sorting" mechanism at the synapse. These considerations also provide additional support to the assumption made in the previous subsection: the SVs contribute to the specific protein delivery to the active zone.

Another aspect of the synapse composition that seems to be regulated through binding to the SVs is protein copy numbers. The copy numbers present in the synapse can differ by several orders of magnitude between different proteins (Wilhelm et al., 2014). It is not clear how these ratios are maintained and how the presence of an appropriate number of molecules of each protein is ensured over time. The data reported here suggest that this can also be regulated by the SVs, through their binding and retention of adequate numbers of protein molecules. This can then scale according to the activity levels: a more active synapse has a larger number of SVs (Murthy et al., 1997; Rey et al., 2020), and therefore can retain more soluble cofactors, which are needed for the high level of activity.

Organization of the synaptic vesicle cluster

An important observation made in Chapter 1 is the fact that protein behavior is drastically different within the synaptic vesicle cluster, compared to the rest of the synapse. The Figure 8 illustrates these differences.

Not only proteins tend to move slower in the synaptic vesicle cluster, but their concentrations there are also higher. While this is true for all proteins, a few stand out significantly: synapsin, intersectin, and dynamin. Synapsin and intersectin have been suggested to be involved in the formation of the synaptic vesicle cluster via liquid-liquid phase separation (LLPS) (Hoffmann et al., 2021; Milovanovic and Camilli, 2017; Milovanovic et al., 2018). Phase separation is a process of matter segregation without the change of the aggregate state that results in two (or more) distinct phases of different composition. In the cellular context this manifests in a formation of membrane-less organelles such as nucleoli, P-bodies and stress granules, and relies on multiple protein-protein interactions, usually involving intrinsically disordered domains (Alberti, 2017; Shin and Brangwynne, 2017). In the last decade LLPS was proposed to

be an important mechanism for formation of various components of a neuron, including the postsynaptic density (Bai et al., 2020; Nott et al., 2015; Zeng et al., 2018), the active zone (Wu et al., 2019, 2020), and the synaptic vesicle cluster (Feng et al., 2021; Milovanovic and Camilli, 2017; Milovanovic et al., 2018; Pechstein et al., 2020; Wu et al., 2020). In the case of the synaptic vesicle cluster the process is thought to rely on the intrinsically disordered region of synapsin and is suggested to be the main mechanism for the vesicle cluster formation (Hoffmann et al., 2021; Milovanovic et al., 2018; Park et al., 2021; Pechstein et al., 2020; Wu et al., 2020).

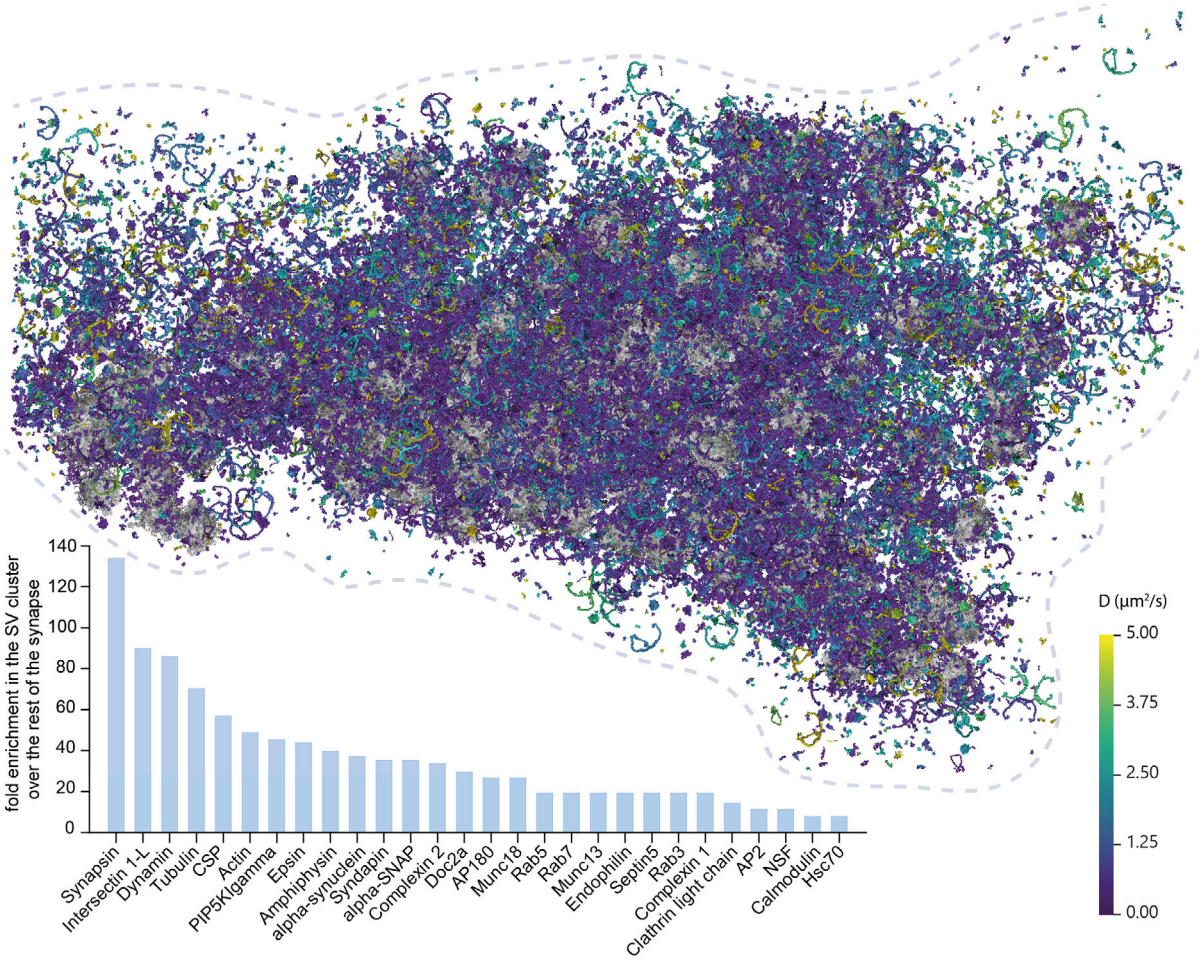

Figure 8. Soluble protein distribution and mobility in the synaptic bouton. Synaptic vesicles (grey) and analyzed soluble proteins (various colored shapes) are shown, with the approximate borders of the synaptic bouton indicated by the dashed line. Proteins are represented in their copy numbers as determined before (Wilhelm et al., 2014), with their positions being determined by their respective mobility model, and are colored according to the diffusion coefficient of each molecule in the position it currently occupies. The graph below quantifies the enrichment of the proteins in the synaptic vesicle cluster, compared to the synaptic space outside the cluster.

While the idea was proposed in 2017, it was not clear until this year whether synapsin-dependent phase separation can happen in a cellular environment. One of the concerns relates to the concentrations of the proteins required for the process to take place, as the initial experiments were performed in an *in vitro* setting with purified synapsin. Our analysis shows that protein concentrations within the synaptic vesicle

cluster, especially such of synapsin, are several orders of magnitude higher than in other parts of the cell on average. This increase in concentration depends on synapsin interactions with the SVs and explanations how he sufficiently high concentrations of synapsin can be achieved locally to induce the phase separation of the synaptic vesicle cluster. The data presented here also provide an additional point of support of the LLPS theory, that relates to the dynamics of the suggested phases. While the LLPS results in two distinct membraneless compartments where transition of a molecule from one phase to another is hindered, both phases remain fluid and protein diffusion is allowed within the phase. This is the characteristic that distinguishes liquid phases from simple aggregates. Experimentally this is usually tested with the help of FRAP experiments, when only a part of the phase is bleached, and the recovery then reflects the degree of protein mobility within the phase. The protein mobility measurements presented here confirm that indeed, protein diffusion is allowed within the synaptic vesicle cluster, in agreement with the suggested LLPS nature of its segregation.

Protein mobility rates and synaptic activity

In addition to providing information on the protein dynamics and spatial organization and the regulation thereof, the mobility rates provided by this work can be used in investigations of the synaptic function. By combining these data with the known protein copy numbers, more accurate models of the synapse can be generated, which would allow studying various synaptic processes and test hypotheses that could not be addressed by *in silico* approaches before.

As an example, mobility rates can be used to determine whether certain proteins are required or not to participate in specific processes to maintain synaptic activity. One process where the protein requirements are not clear is the endocytosis of synaptic vesicles. Suggested modes of synaptic vesicle retrieval from the plasma membrane include clathrin-dependent and independent routes, as illustrated in Figure 9A (Gan and Watanabe, 2018; Kononenko and Haucke, 2015; Milosevic, 2018; Soykan et al., 2016). Using the known data on clathrin copy numbers required for the endocytosis of one vesicle (McMahon and Boucrot, 2011), and present in the synapse (Wilhelm et al., 2014), one can estimate that about 10% of all synaptic clathrin needs to be used to retrieve one synaptic vesicle. Considering that multiple vesicles are being released during a single burst of activity, and that clathrin needs to be removed from the endocytosed vesicles before it can be used again, one can imagine that the availability of clathrin might become a limiting factor for synaptic activity in the case of its obligatory involvement in the retrieval of every synaptic vesicle. The same, in fact, can be true for any protein, and without knowing their mobility rates it is impossible to tell whether it is the case.

Knowing protein mobility rates, their overall copy numbers in the synapse, and the number required for a single endocytic event, one can compute how different modes of synaptic vesicle retrieval can counter-balance vesicle exocytosis during basal activity (Reshetniak et al., 2020). This simulation would look as follows: vesicles are being released at a known rate (Truckenbrodt et al., 2018), and can be considered retrieved either when *(a)* sufficient for one endocytic event number of dynamin molecules has accumulated at the retrieval site, or *(b)* sufficient number of dynamin and clathrin molecules has accumulated at the retrieval site. In the case of the mode *(b)*, the vesicle would be considered uncoated

when a sufficient amount of Hsc70 has accumulated. Until then the clathrin molecules coating this vesicle are removed from the total pool of available clathrin as they are unable to participate in endocytosis of another vesicle.

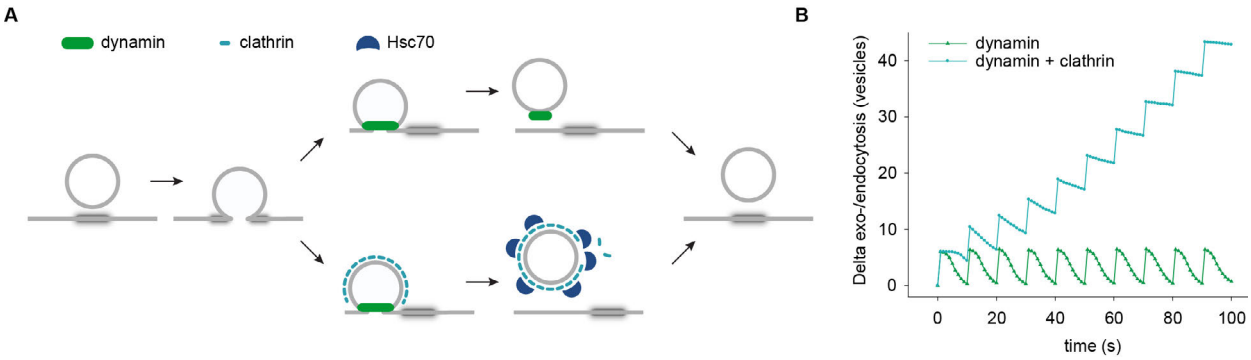

Figure 9. Simulation of protein usage for synaptic vesicle endocytosis during network activity. A, following fusion, the synaptic vesicle material can be retrieved via various mechanisms. The scheme illustrates two options tested in these simulations: either vesicle can be endocytosed when sufficient amount of dynamin is available for membrane fission (top), or the assembly and consequent disassembly of the clathrin coat is required (bottom). **B**, differences in the number of vesicles that are released during spontaneous network activity, and can be retrieved in either of the two pathways presented in **A**. Endo- and exocytosis can be balanced if only dynamin is required for endocytosis, but not if both dynamin and clathrin are required. Figure from Reshetniak et al., 2020.

The ratios between the number of vesicles released and endocytosed in either mods are plotted in Figure 9B. Already after one activity burst, the synapse is not able to retrieve all 6 vesicles if both dynamin and clathrin are required, and the effect accumulates over time, showing that such a synapse would not be able to maintain its normal network activity rate. When only dynamin is required, the synapse is able to effectively retrieve all vesicles and hence dynamin can participate in every endocytosis step. These findings are consistent with *in vivo* observations, and do not only support the idea that, unlike dynamin, clathrin might not be required for the endocytosis of every synaptic vesicle (Kononenko et al., 2014; Newton et al., 2006), but also provide a mechanistic explanation why it cannot be required. This demonstrates that despite seemingly high mobility rates and excessive copy numbers, some proteins might not be able to reach their respective functionally relevant sites in excessive amounts. It remains an open question whether any of such proteins would act as a factor to limit the synaptic activity. It is possible that the differences in protein mobility rates and the extent to which they are affected by the vesicle cluster are the factors that allow preventing such bottlenecks.

This simple example demonstrates how the results reported here can be used to address issues that are difficult to investigate otherwise. I expect that these data will be used by laboratories that specialize in modeling of synaptic physiology to analyze more complex reactions.

Broader implications for synaptic physiology

Taken together, the discussed observations demonstrate that the synaptic vesicle cluster plays a much more diverse role in the synaptic physiology, which is not limited to the storage of the neurotransmitter

and soluble co-factors. It regulates qualitative and quantitative protein compositions of the synapses, mobility and availability of soluble proteins, as well the organization and morphology of the synapse. In this new context, additional interpretations of the previously reported findings become available.

The synaptic vesicles are known to interact with components of the active zone, including presynaptic adhesion molecules as well as other, both soluble and membrane, proteins of the active zone (Fernández-Busnadiego et al., 2013; Scheiffele et al., 2000; Takamori et al., 2006). Considering the SVs' role in the regulation of protein mobility and localization, it is possible that they are also involved in the maintenance of the active zone. Moreover, since the SVs also appear to play a crucial role in the formation of the synaptic vesicle cluster and can detect a contact with a postsynaptic cell via the adhesion molecules (Scheiffele et al., 2000), it is reasonable to suggest that they may be involved in the initiation or regulation of the active zone assembly and synaptogenesis. This can be further reinforced by the vesicles' effects on the local cytoskeleton. The main cytoskeletal component of synapses, actin, is recruited by the strongest vesicle binder, synapsin (Bloom et al., 2003). This implies that the distribution of actin filaments would be heavily affected by the distribution of the SVs. Not only distribution, but also the kinetics of the actin filament assembly can be affected by the SVs (Chieregatti et al., 1996). Additionally, the lipid composition of the SVs influences actin involvement in the endocytic events (Dason et al., 2014). Taken together, these data suggest that the SVs can serve as a hub to coordinate and regulate synaptogenesis, through the formation of the SVs cluster, detection of the contact with a postsynapse, organization of the active zone, and local cytoskeletal rearrangements (Figure 10).

Evidence for the SVs binding multiple proteins and regulating their copy numbers indicates that the synaptic vesicle cluster may also be involved in the homeostatic plasticity. The synaptic strength and size depend on the number of synaptic vesicles and need to be maintained at an optimal level. One possible mechanism relies on the ability of the synapse to detect and remove the SVs that were exocytosed many times (Truckenbrodt et al., 2018). An overly active synapse would lose synaptic vesicles at a high rate, decreasing in size, and vice versa: a less active synapse, whose vesicles do not undergo exocytosis as often, will accumulate vesicles and grow. Together with the vesicles, the necessary soluble cofactors would be either decreased or increased in numbers, to support proper activity levels. Additionally, the growth or shrinkage of the synapse can be caused by the size of the vesicle cluster itself. Larger synapses contain fewer soluble co-factors, relative to their size, than smaller ones (Wilhelm et al., 2014). At the same time, they contain more exocytosis cofactors than endocytosis cofactors, both in total and relative to the required for a single activity event numbers. Larger synapses are therefore expected to be more efficient in releasing than retrieving synaptic vesicles, eventually losing them, and decreasing in size. Small synapses, on the other hand, would increase in size, and as a result the number of synaptic vesicles should stabilize at the optimal level, not allowing the synapse to grow too large or too small. With these, and mentioned in the previous sections points considered, it becomes clear why synapses contain far more synaptic vesicles than they need to release under the physiological conditions.

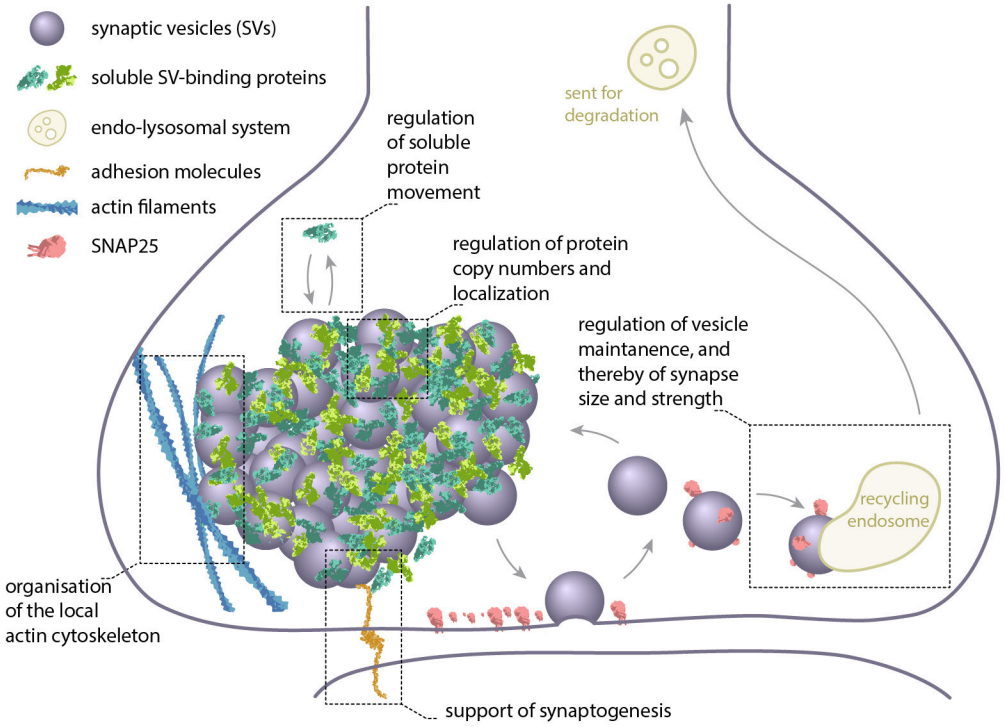

Figure 10. The synaptic vesicle cluster as a key regulator of synaptic organization. The synaptic vesicles bind multiple proteins, including soluble exo- and endocytosis cofactors, cytoskeleton elements, molecules of cellular adhesion, and active zone proteins. This allows the SV cluster to regulate protein distribution and mobility, modulate cytoskeleton organization, and participate in the active zone assembly. Selective SV recycling or degradation links SV cluster regulation with synapse size and strength (figure from Reshetniak and Rizzoli, 2021).

Outcome

To sum up, the data I presented in Chapter 1 and Chapter 2 provide a vast amount of information, with multiple possible applications. Chapter 1 describes a previously unavailable, highly detailed analysis of protein mobility in the synaptic boutons. The generated database contains the mobility rates of 47 different proteins. These are useful for the analysis of the synaptic functions of individual proteins, and provide insight into their biology that was previously difficult to obtain for any individual protein in the presynapse. Additionally, the values can be used for high-precision modeling of synaptic biology.

The analysis of the data I obtained also widens our understanding of the fundamental principles of synaptic physiology. These include the mechanisms of synaptic protein mobility and distribution regulation, which are crucial for the maintenance of neurotransmission. The observations made here allow for new interpretations of previously available data. For example, they enlarge the previous view of the synaptic vesicle cluster as a regulator of protein locations for a few exo- and endocytosis cofactors to a *bona fide* major organizer of the entire presynapse.

Overall, by addressing the questions posed in the introduction, this thesis provides the most detailed view of the dynamic organization of proteins in the synaptic bouton available to date.

REFERENCES

Ahmari, S.E., Buchanan, J., and Smith, S.J. (2000). Assembly of presynaptic active zones from cytoplasmic transport packets. Nat. Neurosci. 3, 445–451.

Alberti, S. (2017). Phase separation in biology. Curr. Biol. CB 27, R1097–R1102.

Albrecht, D., Winterflood, C.M., Sadeghi, M., Tschager, T., Noé, F., and Ewers, H. (2016). Nanoscopic compartmentalization of membrane protein motion at the axon initial segment. J Cell Biol jcb.201603108.

Aravanis, A.M., Pyle, J.L., and Tsien, R.W. (2003). Single synaptic vesicles fusing transiently and successively without loss of identity. Nature 423, 643–647.

Axelrod, D., Koppel, D.E., Schlessinger, J., Elson, E., and Webb, W.W. (1976). Mobility measurement by analysis of fluorescence photobleaching recovery kinetics. Biophys. J. 16, 1055–1069.

Bai, G., Wang, Y., and Zhang, M. (2020). Gephyrin-mediated formation of inhibitory postsynaptic density sheet via phase separation. Cell Res. 1–14.

Basu, J., Shen, N., Dulubova, I., Lu, J., Guan, R., Guryev, O., Grishin, N.V., Rosenmund, C., and Rizo, J. (2005). A minimal domain responsible for Munc13 activity. Nat. Struct. Mol. Biol. 12, 1017–1018.

Betz, W. J., Bewick, G. S., & Ridge, R. M. (1992). Intracellular movements of fluorescently labeled synaptic vesicles in frog motor nerve terminals during nerve stimulation. Neuron, 9(5), 805–813.

Bird, M.M. (1976). Microtubule--synaptic vesicle associations in cultured rat spinal cord neurons. Cell Tissue Res. 168, 101–115.

Bloom, O., Evergren, E., Tomilin, N., Kjaerulff, O., Löw, P., Brodin, L., Pieribone, V.A., Greengard, P., and Shupliakov, O. (2003). Colocalization of synapsin and actin during synaptic vesicle recycling. J. Cell Biol. 161, 737–747.

Blumenthal, D., Goldstien, L., Edidin, M., and Gheber, L.A. (2015). Universal Approach to FRAP Analysis of Arbitrary Bleaching Patterns. Sci. Rep. 5.

Böcking, T., Aguet, F., Harrison, S.C., and Kirchhausen, T. (2011). Single-molecule analysis of a molecular disassemblase reveals the mechanism of Hsc70-driven clathrin uncoating. Nat. Struct. Mol. Biol. 18, 295–301.

van den Bogaart, G., Holt, M.G., Bunt, G., Riedel, D., Wouters, F.S., and Jahn, R. (2010). One SNARE complex is sufficient for membrane fusion. Nat. Struct. Mol. Biol. 17, 358–364.

Borgdorff, A.J., and Choquet, D. (2002). Regulation of AMPA receptor lateral movements. Nature 417, 649–653.

Bouchard, R., Pattarini, R., and Geiger, J.D. (2003). Presence and functional significance of presynaptic ryanodine receptors. Prog. Neurobiol. 69, 391–418.

Brose, N., Hofmann, K., Hata, Y., and Südhof, T.C. (1995). Mammalian Homologues of Caenorhabditis elegans unc-13 Gene Define Novel Family of C2-domain Proteins (∗). J. Biol. Chem. 270, 25273–25280.

Bury, L.A., and Sabo, S.L. (2011). Coordinated trafficking of synaptic vesicle and active zone proteins prior to synapse formation. Neural Develop. 6, 24.

Cambier, C., Banik, S.M., Buonomo, J.A., and Bertozzi, C.R. (2020). Spreading of a mycobacterial cell-surface lipid into host epithelial membranes promotes infectivity. ELife 9, e60648.

Cesca, F., Baldelli, P., Valtorta, F., and Benfenati, F. (2010). The synapsins: key actors of synapse function and plasticity. Prog. Neurobiol. 91, 313–348.

Chamma, I., Letellier, M., Butler, C., Tessier, B., Lim, K.-H., Gauthereau, I., Choquet, D., Sibarita, J.-B., Park, S., Sainlos, M., et al. (2016). Mapping the dynamics and nanoscale organization of synaptic adhesion proteins using monomeric streptavidin. Nat. Commun. 7, 10773.

Chan, K.Y., and Bunt, A.H. (1978). An association between mitochondria and microtubules in synaptosomes and axon terminals of cerebral cortex. J. Neurocytol. 7, 137–143.

Chanaday, N.L., and Kavalali, E.T. (2018). Time course and temperature dependence of synaptic vesicle endocytosis. FEBS Lett. 592, 3606–3614.

Chang, D.T.W., Honick, A.S., and Reynolds, I.J. (2006). Mitochondrial trafficking to synapses in cultured primary

cortical neurons. J. Neurosci. Off. J. Soc. Neurosci. 26, 7035–7045.

Chavan, V., Willis, J., Walker, S.K., Clark, H.R., Liu, X., Fox, M.A., Srivastava, S., and Mukherjee, K. (2015). Central Presynaptic Terminals Are Enriched in ATP but the Majority Lack Mitochondria. PLoS ONE 10.

Chavis, P., and Westbrook, G. (2001). Integrins mediate functional pre- and postsynaptic maturation at a hippocampal synapse. Nature 411, 317–321.

Cheng, Y., Boll, W., Kirchhausen, T., Harrison, S.C., and Walz, T. (2007). Cryo-electron tomography of clathrin-coated vesicles: structural implications for coat assembly. J. Mol. Biol. 365, 892–899.

Chenouard, N., Xuan, F., and Tsien, R.W. (2020). Synaptic vesicle traffic is supported by transient actin filaments and regulated by PKA and NO. Nat. Commun. 11, 5318.

Chieregatti, E., Ceccaldi, P.E., Benfenati, F., and Valtorta, F. (1996). Effects of synaptic vesicles on actin polymerization. FEBS Lett. 398, 211–216.

Cingolani, L.A., and Goda, Y. (2008). Actin in action: the interplay between the actin cytoskeleton and synaptic efficacy. Nat. Rev. Neurosci. 9, 344–356.

Crispino, M., Kaplan, B.B., Martin, R., Alvarez, J., Chun, J.T., Benech, J.C., and Giuditta, A. (1997). Active polysomes are present in the large presynaptic endings of the synaptosomal fraction from squid brain. J. Neurosci. Off. J. Soc. Neurosci. 17, 7694–7702.

Crispino, M., Chun, J.T., Cefaliello, C., Perrone Capano, C., and Giuditta, A. (2014). Local gene expression in nerve endings. Dev. Neurobiol. 74, 279–291.

Dahan, M., Lévi, S., Luccardini, C., Rostaing, P., Riveau, B., and Triller, A. (2003). Diffusion dynamics of glycine receptors revealed by single-quantum dot tracking. Science 302, 442–445.

Darcy, K.J., Staras, K., Collinson, L.M., and Goda, Y. (2006). Constitutive sharing of recycling synaptic vesicles between presynaptic boutons. Nat. Neurosci. 9, 315–321.

Dason, J.S., Smith, A.J., Marin, L., and Charlton, M.P. (2014). Cholesterol and F-actin are required for clustering of recycling synaptic vesicle proteins in the presynaptic plasma membrane. J. Physiol. 592, 621–633.

Denker, A., Kröhnert, K., Bückers, J., Neher, E., and Rizzoli, S.O. (2011). The reserve pool of synaptic vesicles acts as a buffer for proteins involved in synaptic vesicle recycling. Proc. Natl. Acad. Sci. U. S. A. 108, 17183–17188.

Dieck, S., Sanmartí-Vila, L., Langnaese, K., Richter, K., Kindler, S., Soyke, A., Wex, H., Smalla, K.-H., Kämpf, U., Fränzer, J.-T., et al. (1998). Bassoon, a Novel Zinc-finger CAG/Glutamine-repeat Protein Selectively Localized at the Active Zone of Presynaptic Nerve Terminals. J. Cell Biol. 142, 499–509.

Ehlers, M.D., Heine, M., Groc, L., Lee, M.-C., and Choquet, D. (2007). Diffusional trapping of GluR1 AMPA receptors by input-specific synaptic activity. Neuron 54, 447–460.

Evans, L.L., Lee, A.J., Bridgman, P.C., and Mooseker, M.S. (1998). Vesicle-associated brain myosin-V can be activated to catalyze actin-based transport. J. Cell Sci. 111 (Pt 14), 2055–2066.

Evergren, E., Marcucci, M., Tomilin, N., Löw, P., Slepnev, V., Andersson, F., Gad, H., Brodin, L., De Camilli, P., and Shupliakov, O. (2004). Amphiphysin is a component of clathrin coats formed during synaptic vesicle recycling at the lamprey giant synapse. Traffic Cph. Den. 5, 514–528.

Evergren, E., Gad, H., Walther, K., Sundborger, A., Tomilin, N., and Shupliakov, O. (2007). Intersectin Is a Negative Regulator of Dynamin Recruitment to the Synaptic Endocytic Zone in the Central Synapse. J. Neurosci. 27, 379–390.

Ewers, H., Tada, T., Petersen, J.D., Racz, B., Sheng, M., and Choquet, D. (2014). A Septin-Dependent Diffusion Barrier at Dendritic Spine Necks. PLOS ONE 9, e113916.

Faelber, K., Posor, Y., Gao, S., Held, M., Roske, Y., Schulze, D., Haucke, V., Noé, F., and Daumke, O. (2011). Crystal structure of nucleotide-free dynamin. Nature 477, 556–560.

Farías, G.G., Guardia, C.M., Britt, D.J., Guo, X., and Bonifacino, J.S. (2015). Sorting of Dendritic and Axonal Vesicles at the Pre-axonal Exclusion Zone. Cell Rep. 13, 1221–1232.

Fassio, A., Raimondi, A., Lignani, G., Benfenati, F., and Baldelli, P. (2011). Synapsins: from synapse to network hyperexcitability and epilepsy. Semin. Cell Dev. Biol. 22, 408–415.

Feng, Z., Wu, X., and Zhang, M. (2021). Presynaptic bouton compartmentalization and postsynaptic density-mediated glutamate receptor clustering via phase separation. Neuropharmacology 193, 108622.

Fenster, S.D., Chung, W.J., Zhai, R., Cases-Langhoff, C., Voss, B., Garner, A.M., Kaempf, U., Kindler, S., Gundelfinger, E.D., and Garner, C.C. (2000). Piccolo, a Presynaptic Zinc Finger Protein Structurally Related to Bassoon. Neuron 25, 203–214.

Fernández-Busnadiego, R., Asano, S., Oprisoreanu, A.-M., Sakata, E., Doengi, M., Kochovski, Z., Zürner, M., Stein, V., Schoch, S., Baumeister, W., et al. (2013). Cryo–electron tomography reveals a critical role of RIM1α in synaptic vesicle tethering. J. Cell Biol. 201, 725–740.

Fernández-Chacón, R., Wölfel, M., Nishimune, H., Tabares, L., Schmitz, F., Castellano-Muñoz, M., Rosenmund, C., Montesinos, M.L., Sanes, J.R., Schneggenburger, R., et al. (2004). The Synaptic Vesicle Protein CSPα Prevents Presynaptic Degeneration. Neuron 42, 237–251.

Fu, Y., and Huang, Z.J. (2010). Differential dynamics and activity-dependent regulation of alpha- and beta-neurexins at developing GABAergic synapses. Proc. Natl. Acad. Sci. U. S. A. 107, 22699–22704.

Gaffield, M.A., Rizzoli, S.O., and Betz, W.J. (2006). Mobility of Synaptic Vesicles in Different Pools in Resting and Stimulated Frog Motor Nerve Terminals. Neuron 51, 317–325.

Gan, Q., and Watanabe, S. (2018). Synaptic Vesicle Endocytosis in Different Model Systems. Front. Cell. Neurosci. 12, 171.

Garcia, E.P., McPherson, P.S., Chilcote, T.J., Takei, K., and De Camilli, P. (1995). rbSec1A and B colocalize with syntaxin 1 and SNAP-25 throughout the axon, but are not in a stable complex with syntaxin. J. Cell Biol. 129, 105–120.

Gerth, F., Jäpel, M., Pechstein, A., Kochlamazashvili, G., Lehmann, M., Puchkov, D., Onofri, F., Benfenati, F., Nikonenko, A.G., Fredrich, K., et al. (2017). Intersectin associates with synapsin and regulates its nanoscale localization and function. Proc. Natl. Acad. Sci. U. S. A. 114, 12057–12062.

Gordon-Weeks, P.R., Burgoyne, R.D., and Gray, E.G. (1982). Presynaptic microtubules: organisation and assembly/disassembly. Neuroscience 7, 739–749.

Graffe, M., Zenisek, D., and Taraska, J.W. (2015). A marginal band of microtubules transports and organizes mitochondria in retinal bipolar synaptic terminals. J. Gen. Physiol. 146, 109–117.

Graydon, C.W., Zhang, J., Oesch, N.W., Sousa, A.A., Leapman, R.D., and Diamond, J.S. (2014). Passive Diffusion as a Mechanism Underlying Ribbon Synapse Vesicle Release and Resupply. J. Neurosci. 34, 8948–8962.

Greengard, P., Valtorta, F., Czernik, A.J., and Benfenati, F. (1993). Synaptic vesicle phosphoproteins and regulation of synaptic function. Science 259, 780–785.

Groc, L., Heine, M., Cognet, L., Brickley, K., Stephenson, F.A., Lounis, B., and Choquet, D. (2004). Differential activity-dependent regulation of the lateral mobilities of AMPA and NMDA receptors. Nat. Neurosci. 7, 695–696.

Guan, R., Dai, H., and Rizo, J. (2008). Binding of the Munc13-1 MUN domain to membrane-anchored SNARE complexes. Biochemistry 47, 1474–1481.

Hafner, A.-S., Donlin-Asp, P.G., Leitch, B., Herzog, E., and Schuman, E.M. (2019). Local protein synthesis is a ubiquitous feature of neuronal pre- and postsynaptic compartments. Science 364.

Harris, K.M., Spacek, J., Bell, M.E., Parker, P.H., Lindsey, L.F., Baden, A.D., Vogelstein, J.T., and Burns, R. (2015). A resource from 3D electron microscopy of hippocampal neuropil for user training and tool development. Sci. Data 2, 150046.

Haydon, P.G., Henderson, E., and Stanley, E.F. (1994). Localization of individual calcium channels at the release face of a presynaptic nerve terminal. Neuron 13, 1275–1280.

Henne, W.M., Boucrot, E., Meinecke, M., Evergren, E., Vallis, Y., Mittal, R., and McMahon, H.T. (2010). FCHo proteins are nucleators of clathrin-mediated endocytosis. Science 328, 1281–1284.

Herzog, E., Nadrigny, F., Silm, K., Biesemann, C., Helling, I., Bersot, T., Steffens, H., Schwartzmann, R., Nägerl, U.V., El Mestikawy, S., et al. (2011). In vivo imaging of intersynaptic vesicle exchange using VGLUT1 Venus knock-in mice. J. Neurosci. Off. J. Soc. Neurosci. 31, 15544–15559.

Heuser, J.E., and Reese, T.S. (1973). Evidence for recycling of synaptic vesicle membrane during transmitter release at the frog neuromuscular junction. J. Cell Biol. 57, 315–344.

Hilfiker, S., Benfenati, F., Doussau, F., Nairn, A.C., Czernik, A.J., Augustine, G.J., and Greengard, P. (2005). Structural Domains Involved in the Regulation of Transmitter Release by Synapsins. J. Neurosci. 25, 2658–2669.

Hirokawa, N. (1998). Kinesin and Dynein Superfamily Proteins and the Mechanism of Organelle Transport. Science 279, 519–526.

Hirokawa, N., Sobue, K., Kanda, K., Harada, A., and Yorifuji, H. (1989). The cytoskeletal architecture of the presynaptic

terminal and molecular structure of synapsin 1. J. Cell Biol. 108, 111–126.

Hoffmann, C., Sansevrino, R., Morabito, G., Logan, C., Vabulas, R.M., Ulusoy, A., Ganzella, M., and Milovanovic, D. (2021). Synapsin Condensates Recruit alpha-Synuclein. J. Mol. Biol. 433, 166961.

Hua, Y., and Scheller, R.H. (2001). Three SNARE complexes cooperate to mediate membrane fusion. Proc. Natl. Acad. Sci. U. S. A. 98, 8065–8070.

Innocenti, G.M., and Caminiti, R. (2017). Axon diameter relates to synaptic bouton size: structural properties define computationally different types of cortical connections in primates. Brain Struct. Funct. 222, 1169–1177.

Ishikawa-Ankerhold, H.C., Ankerhold, R., and Drummen, G.P.C. (2012). Advanced Fluorescence Microscopy Techniques—FRAP, FLIP, FLAP, FRET and FLIM. Molecules 17, 4047–4132.

Jacob, T.C., Bogdanov, Y.D., Magnus, C., Saliba, R.S., Kittler, J.T., Haydon, P.G., and Moss, S.J. (2005). Gephyrin regulates the cell surface dynamics of synaptic GABAA receptors. J. Neurosci. Off. J. Soc. Neurosci. 25, 10469–10478.

Jahn, R., and Grubmüller, H. (2002). Membrane fusion. Curr. Opin. Cell Biol. 14, 488–495.

Jahn, R., and Scheller, R.H. (2006). SNAREs — engines for membrane fusion. Nat. Rev. Mol. Cell Biol. 7, 631–643.

Jähne, S., Mikulasch, F., Heuer, H.G.H., Truckenbrodt, S., Agüi-Gonzalez, P., Grewe, K., Vogts, A., Rizzoli, S.O., and Priesemann, V. (2021). Presynaptic activity and protein turnover are correlated at the single-synapse level. Cell Rep. 34, 108841.

Jakobsson, J., Gad, H., Andersson, F., Löw, P., Shupliakov, O., and Brodin, L. (2008). Role of epsin 1 in synaptic vesicle endocytosis. Proc. Natl. Acad. Sci. U. S. A. 105, 6445–6450.

Jäpel, M., Gerth, F., Sakaba, T., Bacetic, J., Yao, L., Koo, S.-J., Maritzen, T., Freund, C., and Haucke, V. (2020). Intersectin-Mediated Clearance of SNARE Complexes Is Required for Fast Neurotransmission. Cell Rep. 30, 409-420.e6.

Jordan, R., Lemke, E.A., and Klingauf, J. (2005). Visualization of Synaptic Vesicle Movement in Intact Synaptic Boutons Using Fluorescence Fluctuation Spectroscopy. Biophys. J. 89, 2091–2102.

Kamin, D., Lauterbach, M.A., Westphal, V., Keller, J., Schönle, A., Hell, S.W., and Rizzoli, S.O. (2010). High- and Low-Mobility Stages in the Synaptic Vesicle Cycle. Biophys. J. 99, 675–684.

Kang, M., Day, C.A., Kenworthy, A.K., and DiBenedetto, E. (2012). Simplified equation to extract diffusion coefficients from confocal FRAP data. Traffic Cph. Den. 13, 1589–1600.

Karatekin, E., Giovanni, J.D., Iborra, C., Coleman, J., O'Shaughnessy, B., Seagar, M., and Rothman, J.E. (2010). A fast, single-vesicle fusion assay mimics physiological SNARE requirements. Proc. Natl. Acad. Sci. 107, 3517–3521.

Kawasaki, F., Zou, B., Xu, X., and Ordway, R.W. (2004). Active Zone Localization of Presynaptic Calcium Channels Encoded by the cacophony Locus of Drosophila. J. Neurosci. 24, 282–285.

Kononenko, N.L., and Haucke, V. (2015). Molecular mechanisms of presynaptic membrane retrieval and synaptic vesicle reformation. Neuron 85, 484–496.

Kononenko, N.L., Puchkov, D., Classen, G.A., Walter, A.M., Pechstein, A., Sawade, L., Kaempf, N., Trimbuch, T., Lorenz, D., Rosenmund, C., et al. (2014). Clathrin/AP-2 Mediate Synaptic Vesicle Reformation from Endosome-like Vacuoles but Are Not Essential for Membrane Retrieval at Central Synapses. Neuron 82, 981–988.

Krueger, B.K., Forn, J., and Greengard, P. (1977). Depolarization-induced phosphorylation of specific proteins, mediated by calcium ion influx, in rat brain synaptosomes. J. Biol. Chem. 252, 2764–2773.

Landis, D.M.D., Hall, A.K., Weinstein, L.A., and Reese, T.S. (1988). The organization of cytoplasm at the presynaptic active zone of a central nervous system synapse. Neuron 1, 201–209.

Lee, S., Jung, K.J., Jung, H.S., and Chang, S. (2012). Dynamics of Multiple Trafficking Behaviors of Individual Synaptic Vesicles Revealed by Quantum-Dot Based Presynaptic Probe. PLOS ONE 7, e38045.

Liu, C., Liu, Y.-L., Perillo, E.P., Dunn, A.K., and Yeh, H.-C. (2016). Single-Molecule Tracking and Its Application in Biomolecular Binding Detection. IEEE J. Sel. Top. Quantum Electron. Publ. IEEE Lasers Electro-Opt. Soc. 22, 6804013.

LoGiudice, L., Sterling, P., and Matthews, G. (2008). Mobility and Turnover of Vesicles at the Synaptic Ribbon. J. Neurosci. 28, 3150–3158.

Maas, C., Torres, V.I., Altrock, W.D., Leal-Ortiz, S., Wagh, D., Terry-Lorenzo, R.T., Fejtova, A., Gundelfinger, E.D., Ziv, N.E.,

and Garner, C.C. (2012). Formation of Golgi-Derived Active Zone Precursor Vesicles. J. Neurosci. 32, 11095–11108.

Maeder, C.I., San-Miguel, A., Wu, E.Y., Lu, H., and Shen, K. (2014). In Vivo Neuron-Wide Analysis of Synaptic Vesicle Precursor Trafficking. Traffic 15, 273–291.

McMahon, H.T., and Boucrot, E. (2011). Molecular mechanism and physiological functions of clathrin-mediated endocytosis. Nat. Rev. Mol. Cell Biol. 12, 517–533.

Medine, C.N., Rickman, C., Chamberlain, L.H., and Duncan, R.R. (2007). Munc18-1 prevents the formation of ectopic SNARE complexes in living cells. J. Cell Sci. 120, 4407–4415.

Meier, J., Vannier, C., Sergé, A., Triller, A., and Choquet, D. (2001). Fast and reversible trapping of surface glycine receptors by gephyrin. Nat. Neurosci. 4, 253–260.

Milles, S., Tyagi, S., Banterle, N., Koehler, C., VanDelinder, V., Plass, T., Neal, A.P., and Lemke, E.A. (2012). Click Strategies for Single-Molecule Protein Fluorescence. J. Am. Chem. Soc. 134, 5187–5195.

Milosevic, I. (2018). Revisiting the Role of Clathrin-Mediated Endoytosis in Synaptic Vesicle Recycling. Front. Cell. Neurosci. 12, 27.

Milovanovic, D., and Camilli, P.D. (2017). Synaptic Vesicle Clusters at Synapses: A Distinct Liquid Phase? Neuron 93, 995–1002.

Milovanovic, D., Wu, Y., Bian, X., and Camilli, P.D. (2018). A liquid phase of synapsin and lipid vesicles. Science 361, 604–607.

Missler, M., and Südhof, T.C. (1998). Neurexins: Three genes and 1001 products. Trends Genet. 14, 20–26.

Mizoguchi, A., Nakanishi, H., Kimura, K., Matsubara, K., Ozaki-Kuroda, K., Katata, T., Honda, T., Kiyohara, Y., Heo, K., Higashi, M., et al. (2002). Nectin : an adhesion molecule involved in formation of synapses. J. Cell Biol. 156, 555–565.

Mohrmann, R., de Wit, H., Verhage, M., Neher, E., and Sørensen, J.B. (2010). Fast vesicle fusion in living cells requires at least three SNARE complexes. Science 330, 502–505.

Molliex, A., Temirov, J., Lee, J., Coughlin, M., Kanagaraj, A.P., Kim, H.J., Mittag, T., and Taylor, J.P. (2015). Phase separation by low complexity domains promotes stress granule assembly and drives pathological fibrillization. Cell 163, 123–133.

Monaldi, I., Vassalli, M., Bachi, A., Giovedì, S., Millo, E., Valtorta, F., Raiteri, R., Benfenati, F., and Fassio, A. (2010). The highly conserved synapsin domain E mediates synapsin dimerization and phospholipid vesicle clustering. Biochem. J. 426, 55–64.

Montecucco, C., Schiavo, G., and Pantano, S. (2005). SNARE complexes and neuroexocytosis: how many, how close? Trends Biochem. Sci. 30, 367–372.

Morales, M., Colicos, M.A., and Goda, Y. (2000). Actin-Dependent Regulation of Neurotransmitter Release at Central Synapses. Neuron 27, 539–550.

Murthy, V.N., and De Camilli, P. (2003). Cell biology of the presynaptic terminal. Annu. Rev. Neurosci. 26, 701–728.

Murthy, V.N., Sejnowski, T.J., and Stevens, C.F. (1997). Heterogeneous release properties of visualized individual hippocampal synapses. Neuron 18, 599–612.

Newton, A.J., Kirchhausen, T., and Murthy, V.N. (2006). Inhibition of dynamin completely blocks compensatory synaptic vesicle endocytosis. Proc. Natl. Acad. Sci. 103, 17955–17960.

Nott, T.J., Petsalaki, E., Farber, P., Jervis, D., Fussner, E., Plochowietz, A., Craggs, T.D., Bazett-Jones, D.P., Pawson, T., Forman-Kay, J.D., et al. (2015). Phase transition of a disordered nuage protein generates environmentally responsive membraneless organelles. Mol. Cell 57, 936–947.

Okamoto, M., Schoch, S., and Südhof, T.C. (1999). EHSH1/intersectin, a protein that contains EH and SH3 domains and binds to dynamin and SNAP-25. A protein connection between exocytosis and endocytosis? J. Biol. Chem. 274, 18446–18454.

Orenbuch, A., Shalev, L., Marra, V., Sinai, I., Lavy, Y., Kahn, J., Burden, J.J., Staras, K., and Gitler, D. (2012). Synapsin selectively controls the mobility of resting pool vesicles at hippocampal terminals. J. Neurosci. Off. J. Soc. Neurosci. 32, 3969–3980.

Palay, S.L. (1956). SYNAPSES IN THE CENTRAL NERVOUS SYSTEM. J. Biophys. Biochem. Cytol. 2, 193–202.

Park, D., Wu, Y., Lee, S.-E., Kim, G., Jeong, S., Milovanovic, D., De Camilli, P., and Chang, S. (2021). Cooperative function of synaptophysin and synapsin in the generation of synaptic vesicle-like clusters in non-neuronal cells. Nat. Commun. 12, 263.

Patel, A., Lee, H.O., Jawerth, L., Maharana, S., Jahnel, M., Hein, M.Y., Stoynov, S., Mahamid, J., Saha, S., Franzmann, T.M., et al. (2015). A Liquid-to-Solid Phase Transition of the ALS Protein FUS Accelerated by Disease Mutation. Cell 162, 1066–1077.

Pechstein, A., Shupliakov, O., and Haucke, V. (2010). Intersectin 1: a versatile actor in the synaptic vesicle cycle. Biochem. Soc. Trans. 38, 181–186.

Pechstein, A., Tomilin, N., Fredrich, K., Vorontsova, O., Sopova, E., Evergren, E., Haucke, V., Brodin, L., and Shupliakov, O. (2020). Vesicle Clustering in a Living Synapse Depends on a Synapsin Region that Mediates Phase Separation. Cell Rep. 30, 2594-2602.e3.

Perkins, G.A., Tjong, J., Brown, J.M., Poquiz, P.H., Scott, R.T., Kolson, D.R., Ellisman, M.H., and Spirou, G.A. (2010). The Micro-Architecture of Mitochondria at Active Zones: Electron Tomography Reveals Novel Anchoring Scaffolds and Cristae Structured for High-Rate Metabolism. J. Neurosci. Off. J. Soc. Neurosci. 30, 1015–1026.

Predescu, S.A., Predescu, D.N., Timblin, B.K., Stan, R.V., and Malik, A.B. (2003). Intersectin regulates fission and internalization of caveolae in endothelial cells. Mol. Biol. Cell 14, 4997–5010.

Prekeris, R., and Terrian, D.M. (1997). Brain myosin V is a synaptic vesicle-associated motor protein: evidence for a Ca2+-dependent interaction with the synaptobrevin-synaptophysin complex. J. Cell Biol. 137, 1589–1601.

Rea, R., Li, J., Dharia, A., Levitan, E.S., Sterling, P., and Kramer, R.H. (2004). Streamlined Synaptic Vesicle Cycle in Cone Photoreceptor Terminals. Neuron 41, 755–766.

Reshetniak, S., and Rizzoli, S.O. (2019). Interrogating Synaptic Architecture: Approaches for Labeling Organelles and Cytoskeleton Components. Front. Synaptic Neurosci. 11, 23.

Reshetniak, S., and Rizzoli, S.O. (2021). The vesicle cluster as a major organizer of synaptic composition in the short-term and long-term. Curr. Opin. Cell Biol. 71, 63–68.

Reshetniak, S., Fernández-Busnadiego, R., Müller, M., Rizzoli, S.O., and Tetzlaff, C. (2020). Quantitative Synaptic Biology: A Perspective on Techniques, Numbers and Expectations. Int. J. Mol. Sci. 21, E7298.

Rey, S., Marra, V., Smith, C., and Staras, K. (2020). Nanoscale Remodeling of Functional Synaptic Vesicle Pools in Hebbian Plasticity. Cell Rep. 30, 2006-2017.e3.

Ribrault, C., Reingruber, J., Petković, M., Galli, T., Ziv, N.E., Holcman, D., and Triller, A. (2011). Syntaxin1A Lateral Diffusion Reveals Transient and Local SNARE Interactions. J. Neurosci. 31, 17590–17602.

Richards, D.A., Rizzoli, S.O., and Betz, W.J. (2004). Effects of wortmannin and latrunculin A on slow endocytosis at the frog neuromuscular junction. J. Physiol. 557, 77–91.

Richmond, J.E., Weimer, R.M., and Jorgensen, E.M. (2001). An open form of syntaxin bypasses the requirement for UNC-13 in vesicle priming. Nature 412, 338–341.

Rickman, C., Medine, C.N., Dun, A.R., Moulton, D.J., Mandula, O., Halemani, N.D., Rizzoli, S.O., Chamberlain, L.H., and Duncan, R.R. (2010). t-SNARE protein conformations patterned by the lipid microenvironment. J. Biol. Chem. 285, 13535–13541.

Rizo, J., and Südhof, T.C. (2002). Snares and munc18 in synaptic vesicle fusion. Nat. Rev. Neurosci. 3, 641–653.

Robitaille, R., Adler, E.M., and Charlton, M.P. (1990). Strategic location of calcium channels at transmitter release sites of frog neuromuscular synapses. Neuron 5, 773–779.

Rollenhagen, A., and Lübke, J.H.R. (2006). The morphology of excitatory central synapses: from structure to function. Cell Tissue Res. 326, 221–237.

Rothman, J.S., Kocsis, L., Herzog, E., Nusser, Z., and Silver, R.A. (2016). Physical determinants of vesicle mobility and supply at a central synapse. ELife 5, e15133.

Rothnie, A., Clarke, A.R., Kuzmic, P., Cameron, A., and Smith, C.J. (2011). A sequential mechanism for clathrin cage disassembly by 70-kDa heat-shock cognate protein (Hsc70) and auxilin. Proc. Natl. Acad. Sci. 108, 6927–6932.

Rougon, G., and Hobert, O. (2003). New insights into the diversity and function of neuronal immunoglobulin superfamily molecules. Annu. Rev. Neurosci. 26, 207–238.

Sabo, S.L., and McAllister, A.K. (2003). Mobility and cycling of synaptic protein-containing vesicles in axonal growth cone filopodia. Nat. Neurosci. 6, 1264–1269.

Sakata, J.T., and Jones, T.A. (2003). Synaptic mitochondrial changes in the motor cortex following unilateral cortical lesions and motor skills training in adult male rats. Neurosci. Lett. 337, 159–162.

Sankaranarayanan, S., Atluri, P.P., and Ryan, T.A. (2003). Actin has a molecular scaffolding, not propulsive, role in presynaptic function. Nat. Neurosci. 6, 127–135.

Scarnati, M.S., Kataria, R., Biswas, M., and Paradiso, K.G. (2018). Active presynaptic ribosomes in the mammalian brain, and altered transmitter release after protein synthesis inhibition. ELife 7, e36697.

Scheiffele, P., Fan, J., Choih, J., Fetter, R., and Serafini, T. (2000). Neuroligin Expressed in Nonneuronal Cells Triggers Presynaptic Development in Contacting Axons. Cell 101, 657–669.

Schikorski, T., and Stevens, C.F. (1997). Quantitative ultrastructural analysis of hippocampal excitatory synapses. J. Neurosci. Off. J. Soc. Neurosci. 17, 5858–5867.

Schmidt, T., Schütz, G.J., Baumgartner, W., Gruber, H.J., and Schindler, H. (1996). Imaging of single molecule diffusion. Proc. Natl. Acad. Sci. U. S. A. 93, 2926–2929.

Schneggenburger, R., and Neher, E. (2000). Intracellular calcium dependence of transmitter release rates at a fast central synapse. Nature 406, 889–893.

Schwille, P. (2001). Fluorescence correlation spectroscopy and its potential for intracellular applications. Cell Biochem. Biophys. 34, 383–408.

Scott, D.A., Das, U., Tang, Y., and Roy, S. (2011). Mechanistic logic underlying the axonal transport of cytosolic proteins. Neuron 70, 441–454.

Sengar, A.S., Wang, W., Bishay, J., Cohen, S., and Egan, S.E. (1999). The EH and SH3 domain Ese proteins regulate endocytosis by linking to dynamin and Eps15. EMBO J. 18, 1159–1171.

Shapira, M., Zhai, R.G., Dresbach, T., Bresler, T., Torres, V.I., Gundelfinger, E.D., Ziv, N.E., and Garner, C.C. (2003). Unitary Assembly of Presynaptic Active Zones from Piccolo-Bassoon Transport Vesicles. Neuron 38, 237–252.

Shapiro, L., and Colman, D.R. (1999). The Diversity of Cadherins and Implications for a Synaptic Adhesive Code in the CNS. Neuron 23, 427–430.

Sharma, M., Burré, J., and Südhof, T.C. (2011). CSPα promotes SNARE-complex assembly by chaperoning SNAP-25 during synaptic activity. Nat. Cell Biol. 13, 30–39.

Shen, K., and Meyer, T. (1999). Dynamic Control of CaMKII Translocation and Localization in Hippocampal Neurons by NMDA Receptor Stimulation. Science 284, 162–167.

Shen, J., Tareste, D.C., Paumet, F., Rothman, J.E., and Melia, T.J. (2007). Selective activation of cognate SNAREpins by Sec1/Munc18 proteins. Cell 128, 183–195.

Shepherd, G.M., and Harris, K.M. (1998). Three-dimensional structure and composition of CA3-->CA1 axons in rat hippocampal slices: implications for presynaptic connectivity and compartmentalization. J. Neurosci. Off. J. Soc. Neurosci. 18, 8300–8310.

Shi, L., Shen, Q.-T., Kiel, A., Wang, J., Wang, H.-W., Melia, T.J., Rothman, J.E., and Pincet, F. (2012). SNARE Proteins: One to Fuse and Three to Keep the Nascent Fusion Pore Open. Science 335, 1355–1359.

Shin, Y., and Brangwynne, C.P. (2017). Liquid phase condensation in cell physiology and disease. Science 357.

Shnyrova, A.V., Bashkirov, P.V., Akimov, S.A., Pucadyil, T.J., Zimmerberg, J., Schmid, S.L., and Frolov, V.A. (2013). Geometric catalysis of membrane fission driven by flexible dynamin rings. Science 339, 1433–1436.

Shtrahman, M., Yeung, C., Nauen, D.W., Bi, G., and Wu, X. (2005). Probing Vesicle Dynamics in Single Hippocampal Synapses. Biophys. J. 89, 3615–3627.

Shupliakov, O. (2009). The synaptic vesicle cluster: a source of endocytic proteins during neurotransmitter release. Neuroscience 158, 204–210.

Shupliakov, O., Bloom, O., Gustafsson, J.S., Kjaerulff, O., Low, P., Tomilin, N., Pieribone, V.A., Greengard, P., and Brodin, L. (2002). Impaired recycling of synaptic vesicles after acute perturbation of the presynaptic actin cytoskeleton. Proc. Natl. Acad. Sci. U. S. A. 99, 14476–14481.

Shupliakov, O., Haucke, V., and Pechstein, A. (2011). How synapsin I may cluster synaptic vesicles. Semin. Cell Dev. Biol. 22, 393–399.

Siksou, L., Rostaing, P., Lechaire, J.-P., Boudier, T., Ohtsuka, T., Fejtová, A., Kao, H.-T., Greengard, P., Gundelfinger, E.D., Triller, A., et al. (2007). Three-dimensional architecture of presynaptic terminal cytomatrix. J. Neurosci. Off. J. Soc. Neurosci. 27, 6868–6877.

Singh, N., Bartol, T., Levine, H., Sejnowski, T., and Nadkarni, S. (2021). Presynaptic endoplasmic reticulum regulates short-

term plasticity in hippocampal synapses. Commun. Biol. 4, 1–13.

Sinha, R., Ahmed, S., Jahn, R., and Klingauf, J. (2011). Two synaptobrevin molecules are sufficient for vesicle fusion in central nervous system synapses. Proc. Natl. Acad. Sci. U. S. A. 108, 14318–14323.

Smith, S.M., Renden, R., and von Gersdorff, H. (2008). Synaptic vesicle endocytosis: fast and slow modes of membrane retrieval. Trends Neurosci. 31, 559–568.

Soykan, T., Maritzen, T., and Haucke, V. (2016). Modes and mechanisms of synaptic vesicle recycling. Curr. Opin. Neurobiol. 39, 17–23.

Staras, K., Branco, T., Burden, J.J., Pozo, K., Darcy, K., Marra, V., Ratnayaka, A., and Goda, Y. (2010). A Vesicle Superpool Spans Multiple Presynaptic Terminals in Hippocampal Neurons. Neuron 66, 37–44.

Stepanova, T., Slemmer, J., Hoogenraad, C.C., Lansbergen, G., Dortland, B., De Zeeuw, C.I., Grosveld, F., van Cappellen, G., Akhmanova, A., and Galjart, N. (2003). Visualization of microtubule growth in cultured neurons via the use of EB3-GFP (end-binding protein 3-green fluorescent protein). J. Neurosci. Off. J. Soc. Neurosci. 23, 2655–2664.

Südhof, T.C., Czernik, A.J., Kao, H.T., Takei, K., Johnston, P.A., Horiuchi, A., Kanazir, S.D., Wagner, M.A., Perin, M.S., and De Camilli, P. (1989). Synapsins: mosaics of shared and individual domains in a family of synaptic vesicle phosphoproteins. Science 245, 1474–1480.

Takamori, S., Holt, M., Stenius, K., Lemke, E.A., Grønborg, M., Riedel, D., Urlaub, H., Schenck, S., Brügger, B., Ringler, P., et al. (2006). Molecular Anatomy of a Trafficking Organelle. Cell 127, 831–846.

Tang, J., Maximov, A., Shin, O.-H., Dai, H., Rizo, J., and Südhof, T.C. (2006). A complexin/synaptotagmin 1 switch controls fast synaptic vesicle exocytosis. Cell 126, 1175–1187.

Tang, Y., Scott, D.A., Das, U., Edland, S.D., Radomski, K., Koo, E.H., and Roy, S. (2012). Early and Selective Impairments in Axonal Transport Kinetics of Synaptic Cargoes Induced by Soluble Amyloid β-Protein Oligomers. Traffic 13, 681–693.

Tang, Y., Scott, D., Das, U., Gitler, D., Ganguly, A., and Roy, S. (2013). Fast vesicle transport is required for the slow axonal transport of synapsin. J. Neurosci. Off. J. Soc. Neurosci. 33, 15362–15375.

Tao-Cheng, J.-H. (2007). Ultrastructural Localization of Active Zone and Synaptic Vesicle Proteins in a Preassembled Multi-vesicle Transport Aggregate. Neuroscience 150, 575–584.

Tardin, C., Cognet, L., Bats, C., Lounis, B., and Choquet, D. (2003). Direct imaging of lateral movements of AMPA receptors inside synapses. EMBO J. 22, 4656–4665.

Terada, S., Kinjo, M., Aihara, M., Takei, Y., and Hirokawa, N. (2010). Kinesin-1/Hsc70-dependent mechanism of slow axonal transport and its relation to fast axonal transport. EMBO J. 29, 843–854.

Tokuoka, H., and Goda, Y. (2006). Myosin Light Chain Kinase Is Not a Regulator of Synaptic Vesicle Trafficking during Repetitive Exocytosis in Cultured Hippocampal Neurons. J. Neurosci. 26, 11606–11614.

Truckenbrodt, S., Viplav, A., Jähne, S., Vogts, A., Denker, A., Wildhagen, H., Fornasiero, E.F., and Rizzoli, S.O. (2018). Newly produced synaptic vesicle proteins are preferentially used in synaptic transmission. EMBO J. e98044.

Ungewickell, E., Ungewickell, H., Holstein, S.E., Lindner, R., Prasad, K., Barouch, W., Martin, B., Greene, L.E., and Eisenberg, E. (1995). Role of auxilin in uncoating clathrin-coated vesicles. Nature 378, 632–635.

Van der Kloot, W. (2003). Loading and recycling of synaptic vesicles in the Torpedo electric organ and the vertebrate neuromuscular junction. Prog. Neurobiol. 71, 269–303.

Verhey, K.J., Meyer, D., Deehan, R., Blenis, J., Schnapp, B.J., Rapoport, T.A., and Margolis, B. (2001). Cargo of Kinesin Identified as Jip Scaffolding Proteins and Associated Signaling Molecules. J. Cell Biol. 152, 959–970.

Verstreken, P., Ly, C.V., Venken, K.J.T., Koh, T.-W., Zhou, Y., and Bellen, H.J. (2005). Synaptic Mitochondria Are Critical for Mobilization of Reserve Pool Vesicles at Drosophila Neuromuscular Junctions. Neuron 47, 365–378.

Walling, M.A., Novak, J.A., and Shepard, J.R.E. (2009). Quantum Dots for Live Cell and In Vivo Imaging. Int. J. Mol. Sci. 10, 441–491.

Walsh, F.S., and Doherty, P. (1997). NEURAL CELL ADHESION MOLECULES OF THE IMMUNOGLOBULIN SUPERFAMILY: Role in Axon Growth and Guidance. Annu. Rev. Cell Dev. Biol. 13, 425–456.

Wang, Y., Okamoto, M., Schmitz, F., Hofmann, K., and Südhof, T.C. (1997). Rim is a putative Rab3 effector in regulating synaptic-vesicle fusion. Nature 388, 593–598.

Wang, Y., Liu, X., Biederer, T., and Südhof, T.C. (2002). A family of RIM-binding proteins regulated by alternative splicing: Implications for the genesis of synaptic active zones. Proc. Natl. Acad. Sci. 99, 14464–14469.

Weber, T., Zemelman, B.V., McNew, J.A., Westermann, B., Gmachl, M., Parlati, F., Söllner, T.H., and Rothman, J.E. (1998). SNAREpins: minimal machinery for membrane fusion. Cell 92, 759–772.

Weninger, K., Bowen, M.E., Choi, U.B., Chu, S., and Brunger, A.T. (2008). Accessory proteins stabilize the acceptor complex for synaptobrevin, the 1:1 syntaxin/SNAP-25 complex. Struct. Lond. Engl. 1993 16, 308–320.

White, K.I., Zhao, M., Choi, U.B., Pfuetzner, R.A., and Brunger, A.T. (2018). Structural principles of SNARE complex recognition by the AAA+ protein NSF. ELife 7, e38888.

Wilhelm, B.G., Mandad, S., Truckenbrodt, S., Kröhnert, K., Schäfer, C., Rammner, B., Koo, S.J., Claßen, G.A., Krauss, M., Haucke, V., et al. (2014). Composition of isolated synaptic boutons reveals the amounts of vesicle trafficking proteins. Science 344, 1023–1028.

Wu, X., Cai, Q., Shen, Z., Chen, X., Zeng, M., Du, S., and Zhang, M. (2019). RIM and RIM-BP Form Presynaptic Active-Zone-like Condensates via Phase Separation. Mol. Cell 0.

Wu, X., Ganzella, M., Zhou, J., Zhu, S., Jahn, R., and Zhang, M. (2020). Vesicle Tethering on the Surface of Phase-Separated Active Zone Condensates. Mol. Cell.

Wu, Y.E., Huo, L., Maeder, C.I., Feng, W., and Shen, K. (2013). The Balance between Capture and Dissociation of Presynaptic Proteins Controls the Spatial Distribution of Synapses. Neuron 78, 994–1011.

Younts, T.J., Monday, H.R., Dudok, B., Klein, M.E., Jordan, B.A., Katona, I., and Castillo, P.E. (2016). Presynaptic Protein Synthesis Is Required for Long-Term Plasticity of GABA Release. Neuron 92, 479–492.

Zeng, M., Chen, X., Guan, D., Xu, J., Wu, H., Tong, P., and Zhang, M. (2018). Reconstituted Postsynaptic Density as a Molecular Platform for Understanding Synapse Formation and Plasticity. Cell 174, 1172-1187.e16.

ACKNOWLEDGEMENTS

The work presented here would not be possible without contributions of my colleagues and help and support of all with whom I have shared my path towards this point, and to all of whom I am deeply thankful.

Most of all, my gratitude goes to my supervisor Prof. Dr. Silvio O. Rizzoli. Thank you for this exciting and challenging project, for all the MATLAB scripts I needed for data analysis, as well as for the countless hours you spent developing the simulations used in this project. Thank you not only for your academic guidance and scientific advice, but also for your constant support and mentorship. It means a lot to have a supervisor who cares for your personal success and puts an extra effort to contribute to your development as a scientist, and I could not wish for more from mine. Thank you, Silvio.

Thank you to Prof. Reinhard Jahn and Prof. Andreas Janshoff for all the valuable comments and suggestions during our Thesis Advisory Committee meetings. Thank you to Prof. Nils Brose, Dr. Sarah Adio, and Prof. Carolin Wichmann, for joining the examination board for my thesis defense.

Thank you to the coordination office of the IMPRS Molecular Biology program, Dr. Steffen Burkhardt and Kerstin Grüninger, for their continuous help and support and for the whole excellent experience that it was to be a part of this program.

Thank you to all the co-authors of the papers presented here: Jan-Eike Ußling, Eleonora Perego, Burkhard Rammner, Thomas Schikorski, Eugenio F. Fornasiero, Sven Truckenbrodt, Sarah Köster, Charlotta Lorenz, Christian Hoffmann and Dragomir Milovanović, for their respective contributions to these papers and productive collaborations we had. Special thank you, Eleonora, for the effort and time you put into establishing the protein patterning and the FCS measurements, and for all the time we spent together working on these experiments. Thank you, Sarah, for the support you provided to make this collaboration possible.

Special thank you to Sven Truckenbrodt, with whom this project was conceived, and who guided me through my first days in the lab. I have learned a lot from you and genuinely enjoyed the time we worked together.

Thank you to Silvio Rizzoli, Oleh Rymarenko, Cera McDonald, and Tal Dankovich for their valuable suggestions and comments on the text of my thesis.

Thank you to our great TA team, Dagmar Crzan, Nicole Hartelt, Gabriele Klaehn, Christina Patzelt, and Christina Zeising, for their continuous help that allows maintaining smooth flow of the experimental work in the lab. Especially thank you, Tina, for the preparation of the hundreds of neuronal cultures I needed for my project.

Thank you to our secretariat team, Anita-Karina Jaehnke, Regina Sommer-Kluß, and Christin Wiemuth, for taking excellent care of all the administrative issues. Thank you, Anita, for the extra care you took with my contract extensions.

Thank you to all former and current members of the Rizzoli, Opazo, and Fornasiero groups for the great professional and social atmosphere in the lab. It is a pleasure to work with you and I am thankful for all the help and advice I got from each of you. Special thanks to Eugenio for the unsurpassed amount of scientific advice. Thank you to Kim, Selda, Manuel, Daniëlle, Verena, Sebastian, and Tal for sharing with me their expertise on various topics and methods throughout these years. Thank you, Hanna, Daniëlle, Paola, and Nhu for the warm atmosphere in our office while we shared it. Thank you to Tal for never relocating my pipettes. Thank you, Sinem, Sebastian, Tal, Nhu, and Shama, for your company during our conference trips. Thank you, Verena, Kim, and Sebastian, for not letting me forget what human interaction is in my post-covid office. Thank you all for all the fun we had barbecuing, hiking, boxing, jumping, lasertagging, and celebrating. Every coffee break, short chat, or portable Weihnachtsmarkt are what made the PhD times special. Thank you, Kristina, Ronja, and Nikos, for the lively energy you brought despite the challenges of the pandemics, and for my incredible Doktorhut I can't wait to see.

Thank you to Klaus and Finn, who were always there to comfort, motivate, and cheer me up.

And thank you to Oleh, without whose help, advice, and support this thesis would not exist.

CURRICULUM VITAE

Education

2017 –2021	Doctoral program “Molecular Biology” Georg-August University School of Science, International Max Plank Research School for Molecular Biology
2015 –2017	Master of Science program “Molecular Biology” Georg-August University Göttingen, International Max Plank Research School for Molecular Biology
2010 –2014	Bachelor of Science program “Biology” Taras Shevchenko National University of Kyiv, ESC “Institute of Biology”, Department of Biochemistry

Research experience

since June 2017	PhD thesis project Institute of Neuro- and Sensory Physiology at University Medical Center Göttingen
October – March 2017	MSc thesis project Institute of Neuro- and Sensory Physiology at University Medical Center Göttingen
May – June 2016	IMPRS laboratory rotation Department of Bioanalytical Mass Spectrometry at Max-Plank Institute for Biophysical Chemistry, Göttingen
March – April 2016	IMPRS laboratory rotation Institute of Neuro- and Sensory Physiology at University Medical Center Göttingen
January – February 2016	IMPRS laboratory rotation Department of Cellular Logistics at Max-Plank Institute for Biophysical Chemistry, Göttingen
2014 – 2015	Graduate research assistant Department of Functional Genomics, Institute of Molecular Biology and Genetics of The National Academy of Sciences of Ukraine
2012 – 2014	Undergraduate research assistant, BSc thesis project Department of Functional Genomics, Institute of Molecular Biology and Genetics of The National Academy of Sciences of Ukraine

List of Publications

Perego, E.*, **Reshetniak, S.***, Lorenz, C., Hoffmann, C., Milovanović, D., Rizzoli, S.O., and Köster, S. (2020). A minimalist model to measure interactions between proteins and synaptic vesicles. Sci Rep 10, 21086.

Reshetniak, S., and Rizzoli, S.O. (2019). Interrogating Synaptic Architecture: Approaches for Labeling Organelles and Cytoskeleton Components. Front Synaptic Neurosci 11, 23.

Reshetniak, S., and Rizzoli, S.O. (2021). The vesicle cluster as a major organizer of synaptic composition in the short-term and long-term. Curr Opin Cell Biol 71, 63–68.

Reshetniak, S., Ußling, J.-E., Perego, E., Rammner, B., Schikorski, T., Fornasiero, E.F., Truckenbrodt, S., Köster, S., and Rizzoli, S.O. (2020). A comparative analysis of the mobility of 45 proteins in the synaptic bouton. EMBO J 39, e104596.

Reshetniak, S., Fernández-Busnadiego, R., Müller, M., Rizzoli, S.O., and Tetzlaff, C. (2020b). Quantitative Synaptic Biology: A Perspective on Techniques, Numbers and Expectations. Int J Mol Sci 21, E7298.